Tephrochronology as a tool for assessing the synchronicity of Middle Palaeolithic and Upper Palaeolithic techno-complexes in the Caucasus

Victoria L Cullen
Keble College

A thesis submitted for the degree of Doctor of Philosophy

Archaeological Sciences
Hillary term, 2015

Acknowledgements

Embarking of a DPhil was a personal challenge and the experience, as expected, was an emotional rollercoaster. Many people have contributed in getting me through to the end and I would like to thank them all most sincerely. Two people were particularly influential in my DPhil journey. My supervisor Dr. Victoria Smith has been a constant source of calm and good advice throughout. Her dedication to her students (including myself) is outstanding and I could have not got through without her guidance and encouragement. The second person I would like to thank is my wonderful fiancé Robert Vale. Throughout all my highs and lows he has been an unwavering pillar of support, although I am sure on occasion this has been just as hard on him, thank you! In addition to these two wonderful people I am fortunate to have a number of great friends who have been with me over the last three and half years. I would like to personally thank Dr. Christine Lane for her advice, friendship and support throughout and members of 'Team Tephra Oxford' (Dr. Paul Albert, Dr. Anna Oh, Dr. Cassian Bramham Law and Dr. Richard Staff) for their support, interesting discussions and fun diversions while sieving (oh the never ending sieving). I would also like to acknowledge my many friends in and outside of RLAHA and my family who all need a huge thank you for evenings of distractions, supportive phone calls and talks - I owe you all a drink!

I was able to travel and work in some wonderful locations in the southern Caucasus. I would first like to thank Dr. Simon Blockley for facilitating introductions to work in the region and for his constant positive and supportive attitude. Working in the region was made an enjoyable experience thanks to the organisation and dedication of two brilliant individuals, Prof. Ron Pinhasi and Dr. Daniel Adler. I would like to thank them both most sincerely for allowing me to join their dynamic and interesting projects in Georgia and Armenia and for the hours of learning and enjoyment in the field. Ron and Dan were instrumental in helping me gain access to many of the sites I sub-sampled and being part of their excavation teams was a positive and instructive experience. In no particular order I would also like to thank Dr Nika Tushabramishvili, Dr Tengiz Mesheviliani, Prof. David Lordkipanidze, Dr Medea Nioradze, Dr. Boris Gasparyan and Dr. Andrew Kandel for allowing me access to their sites and Dr. Keith Wilkinson for his helpful comradery at each site while subsampling (and especially around the Georgian toasting table in the evenings). I would also like to thank Dr. Ellery Frahm for help with locating some Armenian volcanic deposits and Dr. Helge Arz for allowing me access to the Black Sea core and for his advice and guidance while writing of our paper. Additional samples from the Caucasus were provided thanks to Dr. Rupert Housley and Prof. David Pyle (EFCHED project) and from members of the RESET project. It was a pleasure to work with members associated with both these exciting projects, and I am grateful for their help and advice. I always felt very welcome in both Georgia and Armenia and this was In large thanks to the Georgian and Armenian collaborators, students, helpers and local hosts who made the whole experience one I will never forget so a final big thanks and gaumarjos and genatzt (cheers) to you all!

Table of content

Figure List

Chapter 1

Chapter 2

Chapter 3

Chapter 4

Chapter 5

Chapter 6

Chapter 7

Chapter 8

Chapter 9

List of Tables

Definition of common abbreviations found in this thesis

AMH - Anatomically Modern Humans

CI - The ~39 ka Campanian Ignimbrite tephra, from the Campi Flegrei, Italy.

TAS – Total Alkali Silica diagram

MIS – Marine Isotope stage (also OIS; Oxygen isotope stage; from ice core data) are alternating cold and warm periods in the Earth's palaeoclimate (glacial and interglacial events).

D-O - Dansgaard–Oeschger cycle; periods of rapid warming (Greenland interstadial; GI) and slow cooling events (Greenland stadial; GS) as seen in the Greenland ice cores.

HE – Henrich Events are increases in iceberg discharged that reduced ocean salinity enough to slow deep water formation and the thermohaline circulation resulting in periods of rapid cooling within the D-O cycle, typically after a warming event.

ka - Thousand years

ka cal BP - Calibrated radiocarbon years before present, or before 1950 in the case of calibrated radiocarbon ages

ka BP - Radiocarbon years before present, uncalibrated.

MP – Middle Paleolithic; MP, typically with a Levellois core technology.

UP- Upper Palaeolithic

IUP –Initial Upper Paleolithic/transitional phase. Assemblages that have MP and UP lithic like characteristics, could be a product of either AMH or Neanderthals.

EUP – Early Upper Palaeolithic. All-encompassing term of the first phase of the Upper Palaeolithic associated with AMH.

LA-ICP-MS – Laser Ablation Inductively Coupled Mass Spectrometry.

WDS-EPMA – Wave-Length Dispersive, Electron Probe Micro Analyser.

Tephrochronology as a tool for assessing the synchronicity of Middle Palaeolithic and Upper Palaeolithic techno-complexes in the Caucasus

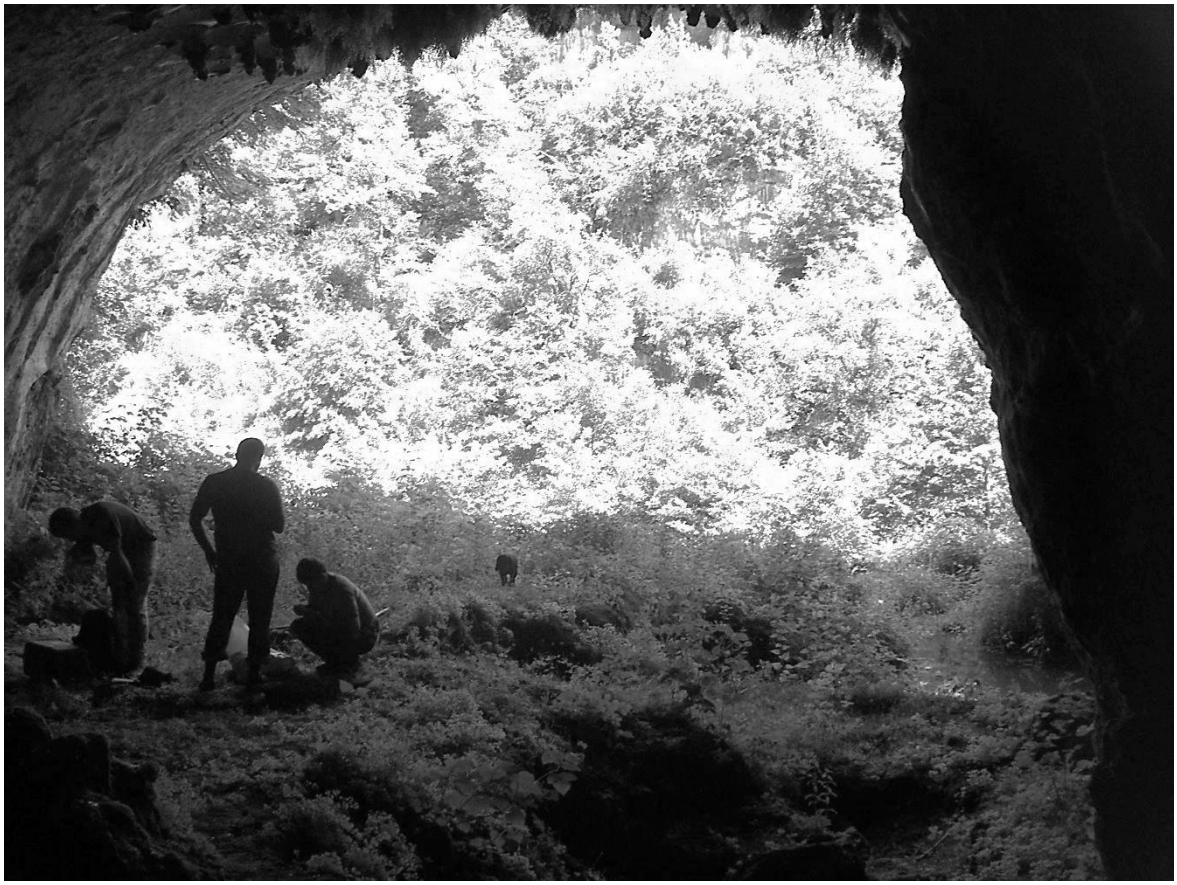

View from Dzudzuana Cave, Georgia

Victoria L Cullen

Keble College, University of Oxford,

Hillary term, 2015

Chapter 1.
Introduction to the study

1.1. Introduction

The Caucasus is a mountainous, ecologically diverse isthmus situated between the Black Sea and Caspian Sea. Given its geographical location, the Caucasus provide a natural land bridge linking Africa to northern Eurasia and is considered to have been a major migratory route for Hominin species. The region has a wide variety of ecological landscapes and niches (forest, steppe/desert) that have supported a diverse range of flora and fauna, and hunter gatherers, demonstrated by a rich Palaeolithic, archaeological record (e.g. Adler et al., 2008; Gasparyan et al., 2014a, b; Golovanova and Doronichev, 2003; Pinhasi et al., 2012). In addition, access to high quality raw materials (including extensive obsidian deposits) for lithics production have been shown to be exploited by early hominins (e.g. Le Bourdonnec et al., 2012).

Over the past decade, the Palaeolithic importance of the Caucasus has been given renewed attention due to new recovery techniques and dating protocols allowing for re-evaluations of previous interpretations, with specific interest focused on the replacement of Neanderthal species by Anatomically Modern Humans (AMH), known as the Middle to Upper Paleolithic “transition” (e.g. Adler et al., 2008; Bar-Yosef et al., 2006; Golovanova et al., 2010a). The period of interest for this studies falls within stages Marine Isotope Stage (MIS) 5e to MIS 3 (~125-30 ka). In this period, there is a greater regional diversity in Neanderthal assemblages found to the north and south of the Great Caucasus Range (e.g. Golovanova and Doronichev, 2003), the eventual demise of the Neanderthal

species and the expansion of AMH (e.g. Adler et al., 2008; Pinhasi et al., 2012) and intense climatic changes seen in the northern hemispheric climate system (e.g. Capron et al., 2010; North Greenland Ice Core Project members, 2004; Rasmussen et al., 2014). Due to limited regional palaeoenvironmental studies and a lack of robust chronological controls, the ability to assess exactly when technologies changed and timing of Neanderthal and modern humans movement though the region is restricted. Furthermore, how these relate to fluctuations in local palaeoclimate is unknown.

To answer fundamental questions of when changes occur in palaeoenvironmental and archaeological records, a robust chronological framework is required. Once a framework has been established, questions of why and how can be addressed. Volcanic ash (tephra) marker layers are a powerful and unique tool for directly synchronising and dating palaeoclimate and disparate archaeological sequences (e.g. Fedele et al., 2008; Lane et al., 2011a; Lowe et al., 2012a; Lowe, 2011), negating temporal uncertainty. The extension of these isochrones by extracting cryptically preserved tephras (those invisible to the naked eye) that can be deposited thousands of kilometres from source, termed cryptotephra, has significantly added to the tephrochronological research field. The application of tephrostratigraphy in European and the Mediterranean archaeological sites to answer when and why changes occurred is becoming more common (see Lowe et al., 2012). Recent studies have shown that visible tephra is present in stratigraphic sequences in the Caucasus and surrounding regions, e.g. Mesmaiskaya Cave (Golovanova et al., 2010a), Lake Van (Sumita & Schmincke 2013a, b) and the Black Sea (Guichard et al., 1993; Kwiecien et al., 2008; Lamy et al., 2006;

Nowaczyk et al., 2012), suggesting this is viable region for using tephrochronology to date and correlate sites. However, few authors have attempted a cryptotephra investigation of their palaeoenvironmental sequences, and even fewer have attempted such an approach in archaeological records in the region.

This DPhil research seeks to assess the potential of using volcanic ash layers to synchronise archaeological sites across the Caucasus during the mid-Middle Palaeolithic (MP) to the Middle-Upper Palaeolithic transition (~125-30 ka). This will be the first attempt to provide a detailed tephrostratigraphic framework for this geographically and archaeologically important region. This framework will be used to assess the relative timing of archaeological events in the region and establish how these related to changes in palaeoclimate.

1.2. The Middle to Upper Palaeolithic transition

One of the most debated archaeological periods in the timeframe of this study is the archaeological change that is commonly referred to as the MP to Upper Paleolithic (UP) 'transition'* at ~ 45 ka BP. At this time there is a significant technological, cognitive and behavioural change that is seen in the archaeological record in Eurasia. Archaeological remains show a diversification of tool kits (lithic and bone), and the appearance of personal adornment with expressions of advanced artistic capability (e.g. Bar-Yosef, 2002). This period is also coincident with the (eventual) biological replacement of an archaic population, Neanderthals, by an expanding population of AMH. Studies into the technological and biological

**The term 'transition' is used to describe the period in time that saw the decline of Neanderthals and the coincident expansion of AMH, and does not imply causality.*

replacement of Neanderthals by AMH, offers archaeologists and paleoanthropologists a unique chance to investigate factors relating to the replacement of one species by another. Big questions such as how and when AMH entered northern Eurasia, the degree of interaction of the two species, where interaction may have occurred, and the how and why Neanderthals became extinct are not fully resolved (e.g. Adler and Jöris, 2008; Fu et al., 2014; Hublin, 2012; Mellars, 2004; 2005; 2011; Villa and Roebroeks, 2014). Genetic studies have shown that there was a limited genetic contribution of Neanderthals to the AMH genome and that contact likely occurred 50 to 60 ka, after the major expansion of AMH out of Africa, and prior to their full expansion across Eurasia (Green et al., 2010; Fu et al., 2014). This interbreeding may have occurred in the Levantine corridor (see Hershkovitz et al., 2015). More recently genetic studies have also revealed admixture of a third species into the genomic make up of both AMH and Neanderthals from a (currently geographically restricted) Siberian species known as the Denisovans (Meyer et al., 2012; Prufer et al., 2014; Reich et al., 2010). This information highlights the increasing complexity of this period in archaeology and human evolution as research improves and focus expands beyond the Eurocentric. Developing robust chronologies in regions where we have the potential records of the early expansion of AMH, such as those across the Caucasus, is essential to test hypotheses related to periods of coexistence and/or replacement by early humans.

In recent years, genetic studies have questioned some models to explain the replacement (e.g. *regional continuity* and *multi regionalism models* whereby indigenous Neanderthals instigated the change and directly evolved into AMH; e.g., Wolpoff et al., 2001), with evidence of limited interbreeding suggesting that

Neanderthals were not simply replaced by AMH. Consequently, focus is now directed towards models of *assimilation*, *acculturation* and *interbreeding.* These models imply a degree of engagement and co-existence (spatially variable) of the indigenous Neanderthals with AMH (e.g. Bar-Yosef, 1998; Higham et al., 2014; Smith et al., 2005; Mellars, 2005; Villa and Roebroeks, 2014). For example, it is now thought the two species may have overlapped for a significant amount of time, ~5000 years in some regions of western Europe (Higham et al., 2014). However, the disappearance of Neanderthals was not temporally and geographically uniform suggesting a complex (as yet unknown) mosaic of replacement that took place across the greater Eurasian region. The reasons why Neanderthals ultimately became extinct are still debated (e.g. Golovanova et al., 2010a; Lowe et al., 2012; Villa and Roebroeks, 2014).

There certainly was a movement of AMH from Africa, and they then proceeded to successfully expand into Eurasia and beyond (e.g. the Out of Africa 2b scenario; Garcea, 2012). Proposed routes for early migrations into Europe and northern Eurasia after leaving Africa have included two routes that circumvent the Mediterranean rim, and one that follows the route of the Danube fluvial corridor (Mellars et al., 2004; 2011; Figure 1.1). These routes are based on the geography and the ages of changing techno-complexes. For example prior to a fully-fledged UP (e.g. the 'classic' Aurignacian in western Europe), there were a number of techno-complexes that show diversity in material culture across Eurasia. These techno-complexes are sometimes referred to as 'transitional' but should be referred to as the initial UP (IUP; e.g. the Uluzzian industry in Italy and the Emiran in the Levant; Kuhn et al., 1999), that was subsequently followed by the early UP (EUP) techno-complexes (e.g. the EUP proto-Aurignacian of west/central Europe

and the Levantine Ahmarian). The scarcity of identifiable human remains securely associated with these IUP/transitional and EUP assemblages and the lack of chronological control means authorship of some of these techno-complexes is still disputed (e.g. Bar-Yosef and Bordes, 2010; Davies, 2001; d'Errico, 2003; Hublin et al., 2012; Mellars, 2005; Zilhão, 2006). However, these proposed passages rarely consider a north-eastern expansion of AMH to northern Eurasia through the Caucasus (see Figure 1.1) that contains an EUP bone and stone techno-complex thought to be similar to the Levantine Ahmarian (Golovanova et al., 2010a, b). There is a significant gap in our current understanding of how, why and when these expansions occurred on a larger scale and how the Caucasus fits into the larger mosaic of spatial and temporal change. Therefore, further investigation is warranted in the Caucasus' unique, geographic corridor.

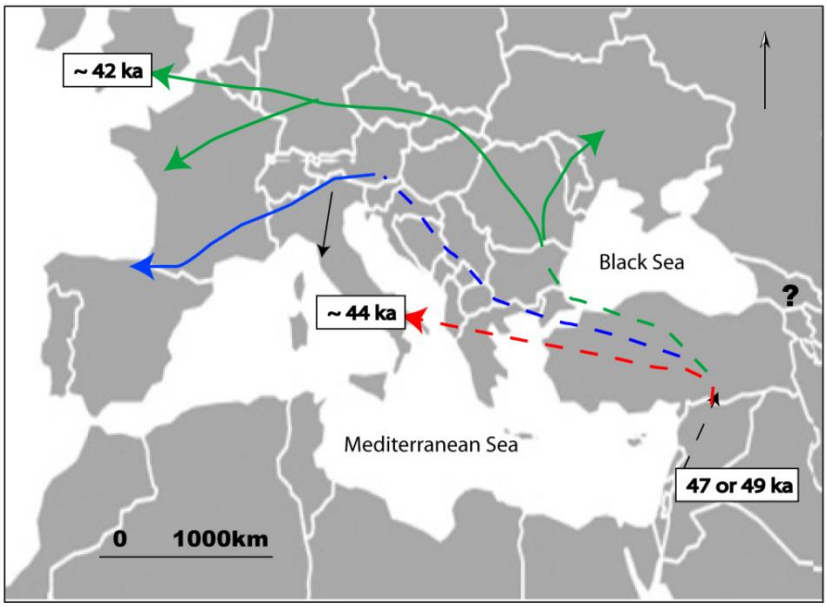

Figure 1.1. Proposed dispersal routes for AMH populations across Europe after Mellars (2011). Two main trajectories are suggested, the northern route tracks the Danube corridor (solid green line) and is associated with UP Aurignacian technologies. The southern expansions follow the Mediterranean rim (dotted red and blue lines) and are associated with bladelet technologies of the EUP, Proto-Aurignacian and the IUP Uluzzian techno complex. Numbers denote calibrated radiocarbon dates BP from Mellars (2011). Question mark symbol shows location of the Caucasus as it is not clear whether it was an early dispersal route. Note that the earlier expansion routes (~>60 ka) of modern humans have also been

proposed through southern Asia, to Arabia and beyond (see Dennell and Petraglia, 2012; Petraglia, 2011).

1.3. The chronological framework

Archaeological information from AMH and Neanderthals derives from the artefactual evidence. Therefore the precise rates of change and the construction of an absolute chronology is key to testing hypothesis relating to the mechanism of technological change. The main method used to date the transitional period is radiocarbon dating. Recent advances in radiocarbon calibration methods in the last 5 years (IntCal09 and IntCal13; Reimer et al., 2009 and 2013) provide more accurate means of establishing a calendar age against which the ^{14}C determination can be directly compared. In addition, the development of pre-treatment methods (e.g., Ultrafiltration, Higham et al., 2006; ABOx-SC, Bird et al., 1999; CarDS, Douka et al., 2010) to remove sample contamination (especially from weathered samples; Higham et al., 2009) has also helped to increase the accuracy of ages of old (>30 ka) samples (e.g. Higham et al., 2009; Wood et al., 2012). Radiocarbon dates produced prior to these advancements should be regarded as a minimum age estimates or rejected (see Blockley et al., 2008; Higham et al., 2009; Mellars, 2006).

This period of replacement of Neanderthals by AMH sits at or close to the current limits of radiocarbon dating (~50 ka), with the MP period beyond this age. Thus, there is a need for other chronological techniques, such as thermo-luminescence (TL), optically stimulated luminescence (OSL) and electron spin resonance (ESR), to provide additional chronological control. These techniques are especially useful in regions where organic finds are lacking. At present, site to site comparisons in

the Caucasus are based on a range of data (e.g. calibrated radiocarbon dates, un-calibrated radiocarbon ages, ESR data and OSL and TL data) with inter-site comparisons based on coarse lithic typologies and/or assumed climatic correlations still common for older sites. These techniques all invariably have different levels of precision and accuracy, and make true temporal comparisons difficult (especially when reaching the limits of radiocarbon calibration curve ~50 ka BP). The most powerful alternative/supporting dating technique is the use of widespread chrono-stratigraphic markers, such as volcanic ash dating (tephrochronology) and the use of palaeomagnetic excursions (e.g. the Laschamp geomagnetic excursion ~ 41 ka; Singer et al., 2009), that allow for the unambiguous synchronisation of disparate sedimentary archives (e.g. Blockley et al., 2014; Lane et al., 2011a; 2013a; Lowe, et al., 2012). The application of tephra as a stratigraphic marker has augmented the ability to test synchronicity of changes (archaeological and palaeoenvironmental) recorded in sediments, negating temporal uncertainty as well as assisting in site specific age models (e.g. Douka et al., 2014; Finsinger et al., 2011, Lane et al., 2012a). The ability to directly anchor archaeological evidence to palaeoenvironmental archives allows for the testing of hypotheses that relate climate and demographic changes (e.g. Lowe et al., 2012). As such, tephra studies in archaeological sites are increasing across the Mediterranean and Europe (e.g. Douka et al., 2014; Karkanas et al., 2014; Lane et al., 2014), with the widespread Campanian Ignimbrite tephra from Campi Flegrei, Italy, indicating a spatial complexity in the timing of the arrival of AMH industries across the Mediterranean, southeast Europe, Africa and Russia (Figure 1.2). Detailed tephra investigations in the corridor regions such as in the Levant and the Caucasus are still however lacking. There is still a disproportionate

amount of work with state of the art techniques, chronological and archaeological conducted in western Europe compared with studies in eastern Europe and the Near East. As such, some would still argue a Eurocentric view could exist for this period of replacement (e.g. Anghelinu and Niţă 2012; Roebroeks, 2008), and how far the East mirrors the West is unknown.

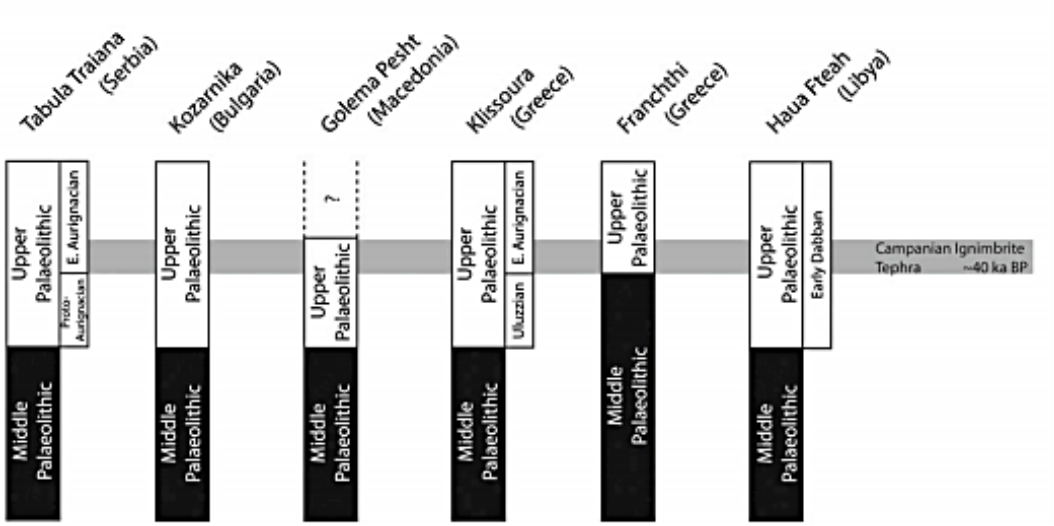

Figure 1.2. An example of using a volcanic ash layer to synchronise records. The widespread ~39 ka BP Campanian Ignimbrite (CI) tephra (from Campi Flegrei, Italy) has been used to correlate various archaeological sites around the Mediterranean. This shows that there are spatial differences in assemblages and that the timing of the technological change that occur prior to ~39 ka and was not simultaneous. Modified from Lowe et al. (2012).

1.4. Aims and objectives

1.4.1. Aim

The aim of this project is to build a detailed tephrostratigraphy for the Caucasus during the Middle to the Middle-Upper Palaeolithic transition (~125 ka to 30 ka) to allow archaeological and palaeoenvironmental records to be correlated. Constructing a tephrostratigraphic framework from these records within the Caucasus will allow us to link sites to assess:

- how synchronous the Neanderthal occupations were within the region;
- the synchronicity of AMHs arrival across the region; and
- to assess whether environmental changes may have affected the expansion and occupation of the hominin species in the region by linking the archaeological records to a detailed palaeoenvironmental record with tephra isochrons.

1.4.2. Objectives

The following objectives have been devised:

- Review the archaeological evidence and chronological data from sites in the region.
- Summarise palaeoenvironmental data to assess the timing of changes in this climatically diverse region.
- Sample cave sites that have assemblages that span from the Mid-Middle Palaeolithic (MP) through to the Upper Palaeolithic (UP) that also have a detailed archaeological or palaeoenvironmental record.
- Obtain a long record for cryptotephra analysis to help build up the tephrostratigraphic framework, preferably a palaeoenvironmental archive so that the climatic information can be directly related to the archaeological sites.
- Establish the volcanic sources and eruptions that are likely to have dispersed ash across the Caucasus.
- Collect, where possible, proximal eruption deposits in the Caucasus for comparison and the identification of the sources.

- Sample material in the sedimentary archives that could be dated using radiometric methods, e.g., especially suitable material (macrofossils) from above and below tephra layers (proximal and distal).
- Collate published chronological data of widespread tephra layers to link the tephrostratigraphic framework to an absolute timescale.
- Chemically characterise (major element analysis) glass shards from tephra units to identify sources.
- Use trace element compositions of glass shards (where possible) to verify correlations based on major element compositions.
- Compare the published information on the techno-complexes in the archaeological sites and link them to high-resolution palaeoenvironmental records using the tephra layers.

Chapter 2

The Caucasus: an environmental and archaeological background

This chapter provides the geographic, environmental and archaeological background of the Caucasus.

2.1. Introduction to the Caucasus and its environments

Traditionally the Caucasus has been split into two geological zones, the northern Caucasus and the southern Caucasus, aligned either side of the Greater Caucasus range (5000 m.a.s.l; Figure 2.1).

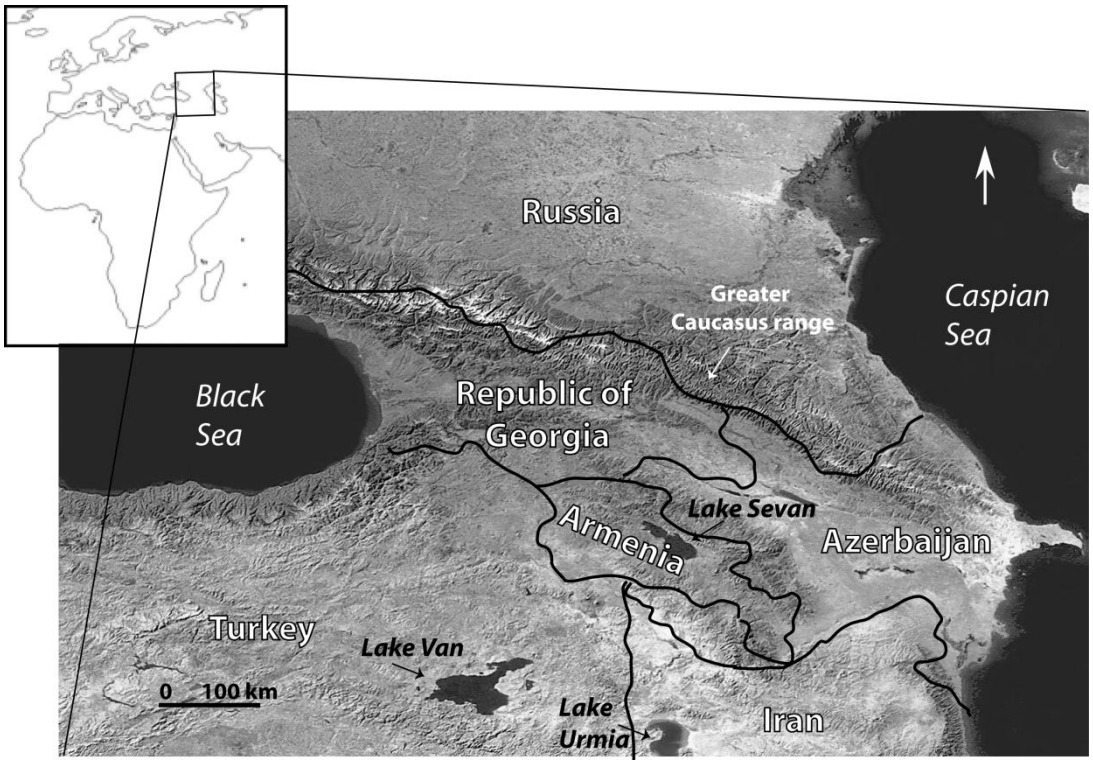

Figure 2.1. A digital elevation map of the Caucasus. This corridor is flanked by the Black Sea in the west and Caspian Sea in the east. The Greater Caucasus range rises ~4800 m above the surrounding topography in some areas forming a barrier through the corridor.

The northern Caucasus comprises modern day southern Russia, and the southern Caucasus comprises modern day Georgia, Armenia and Azerbaijan (Figure 2.1).

The Greater Caucasus range stretches the width of the isthmus, over 1200 km between the Black sea and Caspian Sea on a NNW-SSE transect.

A number of weather systems control the climate in the Caucasus, and this in conjunction with the varying topographical setting has resulted in an ecologically diverse landscape (e.g. Adler et al., 2006a; Joannin et al., 2010). The regions to the north of the Greater Caucasus range are subjected to cold/moderate dry air masses from the Russian plains. The highest peaks of this range are often snow-capped and glaciated throughout the year (Volodicheva, 2002). Consequently, the northern Caucasus has a temperate climate with the Greater Caucasus range forming a climatic and bio-geographical barrier north to south (Figure 2.2). The southern Caucasus is protected from the harsh conditions and this has given rise to a belt of subtropical climate.

In the southern Caucasus there is a further climatic divide which exists east to west. To the west, Atlantic-Mediterranean air masses enter from the Black Sea, while the east is influenced by dry continental air masses coming in from inner Eurasia and the Levant (Asia Minor; Figure 2.2). Precipitation inputs and the mountainous topography of this area also add to the east/west divide. Warm, humid, highly saturated air masses from the Black Sea deposit most of their annual precipitation in the mountainous west. As the precipitation belt continues east over the Surami ridge (see Figure 2.2), much of this rain will have been deposited resulting in a more arid air flow towards the east and Caspian Sea. Consequently, the west of the southern Caucasus (Georgia) is typified by a warm-humid, well-forested and mountainous environment (subtropical), with a continental climate to the east, which is a much drier, arid zone (Armenia and Azerbaijan; Adler et al., 2006a; Shatilova et al., 2011; Volodicheva, 2002). This

information is based on modern day assessments, but it is believed that the similar conditions existed in the Quaternary (Adler et al., 2006a; Volodicheva, 2002).

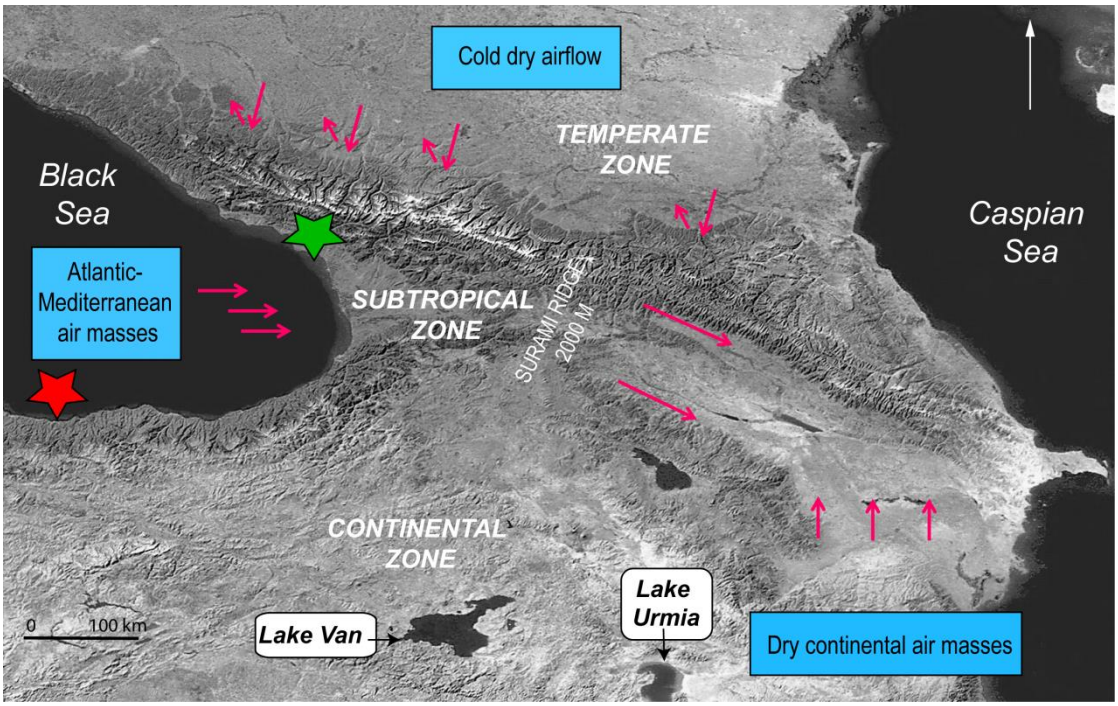

Figure 2.2. Map shows climatic divisions in the Caucasus. North of the Greater Caucasus range has a temperate climate. The western Caucasus receives the greatest amount of precipitation and is more subtropical in its climate. Armenia and Azerbaijan are drier and more arid, with continental climates. Red star shows location of M72/5-25-GC1 core taken from the Black Sea; green star is the Dziguta basin that has undergone coring for palaeo-pollen analysis and locations of Lake Van and Lake Urmia are indicated (sites are mentioned in text). After Adler et al. (2006a).

2.2. Palaeoclimate reconstruction in the Caucasus

Marine records from the northern Atlantic (SPECMAP) and ice core records from Greenland (e.g. GRIP, NGRIP, GISP2 and DYE-3) provide an almost complete northern hemispherical climate stratigraphy from the last interglacial-glacial cycle spanning ~130 to 10 ka BP. The period of interest for these studies falls within Marine Isotope Stage (MIS) 5e to MIS 3 (~125-30 ka; Figure 2.3). This period in

time is punctuated with abrupt environmental transitions (e.g. North Greenland Ice Core Project members, 2004).

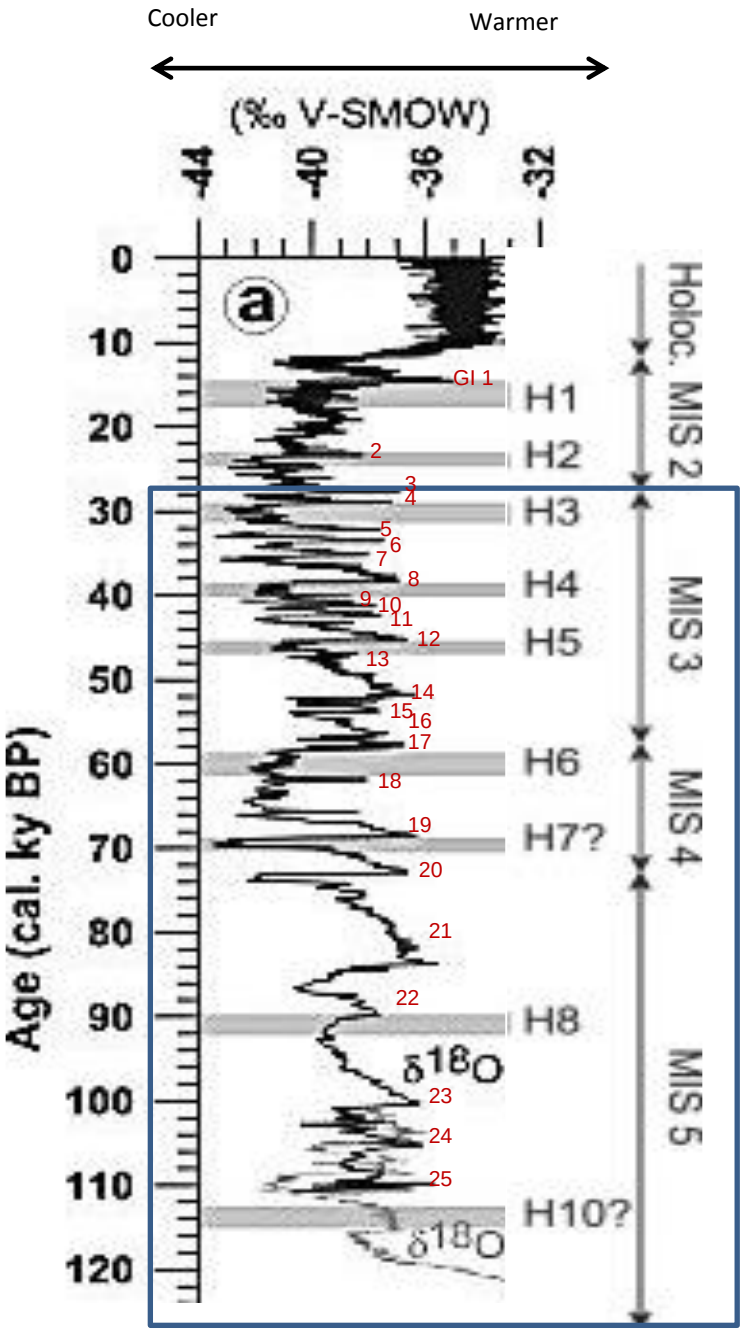

Figure 2.3. Oxygen isotope record ($\delta^{18}O$) from GISP2 (Black) and NGRIP (grey) ice cores from Greenland (a). Changes in $\delta^{18}O$ are a proxy for temperature. There are pronounced oscillations during the Quaternary period. The record is broken down into MIS, also known as Oxygen Isotope Stages (OIS), which refer to generally warm or cool episodes (the Glacial and Interglacial cycle). Within the MIS stages, there are periods of abrupt warming followed by gradual cooling, known as Dansgaard - Oescher events (D-O) or Greenland interstadials (GI; numbered in red) and Greenland stadials (GS cooler troughs between GI events). Grey horizontal lines refer to Heinrich events (e.g., H1). These events are linked to increases in iceberg discharged that reduced ocean salinity enough to slow deep water formation and the thermohaline circulation resulting in periods of rapid cooling within the D-O cycle. Image adapted from Salgueiro et al. (2010).

Climate change models that are derived from palaeoenvironmental records in temperate areas, e.g., in northern Eurasia and to a lesser extent the French Alps, are often used for climate reconstructions of the Caucasus (e.g. Golvanova and

Doronichev, 2003). The Caucasus has a number of different environments (related to subtropical, continental and temperate climates) that would have responded differently to northern hemispheric changes in climate, if at all. Consequently, the previously mentioned climate schemes may be appropriate for the temperate, northern Caucasus but not necessarily for the southern Caucasus.

2.2.1. Paleoclimate data in the Caucasus

There is very limited palaeoenvironmental data direct from the southern Caucasus (e.g. Arslanov et al., 2007, Ollivier et al., 2010; Shatilova et al., 2011), with no detailed palaeoclimate archives from the Northern Caucasus in the time frame of this study. Shatilova et al. (2011) attempted to synthesise palaeoenvironmental information from the Palaeozoic to the Holocene (mainly based on flora) from around Georgia (Figure 2.4). A warm climate with low humidity characterises the Early Karangatian, linked to the Eemian or Riss-Würm interglacial, MIS 5e (Shatilova et al., 2011). By the late Karangatian, conditions become much cooler, including three stages of decreasing temperatures that are observed up to and including the New Euxinian. This period is linked to the start of the Würm glacial or Weichselian, MIS 5d-2 (Shatilova et al., 2011). The latter part of this period experienced severe cooling, and this may be coincident with the last glacial maximum (LGM), but the authors make no correlation (Figure 2.4). The resolution of the research conducted by Shatilova et al. (2011) is not high enough to identify subtle changes in the environment that could be linked to changes in temperatures as exhibited in the marine, ice cores and other records.

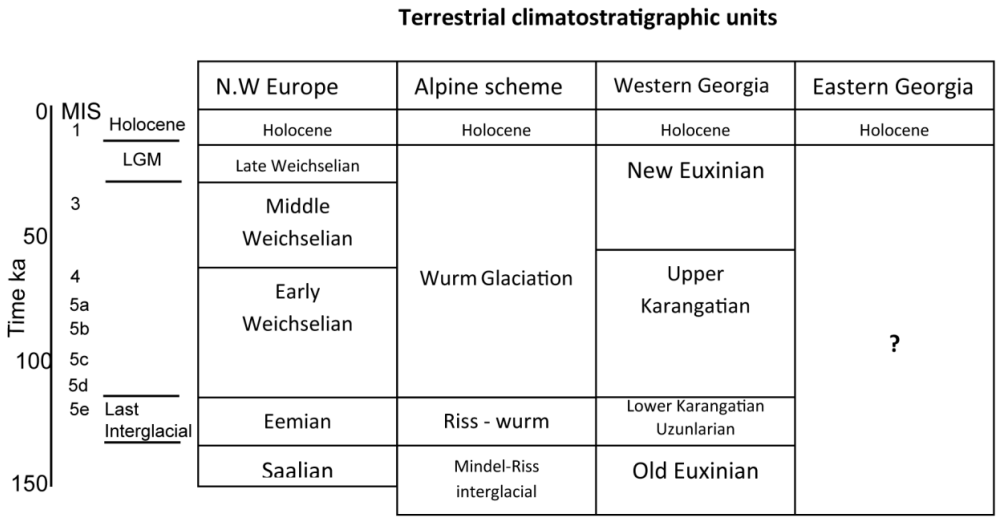

Figure 2.4. Terrestrial schemes for last 150 ka adapted from Shatilova et al. (2011). LGM = Last Glacial Maximum.

Pollen data from buried deposit in the Dziguta river basin (western Georgia; Figure 2.2) ranging from ~ >48 to 10 ka cal BP (calibrated ^{14}C determinations on peat, wood and gyttja) revealed 10 pollen zones (Arslanov et al., 2007). Descriptions of pollen zones 6 to 1 (~> 48 to 16 ka cal BP) are provided in Table 2.1. Arslanov et al. (2007) compare their data to a $\delta^{18}O$ record in the southern Aegean Sea (core 69; Geraga et al., 2005), and suggest the pollen data follows a coherent pattern of climatic change (D-O cycles and possible expressions of climatic cooling coincident with Henrich events). However, Fletcher et al. (2010) and Shumilovskikh et al. (2014) suggest that both records (Dziguta and core 69) do not show a clear D-O pattern. The pollen data suggest there was a well-developed forest environment in the western Caucasus over (at least) the last ~50 ka that experienced periods of change between cold/arid and warm/humid conditions across ~MIS 3 to MIS 2 period. However, there is insufficient chronological control and sample resolution for robust correlations to D-O cycles.

Table 2.1. Pollen zones in the Dziguta river basin from Aslanov et al. (2007)

Pollen zone	Age*	Age cal BP	Identified species	Climate
1	44-48	>48- 47	Dominance of fir with beech. Limited occurrence of alder, hornbeam, elm and lime.	Moderately mild and wet
2	42-44	47- 45	Expansion of coniferous forests species and alder, with reduction in fir	Wet becoming cool
3a	38.5-42 (start of zone)	45- 42	Adler dominated forests with some broad leaved species (e.g., hornbeam, chestnut, and elm).	Moderately mild and wet
3b	38.5-42 (end of zone)	45- 42	Rapid increase in fir and alder forests with beech. Increase in hornbeam, elm and chestnut also.	Moderately mild and wet
4	32-38.5	42- 36	Expansion of pine with alder, with the disappearance of broadleaved species and increase in herbs	Cool and dry
5a	28-32 (start of period)	32- 31	Expansion of fir and alder, limited occurrence of broadleaved species	Moderately mild and wet
5b	28-32 (end of period)	32- 31	Reduction of alder and increase in pine with continual presence of broadleaved species	Mild and drier
6	14-28	31- 16	Pine forest dominates. Middle of period sees rapid expansion of herb species	Pronounced cool and dry period

*Footnote. * Ages shown are un-calibrated ^{14}C determination given in Arslanov et al., 2007. Age cal BP is the calibrated age determination using IntCal 13 on the OxCal4.2.3 platform (Bronk Ramsey, 2009a; Reimer et al., 2013).*

2.2.2. Paleoclimate Data from archives close to the Caucasus

The ~200 ka long lake archive from Lake Urmia, NW Iran (Djamali et al., 2008), a ~600 ka composite lake record from Lake Van, eastern Turkey (e.g., Litt et al., 2014), and the M72/5-25-GC1 core that spans the last ~60 ka extracted from the south-eastern Black Sea (Shumilovskikh et al., 2014), are the most detailed palaeoenvironmental archives closest to the southern Caucasus (see Figure 2.2 for locations). The closest palaeoenvironmental sequences to the northern Caucasus that have been intensively studied include loess deposits derived from four locations, three from Eastern Europe (Moldova V, Ukraine; Mitoch-Malu

Galben, Romania, and Cosautsi in Moldova) and one area in central Siberia (Kurtak; Haesaerts et al., 2003; 2009; 2010). Currently, these are the best archives for high-resolution palaeoclimate reconstruction in the northern Caucasus. Figure 2.5 shows available proxy data including total arboreal pollen (% AP), total organic carbon (TOC) and lithostratigraphic data (for the loess deposits) for the four sets of archives. These data have been compared by authors to the $\delta^{18}O$ records from Greenland (see Haesaerts et al., 2010; Litt et al. 2014; Shumilovskikh et al., 2014; Stockhecke et al., 2014a,b). To date, there is no detailed chronological and/or palaeoenvironmental information published on sediments older than 20 ka from the Caspian Sea and surrounding areas (e.g., Leroy et al., 2014).

Fluctuations in AP data from Lake Urmia are comparable to those seen in the Lake Van pollen record (see Figure 2.5a, d). The section across what appears to be MIS 5 (~125- 70 ka) displays changes in humidity (linked to stadial and interstadial events), with the maximum reached in interstadial stage 5e, thought to correspond to the start of the Eemian warming and again in interstadial 5c, and to a lesser extent 5a (see Figure 2.5). Stages 5d and 5b show increased aridity and represent stadial events (Djamali et al., 2008, Litt et al., 2014). After MIS 5d, abrupt environmental transitions in MIS 4 to 2 (D-O cycle) seen in the Greenland ice core data have not been identified in the AP records. Fluctuations in this time period are often seen in other AP palaeoclimate records in the western Mediterranean and Europe (see review in Fletcher et al., 2010). This could however, be a result of the low resolution sampling; ~ one sample was taken every meter of core (see Djamali et al., 2008, Litt et al., 2014). Rapid climatic fluctuation across this period are however documented in the total organic carbon

(TOC) data from Lake Van (see Stockhecke et al., 2014b; Figure 2.5a; proxy reflects aquatic productivity) and the authors suggest these fluctuations are concurrent to the D-O cycle identified in the Greenland ice core records. The M72/5-25-GC1 core that spans the last ~60 ka provides a higher resolution pollen record (163 samples taken from a 952 cm long core) thought to correspond to the end of ~MIS 4 to the start of the MIS 2 period (Figure 2.5a). Shumilovskikh et al. (2014) identified two major arid phases, one at ~64- 55 and another at 40- 32 ka, and two major humid phases at ~54-45 and 28- 20 ka, with the pollen record interpreted as following a D-O-like pattern (Shumilovskikh et al., 2014, Figure 6e). Based on visual correlation to the $\delta^{18}O$ signal recorded in the GISP2 ice core archive (Greenland; Figure 2.5), Haesaerts et al. (2010) also identify a series of interstadial episodes (thought to correspond to the D-O cycle) between MIS 3 to MIS 2, with severe cooling events believed to represent the effects of H1 to H3 with a possible cooling at H4 identified (Figure 2.5; see Haesaerts et al., 2010).

Figure 2.5 (next page). Total AP against age/depth (ka BP) for (a) Lake Van that is a composite record from two cores, the M72/5-25-GC1 core (f; the grey boxes represent DO events) and Lake Urmia (e). AP is an indicator of moisture availability. These data are used to depict the changes between glacial (moisture deficient periods) and interglacial conditions that have an increased moisture availability (shown by an increase in AP %). The NGRIP oxygen isotope record is shown in d, with the numbers on the right axis depicting the ice core stadial and interstadial events. Total organic carbon (TOC) for Lake Van is shown in c, and depicts pronounced fluctuations during the in MIS3 period (data from Stockhecke et al., 2014b; Shumilovskikh et al., 2014). g shows a schematic of the composite, lithostratigraphic data from loess sites Molodova V (Mol), Mitoch-Malu Galben (MG) and Cosautsi (Cos) from the east Carpathians (modified from Haesaerts et al., 2010). Loess accumulations provide long sedimentary sequences that are comprised of aeolian deposits attributed to dry and cold conditions with inter-bedded paleosols that formed in phases of climatic stability (Haesaerts et al., 2003; 2009; 2010). Palaeoclimate reconstruction from these deposits is based on the sedimentary and pedologic processes (including periglacial features) that have been integrated with pollen and faunal data where possible (see Haesaerts et al., 2003; 2009; 2010). Loess interstitials shown as grey boxing to the right of east Carpathian, sediment profile, correspond to more positive peaks in $\delta^{18}O$ (a proxy for warmer conditions recorded in the ice cores), whilst deep frost and permafrost conditions identified in the sedimentary sequences are aligned with more negative $\delta^{18}O$ vales, linked to cooling events. Fluctuations in all records are thought to correspond to the glacial/interglacial cycle as observed in the Greenland ice core records shown as grey horizontal connector lines between the archives.

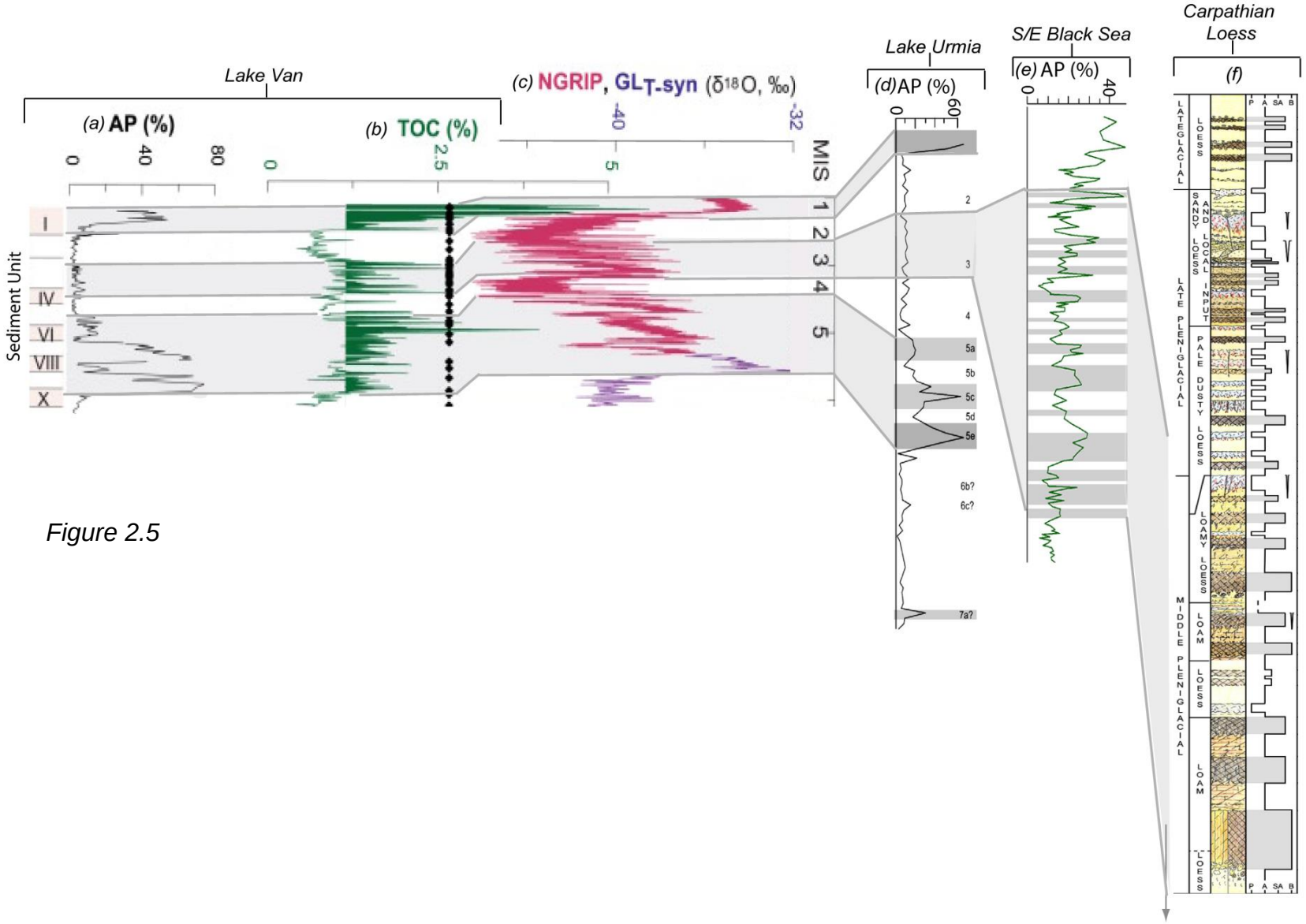
Lake Van
(a) AP (%)
(b) TOC (%)
(c) NGRIP, GL_T-syn (δ18O, ‰)
Sediment Unit
I
IV
VI
VIII
X
MIS
Lake Urmia
(d) AP (%)
S/E Black Sea
(e) AP (%)
Carpathian Loess
(f)
LATEGLACIAL
LOESS
SANDY LOESS
AND LOCAL INPUT
LATE PLENIGLACIAL
PALE DUSTY LOESS
LOAMY LOESS
LOAM
MIDDLE PLENIGLACIAL
LOESS
LOAM
LOESS

Figure 2.5

The above mentioned palaeoenvironmental archives are the only records that can be used to reconstruct the Quaternary palaeoclimate across the northern and southern Caucasus. Collectively, these data suggest that the temperate, northern Eurasia, the southern Caucasus and regions close to the southern Caucasus (encompassing subtropical and continental environments) experienced rapid climate change within the timeframe of this study and that this could be coincident with changes observed in the Greenland ice core records. However, no direct correlations to the Greenland ice cores or between the archives are possible and it should also be noted that all records were tuned or wiggle matched to a global climate archive (e.g. the GISP2 or GICC05 $\delta^{18}O$ records). Although there are some independent chronological controls in the lake records (including the Black Sea data and Lake Van), tuning an archive that contains terrestrial proxies to an archive that records global climate change assumes synchronicity. Therefore, subtle differences in the timing of the changes and the drivers of these changes across wide geographical regions are lost (Blaauw, 2012), which are key to understanding the mechanisms of climate change. Consequently, how synchronous the terrestrial and aquatic responses were to each other in and across the Caucasus region, and how these actually related to the northern hemispheric climate fluctuations is not known.

2.3 The Middle Palaeolithic (MP) and Upper Palaeolithic (UP) of the Caucasus

2.3.1. The Middle Palaeolithic of the Caucasus

The Middle Palaeolithic period (that is associated with Neanderthals in Europe) can be sub-divided into an early phase, the ~250- 128 ka Early MP (EMP) that includes MIS 6 to 7, and two later stages, the Mid-Middle Palaeolithic, (MMP; ~128-71 ka, MIS 5) to the Late MP (LMP) that spans ~71 to 45 ka (MIS 4-3) (Pinhasi et al., 2011a). The more recent stages are dominated by a (geographically variable) Mousterian, flake-based tool industry typified by a Levellois core technology (a term used to describe the removal of flakes from a specially prepared platform) (e.g. Dibble and Rolland, 1990; Shea, 2013). This is also true for the Caucasian assemblages but there are issues with chronology.

The Caucasus is situated in the central to eastern extent of the known Eurasian Neanderthal range (Figure 2.6). MP sites tend to be concentrated in the karst regions, specifically the Imereti (central) region of Georgia and cave systems north of the Greater Caucasian Range (Figure 2.7). There have been a number of significant MP finds in the Caucasus, including several Neanderthal remains ranging from mandible fragments, skeletal remains and teeth (e.g. Faerman et al., 1994; Gabunia and Vekua, [1990-Cited in Pinhasi et al., 2012]; Golovanova et al., 1999; Nioradze, 1991), but unfortunately, direct dating of these Neanderthal remains has been poor due to insufficient collagen preservation (see Pinhasi et al., 2012).

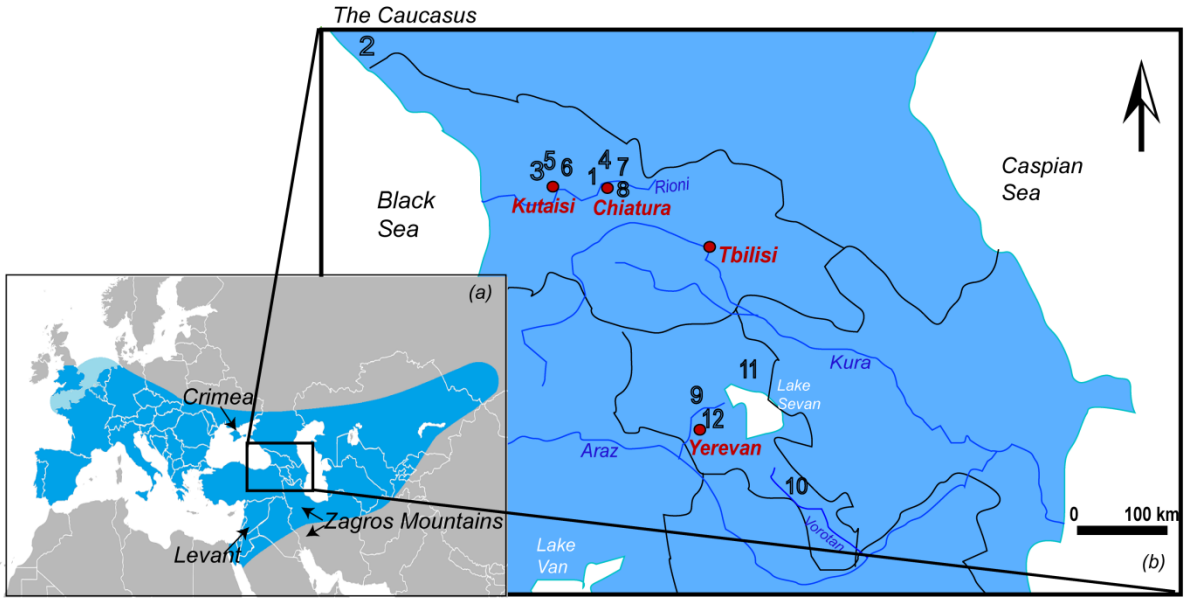

Figure 2.6. (a) Map of the known extent of Neanderthals in northern Eurasia (blue), after Krause et al. (2007). The locations of the Zagros Mountains, Crimea and the Levant that contain assemblages with technological similarities to the Caucasian data are shown. (b) The location of archaeological sites in the Caucasus that are mentioned in text: 1, Ortvale Klde; 2, Mezmaiskaya Cave; 3, Sakajia; 4, Bondi Cave; 5, Ortvale Cave; 6, Bronze Cave; 7, Djruchula cave; 8, Dzudzuana; 9, Lusakert 1; 10, Aghitu 3; 11, Kalavan; 12, Yerevan 1.

Due to differences exhibited in the techno-complexes (tool packages and faunal assemblages) from MP sites in the Caucasus, it is assumed a variable system of settlement and subsistence existed. This is thought to be associated with environmental and topographical differences (e.g. Adler and Tushabramishvili, 2004; Golovanova and Doronichev, 2003). A number of authors have tried to compartmentalise the archaeological evidence into smaller, demographic based techno-complexes. For example, Liubin, Nioradze and Tushabramishvili sub-divided the archaeological evidence of the southern Caucasus into 5 distinct and assumed contemporaneous groups: the Tsopi, Djruchula-Kudaro, Tsutskhvati, Tskhinvali, and the Tskaltsitela (Liubin, 1977; 1989; Nioradze, 1992; Tushabramishvili, 1978 [cited in Adler and Tushabramishvili, 2004, Golovanova

and Doronichev, 2003 and Pinhasi et al., 2012]). Groups were based on differences observed in techno-complexes found in sites, e.g., Levellois vs. non-Levellois techniques or similarities exhibited in the production of blades and data from paleontological analysis (the presence and absence of certain species at each site). What emerged was the concept that several, locally distinct groups subsisted in close proximity to each other that had distinct traditions, beliefs and technological practices. However, Adler and Tushabramishvili (2004a) recognised that true temporal correlation between the groups with analysis of diachronic change in each group was not possible and these initial assessments may be false (see Adler and Tushabramishvili, 2004). More recently, to help simplify this complex situation Doronichev (1993) and Golovanova and Doronichev (2003) assessed all the Caucasus MP evidence together from a regional perspective (north and south), rather than sub-regional one. Doronichev (1993) proposed three 'cultural areas' (Table 2.2; Figure 2.7) that highlight the archaeological variation across the whole Caucasus. In addition, Adler and Tushabramishvili (2004), Golovanova and Doronichev (2003) and Kozlowski (1998) have also made significant steps in trying to synthesise the MP evidence and gain some insight into the MP in the Caucasus, but chronological control and often contextual control at sites is lacking.

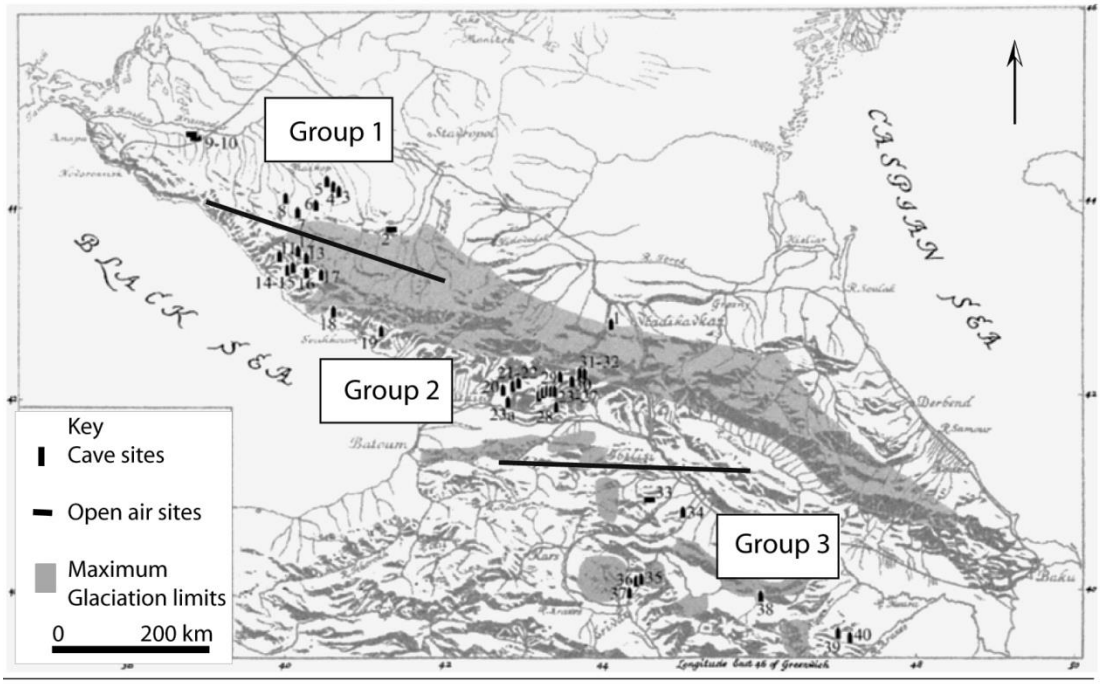

Figure 2.7. Distribution of MP sites (dark lines), and 'cultural groups' 1 to 3 (see Table 2.2 for description) in the Caucasus as proposed by Doronichev (1993). Note the disproportion of sites, east to west and north to south, highlighting some significant gaps in our current understanding of regional occupations. Most sites are situated in the karst systems in the west of the region; Group 2 sits in the Imereti region of Georgia and on the southern slopes of the Greater Caucasus range and Group 1 in the karst region in the north-west, northern Caucasus. There are more cave sites than open air sites but this could be due to the increased visibility of caves. Image adapted from Golovanova and Doronichev (2003).

Table 2.2. MP 'cultural groups' in the Caucuses as proposed by Doronichev (1993) and Golovanova and Doronichev (2003).

'Cultural group'	Geographical location	Distinguishing features	Fauna
Group 1	The northern and north-western Caucasus	Typified by Micoquian tool types. Bifacial tools, broad triangular hand axes, laurel leaf shaped points, bifacial and partly bifacial convergent tools and bifacial side scrapers and knives.	Predominance of bison and the presence of other ungulates (sheep, goats, and cave bears).
Group 2	Southern Caucasus and locations on the southwest Greater Caucasus range; Georgia, southern Ossetia, western Azerbaijan, and the Armenian volcanic highland.	Several local entities, similar but not identical to Levantine and the Karin Mousterian. Some distinct local features identified in lithic production (mainly related to differences in flaking technology), but no Micoquian tool types.	Cave bear is the most common in many cave sites but there is generally heterogeneity in assemblages.

Group 3	The southernmost Caucasus; southern Georgia, Armenia and western Azerbaijan.	Erevan-type industry in Armenia and Taglar-type industry in Azerbaijan. Dominance of truncated-facetted tools that resemble those of the Zagros Mousterian. No Micoquian tool types	Predominance of ungulates from grass and forest environments.

Footnote; Data in table are from Doronichev (1993), with updated information from Adler and Tushabramishvili (2004), Golovanova and Doronichev (2003), and Hoffecker and Clegghorn (2000).

In general it is agreed that the MP techno-complexes observed in sites in the northern Caucasus (Group 1; Table 2.2) do not have the same features as those observed in sites in the southern Caucasus (Groups 2 and 3), and are more similar to the eastern European and Crimean Micoquian technologies (Bar-Yosef et al., 2006; Demidenko, 2008; Golovanova and Doronichev, 2003). The southern Caucasus techno-complexes show more variability, with similarities to MP techno-complexes found in the Levant and Zargos mountains (see Bar-Yosef et al., 2006; Beliaeva and Lioubine, 1998; Golovanova and Doronichev, 2003; Table 2.2; Figure 2.6). True temporal correlations between Neanderthals that produced the variable techno-complexes (north and south) are limited (Adler and Tushabramishvili, 2004).

The significant variation in MP technologies between sites to the north and that to the south of the Greater Caucasus range indicate that the mountains were a significant barrier to Neanderthal populations (Adler and Tushabramishvili, 2004; Bar-Yosef et al., 2006; Golovanova and Doronichev, 2003). This range would have also been glaciated in cooler climates (e.g. stadial MIS 5d, 5b and cooler periods in MIS 4) that likely formed a further barrier (Figure 2.7). Another possible environmental barrier prohibiting movement north/south in the Caucasus is the

transgressions of the Black Sea and Caspian Sea. The Black Sea and Caspian Sea are currently separated, but did flood in the past through the Manych-Kerch spillway (see Figure 2.8).

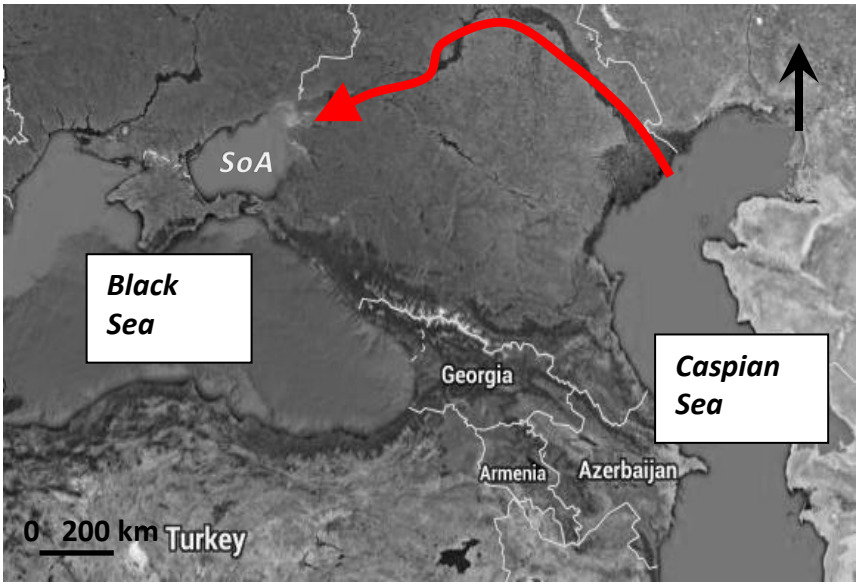

Figure 2.8. The red arrow denotes the low lying Manych-Kerch spillway that has connected the Black Sea via the Sea of Azov (SoA) to the Caspian Sea. Connection of the two seas would have resulted in flooding of the low lying areas, reducing the habitat for native species.

This process occurred through either the transgression of the Black Sea, coinciding with warm climatic episodes due to rising sea levels (increase precipitation in interglacial cycles) or the transgression of the Caspian Sea coinciding with the start of glacial cycles (Kozlowski, 1998). The latter is a result of the increasing size of the Scandinavian ice sheet that subsequently diverted rivers and meltwater into the Caspian Sea (see Mangerud et al., 2004). The extent of these transgressions is not well constrained. However, they are thought to have occurred in MIS 5 (Badertscher et al., 2011; Kozlowski, 1998; Mangerud et al., 2004) and possibly at the start of ~MIS 2 (e.g. Arslanov et al., 2007; Badertscher

et al., 2011; Shumilovskikh et al., 2014) and would have resulted in sporadic flooding and the reduction of habitable areas north of the Greater Caucasus range.

Although Doronichev (1993), Golovanova and Doronichev (2003) and Liubin (1977, 1989) endeavoured to make sense of the Caucasus MP data they failed to take into account differences in excavation techniques, raw materials used, taphonomic considerations and zooarchaeological remains (Adler and Tushabramishvili, 2004). No firm chronometric correlations were made; thus, new chronological and archaeological information will result in a revision and progression of these original ideas in the future. For example, new ages have started to yield new information on both the southern and northern Caucasus MP assemblages (e.g. Adler et al., 2008; Mercier et al., 2011; Pinhasi et al., 2011b; Pinhasi et al., 2012). New TL dates from flint blades found in Djruchula cave (Mercier et al., 2011) indicate that these archaeological assemblages are much older than many of the other techno-complexes within this region (>140 ka and a second occupation at 260-210 ka Mercier et al., 2011). Recent radiometric dating from the sites of Ortvale Klde and Bronze Cave (Adler et al., 2008; Pinhasi et al., 2012) has supported claims of Golovanova and Doronichev (2003) and has shown that Neanderthals who hunted *Capra caucasica* (tur) near the sites of Ortvale Klde and those that hunted predominantly *Bison priscus* near Bronze cave (7.5 km away) were not contemporary. Consequently, prey selection may not have been due to cultural preferences of different hunter gatherer groups at the two sites as previously thought (see Adler and Tushabramishvili, 2004). New radiocarbon data produced by Pinhasi et al. (2011b) also now challenge claims for the late survival of Neanderthals in the northern Caucasus. Subsequently, what was previously

thought about the MP in the Caucasus appears to be changing as less emphasis is based on old dates and techno-typological characteristics that do not always aid relative chronologies.

2.3.2. The Upper Palaeolithic and the arrival of AMH

The most comprehensively dated sites that contain an early UP (EUP) superimposed on to a late MP (LMP) are Ortvale Klde in Georgia and Mezmaiskaya Cave in the north-western Caucasus (Adler et al., 2008; Pinhasi et al., 2011b; Figure 2.6). Age estimates have also recently been obtained for LMP and UP assemblages in the following cave sites, Sakajia Cave, Bondi Cave and Ortvale Cave (also in Georgia; Pinhasi et al., 2012), but preservation is poor and there are still only a few radiometric determinations for each site.

New age information from the re-analysis of samples using more modern techniques (archaeological and chronometric; but not always ultrafiltration for radiocarbon dates) has challenged the presumed '*in situ'* transition to the EUP at sites such as Ortvale Klde and Mezmaiskaya (Adler et al., 2008; Pinhasi et al., 2011b). Pinhasi et al. (2012) recently suggested that, in fact, it is unlikely that Neanderthals survived in Georgia and the northern Caucasus after ~39 ka cal BP, and following this demise or migration of Neanderthals out of the region there was a significant hiatus (chronologically and stratigraphically) prior to the arrival of the AMH (Pinhasi et al., 2012). These dates are consistent with recent estimates from the end of the LMP assemblages across western Europe (Higham et al., 2014). Approximate dates for this technological change in the Caucasus currently fall within ~42 - 37 ka cal BP (Adler et al., 2008; Pinhasi et al., 2012) suggesting AMH branched out into western Europe before inhabiting the Caucasus. Older AMH

remains have been found in Kents Cavern, England (~44 - 41 ka cal BP; Higham et al., 2011) and Grotta del Cavallo, southern Italy (~ 45 - 43 ka cal BP; Benazzi et al., 2011). However, there is a single radiocarbon date on bone from the oldest EUP in the Caucasus (Ortvale Klde, Layer 4d), which suggests some AMH were probably in the region earlier at 44 - 40 ka cal BP (recalibrated with IntCal13). This date could be considered a minimum age as the sample did not undergo an ultrafiltration pre-treatment, but the authors note caution on the arrival of AMH based on one date (Adler et al., 2008).

It appears that the AMHs who arrived in the southern Caucasus had a fully-fledged bone and stone tool package. This techno-complex is similar to the EUP Ahmarian techno-complex that is found in the Levant (e.g. Golovanova et al., 2010a,b; Kozlowski et al., 1998) and dates between ~49- 37.5 ka (e.g. Douka et al., 2013; Rebollo et al., 2011). The Ahmarian techno-complex is defined by highly developed blade and bladelets technology, bone tools and ornaments. Similar tool packages have been found in the EUP Layers at sites Ortvale Klde (Layers 4 and 3), Dzudzuana (Unit D) and Layer 1C/1B in Mezmaiskaya cave (Golovanova et al., 2010a,b; Figure 2.9). No skeletal material has been found within these EUP assemblages in the Caucasus. However, similarities with the Ahmarian culture elsewhere that has AMH remains (e.g., Bergman and Stringer, 1989; Ewing, 1947) and the rapid and intrusive nature of a regional stone and bone assemblage, suggest the Caucasus assemblages can be attributed to AMH. Recently, Otte et al. (2011), Barzgir et al. (2014) and Tsanova. (2013) suggested technological and chronological similarities to another EUP techno-complex found in Iran and the Zagros regions, termed the AMH Baradonstian techno-complex (associated with AMH tooth; Scott and Marean, 2009) that is dated to ~39 ka cal BP. Typological

similarities of the Baradonstian from the cave site Yafteh (Iran) to the early Ahmarian in the Levant have also been made (Barzgir et al., 2014; Tsanova, 2013).

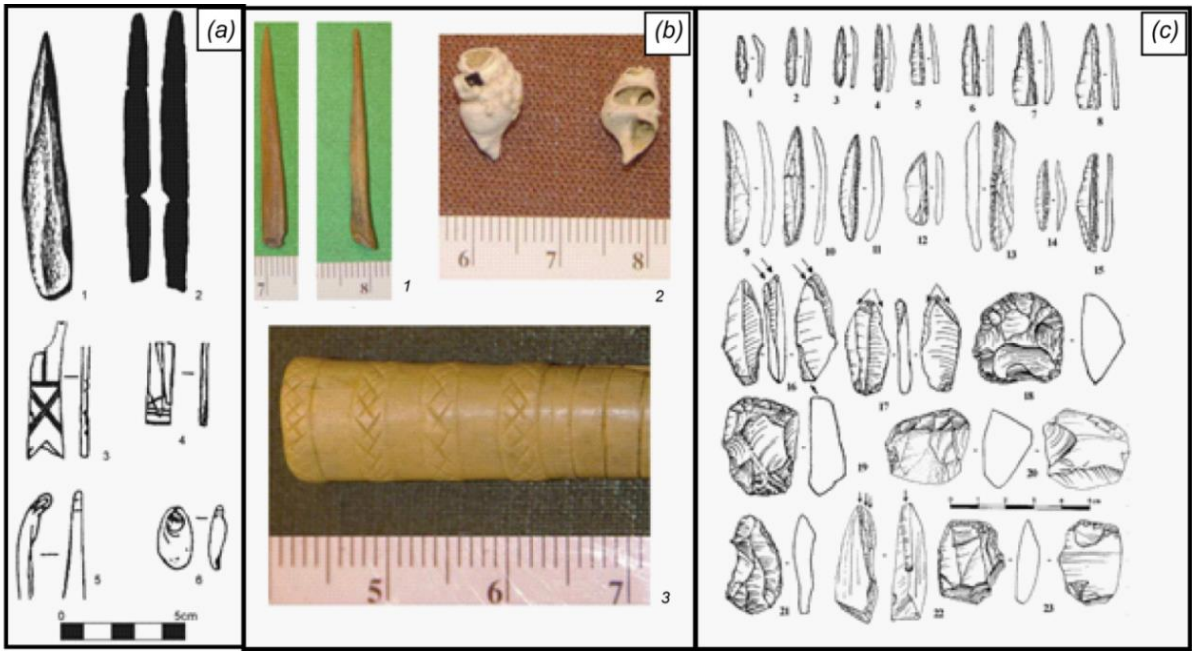

Figure 2.9. Images of similar EUP assemblages that have been found in Ortvale Klde and Dzudzuana (a) and Mesmaiskaya Cave (b, and c). See Golovanova et al. (2010b) for further details.

These data, with recent dates (mainly radiocarbon) from the re-excavated key sites (e.g. Ortvale Klde), provide insight into the first appearance of AMH in the region. Current thoughts conclude that the expansion of AMH was relatively abrupt, and they likely came from the Levant (or Zargos region), arriving in Georgia first and then traversing into the northern Caucasus (Adler et al., 2006a; Adler et al., 2008; Golovanova et al., 2010a, b). Consequently, the Greater Caucasus range, which hindered Neanderthal movements, did not seem to stop the migration of AMH north (e.g. Adler et al., 2008; Bar-Yosef et al., 2006). Zooarchaeological data from site Ortvale Klde also suggest that hunting patterns

and prey selection changed little between the LMP and the EUP (Adler et al., 2006b; Bar-Oz and Adler, 2005), suggesting both populations were equally as adapt at hunting these species. However, the higher concentration of exotic obsidian artefacts (sourced ~180-350 km away) within EUP assemblages in Georgia suggests AMH may have moved around the landscape much more, and probably had larger social networks (e.g. Adler et al., 2006a, b). The latter could have attributed to a demographic advantage of AMH over native Neanderthal species (Adler et al., 2006a, b)

Evidence for the EUP occupation of Armenia and Azerbaijan is limited, and often only comprises a few surface finds (prismatic cores, end scrapers, and burins) often with no specific contexts (see Pinhasi et al., 2008). Currently, Aghitu 3 in Armenia (Figure 9b) is the only published site that has a fully stratified, early UP techno-complex (deposits ~27-35- ka cal BP; Gasparyan et al., 2014a; Kandel et al., 2011; 2014). Kandel et al. (2014) suggested that there are technological similarities between Dzudzuana Cave (layers D and C) and possibly Ortvale Klde (Layers 4c,4b and 3), Mezmaiskaya cave (Layer 1a) and Yafteh (Iran), but excavations and analysis are still ongoing. Interestingly, limited dates from the sites of Lusakert 1 and Yerevan 1 in Armenia (Figure 2.6) imply that MP occupations may have continued throughout MIS 3 (see Table 2.3). These suggest the later survival of Neanderthals may have occurred in the southernmost Caucasus, but chronological control in Armenia is currently poor in comparison to Georgia, making correlation between sites/countries difficult.

Table 2.3. Radiocarbon dates for the Palaeolithic record of Armenia, from Pinhasi et al. (2008).

Techno complex	Site	Layer	Lab. No.	Date uncal BP	±	Material used ^{14}C	Date cal BP (95%) *	Reference
MP	Kalavan 2	7	Poz-20366	34200	360	Bone	39657-37839	Pinhasi et al., 2008
MP	Lusakert 1	C2	GRA-14949/Lyon1006	26920	220	Bone	31282-30731	Fourloubey et al., 2003
MP	Yerevan 1	3	GrN 8028a	32600	800	Charcoal	38760-35010	Pinhasi et al., 2008
MP	Yerevan 1	3	GrN 8028b	31600	800	Charcoal	37854-34120	Pinhasi et al., 2008
MP	Yerevan 1	7	GrN8860	27000	650	Charcoal	32719-29745	Pinhasi et al., 2008
MP	Yerevan 1	7	GrN 8860	28000	500	Charcoal	33253-31095	Pinhasi et al., 2008

**Dates re-calibrated using IntCal13 (Reimer et al., 2013) with OxCal 4.2.3 (Ramsey., 2013). Dates are likely to be underestimates and there are potential issues with old excavation techniques from the site of Yerevan 1 (from Pinhasi et al., 2008).*

2.4. Summary to chapter

The Caucasus has a diverse climate and is composed of a wide variety of ecological landscapes and niches (forest, steppe/desert) that have supported a diverse range of flora and fauna. This contributed to the variable MP techno-complex seen across the region, but how synchronous these MP occupations were is not well constrained. Current published data indicate that last expression of MP assemblages occurred ~40 ka in Georgia and the northern Caucasus, but the manufacture and use of MP techno-complexes could have persisted in Armenia. AMH who arrived in the region arrived abruptly at ~44-37 ka and carried a distinctive bone and stone techno-complex that is similar to the Levantine Ahmarian, suggesting that AMH expanded from the Levant. AMH arrived in Georgia first and then quickly migrated to the north, but whether AMH and

Neanderthals overlapped in the Caucasus remains unclear and is presumed that it was unlikely.

The palaeoclimate data for the Caucasus show fluctuations between cooler/arid and warmer/humid periods suggesting the region experienced environmental change linked to changes in climate. These changes may be coincident with the northern hemispheric climate record as seen in the Greenland ice cores. However, there are no direct linkages between the archives to test how truly synchronous changes were across the region and at present how far these fluctuations may have influenced the archaeological story is not known.

Chapter 3.

Tephrostratigraphy: a new approach to the Caucasus

The following chapter explains the principles and limitations of tephrostratigraphy/tephrochronology and its potential in the Caucasus.

3.1. Principles of tephrostratigraphy

Explosive volcanic events typically generate large plumes of ash and gas that drive fine particles into the upper atmosphere. This material (tephra) is deposited; thicker and coarser fractions are deposited close to the vent while only small amounts of fine material are found in the distal environments. Tephra constitutes the following types based on their decreasing size: Blocks and Bombs (>64 mm), the latter being slightly aerodynamically shaped; Lapilli (2-64 mm); and Ash (<2 mm). These pyroclasts are typically non-consolidated and include crystals, glass and rock fragments. The fine ash of distal tephra deposits is produced from either a sustained eruption column, that extends from vent into the atmosphere (ash fall deposit), or the co-ignimbrite plume that rises up from a pyroclastic flow (ash flow deposits). The largest particles fall out of the column closest to the vent; thus in proximal locations (10s km from vent), volcanic deposits are thick and have a poorly sorted, grain size distribution. As smaller particles remain suspended they are carried long distances by winds, and are often found 1000s km from their source volcano (Thorarinsson, 1954).

In distal to ultra-distal regions volcanic ash layers are very thin and often not visible to the naked eye (Figure 3.1), but the preservation of non-visible volcanic ash layers may also reflect taphonomic circumstances in the sedimentary archive. These cryptically preserved volcanic ash layers are referred to as micro-tephra

(e.g., Turney et al., 1997) or cryptotephra (hereafter used in this study; Lowe & Hunt, 2001), and their presence in sedimentary sequences is only identified through laboratory extraction techniques (e.g., Blockley et al., 2005; Dugmore et al., 1992a). Cryptotephra is composed mostly of vitreous shards (glass) and the size of these is commonly <100 micrometres (Blockley et al., 2005). These particles (emplaced in hours, days or weeks) can be preserved in a variety of sedimentary contexts beneath the plume (e.g., Davies et al., 2012; Lowe 2011; Lowe et al., 2012). These layers form geologically instantaneous isochrones found over wide areas (Figure 3.1). Over time these ash layers are buried due to sedimentation processes, and others may be deposited from the same or different volcanic events higher in the sequence.

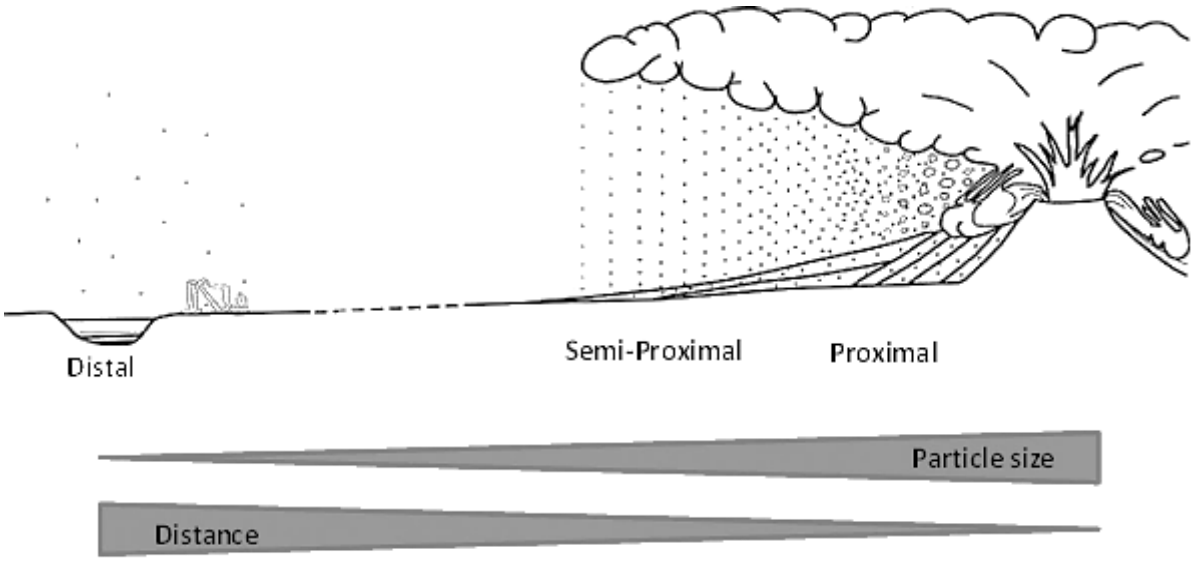

Figure 3.1. Schematic diagram of tephra deposition from an eruption plume. Tephra deposits closest to source are thickest. Distal deposits only record the furthest travelled, fine ash particles. Tephra is continually deposited under the plume forming an isochronous layer as the plume is carried by winds over the biosphere.

The key to tephrostratigraphy is chemically characterising and identifying the sequence of the tephra layers. These layers typically have unique characteristics

that allow them to be correlated between sites and records. The components of tephra deposits (glass) typically have a chemical composition that is unique to the eruption source/event. This reflects the melt composition that is controlled by the amount of crystal fractionation and incorporation of crustal material, and other processes (see Hall, 1996; Rollinson, 1993). In proximal settings lithology, stratigraphy and mineralogy (in conjunction with glass geochemistry) can be employed to identify tephra deposits. However, in distal regions these additional features are absent, and only the glass fraction is present. As such, correlation to source (and between deposits) typically relies on robust geochemical fingerprinting of the glass shards (Shane, 2000; Lowe, 2011).

Compositions can range from primitive (basalt) through to evolved magma (rhyolite / phonolite; e.g., Shane, 2000; Hall, 1996). The common magma melt series, reflecting increasing degree of fractional crystallisation, include the peralkaline (or alkaline) series, *alkali basalt – trachybasalt – trachyte-phonolite*, and the calc-alkaline (or subalkaline) series, *basalt – andesite – dacite - rhyolite* (Hall, 1996; Figure 3.2).

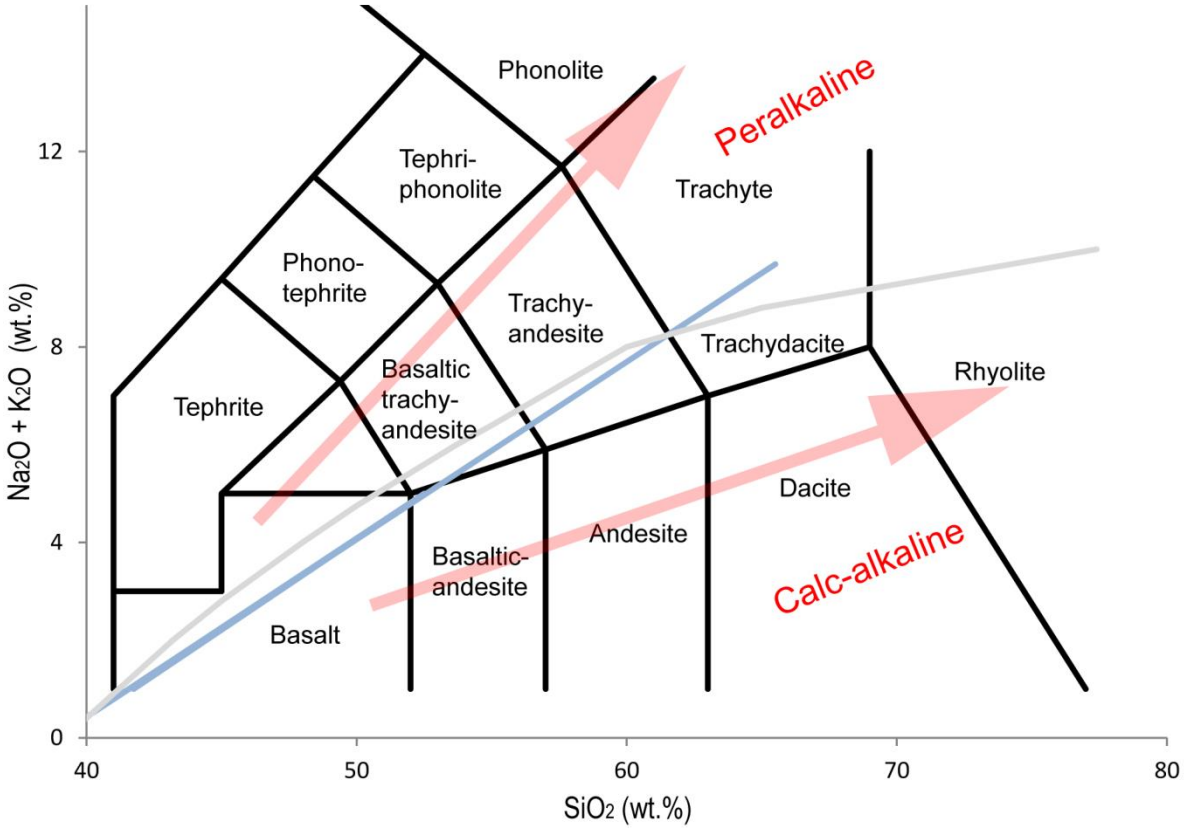

Figure 3.2. Total alkali silica plot with dividing magmatic trend line (coordinates from Rollinson, 1993) for peralkaline (alkaline) and calc-alkaline (subalkaline) series. Arrows show progressive fractionation of the magma melt, from primitive to evolved.

The geochemical composition of tephra is determined by instrumental analysis. Electron probe micro-analysers (EPMA) with the addition of spectrometers (wavelength dispersive; WDS, or energy dispersive; EDS) are used to measure a grain specific (individual shard) relative weight percentage of major and minor elements (e.g. Shane, 2000). EPMA are therefore able to characterise the chemical composition of the tephra deposits (Froggatt, 1992). Bulk techniques (whole rock analysis and/or combining of a number of shards, and sometimes minerals into one sample) have also been employed to measure both major and trace elements (the latter in parts per million, ppm). However, these bulk techniques are unable to detect heterogeneity and provide an average

composition for a sample (Froggatt, 1992), which can lead to incorrect characterisation and/or discrimination of and between samples from proximal and distal settings (e.g. see Tomlinson et al., 2012a). More recently, laser ablation inductively coupled plasma, mass spectrometry (LA-ICP-MS) has been employed to obtain shard specific trace element data. These data are normalised using the WDS-EMPA SiO_2 or CaO content of the specific shard to obtain absolute concentrations (see Tomlinson et al., 2010). Reference glasses are run with unknowns to check instrument performance and to ensure reproducibly, precision and accuracy of all grain specific results. To assess the homogeneity of the tephra samples >30 shards are analysed where possible.

Tephrostratigraphy involves building a framework of stratigraphic positions of tephra units relative to others. This framework is often tied to an absolute chronological scale using radiometric ages, referred to as tephrochronology (Lowe & Hunt, 2001). The ages of the tephra units are often determined at proximal locations but can be determined at distal locations if the source is not known (e.g. Smith et al., 2013)**.** At proximal locations relative ages can be obtained from radiocarbon dating on organic remains in and between the volcanic deposits and/or absolute ages from $^{40}Ar/^{39}Ar$ dating (typically using sanidine or biotite crystals, if present; e.g., Smith et al., 2011a; Mark et al., 2014). At distal locations, relative ages can be established from a number of methods; e.g., varved chronologies, radiocarbon age depth models in lakes and year chronologies from ice cores (e.g., Brauer et al., 1999; Rasmussen et al., 2006; Smith et al., 2013), other chronological techniques such as luminescence dating (e.g., Grapes et al., 2010), or a combination of some of these methods (e.g., Bronk Ramsey et al.,

2014). The use of this chronological information between sites requires precise, chemical correlation between the glass tephra deposits. If the age of the tephra is known then these layers also provide an absolute age that can be used in age models for the sites/archives (e.g., Douka et al., 2014; Lane et al., 2012a; Lowe et al., 2012).

3.2. Limitations and the preservation of tephra

Tephrochronology/tephrostratigraphy has considerable potential as a correlative tool (between archives) and for the formulation of independent, local and regional chronologies. However, as with all chronological techniques, consideration of the limitations and potential obstacles that may affect the precision and accuracy of the method are essential.

Although there is no temporal limit on the use of tephrochronology (as with other chronological methods; e.g. radiocarbon dating, ~50 ka), the technique is limited to, and governed by, the activity and frequency in volcanism at the volcanic centres. Tephrochronology is also spatially restricted by factors that include the following: the type of volcanic eruption (e.g. the magnitude of the event), the strength and direction of prevailing wind and atmospheric winds at the time of the eruption. In addition, tephras are unlikely to be found in geographic regions that are not close to or situated downwind of productive volcanic centres.

Robust chemical characterisation is central to tephra studies. The full range of tephra compositions from an eruption may not always be found at distal locations. This is due to melts of different compositions often being ejected into the atmosphere during the eruption. These are often not erupted simultaneously and instead are sequentially emitted, which can also coincide with a change in wind

direction and therefore dispersal. For example, the Laacher See tephra (LST) in the Eifel region, Germany, erupted multiple compositions, which were each dispersed in a different direction (see Schmincke et al., 1999; van den Bogaard and Schmincke, 1985). Unless the full suite of compositions is known from the proximal deposits (that could be hampered by insufficient characterisation work or removal of older deposits due to subsequent eruptions), this could result in correlations between archives not being made when they should.

Typically tephras have glass compositions that are unique to the volcanic centre and the eruption, that allow for distal deposits to be robustly correlated to each other and to the source volcano (Shane, 2000; Lowe, 2011). However, some volcanic centres are also known to have repeatedly produced tephras with indistinguishable major element chemistry (e.g. Katla, Lane et al., 2012b and Campi Flegrei, Smith et al., 2011b). In these instances, and if the shards are large enough, trace data can be used to help discriminate between them (e.g. Albert et al., 2014); however there are exceptions to this (e.g. Lane et al., 2012b) and miscorrelation may result. Corroborating information such as the tephras stratigraphic position in the climatic record (e.g. the Vedde ash is known to have erupted mid-way through the Younger Dryas stadial; Mangerud et al., 1984) or supporting chronological information can be used to help discern which tephra has been found in the archive (e.g. Lane et al., 2012b).

The chemical stability of natural glasses in the burial environment and during laboratory processing is of key importance (e.g. Blockley et al., 2005; Pollard et al., 2003). Reliable correlation of tephra layers requires high-precision geochemical analysis, but glass is susceptible to chemical alteration from aqueous attack in acidic and basic environments, and at elevated temperatures (see

Pollard et al., 2003). These agents can result in the total loss of natural glasses through dissolution (e.g. the complete destruction of the silica network especially in basic environments; pH >9) and/or can result in cationic leaching from the matrix; e.g. the mobilisation of sodium (Na) in more acidic environments (Blockley et al., 2005; Pollard et al., 2003). Anthropogenic factors such as heating of land surfaces (e.g. from the use of hearths) that contain tephra could also increase alkali exchange in the burial environment (Lane et al., 2014). These processes alter the chemical composition of the glass, rendering them unusable as tephra markers. This in turn has led to concerns over the reliability of chemical data from tephra that have undergone aggressive laboratory separation from their host sediments (e.g. acid digestion and ashing of sediments to remove organics; e.g. Dugmore et al., 1992b; Rose et al., 1996; Roland et al., 2015) and has led to the development of a non-destructive extraction procedure by Blockley et al. (2005). Alkali exchange can however be identified by careful scrutinisation of the WDS-EPMA data (specifically the ratio of Na to potassium, K; e.g. Scott, 1971). The presence of hydration rim or pitting on the external surfaces on the shards (via optical analysis) could also indicate chemical dissolution from the burial environment (see Figure 3.3). Both these tools can be used to assess the reliability of the compositional analysis.

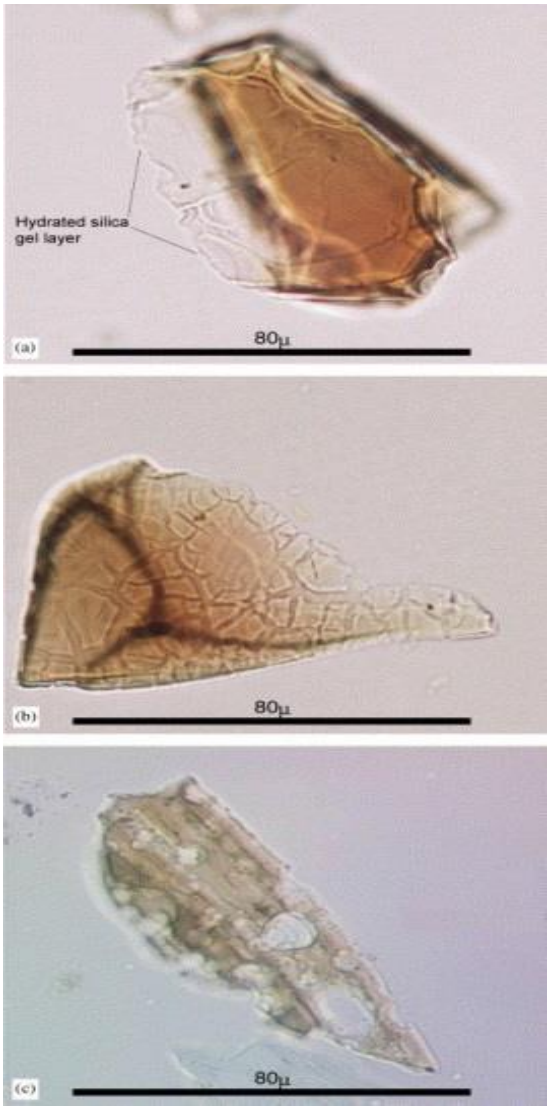

Figure 3.3. Photographs of basaltic shards that have undergone chemical dissolution. (a) shows the formation of a silica gel layer, (b) is the re-crystallisation of leached products that have formed on the surface and (c) shows pitting and corrosion of the shard. Basaltic shards are much more susceptible to chemical alteration. Images from Blockley et al. (2005).

The potential for tephras to become emplaced in sedimentary sequences, and the frequency and discreteness of the tephra horizon preserved, is influenced by the rate of sedimentation. For example, Carter et al. (2005) discuss that cores that were taken from the western bay of the Bay of Plenty, New Zealand (S794, S803), had few, if any discreetly preserved tephras horizons and shards were generally dispersed throughout the host sediment. The sedimentation rate was ~5.8 cm / 1000 yrs. Cores of a similar age (~75 km away) taken from the eastern part of the bay had a sedimentation rate ~14.4 cm / 1000 yrs, and numerous, thicker and discrete tephra horizons were preserved (see Carter et al., 1995 and references

within). As such, tephra deposits are best preserved in low energy or sheltered environments that have a high sedimentation rates. Rapid burial of the tephra in these environments reduces the risk of post-depositional modification and reworking (Carter et al., 1995; Lane et al., 2014). In open air archaeological sites, tephra deposited on land surfaces (that are not rapidly buried) are also likely to be quickly eroded away or remobilised. This is thought to explain the lack of the late glacial (~12.9 ka) LST tephra in the open-air site of Ahrenshöft, northern Germany (see Housley et al., 2012), even though deposits were abundant in nearby lakes (e.g. Riede et al., 2011). In this case, the absence of the LST in the site was likely due to taphonomic conditions (e.g. scouring of the landscape by glacial winds) that would have dramatically reduced sedimentation rates.

The spread of tephra shards in archives could also be an artefact of the methods used in sampling and sub/sampling of deposits. In archaeological sites, samples are collected from the base of a sequence to the top to negate spillage of tephra from higher in the sequence to lower sediments (Lane et al., 2014). For core sections, drilling processes and core cutting with nylon or metal wire can dislocate shards from their initial positon and smear particle down the outside of the sediment column.

Unlike visible deposits, that can be directly targeted and extracted from sedimentary profiles, cryptotephras are identified in the laboratory by processing continuous samples from an archive. This process is time consuming and labour intensive, e.g., processing 4 m of sediment at low resolution (10 cm) could take ~3 weeks (based on laboratory methods outlined by Blockley et al., 2005). As such, many authors have explored less destructive and more time friendly methods for the location of cryptotephras (e.g. see review in Gehrels et al., 2008), but in

practice the most accurate and reliable cryptotephra profiles are still produced through conventional density extraction and microscope identification techniques (Gehrels et al., 2008).

3.3. Tephra in the sedimentary environment

Essential in tephra studies is the correct identification of the primary tephra deposit: the isochron. For tephra deposits that are visible in the sedimentary sequences, the isochron is usually clearly defined. Both Lewis et al. (2012) and Matthews et al. (2012) suggest the following criteria:

- the primary tephra layer is characterised by clearly defined upper and lower contact;
- it is usually sat uniformly, tracing the original land surface;
- the deposits have no, to few, internal features (cross-bedding etc); and
- the layer forms a continuous unit that is dominated by glass shards with no, non-volcanic material (Lewis et al., 2012; Matthews et al., 2012).

For cryptotephra studies, the identification of the isochron and secondary deposition (where shards have been remobilised and re-deposited from the primary location) is more difficult and requires an understanding of the interplay between transport mechanisms, sedimentation, post-depositional process and the tephra (e.g. Davies et al., 2012; Lowe, 2011). For the purposes of this study, taphonomic processes that govern archaeological sites, specifically cave deposits and processes specific to the marine and lacustrine environments are discussed.

3.3.1. Tephra in Archaeological cave sites

Only a handful of studies, predominantly in Europe and across the Mediterranean, have looked for cryptotephras in archaeological sites (Figure 3.4). Of particular importance for this study is the preservation of cryptotephra in the sedimentary sequences of cave deposits. The first published record of cryptotephra in a cave sequence (with associated archaeological artefacts) was from the Billa Surgam cave site in India by Lane et al. (2011b), and more recently Lowe et al. (2012), Douka et al. (2014) and Karkanas et al. (2014) have found numerous tephras, preserved in stratigraphic order, in cave sediments.

Figure 3.4. Map of northern Eurasia and North Africa that shows the location of archaeological sites (cave and open air) that contained cryptotephra and have been published (open circles). Billa Surgam cave, India is not shown. Triangles denote volcanoes that have been active in the Quaternary. Confirmed source volcanoes (darker triangles) for the tephras found in the archaeological sites are indicated with Roman numerals; i. Hekla; ii, Askja; iii, Katla; iv, Laacher See; v, Campi Flegrei Volcanic Zone; vi, Mt. Etna; vii, Pantelleria; viii. Nisyros. Image adapted from Lane et al. (2014).

Caves are ideal for archaeological and tephra studies as they are, by definition, sheltered sites that behave as natural sediment traps (e.g. Lowe and Walker, 1997; Lane et al., 2014). Karstic regions especially can contain sedimentary sequences that have accumulated over long periods of time (often longer than neighbouring open air sites) and therefore have the potential to preserve a number of tephra horizons in stratigraphic order (see Douka et al., 2014; Karkanas et al., 2014).

There are two types of caves: exogene caves (or rock shelters) that form shallow hollows or niches in hillsides and endogene caves that penetrate deep into the ground with chambers and complex passageways (see Lowe and Walker, 1997). Depositional inputs to these caves fall into three categories: clastic detritus, organic detritus (bones, etc.) and carbonate precipitates. For tephra studies the greatest success has been from cave sediments that are mainly composed of allochthonous deposits (exogenous sediments that derive from outside the cave; see Figure 3.5) rather than in caves that are primarily composed of autochthonous (endogenous) sediments from the cave wall. Allochthonous sediments are more commonly found in exogenous caves or rock shelters and in areas towards the cave mouth opening (in endogene caves) and are especially prominent in caves that have a large cave mouth opening. These locations are ideal to ‘collect’ windblown deposits that could include tephras (Figure 3.5).

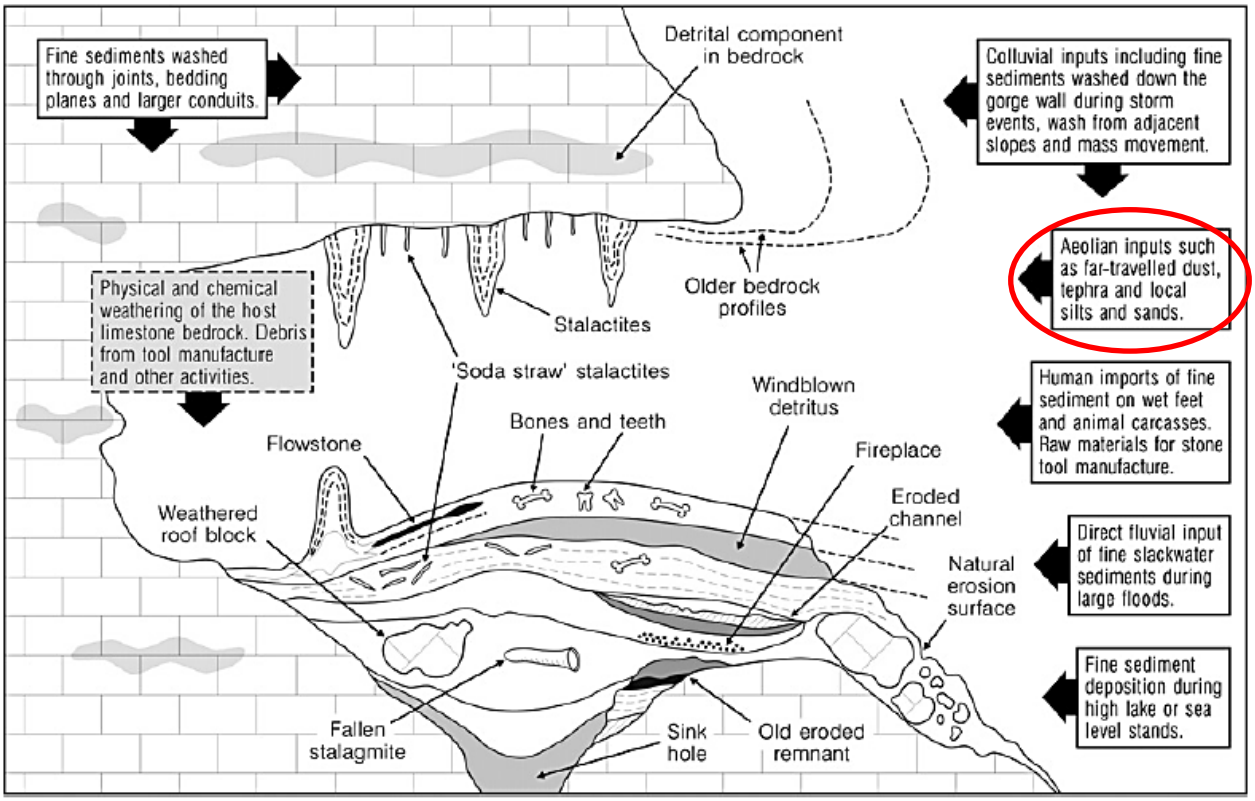

Figure 3.5. Schematic of the types of sediment input and processes of deposition in a limestone cave. Processes can be incredibly complex. Red circle shows the primary process for tephra to enter a cave, but percolation through fissures in the cave roof could also introduce shards to the sediments. Image adapted from Morley and Woodward (2011).

These traps (rock shelters and caves) can receive allochthonous sediment from a number of locations: those within close proximity to the cave entrance and sediments from more distally located sources (that will tend to be more fine grained; Morley and Woodward, 2011; Figure 3.5). Processes responsible for sediment transport into cave and rock shelters include aeolian activity (windblown sediments, primarily through the cave mouth opening), alluvial activity (including rainfall that can also include percolation through the host bedrock and through fissures in the cave walls), colluvial activity (from the surrounding landscape), and biological activity that can introduce organics to the sedimentary sequence (derived from animal and human occupation of these sites). Clastic material (in

various sizes) is also a common feature of cave sedimentation and this is primarily derived from the collapse of the cave wall and continual erosion of the surrounding rocks. Consequently, the stratigraphy in these types of deposits is often complex and hiatuses in the sedimentation are not uncommon (e.g. Theopetra Cave; see Karkanas et al., 2014).

The main agents that are responsible for the complex tephra distributions in caves and rock shelters are:

- Anthropogenic activity such as the construction of hearths and occupation of living surfaces that could displace tephra from its original point of deposition, both laterally and vertically with other debris (Morley and Woodward, 2011; Lane et al., 2014).
- Continual re-working and input from the surrounding landscape after the primary event (Morley and Woodward, 2011; Lane et al., 2014; Lowe, 2011). This can continue until the catchment becomes exhausted. This could be through airborne, colluvial or alluvial activity.
- Low sedimentation rates that enable more reworking of deposits and the decreased resolution of individual tephra horizons.
- Friable and unconsolidated sediments can allow for the migration of shards through the profile. Shards in friable sediments could also be easily displaced during in excavation (this could also contaminate additional profiles but can be prevented in sampling; see methods and Lane et al. (2014).
- Biogenetic activity from animals using the cave (at or around the time of the tephra deposition) and from burrowing animals and micro-organisms and

plant roots (bioturbation). These can displace shards from the original location and could cause mixing of tephra layers.

- The nature of the cave and rock shelter floor at the time of deposition. Uneven surfaces with voids and larger amounts of breccia can affect the stratigraphic integrity of the layer and may result in an artificially thickening and/or thinning of the layers (Morley and Woodward, 2011). At these sites, sampling is normally done at a lower resolution (~ 5cm) as it would be impossible to further constrain the deposition (Lane et al., 2014).

In addition to the limestone cave context described above, the Caucasus, specifically Armenia, has a number of rock shelters that are formed in lava flows. Host sediments in these rock shelters are likely to be composed of volcanic glass eroded from the rock/cave wall surfaces. This would need to be differentiated from exogenous tephra shards. Furthermore, if there is a predominance of artefacts made from obsidian (a volcanic glass) it is possible that increases in anthropogenic activity such as knapping, habitation and trampling of the surfaces etc. could result in fracturing of obsidian producing small flakes of glass. This may appear as an artificial tephra horizon in the site.

3.3.2. Tephra in marine and lacustrine sedimentary archives

Lake and marine archives are often formed from rapidly accumulating sediments that contain a record of past environmental and climate change. These are ideal for the preservation of tephra horizons in a relatively secure stratigraphic order (Lowe, 2011). As such, tephra studies in marine and lacustrine archives are now common in many areas around the world (e.g. Abbott et al., 2011; Bourne et al., 2010; Lane et al., 2011a, 2012a; Lowe, 2011; Smith et al., 2013).

Tephra particles (glass) are instantaneously deposited onto the water surface following a volcanic eruption. These grains quickly overcome surface tension and travel through the water column (with assistance of gravity) to the sea or lake bed and are rapidly covered and preserved. However, there is complexity in the types of processes that control the mode of transport on to the water surface, through the water column and post depositional processes at the lake/ocean floor (e.g., Davies et al., 2012; Griggs et al., 2014; Todd et al., 2014).

The main modes of transport and the processes responsible for the secondary mobilisation of tephra shards in a marine and lacustrine environment are:

- Sea ice rafting or from near shore ice (NSI); production of NSI commonly occurs in large lake bodies and at coastal margins in glacial and cold periods (e.g. Kempema, 1998; Nowaskey et al., 2012). Rafting and subsequent melting (~3-6 month process) from NSI would introduce larger grain sized particles to surficial sediments with tephra that could have collected on and in the ice prior to melting (Kempema, 1998).
- Ocean and water currents. The greater the concentration of the ash that is deposited on the water's surface, the faster a deposit will travel to the bottom of the lake or sea as it is able to overcome strong density currents, termed tephra loading. Less concentrated deposits may take longer (days to weeks depending on depth of water body) but are unlikely to affect the integrity of the final isochron (within the temporal resolution of the sampling precision). Currents at the base of the water column (bottom currents) are likely to cause re-working and remobilisation of shards from surficial sediments (upwelling; see Griggs et al., 2014)

- Bioturbation (burrowing, feeding, defecation and locomotion) from both microscopic and larger animals that live in and on the surface can cause displacement of the surficial sediments and tephras that have been deposited (e.g. Griggs et al., 2014; Todd et al., 2014).
- Unconsolidated sediments that allow for easy, vertical mobilisation of shards below the peak (e.g. Lowe, 2011).
- Low sedimentation rates that could decrease the resolution of individual tephra horizons.
- Remobilisation of shard from the landscape until source is exhausted. This secondary mobilisation of shards from the landscape may also be influenced by climatic regimes; stadial condition with low vegetation could result in periods of continual reworking (Pyne-O'Donnell et al., 2008), with snow entrapment causing a slight temporal lag in the secondary deposition (Davies et al., 2012; restricted to lake environments).
- Coring and sub-sampling could result in smearing of shards from zones that contain a high concentration of shards.

Iceberg rafting is a major concern for marine tephra studies (see Davies et al., 2012; Griggs et al., 2014; Lowe, 2011). In this process, shards of volcanic glass are deposited onto ice sheets in large quantities following an eruption. The ice sheets then undergo calving that produces icebergs and these can transport the tephras into far distal locations. Multiple tephras may have been deposited on the ice sheet prior to calving (Griggs et al., 2014). Temporal delays from the initial deposition on the ice to the final deposition in the distal environment could be millennial to centennial in scale, and tephra would no longer be an isochron (Lowe, 2011). Tephras that are deposited on the ice sheets in large quantities are

likely to be from volcanoes that are in close proximity (e.g. Iceland to Greenland). Fall deposits are typically well sorted and shard size decreases exponentially away from source, and tephra from ice rafted debris (IRD) is poorly sorted with various sizes of shards that are typically compositionally diverse but only if multiple eruptions were deposited prior to calving (e.g. Griggs et al., 2014; Lowe, 2011). However, this is generally restricted to areas with large, long lived ice sheets and should not be an issue for this study.

3.4. Tools of the trade; how we identify primary deposition

Shard concentration profiles are the main tool used to identify a tephra isochron and subsequent reworked shards (e.g., Davies et al., 2012; Lane et al., 2014). These profiles should reflect a contiguous column of sub-samples that encompass the entire sedimentary profile of the archive or site (Davies et al., 2012; Lane et al., 2014). Examples of shard profiles from archaeological sites are given in Figure 3.6 followed by Figure 3.7 that shows similar profiles found in the marine and lacustrine environments. The identification of constrained layers with largely sterile sections of sediment (devoid of volcanic glass) is a good indication of stratigraphic security in the archive (e.g. Douka et al., 2014; Davies et al., 2012); especially if the tephras are geochemically distinct. Cryptotephra concentration profiles often have shards distributed over extended depths (e.g., up to ~10 cm are common in an archaeological site; Lane et al., 2014; Figure 3.6), but the peak in shard concentration is considered the isochron (the timing of the volcanic eruption; Davies et al., 2012; Lane et al., 2014; Lowe, 2011).

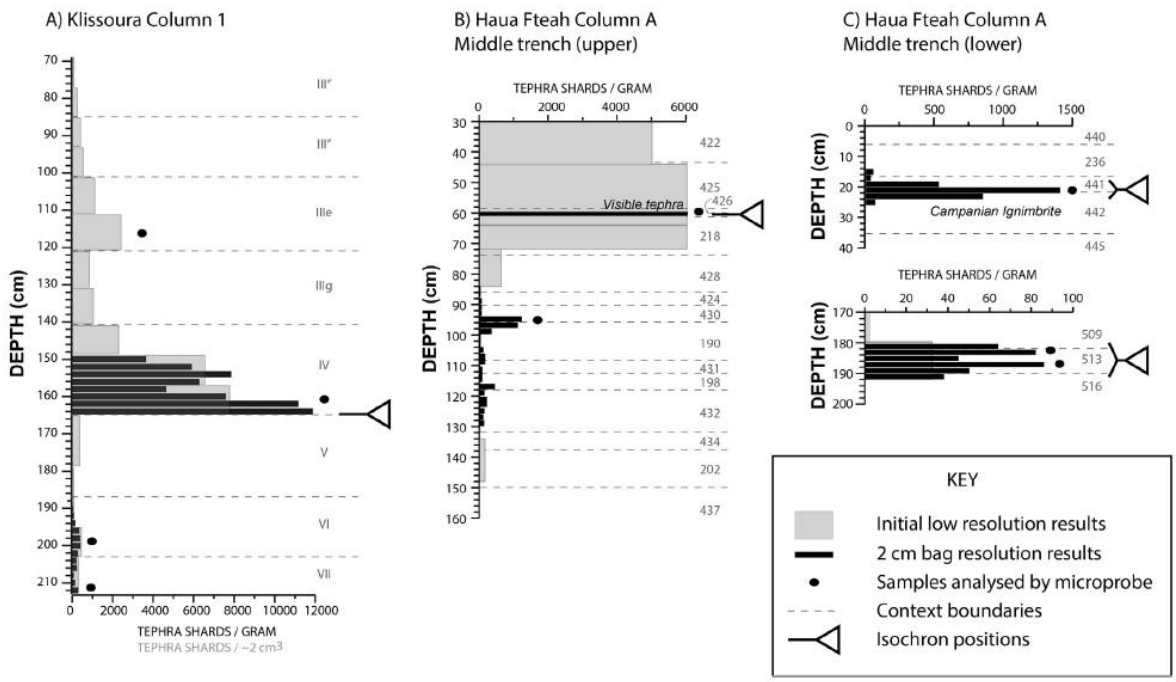

Figure 3.6. Shard concentration profiles, grey bars are shards per gram (s/g) found in the low resolution samples, black line are the s/g in the higher resolution 2 cm bag samples. Profiles are from (a) Klissoura cave that has a sharp boundary at the base of the cryptotephra layer with a tail in cryptotephra above. There is a smaller peak below, which is separated from the larger peak by sterile sediments and it is compositionally and visually distinct (see Lane et al., 2014; Lowe et al., 2012). Tephra profiles from the Haua Fteah cave in Libya are shown in b and c. A thick cryptotephra deposit was found above and below a visible layer in b – the composition of the cryptotephra is the same as the visible deposit and reflects the friable nature of the sediments, which allows for reworking. Two small cryptotephra layers that are both well constrained to ~12 cm depth are seen in profile c. There is some uncertainty on the isochron position, and imported age estimates are applied at context resolution (see Lane et al., 2014). After Lane et al. (2014).

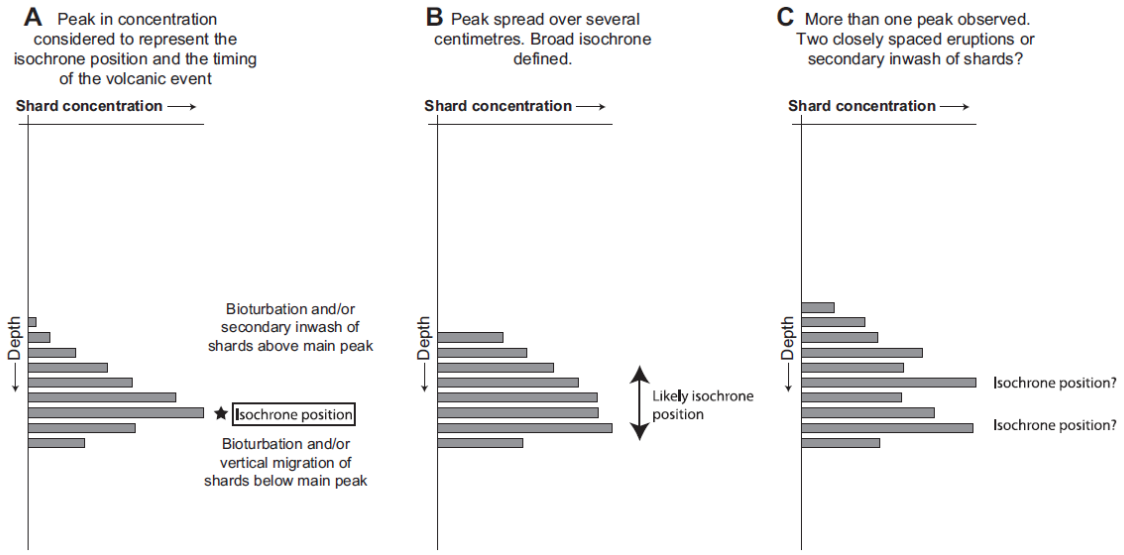

Figure 3.7. Schematic showing different shard concentration profiles that are common to sedimentary sequences in lakes and marine environments. Shard concentrations with a clear peak (a), which is labelled the isochron, (b) and (c) show profiles that do not have a distinct peak and the depositional processes and composition need to be used to assign the position. Image after Davies et al. (2012).

Tephra profiles with a sharp boundary at the base of the distribution (that is indicative of rapid input of tephra, and the primary input) that have an upward tail in decreasing shard concentration tend to reflect anthropogenic activity or large faunal activity at archaeological sites (Figure 3.6). In lacustrine and marine environments this is credited to the remobilisation of shards at the surface by surface currents and/or biological activity. The upwards tailing of shards is also attributed to the continual reworking and secondary mobilisation from the catchment, post the initial eruptive event; the latter is restricted to lakes or near shore environments and archaeological sites (Davies et al., 2012; Griggs et al., 2014; Lane et al., 2014; Pyne-O'Donnell et al., 2008).

Displacement of shards below the largest peak concentration is ascribed to water percolation and/or gravitation, sediment loading (from the sudden influx of high

concentration of shards that were deposited at one time; e.g. Griggs et al., 2014), or can be attributed to gradual, vertical settling of the particles through unconsolidated sediments (Davies et al., 2012; Griggs et al., 2014; Lane et al., 2014). Compaction of the land surfaces by trampling by hominids and /or animals at archaeological sites, could also cause the dislocation of shards below their primary context (Lane et al., 2014; Morley and Woodward, 2012). Bioturbation is another agent responsible for the mobilisation of shards below the main peak in concentration resulting in a downwards tail (Griggs et al., 2014; Lane et al., 2014; Morley and Woodward, 2011). Recent experimental studies in the lacustrine and marine environment have however shown that there is minimal downwards disturbance from bioturbation in these archives; ~1.8 cm from the initial isochron (Todd et al., 2014), and that activity normally ceases in a few months. In some cases, where deposits of volcanic ash are significant (>1 cm in thickness) the ash would smother surface biota and suppress post-depositional bioturbation (Todd et al., 2014; Lowe 2011).

In some shard concentration profiles there is no defined peak (see Figure 3.6c and Figure 3.7c), and the tephra is spread uniformly over a wide area or with multiple peaks with no stratigraphic, sterile break between. This could be a result of several closely spaced eruptions, insufficient sediment rates unable to resolve these and/or reworking from the landscape. A mixture of some or all of these (including bioturbation) should be considered. In this instance the exact location of the isochron cannot be assigned on shard concentration alone (Davies et al., 2012; Griggs et al., 2014; Lane et al., 2014). Compositional analysis (using WDS-EPMA) could be used to help construct the argument for the position of the primary isochron/s. If major element compositions from the main peak are

homogeneous, it is highly likely to be a primary deposit (Davies et al., 2012; Lowe, 2011) and any shards displaced from the main peak (above and/or below) would have the same chemical fingerprint. By comparing the major element chemistry at the top and base of a substantially thick, defuse deposit it can help establish whether the deposit represents one large input with complex reworking or mixing of two or more tephras. If the former is apparent, high resolution tephra processing of the sediments (shard counting at a 1-2 cm resolution) is unlikely to provide extra information on the position of the isochrones (Lane et al., 2014, Figure 3.6). If mixed geochemical compositions are found, this could be a result of reworking or low sedimentation rates, but also could reflect volcanic deposits from a number of eruptions that were closely spaced in time and/or heterogeneity linked to mixing magmas in one eruption (for example, the Vedde Ash from Iceland is composed of both a basaltic and a rhyolitic population; e.g. Mangerud et al., 1984). But the processes responsible for a mixed deposit are hard to resolve, and all possible factors have to be considered on a site to site basis; robust proximal geochemical data can be key in this situation.

A further complementary tool is the visual assessment of the glass shards themselves with high powered optical microscopy. In some cases, glass shards from different eruptions and/or volcanic centres can have a distinctive morphology (Figure 3.8). This is related to the characteristics of the eruption event (highly explosive, gas rich etc.). Differences observed in shard morphologies (although subjective) could be used to discern mixed deposits that derive from different volcanoes and/or differences in eruption mechanics that produced the tephras from the same volcano (e.g. Hamann et al., 2010).

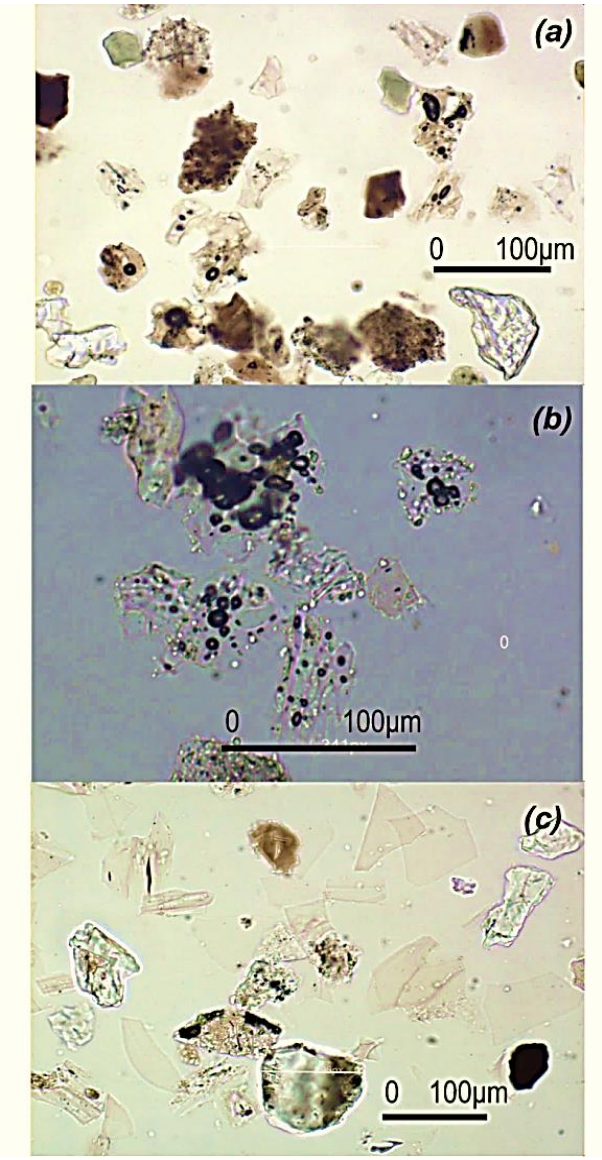

Figure 3.8. Photographs of glass shards from three different eruptions. The Biancavilla ignimbrite from Mt. Etna, Sicily (a) found in the Haua Fteah cave in Libya (Douka et al., 2014). Shards show a range of morphologies, texture and colour, but shards are compositionally homogeneous (trachyte). The LST from Germany (b) found in Endinger Bruch, Germany (Lane et al., 2012a). The shards are distinctively vesicular. And (c) the Campanian Ignimbrite from Campi Flegrei, Italy found in Haua Fteah cave in Libya (Douka et al., 2014). The shards exhibit low relief and there are a large proportion of platy shards in distal locations.

Consideration of other proxies at the site (e.g., palynology) is also recommended as these are likely to be affected by the same processes as tephras (Lowe, 2011; Lane et al., 2014). Micro-morphological techniques can also be useful to discern the types of processes responsible for the dislocation of shards from the main peak (e.g. Griggs et al., 2014).

3.4.1. Realistic resolution of an isochron in sedimentary environments

It is unlikely that a tephra isochron in an archaeological site will be constrained to 1 cm or less (Lane et al., 2014), but can still provide a chronological marker that is

at an appropriate resolution for an archaeological site. Commonly this has a precision that is accurate within an archaeological unit or layer (Lane et al., 2014). The accuracy of an isochron in the marine and lacustrine environment is much more precise; isochrones can commonly be pinpointed to 1 cm depth after careful evaluation of the shard concentration profile and chemistry (Davies et al., 2012; Griggs et al., 2014). The chronological time this 1 cm covers is dependent on the sedimentation rates in the archive at that time, but is equal to (if not more precise) than the sampling resolution for environmental proxies that are sub-sampled from the same archive. In lake sediments that are annually laminated, the resolution can be accurate to the ~varve year (e.g. Van Daele et al., 2014); but varve counting errors have to be included in any age model constructed for the archive.

3.4.2. What constitutes a good tephra horizon?

Once an isochron has been defined in an archive, there needs to be consideration of its potential in that archive, and for the region the archive is from. The following criteria for an ideal tephra layer have been agreed by members of the INtegration of Ice core, MArine and TErrestrial records group (INTIMATE; a INQUA Palaeoclimate commission subgroup):

- The tephra must be robustly dated, and if possible a modelled age from a number of independent methods is used.
- The tephra has a unique geochemical fingerprint with robust, shard specific compositional data (major elements and trace elements where possible).
- Eruption deposits should be widely dispersed (over hundreds of kilometres).

- The tephra sits close to an important environmental and/or archaeological transition.

Although these criteria are very specific, they represent the ideal tephra marker horizon for assessing palaeoenvironmental and archaeological change. The Campanian Ignimbrite tephra (CI) is a good example as it sits close to the onset of a Heinrich Event 4 (HE4) and appears to be coincident with the expansion of modern humans in many sites across Europe and the Mediterranean (e.g. Lowe et al., 2012). It is also dispersed thousands of kilometres east of the vent (in Italy) (see Costa et al., 2012).

3.5. Potential for tephrostratigraphy in the Caucasus

Two cryptotephra layers have been previously found in Mezmaiskaya cave (Middle Paleolithic layer 2B-1, and archaeological sterile Layer 1D) in the Northern Caucasus (Golovanova et al., 2010a, Figure 3.3). Distal facies of the marine Z2 tephra (correlated to the 3.6 ka Minoan eruption of Santorini; Friedrich et al., 2006) and the Late Glacial Y2 tephra (also known as the Cape Riva eruption of Santorini; Druitt et al., 1989) have been identified in north and southwest Black Sea and the Sea of Marmara (Guichard et al., 1993; Kwiecien et al., 2008; Lamy et al., 2006; Wulf et al., 2002). More recently, the Campanian Ignimbrite (CI) tephra (39.3 ± 0.1 ka, Di Vivo et al., 2001) in the southeast Black Sea has also been, tentatively, chemically identified (Nowaczyk et al., 2012) and numerous visible deposits (from Nemrut, east Turkey) have been located in Lake Van (see Stockhecke et al., 2014a, b). Consequently, there is evidence that volcanic plumes have deposited tephra in archaeological and palaeoenvironmental sequences in and around the Caucasus, in the time period of this study.

3.6. Concluding remarks

The Caucasus has been identified as a suitable region for a tephrostratigraphic study. Although there are a number of limitations to tephrostratigraphy, the method is unique from other chronological techniques in its ability to directly anchor disparate archives. A review of the complexity in the identification of the isochron in various depositional environments (cave sites, marine and lacustrine) led to the conclusion that, ideally the isochron should be identified using a combination of shard concentration diagram, visual assessment, compositional analysis and consideration of other proxies data to evaluate if there has been other disturbances in the site sedimentation (including any chronological information). This multifaceted approach is adopted by this study to securely identify primary tephra horizons. It is important to evaluate each new tephra layer identified on a site to site basis and this chapter has highlighted two factors that have yet to be considered in tephra studies: the differentiation of exotic shards of glass (tephra) from endogenous sedimentation of caves formed in lava, and can tephra glasses be clearly differentiated from shards that come from obsidian deposits. Both of these factors will be addressed in this study. Sites selected for tephra analysis are presented in the next chapter. For further discussion of the possible volcanic sources and widespread tephra layers that could be found in the Caucasus see Chapter 6, Volcanic sources of tephra in the Caucasus.

Chapter 4

Site selection

4.1. Introduction

This chapter introduces the archaeological sites and the palaeoenvironmental sequence selected for a cryptotephra investigation. The criteria used to select the archives are given. This is then followed by a description of the archaeological and stratigraphic context of each site that contained tephra*. Previous work on the palaeoenvironmental sequence and some issues with its current age model are then presented.

4.2. Site selection parameters

4.2.1. Archaeological sites

Four primary criteria were used to select sites:

1. Sites were selected from either side of the Greater Caucasus range. This is essential to evaluate the synchronicity of archaeological occupations from a regional perspective.
2. Archaeological sites should have evidence for Mid-Middle Palaeolithic (MMP), Later MP (LMP) and/or an Early Upper Palaeolithic (EUP) occupation (~MIS 5e – ~MIS 3; ~125-30 ka).
3. Sites should have been previously studied, with any archaeological, chronological and stratigraphical information published or available in grey literature.

**Footnote. To be succinct, only sites that contained tephra are summarised in this chapter.*

4. Sites should have a long stratigraphic sequence (constituting a number of archaeological/sedimentological levels) providing the opportunity to locate a number of tephra layers preserved in relative stratigraphic order.

Unfortunately some sites could not be used; for example, we could not get permission to access some sites (e.g. Mesmaiskaya), some sites no longer preserve sediments, excavations had ceased at some sites making them difficult to access and some regions were inaccessible due to current political matters (e.g. Myshtulagty Lagat in Northern Ossetia). Sites that were selected are shown in Figure 4.1, and listed in Table 4.1.

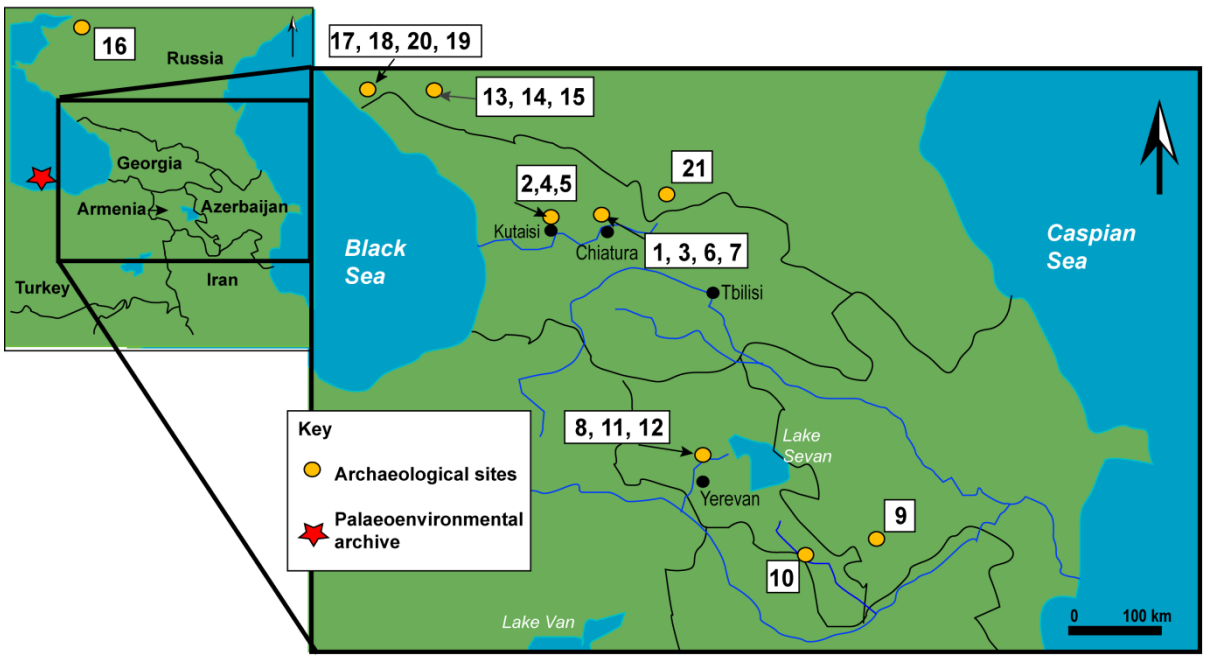

Figure 4.1. Location of the archaeological sites (orange circles) selected for tephra investigations. The location of the M72-25/GC1 core (palaeoenvironmental sequence) is shown by the red star. Numbers next to the orange circles (in white boxes) relate to the site names and these are found in Table 4.1 and in the text next to the site description. Sites were selected from the southern and northern Caucasus.

Table 4.1. Archaeological sites selected for study and applicability to the site selection criteria.

Site Name	Criterion 1 (geographic location)			Criterion 2 (techno-complex)	Criterion 3 (published)	Criterion 4 (long sequence)	Collected by
Ortvale Klde (1)	**Southern Caucasus**	**Republic of Georgia**	Imereti	LMP/EUP	✓	✓	Author
Sakajia cave (2)			Imereti	LMP/UP	✓	✓	Author
Undo cave (3)			Imereti	MP/UP	x	✓	Author
Ortvale cave (4)			Imereti	LMP/UP	✓	✓	Author
Bronze Cave (5)			Imereti	MP	✓	✓	Author
Bondi cave (6)			Imereti	LMP/UP	✓	✓	D. White
Dzudzuana cave (7)			Imereti	EUP/UP	✓	✓	Author
Lusakert 1 (inside and outside the rock shelter) (8)		**Armenia / Azerbaijan**	Hrazdan river gorge	LMP/LMP	**X✓**	✓✓	Author
Azokh cave (9)			Armenia/Azerbaijan (disputed territory),	EMP/LMP/UP	✓	✓	D. White
Aghitu 3 (10)			Syunik region	UP	✓	✓	A. Kandel
Fantan (11)			Hrazdan river gorge	MP	X	x	K. Wilkinson
Kagasi (12)			Hrazdan river gorge	MP	x	X	K. Wilkinson

Gubs rock shelter (13)	**Northern Caucasus**	**Russia**	NW Caucasus, Gubs Ravine	LMP/EUP	✓	✓	EFCHED
Monasheskaya (14)			NW Caucasus, Gubs Ravine	LMP	✓	✓	EFCHED
Barakaevskaya (15)			N Caucasus, North Ossetia	LMP	✓	✓	EFCHED
Biriuchya Balka 2 (16)			Russia steppe, Severski Donets	LMP/ EUP	✓	✓	EFCHED
Navalishensk-aya (17)			NW Caucasus, Sochi	MP/ UP	✓	✓	EFCHED
Kepshinskaya (18)			NW Caucasus, Sochi	MMP?/LMP	✓	✓	EFCHED
Akhshtyr (19)			NW Caucasus, Sochi	EMP/LMP/ UP	✓	✓	EFCHED
Malaya Voronts-ovskaya (20)			NW Caucasus, Sochi	LMP/UP	✓	✓	EFCHED
Myshtulagty Lagat (Weasel Cave) (21)			N Caucasus, North Ossetia	EMP/MMP/ LMP	✓	✓	EFCHED

Footnote: The information, published or otherwise (see criteria 3) for each site differs in quality and quantity. This may affect detailed interpretations of these sites. LMP, Late Middle Palaeolithic; MMP, Mid-Middle Palaeolithic; EMP, Early Middle Palaeolithic; EUP, Early Upper Palaeolithic; UP, Upper Paleolithic. MP-(Middle Palaeolithic) is used if there is no age control but sites contain a MP techno-complex.

4.2.2. Palaeoenvironmental archive

The criteria for the selection of the palaeoenvironmental archive were: the archive must be located in close proximity to the Caucasus; the archive should contain a long palaeoenvironmental sequence, encompasses part or the whole time range for this study (but at least the LMP-EUP transitional period); the archive must be in

good state of preservation that is suitable for high resolution sampling for tephra; and the archive should have detailed palaeoenvironmental work that is published or close to publication at the start of the tephra investigation.

Chapter 2 identified four possible archives (see section 2.2.2). Poor preservation of the Lake Urmia cores means that this record cannot be sampled for cryptotephra analysis. Work on tephras (visible) found in the Lake Van archive/s is ongoing (Schmincke and Sumita, pers comms, 2014), and previous cryptotephra investigations on the eastern European loess from Mitoch-Malu Galben and Molodova V were unsuccessful (previous work on the NERC, RESET project). The M72-25/GC1 core from the south east Black Sea that spans the last ~60 ka was chosen for analysis and its location is shown on Figure 4.1.

4.3. Descriptions of archaeological sites with tephra

4.3.1. Ortvale Klde (Republic of Georgia), site No. 1

The site of Ortvale Klde is situated near the town of Chiatura (Figure 4.1). It comprises two east facing karstic rock shelters. The name ‘Ortvale Klde’ translates as a rock with two eyes and it is positioned ~35 m above the Cherula River, which flows to the Rioni River, via the Kvirila River, to the Black Sea.

Initial excavations conducted by D. Tushabramishvilli and N. Tushabramishvilli found 11 lithostratigraphic layers, with a believed *in-situ* transitional layer between the LMP and EUP occupations. New excavations in 1997 to 2001 by Tushabramishvilli and Adler reinvestigated both the LMP and EUP layers in the southern chamber at the site. They found no evidence for a transitional layer, but identified a stratigraphical and archaeological hiatus at the end of the LMP layers

(Layer 5) and the start of the EUP (Layer 4d; Adler and Tushabramishvili, 2004; Figure 4.2). Investigations in the northern chamber are ongoing (e.g. Moncel et al., 2013). Only the western profile of the southern chamber was sampled for tephra and is described here.

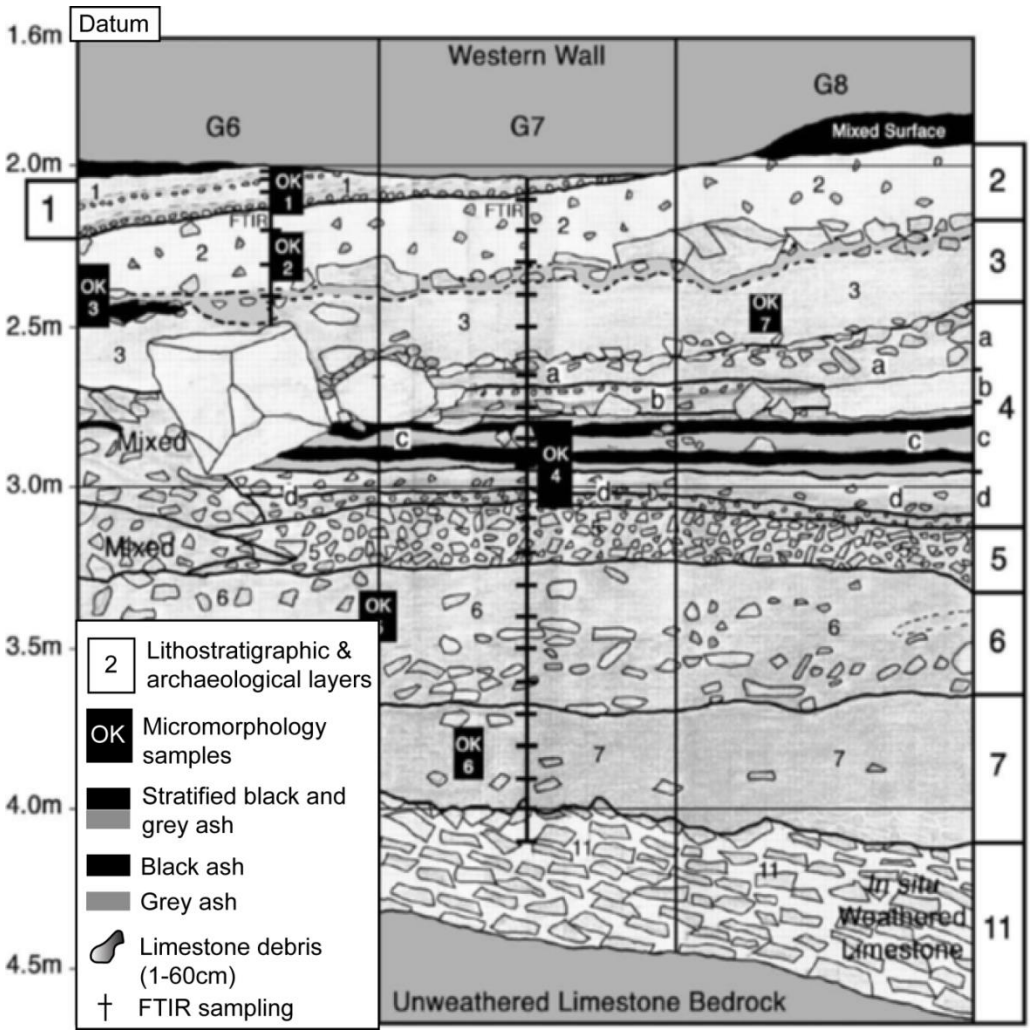

Figure 4.2. Profile of the western wall exposure of Ortvale Klde, with stratigraphic Layers 1-7 and 11 and sub-layers 4d-4a shown. After Adler et al. (2008)

The stratigraphic and archaeological sequence (from the top downwards) of Ortvale Klde (Figure 4.2) is as follows:

- Layer 1. Mixed surface sediments.
- Layer 2-3. There is a clear stratigraphic boundary berteen Layer 2 and 3 of limestone slabs filled with éboulis (broken rock fragments) under which a

light grey, organic ash from was found. Migration between the two layers is unlikely. Some evidence for bioturbation was seen in Layer 3. EUP finds are concentrated towards the top of Layer 3 and the base of Layer 2.

- Layer 4 is ~ 65 cm thick and is subdivided into 4 sublayers; a-d. 4d, contains the first appearance of EUP occupation at the site is composed of a soft brown, grey ash matrix with *in-situ* hearth features. No mixing between 4d and Layer 5 was found. Layer 4c is composed of stratified black and grey organic ash lenses that are rich in faunal and lithics remains. Micropohology indicated some localised, lateral movement in this layer. Layer 4b is overlain by Layer 4a that is situated directly beneath a dense deposit of éboulis at the contact to Layer 3. Layer 4a and 4b are loose yellow sediments with few archaeological finds. No evidence of bioturbation was found in Layer 4.
- Layer 5 contains the last LMP occupation of the site. Sediments are composed of a dense accumulation of small rocks (1-6cm) and are compact and clay-rich. Layer 5 contains numerous archaeological finds, with some evidence of weathering.
- Both Layers 6 and 7 are composed of a black granular matrix, rich in archaeological remains (fauna, lithic and organic remains such as ash and charcoal). Layer 7 contains fewer larger clasts than Layer 6. Evidence of bioturbation is seen in both layers. Layer 7 overlies Layer 11 (in the west section), that is composed of weathered limestone (not sampled).

LMP tool assemblages (Layers 5-11) are dominated by uni-directional, Levellois techniques with the predominance of elongated blanks and scrapers. Tools were produced predominantly (99.6%) from locally sourced high quality local flint, and to

a lesser extent (0.4%) obsidian. The EUP tool assemblage (Layer 4d-2) appears abruptly and constitutes a fully-fledged lithic and bone techno-complex that was never encountered in the LMP layers (Adler et al., 2006a). It contained uni-directional blade cores, end scrapers on blades, rounded flake scrapers, burins, numerous retouched bladelets and backed bladelets. In addition to stone tools, bone/antler tools were also found: three bevel-based bone/antler points, two polished bone/antler abraders and a single polished bone implement with a series of parallel incised lines, similar to that found at the cave site of Dzudzuana (See Figure 2.9). This assemblage is reminiscent of the Ahmarian from the Levant (Golovanova et al., 2010a, b; Kozlowski et al., 1998). Tools made from local flint constituted 95% of the total EUP assemblage (Adler et al., 2006a), with ~5% made from obsidian.

Faunal analysis showed a continuation of subsistence preferences from the LMP to the EUP. This suggests both AMH and Neanderthals, although each had different tool packages, were targeting the same species, *Capra caucasica* (Caucasian tur) a locally abundant, seasonal migrating mammal, and to a lesser extent Bison, Red and Roe deer (Adler et al., 2006b; Bar-Oz and Adler, 2005). Consequently, the site was seasonally occupied and was part of a larger settlement system for both hominins (Adler and Bar-Oz, 2009). Evidence for bone marrow extraction, butcher marks, dismemberment and skinning were found on the faunal assemblages with evidence for burning from abundant charred material in layers Layer 4 (EUP) and 5-7 (LMP). Low resolution pollen studies suggest four zones that reflect oscillations between warm and cold stages from the MP to the UP (see Adler and Tushabramishvili 2004).

Chronological investigations of the site have included radiocarbon dating of bone and charcoal (no ultrafiltration or ABOx dates), TL dating of flints and ESR dating of teeth (See Adler et al., 2008 for full details). The age estimate for the first appearance of AMH in the site is 40 to 44 ka cal BP (calibrated radiocarbon, bone date from Layer 4d with IntCal13).

4.3.2. Sakajia Cave (Republic of Georgia), site No. 2

Sakajia Cave is located above the Tskhaltsitela River (222 m.a.s.l) ~10 km northeast of Kutasi (Figure 4.1). The cave was discovered in 1914 by Schmidt and Koslowski, but initial excavations led by G. Nioradze did not commence until 1936 to 1937. These excavations revealed the presence of an EUP layer (Layer 2) but work was then halted due to WWII. In the late 70's & early 80's under the direction of M. Nioradze, LMP layers were found (Layers 3a-f in ~5 meters of sediments; Figure 4.3). In total, 9 layers have been identified, but Layer 4 is archaeological sterile (Nioradze, 1991; Nioradze and Otte, 2000; Pinhasi et al., 2012). Sediments preserved in the cave are described as yellow to brown sands with varying degrees of rocky clasts; with the denses accumulation in Layer 3a, and towards the top of Layer 3d (Pleurdeau et al., 2007).

Lithics were predominantly made using local flint (with the Sakajia literally translating as 'place of flint') but quartzite and obsidian were also used (Pleurdeau et al., 2007). In total ~ 3000 LMP lithics were recovered, with the largest concentration found in Layer 3a and 3b (~75 % of the LMP assemblage) with only isolated artefacts recovered from Layers 3e and 3f (Golovanova and Doronichev, 2003). Neanderthal remains have been recovered from Layer 3a (parts of a skull),

Layer 3b (a lower molar) and a maxillary fragment that contained teeth was recovered from layer 3d (Nioradze, 1991; Pinhasi et al., 2012).

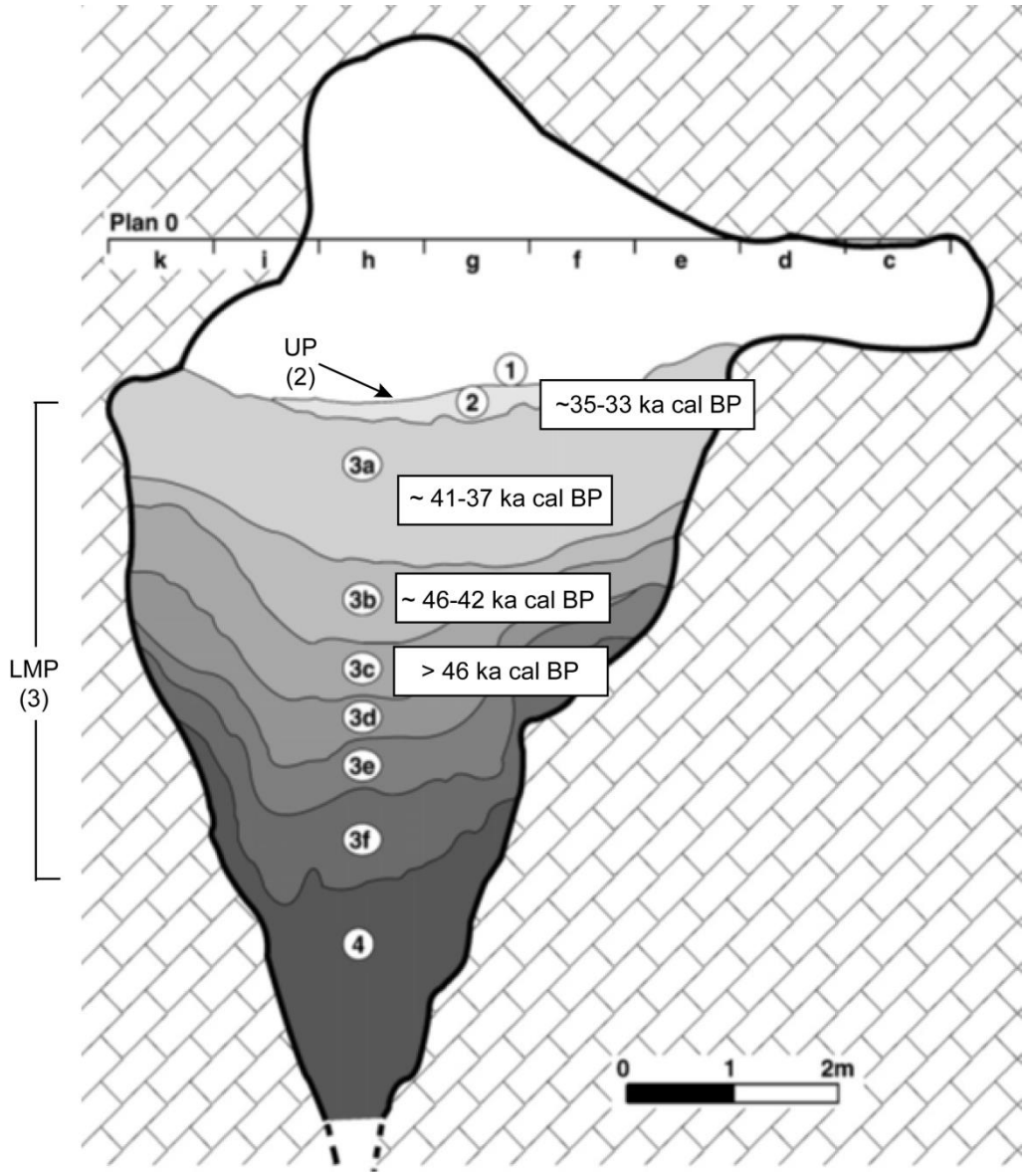

4.3. Stratigraphic profile of Sakajia cave sediments from Pleurdeau et al. (2007). Layer 2 contains UP artefact, while layers 3a-3f are associated with the LMP. Calibrated date ranges for layers 2, 3a, 3b and 3c (radiocarbon determinations on bone, with an ultrafiltration pre-treatment) are from Pinhasi et al. (2012), calibrated with IntCal13.

Tools are characterised as (predominantly) laminar faceted (flake removal from a flatter prepared surface), using Levellois core technology (see Golovanova and Doronichev, 2003). LMP tools were generally formed on blades but retouched

points, side scrapers and denticulate notched tools were also found. Recovered debitage suggest tools were made or re-touched at the site, with some pre-made tools brought to the site (Pleurdeau et al., 2007). Bone points and personal ornaments were recovered from UP Layers (Nioradze and Otto, 2000), with the lithic assemblages (~26,000 recovered) described as 'reminiscent of the European Gravettian type' by Nioradze and Otto (2000).

Fauna at the cave is dominated by cave bear suggesting the cave was also used as a den. The use of the cave by Neanderthals likely occurred seasonally, when it was not used by the bears (Patou-Mathis, 2012; Rivals and Arellano, 2010). Other faunal remains from Layer 3a-3c show Neanderthals hunted deer, large bovine and small cattle.

Radiometric dating of the site has been difficult due to poor preservation of collagen in bones (e.g. Pinhasi et al., 2012) but there are some dates (see Figure 3). Ages suggest Mousterian Layer 3c is likely beyond the limits of radiocarbon (> 46 ka cal BP) with the end of Neanderthal occupation at the site ~41- 37 ka cal BP (boundary between Layer 3a and the onset of UP, Layer 2, Pinhasi et al., 2012). Ages in Figure 4.3 have been recalibrated from Pinhasi et al. (2012), but have not been modelled.

4.3.3. Undo Cave (Republic of Georgia), site No. 3

Undo Cave is situated near the town of Chiatura above the Tabagrebi River Valley (Figure 4.1). There are currently no publications or radiometric dates on the site, and current age estimates are based on typological analysis from lithic stone tools. This site comprises of a deep MP section in the front of the cave (~2 m in depth). Sedimentary deposits derive from colluvial activity with some evidence of paleosol

development between (Figure 4.4). A second, smaller test pit was excavated in the mouth of the cave, which contains UP blades and has three stratigraphic layers (Layer II-IV) below the current trample surface (I).

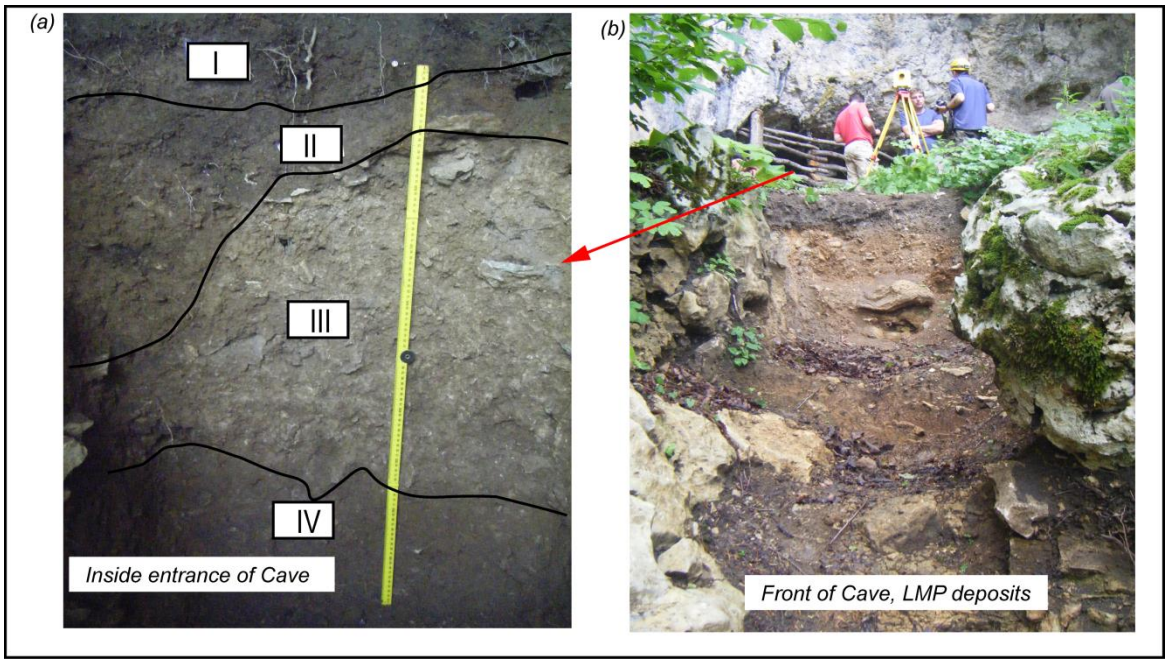

Figure 4.4. Photograph of the test trench sunk into the interior of Undo Cave (a) situated behind wood fence seen in b (base of the red arrow). An UP blade was recovered from Layer III. (b) photograph of the banded sediment section that was excavated front of the cave mouth, which contains MP lithic material. Yellow ruler (a) is 1 meter.

4.3.4. Ortvale Cave (Republic of Georgia), site No. 4

Ortvale Cave was discovered by Korlowaki in 1914 and is ~ 1 km north-east of Sakajia cave. The cave has one entrance that, at ~11 m, splits into two galleries. The right gallery is ~40 m long and the left gallery is 20 m long. Excavations took place in 1974 -1975 and again at 1980-1989 and both were led by M. Nioradze. Evidence for LMP occupations (Layer 3, 3a- 3d) were discovered overlain by an UP Layer (Layer 2) (Nioradze, 1992 [cited in Pinhasi et al., 2012 and Pleurdeau et al., 2007]; Nioradze, 1991; Figure 4.5). Layer 1 was identified as Chalcolithic and

Bronze Age while Layer 4, developed into bedrock, was archaeologically sterile. Sediments are described as dark brown to grey and composed of a granular, sandy matrix. Éboulis was concentrated at the base of Layer 3c and in 3d, but Layer 2 was largely devoid of a rocky content.

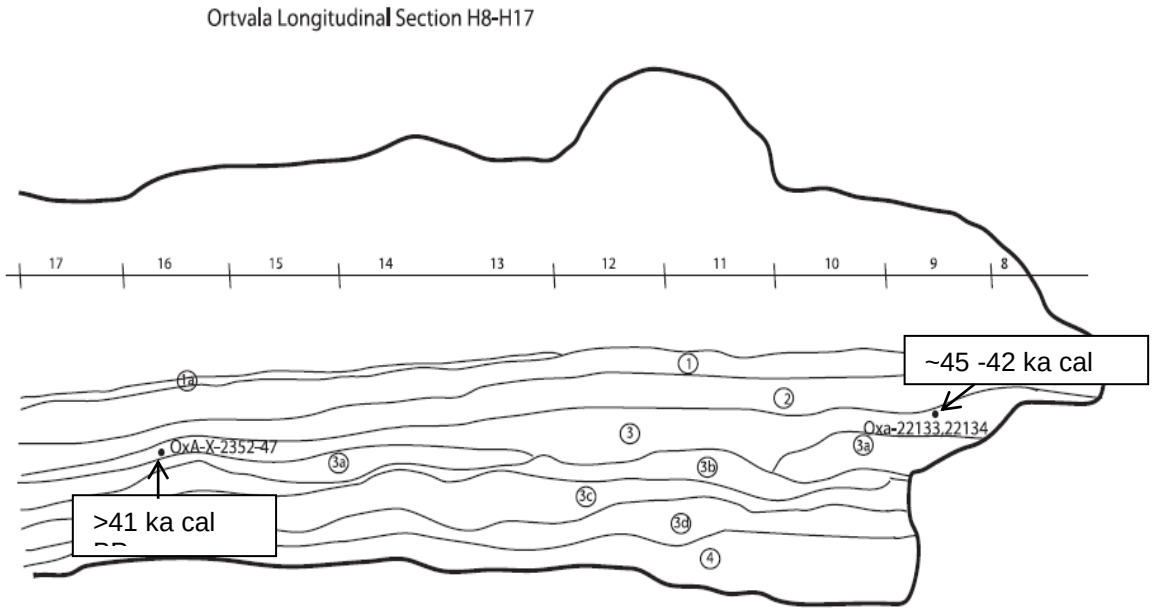

Figure 4.5. Stratigraphic units at Ortvale Cave (right gallery). Layers 1-4 are shown with the location of two bone samples that were radiocarbon dated (with a ultrafiltration pre-treatment). The re-calibrated ages from Pinhasi et al. (2012) for these samples are in the white boxes.

Two Neanderthal teeth were recovered from the top of Layer 3a (Nioradze, 1991). The teeth have not been directly dated but Layer 3 that is stratigraphically above Layer 3a has two radiocarbon dates on bone of ~ 45 to 42 ka cal BP and > 41 ka cal BP (Pinhasi et al., 2012). There are no dates for the UP occupation of the site (Layer 2).

A total of ~ 450 lithics were recovered from the site. These were produced with local flint. The assemblage was dominated by debitage, with the highest accumulations in Layer 3c and 3d. Retouched points, side-scrapers and denticulate tools were found in the LMP layers and Levellois flake technologies

were prevalent (Pleurdeau et al., 2007). Faunal assemblages were less diverse than those seen in the neighbouring Sakajia cave, but occupation of the cave is likely split between cave bear (and possibly other carnivores) with the seasonal occupation of Neanderthals (Rivals and Arellano, 2010). The UP Level 2 had a greater presence of blades with no evidence for Levellois production techniques (Pleurdeau et al., 2007).

4.3.5. Lusakert 1 rock shelter (Armenia), site No. 8

Lusakert 1 and Lusakert 2 (~ 25 m away from Lusakert 1) are both rock shelters in the base of a ~200 ka basalt flow (Wilkinson pers comms, 2013) that is located in the Hrazdan Gorge, north of the city of Yerevan (Figure 4.1). Archaeological remains have been discovered in both sites, but detailed excavations have been carried out at Lusakert 1.

In 2008-2009 fieldwork led by Adler, Pinhasi and Yeritsyan re-exposed old sections located outside Lusakert 1 rock shelter to clarify previous work by Yeritsyan, and to assess the future potential. Previous excavations found several thousand LMP lithics that were recovered at the base of Units C and D (archaeological deposits differ typologically between the units), but poor site recording, the lack of rigorous post-excavation storage and evidence for reworking of the assemblage has hindered analysis (Birtwistle and Yeritsyan, 2012). Four lithostratigraphic units (A at the top, to D at the base) were re-identified outside the rock shelter. New geological interpretations of Units A-B indicate that they are mixed, therefore unsuitable for dating (Adler et al., 2012). The new excavations revealed poor faunal preservation outside the rock shelter. Initial OSL estimates from C (alluvial deposits, composed of fine sands and sub-angular basalt pieces)

suggest an age of ~36 ka, older than a previous AMS age of ~31 ka cal BP (Fourloubey et al., 2003). However, radiocarbon dates should be considered minimum ages as the bones did not undergo ultrafiltration. Furthermore, the OSL age was acquired using with single aliquot method rather than the single grain method, which is not precise. Analysis of the newly excavated lithic assemblages is ongoing, but are LMP.

Given the issues outside the cave a new sondage was dug in the interior. A well stratified, archeologically-rich section was located. Six archaeological layers that have subdivisions within (Figure 4.6) were identified, with a collective depth of ~ 140 cm. Unit 1 (2cm thick) is a fine, light brown yellow, poorly sorted silt/clay that contains charcoal and obsidian pebbles. This layer is likely to be formed of mixed deposits and is disturbed due to modern surface activity. Units 2-7 are largely formed from debris from the basalt cave walls with an allochthonous component (material derived from outside the cave). There is also evidence of possible soil development in Units 2 (that also shows animal burrows) and in Unit 3. There is little evidence for modern bioturbation in the site (Adler et al., 2012). Unit 10 is archaeological sterile, and is solely composed of endogenous cave earth.

Lithic assemblages (n=4127 from 2008-2009 excavations) are composed solely of obsidian and showed the predominance of Levellois and Kombewa flake and blade technology, with both facetted and plain platforms (Adler et al., 2012; Gasparyan et al., 2014b). Moderate occurrences of formal tools (including denticulates, side scrapers, burins, end scrapers) with few cores and a low frequency of cortex were present, but the high percent of micro-debitage suggest manufacture and modification of stone tools took place in the rock-shelter (Adler et al., 2012). Abundant faunal remains, including microfauna have been recovered

that show evidence for intensive processing by hominins (e.g. cut mark, impact fractures and green breaks), but collagen preservation was low.

Excavations have not found any discernible EUP assemblages inside or outside the rock shelter (Adler et al., 2012; Adler pers comm., 2013; Birtwistle and Yeritsyan, 2012). No hominin skeletal remains have been uncovered and as the techno-complex is unique in comparison to other MP techno-complexes in the Caucasus, and to those found outside the rock shelter, creators of the rock shelter MP assemblage is unclear (Adler pers coms, 2013).

Current age estimates for the internal sondage are limited. OSL dating proved to be inconclusive (e.g. Lukich, 2012), and only two radiocarbon samples taken from Unit 4.1 (charcoal) and Unit 5 (bone) produced ages, ~ 35 to 33 ka cal BP and > 45 ka cal BP age, respectively (Figure 6). One visible tephra layer was found in the site, Layer 6.5 (Figure 4.6). Further dating and analysis of the archaeological finds is pending (Adler et al., 2012; Gasparyan et al., 2014b), but currently the Lusakert 1 rock shelter comprises the most archaeologically rich, in-situ, stratified LMP cave site in Armenia.

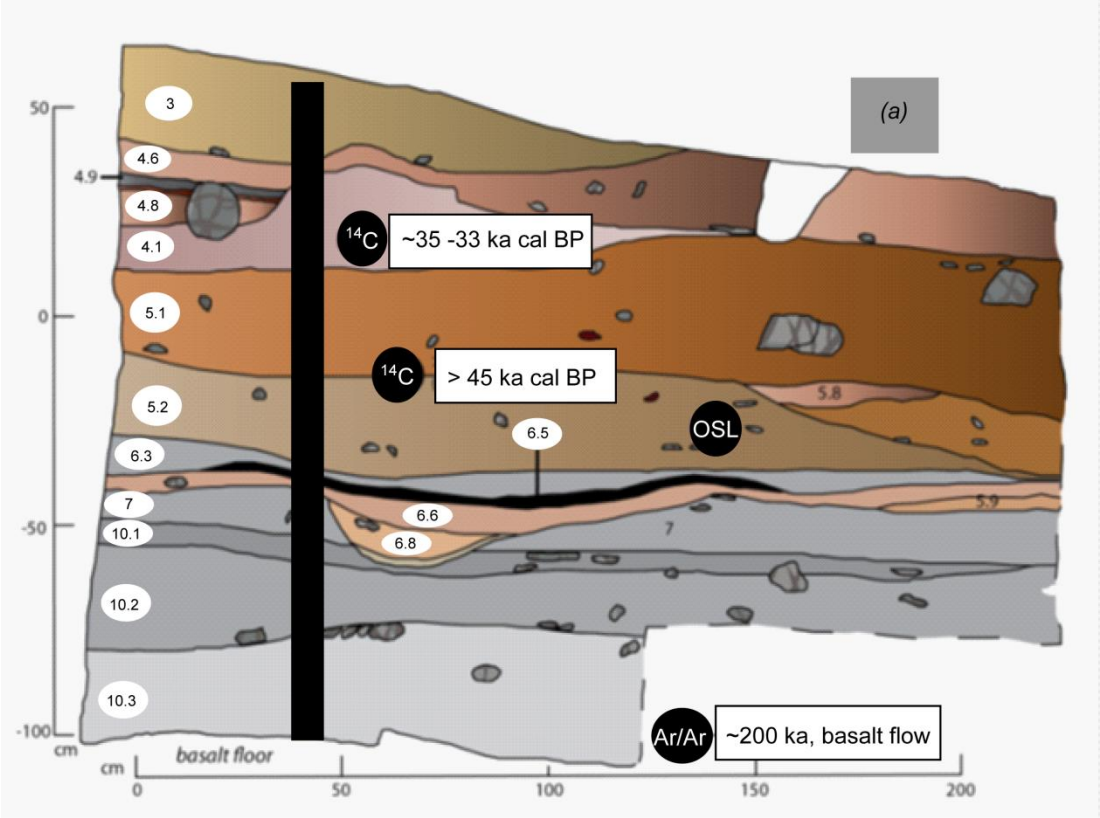

Figure 4.6. Stratigraphic profile of the Lusakert 1 rock shelter sediments (a). The lithological and archaeological layers are shown in white circles. Black boxing is position of tephra sampling column. Position where previous radiometric dating samples were collected (black circles) with calibrated dates given in white boxes. The cave is formed in a basalt flow.

4.3.6. The Azokh caves (Azerbaijan / Armenia, disputed territories), site No. 9

The Azokh cave system, close to the village of Azhok, is located in the mountainous terrain of the Nagorno-Karabakh region (Figure 4.1). The cave system has three entrances: Azokh 1, 2 and 5. Initial excavations of Azokh 1 were conducted by Huseinov in 1960s with continued excavations run by joint Russian and Azerbaijan teams until 1988. Ten stratigraphic horizons were found with a large number of faunal, lithic and hearth remains, ranging from Acheulean to MP and to a lesser extent UP. Later these archaeological horizons were increased to 17 and then 25. Due to the complexity of the site and lack of excavation since the

1980s, an international team was invited to re-excavate the site in 2002. Their results and initial conclusions will be discussed below.

The remaining, unexcavated sediments had 11 lithological units preserved across two sections. Units IX – VI are observed in section 1; and Units V-I in section 2 (Murray et al., 2010; Figure 4.7). A mandible believed to be from *Homo Heidelbergensis* dated to ~300 ka, was discovered in Unit V (Murray et al., 2010). Consequently, Azokh is believed to contain a nearly continuous stratigraphic deposits from >300 ka to the Holocene (Fernández-Jalvo et al., 2010). Units II and I represent the LMP and possibly UP. Radiometric dating from Units II and I proved difficult, believed to be due to the abundance of bat guano chemically degrading bone collagen in faunal remains (Fernández-Jalvo et al., 2010). Consequently, the chronology of Azokh cave 1 Units I–II is poor and based on tool typologies.

The limestone bedrock provides good quality flints and consequently many tools are made from this. Obsidian tools were also located in Units II, but obsidian outcrops are not found in the local area indicating movement of Neanderthal species (Murray et al., 2010). Units II and III contain MP Mousterian-type lithics, with a transfer to the Levellois technique observed in Unit II. Unit I sits unconformably above Unit II suggesting modification or an erosional horizon, representing a hiatus of unknown length. Additionally, Unit I has evidence for bioturbation and possible mixing. Unit I is believed to be UP to Holocene (at the top) in age, with the finding of a classic UP end scraper in the contact between Unit I and II (Fernández-Jalvo et al., 2010). There are numerous faunal remains, including bones bearing butchery marks and intermittent hearth layers and

abundant charcoal (Units V-I), suggesting continued human occupation at the site (Murray et al., 2010).

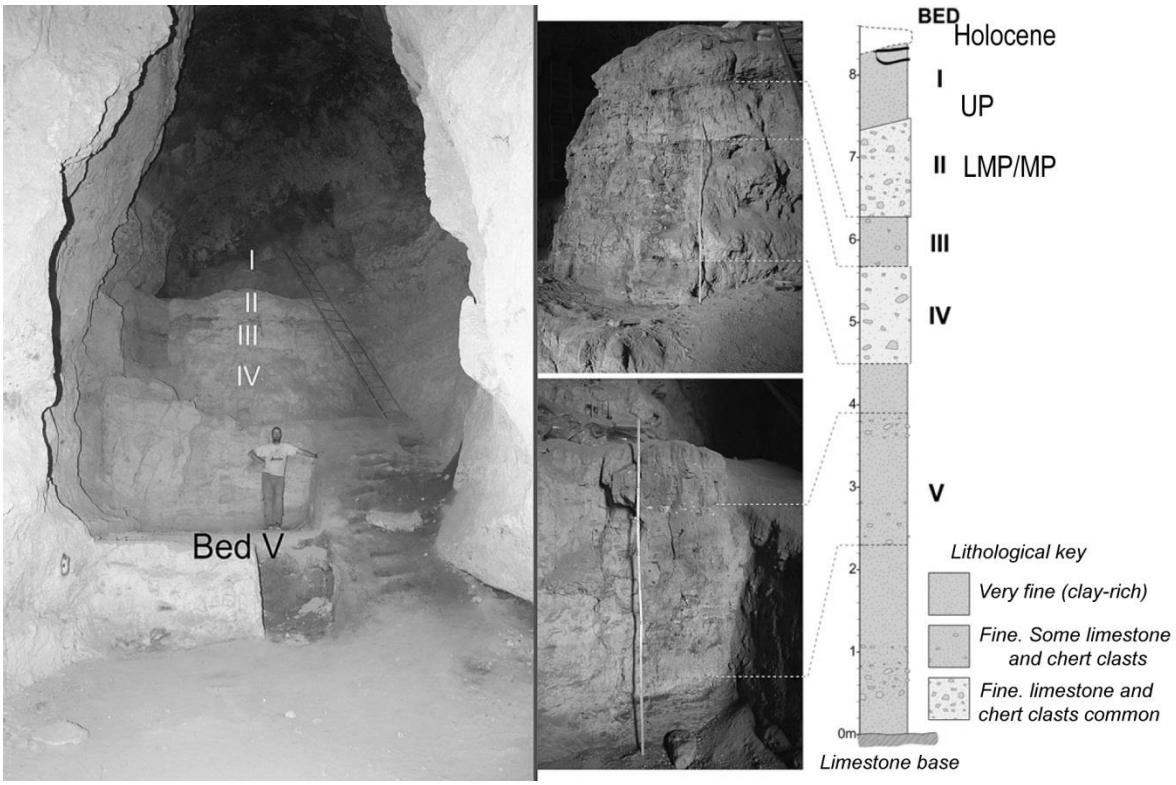

Figure 4.7. Left is a photograph of Azokh 1 cave, upper sequence (Units I-V). The composite stratigraphic profile is shown right of photographs with lithological units in Roman numerals. See key for sediment descriptions. The archaeological entities are shown to the right of the Roman numerals. After Fernández-Jalvo et al. (2010).

4.3.7. Aghitu 3 (Armenia), site No. 10

The site of Aghitu 3 was discovered during the 2008 field survey of the Vortan valley, in the Syunik region of southern Armenia (Figure 4.1). Located ~5 km from the village of Aghitu, at an elevation of 1601 m.a.s.l, the site is one of seven caves that have formed in the base of a ~30 m high lava flow (Kandel et al., 2011; 2014). Excavations started in 2009 by a joint German and Armenian team (The Tübingen–Armenian Paleolithic Project; TAPP) and are ongoing.

Initially, six geological and six archaeological horizons were identified. Since then, further work on the same section has revealed a more complex sedimentological stratigraphy, with 10 geological horizons (GH) that encompass six archaeological horizons (AH; Kandel et al, 2011, 2014; Figure 4.8). This site contains two horizons that are suspected to be volcanic in origin: a grey unit (GH 8a) and a black unit (GH 8d). Radiocarbon ages of ~31 - 30 ka cal BP have been assigned to these layers (Figure 4.8). This is the first site found in Armenia to contain a stratified and well dated UP sequence (AH III-VI). Charcoal found at the base of GH-10 (AH VI) has been radiocarbon dated to ~35 to 34 ka cal BP with a charcoal age of ~28-27 ka cal BP for AH IIIa towards the top of the sequence (Kandel et al., 2014; Figure 4.8).

The recovered lithic assemblage is made from obsidian (nearest source 40 km away) and chert and comprises ~1970 chipped stone artefacts. The majority of chipped artefacts found are laminar flakes and blades, and it is likely these were prepared and then brought to the site (Kandel et al., 2014). Bone tools consist of a one-eyed bone needle, one bone point and one bone awl that were found in AH III with six perforated shells (Gasparyan et al., 2014a).

Preliminary analysis of faunal remains suggests the predominance of wild sheep/goat, with evidence for both humans and carnivore activity (Kandel et al., 2011; 2014). The small amount of fauna and the low concentrations of pre-made tools suggest the site was sporadically occupied by humans, possibly seasonally. AH III was the most intensively occupied layer, with environmental reconstruction suggesting a cold and dry climate (based on pollen, microfauna and sedimentological analysis). Layers AH IV – V below, dated between 31-28 ka cal BP, also contained evidence for a cold dry climate, but had fewer finds. The oldest

Layer, AH VI (GH 10; 35-31 ka cal BP) at the base of the sequence has evidence for spatially isolated occupations and conditions were warmer (Gasparyan et al., 2014a). Analysis is still on-going at the site (Kandel et al., 2014).

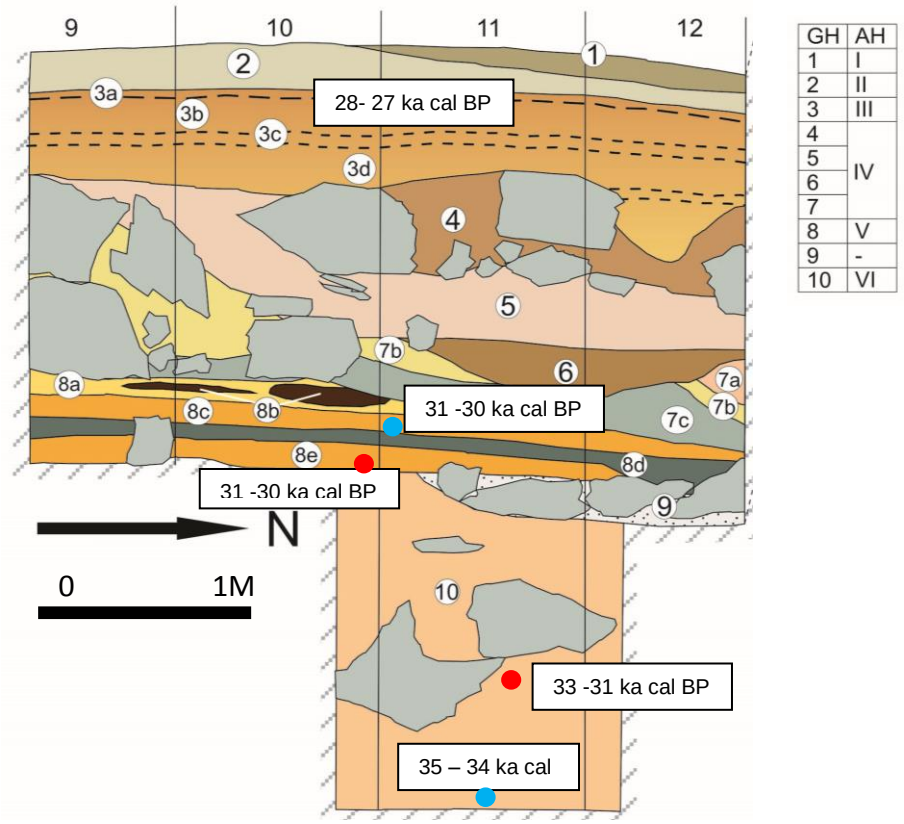

Figure 4.8. Drawing of west profile in Aghitu 3 Cave. The 10 geological horizons (GH) shown on the drawing (white circled numbers) correspond to archaeological horizons (AH) I–IV (table top right). Red dots are radiocarbon dates on bone, while blue dots indicate the position of charcoal taken for ^{14}C dating. Calibrated ages are shown in boxes next to each dot. GH 8d and 8a are the suspected volcanic ash layers. Grey objects represent basalt rocks (endogenous) in the section. After Kandel pers comms (2014).

4.3.8. Fantan and Kagasi (Armenia), sites No. 11 and 12

The open air sites of Fantan and Kagasi were discovered during the 2008/2009 survey of the Hrazdan gorge by Adler, Wilkinson and colleagues. No formal

excavation of the sites has taken place. Fantan consists of an outcropping of a rhyolitic obsidian dome (~8 m in height), south of Gutansar volcano. A road cutting around the dome revealed a sequence of two large tephra deposits (FU_AM and FL_AM) with one paleosol between them (Figure 4.9a). Small scale test pits in to the paleosols have revealed the presence of MP artefacts produced with a Levellois technology. The age of these artefacts is unknown, but based on initial typological assessment they could be Early and possibly Mid-MP (Adler pers comms, 2013).

The sediment profile of Kagasi is exposed adjacent to a large refuse tip and can be accessed by foot. There are three visible tephra layers that have sediments separating them (including paleosols; Figure 4.9b). The upper ash (KGU_AM) is light in colour and sits on top of a unconformity. It is 1 m thick but pinches out across in the section. The middle ash (KGM_AM) is found ~0.8 m beneath the upper ash unit, it is 10-15 cm thick, moderately sorted and distinctly sandy, course and looks basaltic. Some crystals are observed within the volcanic ash. The lower ash (that is separated by a dark paleosol that grades into a lighter brown material; KGL_AM) is also basaltic looking, with signs of weathering. It is dark in colour and well sorted. Ages of the tephra units are unknown, but a lithic recovered from the paleosol between the KGL_AM and KGM_AM ash layers suggest they are Early to Mid-MP (Adler pers comms, 2013).

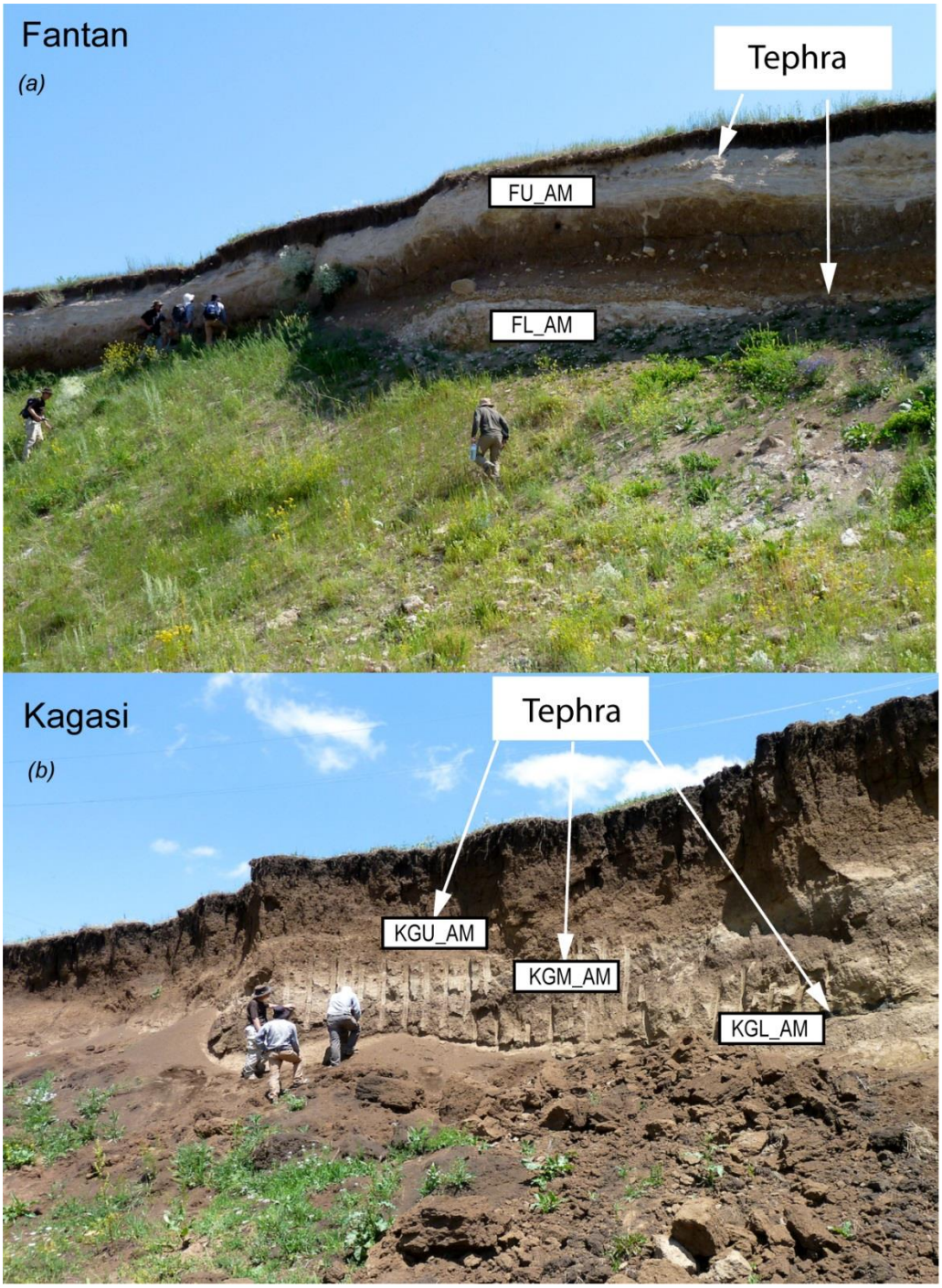

Figure 4.9. (a) The tephra layers at Fantan. (b) The three tephra layers at Kagasi.

4.3.9. Gubs rock shelter 1 (northern Caucasus), site No. 13

Gubs rock shelter 1 is one of 11 south facing caves that form a complex located in the limestone terraces of the Gubs George, ~ 40-45 km east of Maikop (Figure

4.1). The sites were originally located by Autlev in 1961 and excavations were conducted by Liubin and Muratov in 1964 and again in 1986 by Amirkhanov.

Muratov excavations identified eight lithological horizons in a ~2 m deep section (Figure 4.10). Layer 2 is a fine, yellowish sand with a small component of gravel (~1-3 cm) and contains 2 intercalated deposits (Layers 3 and Layer 4) in its matrix (Burbidge et al., 2005). Layer 3 is a dark, buried humifed horizon, while Layer 4 is reddish sandy loam that contains gravel and angular pices of limestone up to 15 cm in diameter (see review, Burbidge et al., 2005). Layers 5 to 7 are composed of fine yellowish brown sands, and contain densly packed, limestone rubble. Layer 5 also has a sandy loam component (up to 40% of the matrix; Burbidge et al., 2005). Layer 8 is archaeologically sterile and sits on top of the limestone base. Layers 2-4 contain UP artefacts, and Layers 5-7 contain MP material (Figure 4.10). This is the only site in the northern Caucasus with a UP and MP sequence.

UP excavated material amounted to ~ 4500 pieces that include cores (55) and ~160 tools. Excavations by Amirkhanov also identified two UP ‘cultural’ layers including the presence of hearths and bone points that were found in cultural layer 1 (the latter, likely to be LUP; Amirkhanov, 1986 [cited in Burdidge et al., 2005]). Further analysis on the UP artefacts is unpublished and the site has no chronometric ages. The MP lithic assemblages are believed to represent the latest stages of the Micoquian industry in the northern Caucasus (LMP; Golovanova and Doronichev, 2003). A single sub-triangular handaxe was the only bifacial tool (typical of Micoquian industry) found and other tools consist of simple side scrapers and end scrapers; ventral and dorsal thinning of tools is common (Golovanova and Doronichev, 2003). Levellois flakes and blades are also present.

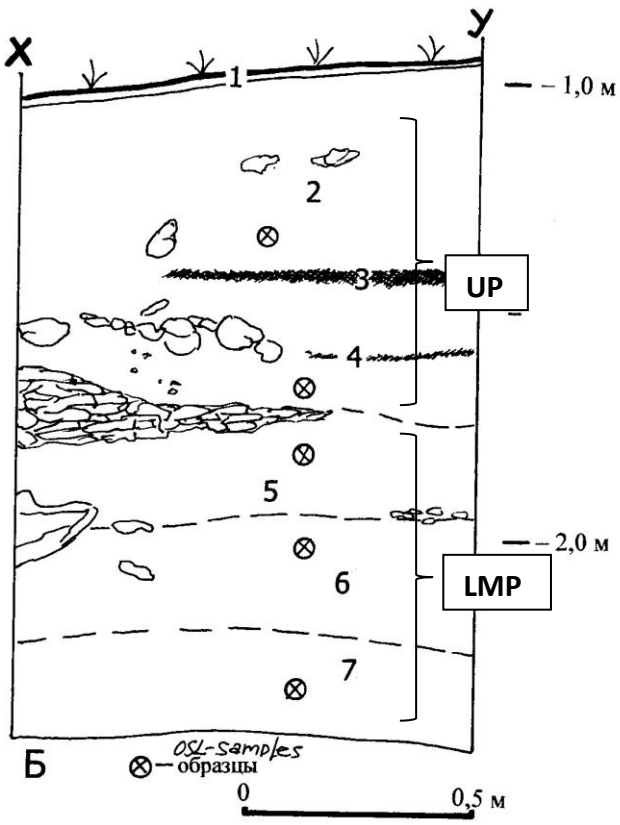

Figure 4.10. Section drawing of Gubs rock shelter 1 by Burbridge et al. (2005) with OSL sampling positions (circles with x). Dates from these samples have not been published. Layer 2-4 contained UP artefacts, Layers 5 to 7 contain a LMP Micoquian industry.

Faunal remains from the site were limited but bison, horse, vole, squirrel and sheep/goat are present in the UP assemblages, and passerine bird and a hamster-like rodent in the MP assemblages (Burbridge et al., 2005).

4.3.10. Myshtulagty Lagat, Weasel cave (northern Caucasus), site No. 21

The site of Myshtulagty Lagat (Weasel cave) was discovered by Hidjrati in 1987. The site is situated in the central, northern Caucasus (northern Ossetia) close to the Terek Gorge (Figure 4.1). The cave complex consists of two chambers known as the Dormouse Hall and another large chamber that has collapsed (Hidjrati et al., 2003). Both chambers are west-facing and have developed in Jurassic dolomite. The site contains three deep sections and 36 archaeological layers have been identified: the Lower Palaeolithic (LP), Layers 22-36; MP, Layers 21 - 5; and

Layers 1-3 span the later part of the Holocene and include Medieval archaeology. Layer 4 is archaeologically sterile and believed to correspond to the late glacial period (Hidjrati et al., 2003). The MP layers have been further sub-divided into two different groups: the upper ensemble, Layers 5-11, and Layers 12-21 that constitute middle ensemble (Figure 4. 11).

The upper ensemble constitutes typical denticulate Mousterian assemblages produced from quartzite but is devoid of a blade component. No evidence of the Levellois technique is present. Dates for the end of this period (LMP, Layer 5) range from ~41 to 34 ka cal BP; possibly suggesting the late survival of Neanderthals within the region (Hidjrati et al., 2003). However, the dates were prepared and dated using old radiocarbon techniques with no pre-treatment, and should be considered a minimum age. The middle ensemble (Layers 12 to 21), contain more artifactual evidence for Neanderthal occupation (Hidjrati et al., 2003). Both denticulate Mousterian with Levellois techniques are observed, including blade tools and points. Layers 12-14 have been dated based on faunal and pollen profiles to ~128 - 70 ka, and assigned to Isotope stage 5e (MMP; Hidjrati et al., 2003). Ten volcanic ash layers have been documented in the lower Palaeolithic layers, and were dated using $^{40}Ar/^{39}Ar$ to >200 ka (Layer 18) and >500 ka for Layer 24 (Hidjrati et al., 2003; see Figure 4.11). Microware analysis of stone tools from Layer 5-14 (taken from both chambers) and faunal studies suggest wood-working (including hafting of tools), butchering and the scraping of hides were the main activities at the site (Faulks et al., 2011; Hidjrati et al., 2003).

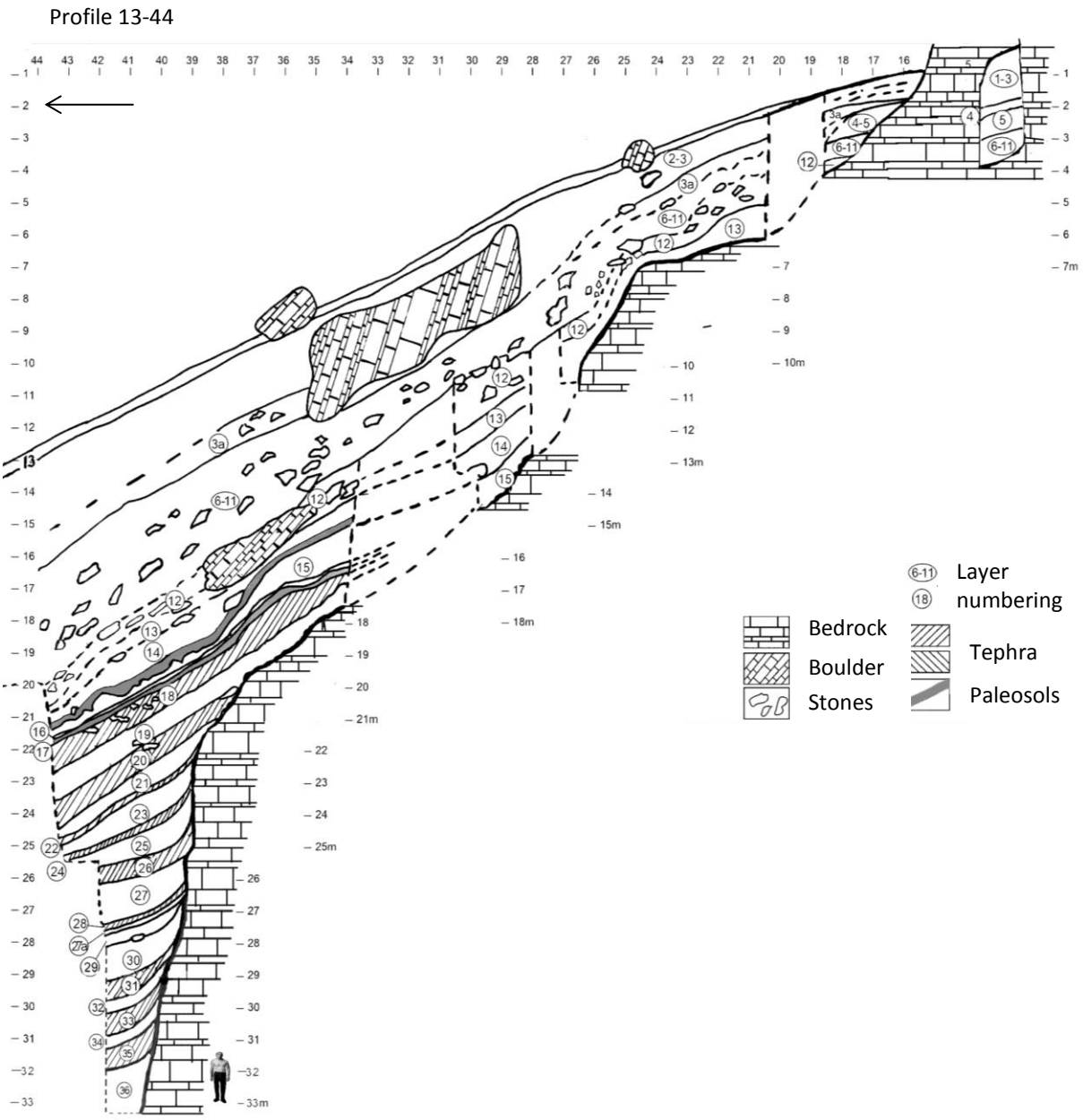

Figure 4.11. The Myshtulagty Lagat sediment stratigraphy, after Hidjrati et al. (2003).

4.4. The M72/5-25-GC1 Black Sea core

The Black Sea is situated between Europe and Asia and the sediments preserve a detailed temporal record of the palaeoenvironmental change in the region. The Black Sea has oscillated between being predominantly fresh water and marine,

believed to be coincident with the glacial–interglacial cycles (Schrader, 1979). The M72/5-25-GC1 core is one of six gravity cores taken from southeast Black Sea during the 2007 German RV Meteor-cruise (Figure 4.12). It is 12 cm in diameter and 952 cm in length. The core was extracted from a water depth of 418 m on the Archangelsky ridge at 42°06.21'N 36°37.43'E. The Late Glacial and Holocene sections of the cores extracted during the M72/5 expedition all record the same basin-wide sequence (Nowaczyk et al., 2012). Late glacial deposits are lacustrine clayey muds (Unit III), and the Holocene sediments are comprised of marine sapropels (Unit II) and coccolith oozes (Unit I). Pre-Unit III sediments are predominantly fine-grained and comprised of siliciclastic material with variable amounts of calcium carbonate content (~15-40%, Nowaczyk et al., 2012). Iron sulphides with a 'deep black sediment colour' (greigite, Fe_3S_4) were observed during core sectioning (Nowaczyk et al., 2013). These have oxidised and are now either very faint or not visible. There are two suspected sedimentary hiatuses in the M72/5-25-GC1 core, one at 180 cm (~2 ka) and a second at 50 cm of unknown time (Arz pers comms, 2014).

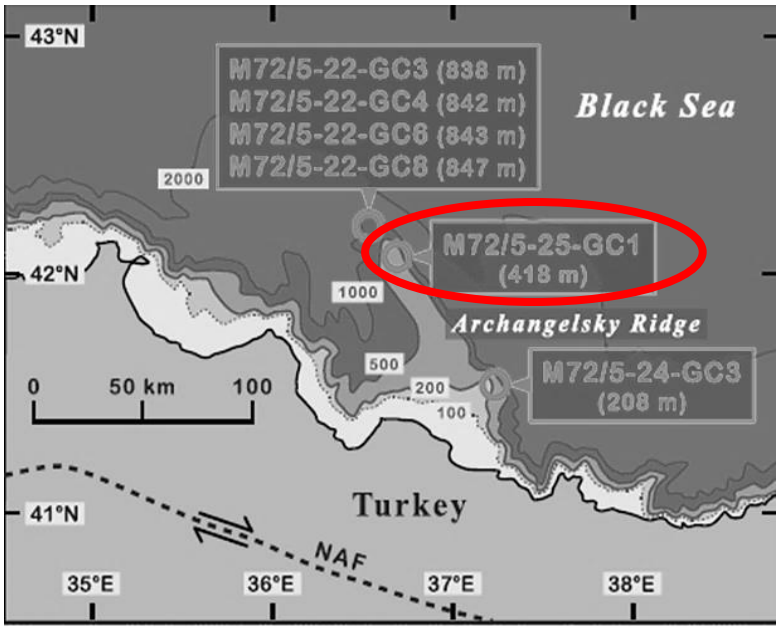

Figure 4.12. A bathymetric map of the southeast Black Sea (contours in meters). Core sampling locations shown with water depths (in brackets). NAF refers to the North Anatolian Fault. The M72/5-25-GC1 is circled in red Nowaczyk et al. (2012).

Palaeoenvironmental reconstruction for the past ~60 ka was established using ice rafted debris (IRD), carbonate data and pollen data (Nowaczyk et al., 2012; 2013; Shumilovskikh et al., 2014). Calcium X-Ray fluorescence counts (Ca-XRF), magnetic susceptibility and relative palaeointensity profiles were also produced for the core (Figure 4.13). These data were used to anchor the 6 cores together, with the latter data used to identify palaeomagnetic excursions that were recorded in the sediments.

Increases in average grain size were interpreted as IRD*. This is thought to be a result of the seasonal melting of coastal, and fluvial winter ice that forms in cold periods. $CaCO_3$ can be used as a measure of water productivity linked to CO_2 assimilation and pH-increase by phytoplankton bloom activity (Bahr et al., 2005; Leng and Marshall, 2004). In warm periods, there is an increase in photosynthetic activity that leads to carbonate supersaturation and precipitation in the water column. Consequently, higher values of inorganically-precipitated carbonates ($CaCO_3$) are thought to reflect warmer periods when productivity would have increased, and lower values represent cooler periods when activity is reduced (e.g. Bahr et al., 2005; Nowaczyk et al., 2012). Nowaczyk et al. (2012) note an increase in IRD counts that are concentrated in intervals when inorganically-precipitated carbonates are reduced or absent (cooler periods) in the M72/5-25-GC1 core sediments (Nowaczyk et al., 2012; 2013).

** Nowaczyk et al. (2012) interpret the increases in grain size in the core resulting from the melting of coastal winter ice, and not from icebergs. These deposits are not IRD sensu stricto as they are not from large icebergs from long-lived ice sheets (see section 3.3.2).*

These changes are thought to represent a pattern of warmer and cooler climates, (Figure 4.13) that are believed to correlate to D-O events that are recorded in the Greenland ice cores (~MIS 3). Visible tephra have been identified between what is thought be GI 8 and GI 9 (Nowaczyk et al., 2012; 2013).

Creating a reliable age model for palaeoclimatic events recorded in Black Sea sediments has been problematic as there is a lack of material that can be dated using conventional techniques (e.g. radiocarbon; Kwiecien et al., 2008). Furthermore, there are unknown reservoir offsets that affect radiocarbon dates (e.g. Bahr et al., 2005; Kwiecien et al., 2008) and the younger deposits do not have continuous 'annual' laminations to create a varve chronology (Kwiecien et al., 2008).

The current chronology for the M72/5-25-GC1 core is based on the position and ages of the 39.28 ± 0.11 ka CI eruption (De Vivo et al., 2001), and the reservoir corrected radiocarbon ages from the parallel M72/5-25-GC3 core (correlated to M72/5-25-GC1 using magnetic susceptibility profiles). The palaeoenvironmental data (IRD and carbonate content; Nowaczyk et al., 2012) from the core was then used to compare and tune the record to the Greenland ice cores so that the GICC05 $\delta^{18}O$ time scale could be used (see also Figure 4.14). However, it should be noted that although Nowaczyk et al. (2012) used an independent age marker (the CI tephra) they still assume synchronicity to global, climatic oscillations and tune the final model. Furthermore, the reservoir correction applied to the 16 interpolated, AMS ^{14}C ages of juvenile bivalve shells (*Dreissenia rostiformis* species) is based on correction factors derived for samples in the southwest Black Sea by Kwiecien et al. (2008). These radiocarbon samples were calibrated using

IntCal09 that is now known to slightly diverge from the new IntCal13 between the periods of ~45-27 cal ka BP (see Reimer et al., 2013), and therefore need to be recalibrated.

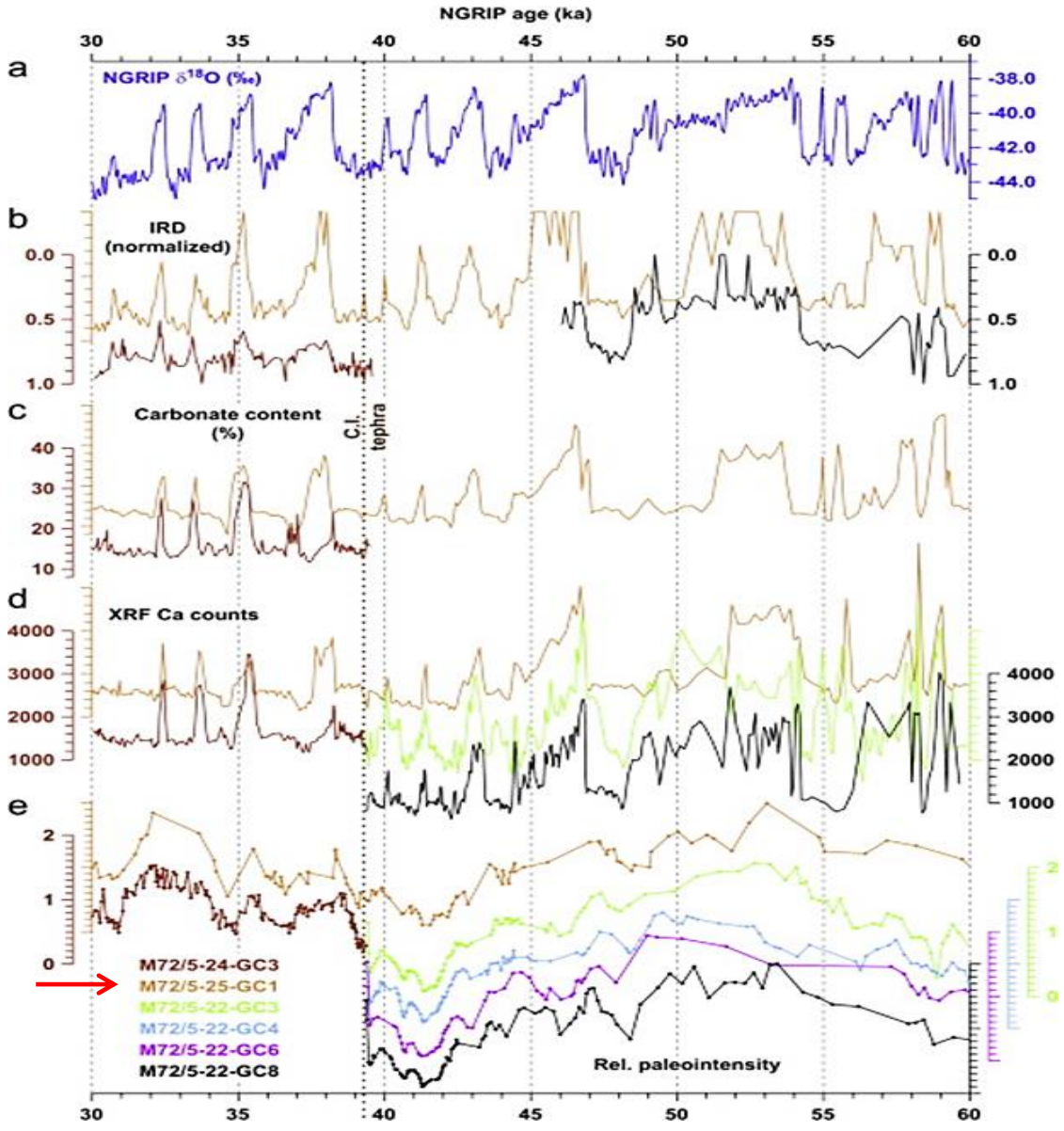

Figure 4.13. IRD, carbonate content and Ca-XRF palaeoclimate data for the M72/5 cores (b-d) that are tuned to the NGRIP $\delta^{18}O$ record (a) for the period between 60 -30 ka. Palaeointensity profiles for the cores are shown in e. Dashed black line is the visible tephra that was located in the M72/5-25-GC1 and M72/525-GC3 cores; this tephra has not been found in the Greenland ice cores. Image after Nowaczyk et al. (2012).

Kwiecien and colleagues combined AMS radiocarbon dating of marine shells with tephrochronology to attempt to study effects of differential water inputs to the Black Sea as a means to study reservoir age changes through the Late Glacial to the Holocene. Results showed a complex and variable reservoir age over the Late Glacial, with reservoir ages intrinsically linked to the hydrology of the Black Sea. Tephrochronology was central in assisting the estimation of marine water reservoir offsets by providing an independent marker layer for radiocarbon dated sediments either side of the ~22 ka Y2 tephra (from Santorini) that was found in the core. Estimates showed a ~1450 ^{14}C yrs reservoir offset for these glacial sediments. A reduced correction factor of ~1000 ^{14}C yrs was calculated for the younger part of the composite core. This latter reservoir estimate was based on the assumption that fluctuations in the proxy data (thought to be coincident with the Bølling / Allerød warm periods) were synchronous to the GISP2 Greenland ice core. The calculated difference in age between the Black sea ^{14}C ages to the 'onset' date for these climate events (derived from the ice cores) was used as the reservoir offset. This reservoir correction was thought to reduce towards the Younger Dryas period (~ 0 to 900 yrs). The correction factor for interglacial sediments is therefore reliant on the assumption that fluctuations in the proxy data are synchronous to changes observed in the Greenland ice core data. This also assumes that the hydrological regime in the west and east Black Sea would be the same, despite having different sedimentary inputs. Consequently, there are potential issues with the current M72/5-24-GC1 chronology, with further independent testing needed.

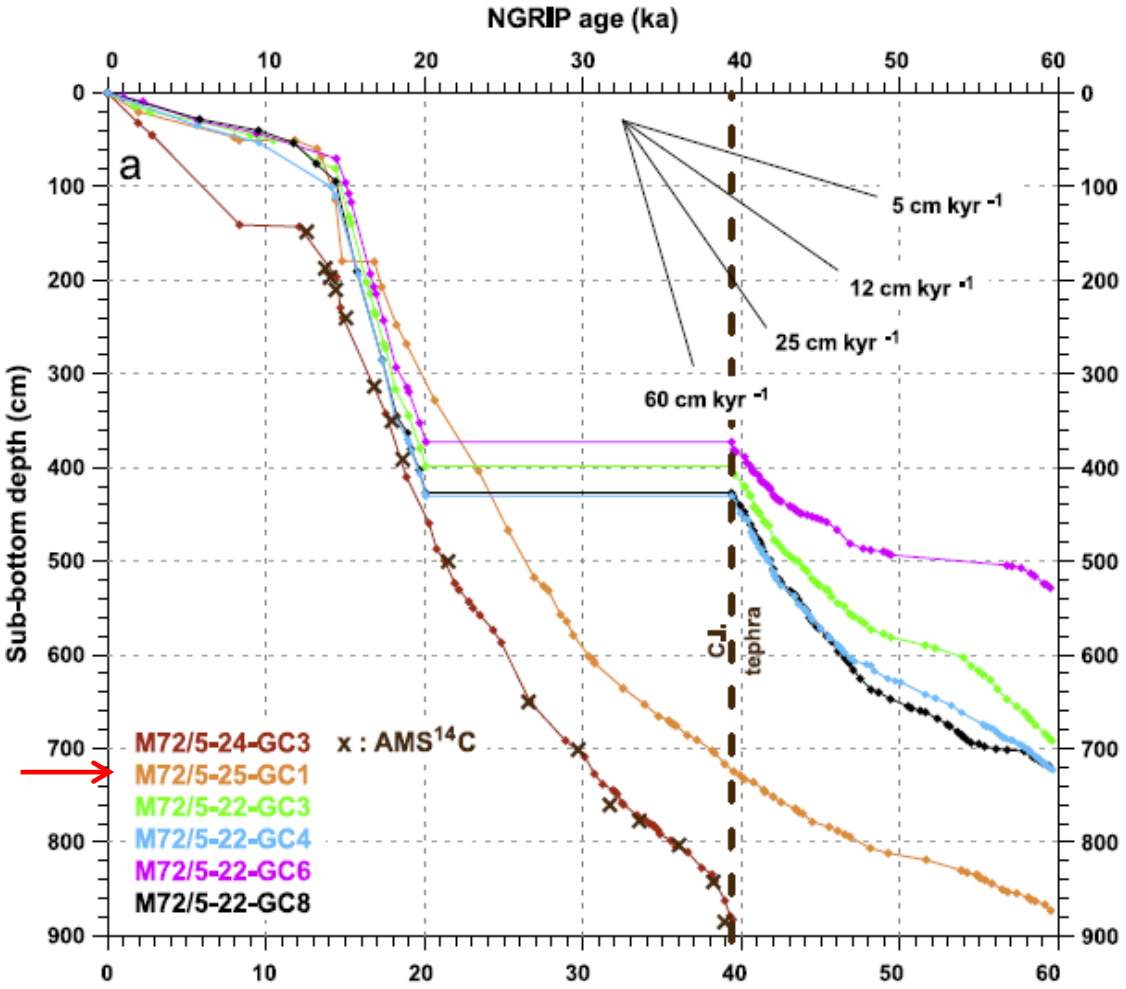

Figure 4.14. Age models for the M72/5 cores. Dark brown crosses indicate locations of ^{14}C dates obtained from core M72/5-24-GC3. The cores were correlated using magnetic susceptibility measurements. The position of the CI tephra (dotted black line) is shown. Calculated sedimentation rates are shown in the top right. Records have been 'tuned' to the the $\delta^{18}O$ record from NGRIP. After Nowaczyk et al. (2012).

4.5. Summary to chapter

Twenty-one archaeological sites located on a north to south transect across the Caucasus and one long palaeoenvironmental sequence from the southeast Black Sea (~ 60 ka) were selected for tephra analysis. The M72/5-25-GC1 palaeoenvironmental core has been selected for tephra analysis as this is close to the region and could potentially link the archaeological archives across the region to a dated sequence with palaeoenvironmental data. It is clear that the amount of

chronological and archaeological information for the cave and open air sites varies considerably. Tephra data from these archives will assist in the construction of the first tephra lattice for the region and could aid in the synchronisation of the archaeological occupations.

Chapter 5

Methods

5.1. Introduction

In order to build a robust tephrostratigraphic framework to correlate records it is very important that the tephra units are correctly identified. The methodological procedures that were used to collect, process, identify and characterise all tephra samples is described in this chapter. These methods are based on those published (e.g. Blockley et al., 2005 and Lane et al., 2014) but have been adapted to take into account sample specific needs for the different types of archives (archaeological sites, a marine core and proximal eruption deposits) investigated in this study.

5.2. Sampling the archaeological, marine and proximal deposits

5.2.1. Sampling of the archaeological (cave and open air) sites

Methods for subsampling archaeological sites follow Lane et al. (2014). Sections that had evidence of Middle Paleolithic (MP) and/or Upper Paleolithic (UP) occupation were selected (see Chapter 4) and the exposed sections were cleaned with a trowel prior to sampling. At each site, the contacts between the archaeological units in the sites stratigraphy was identified (through consultation with the archaeologists at the site and/or using published information) and, the contact was then marked directly on to the profile (a drawn line in the sediment using a knife or trowel) with a note that had the relevant unit information (Unit 1, 2, etc.) that was held in place with a nail at the base of each unit (Figure 5.1). A tape measure was run the length of the section as a guide prior to sampling.

Figure 5.1. Photograph of the trench sampled for cryptotephra at the Lusakert archaeological site, Armenia. A tape measure is used as a guide so that the profile can be subsampled contiguously every 2 cm from base to top. The yellow tickets denote the archaeological units. Samples were recorded in a field notebook and double bagged. Image V Smith.

The archaeological sites typically contain large clastic material from weathered surrounding rocks and artefacts (bones and lithic materials etc.). These objects hampered the collection of sediment in large continuous tins or monoliths (Figure 5.2). As such, a small amount of sediment (~10-20 grams) was sampled using a small metal tool (knife or spoon) and placed in a labelled small bag. This method allows the navigation around obstacles in the archaeological sites (see Lane et al., 2014; Figure 5.2). Sampling was contiguous at 2 cm resolution that was increased to ~5 cm around higher concentrations of clastic material. Sampling always started at the base of the profile to ensure that there was no contamination from sediment falling from above (Lane et al., 2014).

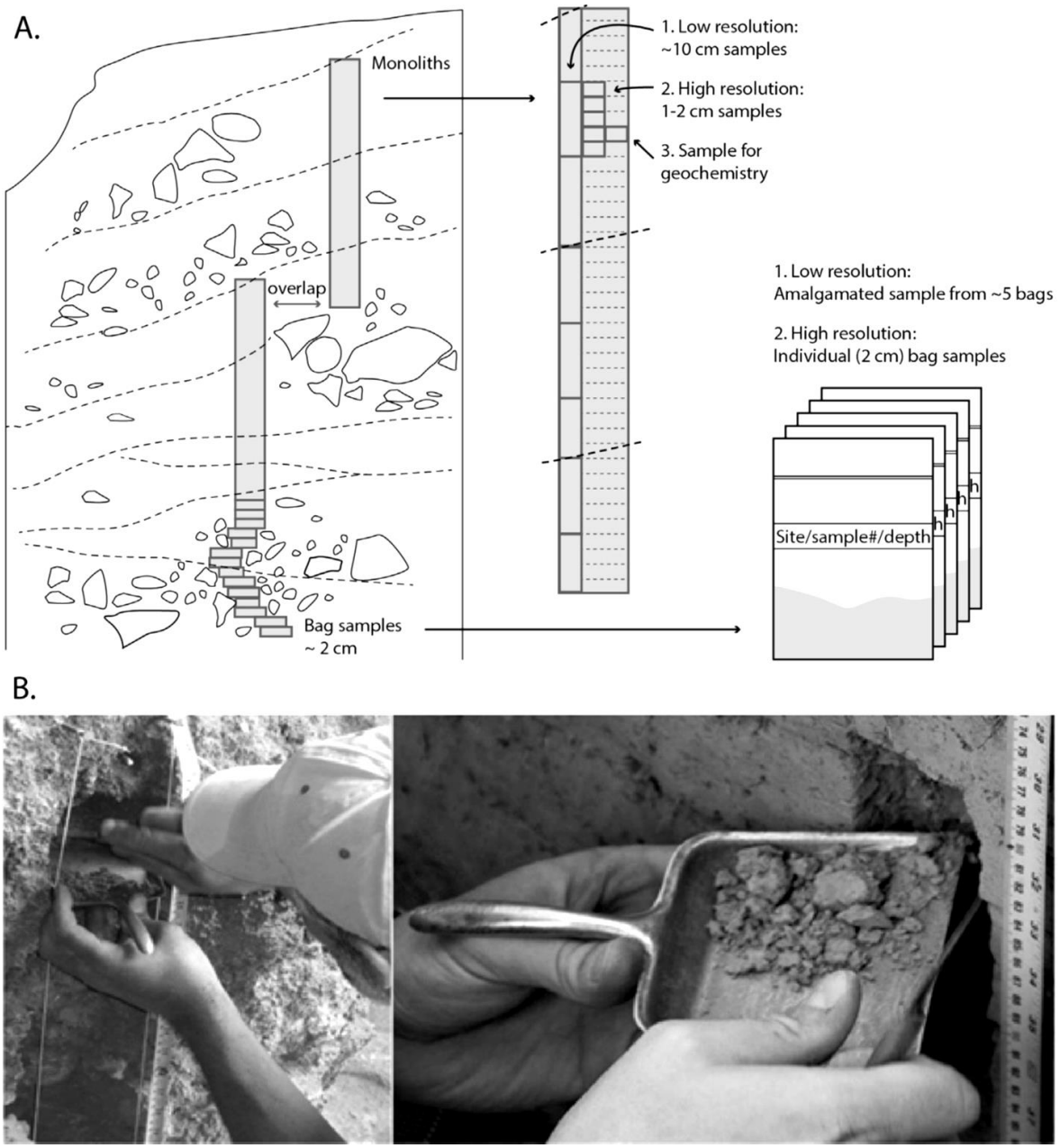

Figure 5.2. Illustration of the two different methods for sampling archaeological sites are shown in a. The 1-2 cm contiguous bag method is used on loosely compacted sediment or sections that have a high concentration of clastic material and/or archaeological artefacts (method adopted in this study). Tin or monolith sampling is a quicker and more efficient way to sample a site but requires consolidated sediments that are devoid of large amounts of clastic or archaeological artefacts (see Lane et al., 2014). Subsampling of the tins is done within a laboratory. Photos show samples been collected by D. White (b). Samples are always collected from the base of the sequencing upwards through sampling column. Image Lane et al. (2014).

Sediment samples from sites in the Northern Caucasus were collected as part of the NERC funded “Environmental Factors in the Chronology of Humans Evolution

and Dispersal" (EFCHED) project in 2004. Some of the archive material (stored at Royal Holloway, University College London) that was relevant to this study was used. These samples were collected by others at different sample resolutions (~3-5 cm), but were contiguous.

5.2.2. Subsampling the M72/25-GC1 Black Sea marine core

U-channels (1cm x 1cm x 1 m) from the 952 cm long M72/25-GC1 sediment core were provided by Prof. Helge Arz (The Leibniz Institute for Baltic Sea Research, Warnemünde, Germany) (Figure 5.3). They were stored in a cold store to ensure no drying and/or shrinking of the channels. The surface of each U-channel was only exposed for short periods of time (~10-30 minutes) whilst been subsampled.

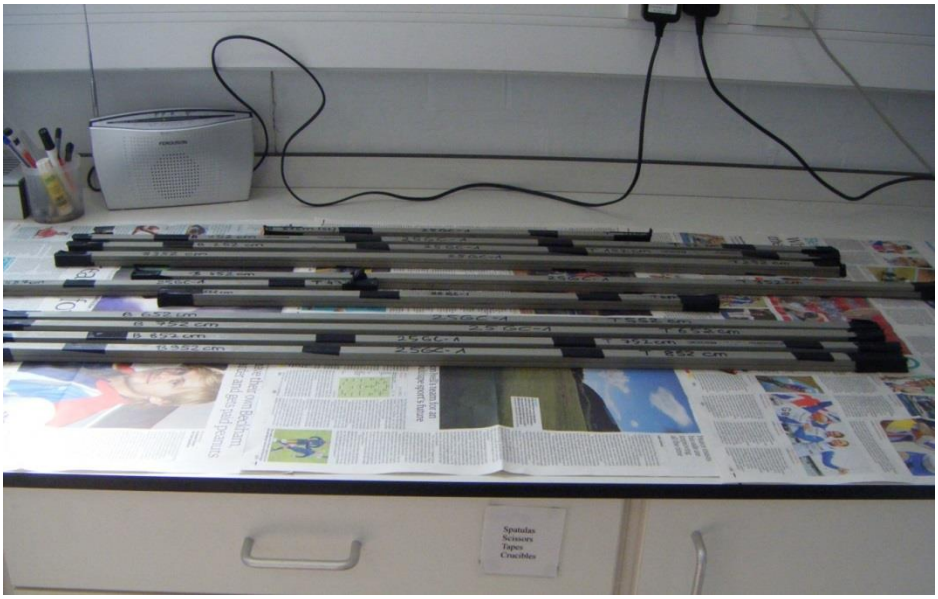

Figure 5.3. Photo of 1 m long U-channels of the M72/25-GC1 core from the Black Sea that were sent to Oxford for cryptotephra investigation.

The exposed sediment face was cleaned prior to sampling to ensure there was no contamination or smearing of the sediments down the core. Initial, low resolution samples were taken to establish if there were any cryptotephra layers. Small

amounts of sediment that encompassed the equivalent of 10 cm in depth were taken and amalgamated to form one sample (~0.5 g). Sampling was done using a scalpel and care was taken not to smear the sediments down core when subsampling. This process continued contiguously from 952 cm to the top of the core at 2 cm (the last 2 cm of core were absent). The position of each sample taken was marked on the side of the U-channel with a permanent marker so that the same section could be resampled if needed.

5.2.3. Proximal deposits

Glass compositional data from outcrops proximal to the volcanic centres, where the eruptions stratigraphy is well established, is used in comparisons in this thesis to identify source and eruption. A proximal glass dataset was compiled from the literature, and some samples were collected at proximal locations. Only single shard glass data, analysed using a wavelength-dispersive electron microprobe (WDS-EPMA), from the literature were used so that they were directly comparable to data produced in this study. Relevant eruptive centres include the volcanic provinces in Italy, Greece, Turkey, Romania, Armenia, Georgia and on the Greater Caucasus range. The focus for the dataset was to obtain data from large eruptions that occurred in the timeframe of this study to compare to the tephras found in the Caucasus. Where this information was not available, glass data from the volcanic centre was used for comparison, to assess whether a tephra found in the Caucasus had a similar composition and could therefore be a product of other eruptions from that centre. Tephras from the same volcanic province often have the same or similar glass compositions (Pearce et al., 2004).

In addition to published datasets, proximal samples were collected from four volcanoes; the Ciomadul volcano in the East Carpathians, Romania; Gutansar volcano in the Geghama highlands, Armenia; Santorini in the Aegean Arc, Greece; and Nemrut Volcano, East Turkey. With the exception of samples from Gutansar volcano, the proximal deposits were collected by colleagues and subsamples were sent to the University of Oxford.

5.3. Laboratory procedures for tephra analysis

5.3.1. Laboratory processing of cryptotephra deposits

Processing of samples for cryptotephra investigation from the archaeological sites and the M72/25-GC1 core followed the non-destructive, physical separation technique outlined in Blockley et al. (2005; see Figure 5.4).

Initially, sediments from the archaeological sites and the M72/25-GC1 core were subsampled at 'low resolution' so that the archives could be efficiently processed to check for the presence or absence of tephra. Low resolution samples from the archaeological site were collated as follows; some material of each contiguous bag sample across ~10 cm (i.e. from 5 samples) was subsampled and amalgamated to form a single sample (~ 1g) and placed in 50 mL test tube with a lid. An adapted flow diagram of the full laboratory procedure as outlined by Blockley et al. (2005) is given in Figure 5.4. The sample-specific adaptions to these methods are described below.

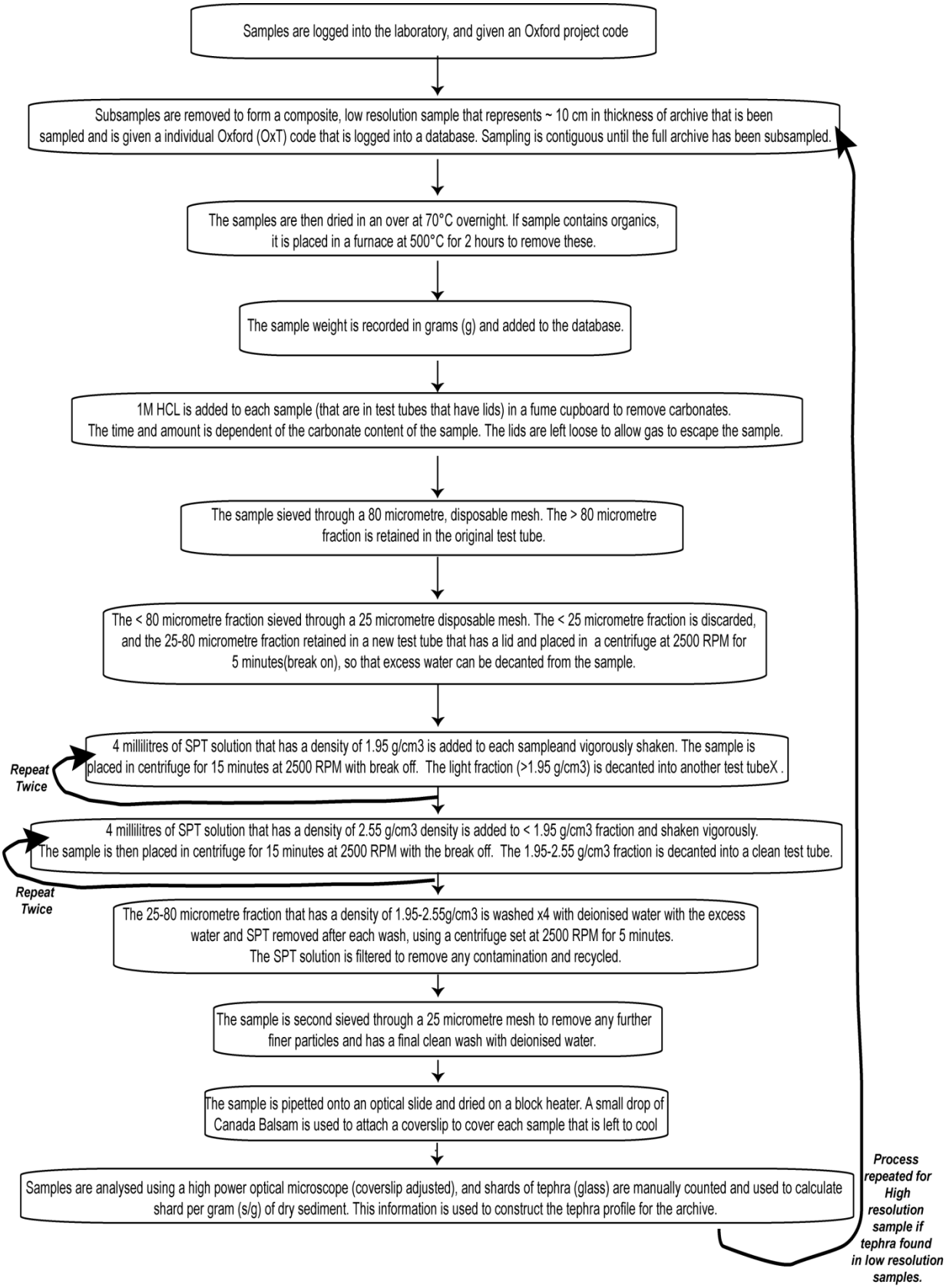

Figure 5.4. A flow diagram of the laboratory methods used in this study to isolate shards of volcanic glass from the host material, modified from Blockley et al. (2005).

All samples were dried in an oven overnight (~70 °C). Once dry, the samples were weighed (g). Any small stones or archaeological material (bones, lithics etc.) were removed prior to weighing the archaeological samples so the sediment weight was accurate, and comparable to all other samples (Lane et al., 2014). It was not necessary to ash the samples (see Figure 5.5), as there was no organic content in the samples. 1 Molar hydrochloric acid (HCl) was then added to each sample (enough to cover the sample) to remove any carbonates in the host material. Additional acid was added until the fizzing had stopped (Blockley et al., 2005).

Samples were then sieved to isolate the size fraction that cryptotephra is commonly found, 25-80 micrometres (Blockley et al., 2005). The archaeological samples were initially sieved through an 80 micrometre mesh using a plastic spatula with tap water and a mild soap to assist in the disaggregation of consolidated sediment. The >80 micrometre fraction was retained and the <80 micrometre fraction (that was then suspended in water) was then sieved through a 25 micrometre mesh. The 25-80 micrometre fraction was taken to the next stage in processing, and the <25 micrometre fraction was discarded as they are too small to analyse. The M72/25-GC1 sediments are very fine grained and therefore only needed to be sieved through 25 micrometre mesh (retaining the >25 micrometre fraction). Little sample remained post-sieving so the density separation to extract glass shards was not necessary (see next step; Figure 5.4). The sieving mesh used for all samples is disposable, and is never used twice so no cross contamination could occur. Additionally, all equipment was thoroughly cleaned after every sample and a ‘blank’ sample was introduced (that undergoes the same

methodological procedure; including exposure to all reagents) every tenth sample to monitor for contamination.

These archaeological samples were then density separated (Figure 5.4). This method separates glass shards (tephra) based on their density from the host sediments. Volcanic glass has a density between 1.95 g/cm^3 and 2.5 g/cm^3 (Blockley et al., 2005) and this range was separated using sodium polytungstate (SPT) that can be made to the required density. This is a two-step procedure using two densities of SPT (2.5g/cm^3 and then 1.95g/cm^3) to isolate the material of the required density (see Figure 5.4). After density separation, the remaining sample (25 - 80 micrometres in size with a density of 1.95 to 2.5 g/cm^3) is thoroughly cleaned with deionised water and both the Black Sea and archaeological samples were mounted using onto optical slides with Canada balsam. Water remaining in the blank sample was also mounted for optical analysis.

Vitreous grains (tephra) were identified using a high-powered, polarising (and cross polarising), optical microscope with a rotating stage. Tephra shards were identified by morphological characteristics exhibited by the glass, i.e., non-crystalline, vitreous lustre, and irregular structure with vesicles or ‘platy’ shape (Figure 5.5; Lowe, 2011). Tephra shards in each sample were manually counted and the number of shards per gram of dry sediment (s/g; based on initial, dry weight of the sample) was established. No tephra was found in the blank samples used to monitor cross contamination.

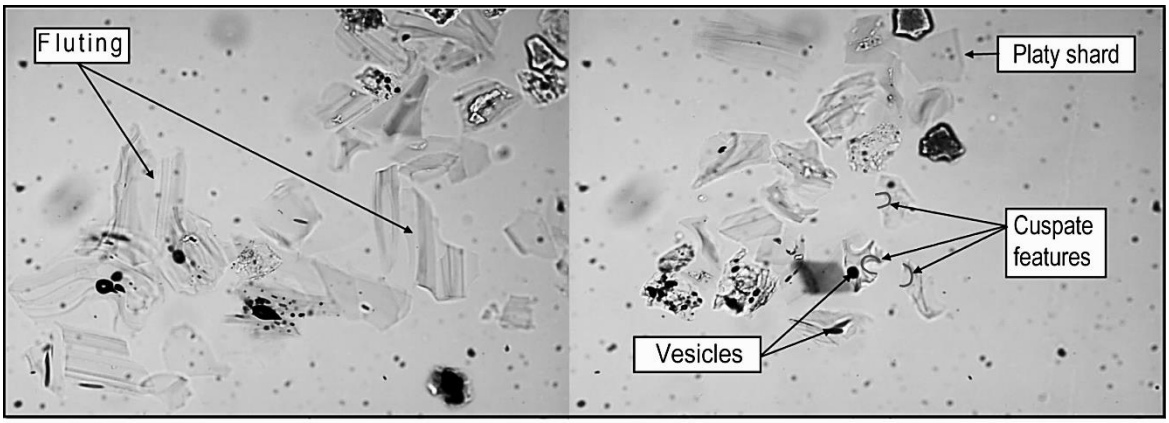

Figure 5.5. Images of shards of tephra (glass) from the CI eruption. Shards have a vitreous lustre and are irregular in form. Some of the key features that are used to identify shards of volcanic glass are highlighted on the images. The pink colour is an artefact (associated with the refraction index) of the Canada balsam that is used to mount the samples. Shards are typically clear but low silica glasses are darker (brown) in colour.

If glass shards were identified in the amalgamated samples, high-resolution sampling was carried out. For the M72/25-GC1 core, the 10 cm section was contiguously resampled at 1 cm resolution, and for the archaeological samples ~1 g of sediment was taken from each individual bag included in the low resolution scan sample (typically spanning 2-5cm). All samples were then processed in the same way as outlined above to establish the exact stratigraphic position of the tephra layer. Tephra 'peaks' were determined by visual analysis of the shard concentration profiles, expressed as s/g (see Chapter 3.4 for discussion on the identification of tephra peaks).

5.3.2. Laboratory processing of proximal tephra deposits

Proximal volcanic deposits were broken up to obtain a small representative sample for analysis. The sample was placed in a clean pestle and mortar and ground to disaggregate it and was then wet sieved through an 80 micrometre mesh with tap water to remove the <80 micrometre fraction. The >80 micrometre

fraction was placed in a beaker and was dried at 70°C in an oven overnight. Proximal samples were not prepared in the same laboratory as any cryptotephra samples. The proximal sample from Nemrut was sieved by Sumita and Schmincke (pers comms, 2014), and the 80 to 125 micrometre fraction was sent to Oxford.

5.4. Preparation for geochemical analysis

5.4.1. Procedures for mounting cryptotephra deposits

Once a tephra layer had been identified, glass shards in high-resolution samples were isolated from the remaining host sediment and concentrated ready for compositional analysis. Each sample was re-processed as outlined above, but did not undergo the mounting stage (Figure 5.4). The sample (that was then suspended in water) was then pipetted on to a welled optical slide and placed under a high power optical microscope. Individual shards of volcanic glass were extracted from the water using a specially prepared gas chromatography (GC) syringe that was attached to a micromanipulator for stability, and shards were deposited onto a pre-made resin stub (Figure 5.6; see Lane et al., 2014). Once all the tephra shards had been extracted, the water was left to evaporate and the shards of glass (tephra) were then ‘capped’ with a fresh layer of resin (Specifix-40 by Stuers) and cured in the oven at >40°C for 3.5 hours.

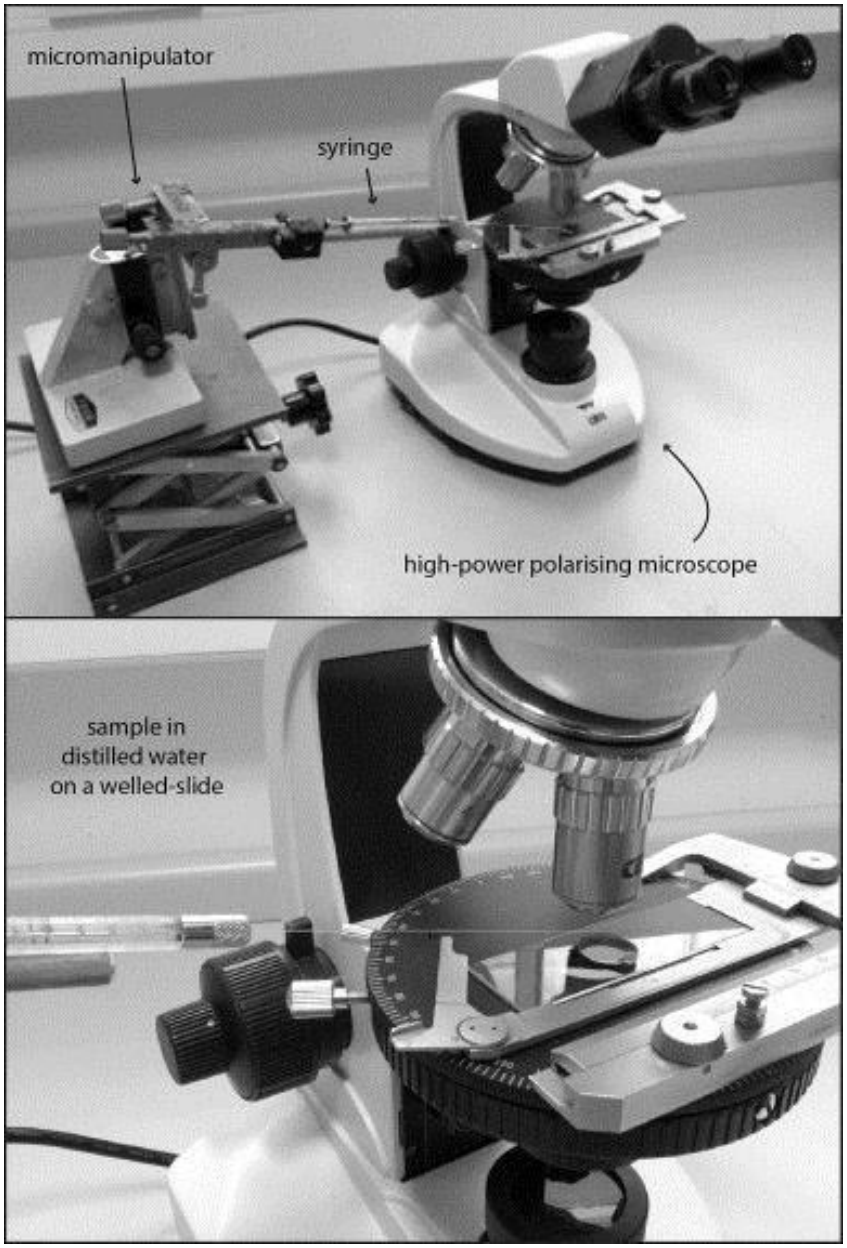

Figure 5.6. Images of the equipment that was used to manually pick shards of volcanic glass from host material. Image taken from Lane et al. (2014)

5.4.2. Procedures for mounting proximal / visible deposits

Proximal deposits that had been ground and sieved (and any visible tephra layers) were mounted in pre-prepared multi-hole resin stubs as outlined in Figure 5.7. This method of preparation allows for more samples to be analysed in a single run

on the WDS-EPMA. Struers Specifix-20 cold setting resin was used to mount the samples.

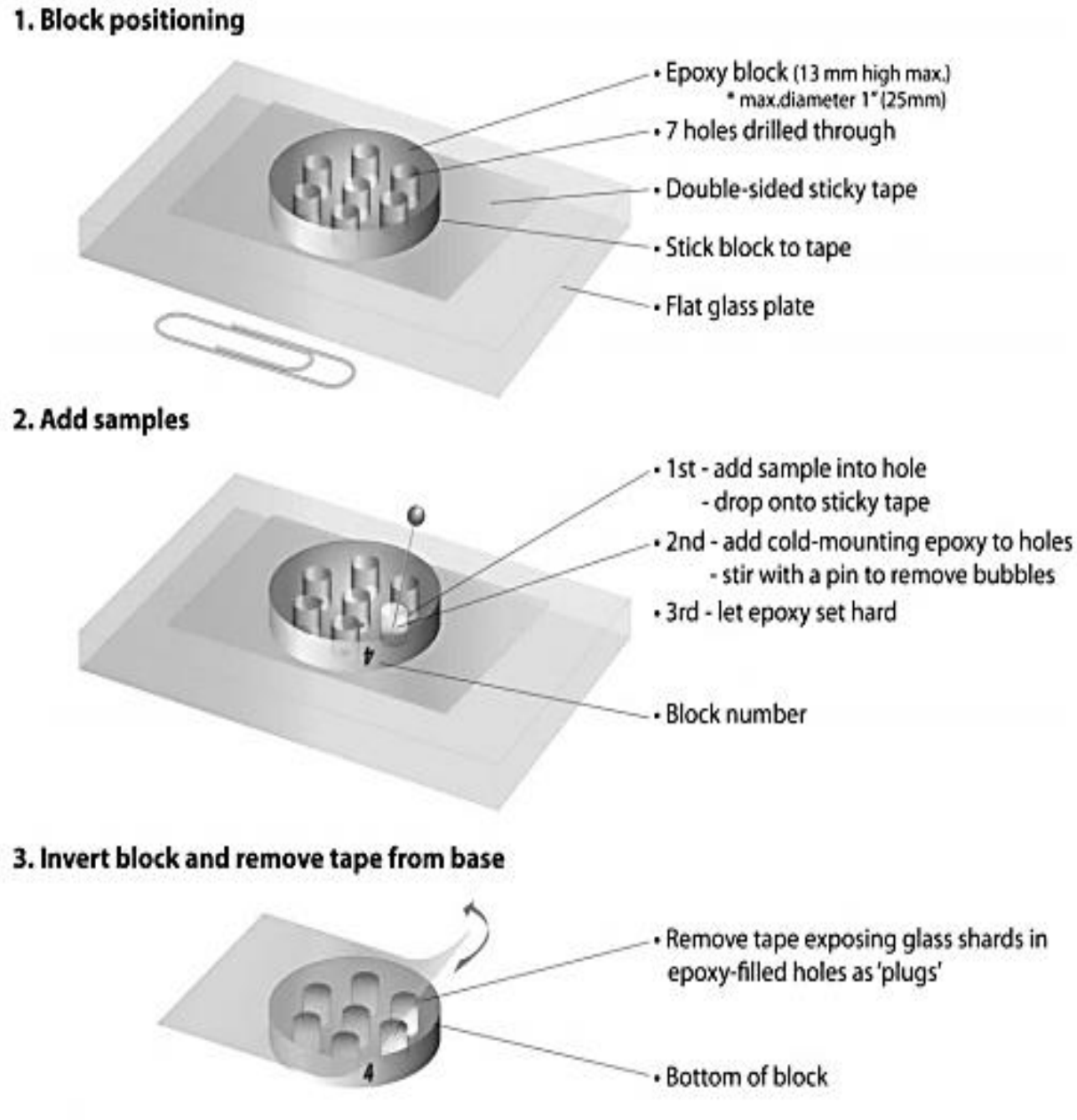

Figure 5.7. Schematic illustration of the procedures used to prepare multi-sample resin blocks for visible tephra deposits. Once tape is removed from the sample surface (3) and the sample is ground and polished (see below), the sample surface is scored with a scribe so that each sample can be easily identified during WDS-EMPA. Image from Lowe (2011)

For the pumice samples (that were broken into small fragments), double sided sticky tape was placed on the glass plate and an empty plastic ring (that is the correct size for the WDS-EPMA holder) was stuck to the tape. Individual pieces of pumice were then placed in the ring, in rows (approximately 4 rows with 6 pieces of pumice in each row). The ring was then backfilled with cold curing resin and left to cure overnight.

5.4.3. Grinding and polishing of samples for WDS-EPMA analysis

All stubs were ground by hand using silicon carbide papers to expose a flat section through the tephra shards. The stubs where then polished on a lap with 3 micrometre diamond paste at 150 rpm for ~3 minutes (cryptotephra stubs) and ~10 minutes for proximal deposits (visible tephra stubs). Times varied somewhat depending on the quality of the polish, and a 6 micrometre and a 1 micrometre diamond polish were used when needed.

For proximal samples or samples that had sufficient glass shards, grinding ceased when at least 30 grains were exposed. The cryptotephra samples that were manual picked often only had a few glass shards exposed although others were deeper in the resin. Therefore, the sample was analysed and polished multiple times to ensure the maximum number of analysis for each deposits was achieved.

5.5. Geochemical analysis for Major element concentrations

5.5.1. Major and minor element analysis using a wavelength-dispersive electron microprobe analyser (WDS- EPMA)

Analysis of 11 major elements (Na, Mg, Al, Si, P, Cl, K, Ca, Ti, Mn and Fe) for each sample was carried out using an electron microprobe with 4 wavelength dispersive spectrometers, housed at the Research Laboratory for Archaeology and History of Art (RLAHA), University of Oxford. The advantage of using WDS-EMPA is the ability to obtain precise grain specific analysis (Lowe, 2011).

5.5.2. Instrument conditions and secondary standards.

Data from the WDS-EPMA were converted to wt. % oxide for each element by the electron microprobe SAMx computer software. Operating conditions were as follows, 15keV, 6nA with a 10 micrometre beam with peak count times of 10-60 seconds per analysis. Prior to analysis the microprobe was calibrated for each element using primary standards (mineral and oxides). The calibration was tested using analysis of secondary standard glasses, ATHO-G, GOR132/5 and St/Hs6/80-g from the MPI-DING collection (Jochum et al., 2006) for which there are published preferred values (quoted with a 95% confidence level). Secondary standards were run alongside the 'unknown' samples to assess and monitor precision and accuracy of chemical data obtained throughout the run.

5.5.3. WDS-EPMA data reduction

Analytical totals are always <100% as the glass shards contain elements that are not analysed, including dissolved volatiles (e.g., H_2O – magmatic and secondary

hydration; Shane, 2000) and trace elements. Weight % totals of >93 % are normalised to 100% to account for secondary hydration; those <93% were discarded as they most likely reflect poor analyses (Shane, 2000). Post-eruption alteration including devitrification (formation of crystalline structure within the glass) and alkali exchange (enrichment of K and loss of Na) can be identified by optical analysis (using cross polarised light) and in the compositional data, respectively (Shane, 2000; Scott, 1971). Thus, these samples were not analysed or the data were discarded. All data, including analyses of the secondary standards, are provided in Appendix 1.

5.6. Geochemical analysis for trace element concentrations

5.6.1. Laser Ablation Inductively Coupled Plasma Mass Spectrometer (LA-ICP-MS)

Analysis of trace elements for samples BSC_411, BSC_394, and the visible tephra deposits from the archaeological sites of Lusakert, Fantan and Kagasi (Armenia) were carried out over three days using an a LA-ICP-MS housed at the Department of Geology, Trinity College Dublin. The LA-ICP-MS is a multi-element analytical technique commonly used in tephra studies (e.g. Pearce et al., 2004; Perkins et al., 1997; Tomlinson et al., 2010).

5.6.2. Instrument conditions and secondary standards.

Trace element analysis was carried out on a Thermo Scientific iCAP Q ICM-MS, coupled to a Photo Machines analyte 193 nm eximer laser ablation system, with a Helix two volume cell that is housed in the Department of Geology, Trinity College,

Dublin. Spot sizes 24, 30 and 36 micrometres were selected based on the size of the exposed shard. A 5 Hz pulse was used, with a count time of 40 s (200 pulses) per spot and 30 s on the gas blank (introduced between each sample to allow for aerosols to be flushed from the system, prior to the next analysis). Analysis of NIST612 glass allowed for instrument calibration and ^{29}Si and ^{43}Ca (determined using EMPA) were the internal standards. The MPI-DING reference glasses (ATHO-G, StHs6/80-G, and GOR128-G; Jochum et al., 2006 that have published known assays) were employed to monitor accuracy between runs (~20 'unknowns' were run between sets of standards). The sample surface was mapped prior to WDS-EPMA and the same grain was targeted for LA-ICP-MS analysis so that there was internal consistency between the internal reference element (^{29}Si or ^{43}Ca) from each shard that was analysed.

5.6.3. Data Reduction for the LA-ICP-MS

Isotope intensity profiles (that are produced with each ablation) are used to reduce LA-ICP-MS data. Parts of the ablation profiles that showed evidence for 'negative ablation' (where the laser has ablated through a sample) or evidence for the accidental ablation of crystal inclusions were deleted for data reduction. In some cases, these parts of ablation analysis can be removed, but typically the whole analysis was rejected (Albert et al., pers comms 2014; Tomlinson et al., 2010).

To obtain absolute element concentration in parts per million (ppm) for each trace element (that is measured as count per second on the LA-ICP-MS), an external matrix matched secondary standard (NIST612 glass) and a previously quantified, internal standard are needed for calibration and data reduction. The latter is commonly ^{29}Si or ^{43}Ca that are determined on the WDS-EPMA (Lowe, 2011). For

this study data reduction was performed using the method outlined in Tomlinson et al. (2010) and calculations were performed using a computer program designed by Tomlinson (Tomlinson pers comms., 2014). Internal standards used were ^{29}Si for the rhyolitic samples from the Black Sea (BSC_411 and BSC_394) and ^{43}Ca for samples from Armenia.

5.7. Data analysis and presentation

The following section describes the key ways in which the data produced in the study will be presented and methods used for chemical classification and sample correlation and discrimination. These are the methods that will be used in the results chapters (Chapters 6-8). Methods used in this thesis to monitor data quality and those used to calculate errors have been provided in previous sections (section 5.5.2 and 5.6.2).

5.7.1. Visualisation of geochemical data

Glass compositional data that has been produced as part of this study has been presented on major and trace element plots. Specifically selected pairs of elements are presented together to allow for compositional gradients in the melt to be identified. For example, a total alkalis (Na_2O + K_2O wt. %) versus silica (SiO_2 wt. %) diagram (referred to as a TAS plot) is used to classify tephras and show trends in the fractionation of the source magma through the eruption (e.g. data plots from a rhyolite to andesite on a linear trend). The limitation when working in two dimensions is that the full suite of elements needs multiple plots.

For this study, a TAS plot has been presented for all data for classification (after Le Bas et al., 1986), with discrimination lines (data from Rollinson, 1993) for calc-alkaline and peralkaline magma added to identify melt series. In addition, a suite of other plots of different elements have been produced for each sample. These are standardised with the element that has the potential of the maximum variability plotted on the X-axis; SiO_2 wt.% for major data (also called Harker diagrams) and Th ppm from trace data, and are plotted against all other elements (that are plotted on the Y-axis). Both these elements (SiO_2 and Th) often show the greatest range in data-set that can allow for discrimination of tephras from a (potentially) varied number of unknown sources (Rollinson, 1993). These plots allow for easy comparison and discrimination between data sets.

In addition to biplots, trace element compositional data (from 23 elements, see Appendix 1) have been presented in a multi-element spider diagram. In this thesis the trace data were normalised to the primitive mantle (data are from Sun and McDonough, 1989). These diagrams can highlight contributions, in the various tectonic sources, to the melt (see Rollinson, 1993; Sun and McDonough, 1989).

Data produced from glasses found in the Black Sea M72/25-GC1 core are presented in black and grey scale; data from proximal deposits is presented as chemical envelopes and data from tephra shards horizons that have been found each archaeological site were assigned coloured symbols, with different tephra layers from the same site having the same symbol in different colours. All data are provided in Appendix 1, and average compositional data (with 1 σ uncertainties) or full data sets if there were only a few analyses are provided in tables in the Results Chapters 6-8. All data presented in figures and tables were normalised to 100% (anhydrous) for comparative purposes. Error bars shown with WDS-EPMA

data in figures are at 2σ (unless otherwise stated). These values were calculated from data from cumulative runs of a reference glass, ATHO-G from the MPI-DING collection (Jochum et al., 2006).

Chapter 6

Volcanic sources of tephra in the Caucasus

6.1. Introduction

This chapter provides information on the tephras that could have been dispersed across the southeast Black Sea and the Caucasus. This is essential for the identification of tephras found in the archaeological sites and palaeoenvironmental archives in the region. The following results are derived from both an extensive literature review of available glass chemical data and new data produced as part of this study.

6.2. Exploration of potential proximal sources

Since tephra can be dispersed far from source, and the dominant wind direction is often eastwards (current global circulation pattern), tephras from the following volcanic regions to the west of the Caucasus need to be considered: the Italian provinces (Campi Flegrei, Pantelleria, Vesuvius); the Aeolian islands (Lipari, Vulcano and Salina); the Hellenic arc (Santorini, Nisyros, Yali and Kos); Turkey (Mt Ararat, Nemrut, Tendürek, Süphan, Hasan Dagi, Acigöl, Göllü Dagi, Erciyes Dagi and Gölcük) and the East Carpathians (Ciomadul volcano; Figure 6.1). Volcanoes within these centres are known to have erupted, with varying degrees of explosivity, within the last 200 ka (see summary Table 6.1). Volcanic centres in the southern Caucasus (e.g. the Geghama range, Armenia) and on the Greater Caucasus range (volcanoes include Elbrus, SW Russia, and Kasbek and the Keli highlands in Georgia) are also known to have been active within the Quaternary (Figure 6.1, Table 6.1). Unfortunately, geochemical and chronological data for many of these eruptions are limited.

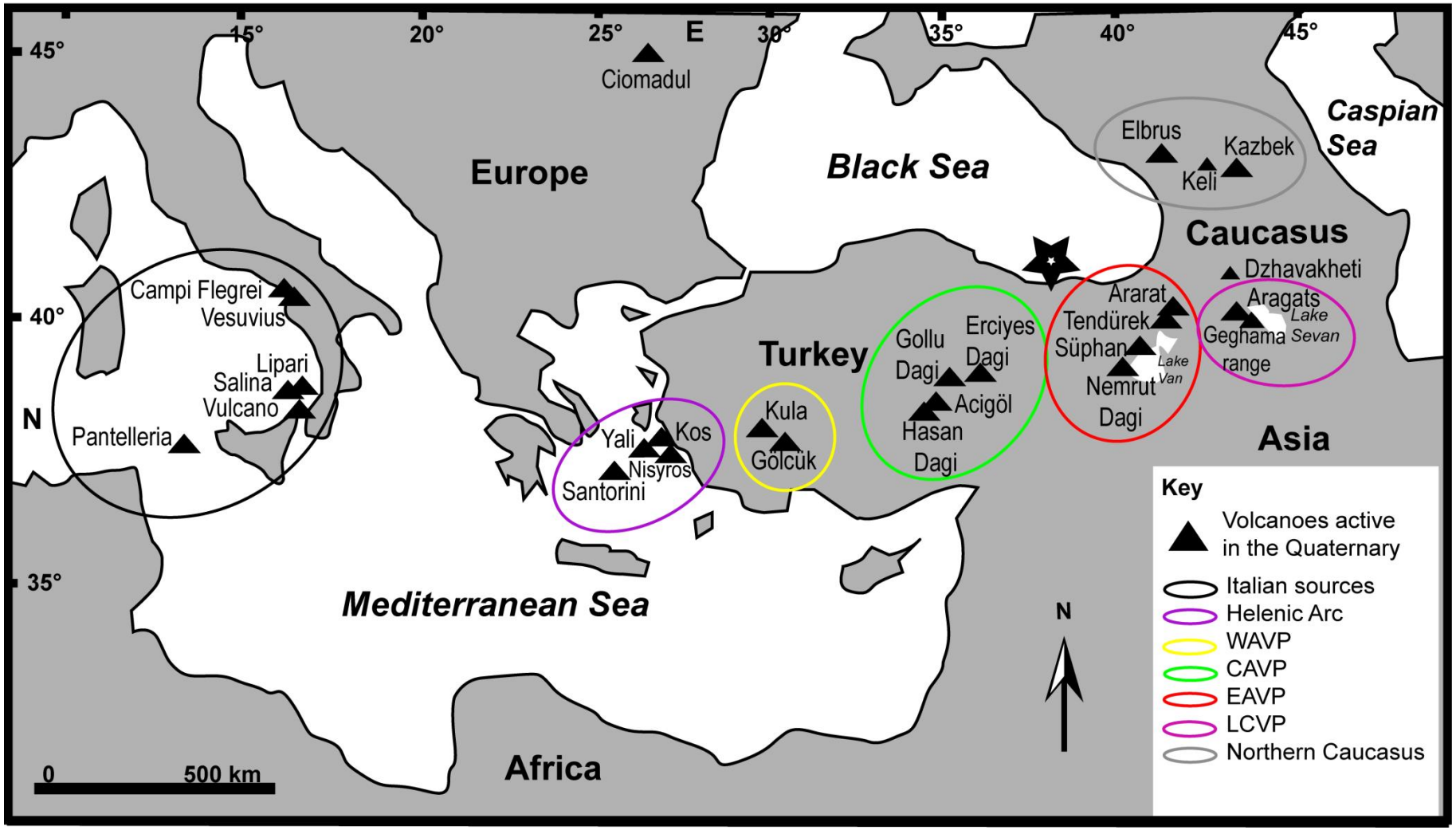

Figure 6.1. Map of Quaternary volcanoes that are upwind of the Caucasus and southeast Black Sea M72/5-25-GC1 core (star on map). Coloured circle denote the volcanic regions. WAVP = West Anatolian Volcanic Province; CAVP = Central Anatolian Volcanic Province; EAVP = East Anatolian Volcanic Province and LCVP is the Lesser Caucasus Volcanic Province.

Table 6.1. Summary information of both widespread and specific eruptions from volcanic centres that are upwind of the Caucuses.

Country	***Region / Source Volcano***	***Eruption / Marker Layer***	***Age of eruption (ka) or phases of activity #***	***Magma series***	***TAS classification***	***Glass data references****	***Age information references***
Italy	CVZ / Campanian	/ X6	~108. 3 ± 5.4 ka (varve age)	P	High K trachyte-phonolite	Wulf et al., 2012	Wulf et al., 2012
	CVZ / Campanian	/ X5	~105.5 ± 5.3 ka (varve age) ; 105 ± 2 ka and 106 ± 1 ka (^{39}Ar/^{40}Ar)	P	High K-Trachyte	Wulf et al., 2012	Wulf et al., 2012; Kraml, 1997, Giaccio et al., 2012
	CVZ / Campi Flegrei	Tlf, Tlc and Tla	Tla; = 58.9 ± 1.8 ka (^{39}Ar/^{40}Ar)	P	phonolite	Tomlinson et al., 2012b	Pappalardo et al., 1999
	CVZ / Campi Flegrei	Campanian Ignimbrite / Y5	39.3 ± 0.1 ka (^{39}Ar/^{40}Ar)	P	High K trachyte-phonolite	Tomlinson et al., 2012b	De Vivo et al., 2001
	CVZ / Campi Flegrei	/ Y3	29.1 ± 0.2 cal ka BP (modelled age)	P	High K trachyte-phonolite	Albert et al., 2014	Bronk Ramsey et al., 2014
	CVZ / Ischia	Mt. Epomeo Green Tuff (MEGT) / Y7	55 ± 2 ka (^{39}Ar/^{40}Ar)	P	Trachyte-phonolite	Tomlinson et al., 2014b	Watts et al., 1996
	Pantelleria	Green tuff / Y6	45.7 ± 1.0 ka (^{39}Ar/^{40}Ar)	P	Bimodal, trachyte and pantellerite	Tamburrino et al., 2012	Scaillet et al., 2013
	Pantelleria	/ P-11	~ 130.6 ± 5 ka (tuned age)	P	Bimodal, trachyte and pantellerite	Tamburrino et al., 2012	Paterne et al., 2008
	Aeolian islands / Lipari	Lower and Upper Monte Pilato®	Explosive activity 220-98 ka- and ~42 - Holocene	C	Rhyolite (older activity andesite)	Albert et al., 2012a,b	Crisci et al., 1991; 1983; Gioncada et al., 2003.
	Aeolian islands / Salina	Lower Pollara®	<27.6 ± 0.8 ka BP and >26.3 ±0.8 ka cal BP (^{14}C)	C	Andesite, dacite, rhyolite	Albert et al., 2012b	Albert et al., 2012a; Crisci et al., 1983; Morche, 1988

	Aeolian islands / Salina	Grey Porri Tuff	68.5 ± 1.5 ka (K-Ar)	C	Dacite	Albert et al., 2012b	Luccin et al., 2008
	Aeolian islands / Vulcano	Palizzi A®	Explosive activity ~ 80 ka-Holocene	P	Trachyte	Albert et al., 2012a,b	Gioncada et al., 2003; See, Luccin et al., 2008
Greece	Hellenic arc / Santorini	Minoan / Z2	~ 3.6 cal ka BP (^{14}C modelled age)	C	Rhyolite	This study; Tomlinson et al., 2014a	Friedrich et al., 2006; Manning et al., 2006
	Hellenic arc / Santorini	Cape Riva / Y2	~ 22,024 ± 321 (modelled age)	C	Rhyodacite	Aksu et al., 2008; Margari et al., 2007; Tomlinson et al., 2014a; Wulf et al., 2002	Bronk Ramsey et al., 2014
	Hellenic arc / Santorini	/ V1	~170 ka (sapropel age)	C	Rhyodacite	Aksu et al., 2008	Narcisi and Vezzoli, 1999
	Hellenic arc / Santorini	/ W2	~150 ka (sapropel age)	C	Trachy-dacite	Aksu et al., 2008	Narcisi and Vezzoli, 1999
	Hellenic arc / Nisyros	NUP	47.7 cal ka BP or >50 ka cal BP (^{14}C)	C	Rhyolite	Tomlinson et al., 2012a	Karkanas et al., 2014; Limburg & Varekamp, 1991; Tomlinson et al., 2012a
	Hellenic arc / Nisyros	NLP	~47 - 161 ka (constrained between 2 ^{39}Ar/^{40}Ar ages)	C	Rhyolite	Tomlinson et al., 2012a	Smith et al., 1996
	Hellenic arc / Yali	Yali-C	~31 ka (Oxygen isotope stratigraphy)	C	Rhyolite	Aksu et al., 2008; Federman and Carey, 1980	Federman and Carey, 1980
	Hellenic arc / Kos	Kos plateau tuff / W3	~160 ka (sapropel age)	C	Rhyolite	Aksu et al., 2008	Narcisi & Vezzoli, 1999
Turkey	CAVP / Acigöl	Korudağ and Guneydağ	~24.9 ± 0.9 ka; 23.8 ± 0.9 ka (U-Th/He zircon) (possible late glacial - Holocene eruptions)	C	Rhyolites	Tomlinson et al., 2014a	Kuzucuoglu et al., 1998; Mouralis et al., 2002; Schmitt et al. 2011

	CAVP / Acigöl	First phase activity®	~65-200 ka (U/Th)	C	Rhyolites	Tryon et al., 2009	Druitt et al., 1995;Tyron et al., 2009; Mouralis et al., 2002
	CAVP / Hasan Dagi	®	~ 13-7 Ma, 1-0.15 Ma, <120 Ka. Younger eruptions 28.9 ± 1.5 ka; 8.97 ± 0.64 ka (U-Th/He zircon)	C	Rhyolites andesite and dacite	Tryon et al., 2009	Deniel et al., 1998 Schmitt et al., 2014
	CAVP / Erciyes Dagi	Perikartini, Dikkartin and Karagüllü ®	7-10 ka (^{14}C and ^{36}Cl)for Perikartini, and Karagüllü. Dikkartin = 8.8 ka cal BP (^{14}C)	C	Rhyolites	Hamann et al., 2010; Tomlinson et al., 2014a	Sarikaya et al., 2006 Hamann et al., 2010
	CAVP / Göllü Dagi	®	1.5 Ma - ?	C	Rhyolites	Tryon et al., 2009	Mouralis et al., 2002
	WAVP / Gölcük	Cycle III	72.7 ± 4.7 ka – 24 ± 2 ka (^{39}Ar/^{40}Ar)	P	Trachyte	Tomlinson et al., 2014a	Platevoet et al., 2008
	EAVP / Nemrut	Nemrut formation (NF)	~30 ka (^{39}Ar/^{40}Ar)	P	Trachyte and rhyolite	Sumita & Schmincke 2013a,b.	Sumita & Schmincke 2013a,b
	EAVP / Nemrut	Tatvan Ignimbrite (TI)	45.1 ± 2.1 ka (^{39}Ar/^{40}Ar)	P	Rhyolite	This study	Sumita & Schmincke 2013a,b
	EAVP / Nemrut	Ahlat Pumice 6 – Halepkalesi Pumice 10 (AP-6/HP-10)	61.60 ± 2.55 ka (^{39}Ar/^{40}Ar)	P	Trachyte	This study	Sumita & Schmincke 2013a,b
	EAVP / Nemrut	Ahlat Pumice 8b (AP-8b)	59.4 ± 10 ka (^{39}Ar/^{40}Ar)	P	Rhyolites	This study	Sumita & Schmincke 2013a,b
	EAVP / Süphan		Started ~2 Ma. Last activity ~10 ka	C	Basaltic trachy andesite to rhyolites		Yilmaz et al., 1998

	EAVP / Tendürek		Started ~700 Ka. Last activity ~2.5 ka	P	Trachy andesite-phonolite		Yilmaz et al., 1998
	EAVP / Ararat		Started ~1.5 Ma. Last activity Holocene	C	Basaltic andesite-rhyolites		Yilmaz et al., 1998; Karakhanian et al., 2003
Romania	East Carpathians / Ciomadul	Older Turia / Tusand	41.6-44.9 ka cal BP / 41.7 - 44.5 ka cal BP (^{14}C)	C	Rhyolite	Wulf & Veres pers comms, 2014; this study	Harangi et al., 2010; Wulf & Veres pers comms, 2014
	East Carpathians / Ciomadul	Younger Turia / Bixad	30.8-31.5 ka cal BP / 30.7 - 33.1 ka cal BP (^{14}C)	C	Rhyolite	Wulf & Veres pers comms, 2014	Harangi et al., 2010; Wulf & Veres pers comms, 2014
Armenia	Southern Caucasus/ Gutansar Volcano in the Geghama range	®	Quaternary phases of activity for Geghama range; ~700 ka, 550-480 ka, 190-150 ka, 110-70 ka and <50 ka (K-Ar). Possible Holocene activity.	C / mildly acidic	Basaltic Trachy andesite - trachy andesite and rhyolites	This study	Arutyunyan et al., 2007; Karakhanian et al., 2003; Lebedev et al., 2013
	Southern Caucasus/ Aragats		Phases of activity stared at ~5 Ma, youngest volcanism ~900 - 450 ka and Holocene (K-Ar and radiometric)	C	Andesite dacite rhyolites		See Karakhanian et al., 2003; Lebedev et al., 2011a
Georgia	Dzhavakheti volcanic range (Samsari Ridge)		Quaternary volcanism 800-~50 ka (possibly Holocene). (K-Ar, Rb-Sr)	C	Mainly dacite with some basalt, rhyolite		Lebedev et al., 2004a; 2011a
	Northern Caucasus / Kasbek		180-250 ka modern Kazbek formed. Activity ~70-6 ka (K-Ar ages)	C	Dominance of andesite but also dacite		See Lebedev et al., 2007; 2011a
	Northern Caucasus / Keli volcanic centre		Phases of Quaternary activity at ~170-245, 70-137 ka, and <30 ka (K-Ar)	C	Dacite - Andesite, - trachy andesite		Lebedev et al., 2011a,b.

					rhyolite		
SW Russia	Northern Caucasus / Elbrus		Phases of Quaternary activity at 900, 170-255, 70-110 and >35 ka - Holocene (K-Ar)	C	Dacite and rhyolites		Chernyshev et al., 2002; Lebedev et al., 2010; 2011a

*Footnote; CVZ =Campanian Volcanic Zone (Campi Flegrei, Ischia and Vesuvio); P= peralkaline; C= calc-alkaline; # age of the specific eruption and/or the eruptive phases from the volcano (radiocarbon ages have been calibrated using IntCal13); * Glass chemistry of individual shards analysed using a WDS-EMPA; ® EPMA glass data from the volcano is from an eruption that may be younger or older than the project parameters, and is the only representative EPMA data.*

6.3. The Italian Sources

6.3.1. Campanian Volcanic Zone (Campi Flegrei, Vesuvius, and Ischia)

Numerous explosive eruptions have occurred in the Campanian Volcanic Zone (CVZ) over the last ~200 ka years, ranging from Plinian eruptions (that formed large calderas) to pumice surges and minor fall deposits (e.g. Orsi et al., 1996; Pappalardo et al., 1999; Rolandi et al., 2003; Scandone et al., 1991). Explosive eruptions that could have dispersed ash into the Black Sea and Caucasus include the widespread Campanian Ignimbrite (CI), the Y3 tephra, the X5 and X6 tephras and the Mt Epomeo Green Tuff (MEGT or Y7) tephra from Ischia.

The largest eruption from the Mediterranean in last 200 ka years is the caldera forming eruption known as the CI (Barberi et al., 1978) that is dated to ~39 ka (De Vivo et al., 2001). This eruption was from Campi Flegrei, west of Naples (Figure 6.1; Fisher et al., 1993; Orsi et al., 1996) and generated a Plinian eruption column that extended > 44 km into the atmosphere (Rosi et al., 1999), a widespread pyroclastic density current (PDC) and fine ash fall termed co-ignimbrite associated with the PDC (Fisher et al., 1993; Rosi et al., 1999). Distal facies of tephra ejected during the eruption from the Plinian and co-ignimbrite fallout have been found in the Palaeolithic site of Kostenki in Russia (Pyle et al., 2006), in the Middle Stone Age (MSA) site of Haua Fteah in Libya (Douka et al., 2014) and throughout the Mediterranean and eastern Europe in various lacustrine, marine and terrestrial sequences (e.g. Costal et al., 2012; Lowe et al., 2012; Figure 6.2). Modelled dispersal maps of Costa et al. (2012) suggest that the CI could have reached the Caucasus (Figure 6.2), and recently a visible deposit was tentatively identified as the CI by Nowaczyk et al. (2012) in the south-east Black Sea.

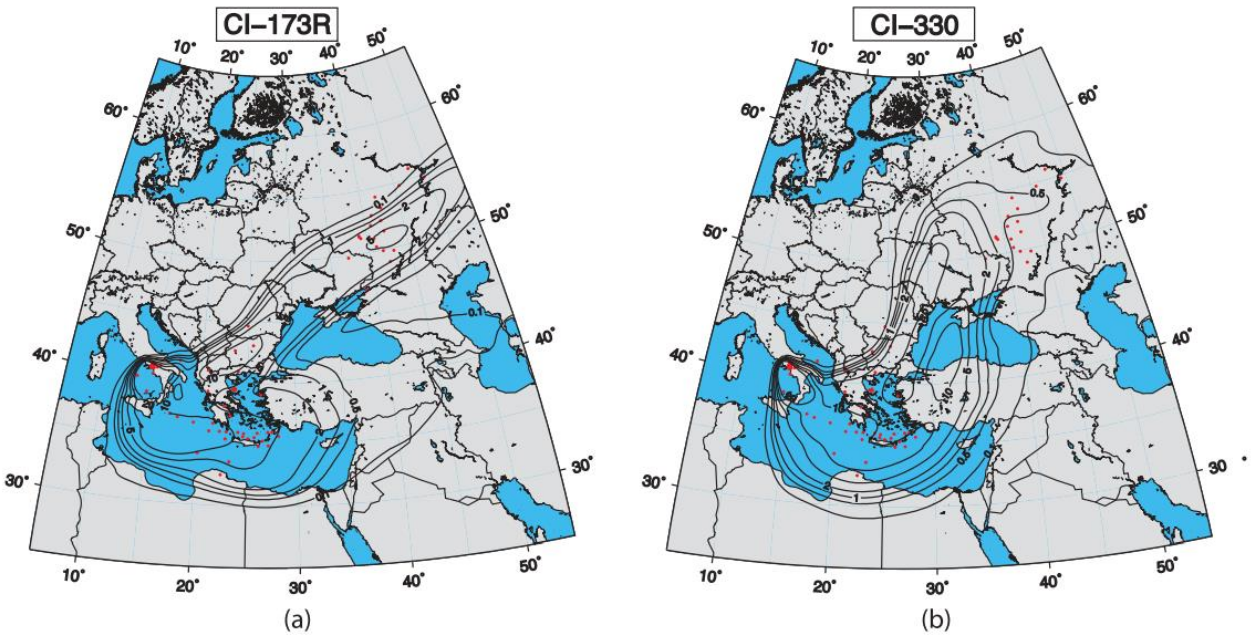

Figure 6.2. Isopach maps showing the simulated thicknesses of CI ash. These are the two best fit simulations for the CI dispersal modelled using FALL3D (see Costa et al., 2012). The locations with visible tephra deposits are indicated by red dots.

A second large eruption that originates from the CVZ is the distally named and chemically characterised Y3 tephra (Albert et al., 2014; Keller 1978; Zancehtta et al., 2008). The Y3 was first identified in an Ionian marine core (climate zone Y; Keller 1978). This tephra was erupted ~29 ka cal BP (Bronk Ramsey et al., 2014) and is found on an easterly and southerly dispersal axis across the Mediterranean. The most distal record of this tephra is a cryptotephra in the long, terrestrial palaeoenvironmental archive from Tenaghi Philippon, Greece (Albert et al., 2014).

Both the CI (also known as the Y5 marine tephra; Keller et al., 1978) and the Y3 are high K-trachytes that straddle the phonolite boundary (Figure 6.3). They have SiO_2 compositions that range from 60-63 wt. % (Albert et al., 2014; Tomlinson et al., 2012b), and CaO and FeOt compositions that are suggestive of a Campanian origin (1.3-2.8 and 2.45–3.8 wt. %, respectively; Albert et al., 2014; Tomlinson et al., 2012b). These CaO, FeOt and MgO contents differentiate Campi Flegrei (CF)

deposits from those of Somma Vesuvius (that has no known eruption >22 ka; e.g. Santacroce et al., 2008) and Ischia (see, Albert et al., 2014; Tomlinson et al., 2014b). In addition, CF tephra typically have K_2O compositions that are greater than the Na_2O contents (e.g. Wulf et al., 2004).

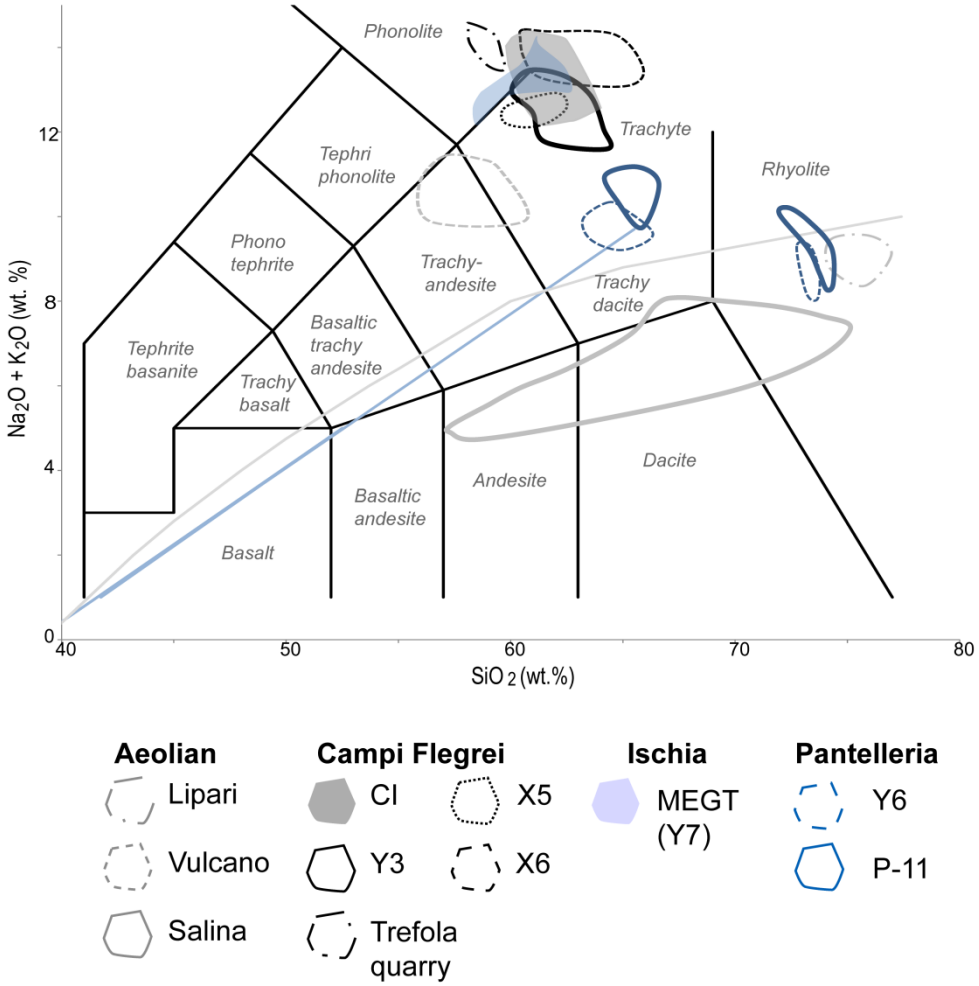

Figure 6.3. TAS plot of published, glass compositional data for the Y5, Y3, X6, X5 and the pre-CI (Tlf, Tlc and Tla; labelled Trefola Quarry) eruptions from Campi Flegrei; the MEGT (Y7) from Ischia; the Y6 and P-11 from Pantelleria; the Lower and Upper Monte Pilato (Lipari), the Palizzi A (Vulcano) and the Lower Pollara and Grey Porri Tuff (Salina) from the Aeolian archipelago (see Table 6.1 for references).

Less is known on the extent of dispersal of the pre-CI eruptions from the CVZ. These events, like the Y3, are found and chemically defined from locations away from the caldera (medial and distal deposits) as proximal deposits were likely

destroyed or buried by the subsequent CI eruption. It is believed these eruptions were highly explosive and were Plinian to sub-Plinian in character (Pappalardo et al., 1999). Glass chemical data from pre-CI deposits in the Terfola quarry; Tlf, Tlc and Tla (the latter dated to ~58.9 ± 1.8 $^{39}Ar/^{40}Ar$; Pappalardo et al., 1999) are phonolitic in composition, with SiO_2 contents of 55 to 60 wt.% and, like other Campanian tephras, have greater K_2O contents than Na_2O (Tomlinson et al., 2012b). The Trefola tephras that have been chemically characterised are easily distinguishable from the CI and Y3 on major element chemistry (see Tomlinson et al., 2012b; Figure 6.3). Additional, older eruptions from the CVZ that fit within the timeframe of this study (~125-30 ka) are the X5, X6 and Y7 (or MEGT) (Keller et al., 1978).

The X5 is a high K-trachyte (Wulf et al., 2012) and is dated to ~106-105 ka (see Table 6.1). The X5 was recently identified in Lake Ohrid, in the Balkans, by Sulpizio et al. (2010). The X6 is a phono-trachyte and glasses have CaO contents that span a wide range (1.6 to 2.1 wt. %; Wulf et al., 2012). Co-ignimbrite deposits in LGdM date this eruption to ~108.3 ± 5.4 ka (Wulf et al., 2012). The X6 is a widespread marker layer and has been found in the Ionian Sea (Keller et al., 1978), in central and southern Italy (Giaccio et al., 2012) and in the Balkans (Lake Ohrid; Sulpizio et al., 2010). The Y7 or MEGT tephra from island of Ischia (Gillot et al., 1982) dates to ~55 ka (Watts et al., 1996). This Ultra-Plinian eruption is the largest from the island (Brown et al., 2008) and has been located distally in marine records across the Mediterranean (see Narcisi and Vezolli, 1999; Keller et al., 1978; Bourne et al., 2010). Tephras from Ischia are phonolitic to trachytic in composition (e.g. Tomlinson et al., 2014b; Figure 6.3), and can be differentiated from tephras from the Campi Flegrei volcanic centre on CaO versus MgO and

Na_2O versus SiO_2 bi-plots (see Albert et al., 2014 and also Tomlinson et al., 2014b).

6.3.2. Pantelleria

Tephras from the volcanic island of Pantelleria are the 45.7 ± 1.0 ka 'Green tuff' also known as the marine Y6 tephra (Keller et al., 1978; Scaillet et al., 2013) and the P11 tephra that is dated to ~131-128 ka (Paterne et al., 2008). Both tephras are bimodal in composition, with a trachyte component with ~64-65 wt.% SiO_2 and a distinctive rhyolite component that is compositionally low in Al_2O_3 and high FeOt (~8 wt.% and 7-8 wt.%, respectively; e.g. Tamburrino et al., 2012; Figure 6.3). Both these tephras have been found distally in the Balkans (Sulpizio et al., 2010) and in the archaeological site of Theopetra Cave, Greece (Karkanas et al., 2014). The P-11 has also been found in sediments in the island of Lesvos, close to Turkey (Margari et al., 2007). Although other eruptions are known to have occurred on Pantelleria (see Tamburrino et al., 2012), the Y6 and P11 are the only known widespread layers.

6.3.3. Aeolian islands

Explosive eruptions from the Aeolian island archipelago are generally dominated by mid - to low intensity eruptions (sub-Plinian; see Albert et al., 2012a). The main phase of explosive activity commenced at ~ 80 ka and extended into the Holocene (see Table 6.1), but older activity (~200 ka) is recorded from Lipari (Crisci et al., 1991). Glass data are available from Albert et al. (2012a, b) and from three volcanic edifices: Lipari, Vulcano and Salina (Figure 6.3). The tephras generally follow a calc-alkaline to high-K calc-alkaline trend and are classified as trachy-

andesite (Vulcano) and andesite to rhyolite (Salina and Lipari; Figure 6.3). The extent of eruptive deposits from these volcanoes is unknown.

6.4. Aegean / Hellenic arc volcanoes

The Hellenic arc is composed of a number of volcanoes that have formed due to a complex subduction-related tectonics (e.g. Fytikas et al., 1984). In the Quaternary, explosive volcanism is known from the islands of Methana, Milos, Santorini, Kos, Yali and Nisyros (Druitt et al., 1999; Table 6.1 and Figure 6.1).

6.4.1. Santorini

There have been ~12 major explosive eruptions from Santorini in the last ~300 ka, all of which are calc-alkaline in composition (Druitt et al., 1999). Two of the younger eruptions from Santorini are the large Plinian event known as the Cape Riva eruption (or Y2 marker layer) that is dated to ~22 ka (see Bronk Ramsey et al., 2014) and the ~3.6 ka Z2 tephra (more commonly referred to as the Minoan eruption; Friedrich et al., 2006; Manning et al., 2006). Both these Santorini tephra layers (Z2 and Y2) have been identified in the Black Sea (Guichard et al., 1993; Kwiecien et al., 2008; Lamy et al., 2006). This is consistent with a easterly, north-easterly dispersal axis of the volcanic deposits (see Wulf et al., 2002; Zanchetta et al., 2011).

The Y2 and Z2 tephras (glass data) are calc-alkaline, rhyodacites (Aksu et al., 2008; Margari et al., 2007; Tomlinson et al., 2014a; Wulf et al., 2002; and new data, this study Figure 6.4). Glass data from the Y2 tephra have SiO_2 contents

ranging from ~64 wt.% in the proximal settings to a more evolved component ~71-72 wt.% that is also found in proximal settings and dominates in the more distal locations. The Z2 glasses have higher SiO_2 contents than those of the Y2 (72-74 wt.%; Figure 6.4), and the Y2 glasses are generally higher in CaO than those of the Z2 (>1.7 wt.%, <1.5 wt.% respectively). Both the Y2 and Z2 have Na_2O compositions that are greater than the K_2O contents.

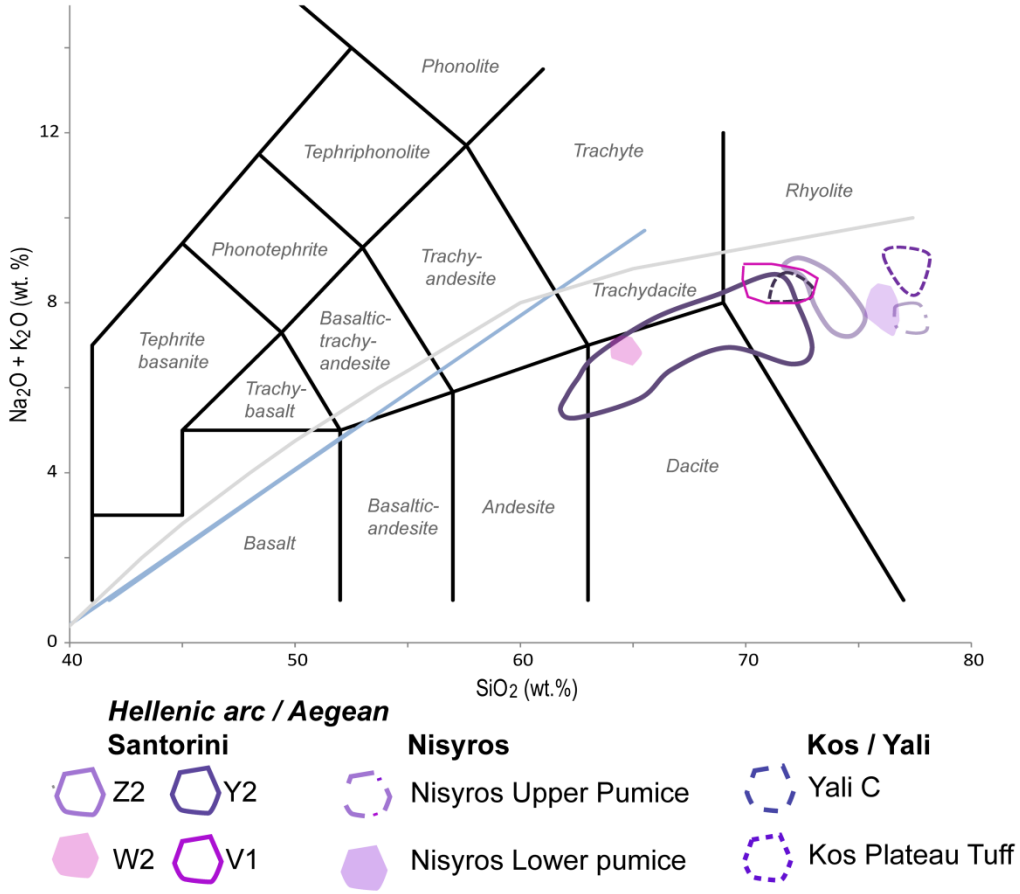

Figure 6.4. TAS plot of glass compositional data for the Z2, Y2, W2 and V1 eruptions from Santorini, the Nisyros Upper Pumice and the Nisyros Lower Pumice from the island of Nisyros, and the Yali C and Kos Plateau Tuff from the Kos and Yali volcanoes. All data are from published sources (see Table 6.1 for references) with the exception of the Z2 that was produced for this study (Appendix 1).

Older eruptions from Santorini that have published (although limited) comparable glass chemistry are the marine defined W2 and V1 tephras (Keller et al., 1978).

These eruptions have age estimates of 150 ka and 170 ka, respectively (Narcisi and Vezzoli, 1999). W2 has SiO_2 compositions of ~64-66 wt. % and is a dacite/trachy-dacite (Figure 6.4), and the V1 tephra is described as a rhyodacitic with ~71 wt. % SiO_2. Both tephras have Na_2O compositional values that are higher than the K_2O wt. % content that distinguishes tephras from Santorini from the other Hellenic arc volcanic deposits (e.g. Nisyros, Yali and Kos).

6.4.2. Nisyros

The island of Nisyros is part of the Kos-Yali-Nisyros volcanic field and is associated with a number of effusive and explosive eruptions in the Quaternary period (Di Paola, 1974; Hardiman, 1999; Limburg and Varekamp, 1991). There are two large Plinian eruptions from Nisyros known as the Upper Nisyros Pumice (UNP) and the Lower Nisyros Pumice (LNP); the former is believed to have resulted in the formation of a caldera (Di Paola, 1974; Limburg and Varekamp, 1991; Tomlinson et al., 2012a). Distal tephra deposits of the UNP have been found throughout eastern Mediterranean in both terrestrial (e.g. Karkanas et al., 2014; Magari et al., 2007) and marine sequences (e.g. Asku et al., 2008) on a northerly dispersal axis from the volcano. The date of the UNP eruption is ~47.7 cal ka BP (Limburg & Varekamp, 1991) but possibly older (>50 ka: Karkanas et al., 2014). Tomlinson et al. (2012a) demonstrated that previous reports of distal LNP deposits (e.g. Magari et al., 2007) were in fact the UNP. LNP deposits are not found in the same archives that record the UNP tephra and this either insinuates that the LNP eruption is significantly older than UNP (current age estimates are between ~161- 47 ka; Smith et al., 1996) and therefore beyond the limit of the distal archives, or that the dispersal axis was different (Tomlinson et al., 2012a).

The two eruptions can be distinguished on glass major element chemistry (Tomlinson et al., 2012a). Both tephras are high K-rhyolites, but show compositional divergence on SiO_2, Al_2O_3 and NaO_2 wt. % (Tomlinson et al., 2012a; Figure 6.4). The UNP has higher SiO_2 (76-77 wt. %) and lower in Al_2O_3 and Na_2O (11-13 wt. % and ~3.3 wt. %, respectively) than the LNP, which has SiO_2 of ~75-76 wt. % and an Al_2O_3 contents >12 wt. % (Tomlinson et al., 2012a).

6.4.3. Yali and Kos

Eruptive deposits from Yali and Kos that have been located distally are ~31 ka, Yali C (Federman & Carey, 1980) and the Kos Plateau Tuff (also known as the W3 that has an extrapolated age of ~160 ka; Narcisi & Vezzoli, 1999). The Yali C tephra is compositionally similar to the Z2, but has higher MgO and CaO values (~0.6 and ~2 wt. %, respectively; Aksu et al., 2008) with Na_2O and K_2O concentrations that are similar (~4 wt.%). Eruptive glasses from Kos are distinctive with low FeOt and very low TiO_2 and MgO (<0.6, <0.3 and < 0.04 wt. %, respectively; Aksu et al., 2008). The W3 has been found only in cores in the eastern Mediterranean, close to the volcano (Federman & Carey, 1980; Narcisi & Vezzoli, 1999), and the current known dispersals of both eruptions are limited (Federman & Carey, 1980).

6.5. Turkey (Anatolia)

Turkey, southwest of the Caucasus (Figure 6.1), contains a number of volcanoes that were active in the Quaternary. The region is tectonically complex and was formed through the interactions of three major plates, Africa, Arabian and the Eurasian, that has resulted in a number of complex continental collisions zones

and subduction zones (e.g. Deniel et al., 1998; Keskin et al., 1998; Pasquarè et al., 1988).

Turkey can be divided into three volcanic sub-regions that are characterised by the dominant magma series of their volcanic products: the Western Anatolian Volcanic Province (WAVP), the Central Anatolian Volcanic Province (CAVP) and the Eastern Anatolian Volcanic Province (EAVP) (see Figure 6.1). In the late Quaternary the EAVP and the WAVP are characterised by peralkaline volcanism (with the exception of Süphan and Ararat in the east) and magmas from the CAVP are calc-alkaline in composition (e.g. Yilmaz, 1990; Yilmaz et al., 1998). There are some glass data available for specific eruptions, but like other volcanoes, whole rock data dominates the literature (e.g. Sumita & Schmincke 2013a, Siebel et al., 2011; Yilmaz et al., 1998). A combination of glass data from specific eruptions (that have good age controls) and other glass data collected from the volcano are presented below for the Turkish data (Figure 7; Table 6.1).

6.5.1. CAVP

Many authors suggest distinct periods of volcanic activity for the CAVP (e.g., Bigazzi et al., 1993; Druitt et al., 1995; Kuzucuoglu et al., 1998; Mouralis et al., 2002). However, there are discrepancies in the ages obtained for the same eruption using different dating methods; e.g. the U/Th age of the Korudağ eruption (Acigöl) is ~24.9 ± 0.9 ka (Schmitt et al., 2011), and the obsidian fission track age is ~16.0 ± 0.3 ka (Bigazzi et al., 1993). Unfortunately, precise ages and the relative ordering of eruptions from the CAVP are not known.

6.5.1.1. Acigöl rhyolite complex

Schmitt et al. (2011) and Siebel et al. (2011) define two eruptive phases from the Acigöl rhyolite complex. The first phase ~200-150 ka (based on U/Th ages; Schmitt et al., 2011) originates from the eastern extent of the Acigöl rhyolite field producing compositionally less evolved tephra deposits with ~74-76 wt.% SiO_2 (Siebel et al., 2011; Tryon et al., 2009). The second phase occurred at ~25-20 ka (Schmitt et al., 2011) and originated in the west and produced more evolved rhyolites, ~> 77 wt.% SiO_2 (Sieble et al., 2011). There is only glass chemistry available for the Korudağ and Guneydağ (from the younger phase of Acigöl activity) eruptions (Tomlinson et al., 2014a) and the older (~200-150 ka) phase (Tryon et al., 2009; Figure 6.5 and 6.6). The more evolved, younger tephras (Korudağ and Guneydağ) have distinctively low CaO compositional values (< 0.4 wt. %) that distinguish these young Acigöl glasses from other CAVP tephras (Figure 6.6). The older tephras from Acigöl have CaO glass contents between 0.8 and 1 wt.%, and combined with FeOt contents (0.7-1.4 wt.%) can be differentiated from other CAVP products (Figure 6.6).

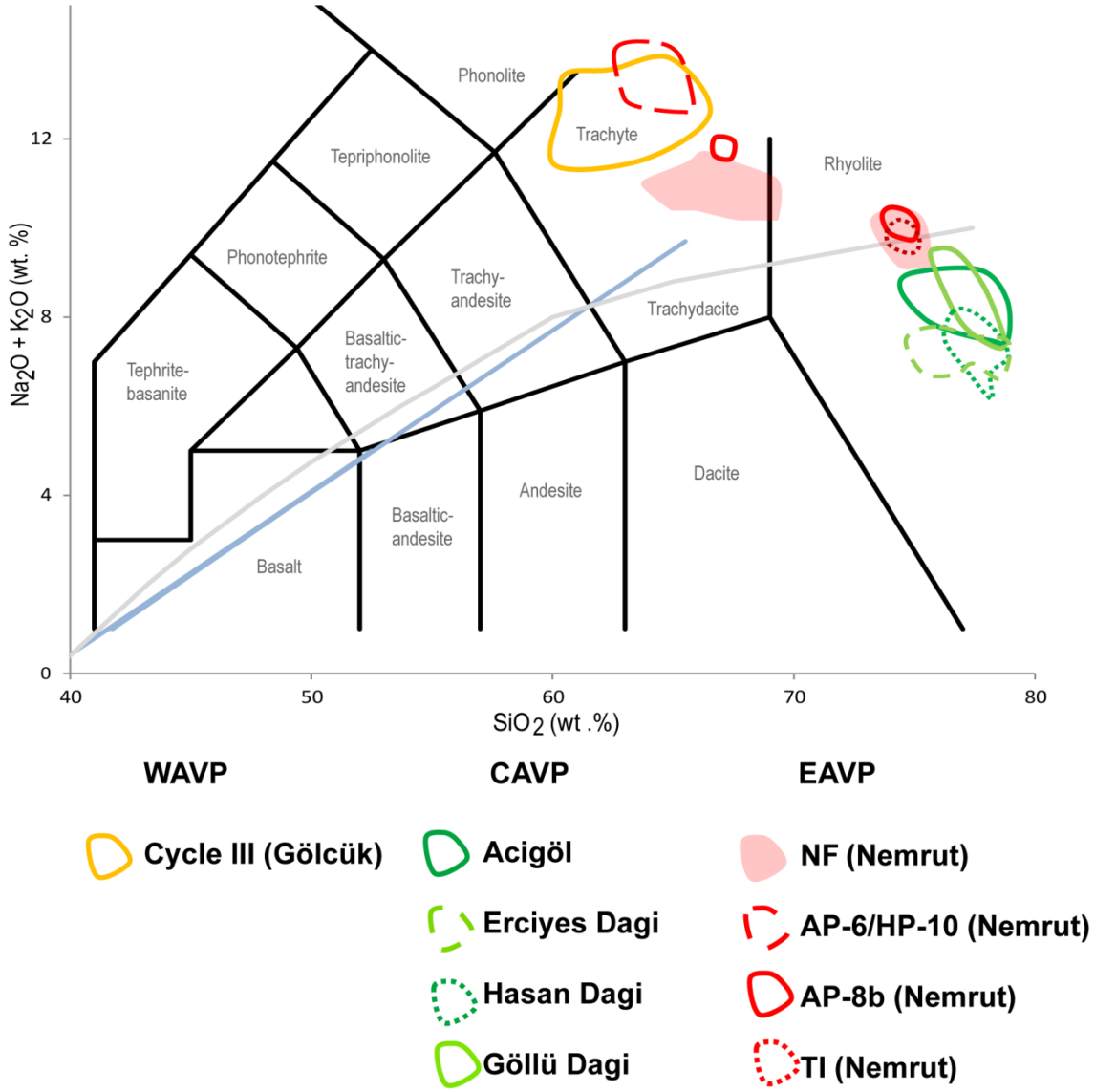

Figure 6.5. TAS plot of glass compositional data collected from published sources for the CAVP (Acigöl, Erciyes Dagi, Hasan Dagi, Göllü Dagi), WAVP (Gölcük volcano) and the NF (Nemrut Formation tephra), Nemrut, Turkey. See Table 6.1 for references. New compositional data for the Tatvan Ignimbrite (TI), Ahlat Pumice 6/Halepkalesi Pumice 10 (AP-6/HP-10) and the Ahlat Pumice 8b (AP-8b) from the Nemrut volcano was produced in this study, see Appendix 1 for full data.

6.5.1.2. Hasan Dagi and Erciyes Dagi

Hasan Dagi and Erciyes Dagi are the only stratovolcanoes in the CAVP. Both are thought to have a long eruptive history that continued in the Quaternary (e.g. Deniel et al., 1998; Innocent et al., 1975; Sarikaya et al., 2006; Schmitt et al., 2014). However, there is limited chronological data and glass compositional data

from both these volcanoes. The only EPMA glass data available from Erciyes Dagi is from three Holocene eruptions – the Karagüllü, Perikartini and Dikkartin (Hamann et al., 2010; Tomlinson et al., 2014a). Volcanic glasses from the Karagüllü and Perikartini eruptions both have SiO_2 contents that are between ~75-78 wt.%, high CaO contents (>1 wt.%), and similar Na_2O and K_2O contents of ~3.5 wt.% (Hamann et al., 2010; Tomlinson et al., 2014a). The known dispersal of the Karagüllü and Perikartini eruptions is limited and stratigraphic relationship between these tephras is not clear in the literature. Age estimates for the Karagüllü and Perikartini are 9971-9594 cal ka BP and 9984-9596 cal ka BP (charcoal) with lava ages (cosmogenic radionuclides, ^{36}Cl) that range from ~10.3 to 7.3 ka (Sarikaya et al., 2006). A third eruption, Dikkartin (~8.8 cal ka BP,^{14}C on planktonic foraminifera; Hamann et al., 2010) has lower SiO_2 contents (~75-76 wt.%) than glasses from the Karagüllü and Perikartini eruptions. Distal deposits of Dikkartin have been found in the Levant, suggesting a southerly dispersal (Hamann et al., 2010).

Glass data indicate that Hasan Dagi volcano erupts calc-alkaline rhyolites (Tyron et al., 2009; Figure 6.5), but whole-rock data indicate that andesite and dacite have also been erupted in the Quaternary (Deniel et al., 1998). Glass shards from Hansen Dagi and Erciyes Dagi have indistinguishable SiO_2 contents (~75-78 wt.%) but have different CaO contents - Hasan Dagi has 0.9-1 wt.% and Erciyes Dagi has 1-1.6 wt.% (Figure 6.6).

6.5.1.3. Göllü Dagi

Göllü Dagi is situated between the Acigöl and Hasan Dagi volcanic fields (Figure 6.1). Activity of this volcano is thought to have commenced ~1.5 Ma (Mouralis et al., 2002) and extended into the late Quaternary, but very little is known. Glass compositions of Göllü Dagi tephra are calc-alkaline rhyolites, with distinctive CaO compositions of 0.5-0.8 wt. % (Figure 6.6; data from Tryon et al., 2009).

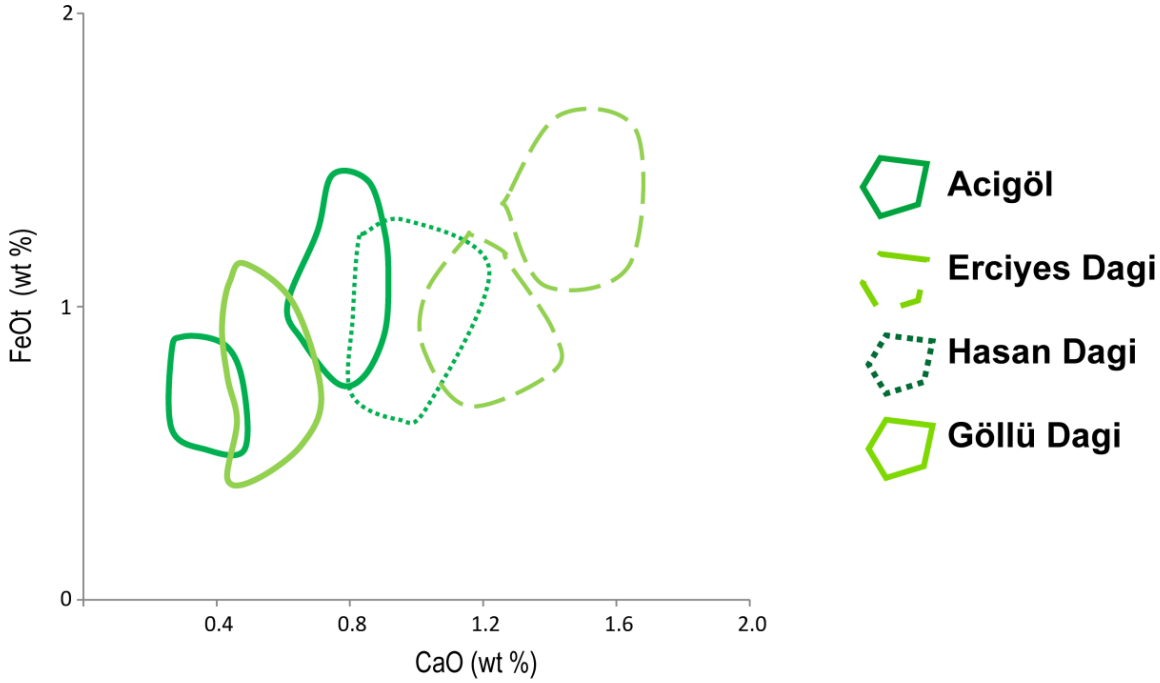

Figure 6.6. FeOt vs CaO bi-plot of glass compositions from the CAVP calc-alkaline volcanoes.

6.5.2. WAVP

Gölcük volcano is situated in southwest Turkey and had three main eruptive phases in the Quaternary: Cycle I, a major caldera forming event ~200 ka, Cycle II, that occurred between 115 ± 3 ka and 62 ± 2 ka, and a final phase (Cycle III) of explosive activity between 72.7 ± 4.7 ka and 24 ± 2 ka ($^{40}Ar/^{39}Ar$ dates from Platevoet et al., 2008). Only glass compositional data from Cycle III eruptions are

published (Tomlinson et al., 2014a). Glasses are peralkaline and trachytic with SiO_2 compositions that range from 63 to 65 wt.% with Na_2O and K_2O contents that are similar (~6-7 wt.%; Tomlinson et al., 2014a; Figure 6.5). Cycle III is thought to be associated with several highly explosive, phreatoplinian eruptions with an axis of dispersal to the north and northeast, but the extent of tephra dispersal is unclear (Platevoet et al., 2008).

Kula volcano (Figure 6.1) is also found in the WAVP and has volcanic products that are SiO_2 poor, alkaline basalts (~40-50 wt. %; whole rock data, Tokçaer et al., 2005). These magmas would have only fuelled small eruptions that would have not dispersed tephra far from source. In addition, there is no comparable glass data for the deposits so the activity from this volcano is not discussed further.

6.5.3. EAVP

Nemrut, Süphan, Tendürek and Ararat are the major volcanic centres that form part of a long (~220 km) chain of Quaternary volcanoes that extends across eastern Anatolia (e.g. Yilmaz et al., 1998; Figure 6.1). The glass compositions of tephra from these volcanoes span a wide compositional range. Those from Ararat and Süphan are calc-alkaline, while Nemrut and Tendürek erupt predominantly peralkaline compositions (e.g. Sumita and Schmincke 2013a & b; Yilmaz et al., 1998).

6.5.3.1. Nemrut

The historically active Nemrut volcano, situated close to Lake Van, has been active for the last ~400 ka (Sumita and Schmincke 2013a & b; Yilmaz et al., 1998).

One of the largest eruptions from Nemrut, the Nemrut Formation tephra (NF, as defined by Sumita & Schmincke, 2013) occurred at ~30 ka and formed the present caldera. The glass compositions of the three phases of the NF are different: the initial plinian fallout (lower NF; L-NF) erupted peralkaline rhyolite (~74 wt.% with high FeOt; 3.8-4.2 wt.% and Al_2O_3 concentrations ~11 wt.%), the middle phase (Middle NF; M-NF) is rhyolitic to trachytic (with an ignimbrite rhyolitic flow deposit with ~12 wt. % Al_2O_3), and the pyroclastic density current (PDC) and a final fall and surge deposits (Upper NF; U-NF) produced darker and denser deposits with SiO_2 contents that range from 64 to ~68 wt.% and have ~16 wt.% Al_2O_3 (see Sumita and Schmincke 2013 a, b and Figure 6.6 and Figure 6.7). This large caldera eruption has an easterly dispersal axis.

Older peralkaline eruptions from Nemrut are the alkaline, rhyolitic Tatvan Ignimbrite (TI) $^{40}Ar/^{39}Ar$ dated to 45.1 ± 2.1 ka, the Ahlat Pumice 8b (AP-8b) tephra ($^{40}Ar/^{39}Ar$ age of 59.4 ± 10 ka) that also has a trachyte component and the trachytic Halepkalesi Pumice 10/ Ahlat Pumice 6 (HP-10/AP-6) tephra (61.60 ± 2.55 ka). New glass data from these eruptions has been produced as part of this study (Figure 6.5 and 6.7, and Appendix 1). The TI and the AP-8b rhyolites are indistinguishable from each other on major element glass chemistry, and both have very homogeneous SiO_2 contents (~74.02 to 74.82 wt. %) and are high in FeOt (~3.9-4.28 wt. %; Figure 6.5 and 6.7). One data point from AP-8b is trachytic, with 66.96 wt. % SiO_2 and 15.10 wt. % Al_2O_3 (the AP-8b and TI rhyolites have Al_2O_3 contents ~10 wt. %; Figure 6.7). Glass shards from the AP-6/HP-10 tephra are trachytic with SiO_2 contents between ~63-64 wt. % and they have higher Na_2O contents than K_2O (~7.8-8.5 wt. %, ~4.88–5.46 wt. %; respectively).

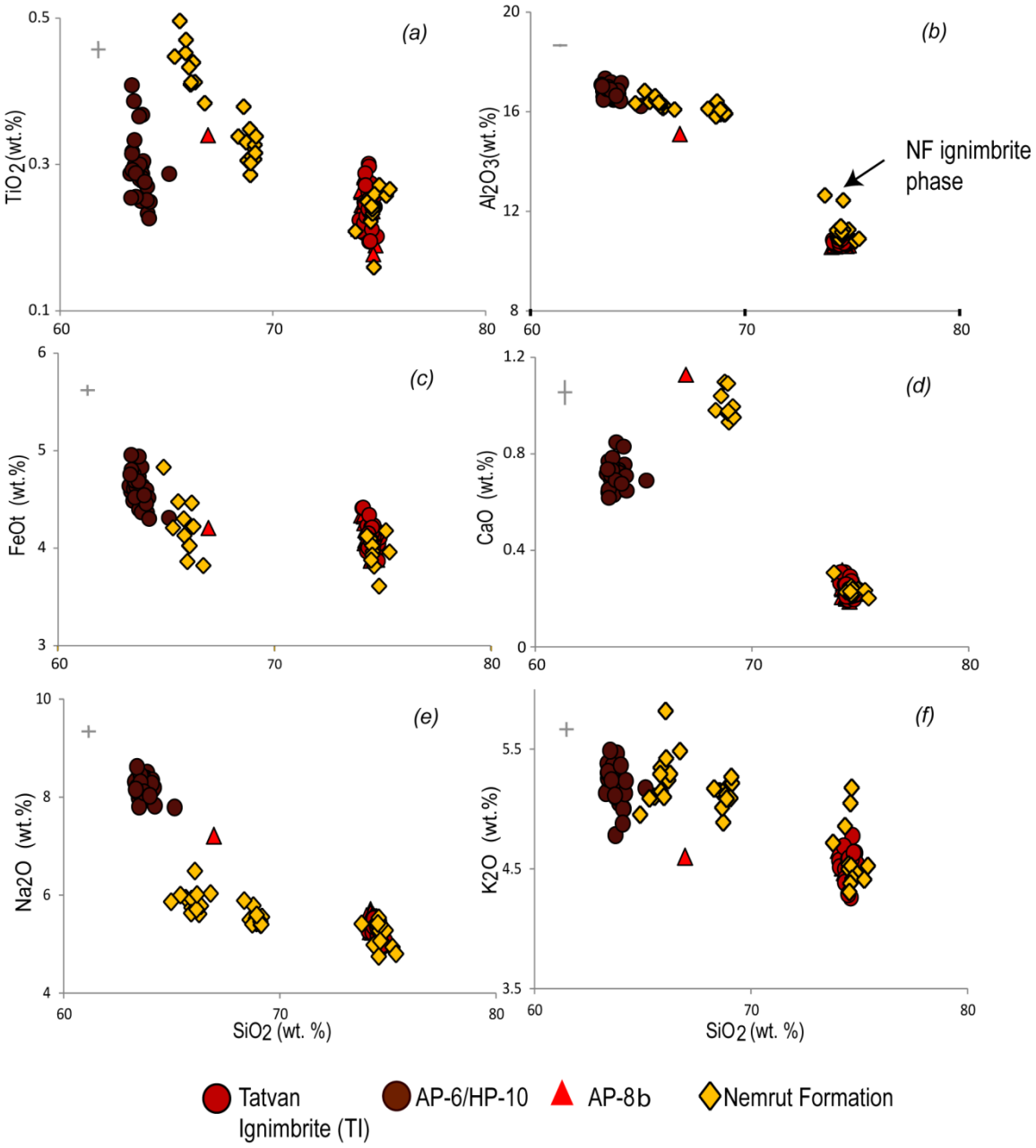

Figure 6.7. Glass compositional data from the AP-8b (~59 ka), AP-6/HP-10 (~61 ka), and the ~45 ka TI tephra from Nemrut volcano (a-f). Samples courtesy of Sumita and Schmincke, pers comms (2014). NF Trachyte is distinct from the other Nemrut tephras (a-f) (data from Sumita & Schmincke, 2013a, b). The NF rhyolite glasses can be differentiated from the other Nemrut rhyolites by the higher Al_2O_3 (~12 wt.%; b) concentrations from the ignimbrite phase of the eruption (MNF). Errors are 1 σ.

Other eruptions have been identified from Nemrut (see Sumita and Schmincke, 2013 a, b) but only average, X-ray fluorescence (XRF) glass chemical data for

these are currently available (Sumita & Schmincke 2013a & b). Sumita & Schmincke (2013a) also produced limited XRF glass chemical data on rhyolitic glasses from Süphan volcano. These glasses have SiO_2 contents of ~71-74 wt. % and have lower TiO_2 and FeOt contents than the younger Nemrut rhyolites (~0.07-0.25 and 1.38-2.56 wt. %, XRF data corrected for LOI; Sumita & Schmincke 2013a).

6.5.3.2. Süphan, Tendürek and Ararat

Only whole rock data is available for the remaining EAVP volcanoes; Süphan, Tendürek and Ararat (e.g. Pearce et al., 1990; Yilmaz et al., 1998). Süphan, Tendürek, and the two volcanoes that form Ararat were all active in the Quaternary, with the last known activity from each in the late glacial and Holocene (e.g. Pearce et al., 1990; Yilmaz et al., 1998). Sumita & Schmincke (2013a) identify Süphan tephras inter-bedded with young Nemrut tephras, but no further age information is provided, and the stratigraphic relationships are unclear. Activity is believed to be Plinian and sub-plinian in character (Yilmaz et al., 1998) and whole rock data from Pearce et al. (1990) and Yilmaz et al. (1998) suggest compositional differences between these volcanic centres. Tendürek is peralkaline and erupts mainly trachy-andesite, trachytic to phonolitic products, whereas Süphan and Ararat magmas are calc-alkaline, with basaltic–andesitic and trachy-dacitic to rhyolitic compositions (Pearce et al., 1990; Yilmaz et al., 1998).

6.6. Romania

6.6.1. Ciomadul Volcano

The Carpathian-Pannonian region in Romania contains a number of volcanic centres have been active over the last 20 Ma years (Pécskay et al., 2006). The

centre that has experienced activity in more recent times is the Ciomadul volcano (see Harangi et al., 2010; Szakács et al., 2002 and references within; Figure 6.1). Ciomadul is located on a 100km long volcanic chain in the East Carpathians and produced calcalkaline volcanic products (Harangi et al., 2010). Szakács et al. (2002) suggest volcanism from Ciomadul started ~1 Ma ago, and the final two eruptions have been radiocarbon dated to ~29.5 ± 0.3 ka cal BP (Bixad pyroclastic flow) and ~41.3 ± 1.0 ka cal BP (charcoal date from volcanic deposits at Tusand; Harangi et al., 2010). Harangi et al. (2010) suggest that tephra from the Ciomadul volcano are high K-dacites and rhyolites (bulk compositional data on rocks and groundmass pumices), and that tephras from older (Tusand) eruption are generally more silicic than the younger Bixand eruption.

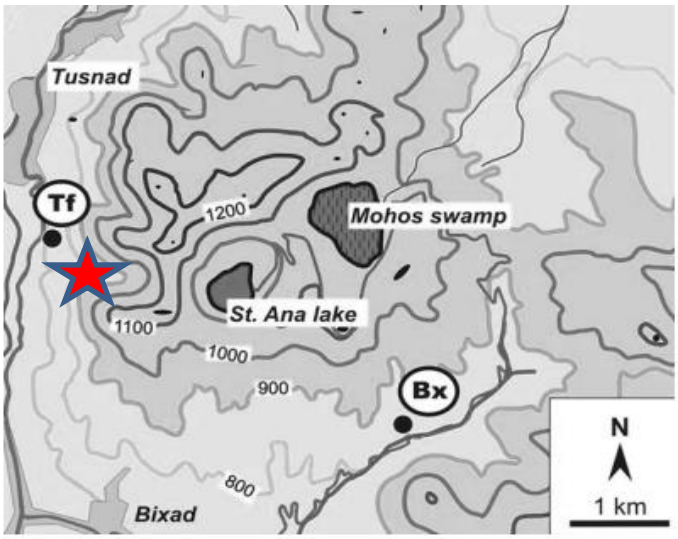

Figure 6.8. Topographical map of the Ciomadul volcano. Bx (Bixad) and Tf (Tusnad) are the locations of samples taken for ^{14}C dating by Harangi et al. (2010). Red star is location of pumice samples analysed in this study (ROM_C).

New, unpublished glass and radiocarbon data (Wulf and Veres, pers comms, 2014) corroborate conclusions from Harangi et al. (2010). Single grain, glass data from the older tephras (re-dated to ~ 44.5- 41.7 ka cal BP) are generally more evolved with SiO_2 compositions of ~74-78 wt. % (Figure 6.9). Glasses from the younger eruption (~ 33.1- 30.7 ka cal BP) are less evolved; 71-75 wt. % SiO_2

(Figure 11; Wulf and Veres pers comms, 2014). These are likely to represent the same two events as described by Harangi et al. (2010) but have been re-named as the Younger Turia and Older Turia by Wulf and Veres (pers comm*;* 2013). Limited glass data was produced in this study from pumices that were collected northwest of the St Ana crater (samples collected by Prof. M. Menzies; Figure 6.8) and have SiO_2 contents between ~ 73-75 wt. %, with ~1.7 wt. % CaO and are low in FeOt (0.6-0.9 wt. %). This is consistent with the Older Turia (Tusand) population (Figure 6.9). How far tephras travelled from both these eruptions is unknown but is presumed not far and further more detailed analysis of the tephras is ongoing.

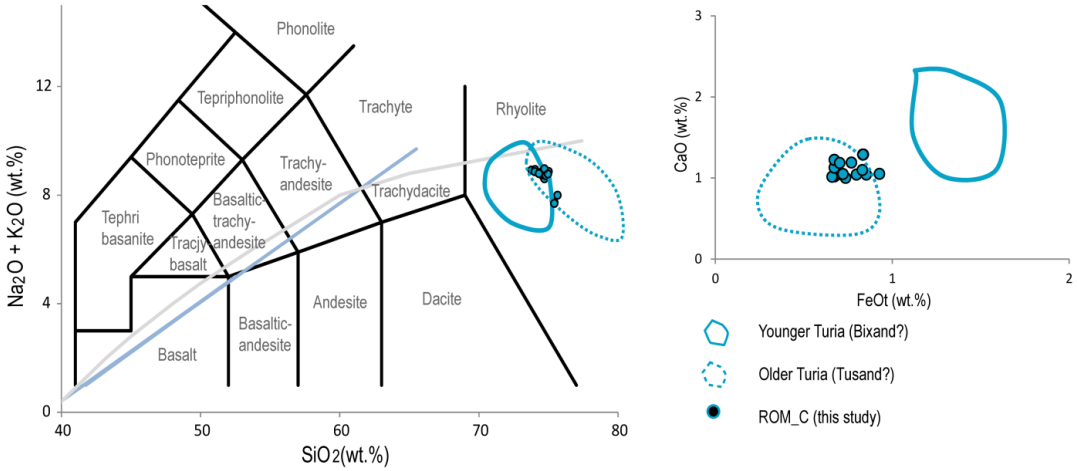

Figure 6.9. Glass compositions of the Younger Turia and Older Turia eruptions from Ciomadul Volcano (data from Wulf & Veres, pers comms., 2014).

6.7. The Caucasus

Quaternary volcanism in the Caucasus is thought to have started at ~1.5 Ma with sporadic activity across the region, some of which continued through into the Holocene (e.g. Karakhanian et al., 2002, 2003; Lebedev et al., 2011a; Figure 6.10). Much of the recent work in the region has focused on dating volcanic rocks to establish phases of activity for volcanic hazard assessments (e.g. Karakhanian et al., 2003; Lebedev et al., 2013) and producing whole rock geochemical data for

volcanoes (e.g. Lebedev et al., 2013). There has been considerably less attention paid to constructing individual eruption histories of the volcanoes or mapping the distribution of tephra products; therefore a tephrostratigraphy for the Caucasus region is lacking.

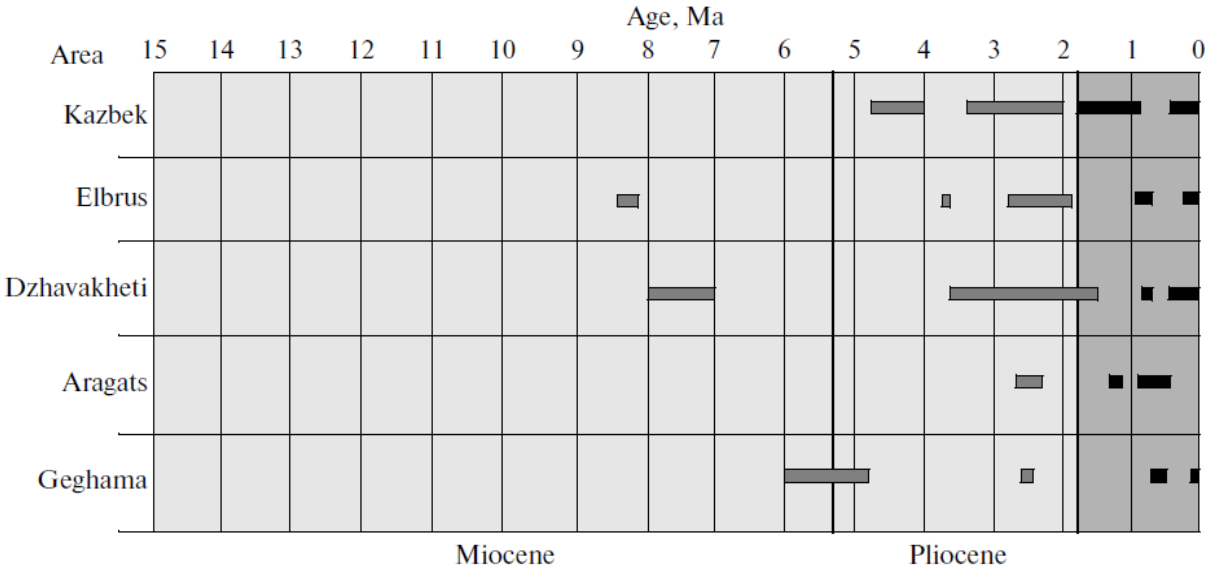

Figure 6.10. Approximate phases of volcanism across the Caucasus. Image after Lebedev et al. (2011a).

Glass data for some eruption deposits in the region are available, but these are only for obsidians (lava domes or flows) with data analysed using neutron activation analysis (NAA), LA-ICP-MS and XRF. These data are commonly used to elucidate sourcing of raw material for stone tool production in the past (e.g. Chataigner & Gratuze, 2014; Le Bourdonnec et al., 2012). These data is not of much use for tephrostratigraphy as lavas are not necessarily associated with explosive, tephra-generating eruptions or widely dispersed. Furthermore, the analytical techniques used to characterise obsidians typically produce data that are not as precise as those required for characterising tephra deposits.

6.7.1. Armenia

Adjacent to the WAVP is the Lesser Caucasus Volcanic Province (LCVP) in Armenia. Volcanism in the region is controlled by the same continental collisions as the EAVP (e.g. Artyunyan et al., 2007; Lebedev et al., 2011a). The LCVP is divided into six volcanic areas: Erusheti-Arsiani, Javakheti regions (both northwest Armenian, on the border with the Republic of Georgia) and Aragats, Geghama volcanic range, Vardenis volcanic range and the Syunik volcanic range (in southeast Armenia; Artyunyan et al., 2007).

Activity started at these centres in the Miocene and some have continued to be active into the Holocene (e.g. Karakhanian et al., 2002; 2003; Figure 6.10). Quaternary volcanism in Armenia is characterised by eruptions along fissures producing long lava flows (e.g., lava flows in the Hrazdan river gorge); central vent eruptions that formed large stratovolcanoes (e.g., Aragats); and monogenetic fields with small cones (e.g., on the western and northern slopes of Aragats; see Karakhanian et al., 2003). Quaternary volcanic deposits from the region have calc-alkaline whole-rock compositions that range from basaltic through to rhyolitic in composition, and mildly acidic compositions that are predominantly basaltic-trachy-andesite to trachy-andesite dacite (e.g. Arutyunyan et al., 2007; Karakhanian et al., 2003).

6.7.1.1. The Geghama volcanic range and Gutansar volcano

The only glass data from tephra deposits in Armenia is from the limited proximal work on Gutansar volcano produced in this study. Tephra deposits (fall and flow) from the Gutansar volcano (close to the archaeological site of Lusakert, see Figure 6.11) were identified, and subsequently subsampled in the Geghama

volcanic range (Figure 6.12; Table 6.2). In the Quaternary, the Geghama range (that is composed of ~100 small to middle sized volcanoes that cluster in the east, west and central area of the range; Karakhanian et al., 2003) has had five known phases of activity from ~700 ka to <50 ka and possibly during the Holocene (see, Table 6.1; Arutyunyan et al., 2007; Karakhanian et al., 2003; Lebedev et al., 2013). The Gutansar cone (one of 14 in the western cluster of the Geghama range) was formed in first phase of activity (~700 ka). Activity across the Geghama range peaked at ~200 ka, when there were more explosive eruptions (Arutyunyan et al., 2007) and is thought to continue till >50 ka (Lebedev et al., 2013). There are no precise dates for the volcanic activity from the Gutansar volcano.

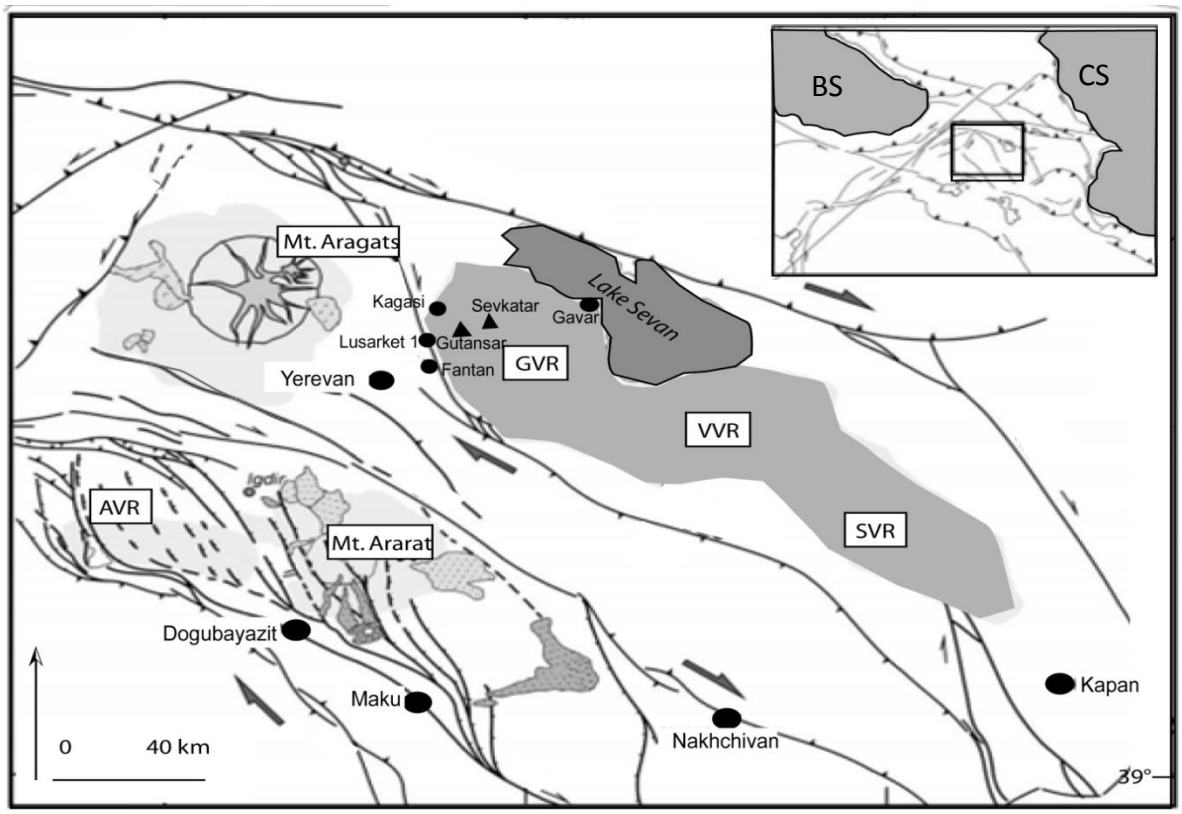

Figure 6.11. Map shows active faults and volcanic ranges in Armenia that borders Turkey. GVR, Geghama Volcanic Range; VVR, Vardeniss Volcanic Range; SVR, Siunik Volcanic Range; AVR, Agri Dag Volcanic Range (Turkey); BS, Black Sea; CS, Caspian Sea. Gutansar is located in the GVR, and is close to the Lusakert 1

archaeological site. See Karakhanian et al. (2002) and Arutyungan et al. (2007) for further details.

Samples were collected from a large ~40 meter banded fall deposit from the side of the Gutansar volcano, and an additional ash sample was taken from a pyroclastic block and ash flow deposits that was associated with obsidian lava flows (the latter is also believed to be associate with Gutansar; Frahm pers comms, (2013; Figure 6.12, Table 6.2).

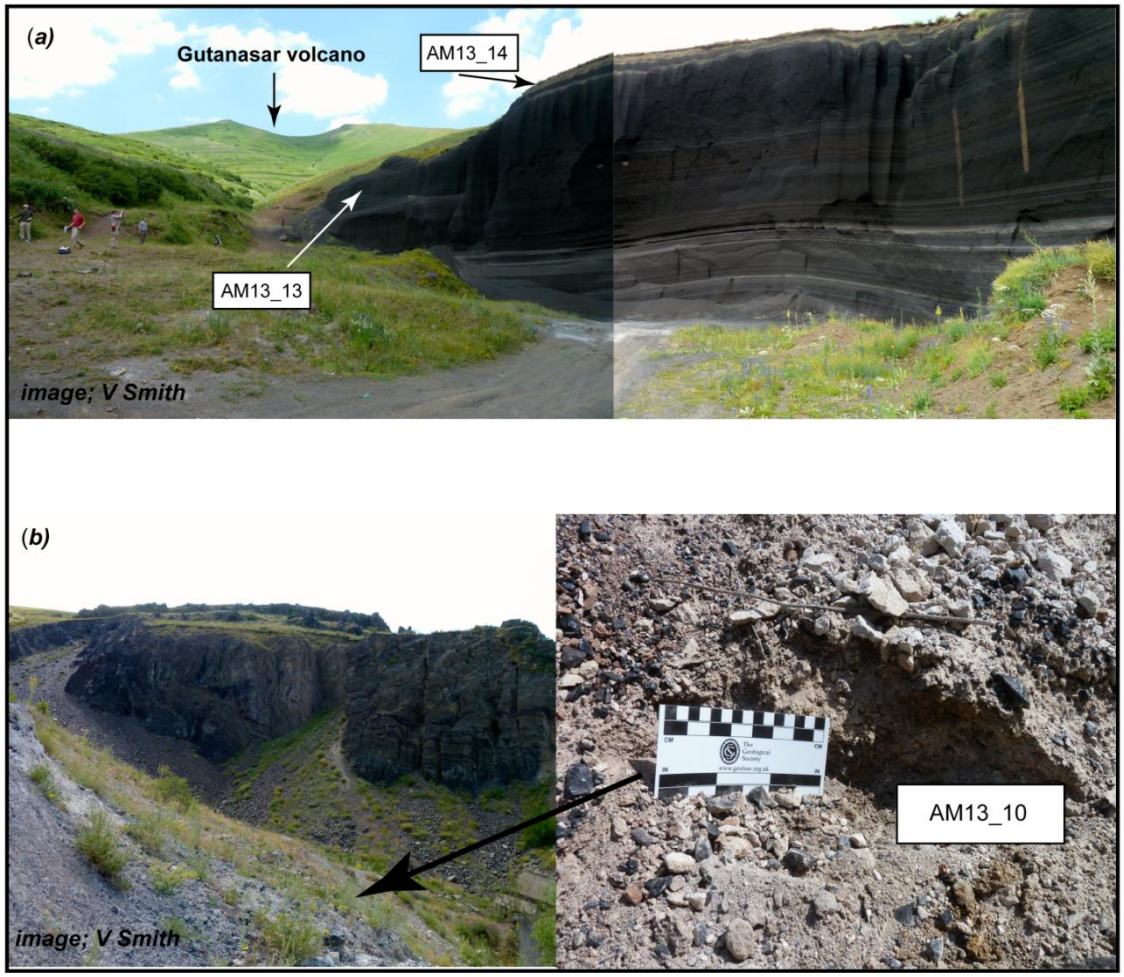

Figure 6.12. (a) ~40 m banded fall deposits exposed close to Gutansar volcano (seen in the background). Sample AM13_14 was taken from a lighter 'yellowish' band of tephra that was at the top of the darker, mafic fall deposits and AM13_13 was taken from the top of the dark fall deposits. (b) shows a block and ash flow deposit from the Gutansar volcano (Frahm pers comms, 2013) where sample AM13_10 was collected. Images V. Smith.

Table 6.2. Proximal samples collected from Gutansar volcano

Sample code	Volcano	Sampling grid reference	Sampling location	Details
AM13-10	Gutansar 44 69'30"N, 47 46'59"E	40 22'37" N, 44 36'36"E.	Pyroclastic block and ash flow (Figure 16b); Close to pipes from hydroelectric station. ~4 km from Lusakert 1 (SW direction)	Block and ash flow off the front of banded obsidian rich lava flow. Lave shows dark black and large oxidised bands in flow. Poorly sorted matrix component (mostly ash) was collected.
AM13-13	Gutansar 44 69'30"N, 47 46'59"E	44 69'30"N, 47 46'59"E.	Quarry at the base of the Gutansar volcanic cone (Figure 16a). Sample taken from top ~8 m of mafic fall deposit.	Thick (~30 m) outcrop of bedded, dark fall deposit at the base of the Gutansar volcanic cone (Figure 16). Middle of the section is comprised of well to poorly sorted beds (thin grey layers). Top of sequence well sorted mafic fall deposits.
AM13-14	Gutansar 44 69'30"N, 47 46'59"E	44 69'30"N, 47 46'59"E.	Quarry at the base of the Gutansar volcanic cone (Figure 16a). Light yellow fall deposit on top of dark mafic fall deposit (Figure 16a)	Moderately sorted tephra deposit, ~2 m thick. Fall is on top of dark banded fall deposit. Different eruptive event. Sandy yellow in colour. Possible alteration?

The EPMA results of glass shards from the two fall samples (AM13_13 and AM13_14; see Figure 6.12) are compositionally identical. They are both basaltic-trachy andesite to trachy-andesite with SiO_2 contents between ~54-56 wt. % and are both high in CaO and FeOt (~6 wt. % and ~8 wt. %, respectively; Figure 6.13). Glass shards from the block and ash flow deposit (AM13_10; Figure 6.12, Table 6.2) are calc-alkaline rhyolites with ~74-75 wt.% SiO_2, Na_2O and K_2O contents of ~4 wt.%, and low CaO contents (~0.9-1.07 wt. %; Figure 6.13).

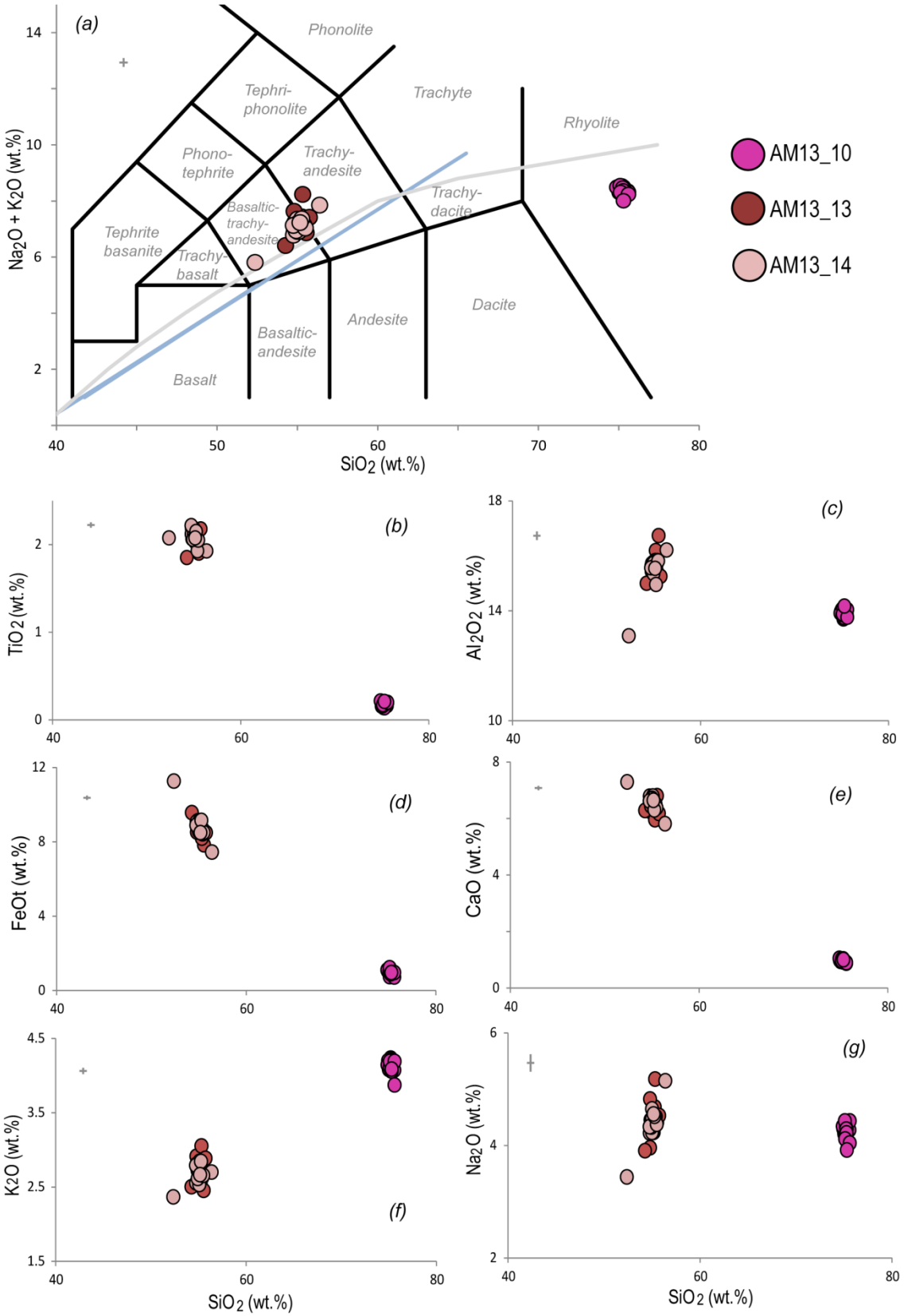

Figure 6.13. Glass compositions of tephra exposed close to Gutansar volcano (a-g).

Volcanic deposits from volcanoes in the Geghama range have been found associated with archaeological deposits. For example, sediments located south of the town of Gavar (~30 km from Lusakert; see Figure 6.11) that contained Mousterian, obsidian tools where 'capped' by a lava flow thought to derive from the eastern volcanic cluster (Karakhanian et al., 2003). A charcoal sample from this sediment layer has a date of ~35.1 – 33.3 ka cal BP (Karapetian, 1983 [cited in Karakhanian et al., 2003]). Karakhanian et al. (2003) also describe lava flows from the central cluster (possibly Sevkar volcano, 14 km east of Lusakert 1 rock shelter) that overlie the Mousterian site of Kapoutan found by Karapetian (1983) but no age estimates are given for the site or the lava flow. However, this suggests frequent volcanic activity in the Geghama range in the time frame of this study, but there are no details on the explosive activity or the archaeological sites mentioned in Karakhanian et al. (2003).

6.7.2. Georgia

6.7.2.1. The Dzhavakheti volcanic range

K-Ar and Rb-Sr dating of lavas from the Dzhavakheti volcanic range (southern Georgia) suggest there are three phases of activity: ~8 to 7 ma; 4 to 2 Ma (that is associated with the emplacement of hominids at the site Dmanisis; Ferring et al., 1996) and a final Quaternary phase at ~800-50 ka (Lebedev et al., 2004a). Evidence of activity in the centre of the range also extends into the Holocene (Lebedev et al., 2004a). The youngest, Quaternary phase is mainly composed of calc-alkaline volcanism, with dacitic products predominating (SiO_2 64-72 wt%; whole rock data; Lebedev et al., 2004a). The extent of any tephra deposits is not discussed.

6.7.3. The Greater Caucasus range

There are two stratovolcanoes on the Greater Caucasian range, Elbrus (SW Russia) and Kazbek (Georgia), that have both remained active into the Holocene (Figure 6.1; Figure 6.10). Quaternary activity of the Elbrus stratovolcano commenced activity at ~900 ka, with later activity taking place in three phases: 225- 170, 110- 70 and >35 ka (Chernyshev et al., 2002; Lebedev et al., 2010; 2011a). The latter two stages of activity produced calc-alkaline dacitic and rhyolitic volcanic products (based on whole rock data). The Kazbek volcanic field extends both sides of the Greater Caucasian range. The modern Kazbek volcano formed in the caldera of the Paleo-Kazbek (~250 to 180 ka) and is associated with small scale volcanic activity from ~70 to 6 ka (Chernyshev et al., 2002; Lebedev et al., 2011a and references within). The volcanic products are trachy-andesite to dacite (whole-rock data; Lebedev et al., 2011a) and there is little information on the dispersal of any explosive deposits.

A third volcanic cluster is the explosive Keli volcanic centre (Figure 6.1), that is located between the two stratovolcanoes, part of the Kazbek neovolcanic area (Lebedev et al., 2004b). Activity has been recorded between 245- 170, 137 to 70 ka, with a second phase of activity (smaller eruptions) commencing at <30 ka (Lebedev et al., 2011a,b). Whole-rock data indicate that the volcanic products are calc-alkaline (andesitic/trachy-andesitic to dacitic) in composition (e.g. Lebedev et al., 2004b; 2007; 2008; 2011a, b) and are unlikely to be far travelled given the low viscosity of these magma compositions and the lack of water/ice to enhance the explosivity of the eruption. There are also a number of other volcanic edifices on the Greater Caucasus range. Volcanic activity from these includes lava flows and small fissure eruptions through to more explosive volcanism (see Chernyshev et

al., 2002; Lebedev et al., 2011a). There is little information on these and there is no single grain glass compositional data for any volcanic deposits in the region.

6.8. Summary of chapter; what can we expect to find?

Tephras that could be found in the Caucasus and the southeast Black Sea are from both the peralkaline and calc-alkaline centres. The most common composition is calc-alkaline rhyolites. Rhyolites tend to be associated with highly explosive eruptions, due to the high viscosity of the felsic magma, and therefore widely dispersed (e.g. tephra from the Vedde ash, Iceland, was found in lacustrine sediments in Slovenia; Lane et al., 2011a). Rhyolitic tephras in the Caucasus and the Black Sea could be from a number of volcanic centres, including Turkey and the Caucasus and those from more distal volcanoes, e.g. Nisyros and Santorini (in the Hellenic arc), Ciomadul (Romania) and possibly Pantelleria. Distinguishing rhyolites from different volcanic centres is possible using the major element glass compositions (e.g. Figure 6.14). The eruption history and the range of geochemical compositions erupted from centres within the Caucasus and Turkey is not well constrained.

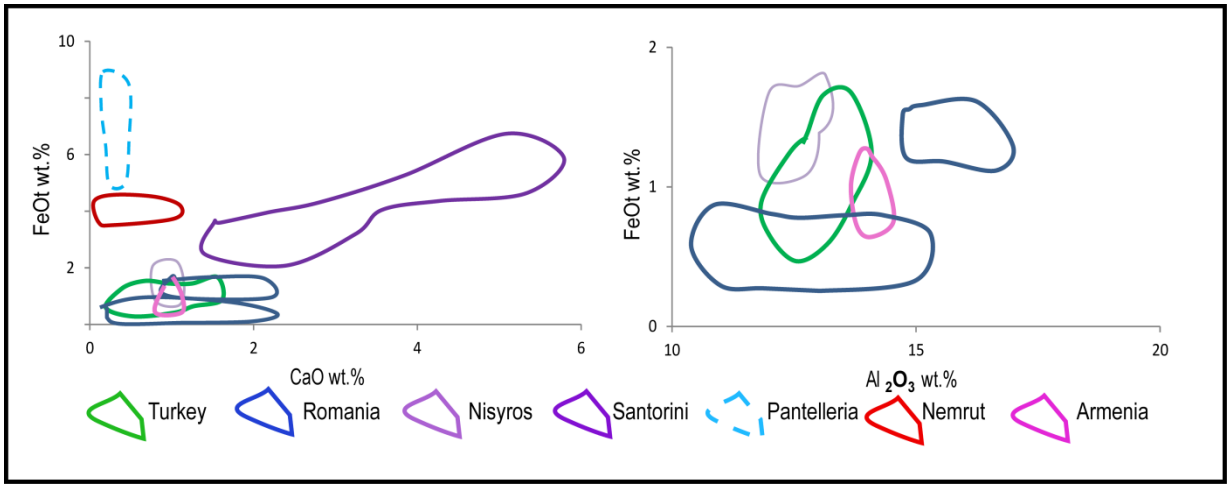

Figure 6.14. Glass compositions of rhyolitic tephras in different volcanic regions. See Table 6.1 for references of data sources.

Trachytic tephras from the Italian centres (e.g. the CI, Y3, X5, X6 and Y7) derive from explosive eruptions and are commonly found across the Mediterranean. As such, tephras from some of these eruptions could be found in the southeast Black Sea and possibly as far as the Caucasus. It is highly probable that the CI would have been dispersed in the Caucasus as it is found in Russia (Kostenki; Pyle et al., 2006) and is consistent with one of the modelled dispersal predictions by Costa et al. (2012). Trachyte (and peralkaline rhyolites) tephras from Nemrut are also highly likely to be preserved in the Caucasus given its proximity to the region and frequency of eruptions (e.g. Sumita and Schmincke; 2013a, b). However, Nemrut is east of the Black Sea and wind dispersal is normally west to east so the tephra may not be found in the Black Sea.

The least evolved tephras (e.g. basaltic - trachy-andesite) are less likely to be far travelled, because eruptions associated with these glass compositions tend to be less explosive. Therefore, discovery of tephra with less evolved compositional values imply that these tephras are from more proximal to medial sources, e.g. volcanoes in Armenia and the on the Greater Caucasus range and possibly some

centres in the EAVP (e.g. Tendürek and Ararat?). The dispersal and the size of these explosive eruptions is not well documented in the literature.

Chapter 7

Tephrostratigraphy of the M72/25-GC1 Black Sea core

7.1. Introduction

The following chapter presents the results from a cryptotephra investigation of the M72/5-25-GC1 core that was extracted from the southeast Black Sea. Environmental reconstructions based on proxy data (pollen, $CaCO_3$ and IRD) and the current age model for the core has been discussed in section 4.4.

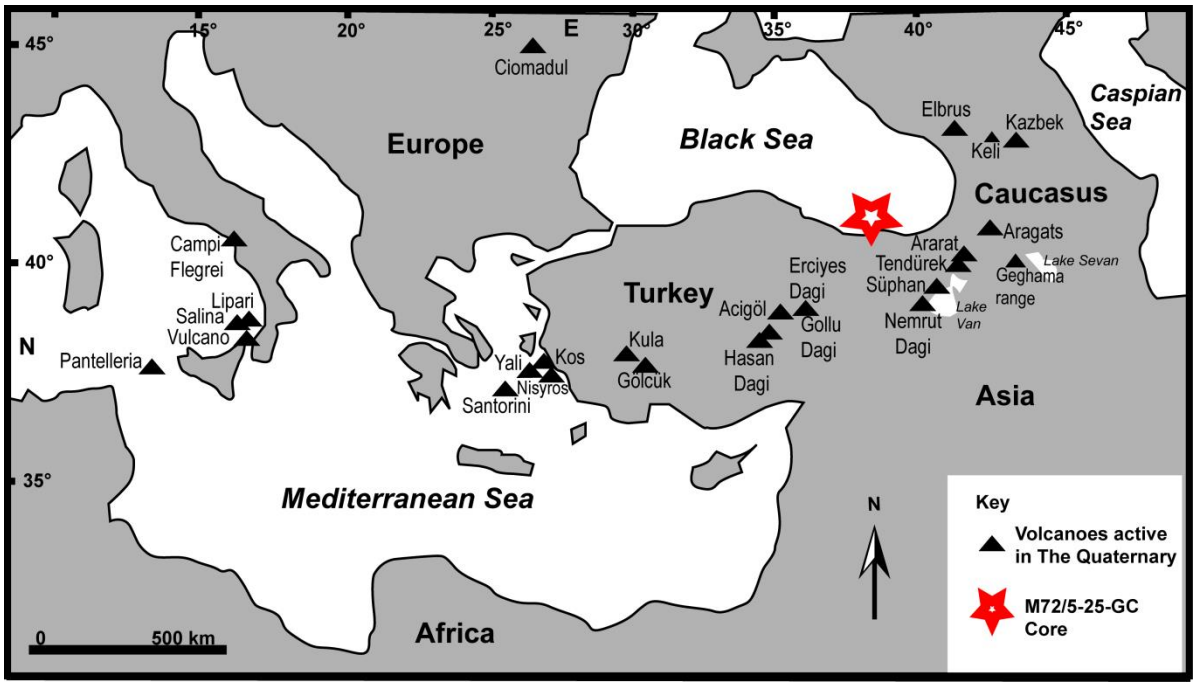

Figure 7.1. Map of the eastern Mediterranean and the Caucasus. The star shows location of M72/5-25-GC1 core, which was taken at a water depth of 418 m at the Archangelsky ridge (42°06.21'N, 36°37.43'E). The triangles denote the location of the volcanoes that have been active in the Quaternary (see previous Chapter).

7.2. Cryptotephra results for the M72/5-25-GC1 core

Prior to the cryptotephra investigations, the M72/5-25-GC1 core was subsampled into 1 cm U-Channels and sent to Oxford where it is stored under reduced temperatures (~5 °C). Methods of subsampling, cryptotephra preparation and

identification are provided in Chapter 5. All tephra concentrations are expressed as glass shard concentration per dry gram of sediment (s/g) and tephra layers have been labelled according to the base depths of the highest peak concentration in the core (e.g. BSC_'cm', Table 7.1, Figure 7.2). The whole core was processed by the author (952 to 2 cm) and twenty-two tephra horizons were identified. Only one of the layers is a visible layer, BSC_721, and all others are cryptotephra horizons.

Table 7.1. Information relating to the visible and cryptotephra layers identified in the M72/5-25-GC1 core.

Group	Tephra label*	Shards per gram of dry sediment (s/g)	Number of EPMA analysis (n=)	EPMA analysis performed by	Number of LA-ICP-MS analysis (n=)	LA-ICP-MS analysis performed by	Composition
Group C	*BSC_008*	150	16	Author	-		CAR
	BSC_022	2683	17	Author	-		CAR
	BSC_079	53000	15	Author	-		CAR
	BSC_139	150	5	Author	-		CAR
	BSC-154	320	8	Author	-		CAR
	BSC-158	340	22	Author	-		CAR
	BSC-179	300	23	Author	-		CAR
Group B	*BSC-394*	306425	37	Author	8	P. Albert	CAR
	BSC-411	22867	30	Author	9	P. Albert	CAR
Group A2 tephras	*BSC-651*	180	42	Author	-		CAR/PR
	BSC-660	50	4	Author	-		CAR
	BSC-674	40	14	Author	-		CAR
	BSC-683	67	8	Author	-		CAR
	BSC-694	81	5	Author	-		CAR
	BSC-698	38	2	Author	-		CAR
	BSC-705	55	7	Author	-		CAR
Visible layer	*BSC-721*	Visible	23	Author	-		TR/Ph
Group A1	*BSC-729*	106	11	Author	-		CAR
	BSC-740	78	10	Author	-		CAR
	BSC-752	71	17	Author	-		CAR
	BSC-778	150	5	Author	-		CAR
	BSC-807	38	2	Author	-		CAR

Footnote: CAR, calc-alkaline rhyolite; T, trachyte; Ph, phonolite; PR, peralkaline rhyolite; see Figure 7.3 and 7.4.

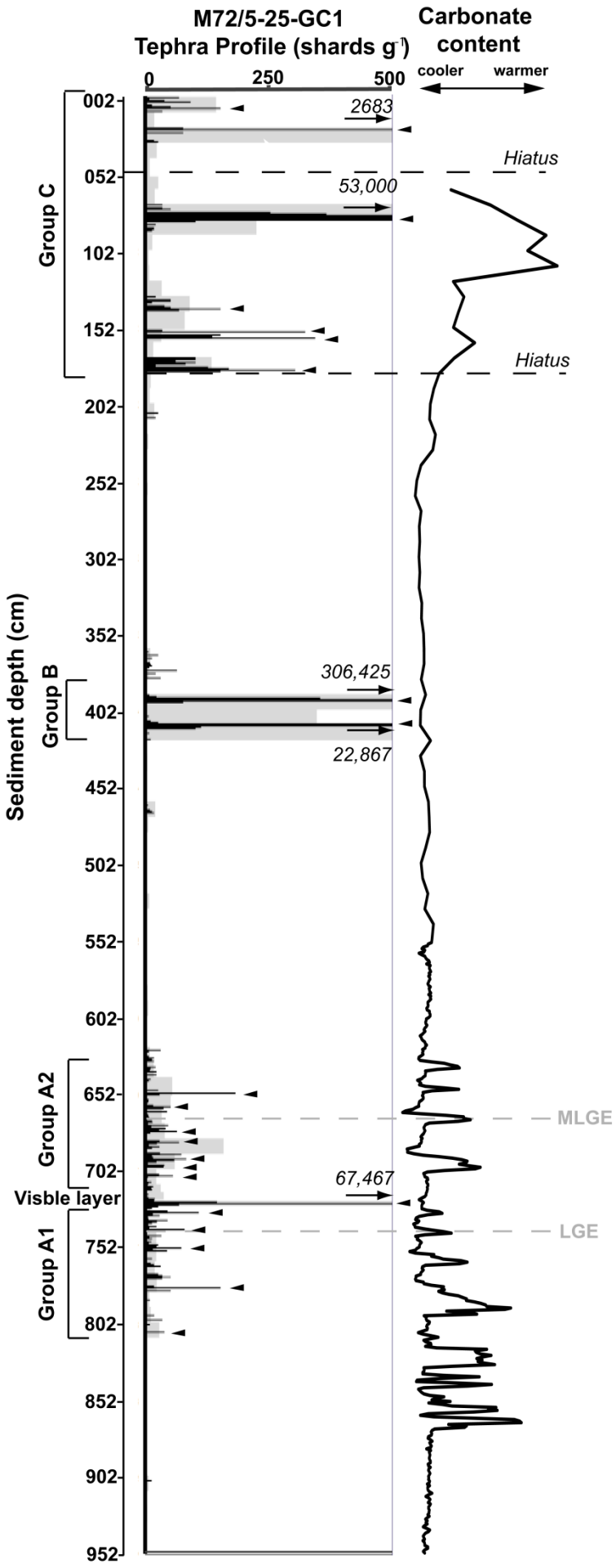

Figure 7.2. The glass shard concentration profile (s/g) for the M72/5-25-GC1 core. Grey boxes indicate the counts from the initial low resolution (~10 cm) samples, and black lines are concentrations in 1cm samples. Samples that have concentrations >500 s/g are marked with an arrow and the concentration is reported. There are distinct periods in volcanism (Groups), separated by sterile sediment. Tephra layers that were analysed (glass chemistry) are shown by black arrows heads. The $CaCO_3$ data (a proxy for water productivity; see 4.4) is plotted on the right of the tephra profile. The positions of the Laschamp geomagnetic excursion (LGE) and the Mono Lake geomagnetic excursion (MLGE) are labelled (from Arz pers comms, 2014; Nowaczyk et al., 2012; 2013).

For simplicity, the tephras have been stratigraphically grouped (Figure 7.2 and Table 7.1). These groups, labelled A at the base to C at the top of the core, are demarcated by sections of sediment that are largely sterile. When dealing with peaks in shard concentration it is important to consider reworking, both above and below the peak as this could be associated with processes such as bioturbation or linked to disturbance during coring (see Chapter 3.3.2). Thus, it is important to look at chemical compositions of the tephra horizons around the major peaks and see if they are repeated within the same stratigraphic group. These groups are therefore useful for comparison of geochemical data to evaluate whether the tephra in some sections has been reworked.

Shards within the largest peaks in concentration, identified during microscope scanning, were picked, mounted and analysed (black arrow heads, Figure 7.2). The extractions of shards from zones with very low tephra concentrations, i.e., at ~375 cm, ~468 cm, ~903 cm and towards the top of the core (~4 cm) were unsuccessful (Figure 7.2). Physical characteristics, shard sizes (based on longest axis), and the geochemical composition of tephra and cryptotephra layers are provided in text and corresponding Tables. All data presented in figures and tables have been normalised to 100% (anhydrous) for comparative purposes. Tabulated, full compositional tables are provided in Appendix 1. Error bars shown with WDS-EPMA data in figures are at 2σ. Presentation of data follows the methods outlined in Chapter 5.

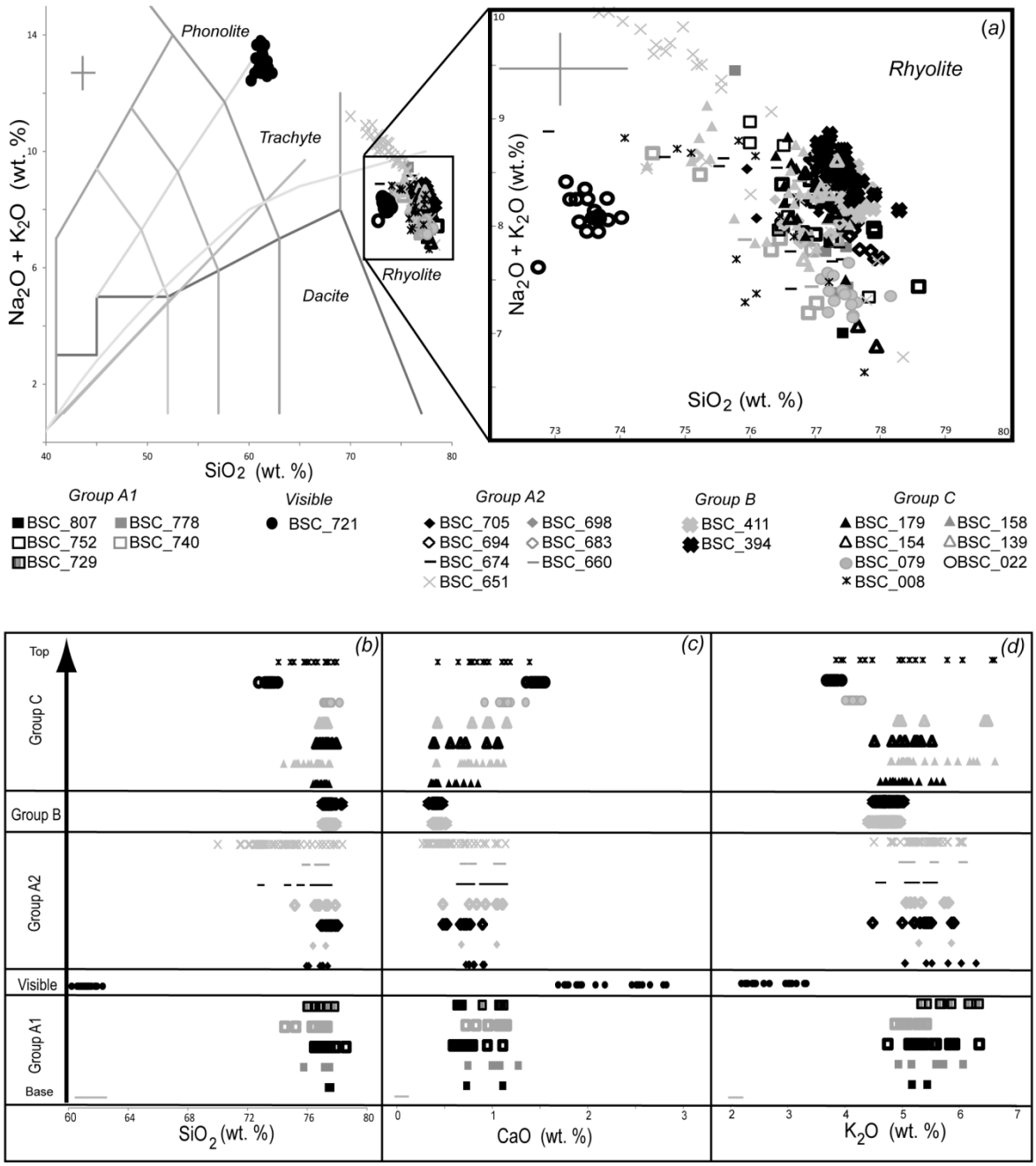

Figure 7.3. TAS plot of glass compositions of tephras found in the M72/5-25-GC1 Black Sea core (a). The visible BSC_721 tephra is trachytic to phonolitic in composition but all the cryptotephra layers are calc-alkaline rhyolites with the exception of one population (<76 wt. %) of BSC_651 that is more alkaline. The range in glass compositions vertically though the core (c) SiO_2, (d) CaO, and (e) K_2O is shown. Coordinates for magma series lines (peralkaline above, calc-alkaline below) are from Rollinson, (1993).

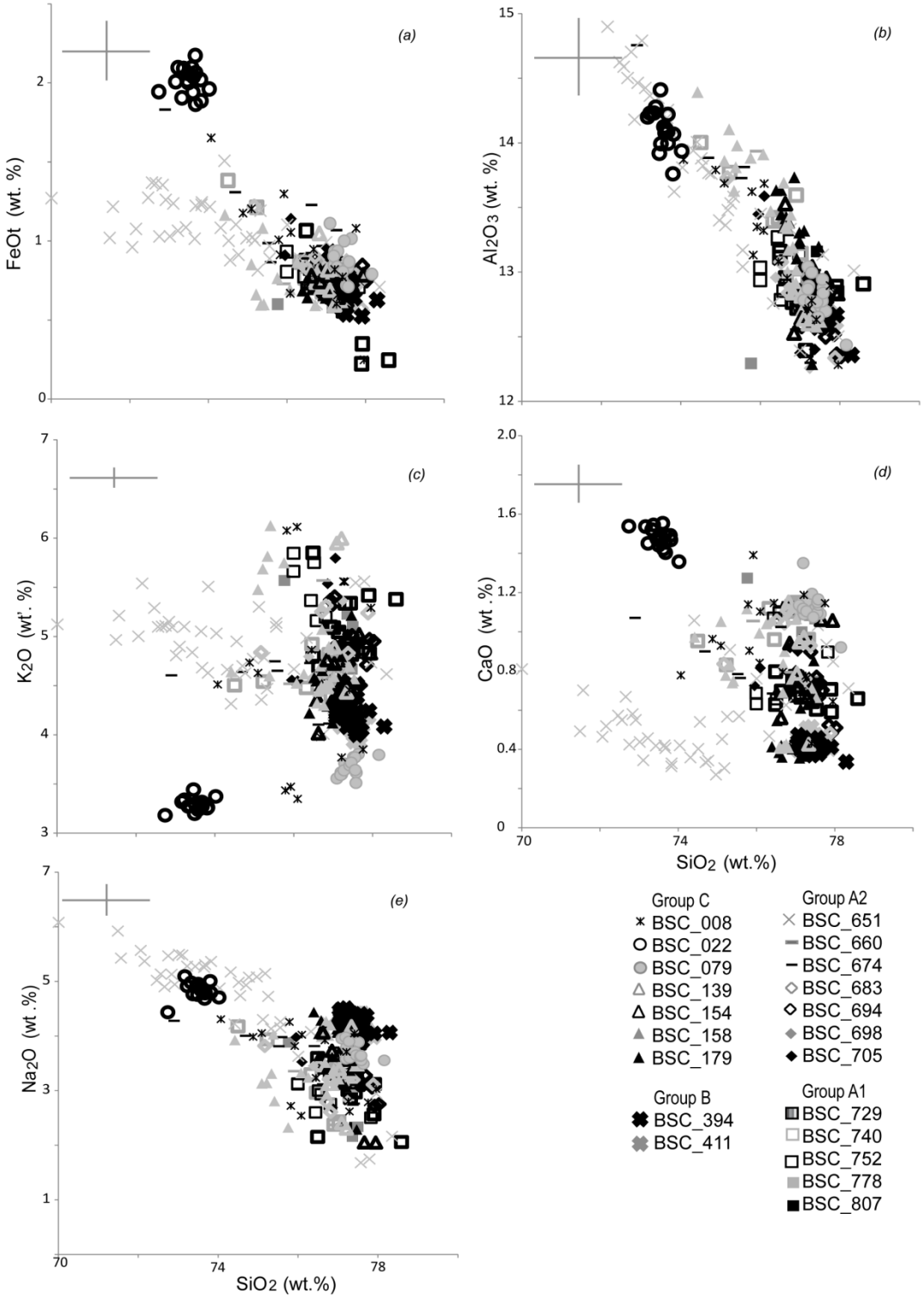

Figure 7.4. Harker diagrams of compositional glass data for tephra (a-d) in the M72/5-25-GC1 core. BSC_721 has not been included as it is easily distinguishable from other tephras in the core.

7.2.1. Group A tephras

Group A includes all tephra horizons between 807 cm and 622 cm sediment depth (Figure 7.2; Table 7.1). This group has been subdivided on plots and in the discussion at the visible tephra layer, with layers below falling into group A1 (BSC_729 to BSC_807) and those above into A2 (BSC_651 to BSC_705). Tephra peaks in Group A1 and A2 were intermittently spaced across 185 cm (Figure 2), with sterile sections of core ranging from 3 to 9 cm between many of the peaks. The highest tephra concentration of 180 s/g observed in Group A was found at 650 – 651 cm (BSC_651). Visual analysis of the tephra shards showed no discernible differences between different peaks (Figure 7.5). All horizons have colourless shards that are very irregular with some expanded vesicles, cuspate features, and fluting. BSC_698, BSC_752 and BSC_807 also contained some platy shards. Shards commonly ranged from 50-100 micrometres across the longest axis, but BSC_729 had shards up to ~130 micrometres (Figure 7.5).

Glass compositions of tephras in Group A1 and A2 are calc-alkaline rhyolites (Figure 7.3) with the exception of one population of BSC_651. These rhyolites have ~76-78 wt. % SiO_2, 4.02 – 5.85 wt. % K_2O, and low FeOt concentrations (0.22 - 1.84 wt. %; Figure 7.3, 7.4; Table 7.2). BSC_651 has two compositional populations, one with >76 wt. % SiO_2 and another with <76 wt. % SiO_2. The lower SiO_2 population also has higher Al_2O_3, FeOt, and Cl (Figure 7.4, Table 7.2), and is distinctive from other tephras in this group (and the core). It displays an inverse correlation between total alkali (Na_2O + K_2O) and SiO_2 content, most pronounced on Na_2O (Figure 7.3a, 7.4e). This suggests a progressive crystal fractionation of feldspar in the magma evolution. BSC_651 has a unique chemical fingerprint within this study.

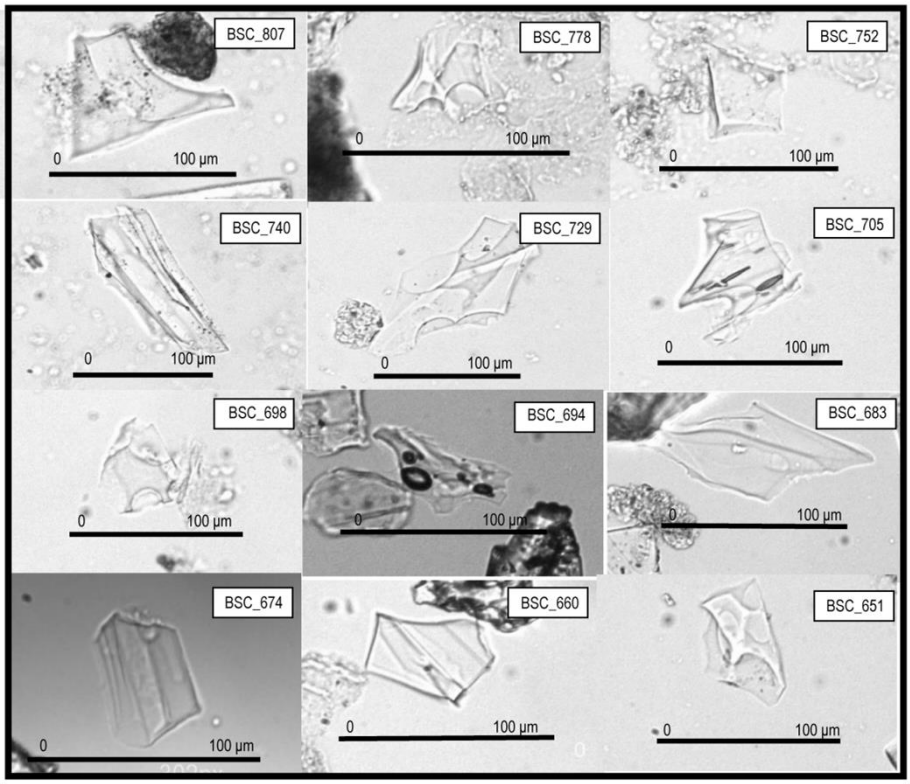

Figure 7.5. Photos of tephra shards from layers (labelled in top right corner) in Groups A1 and A2.

Table 2 (below). Average glass compositions (with 1σ) of tephra layers in Group A1 and Group A2.

Group A1										
Code	BSC_807		BSC_778		BSC_752		BSC_740		BSC_729	
	n=2	*1σ*	n=5	*1σ*	n=10	*1σ*	n=10	*1σ*	n=11	*1σ*
Major (wt. %)										
SiO_2	77.5	*0.11*	77.05	*0.73*	77.26	*0.55*	76.47	*0.91*	76.68	*0.54*
TiO_2	0.13	*0.06*	0.11	*0.03*	0.12	*0.1*	0.14	*0.03*	0.15	*0.04*
Al_2O_3	12.9	*0.36*	12.73	*0.25*	12.82	*0.2*	13.26	*0.44*	12.89	*0.15*
FeOt	0.68	*0.13*	0.69	*0.10*	0.69	*0.23*	0.86	*0.24*	0.77	*0.08*
MnO	0.08	*0.00*	0.10	*0.05*	0.05	*0.04*	0.05	*0.03*	0.07	*0.04*
MgO	0.10	*0.04*	0.13	*0.03*	0.09	*0.03*	0.12	*0.03*	0.13	*0.02*
CaO	0.92	*0.27*	1.03	*0.19*	0.73	*0.13*	1.00	*0.14*	0.88	*0.22*
Na_2O	2.72	*0.55*	2.97	*0.72*	3.09	*0.47*	3.27	*0.58*	2.89	*0.22*
K_2O	4.81	*0.19*	5.00	*0.45*	4.99	*0.38*	4.64	*0.19*	5.35	*0.35*
P_2O_5	0.02	*0.00*	0.01	*0.02*	0.02	*0.02*	0.02	*0.02*	0.03	*0.01*
Cl	0.15	*0.00*	0.17	*0.02*	0.14	*0.07*	0.17	*0.03*	0.18	*0.03*

Table 2 continued.

Group A2																
Code	BSC_705		BSC_698		BSC_694		BSC_683		BSC_674		BSC_660		BSC_651 (<76 wt. %)		BSC_651 (>76 wt. %)	
	n=7	*1σ*	n=2	*1σ*	n=12	*1σ*	n=8	*1σ*	n=12	*1σ*	n=4	*1σ*	n=32	*1σ*	n=9	*1σ*
Major (wt. %)																
SiO_2	76.76	*0.58*	76.81	*0.61*	77.53	*0.26*	76.65	*0.87*	76.83	*0.67*	76.7	*0.56*	73.62	*1.34*	77.22	*0.78*
TiO_2	0.13	*0.04*	0.15	*0.00*	0.08	*0.04*	0.11	*0.04*	0.14	*0.08*	0.11	*0.04*	0.12	*0.05*	0.13	*0.06*
Al_2O_3	12.92	*0.47*	12.61	*0.50*	12.62	*0.15*	12.9	*0.40*	13.22	*0.66*	13.26	*0.46*	14.2	*0.7*	12.93	*0.35*
FeOt	0.78	*0.19*	0.87	*0.04*	0.71	*0.08*	0.83	*0.19*	0.98	*0.33*	0.71	*0.03*	1.12	*0.16*	0.76	*0.19*
MnO	0.05	*0.04*	0.08	*0.00*	0.06	*0.04*	0.07	*0.04*	0.05	*0.05*	0.09	*0.05*	0.05	*0.03*	0.05	*0.04*
MgO	0.08	*0.02*	0.12	*0.02*	0.08	*0.02*	0.11	*0.05*	0.12	*0.06*	0.11	*0.04*	0.06	*0.03*	0.10	*0.04*
CaO	0.81	*0.07*	0.86	*0.26*	0.68	*0.11*	0.92	*0.22*	0.85	*0.16*	0.91	*0.19*	0.50	*0.17*	0.80	*0.21*
Na_2O	3.15	*0.52*	3.14	*0.44*	3.18	*0.31*	3.17	*0.37*	3.53	*0.49*	2.99	*0.48*	5.06	*0.47*	3.03	*0.97*
K_2O	5.10	*0.47*	5.08	*0.40*	4.86	*0.36*	4.93	*0.30*	4.63	*0.32*	4.95	*0.47*	4.94	*0.30*	4.78	*0.52*
P_2O_5	0.01	*0.01*	0.02	*0.01*	0.02	*0.02*	0.01	*0.01*	0.01	*0.02*	0.01	*0.01*	0.01	*0.01*	0.01	*0.01*
Cl	0.20	*0.05*	0.26	*0.16*	0.2	*0.08*	0.14	*0.04*	0.19	*0.05*	0.15	*0.02*	0.31	*0.07*	0.17	*0.04*

7.2.2. BSC_721 visible tephra layer

BSC_721 is the only visible tephra layer in the core (~0.1 cm thick) and is brown/black in colour. High concentrations of glass shards are found over 7 cm, from 719 cm to 726 cm, reflecting some reworking of shards above and below the visible layer. The shards are platy to irregular in shape, with some light fluting and open, expanded vesicles. They range from 30 to 120 micrometres in size and do not display much optical relief (Figure 7.6).

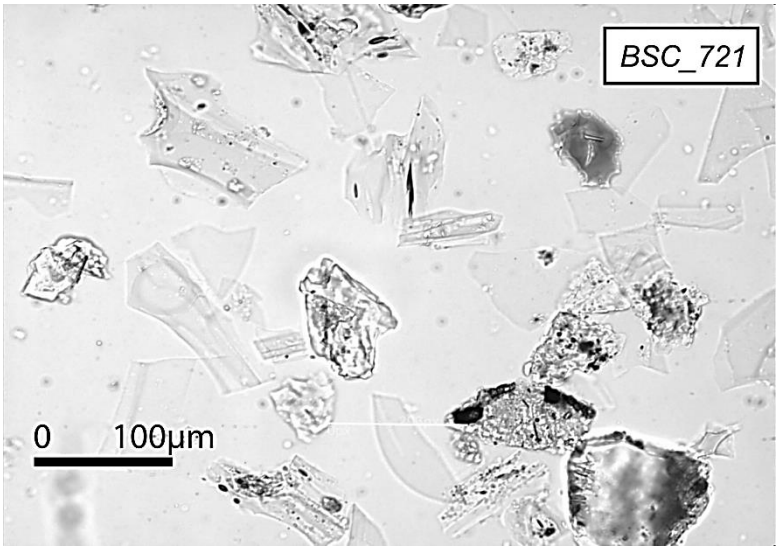

Figure 7.6. Photo of the glass shards in the visible Layer BSC_721. Shards exhibit low relief in optical analysis.

Compositionally the layer is a peralkaline trachyte that straddles the phonolite field (see Figure 3). The shards have a lower SiO_2 composition (60.59 – 62.30 wt.%) and higher K_2O (6.69 - 9.98 wt.%), FeOt (1.69 - 2.79 wt.%), and CaO (2.61 - 3.49 wt.%) concentrations than other tephra layers in the core (Table 7.3, Figure 7.3). This tephra is clearly distinguishable from other glass shards in the core. It is also compositionally bimodal, clearly observed in K_2O and CaO (Figure 7.3c, 7.d).

Table 7.3. Average glass shard compositions (with 1σ) of tephra from the visible layer, BSC_721 in the M72/5-25-GC1 core.

Visible Layer				
BSC CODE	BSC_721 (> 2.46 CaO)		BSC_721 (<2.18 CaO)	
	n=9	*1σ*	n=14	*1σ*
Major element				
SiO_2	60.87	*0.33*	61.44	*0.39*
TiO_2	0.39	*0.06*	0.40	*0.02*
Al_2O_3	18.59	*0.24*	18.74	*0.26*
FeOt	3.32	*0.13*	2.86	*0.15*
MnO	0.11	*0.04*	0.19	*0.06*
MgO	0.70	*0.05*	0.37	*0.09*
CaO	2.60	*0.13*	1.86	*0.14*
Na_2O	3.39	*0.51*	5.76	*0.83*
K_2O	9.46	*0.66*	7.54	*0.62*
P_2O_5	0.16	*0.02*	0.06	*0.03*
Cl	0.41	*0.04*	0.77	*0.18*

7.2.3. Group B tephras.

The next major tephra concentration was located ~240 cm above BSC_651 and there is ~209 cm of sterile sediment located above Group A and before Group B tephras. Group B includes all tephra horizons between 413 cm and 379 cm sediment depth. There are two substantial cryptotephra peaks in Group B; BSC_394 with 306,425 s/g and BSC_411 with 22,867 s/g (Figure 7.2, Table 7.1). These layers are separated by 11 cm of sterile sediment. Shards in both layers are 50-200 micrometres in size and have some expanded and closed vesicles (Figure 7.7). Distinct heavily fluted shards are found in higher concentrations in BSC_394 relative to BSC_411.

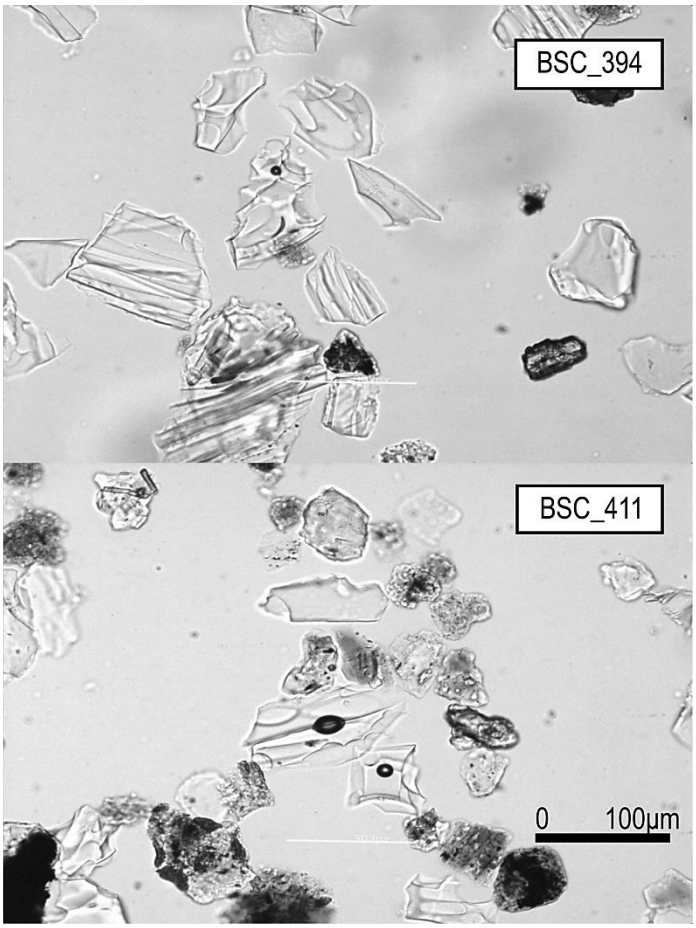

Figure 7.7. Photos of glass shards that comprise tephra layers BSC_411 and BSC_394. Glass shards in BSC_394 exhibited more fluting (top image) than shards in BSC_411 (bottom image).

Glass shards in BSC_394 and BSC_411 are compositionally indistinguishable on major elements. They are both chemically homogeneous, calc-alkaline rhyolites with ~76 -77 wt.% SiO_2, 3.90 - 4.41 wt.% Na_2O, 3.92 – 4.46 wt.% K_2O, and lower CaO concentrations (<0.6 wt.%) than the majority of other tephra layers in the Black Sea core (see Figures 7.3 and 7.4; Table 7.4)

Table 7.4. Average glass shard compositions of tephra from Group B tephras (BSC_411 and BSC_394) in the M72/5-25-GC core.

Group B				
	BSC_411		BSC_394	
	n=30	*1σ*	n=36	*1σ*
Major (wt. %)				
SiO_2	77.53	*0.19*	77.43	*0.25*
TiO_2	0.04	*0.02*	0.03	*0.02*
Al_2O_3	12.71	*0.06*	12.72	*0.10*
FeOt	0.76	*0.07*	0.73	*0.08*
MnO	0.08	*0.04*	0.07	*0.03*
MgO	0.02	*0.01*	0.02	*0.01*
CaO	0.43	*0.03*	0.41	*0.03*
Na_2O	4.23	*0.15*	4.26	*0.16*
K_2O	4.21	*0.14*	4.25	*0.13*
P_2O_5	0.01	*0.01*	0.01	*0.01*
Cl	0.09	*0.02*	0.08	*0.02*

7.2.3.1. Trace data BSC_394 and BSC_411

A number of glass shards from BSC_394 and BSC_411 were large enough for trace element analysis using LA-ICP-MS with a ~30 micrometre beam. This was done to assess if trace element data could differentiate between the two tephra layers that form Group B. The trace element concentrations for BSC_411 and BSC_394 are also indistinguishable, with 29– 37 Th ppm, 249 - 320 ppm Rb, 28 - 41 ppm Y, 62 – 78 ppm Zr, and 12 – 15 ppm La (see Figure 7.8; Table 7.5; Appendix 1 for full data).

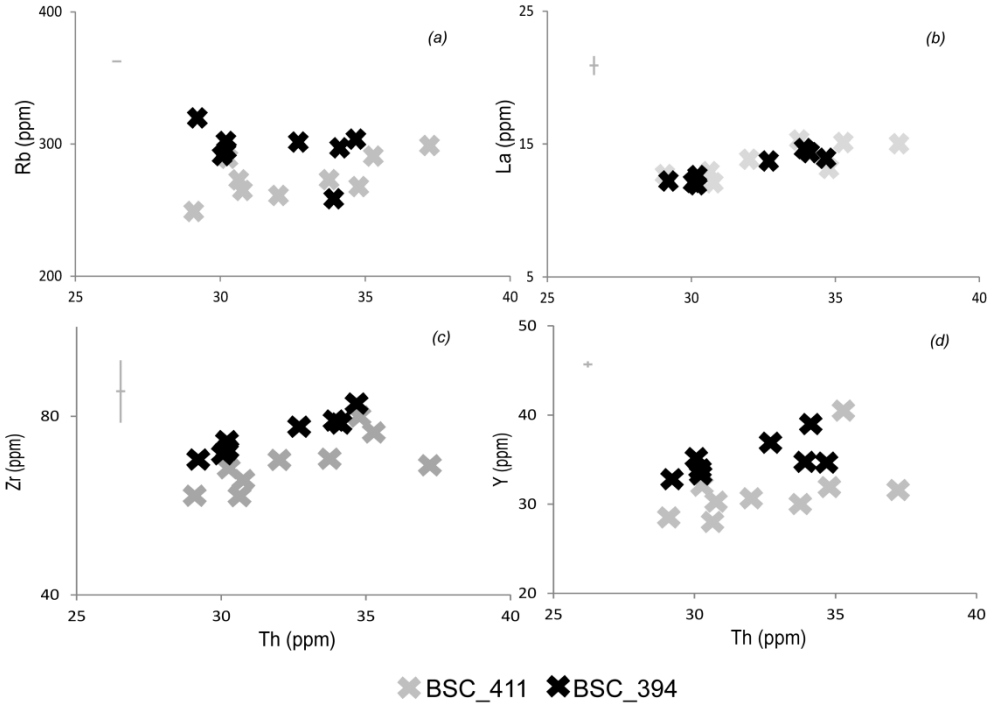

Figure 7.8. Selected plots for incompatible (a) and compatible (b, c, d) glass shards from BSC_411 and BSC_394 that form Group B.

Table 7.5. Compositional ranges for trace element data (ppm) for BSC_394 and BSC_411 glasses

BSC code	BSC_394	BSC_411
	n=8	*n=9*
Trace element (ppm)		
Rb	259 - 320	249 - 291
Y	32.8 - 39.0	28.0 – 41.0
Zr	70.3 - 78.3	62.2 - 76.4
Nb	35.2 – 40.0	31.01 – 42.0
Ba	1.7 - 4.2	1.9 -5.6
La	12.0 - 14.7	12.1 - 15.3
Ce	28.4 - 31.1	28.4 - 36.5
Pr	3.0 - 4.1	3.0 - 3.9
Nd	10.6 - 14.7	12.1 - 15.2
Yb	3.6 - 4.9	3.3 - 4.2
Hf	3.23 - 4.32	2.92 - 4.47
Ta	3.7 - 4.2	3.3 - 4.0
Th	29.2 - 34.7	29.1 - 37.2
U	11.3 - 14.1	10.9 - 13.1

Light Rare Earth Elements (LREE) are enriched relative to Heavy Rare Earth Elements (HREE) in both tephras; BSC_411, 3.09 – 4.06 La/Yb and BSC_394, 2.78 – 3.59 La/Yb. Mantle normalisation diagrams show a deep negative anomaly for Ba in BSC_411 that is suggestive of crystal fractionation (Figure 9; Ba in BSC_394 fell below the limits of detection). Negative anomalies are seen in Nb (in both BSC_411 and BSC_394) and indicate some crustal contamination. Both glasses have slight negative anomalies at Zr with a positive anomaly at Hf (Figure 7.9).

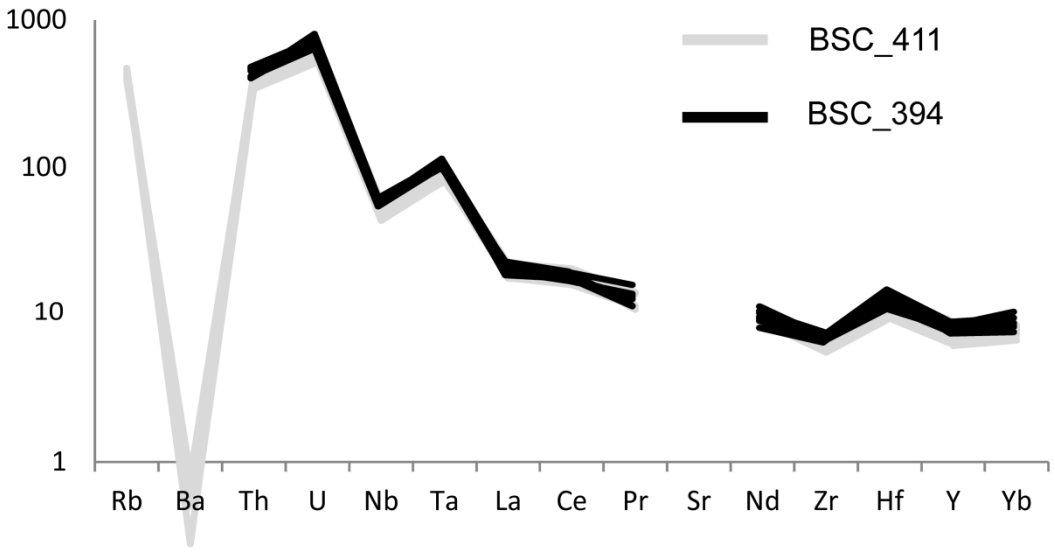

Figure 7.9. Primitive mantle normalised diagram of glass shards in BSC_411 (grey lines) and BSC_394 that are shown as black lines. Sample values are normalised to primitive mantle compositions (Sun & McDonough, 1989). Tephras show identical profiles.

7.2.4. Group C tephras

There is 173 cm of sterile sediments between Group B and the start of Group C tephras (Figure 7.2). Group C includes 7 cryptotephra horizons between 206 cm (sediment depth) and the top of the core (2 cm). There are some sterile sections of

the core (spanning ~1-4 cm) between peaks in tephra concentration (Figure 7.2). Group C tephras include BSC_179 (300 s/g), BSC_158 (340 s/g), BSC_154 (320 s/g), BSC_139 (150 s/g), and a substantial peak at 79-80 cm (BSC_079, 53,000 s/g) but the tephra is spread across 7 cm (Figure 7.2). The next substantial peaks in the group are at 22-21 cm, BSC_022 with 2683 s/g, and BSC_008 with a shard count of 150 s/g (Table 7.1, Figure 7.2). Tephra shards in Group C range from 50 to 150 micrometres in size, and most are slightly vesicular with some expanded vesicles and fluting (BSC_179, BSC_158, BSC_154, BSC_139; Figure 10). BSC_022 and BSC_008 contain shards that are platy with some fluting, and range from 50 to 110 micrometres in size (Figure 7.10).

Compositionally, BSC_008, BSC_139, BSC_154, BSC_158, BSC_179 tephras are calc-alkaline rhyolites and all have a similar major element composition, with ~74 - 77.96 wt.% SiO_2, 3.35 - 6.13 wt.% K_2O, and 0.38 – 1.39 wt.% CaO (Table 7.6; Figure 7.3 and Figure 7.4). Na_2O compositions of BSC_179 are bimodal. BSC_158 is also compositionally diverse, with two mixed compositional populations that plot along different Al_2O_3 trends (see Figure 7.4). The most evolved BSC_158 population (> 76.5 wt. % SiO_2) is identical in composition to the most evolved populations of BSC_154 and BSC_179. BSC_008 is separated from BSC_154 by two substantial layers (BSC_079 and BSC_022), but is compositionally similar to the older tephras in this group (Figure 7.3 and 7.4).

The most substantial peaks in Group C, BSC_079 and BSC_022, are both chemically distinct from other tephras in the core. BSC_079 is a homogenous, calc-alkaline rhyolite with SiO_2 values ranging from 77.16 to 78.16 wt. %. Compositionally, it has lower K_2O values than other tephras in the core (< 4 wt. %) with the exception of BSC_022 (Figure 7.4; Table 7.6). However, the latter is

easily distinguishable from BSC_079 and other tephra in the core based on its lower SiO_2.

values (72.74 – 74.02 wt. %) and higher CaO concentrations (1.36-1.35 wt. %; Table 7.6; Figure 7.3b, c and Figure 7.4).

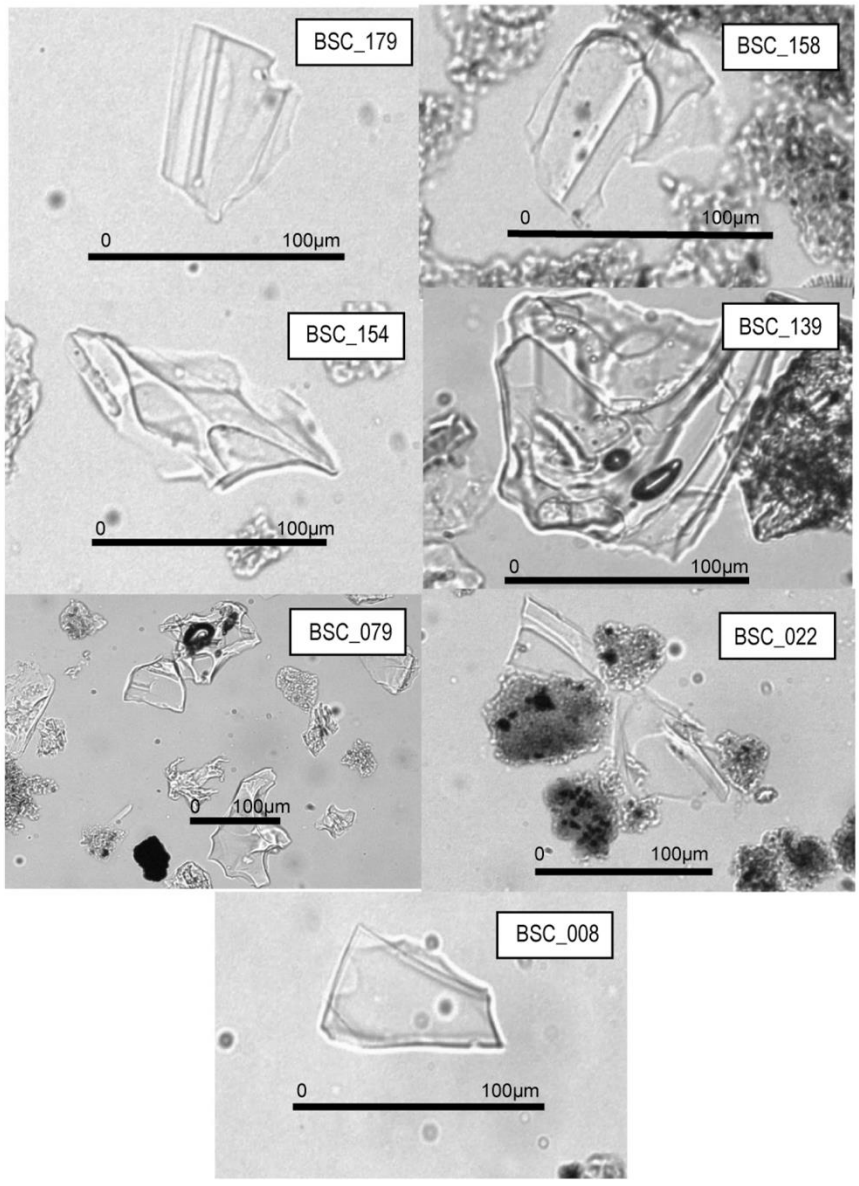

Figure 7.10. Images of tephra shards that form the Group C tephras.

Table 7.6. Average glass shard compositions (with 1σ) of Group C tephras (BSC_179, BSC_158, BSC_154, BSC_139, BSC_079, BSC-022 and BSC_008).

Group C														
Code	BSC_179		BSC_158		BSC_154		BSC_139		BSC_079		BSC_022		BSC_008	
	n=21	*1σ*	n=21	*1σ*	n=8	*1σ*	n=5	*1σ*	n=14	*1σ*	n=17	*1σ*	n=16	*1σ*
Major (wt. %)														
SiO_2	76.94	*0.31*	76.29	*0.83*	77.25	*0.43*	77.1	*0.19*	77.45	*0.26*	73.51	*0.29*	76.34	*1.13*
TiO_2	0.06	*0.06*	0.1	*0.05*	0.1	*0.06*	0.1	*0.05*	0.13	*0.02*	0.31	*0.03*	0.15	*0.05*
Al_2O_3	13.2	*0.33*	13.43	*0.5*	12.89	*0.3*	12.72	*0.11*	12.8	*0.15*	14.17	*0.34*	13.15	*0.53*
FeOt	0.72	*0.07*	0.77	*0.14*	0.75	*0.07*	0.8	*0.17*	0.88	*0.11*	2.01	*0.08*	0.92	*0.34*
MnO	0.07	*0.05*	0.06	*0.04*	0.05	*0.03*	0.07	*0.03*	0.04	*0.03*	0.06	*0.04*	0.05	*0.04*
MgO	0.04	*0.04*	0.08	*0.05*	0.08	*0.06*	0.1	*0.06*	0.17	*0.04*	0.3	*0.03*	0.13	*0.08*
CaO	0.5	*0.16*	0.78	*0.24*	0.72	*0.27*	0.86	*0.27*	1.13	*0.09*	1.48	*0.05*	0.94	*0.25*
Na_2O	3.82	*0.52*	3.45	*0.5*	3.42	*0.88*	3.1	*0.77*	3.7	*0.16*	4.83	*0.15*	3.46	*0.66*
K_2O	4.52	*0.29*	4.89	*0.54*	4.59	*0.32*	5.15	*0.77*	3.67	*0.09*	3.29	*0.06*	4.64	*0.94*
P_2O_5	0.01	*0.01*	0.02	*0.01*	0.01	*0.01*	0.01	*0.02*	0.04	*0.03*	0.04	*0.02*	0.02	*0.01*
Cl	0.13	*0.06*	0.14	*0.04*	0.13	*0.05*							0.19	*0.06*

7.3. Distinguishing primary and re-worked tephras

Group A1 and A2 represent two zones of near continuous but limited tephra deposition (concentrations <30 s/g) separated by a visible tephra deposit. These tephras have indistinguishable major element compositions (with the exception of < 76 wt.% SiO_2 population from BSC_651) but are chemically distinct from the visible layer. It is relatively common for volcanoes to erupt tephra layers with similar major element chemistry over long periods of time (e.g. Lane et al., 2012b; Smith et al., 2011b). Trace element compositions often help to discriminate between these (e.g. Albert et al., 2014) but the trace element composition of many Black Sea tephras could not be determined as the shards were too small. Therefore, it is unclear whether these cryptotephra layers represent material reworked within the catchment or are associated with separate small eruptions from a frequently active volcanic centre. The peaks that form Group A1 and A2 are, for the most part, separated by sterile sections of core that suggests no vertical mixing or prolonged reworking from the landscape. Additionally, shards from the visible tephra layer (constrained to 7 cm) form a well-defined peak and are not found in either Group A1 or A2. Thus, these layers are likely to be associated with frequent, small eruptions from a medial source. The youngest tephra layer in Group A2 (BSC_651) is compositionally bimodal, with two very distinctive compositions. The SiO_2-poor population (<76 wt.%) is distinct from other tephras in this group and those in the rest of the core. This suggests the tephra is probably associated with a different volcanic source. The distinct populations could indicate two coeval eruptions, or the SiO_2-rich (>76 wt.%)

population (compositionally similar to other tephras in the group) is comprised of reworked shards.

BSC_411 and BSC_ 394 (Group B) are stratigraphically isolated in the core, and the shards in each peak are different in morphology. They are both homogeneous calc-alkaline rhyolites with low CaO concentrations (<0.5 wt.%). These layers represent two different events but since they have a similar chemistry they are most likely from the same source volcano.

Group C tephras show the greatest chemical variability, with smaller sterile, stratigraphic breaks (~1-4 cm) separating the peaks in tephra concentration. BSC_139, BSC_154, BSC_158 and BSC_179 glass shards have similar low CaO and high SiO_2 concentrations (<0.5 wt.% and >76 wt.%, respectively) compared to tephras of Group B. The BSC_158 chemical compositions are bimodal, with one population similar to other Group B tephras. These tephras layers are likely to be associated with frequent, small eruptions from a medial source/s. As BSC_179 sits stratigraphically after an extensive sterile period in the core, it probably represents a primary event. BSC_079 is a substantial tephra that is chemically distinct (with K_2O < 4 wt.%) from other tephras in the core (Figure 7.3, 7.4) and thus should be considered a primary air-fall event. The next substantial layer, BSC_022 is also chemically distinct with ~73 wt.% SiO_2, lower total alkali values, and higher CaO than all other tephras in the core (Figure 7.4 and Figure 7.5) and thus is sourced from a distinct volcanic source. BSC_008, the youngest ash layer in the core, is chemically distinct from BSC_022. Compositionally, it has similarities to the early tephras in the group, but it also has a population that is distinctive in K_2O (<3.5

wt.%) and has ~75 wt% SiO_2 (Figure 7.3). The BSC_008 tephra is compositionally heterogeneous and is likely to be a mix of volcanic deposits, possibly from eruptions closely spaced in time. Tephra layers from the youngest section of Group C are not likely to be a result of bioturbation as the Black Sea basin was anoxic during the late Holocene and therefore there was no biological activity (Demaison & Moore, 1980), but some limited movement could have occurred as the tephra was deposited on the surface prior to burial (see sections 3.3.2 and 3.4).

7.4. Summary of results

Results from this study reveal that there are 21 cryptically preserved, previously unidentified tephra layers in the M72/5-25-GC1 Black Sea core with one visible deposit. Major element chemical analysis of these tephra layers shows that they are predominantly calc-alkaline high-silica rhyolites (Figure 7.3). The exceptions are the visible tephra layer that is trachytic/phonolitic in composition and the less evolved population of BSC_651 (<76 wt. % SiO_2) that is more alkaline in composition. The shard concentrations vary considerably through the core, with some sterile layers up to 153 cm thick followed by zones with numerous tephra peaks with high shard concentrations (e.g., Group B has two cryptotephra peaks with concentrations >22,000 s/g, and Group C has a layer with concentrations >50,000s/g).

Chapter 8

Results of tephras that have been found in archaeological sites in the Caucasus.

8.1. Introduction

The following chapter provides the results from a comprehensive tephra investigation of archaeological cave and open air sites across the Caucasus. Sites that have a Middle and/or Upper Palaeolithic techno-complex preserved with a good stratigraphic control and published archaeological, chronological or sedimentological data were selected (see Chapter 4).

8.2. Tephra Results of cave and open air sites

Sites that have undergone analysis for tephra and those that contained tephra are shown in Table 8.1. Sites from the Republic of Georgia, Azerbaijan and Armenia were collected by the author, unless otherwise stated. Samples from the north and northwest Caucasus were subsampled from archive material stored at Royal Holloway, University College London, that were previously collected as part of the EFCHED project.

Table 8.1. Table shows sites that underwent a tephra investigation and results. Number in brackets next to the site name refers to site location on map, Figure. 8.1.

Site Name	Latitude (°N)	Longitude (°E)	Sample processed by	**Tephra Present**
Ortvale Klde (1)	42 19.370	43 17.100	Author	**YES**
Sakajia cave (2)	42 16.430	42 46.200	Author	**YES**
Undo cave (3)	42 19.370	43 17.100	Author	**YES**
Ortvale cave (4)	42 16.430	42 46.200	Author	**YES**
Bronze cave (5)	42 16.220	42 51.094	Author	**NO**
Bondi cave (6)	42 19.370	43 17.010	Author	**NO**
Dzudzuana cave (7)	42 19.370	43 17.100	Author	**NO**
Lusakert 1 and Lusakert rock shelter (8)	40 21.490	44 35.390	Author	**YES/YES**
Azokh cave (9)	39 37.090	46 59.190	Author	**YES**
Aghitu 3 (10)	39 30.490	46 4.550	Author	**YES**
Fantan (11)	40 20.270	44 38.160	Author	**YES**
Kagasi (12)	40 28.580	44 46.500	Author	**YES**
Gubs rock shelter (13)	44 16.043	40 26.039	Author	**YES**
Monasheskaya (14)	44 16.043	40 26.039	Author	**NO**
Barakaevskaya (15)	44 16.099	40 26.051	Author	**NO**
Biriuchya Balka 2 (16)	47 48.365	41 07.846	Author	**NO**
Navalishenskaya (17)	43 33.188	39 55.857	Author	**NO**
Kepshinskaya (18)	43 36.750	40 02.913	Author	**NO**
Akhshtyr (19)	43 31.229	39 59.743	Author	**NO**
Malaya Vorontsovskaya (20)	43 36.750	40 02.913	Author	**NO**
Myshtulagty Lagat (21)	43 11.000	44 14.000	Author	**YES**

In total sediments from 18 cave/rock shelter sites and three open air sites have undergone a physical separation technique that was developed to find tephra (if any) in host sediments. Nine cave sites and two open air sites have shown to have tephra, including visible tephra layers (found solely in Armenia). Multiple tephra units have been found at some sites (see Table 8.2).

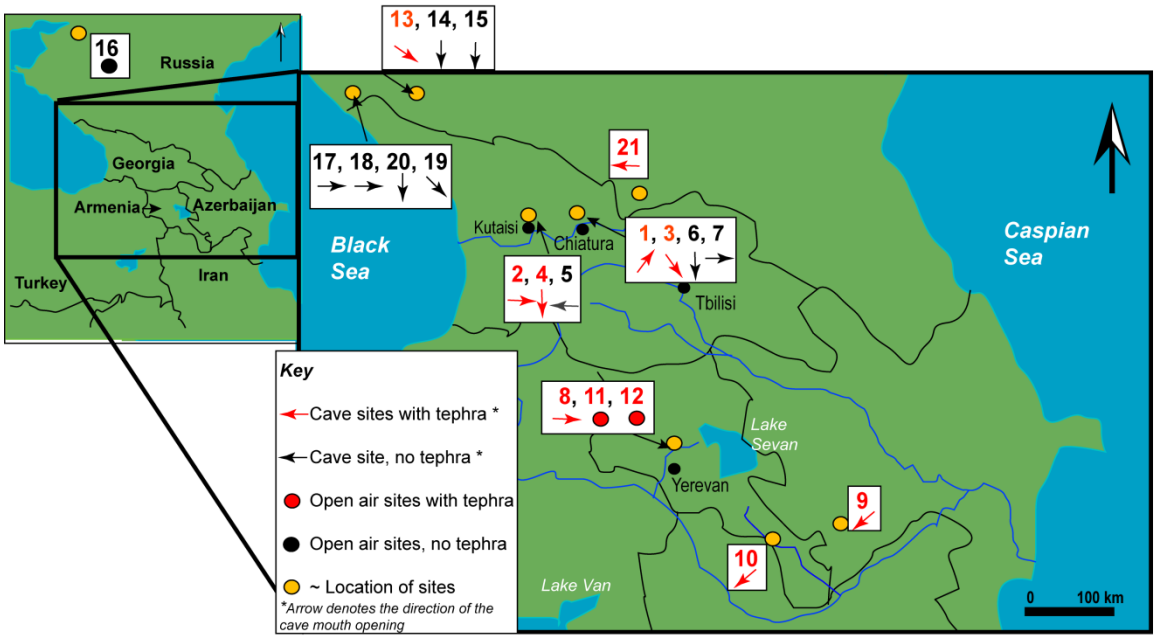

Figure 8.1. Map shows location of sites (orange circle). Each site has a number (see Table 8.1) with a corresponding arrow or circle beneath. The direction of the arrow reflects the direction of the cave mouth, open air sites are represented as a circle. Red indicated the site contained tephra, black indicate the site was devoid of a tephra component.

Tephras (glass shards) with both peralkaline and calc-alkaline compositions have been found in the region (Figure 8.2). Calc-alkaline rhyolite compositions dominate the northern Caucasus (Figure 8.1 and 8.2), but were also found alongside other compositions in the southern Caucasus. Basaltic trachy-andesite to trachy-dacite and peralkaline rhyolites tephras were found in sites in Armenia and Georgia, but phonolite and trachyte tephras were not found in Georgia (Figure 8.2).

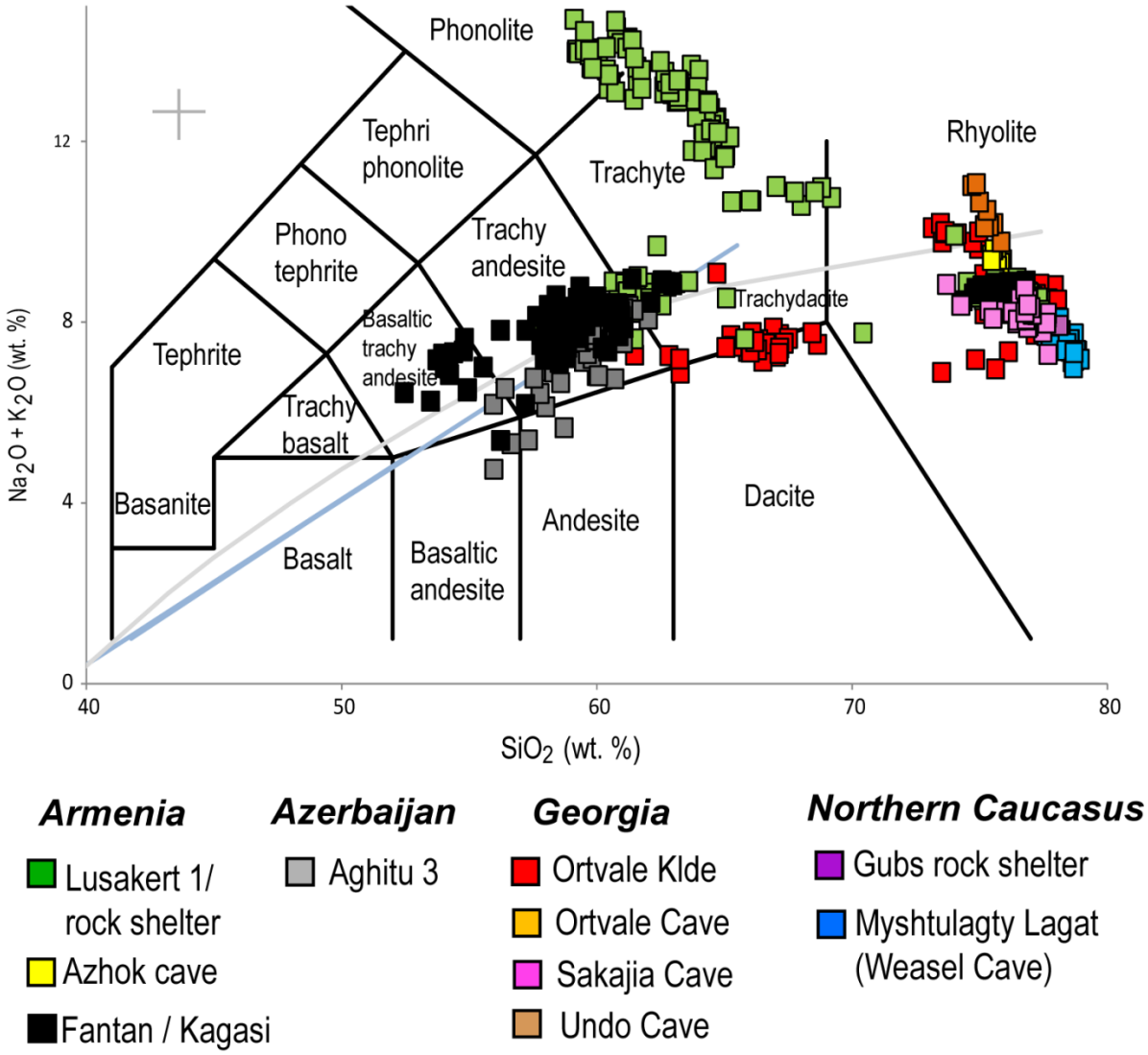

Figure 8.2. Glass compositions of shards found in archaeological sites in the Caucasus. Each site is represented as one colour for simplicity, with geochemical data from Fantan and Kagasi grouped. Glass data from Lusakert includes both the outside of the rock shelter (now called Lusakert 1) and inside of the rock shelter, called Lusakert rock shelter in the text. Specific information on individual (and multiple) horizons that have been located in each site is provided in text.

The following results describe the physical characteristics and chemical compositions of volcanic glasses (tephra) found in archaeological sites listed in Table 8.1. Sites in each region (The Republic of Georgia, Armenia, Azerbaijan and the northern Caucasus) are described separately. Collation and discussion of these results together with results from Chapters 6 and 7 is given in Chapter 9; Discussion.

Tephra horizons were named according to the site's name and the archaeological horizon that the tephra was preserved in; e.g. tephra horizon in Layer 4c of Ortvale Klde is OK_4c (see Table 8.2). Tephra compositional values in tables are presented as averages (with 1σ). Tabulated, full compositional tables are provided in Appendix 1. All data presented in figures and tables have been normalised to 100% (anhydrous) for comparative purposes. Error bars shown with WDS-EPMA data in figures are at 2σ (unless otherwise stated). Presentation of data follows the methods outlined in Chapter 5.

Table 8.2. Information relating to the visible and cryptotephra layers identified in archaeological sites.

Site Name	Tephra label	s/g dry sediment	Populations (n=)	Number EPMA analysis (n=)	Number of LA-ICP-MS analysis (n=)	Composition	LA-ICP-MS & EPMA analysis by
Ortvale Klde (1)	OK_3 OK_4c OK_5 OK_6 OK_7	6 238 8 5 3	2 3 1 1 1	22 40 11 9 1	-	PR/CAR CAR/PR/D CAR CAR TD	Author
Sakajia cave (2)	SK_2 SK_3a	20 3	3 1	32 1	-	CAR CAR	Author
Undo cave (3)	UC_II	118	Altered	9	-	CAR	Author
Ortvale cave (4)	OT_3	5	1	4	-	CAR	Author
Lusakert rock shelter (8)	LKI_3 LKI_4.1 LKI_5.1 LKI_5.2B LKI_6.5 LKI_7	64628 40717 81020 30662 Visible 51507	1 6 3 2 1 2	14 39 25 25 30 13	- - - - 12 -	TR TR/PRCAR/D TR-Ph/TR/CAR TR-Ph/CAR TA-TD TR-Ph/CAR	Author
Lusakert 1 (outside) (8)	LKO_CT LKO_CB LKO_D	23 221 105	1 1 1	14 35 21	-	CAR CAR CAR	Author
Azokh cave (9)	AZ_1 AZ_2a	>5225 >9943	1 (bimodal) 1 (bimodal)	14 16	-	CAR CAR	Author
Aghitu 3 (10)	AG3_8A AG3_8D	Visible Visible	1 1	15 15	7 8	BA-TD BA-TD	Author
Fantan (11)	FU_AM FL_AM	Visible Visible	1 1	27 12	4 -	CAR TA	Author
Kagasi (12)	KGU_AM KGM_AM KGL_AM	Visible Visible Visible	1 1 1	12 24 19	4 11 8	BTA TA-TD TA	Author

Gubs rock shelter (13)	Gub_3	8	1	3	-	CAR	Author
Myshtulagty Lagat (21)	WCEP _12	12	1	22	-	CAR	Author

Footnote: CAR, Calc-alkaline rhyolite; PR, Peralkaline rhyolite; TR, trachyte; TR-Ph, trachytic that extends to phonolite; TA, trachy andesite; D, dacite; BTA, basaltic trachy andesite; TD trachy dacite; BA, basaltic andesite. A number of compositionally distinct tephra populations were found in some layers; these reflect either different source volcanoes and/or different eruptions from the same volcano. Population column shows the number that were found in each layer. See text for details.

8.3. Ortvale Klde (Republic of Georgia), site No. 1

Cryptotephra was found within Layer 3 (between 30-38 cm, with highest peak at 30-32 cm), and layer 7 between 164-170 cm. Both peaks are surrounded by sterile sections of sediment and had peaks containing only a few glass shards per gram of sediment (s/g), 6 and 3 respectively (Figure 8.3). There was spread of tephra between layers 6 and 4b, but the highest concentrations were observed in layer 4c with a prominent increase in shard concentration at the contact between Layer 4d and Layer 4c (Figure 8.3). Layer 4c contained two closely spaced peaks, one at 98-96 cm (208 s/g) and one at 92-94 cm (238 s/g). The highest concentration of shards in Layer 5 and Layer 6 is directly above the contact between the two layers (base of Layer 5, see Figure 8.3). There are negligible amount of tephra between the top of Layer 5 and in Layer 4d (~1 s/g).

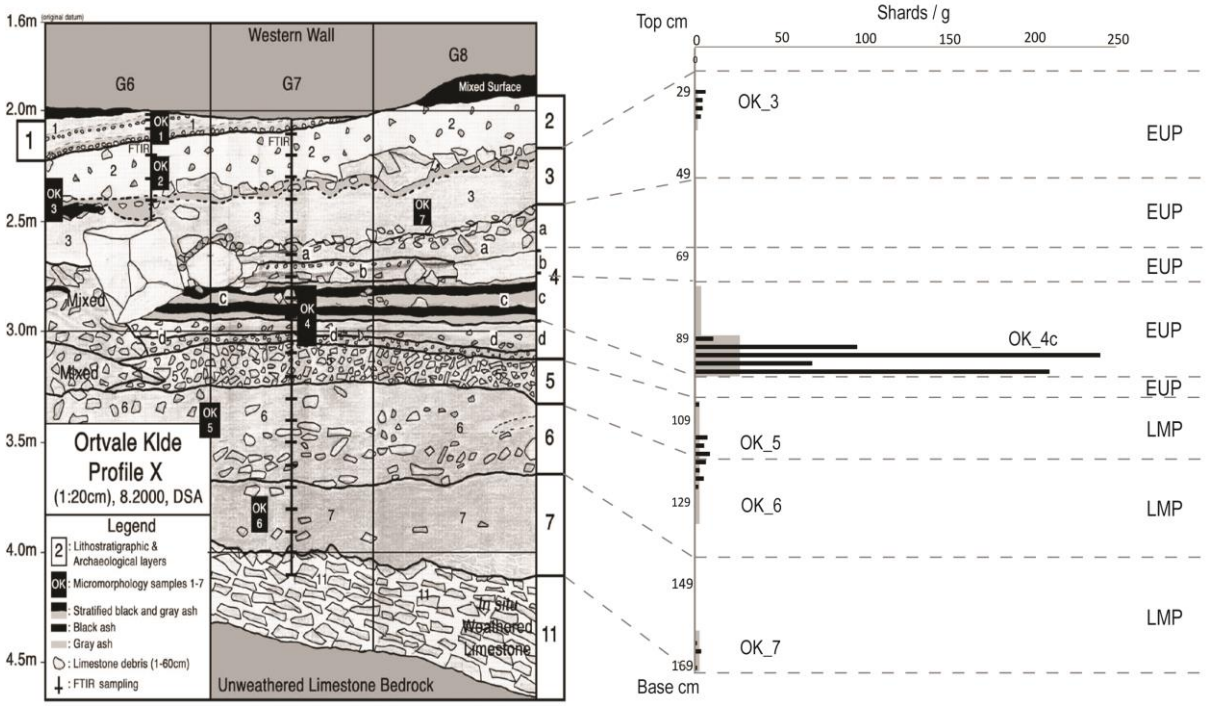

Figure 8.3. Site profile of the western section of Ortvale Klde (left; Profile image from Adler et al., 2008). Right shows the tephra profile and the tephra stratigraphy (glass shards concentrations). Grey boxes are the s/g concentration from the initial, low resolution samples, black lines are the s/g concentration of glass shards found in each 2cm (high resolution) bag of sediment (see methods Chapter 5). Far right on the tephra profile indicate archaeological techno-complex associated with each layer: LMP, Late Middle Paleolithic; EUP, Early Upper Palaeolithic.

Visual analysis of the tephra layers showed no discernible differences between the samples (Figure 8.4). All samples exhibited colourless shards ranging from 40-100 micrometres across the longest axis. Shards are very irregular with some evidence of expanded vesicles, cuspate features and some fluting. OK_5 also contained some platy shards. Brown shards were also found in sample OK_4c.

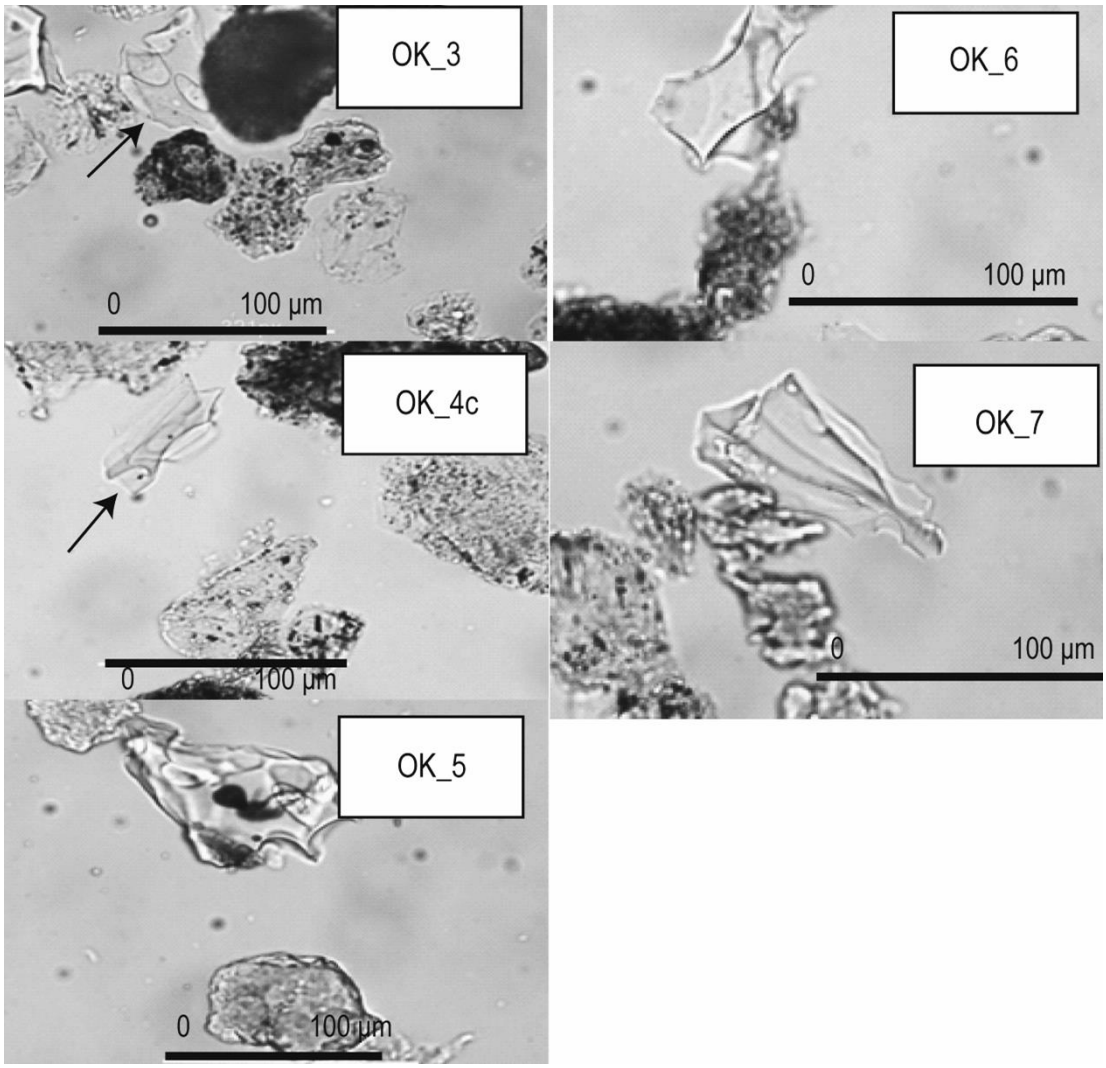

Figure 8.4. Images of glass shards in Ortvale Klde. Shards display similar morphologies.

The chemical results show four tephra compositions in Ortvale Klde (Figure 8.5). Average compositional values are given in Table 8.3.

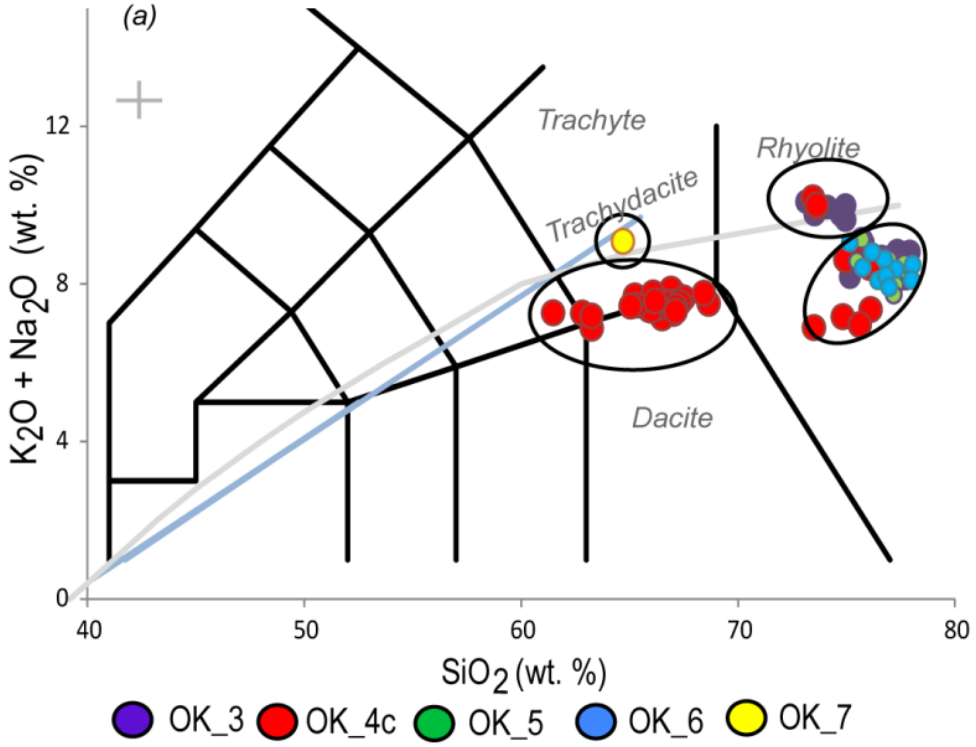

Figure 8.5. TAS of Ortvale Klde glass (tephra) compositions. There are four compositional grouping. Average numerical values for populations (wt. %) are shown in Table 8.2.

OK_7 is the oldest tephra preserved at in the site. Only one analysis was possible due to the low shard concentrations and small size of glass shards within the sediment. OK_7 is trachy-dacitic in composition (Figure 8.5; Table 8.3) with a SiO_2 value of 64.71 wt. %. This is similar to the dacite population of OK_4c (p3; Table 8.2) but it can be differentiated based on high Na_2O and Cl wt. % (5.97 and 0.21, respectively, Figure 8.6 g and h).

OK_5 and OK_6 are both calc-alkaline rhyolites that are compositionally identical, with ~75-78wt. % SiO_2, 4.09–5.63 wt. % K_2O and both show bimodality on FeOt totals (~0.3-0.6 and ~1 wt.%; Figure 8.5, 6 a-h, Table 8.3). The highest concentration in glass shards (8 s/g) was found at 120-112 cm which is the boundary of Layer 6 and 5 in Ortvale Klde (Figure 8.3).

OK_4c has three populations. Two populations are rhyolitic (p1 and 2; Table 8.3) and the other is a dacite (p3; Table 8.3; Figure 8.5). The rhyolitic populations can be split based on their total alkali values (see Figure 8.5); p2 more alkali-rich with higher FeOt compositions (3.08-3.28 wt.%) and is mildly peralkaline in comparison to p1 that is calc-alkaline (Table 8.2, Figure 8.6). The dacite population has 61.48-68.65 wt. % SiO_2 and high CaO and FeOt contents (2.78-5.78 wt. % and 4.16-6.03 wt. %, respectively Figure 8.5, 8.6c, d Table 8.2). This glass composition is distinct from other tephras in the Ortvale Klde sequence (Figure 8.5).

EMPA results from OK_3 indicate it has two compositional populations. One population (p1; Table 8.2) is readily distinguishable from all other chemical groupings in the sequence, with elevated FeOt composition (~4 wt. %), coupled with Al_2O_3 compositions of ~10 – 12 wt. %. These shards are peralkaline rhyolites (see Table 8.2, Figures 5a-c). Population two (p2) in OK_3 is slightly more evolved than p1 glasses (~75 – 77.93 wt. % SiO_2) and has higher Al_2O_3 compositions (>12.33 wt. %), but lower FeOt values (0.39 – 1.29 wt. %). These shards are compositionally similar to shards from OK_5, OK_6 and one chemical group of OK_4c (p1). OK_3, p1 is also similar to OK_4c p2, but has higher FeOt values (Figure 8.5c).

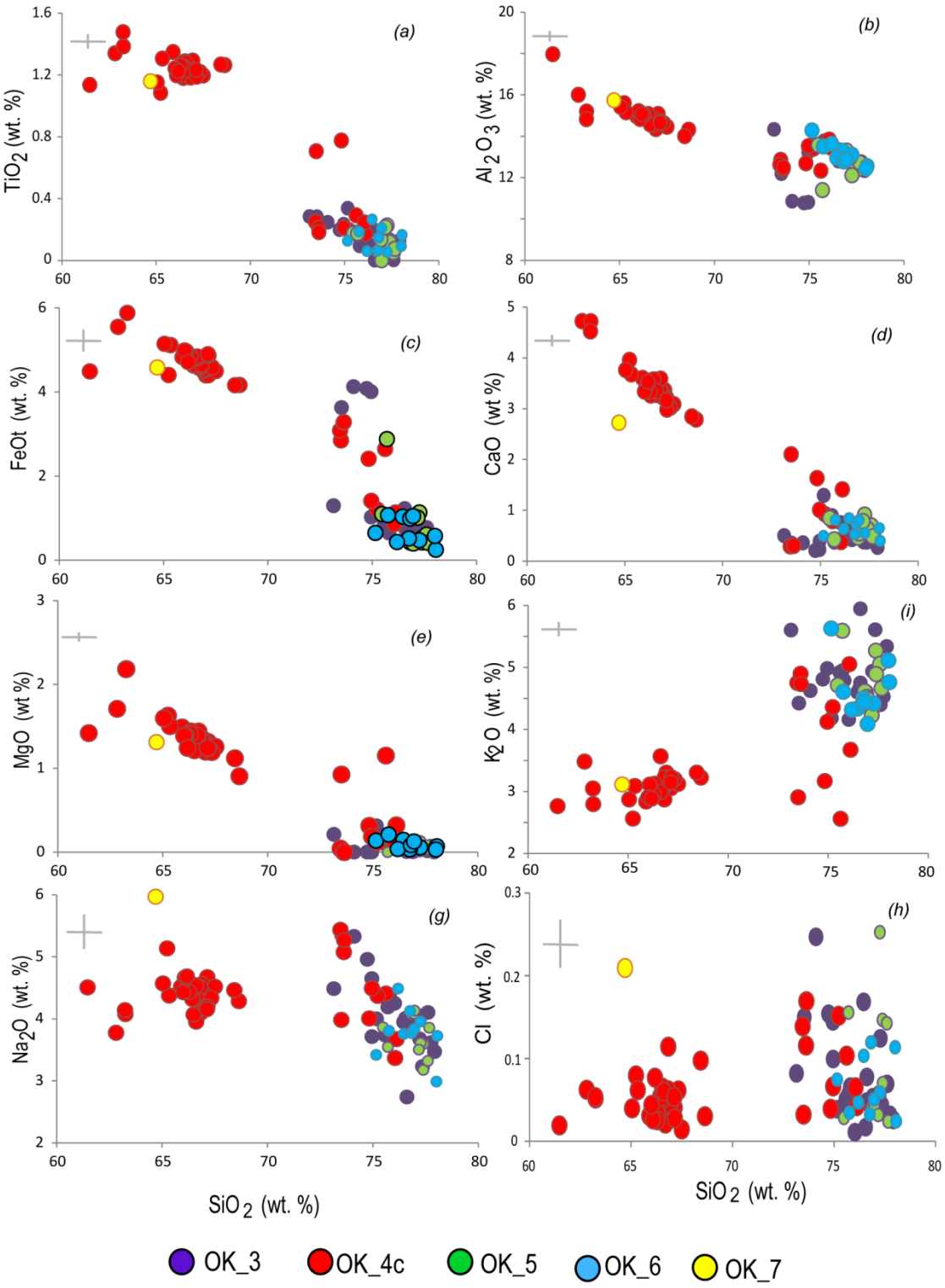

Figure 8.6. Harker diagrams of glass compositional data from tephras in Ortvale Klde.

Table 8.3. (next page) Average glass shard compositions (with 1σ) for tephras in archaeological layers from Ortvale Klde. Full data are presented in Appendix 1; descriptions are based on the full data set.

Sample No.	OK_3				OK_4C					
Population	p1 n=18	*1σ*	p2 n=4	*1σ*	p1 n=7	*1σ*	p2 n=3	*1σ*	p3 n=30	*1σ*
Major (wt. %)										
SiO_2	74.34	*0.64*	76.35	*1.17*	75.19	*0.90*	73.58	*0.10*	66.15	*1.57*
TiO_2	0.24	*0.04*	0.14	*0.09*	0.37	*0.26*	0.21	*0.03*	1.24	*0.08*
Al_2O_3	11.15	*0.69*	13.16	*0.53*	13.15	*0.54*	12.50	*0.11*	14.96	*0.68*
FeOt	3.96	*0.23*	0.81	*0.23*	1.78	*0.82*	3.21	*0.11*	4.78	*0.42*
MnO	0.08	*0.04*	0.05	*0.04*	0.03	*0.01*	0.07	*0.02*	0.07	*0.04*
MgO	0.00	*0.00*	0.08	*0.08*	0.44	*0.42*	0.01	*0.02*	1.40	*0.26*
CaO	0.28	*0.08*	0.54	*0.24*	1.18	*0.58*	0.30	*0.01*	3.55	*0.62*
Na_2O	5.07	*0.33*	3.88	*0.42*	4.04	*0.42*	5.26	*0.18*	4.39	*0.26*
K_2O	4.71	*0.24*	4.91	*0.59*	3.69	*0.88*	4.79	*0.09*	3.06	*0.21*
P_2O_5	0.01	*0.01*	0.01	*0.01*	0.07	*0.06*	0.02	*0.01*	0.36	*0.05*
Cl	0.17	*0.05*	0.06	*0.04*	0.07	*0.04*	0.14	*0.03*	0.05	*0.02*

Sample No.	OK_5 n=11	*1σ*	OK_6 n=9	*1σ*	OK_7 n=1
SiO_2	76.95	*0.72*	76.69	*0.95*	64.71
TiO_2	0.12	*0.07*	0.15	*0.07*	1.16
Al_2O_3	12.76	*0.63*	13.14	*0.59*	15.74
FeOt	0.85	*0.73*	0.70	*0.31*	4.58
MnO	0.06	*0.04*	0.05	*0.07*	0.13
MgO	0.07	*0.05*	0.10	*0.06*	1.31
CaO	0.63	*0.16*	0.65	*0.16*	2.72
Na_2O	3.70	*0.32*	3.77	*0.42*	5.97
K_2O	4.76	*0.41*	4.64	*0.47*	3.11
P_2O_5	0.01	*0.01*	0.02	*0.02*	0.37
Cl	0.09	*0.07*	0.07	*0.04*	0.21

8.3.1. Discrimination of primary and secondary deposition

OK_3 is stratigraphically discrete and contains two populations, one that is peralkaline and one that is calc-alkaline. These tephras are primary fall deposits from two different volcanoes, either spaced closely in time or unresolved due to low sedimentation rates. The spread of shards could also be a result of animal activity identified in the layer or reworking from the landscape (see sections 3.3.1 and 3.4).

Layer 4c has three populations that are confined within its boundaries; no tephra was found in Layer 4b. Positioning of the isochron is difficult as there are two peaks in shard concentration so it is conservatively placed at the base of Layer 4c, encompassing both peaks. Chemical compositions were the same in both peaks with no visual differences. Micro-morphological results indicate some limited, localised horizontal movement (likely water borne) in Layer 4c that could result in dislocation of shards and could account for the formation of two peaks. The limited tailing of shards above is due to remobilisation from the landscape and/or anthropogenic or animal activity at the site. The presence of peralkaline and two distinct calc-alkaline tephras would suggest at least two volcanic sources for the tephras found with eruptions that were closely spaced in time.

OK_5 and OK_6 are identical calc-alkaline rhyolites. The highest tephra concentration was found at 120-112 cm (boundary of Layer 6 and 5) with some reworking of shards vertically through the sequence (~10 cm in total). This tephra represents the same eruptive event, with the isochrones falling at the start of Layer 5. Vertical movement down could be a result of bioturbation noted in the site, but also trampling from anthropogenic activity. Dislocation of shards above

the peak could be due to the remobilisation of shards from the landscape (until the catchment becomes exhausted). OK_7 is distinguishable (chemically and stratigraphically) from all other tephra horizons in Ortvale Klde: this represents a primary deposit.

8.3.2. Radiocarbon dating results.

Tephras in Layer 4c (OK_4C p1 to p3) are positioned stratigraphically above the earliest evidence for AMH in the Caucasus (Layer 4d; see section 4.3.1 and 2.3.2). Previous radiocarbon ages for Layer 4c (charcoal ages without an ABOXs pre-treatment) and Layer 4d (bone sample that did not undergo ultrafiltration) could be underestimates (see section 1.3). To provide a more robust age for these tephra, 11 new bone samples from Layers 4d-4b were collected from the 2008 excavation archive material housed at the Georgian National Museum, Tbilisi. Samples were sent to the Oxford Radiocarbon Accelerator Unit (ORAU) and all underwent an ultrafiltration pre-treatment. Results are shown in Table 8.4.

Table 8.4. Radiocarbon results from Ortvale Klde.

Lab Code OxA-	Layer, Spit, depth (cm)	Code	Pass or fail	Date ± error*	$\delta^{13}C$	Date cal BP#
	4b	1OKC	Fail due to low yield			
27863	**4c, G8A 278-285**	**2OKC**	**Pass**	**39600±1100**	**-18.6**	**41976-45559**
	4c, G8A 278-285	3OKC	Fail due to low %N			
	4c, G8A 285-291	4OKC	Fail due to low %N			
27931	**4c, G8A 285-291**	**5OKC**	**Pass**	**34650±600**	**-18.5**	**37900-40744**
	4c, G8A 300-305/312	6OKC	Fail due to low yield and high CN			
	4c, G8A 300-	7OKC	Fail due to low %N			

	305/312					
27864	**4c, G8A 300-305/312**	**8OKC**	**Pass**	**43200±1700**	**-18.6**	**44470-49968**
	4d, G6c 299-308	9OKC	Fail due to low %N			
27932	**4d, G6c 299-308**	**10OKC**	**Pass**	**22480±150**	**-18.8**	**26364-27245**
	4d, G6c 299-308	11OKC	Fail due to low yield and high CN			

*Footnote: *ages shown are un-calibrated age determinations. # Ages calibrated with IntCal13 on the OxCal 4.2.3. platform (Bronk Ramsey, 2009; Reimer et al., 2013) and are show at 94.5% confidence. These ages are not modelled (see section 9.5).*

Due to the poor preservation of collagen, radiocarbon determinations were only possible on four bones. Layer 4c is older than previous ages (see Adler et al., 2008). Sample 10OKC (Layer 4d) is too young and is likely an intrusive deposit due to bioturbation in the site.

8.4. Sakajia Cave (Republic of Georgia), site No. 2

Negligible amounts of tephra were found in MP Unit 3e (~1 s/g) between 314-324 cm and 3a (~4 s/g) between 150 - 140 cm, but larger concentration of shards were found between 0-20 cm (~20 s/g) in Unit 2 that is associated with UP activity at the site (Figure 8.7). Two samples from Unit 2 - the lowest s/g 'peak' at ~ 16-18 cm (SK_2b) and a higher one at 8-10 cm (SK_2t; Figure 8.7) - were prepared for WDS-EPMA analysis. Shards of tephra were also extracted from Unit 3a from an amalgamation of sediments across 8 cm (~140-148 cm) to maximise the number of shards from this Unit (SK_3a). No further shards could be extracted from Unit 3e.

Shards in Unit 2 and 3a (SK_2t, SK_2b and SK_3a) are irregular in form with expanded and sometimes closed vesicles with fluting a common feature (Figure

8.7). SK_3a appeared to have a higher relief in optical analysis than Unit 2 tephras and shards were generally smaller in size (~40-60 micrometres across the largest shard diameter) compared to 50-100 microns for Unit 2 tephras (Figure 8.7).

SK_2b and SK_2t are both calc-alkaline rhyolites (Figure 8.8). SK_2t has three populations: population 1 (p1), ~74 wt. % SiO_2, population 2 (p2), 75-76 wt. % and population 3 (p3) with SiO_2 composition of > 76 wt. % (Figure 8.9 a-j, Table 8.5). These tephras are all compositionally low in FeOt (< 1 wt. %; Figure 9c). SK_2t, p1 is elevated in Al_2O_3 (> 14 wt. %) compared to p2 and p3. SK_2b is chemically indistinguishable from p3 of SK_2t (Figure 8.8, 8.9 and Table 8.5). Only one analysis was obtained from the tephra found in Unit 3a. SK_3a is a calc-alkaline rhyolite with 75.87 wt. % SiO_2 and is distinguishable from Unit 2 tephras with a higher FeOt content (2.82 wt. %) and lower CaO content (0.25 wt. %; Figure 8.8, 8.9c, d).

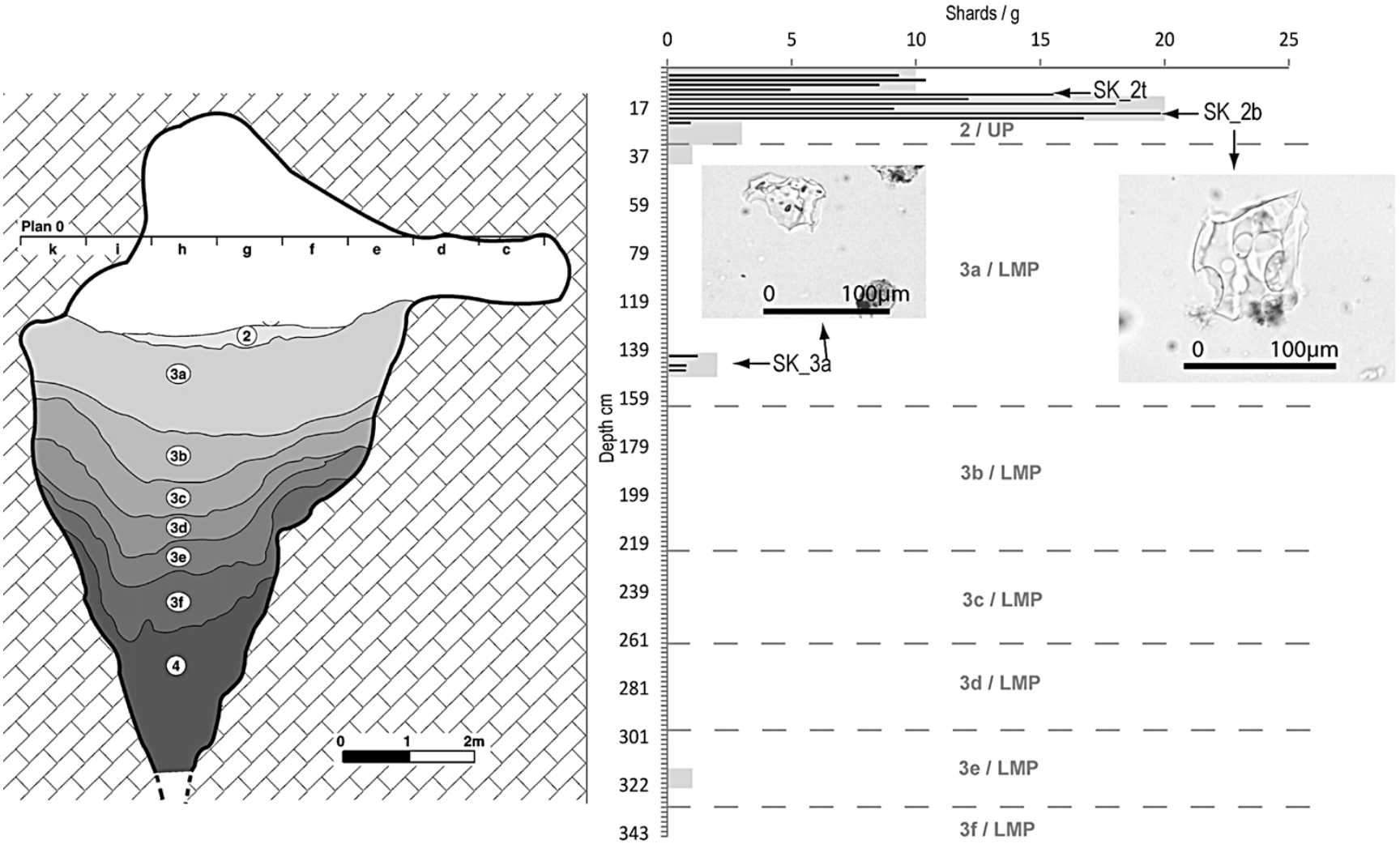

Figure 8.7. Site profile of Sakajia cave showing the defined archaeological horizons (left). Right shows tephra profile alongside the interpreted archaeological techno-complexes (adapted from Pleurdeau et al., 2007) and two images of representative glass shards from the layers selected for EPMA analysis.

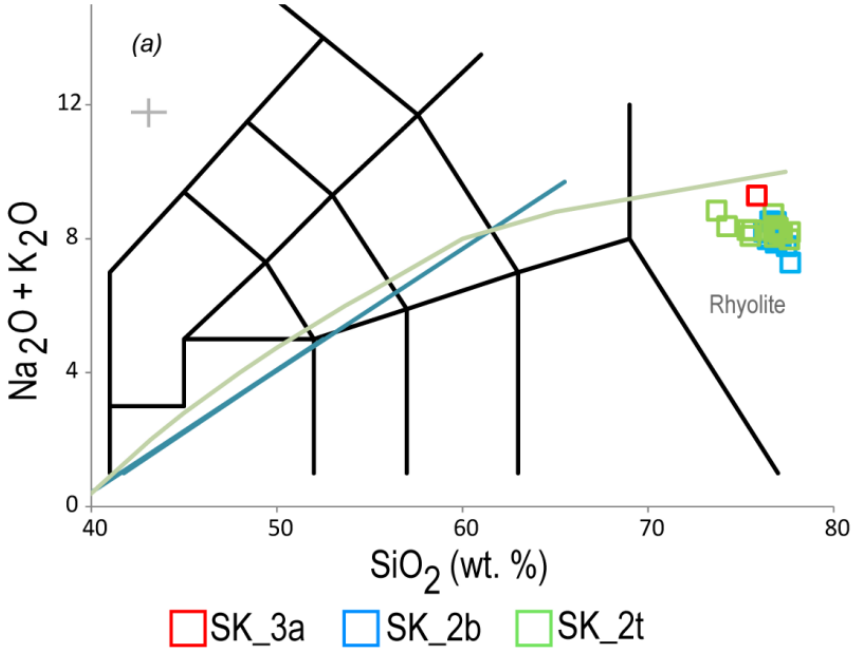

Figure 8.8. TAS plot with glass compositions of tephra found at Sakajia Cave.

Table 8.5. Average Glass compositions from tephras in Unit 2 and 3a of Sakajia Cave

Sample No.	SK_2b		SK_2t						SK_3a
Population			p1		p2		p3		
	n=17	*1σ*	n=2	*1σ*	n=3	*1σ*	n=10	*1σ*	n=1
Major (wt. %)									
SiO_2	76.86	*0.37*	73.98	*0.40*	75.50	*0.13*	77.09	*0.35*	75.87
TiO_2	0.15	*0.07*	0.30	*0.00*	0.23	*0.05*	0.17	*0.06*	0.18
Al_2O_3	12.98	*0.19*	14.39	*0.19*	13.58	*0.39*	12.64	*0.28*	11.33
FeOt	0.86	*0.13*	0.99	*0.26*	1.01	*0.04*	0.84	*0.13*	2.82
MnO	0.04	*0.03*	0.07	*0.03*	0.01	*0.01*	0.02	*0.02*	0.11
MgO	0.10	*0.06*	0.29	*0.01*	0.19	*0.03*	0.11	*0.04*	0.00
CaO	0.83	*0.09*	1.24	*0.02*	1.15	*0.23*	0.79	*0.08*	0.25
Na_2O	3.45	*0.30*	4.12	*0.11*	3.56	*0.14*	3.37	*0.26*	4.77
K_2O	4.63	*0.11*	4.48	*0.22*	4.63	*0.07*	4.87	*0.38*	4.51
P_2O_5	0.02	*0.02*	0.04	*0.05*	0.04	*0.01*	0.02	*0.01*	0.00
Cl	0.07	*0.03*	0.10	*0.00*	0.11	*0.05*	0.07	*0.02*	/

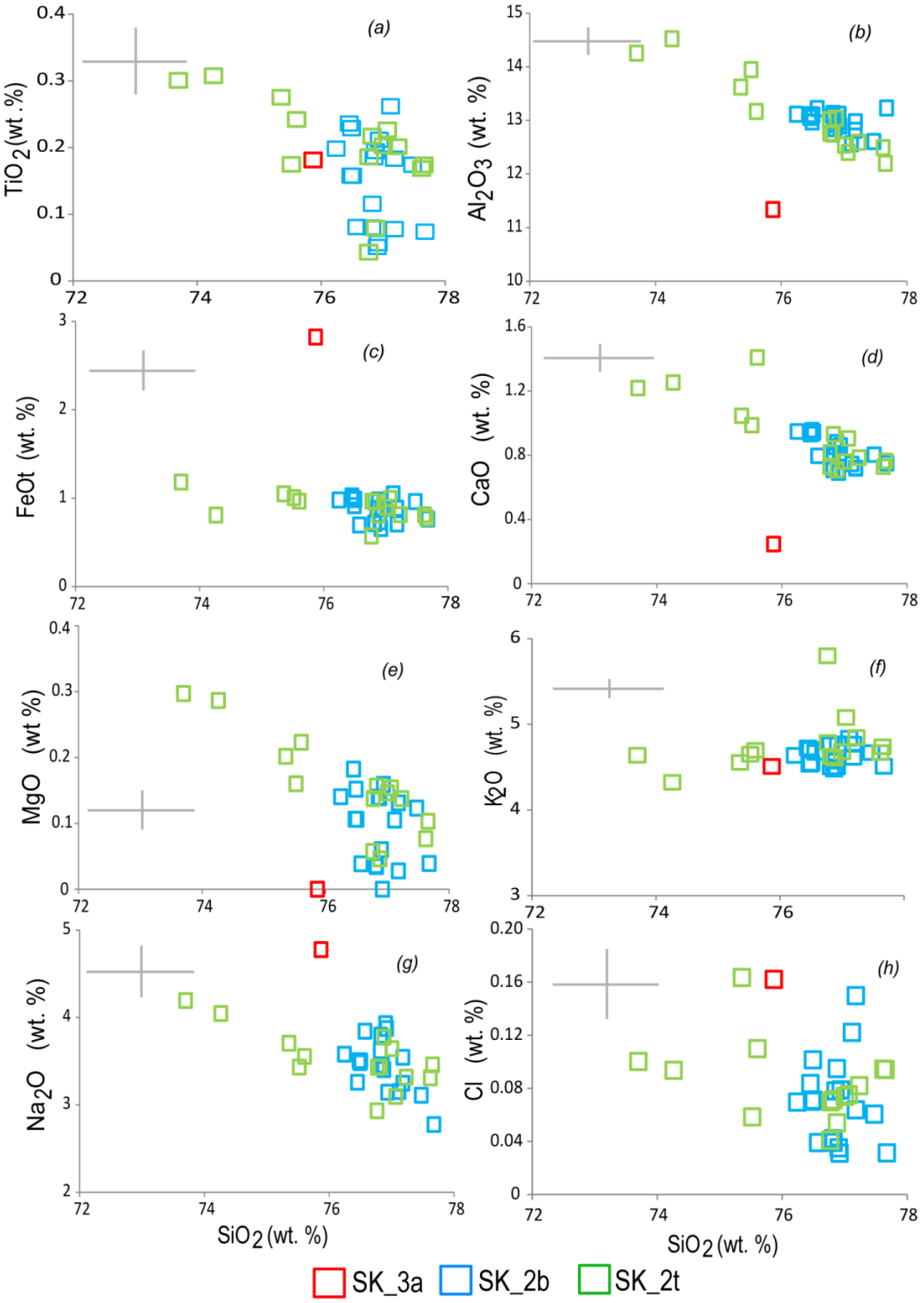

Figure 8.9. Grain specific glass compositional data plotted in Harker diagrams of tephra shards found in Layer 2 and 3a in Sakajia Cave, Georgia.

8.4.1. Discrimination of primary and secondary deposition

SK_3a is stratigraphically and compositionally distinct from the glasses in Unit 2, with ~102 cm of sterile sediments that separates them. This tephra deposit is a primary deposit. There are three tephra compositions in Unit 2. SK_2t is composed of all three, while SK_2b is identical to SK_2t, p3. Glass shards compositions from SK_2t and SK_2b sit on the same trend (Figure 8.9) suggesting the same volcanic source, with a number of closely spaced eruptions recorded in Layer 2. Tephras were deposited during the development of Unit 2, as there is a clear and sharp introduction of tephra at the base of Unit 2/Unit 3a (with little downwards dislocation of shards). No single isochron can be defined. The spread of tephra could be a result of reworking from the landscape or faunal / anthropogenic activity.

8.5. Undo Cave (Republic of Georgia), site No. 3

Samples were taken from a deep sondage (associated with MP archaeology) outside the cave and from a test trench that was dug at the mouth of the cave (Figure 10). Samples from outside the cave did not contain tephra. Inside the cave, cryptotephra was found between 14 and 40 cm, with a peak in shard concentration (~118 s/g) at 18-20 cm that is associated with a UP type lithics (UC_II, Figure 8.10). Visual analysis of shards showed they ranged from 40-70 micrometres across the longest axis and were colourless and morphologically fluted (Figure 8.10).

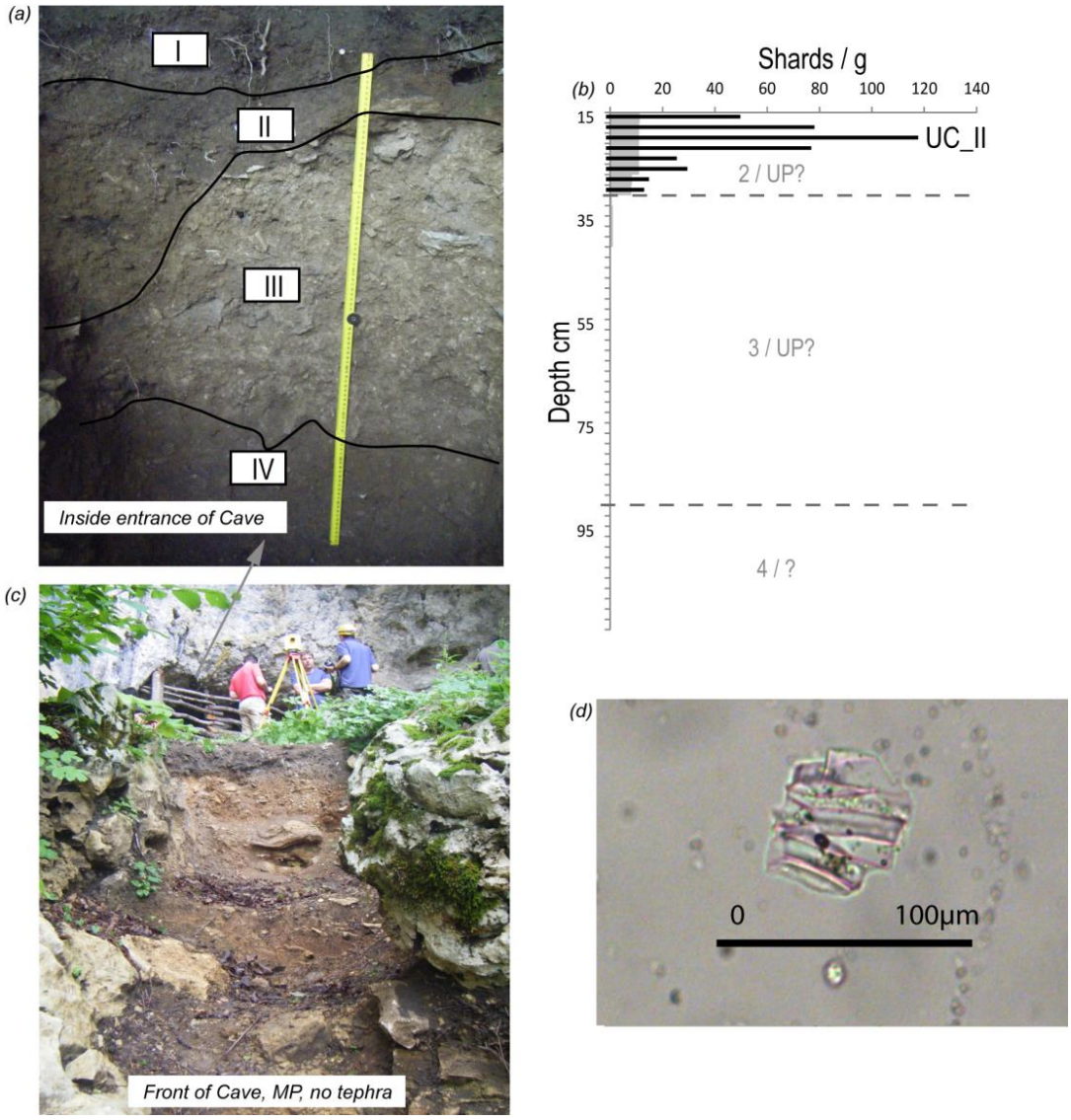

Figure 8.10. Photo of profile that was dug inside the entrance to Undo Cave (a). UP artefacts were found associated with these layer, but formal excavation had not occurred at time of sampling. (b) shows the tephra profile from this section, while (c) shows section at the front of the Cave that is associated with MP finds. No tephra was found. Photo (d) is a representative glass shard.

The major element composition of UC_II is variable and clearly experienced alkali exchange, mobilisation of Na_2O and K_2O (highlighted in Table 8.6). This may be related to the acidic composition of the host sediment. Consequently, this tephra cannot be reliably linked to a source or other tephra deposits.

Table 8.6. WDS-EPMA, Major glass compositional data from 9 shards analysed from Undo Cave. Alkali exchange between Na_2O and K_2O is clearly evident in all shards.

Undo Cave (n=9)									
Major elements (wt. %)									
SiO_2	75.84	75.56	75.19	75.38	75.19	75.29	74.99	74.69	74.87
TiO_2	0.05	0.06	0.06	0.04	0.02	0.08	0.10	0.05	0.06
Al_2O_3	12.73	12.78	13.10	13.01	13.15	12.71	12.84	12.85	12.76
FeOt	0.76	0.61	0.62	0.70	0.73	0.66	0.70	0.75	0.61
MnO	0.04	0.09	0.10	0.05	0.06	0.03	0.03	0.02	0.06
MgO	0.05	0.03	0.05	0.02	0.03	0.03	0.02	0.00	0.04
CaO	0.72	0.65	0.69	0.62	0.65	0.68	0.63	0.56	0.48
Na_2O	1.56	0.84	0.66	0.65	0.59	0.00	0.07	0.27	0.29
K_2O	8.21	9.33	9.47	9.48	9.51	10.47	10.58	10.75	10.77
P_2O_5	0.00	0.00	0.02	0.01	0.04	0.01	0.00	0.02	0.02
Cl	0.05	0.04	0.05	0.05	0.03	0.04	0.05	0.04	0.04

8.6. Ortvale Cave (Republic of Georgia), site No. 4

Cryptotephra was found preserved between 90-116 cm in Unit 3 of Ortvale Cave (Figure 8.11). Sediments either side of the deposit were sterile. Unit 3 has evidence of a MP type techno-complex associated with Neanderthal teeth (see Chapter 4.3.4). The shard count was low across these depths with a maximum of 2 s/g between 90-100 cm. The high resolution samples showed the concentration of tephra to be constrained to 2cm of sediment (~5 s/g) between 98 and 100 cm (Figure 8.11).

Shards were 50-150 micrometres in size and have an irregular morphology with some expanded vesicles (Figure 8.11). Shards were isolated from the host sediment with techniques outlined in Chapter 5 and prepared for WDS-EPMA

analysis. Due to the low shard concentrations and the small size of the glass shards in Unit 3, only 4 analyses were obtained for Ortvale Cave; labelled OT_3.

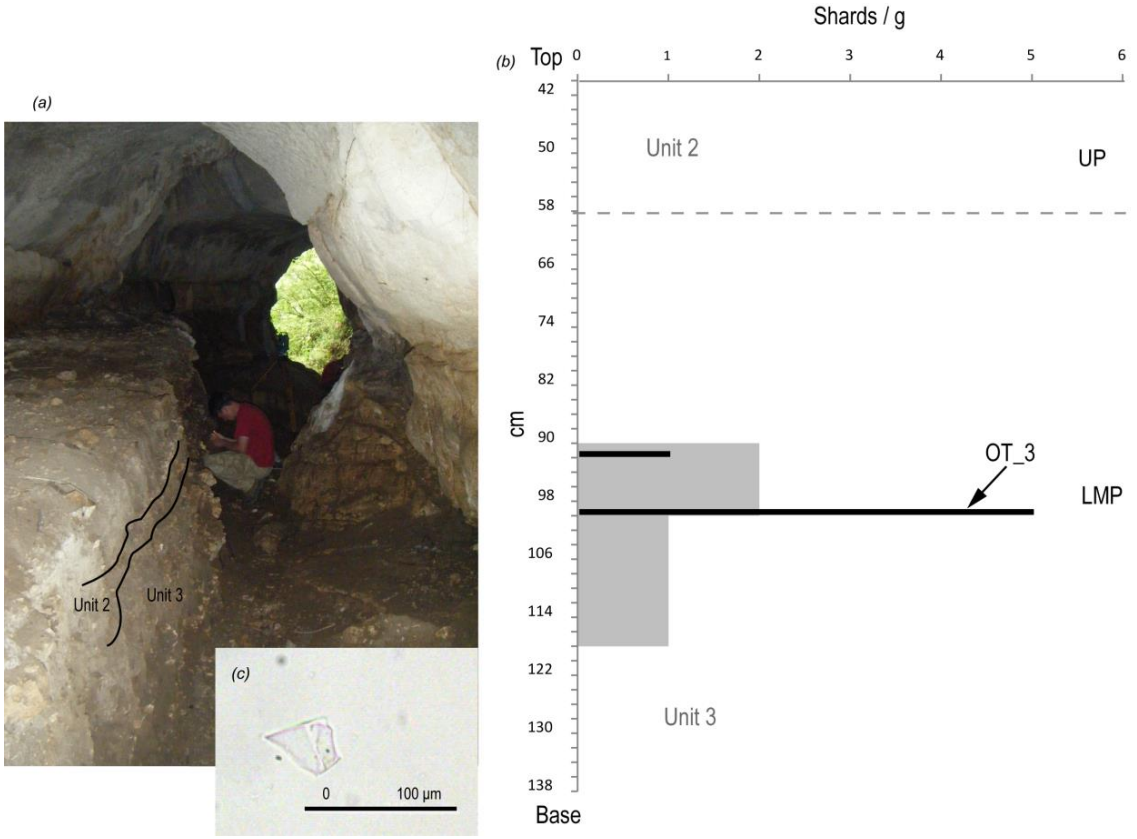

Figure 8.11. (a) image taken from inside the cave showing the cave mouth in the background and the sediment section that was sampled on the left. The tephra profile for Ortvale Cave is shown in (b) (right). Tephra (c) was preserved in sediments associated with a MP techno-complex.

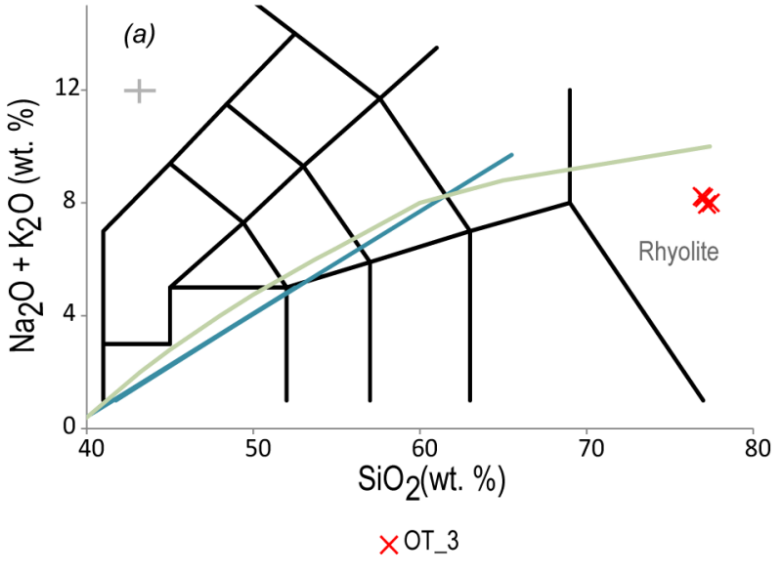

Figure 8.12. TAS of glass shard compositions of tephra from Ortvale Cave.

OT_3 is a homogeneous calc-alkaline rhyolite with a SiO_2 composition between 76.92 – 77.45 wt. % (Figure 8.12) that is compositionally low in FeOt (~ 0.71-0.86 wt. %). Across all four analysis, Na_2O compositional values are consistently <4 wt. % with K_2O > 4 wt. % (Table 8.7).

Table 8.7. WDS-EPMA, Major element, glass compositional data of 4 tephra shards extracted from Ortvale Cave.

Ortvale Cave (n=4)				
Major elements (wt. %)				
SiO_2	77.45	76.92	77.23	77.05
TiO_2	0.16	0.19	0.16	0.08
Al_2O3	12.52	12.72	12.67	13.06
FeOt	0.86	0.81	0.85	0.71
MnO	0.00	0.06	0.02	0.06
MgO	0.13	0.14	0.14	0.06
CaO	0.80	0.81	0.89	0.67
Na_2O	3.20	3.38	3.30	3.63
K_2O	4.80	4.84	4.64	4.55
P_2O_5	0.02	0.02	0.03	0.06
Cl	0.07	0.10	0.07	0.07

8.6.1. Discrimination of primary and secondary deposition

OT_3 is well constrained within 2 cm of sediment, with sterile sections either side. WDS-EPMA analysis was performed over 2 days (see methods Chapter 5) and consistently showed OT_3 to be a homogenous, calc-alkaline rhyolite. Tephra found in Unit 3 is from one primary event. It was not possible to extract shards from the second higher peak.

8.7. Lusakert 1 rock shelter (Armenia), site No. 8

Samples were taken from outside and inside the rock shelter of Lusakert 1 to see if tephrostratigraphy could assist on linking the two sondages that contain a different MP techno-complex. Results will be discussed separately. For simplicity, the Lusakert rock shelter (LKI_?) will be referred to as such, but the outside profile will be called Lusakert 1 (LKO_?).

Lusakert rock shelter has formed in the base of a lava flow and preserves a unique MP type technology produced solely with obsidian (Adler *pers comm*., 2013; section 4.3.5). As such, a background of volcanic glass was expected in the sediments that may mask exogenous tephra deposits (see section 3.3.1). The following criteria and methodological approach were applied when choosing appropriate horizons for WDS-EPMA analysis.

Samples were processed at individual 2 cm bag resolution (n=70); initial scan samples were deemed inappropriate due to the expected background. Visual analysis played a key role in the identification of possible exogenous tephra inputs to the cave sediments. Optical assessment of tephra that formed the archaeologically sterile section (Unit 10) was used as a control. This layer is believed to be formed through endogenous sedimentation and as such acted as a visual control that other samples were compared to (section 4.3.5). Shards from Unit 10 were fluted and irregular in form with lots of micro-crystal inclusions in some glass shards. Brown shards were also found; they were platy to irregular with some micro-crystals. Approximately a 2:1 ratio of clear to brown shards were found in control layers (Figure 8.13). Any changes in visual characteristics of shards through the profile were noted as samples were counted. In addition, the

dense fraction (> 2.55 cm/g^3, see methods) was checked for all samples to assess if denser basaltic/brown shards were present. Once s/g concentrations of each 2 cm sample through the profile was established and peaks in shard concentrations were established, these data was then compared to any visual changes in shard morphology. Choices of horizons for EPMA are based on both these criteria. Background samples were selected randomly from Unit 10 for WDS-EPMA analysis to compare to the other chemical results. Pieces from obsidian debitage found in the site were also collected and crushed for visual and WDS-EPMA analysis (see section 3.3.1).

8.7.1. Tephra results from the Lusakert rock shelter.

A mix of clear and brown shards were found throughout the sequence, but six cryptotephra peaks and one possible visible layer were chosen for EPMA (Figure 8.14).

A large concentration of clear shards (~51,507 s/g) was found at the base of Unit 7 (100-102 cm) at the contact with Unit 10 (Figure 8.14; LKI_7). Shards in this peak have a different morphology. They are very vesicular in form with some fluting and do not contain micro crystals (Figure 8.13). Shards range from 40 – 90 micrometres in size and have a low relief. No visual change was noticed again until Unit 6.5, where there was a significant decrease in clear shards and, upon analysis of the dense fraction a significant increase in the concentration of brown shards was noticed (~186,540 s/g; Figure 14). LKI_6.5 forms a continuous dark brown deposit that is approximately 1 cm thick and has previous been considered a visible, tephra layer in the site. Shards ranged from 50-90 micrometres in size and were predominantly dark brown to brown in colour with platy to vesicular

morphology and some shards contained microcrystals. Shards from this layer were well constrained within 2-4 cm indicate little mobilisation of shards either side of the main 1 cm peak (Figure 8.14).

The next visual change was noticed at 83-84 cm in Unit 5.2 which was accompanied by an increase in clear shards (30,662 s/g) and labelled LK_5.2B (B=base of Unit). Visually this peak was identical to LK_7 (Figure 8.14). Unit 5.2 contained a second peak in clear shards towards the top that had a concentration of ~29,493 s/g and was labelled LKI_5.2T (T=top; Figure 8.14). Shards exhibited more fluting and were 50-180 micrometres in length, but were otherwise morphologically similar to LKI_5.2B with some microcrystals present in some of the glass shards.

At 36-38 cm (towards the top of Unit 5.1) an input of fresh looking shards with a vitreous lustre was noticed. Shards have a higher optical relief than seen previously and are vesicular to strongly fluted in form, ranging from 60-150 micrometres in size. The main peak was at 38-40 cm (LKI_5.1), which was followed by a decrease in shards towards the contact between Unit 5.1 and Unit 4.1.

Unit 4.1 contains a spread of tephra that has three peaks all with a s/g count >20,000 (Figure 8.14). The first peak at ~30-32 cm found at the base of Unit 4.1 looks visually similar to tephra in Unit 10, the background sample, so was not chosen for WDS-EPMA analysis. At 26-28 cm a visual changed was noted, with some shards exhibiting low relief while other shards were heavy fluted suggesting a mix in population of shards (~40,700 s/g). Shards generally ranged from 50-140 micrometres in size and this peak was chosen for WDS-EPMA analysis (LKI_4.1).

The largest and final peak was found at 24-26 cm towards the top of the unit with a shard/g count of ~42,923. This third peak in Unit 4.1 contained less, low relief shards, and had a population of shards that visually similar to the base of this unit; as such it was not chosen for geochemical analysis.

The final micro tephra layer selected was at the base of Unit 3 (~8-10 cm down the profile), LKI_3. Shards were fresh looking with very low relief on optical analysis and ranged from 60-160 micrometres in size and were morphologically vesicular with fluting (Figure 8.13); LK_3 had a s/g count of ~61,628.

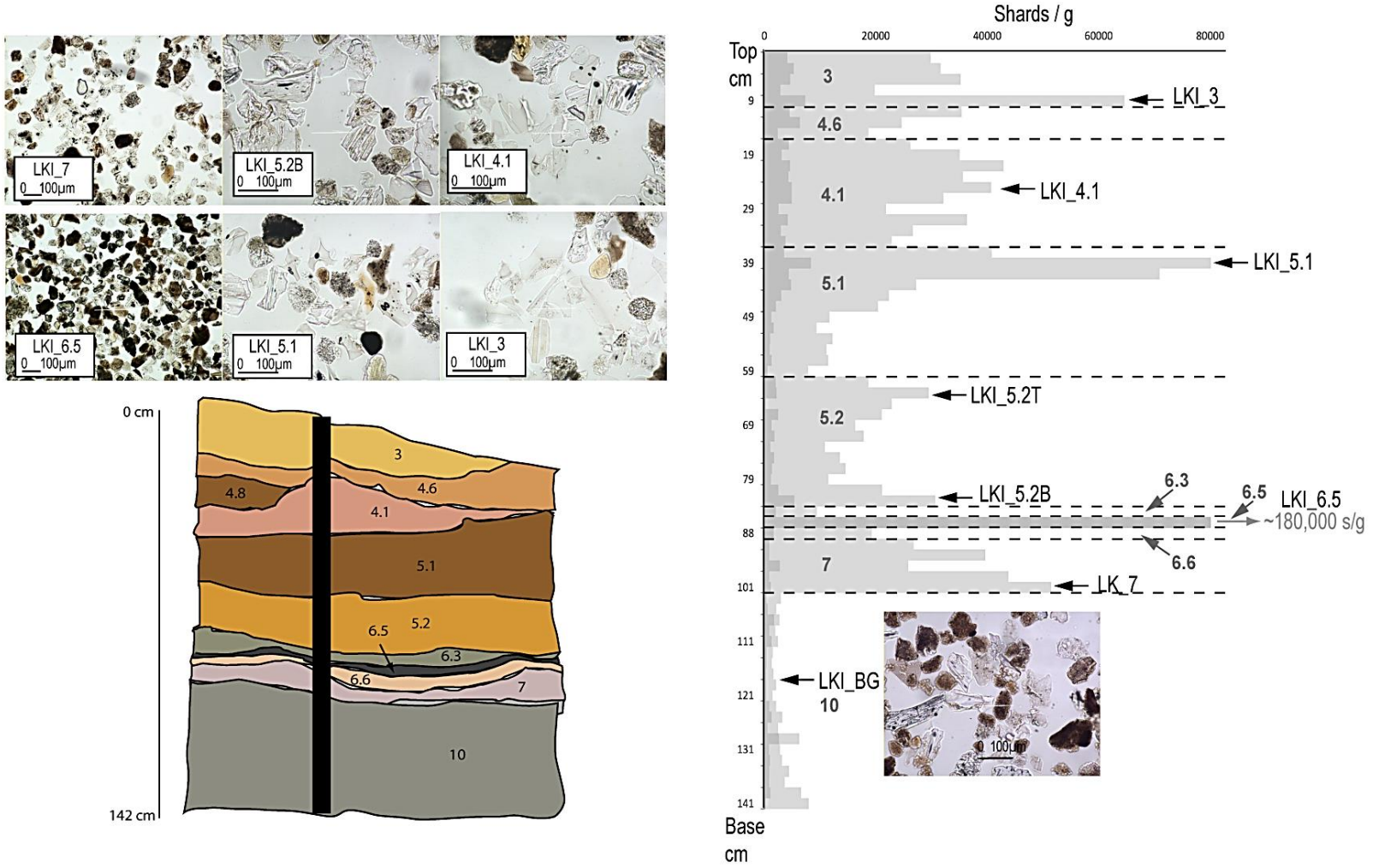

Figure 8.13. Top left shows representative images of tephra shards from each layer in Lusakert rock shelter. Note a visual difference in morphology. Left, bottom is a schematic of the Lusakert section profile (inside rock shelter) that was sampled; along the black box. Right shows the tephra profile of Lusakert; light grey bars show the concentration of clear shards, the darker grey denotes shards counted (s/g) in the dense fraction of each 2 cm sample. There was a continuous tephra presence through the site profile. Peaks in shard concentration that were accompanied with a visual change were chosen for WDS-EPMA analysis. These are labelled on the profile (right). Bottom of profile is an image of shards that are representative of the background content.

There are 11 compositional units preserved within the Lusakert sediments. LKI_5.2T showed a high degree of compositional scatter based on major elements and has been excluded from further analysis (see Figure 8.14a).

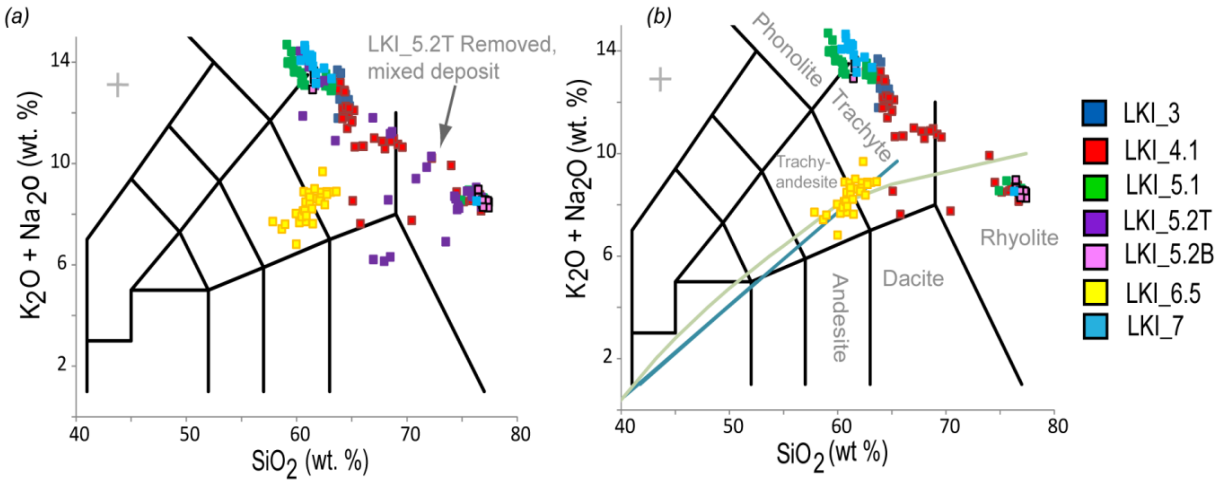

Figure 8.14. Compositional data from glass shards extracted from Lusakert. Sample LKI_5.2T shows scatter (a) so this sample has been excluded from further discussion (b) as this represented a mixed deposit and no further information could be gained.

Both LKI_7 and LKI_5.2B have two populations that are compositionally similar, both with a peralkaline and calc-alkaline component (Figure 8.14b). Population one (p1) from both units is alkaline-rich and straddles the trachyte, phonolite boundary with ~60-62 SiO_2 (wt. %), low CaO (~0.5–1 wt. %), and high FeOt (~4–6.27 wt. %). Population 2 (p2, calc-alkaline) has higher SiO_2 compositions (76-77.40 wt. %) and has generally lower Na_2O values (~3-4 wt. %) than p1 (Figure 8.15, Table 8.8). But LKI_7 p2 has greater FeOt that LKI_5.2B p2 (1.22 and 0.39-0.79 wt. % respectively).

LKI_6.5 (situated between LKI_7 and LKI_5.2B) is the only suspected visible deposit in Lusakert and is readily distinguishable from all other tephras found

preserved within the sedimentary sequence (Figure 8.15a-h). LKI_6.5 straddles the trachy-andesite, trachy-dacite boundary (Figure 8.14b) and has lower K_2O (2.67–4.17 wt. %) and higher CaO and MgO in comparison to other tephras in the Lusakert rock shelter (3.22–5.83 and 1.36–3.53 wt. % respectively: Table 8.8).

The next tephra horizon in the sequence, LKI_5.1, has one calc-alkaline rhyolite population (p3) that is chemically identical to p2 of LKI_7 and LKI_5.2B (Figure 8.14b, 8.15a-j). LKI_5.1 also has two peralkaline populations. P1 has shards with <60.74 wt. % SiO_2 that have elevated Na_2O (~7.77–9.33 wt. %) and CaO wt. % concentrations between 0.94-1.25 wt. % and straddle the trachyte, phonolite boundary. Population two (p2) that has higher SiO_2 contents (>62 wt. %) is trachytic in composition, with CaO concentrations ~0.8 wt. % (Figure 8.14b, Table 8.8 and Appendix 1).

LKI_4.1 has six compositional groupings, again containing both peralkaline and calc-alkaline shards (Figure 8.14b). Peralkaline populations one to three (p3, p2 and p1) are progressively more alkali-rich (~10.58–11.00, 11.39–12.25 and >12.83 wt.%, respectively based on $Na_2O + K_2O$ wt.%) and p1 and p2 have SiO_2 compositions generally < 65 wt.% (Figure 8.15, Table 8.8). All three populations are compositionally similar on all other major elements. Populations four and five (p4 and p5) are both rhyolites. P4 has higher Na_2O (5.30 wt. %) and FeOt (3.12 wt. %) compositions than p5 and is peralkaline rhyolite with lower CaO (0.33 wt. %) contents. P5 is compositionally identical to p2, from LKI_7, 5.2B and p3 from LKI_5.1 (Figure 8.15, Table 8.8). The final population in LKI_4.1 (p6) is a dacite (Figure 8.14b). This population (although less tightly grouped) has consistently higher CaO (>3.3 wt. %), MgO (> 0.66 wt. %) and P_2O_5 (0.14 wt. %) compositions

than all other shards in LK_4.1 and, with the exception of LKI_6.5 all other tephra's preserved in Lusakert rock shelter.

The final tephra horizon in Lusakert rock shelter is a homogeneous, peralkaline trachyte (Figure 8.14b), LKI_3. LKI_3 is alkali-rich with a SiO_2 range of 63.91–64.81 wt. % (Table 8.8). LKI_3 has chemical similarities to p1 of LKI_5.1 and LK_7 and some tephras in LKI_4.1 (Figure 8.14b, 8.15).

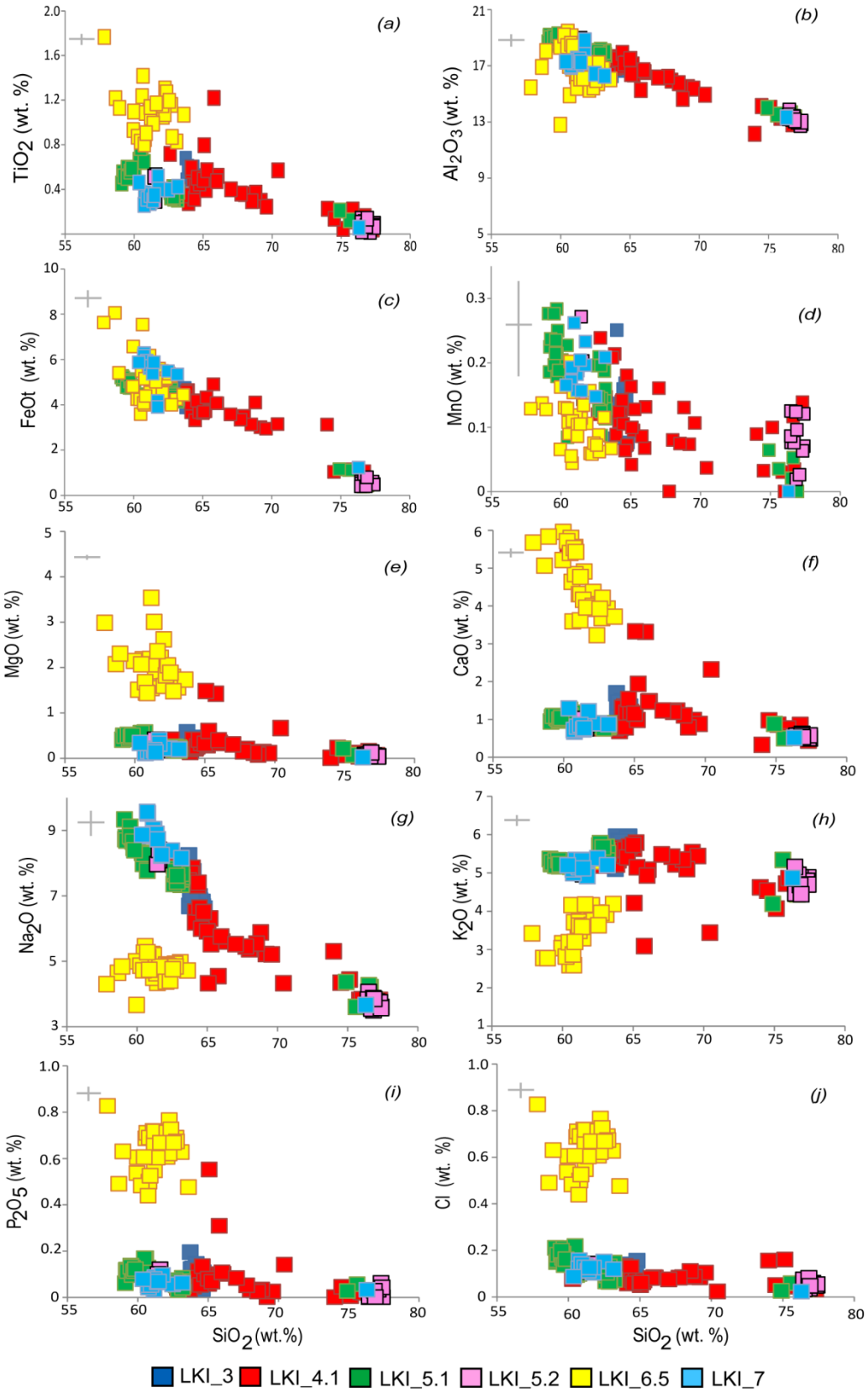

Figure 8.15. Harker diagrams of glass shard compositions of tephras layers analysed from inside the Lusakert profile.

Table 8.8 (next page). Average glass shard concentrations (with 1σ) of tephras found in the Lusakert rock shelter

Sample No.	LKI_3		LKI_4.1								
Population			p1		p2		p3		p4	p5	
	n=14	*1σ*	n=8	*1σ*	n=10	*1σ*	n=10	*1σ*	n=1	n=7	*1σ*
Major (wt. %)											
SiO_2	64.29	*0.39*	63.62	*0.66*	64.64	*0.37*	67.63	*1.48*	74.01	76.03	*0.96*
TiO_2	0.49	*0.10*	0.39	*0.14*	0.48	*0.06*	0.39	*0.10*	0.23	0.11	*0.07*
Al_2O_3	16.80	*0.17*	17.12	*0.30*	17.42	*0.24*	15.91	*0.62*	12.15	13.43	*0.49*
FeOt	3.90	*0.30*	4.50	*0.38*	3.75	*0.24*	3.60	*0.51*	3.12	0.92	*0.30*
MnO	0.13	*0.05*	0.16	*0.05*	0.11	*0.04*	0.10	*0.05*	0.09	0.06	*0.05*
MgO	0.35	*0.10*	0.22	*0.08*	0.34	*0.05*	0.24	*0.16*	0.01	0.10	*0.07*
CaO	1.24	*0.25*	0.79	*0.06*	1.22	*0.15*	1.23	*0.34*	0.33	0.70	*0.21*
Na_2O	6.92	*0.49*	7.67	*0.25*	6.25	*0.24*	5.50	*0.21*	5.30	4.01	*0.31*
K_2O	5.67	*0.23*	5.37	*0.14*	5.64	*0.10*	5.27	*0.20*	4.62	4.56	*0.25*
P_2O_5	0.10	*0.04*	0.06	*0.01*	0.09	*0.02*	0.05	*0.04*	0.00	0.01	*0.02*
Cl	0.10	*0.03*	0.11	*0.02*	0.06	*0.01*	0.09	*0.01*	0.16	0.06	*0.04*

Sample No.	LKI_4.1		LKI_5.1					
Population	p6		p1		p2		p3	
	n=3	*1σ*	n=17	*1σ*	n=13	*1σ*	n=5	*1σ*
Major (wt. %)								
SiO_2	67.10	*0.86*	59.81	*0.51*	62.96	*0.36*	76.12	*0.84*
TiO_2	0.86	*0.33*	0.57	*0.08*	0.36	*0.03*	0.12	*0.06*
Al_2O_3	15.53	*0.77*	18.91	*0.15*	17.89	*0.16*	13.61	*0.25*
FeOt	3.91	*0.90*	4.83	*0.34*	4.36	*0.15*	0.70	*0.39*
MnO	0.07	*0.03*	0.20	*0.06*	0.15	*0.03*	0.03	*0.03*
MgO	1.19	*0.46*	0.48	*0.05*	0.21	*0.03*	0.09	*0.07*
CaO	2.98	*0.58*	1.07	*0.08*	0.84	*0.03*	0.59	*0.16*
Na_2O	4.39	*0.13*	8.59	*0.39*	7.53	*0.14*	4.05	*0.32*

K_2O	3.57	*0.57*		5.24	*0.06*	5.55	*0.11*	4.64	*0.45*
P_2O_5	0.33	*0.21*		0.12	*0.02*	0.06	*0.01*	0.02	*0.03*
Cl	0.05	*0.03*		0.16	*0.04*	0.09	*0.02*	0.04	*0.01*

Sample No.	**LKI_5.2B**				**LKI_6.5**		**LKI_7**	
Population	**p1**		**p2**				**p1**	
	n=3	***1σ***	**n=22**	***1σ***	**n=30**	***1σ***	**n=13**	***1σ***
Major (wt. %)								
SiO_2	61.54	*0.07*	76.87	*0.36*	61.22	*1.28*	61.40	*0.73*
TiO2	0.44	*0.13*	0.08	*0.04*	1.09	*0.20*	0.36	*0.07*
Al_2O_3	18.42	*0.65*	13.21	*0.27*	16.87	*1.27*	17.29	*0.64*
FeOt	4.61	*0.73*	0.55	*0.12*	5.16	*1.05*	5.51	*0.68*
MnO	0.21	*0.06*	0.08	*0.03*	0.10	*0.04*	0.19	*0.03*
MgO	0.33	*0.13*	0.06	*0.03*	2.01	*0.50*	0.20	*0.09*
CaO	0.92	*0.14*	0.55	*0.03*	4.56	*0.78*	0.86	*0.18*
Na_2O	8.15	*0.23*	3.74	*0.16*	4.82	*0.28*	8.81	*0.44*
K_2O	5.15	*0.16*	4.80	*0.20*	3.53	*0.60*	5.19	*0.14*
P_2O_5	0.10	*0.02*	0.02	*0.02*	0.63	*0.10*	0.07	*0.02*
Cl	0.13	*0.02*	0.06	*0.02*			0.12	*0.02*

Glass shard compositions of LKI_7 to LKI_3 were compared to WDS-EPMA data from the bulk sample extracted from Unit 10 (the background/control sample) that is believed to represent endogenous sedimentation at the site (Figure 8.16). The background sample showed considerable spread and a mix of compositions. These data were distinguishable from the majority of the tephras (Figure 8.16). However, there are some similarities to some of the calc-alkaline rhyolitic shards in the tephras (n=3; Figure 8.16), but this was limited and exotic tephras typically formed clustered groups.

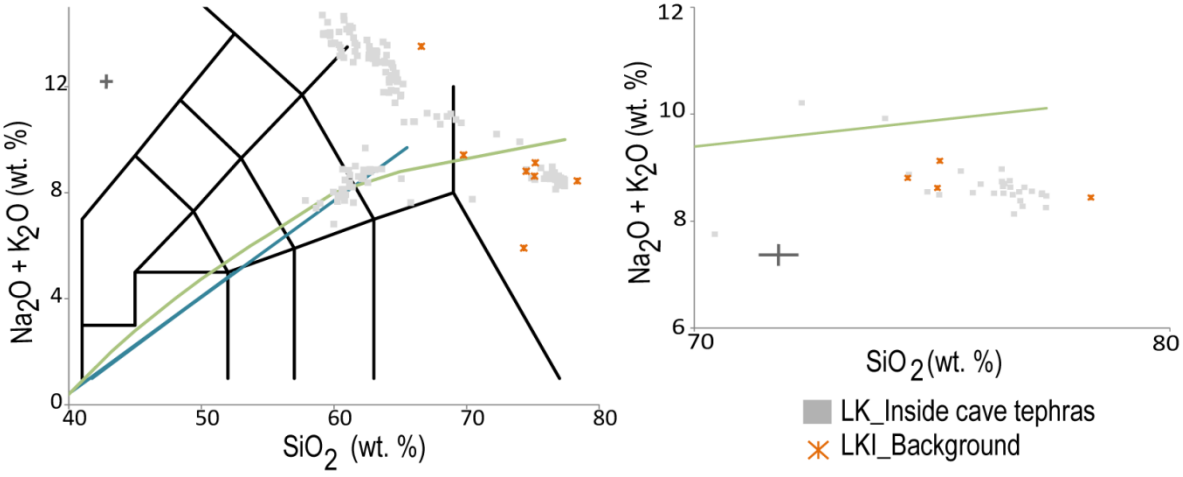

Figure 8.16. Grey points are WDS-EPMA compositional analysis of all samples from the inside of Lusakert 1 (excluding LKI_5.1T, as discussed previously). Orange crosses are from LKI_BG sample taken from Unit 10. Within errors (1σ), ~3 shards have compositional similarities to some of the rhyolites analysed in the layers.

Obsidian (volcanic glass) was the only raw material used for stone tool production at the site the Lusakert rock shelter (see section 4.3.5). To test if shards of glass produced through anthropogenic activity could be differentiated from glass shards of tephra (section 3.3.1) lithic debitage collected at the site was struck and trampled to produce smaller shards. These were collected, sieved with a 25

micrometre mesh and mounted with Canada Balsam for optical analysis (Figure 8.17). Samples were also prepared for major element, WDS-EPMA analysis to compare to the Lusakert rock shelter tephras (Figure 8.18).

Shards of obsidian glass are visually distinct from tephra glasses (Figure 8.17). The obsidian shards had edges that were rough with multiple fracturing scars and commonly showed conchoidal fracture marks*. These features are not observed in glass shards produced from explosive volcanic eruptions. Gas bubbles (vesicles) were seen in the obsidian shards, but were small and there were no large cuspate features, common in tephra shards. A combination of the 'roughness' of the edges the conchoidal fracture marks and the absence of large cuspate features can be used to differentiate between volcanically erupted and anthropogenically produced shards of glass in the site.

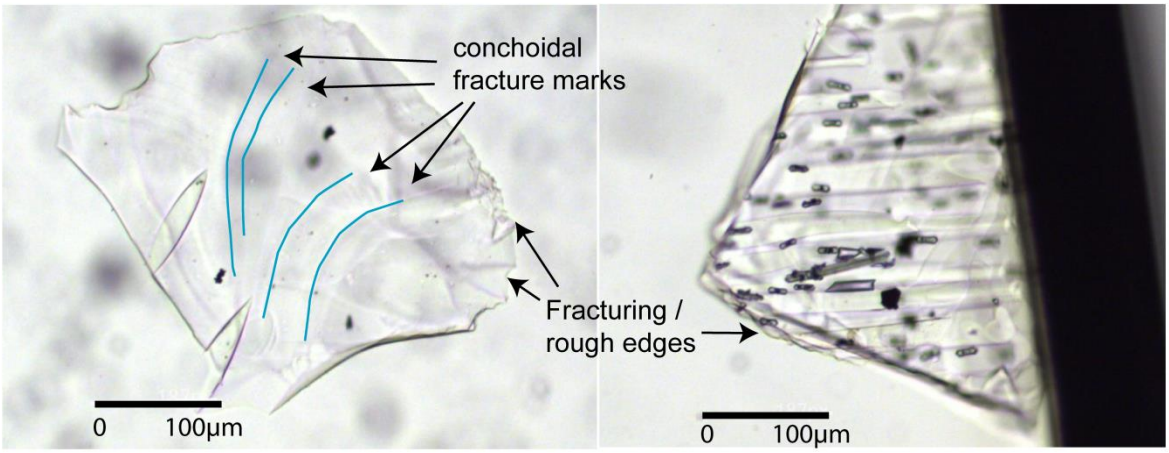

Figure 8.17. Images of shard of obsidian (produced by crushing and striking large pieces with a stone) under high powered optical microscopy. Images show conchoidal fracture marks (blue lines) and rough edges that are not found in glass that has been explosively erupted from a volcano.

**Conchoidal fracture marks are smooth curving features. These are common in fine grained material like glass that do not have internal planes of weakness to allow a clean break to occur when pressure is applied.*

Compositionally, the obsidians are rhyolitic with ~74 wt % SiO_2, 4.01-4.55 wt % Na_2O and 3.87-4.27 wt % K_2O. Figure 8.18 shows the obsidian debitage is chemically distinct from tephra found in the Lusakert sediments, with the exception of ~two data points from LKI_5.1.

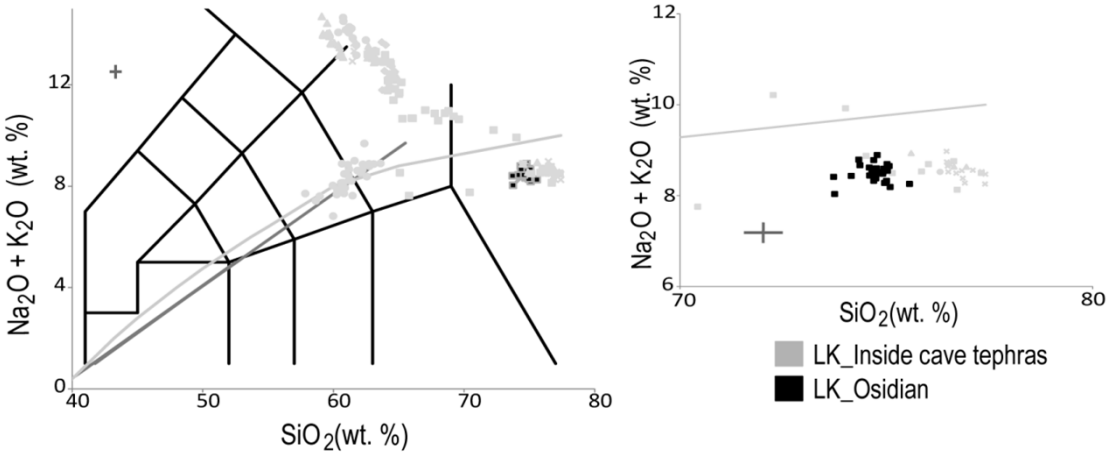

Figure 8.18. Grey points are EPMA compositional analysis of all samples from the inside of Lusakert (excluding LKI_5.1T). Black squares are EPMA data from obsidian debitage taken from Lusakert. ~2 shards have compositional similarities (within errors, 1σ), but can be visually differentiated.

8.7.2. Trace element data for LKI_6.5

Although trace element analysis (using a LA-ICP-MS) requires large glass shards, we attempted to analyse some of the shards of LKI_6.5. A number of elements fell below the limits of detection (mirrored in the secondary standards, Appendix 1. Primitive mantle normalised diagram for the LKI_6.5 glasses (Figure 8.19) shows a “trough” or negative anomaly in Ta with a moderate, negative anomaly in Sm and a positive anomaly in Pb. This suggests that the tephra originates from subduction or post subduction volcanism (Rollinson, 1993; Sun & McDonough 1989; Tomlinson et al., 2014a). Nb and Ti (further indicators of the lithosphere

contamination in the magma melt) were below the limit of detection (LOD). This was also true in the secondary standards on the day, and may not be a precise reflection of LKI_6.5 glasses. A slight, negative anomaly was also noted in Eu. This alongside a small Sr negative anomaly that suggests a slight fractionation of mineral into the magma melt (possibly of feldspar; plagioclase?), that is consistent with fractionation trends in andesitic liquids (Rollinson, 1993)

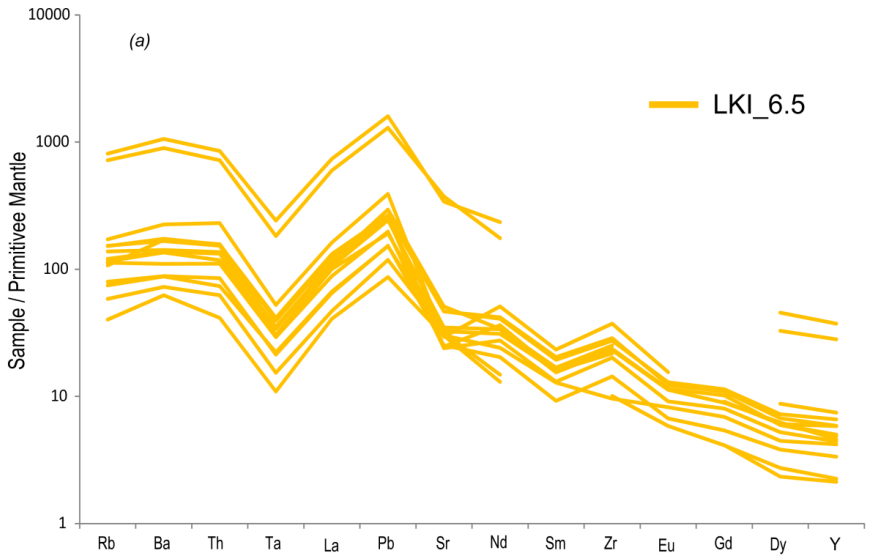

Figure 8.19. Mantel normalisation diagram for LKI_6.5 glasses. Sample values are normalised to primitive compositions (Sun & McDonough, 1989). A deep trough is seen at Ta and to a lesser extent Sm and Eu.

Compositional heterogeneity is observed across all elements (n=12), with Figure 8.20 that shows Th ranges from 5.31-19.58 ppm with 37-13-108.93 ppm Rb, 427-1572 Ba ppm, 2-6 ppm Y, 101-418 ppm Zr, and 32.18–111.15 ppm La (Figure 8.20, Appendix 1).

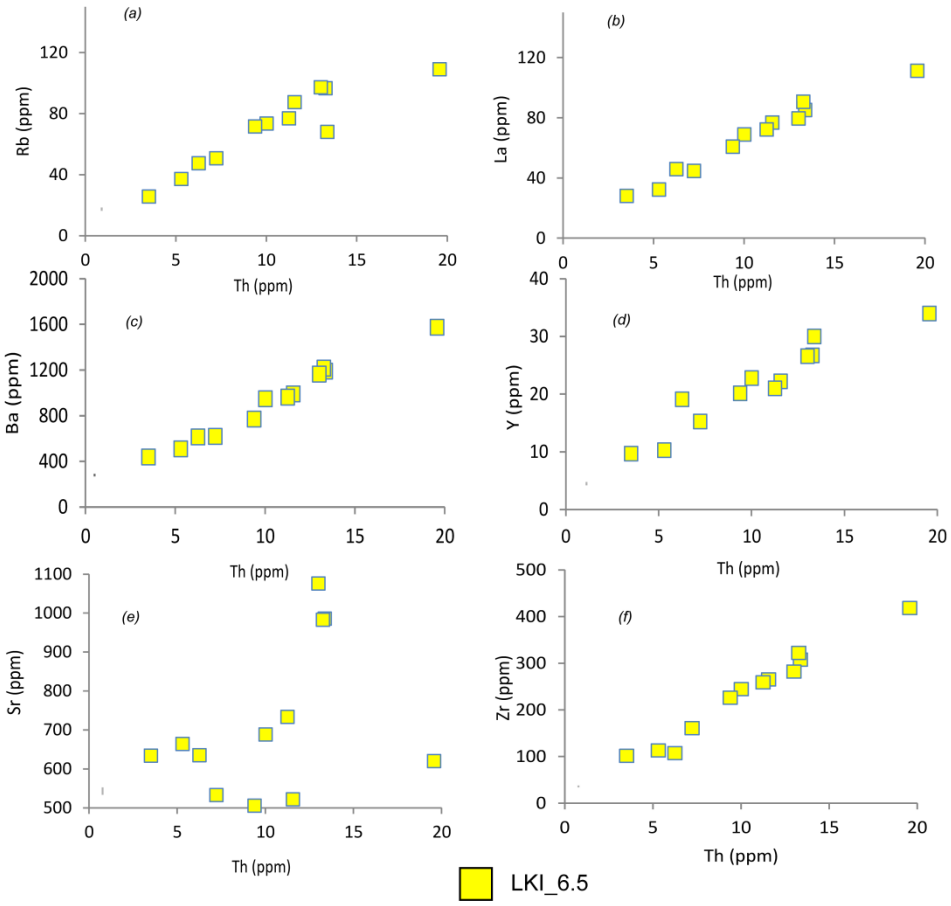

Figure 8.20. Selected bi-plots of glass trace element data form Lusakert rock shelter. Incompatible trace elements (left a, c, e) and compatible element (right; b, d, f). Errors are 2σ of MPI-DING, StHs6/80 analysis run alongside sample. See Appendix 1 for full data.

8.7.3. Discrimination of primary and secondary deposition

Peaks in glass shards concentrations in the Lusakert rock shelter are compositionally and visually distinct from the host sediment and shards of obsidian debitage. These data would suggest they are from external sources and are primary tephra deposits. Micromorphological analysis of the site sediments indicates the main agent's of disturbance (cryoturbation and bioturbation) caused little disturbance through the sites stratigraphy where sampling occurred (Adler

pers comms. 2013), but this could account for the tailing in shards from all the larger peaks in glass shard concentrations, and reworking from the landscape should also be considered. The constant background of glass shards is due to endogenous sedimentation from the cave walls.

Archaeological Units that contained a number of different, compositional populations (e.g. LKI_4.1, LKI_5.1, LKI_7, LKI_5.2B; see Table 8.7) often contain both calc-alkaline and peralkaline deposits that would have come from different volcanic sources. This suggests there were a number of closely spaced eruptions from different volcanoes or that rates in sedimentation were not sufficient to resolve these. Layers that showed repeat compositions e.g. LKI_7 and LKI_5.2B were stratigraphically distinct and are typically separated by a) another distinct tephra composition (e.g. LKI_6.5) or b) by an expanse of sedimentation with no discernible peak, and therefore these reflect sequential eruptions from the same/similar sources, deposited through time.

8.7.4. Tephra from Lusakert 1 (outside profile)

Three peaks in tephra concentration were chosen for WDS-EPMA analysis from Lusakert 1 (Figure 8.21). Layer C contained two peaks, one situated toward the top of the unit (LKO_CT; 8.23 s/g) and one towards the base of the unit; LKO_CB with a shard concentration of 221 s/g. The highest concentration of shards preserved in Layer D was found towards the base of this unit (~105 s/g; LKO_D; Figure 8.21). Tephra shards from all layers were vesicular with a vitreous lustre with some fluted features ranging from 50 to 120 micrometres, but there were some shards in Unit D that were ~150 micrometres in length.

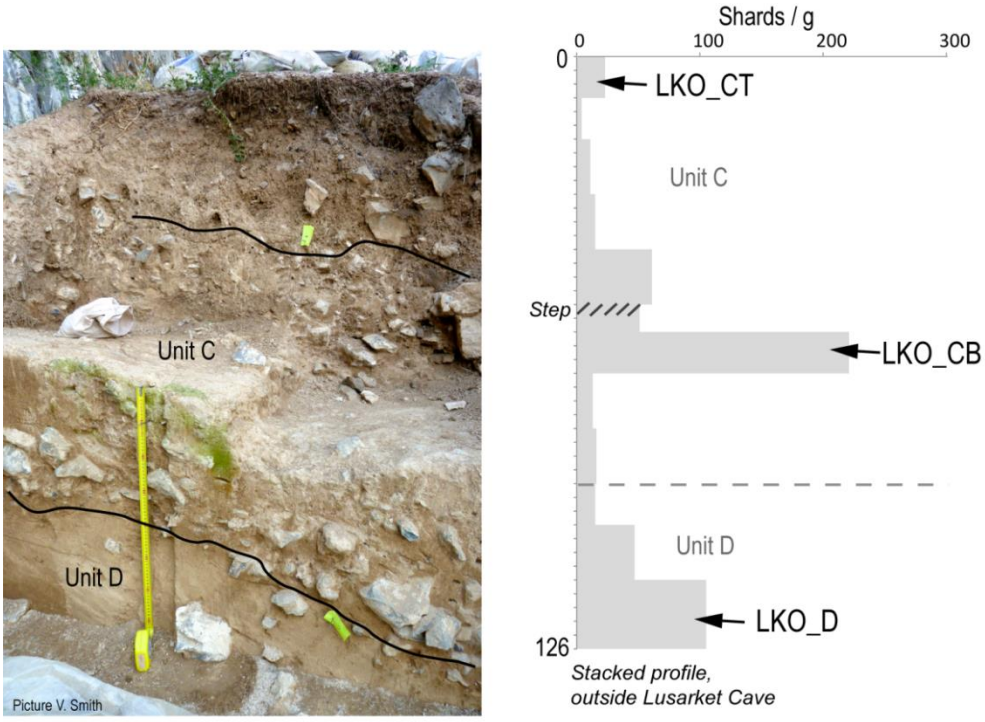

Figure 8.21. Left: annotated photo of the Lusakert 1 section that contains MP technology, distinct from the rock shelter assemblage. Right: tephra profile of Lusakert 1 section that shows where sample were taken for WDS-EPMA.

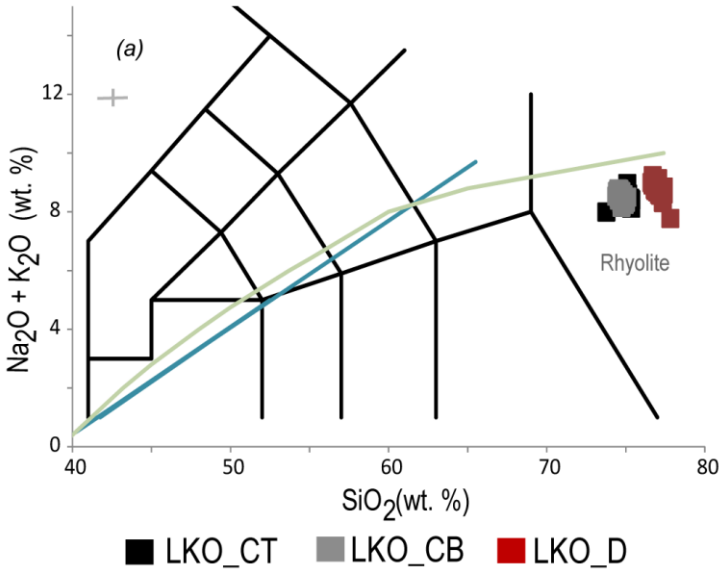

Figure 8.22. TAS shows that tephras (glass shards) found in sediments located in Lusakert 1 are solely calc-alkaline rhyolites.

Compositionally, LKO_CT and LKO_CB are identical, homogenous calc-alkaline rhyolites (Figure 8.22, Table 8.9) that have ~73.78-75.37 wt. % SiO_2 and similar K_2O and Na_2O compositions, ~4 wt. %. LKO_D is also a calc-alkaline rhyolite and

is more evolved (>76 wt. % SiO_2) with generally lower Al_2O_3, CaO and MgO composition than layer C tephras: <13.05, <0.6 and <0.09 wt. % respectively (Figure 8.23 a-i; Table 8.9).

Table 8.9. Average glass compositional data (with 1σ) for tephra found in the sediment of Lusakert 1

Sample No.	LKO_CT n=14	1σ	LKO_CB n=35	1σ	LKO_D n=21	1σ
Major element (wt. %)						
SiO_2	75.05	*0.40*	74.75	*0.17*	77.03	*0.29*
TiO2	0.17	*0.03*	0.18	*0.03*	0.08	*0.03*
Al_2O_3	13.83	*0.15*	14.17	*0.12*	12.86	*0.22*
FeOt	1.05	*0.30*	1.04	*0.09*	0.53	*0.07*
MnO	0.09	*0.05*	0.09	*0.03*	0.08	*0.04*
MgO	0.25	*0.22*	0.22	*0.02*	0.05	*0.02*
CaO	0.98	*0.08*	0.98	*0.05*	0.55	*0.03*
Na_2O	4.21	*0.18*	4.21	*0.14*	3.98	*0.37*
K_2O	4.27	*0.11*	4.26	*0.08*	4.78	*0.21*
P_2O_5	0.04	*0.01*	0.04	*0.02*	0.02	*0.02*
Cl	0.06	*0.02*	0.06	*0.02*	0.05	*0.01*

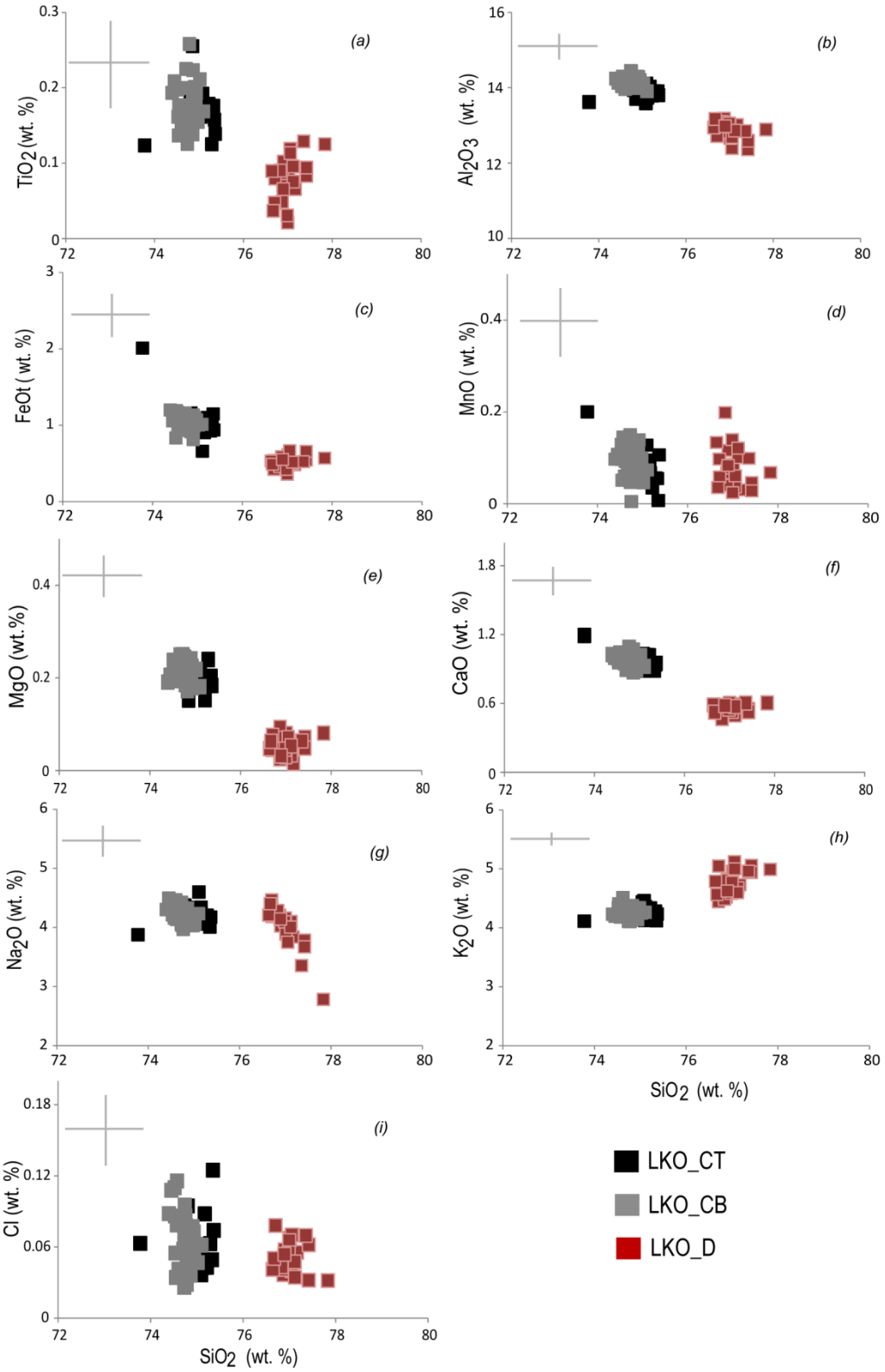

Figure 8.23. Glass shard compositions of cryptotephra in Lusakert 1. LKO_CT and LKO_CB are compositional identical. LKO_D is clearly distinct and is a more evolved rhyolite.

8.7.5. Discrimination of primary and secondary deposition

Glasses found at the top of Layer C (LKO_CT) are chemically identical to glasses found towards the base of the Layer (LKO_CB). LKO_CB was the largest peak in glass shard concentration and is likely to be a primary input. Reworking above and below could be attributed to the continual reworking from the landscape (possibly through fluvial or colluvial activity; see section 4.3.5). LKO_CT found above is likely to represent a second events from the same source given the increase in shard concentration and the distance between the two peaks. Tephra from Layer D (LKO_D) is compositionally distinct and stratigraphical separated by a rocky layer from glasses in Layer C and is a primary deposit. Displacement of shards above LKO_D could be a result of reworking from the landscape or anthropogenic activity.

8.8. Azokh Cave (Azerbaijan), site No. 9

Sediment samples from both Azhok Cave 1 (UP, Unit I) and Azhok Cave 5 (UP, Units A and B) were prepared for cryptotephra analysis. Azhok Cave 5 sediments were sterile for tephra in Unit B, with negligible amounts of tephra shards found in the initial scan samples (n=1) in Unit A. Unit A was re-prepared at bag resolution (2 cm) but failed to produce any further tephra; no further action was taken on Azhok cave 5.

Unit I to the contact to Unit II from two columns (column 1 and 2a) from Azhok Cave 1 were sampled. Both Units contained a tephra deposit that was dispersed through the entire sample's sequence (Figure 8.24). The highest input was at 2.18-2.28 cm with >5225 s/g in column 1 (AZ_1) and at 1.88-1.98 cm with > 9943 s/g count in column 2a (AZ_2a. Figure 8.24).

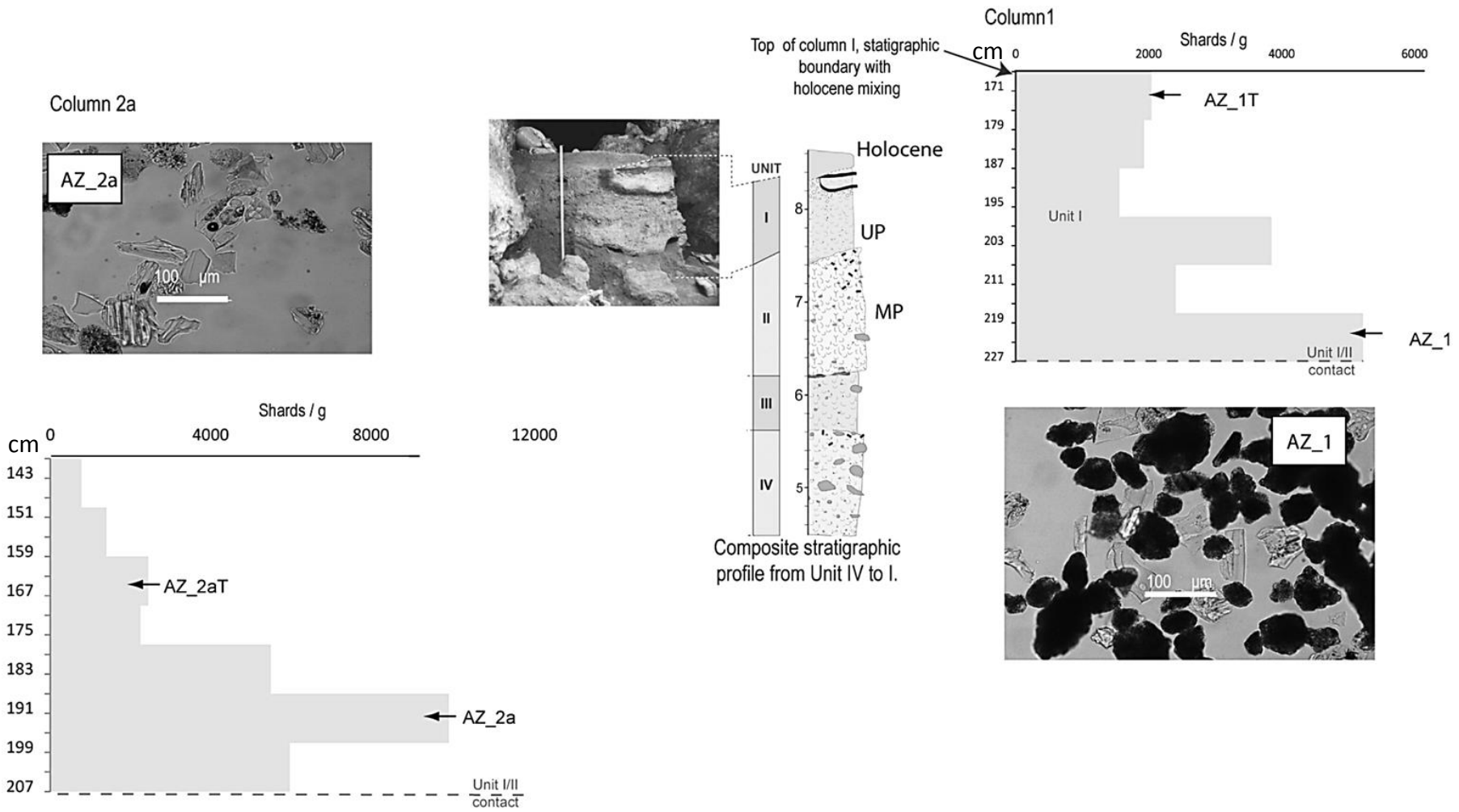

Figure 8.24. The composite profile in centre of figure (from Unit I-IV)shows the top four units at the site, but only Unit I was sampled for cryptotephra. Samples were collected from two columns, 2a and 1 both started at the contact of Unit II and Unit I. Both sequences contain a large concentration of glass shards. Sampling was conducted by D. White.

Visual analysis showed shards were uniform in appearance throughout Unit I, across the two columns, and shards ranged in size from 40-110 micrometres. Shards were irregular and colourless with wide and often enclosed vesicles (Figure 8.24). Some shards in AZ_1 (column 1) appeared altered, with a mottled surface (Figure 8.24). The highest peaks in shard concentration in each column were prepared for WDS-EPMA analysis to see if both columns contained the same tephra. Additional samples from higher in each profile of each column (AZ_1T, AZ_2At, see Figure 8.24) were also prepared for WDS-EPMA analysis to check if the same tephra was dispersed throughout Unit 1.

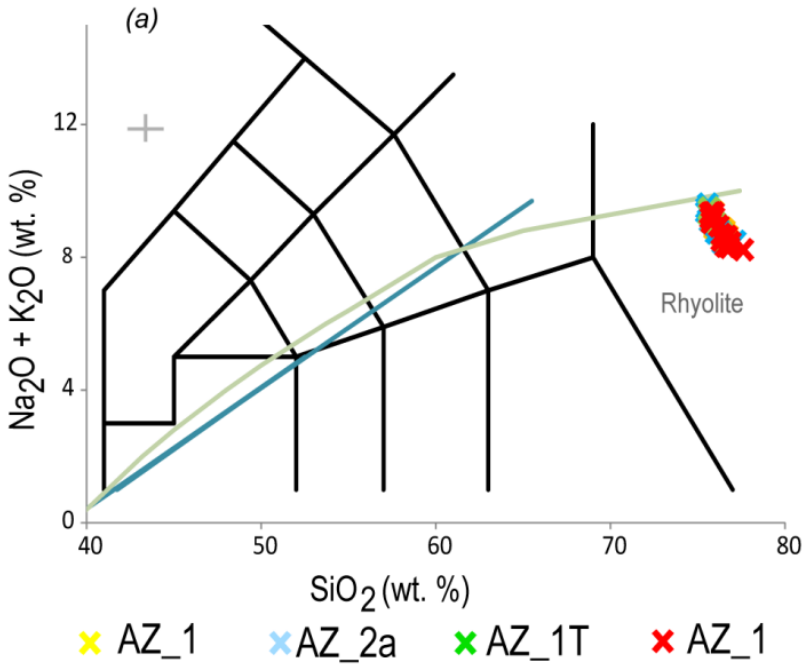

Figure 8.25. TAS plot for all four tephra horizons (glass shards data) from Azhok cave. All four are all identical calcalkaline rhyolites.

Chemical data from AZ_1 shows no evidence of chemical alteration (Table 8.10). AZ_1, AZ1_2a and AZ_1T, AZ_2At (samples from the top of the sequences) are compositionally identical calc-alkaline rhyolites (Figure 8.25, 8.26). All the tephras

have SiO_2 compositional values between ~75.47-77.16 wt. % and are bimodal, seen most clearly on FeOt (~1 wt.% difference; Figure 8.26c), Cl and Al_2O_3 (~1.10 wt.% difference; Figure 8.26g and b) . High resolution sampling (2 cm) has not been done given the size and dispersal of the same tephras in both columns (~56 cm, column 1 and 36 cm column 2a).

Table 8.10. Average compositional data (with 1σ) for tephra extracted from Azokh Cave 1 sedimentary sequence.

Sample No.	**AK_1**		**AK_2a**		**AK_2at**		**AK_1t**	
	n=14	***1σ***	**n=16**	***1σ***	**n=14**	***1σ***	**n=20**	***1σ***
Major (wt. %)								
SiO_2	76.25	*0.41*	76.09	*0.52*	75.96	*0.37*	76.22	*0.52*
TiO_2	0.08	*0.08*	0.11	*0.07*	0.15	*0.08*	0.12	*0.08*
Al_2O_3	12.73	*0.85*	12.35	*0.84*	12.00	*0.80*	12.24	*0.92*
FeOt	1.52	*0.87*	2.00	*0.88*	2.31	*0.80*	2.04	*0.94*
MnO	0.05	*0.04*	0.05	*0.05*	0.06	*0.05*	0.05	*0.01*
MgO	0.02	*0.02*	0.01	*0.02*	0.01	*0.01*	0.01	*0.01*
CaO	0.40	*0.10*	0.33	*0.13*	0.30	*0.11*	0.31	*0.11*
Na_2O	4.15	*0.45*	4.26	*0.58*	4.53	*0.50*	4.31	*0.59*
K_2O	4.72	*0.22*	4.67	*0.25*	4.55	*0.19*	4.58	*0.20*
Cl	0.06	*0.06*	0.09	*0.07*	0.13	*0.06*	0.11	*0.07*

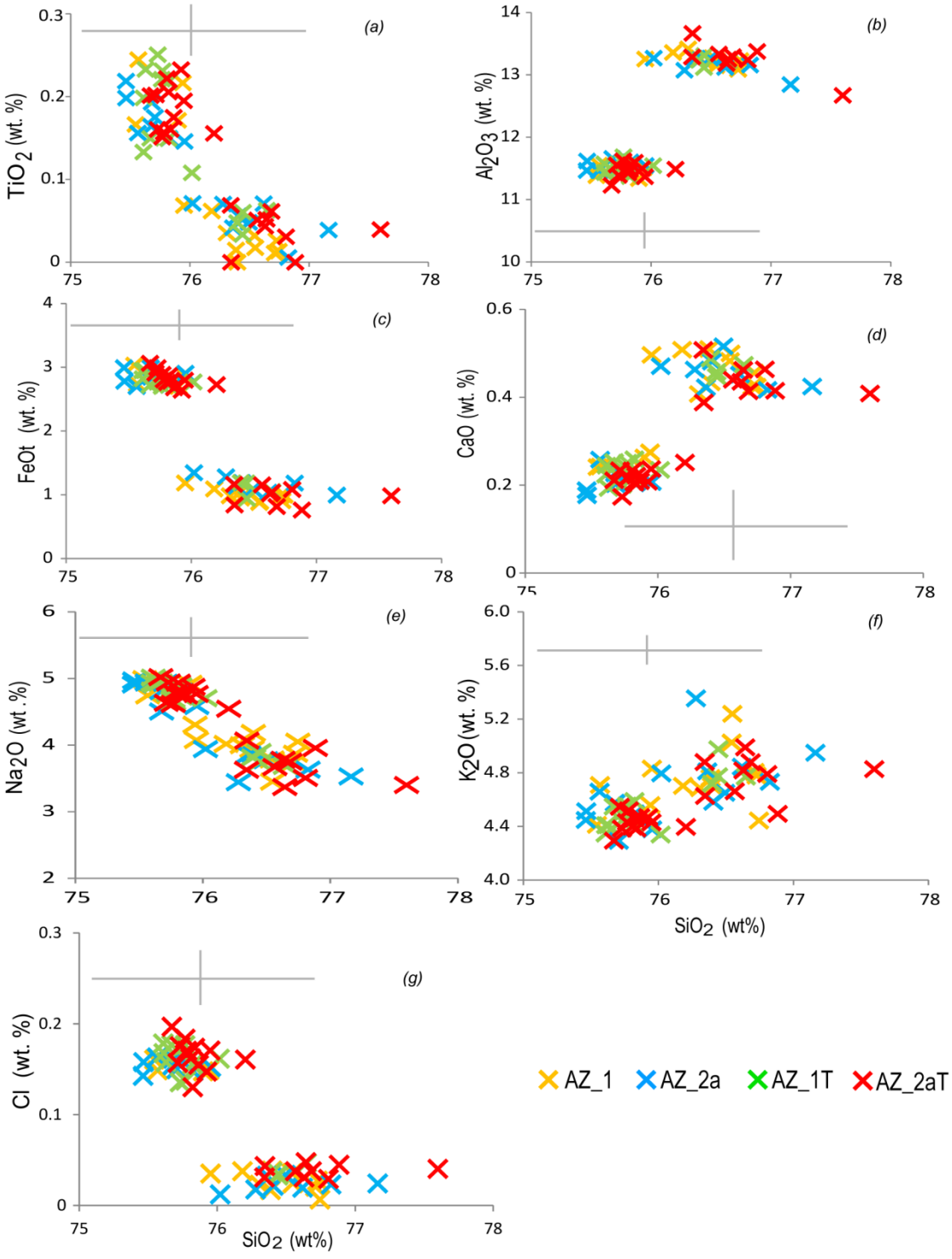

Figure 8.26. Glass composition of AZ_1, AZ_2a, AZ_1T and AZ_2At. It is clear all four samples are compositionally bimodal.

8.8.1. Discrimination of primary and secondary deposition

Peaks in tephra concentration from both columns are towards the base of Unit I, suggesting a primary, uniform deposition. No samples were taken from Unit II below, but a suspected sedimentological hiatus separates both these Units. As such, this tephra must have been deposited during the formation of Unit 1. Both columns preserve glasses that are identical in composition and show a distinctive bimodality. These glasses are very similar and either represents one eruption with increased fractionation during the eruption event and/or they represent two closely spaced eruptions from a similar source. The large spread of tephra above is likely due to the extensive friable nature of the sediments, but reworking from the landscape should also be considered.

8.9. Aghitu 3 (Armenia), site No. 10

There are two visible tephra layers that have been described in the basalt rock shelter of Aghitu 3, Armenia. Presently no contiguous cryptotephra analysis has been performed. These suspected visible layers had previously been assigned individual geological horizons according to the sites numbering convention: GH 8A (tephra code AG3_8A) and GH 8D that is ~10-20 cm above GH 8A that will now be referred to as AG3_8D (Figure 8.27).

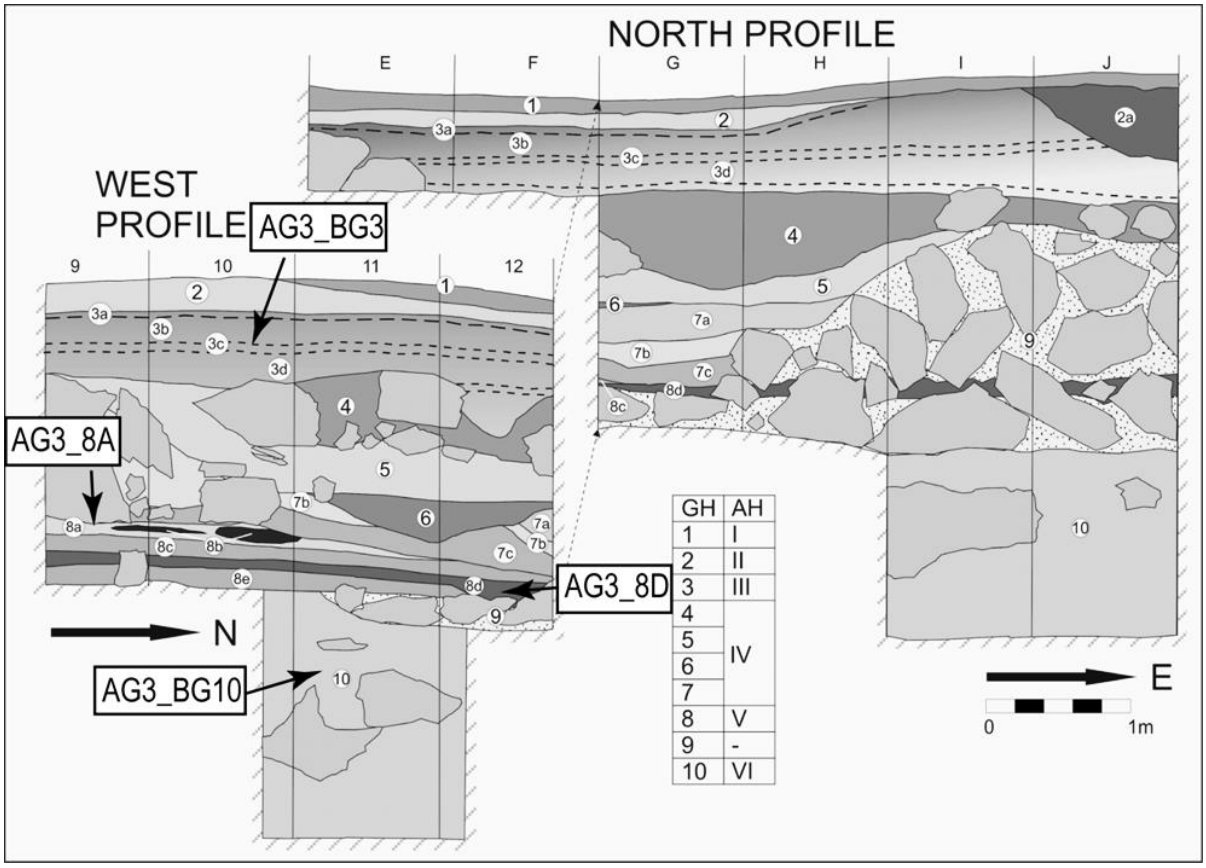

Figure 8.27. West and north sedimentary profile of Aghitu 3 Cave, Armenia. Bag samples from layers GH 10, 8A, 8D and 3C were sent to Oxford curtesy of Andrew Kandel and have been prepared for WDS-EPMA analysis (labelled on image). GH in the table are the geological horizons (seen as circled numbers on the profiles) and the AH are the associated, UP archaeological horizons. Image adapted from A. Kandel.

AG3_8A is described as a 'grey volcanic ash at site' and the deposit is ~8 cm thick. This layer is visible in the west profile, but not found in the North profile. AG4_8D is situated below AG3_8A and forms a continuous dark grey 'band' (~10 cm thick) across both profiles at the sites. Excavations at the site are ongoing so the current extent of the layers is unknown in the east and south profiles. Aghitu 3 formed in the base of a basalt flow, so a constant background of volcanic glass could be expected (see Lusakert rock shelter above). To help differentiate endogenous and exotic volcanic products, samples from geological horizons GH 3

and GH 10 that are representative of the host sediments, (Kendal per comms., 2013) were prepared as controls (see Figure 8.27).

The float samples with a density of 1.95-2.55 g/cm^3 from all four samples are visually similar (Figure 8.28 a-c). The shards are irregular in form with expanded and sometimes closed vesicles, and some with fluting. All shards range in size from 20-120 micrometres across the longest axis and both clear and brown tephra shards were recorded in all four float samples. The dense fraction of AG3_8A and AG3_8D had lots of dark brown shards that are > 2.55 g/cm^3. These shards were irregular in form with expanded vesicles (Figure 8.28a, b). The shards ranged ~40–120 micrometres in size and were rich in microcrystals. This was is stark contrast to the 'background' samples (AG3_BG10, AG3_BG3) that had negligible amounts of degraded tephra shards present, and a predominance of detrital material from the host sediments (Figure 8.28c). Bulk samples from all four layers were prepared for WDS-EPMA analysis.

AG3_8D and AG3_8A are compositionally identical (Figure 8.29, 8.30; Table 8.11). Shards in both layers are predominantly trachy-andesite (Figure 8.30). Shards have ~55.95–61.06 wt. % SiO_2 and are high in MgO and FeOt (~1.38-6.91 and 3.95–8.29 wt. %, respectively; Figure 8.30). These compositions were not found in the background samples (Figure 8.29).

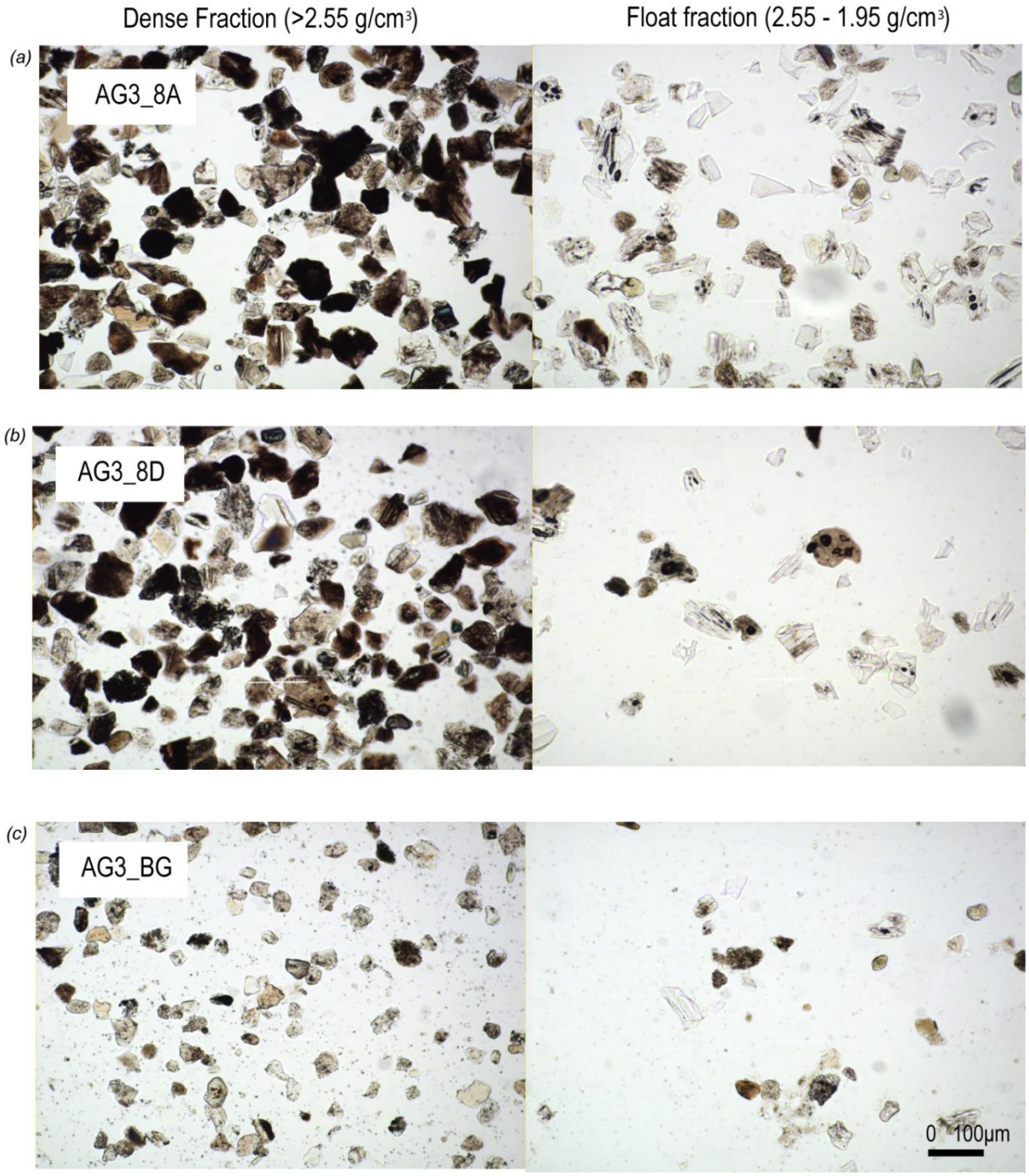

Figure 8.28. Images taken of extracted shards (see methods). The top four images (a, b) show numerous dark brown to brown shards are preserved in the dense fraction of both samples, and a few clear shards in the floatation sample. The bottom two images (c) are of the background samples. They have some clear shards in the float fraction, but no shards were found in the dense fraction.

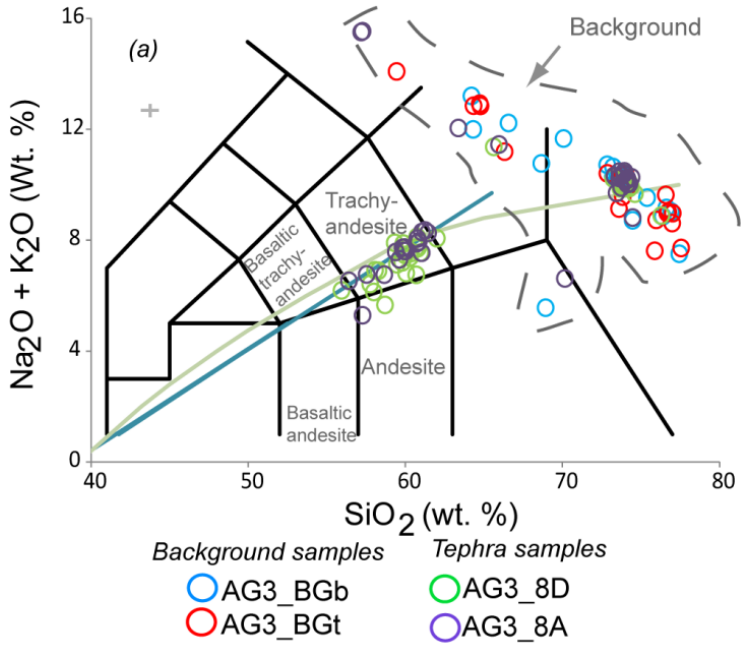

Figure 8.29. Glass compositions of samples from Aghitu 3 Cave. The glass shards that had the same composition as the background samples are removed from further plots and will not be discussed further as they represent reworked tephra.

Table 8.11. Average glass compositions (with 1σ) of the dense fraction from Aghitu 3 (AG3_8D and AG3_8A).

Sample No.	**AG3_8D n=15**	***1σ***	**AG3_8A n=15**	***1σ***
Major element (wt. %)				
SiO_2	59.38	*1.56*	59.64	*1.53*
TiO_2	1.04	*0.15*	1.08	*0.17*
Al_2O_3	16.43	*2.52*	16.44	*1.42*
FeOt	5.78	*1.22*	5.82	*0.73*
MnO	0.11	*0.05*	0.14	*0.05*
MgO	3.44	*2.02*	3.07	*1.49*
CaO	6.38	*1.43*	5.98	*1.42*
Na_2O	4.08	*0.55*	4.30	*0.43*
K_2O	2.98	*0.45*	3.11	*0.53*
P_2O_5	0.34	*0.05*	0.37	*0.06*
Cl	0.05	*0.01*	0.05	*0.03*

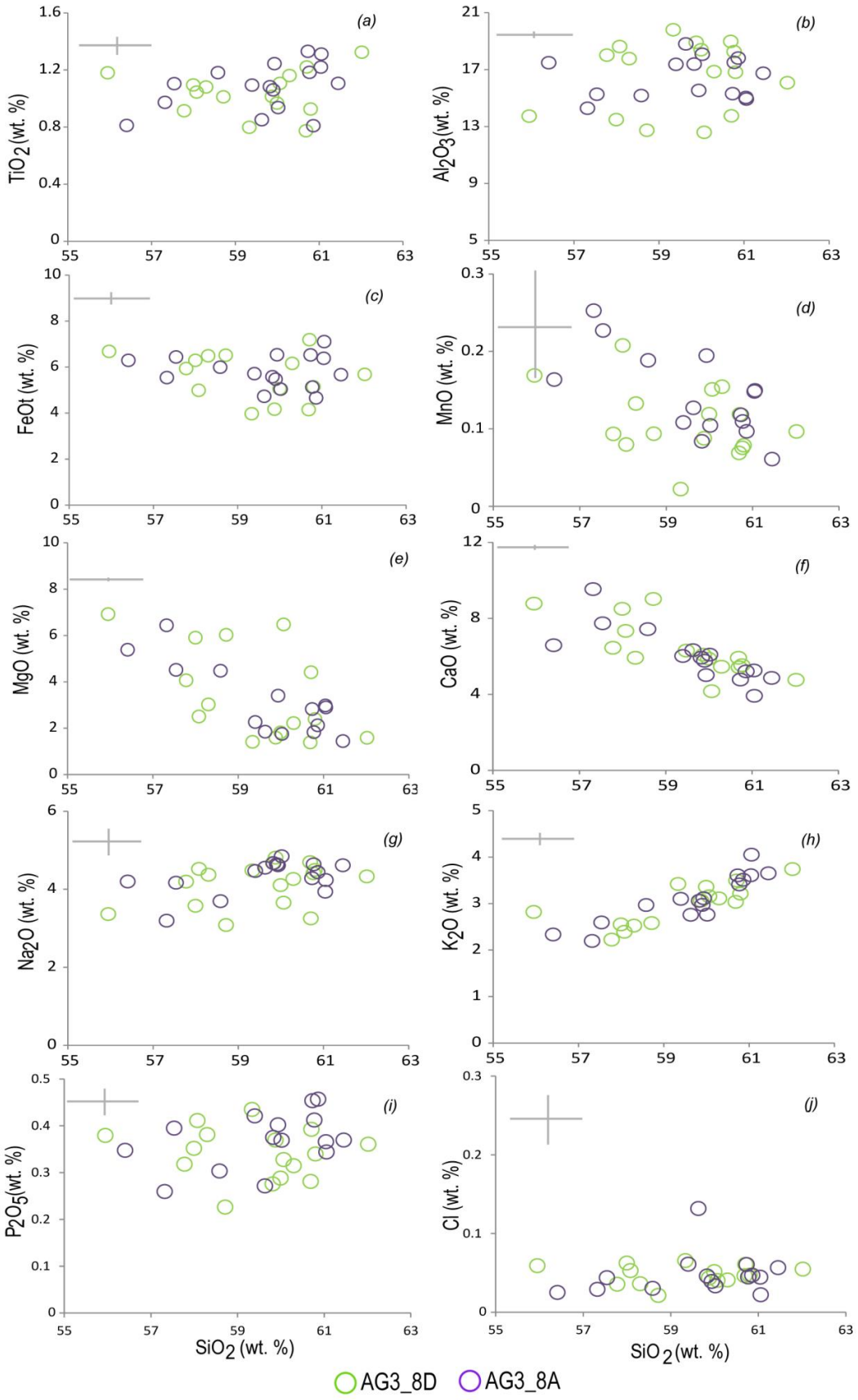

Figure 8.30. Glass compositional data of tephra in AG3_8D and AG3_8A. They are compositionally identical.

8.9.1. Trace element data from AG3_8D and AG3_8A

Trace data from glasses in AG3_8D and AG3_8A was obtained to see if they could be differentiated. Given the high proportion of microcrystals preserved in AG3_8D and AG3_8A volcanic glass, trace element analysis was difficult and only a small number of analysis were obtained (n= 8, AG3_8D and n= 7, AG3_8A on a 32µm beam; see methods). AG3_8A was run on the same day as LKI_6.5; again the precision on the day was poor with only a limited number of elements above the LOD. AG3_8D and AG3_8a both show compositional heterogeneity, and are indistinguishable on trace data (only elements in both sets of glasses that have data have been compared; Figure 8.31). Trace element ranges of both tephras are, ~45-264 ppm Rb, 7-24 Th ppm, 343-1433 Ba ppm, 8.86-38.92 ppm Y, 62.47 - 357.29 ppm Zr, and 14.81 -94.26 ppm La (Figure 8.31).

Mantle normalisation diagrams show a negative anomaly for Ba in both tephras (Figure 8.32). Negative anomalies for Nb, Ta and Ti in AG3_8D strongly suggest this tephra is a product of subduction or post-subduction volcanism, with a negative anomaly also in Ta in AG3_8A with the addition of a positive anomaly in Th (also seen in AG3_8D with another at U) that also suggest AG3_8A is from subduction or post subduction type volcanism (Tomlinson et al., 2014a).

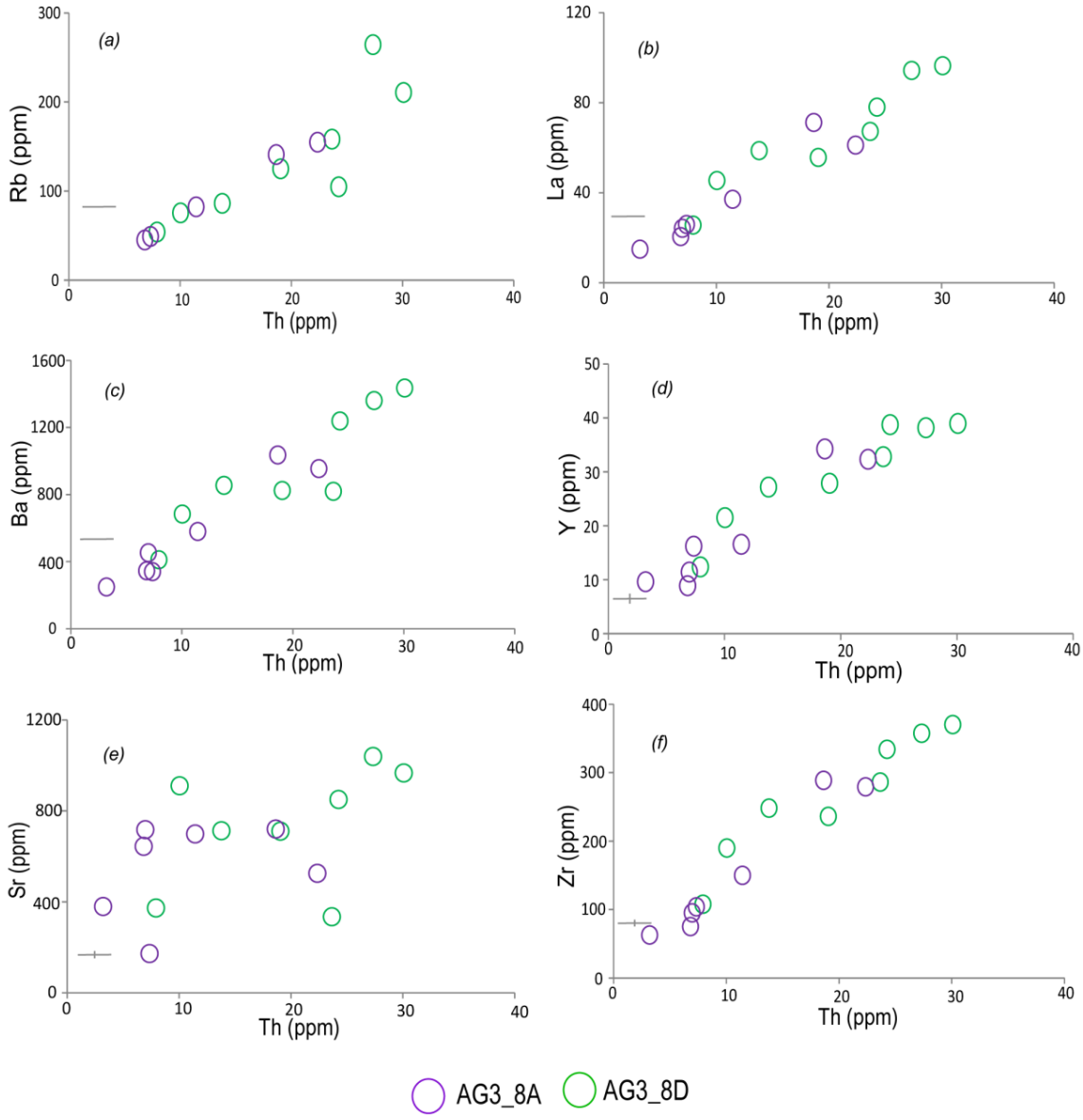

Figure 8.31. Selected bi-plots of glass, trace element incompatible (left a, c, e) and compatible (right; b, d, f) data from AG3_8A and AG3_8D.

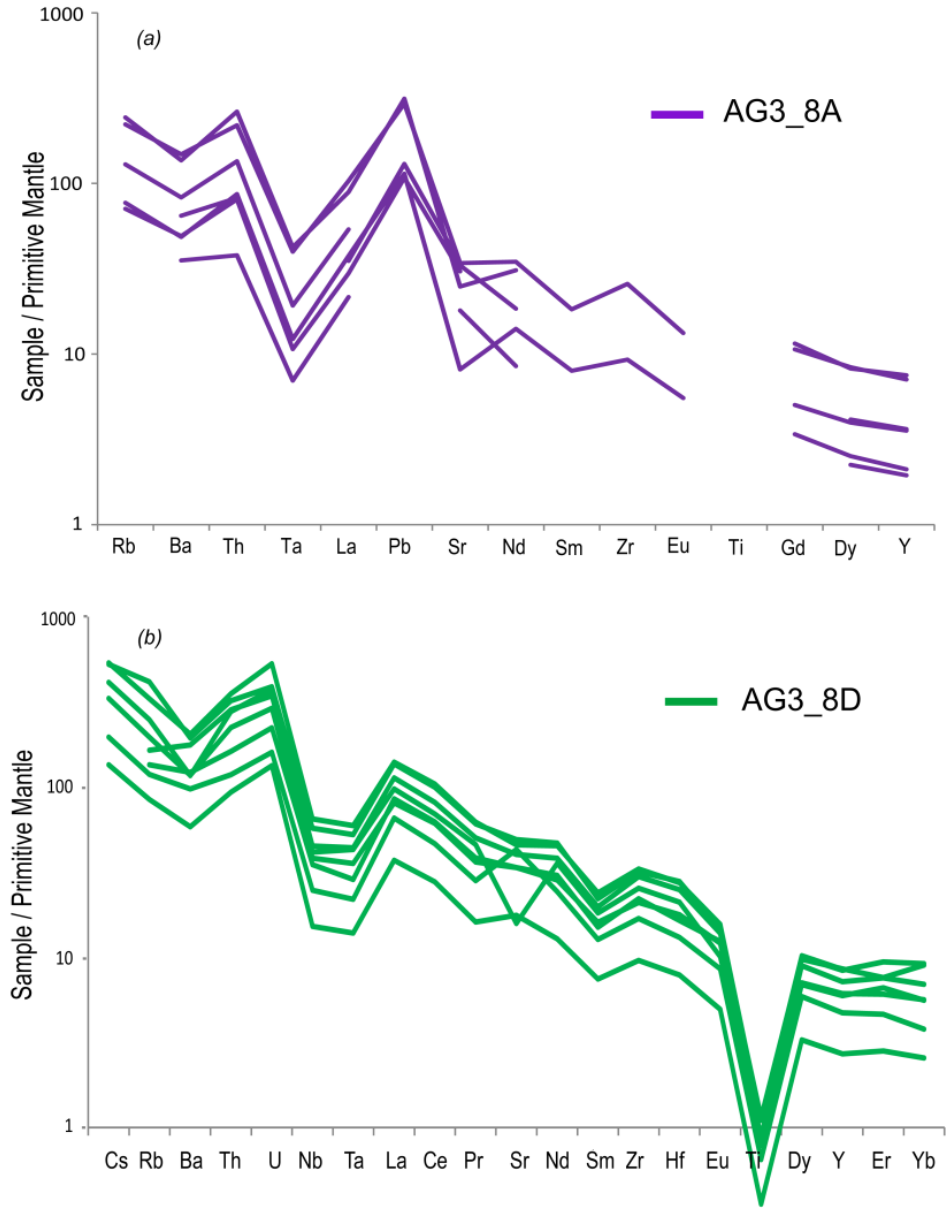

Figure 8.32. Primitive mantle normalised diagram for AG3_8A (a) and AG3_8D (b). Sample values are normalised to primitive mantle compositions (Sun & McDonough, 1989). (b) is clearly suggestive of subduction or post-subduction volcanism.

8.9.2. Discrimination of primary and secondary deposition

AG3_8D and AG3_8A are compositionally and visually identical, but stratigraphically distinct. AG3_8D is ~10-20 cm below layer AG3_8A and is a visible and primary event that extends across the site. AG3_8A is likely to be a second eruption (close in time) from the same volcano. Sedimentological features (charcoal rich layers) in the volcanic horizon (see section 3.3) are from a hearth feature that were on the land-surface prior to the deposition of the tephra (Kandle pers comms. 2013). The tephras are not likely to be far-travelled.

8.10. Fantan and Kagasi (Armenia), site No. 11 & 12

The sites of Fantan and Kagasi were discovered as part of a survey of the Hrazdan Gorge (Figure 8.33). The sites are located in quarried sections and have been shown to contain a number of visible tephra layers that contain a MP-type tool assemblages in places (Adler pers comms., 2013; Figure 8.33). As the sites have had no formal excavation, subsamples from the visible deposits were taken to ascertain any correlation with other tephra-bearing sites in this study.

Three subsamples were taken by Dr. K. Wilkinson from the lower, middle and upper deposits in the exposed section at Kagasi (KGL_AM, KGM_AM and KGU_AM) and two samples from the lower and upper section of Fantan (FL_AM and FU_AM; Figure 8.33). All samples were sieved through a 25 micrometre mesh and then mounted for single grain WDS-EPMA chemical analysis.

In general, tephra shard sizes range from ~50–300 micrometres in all 5 samples, but there were some shards in KGL_AM and FL_AM that were ~400 micrometres in length across the longest axis. With the exception of FU_AM that contains only

clear tephra shards (these are irregular in form with expanded vesicle and some fluting), all other samples have a mix of brown and clear shards. Microcrystals are common in the brown shards and this is a common feature in all the samples. Shards in these samples are generally fluted and irregular in form with some expanded vesicles.

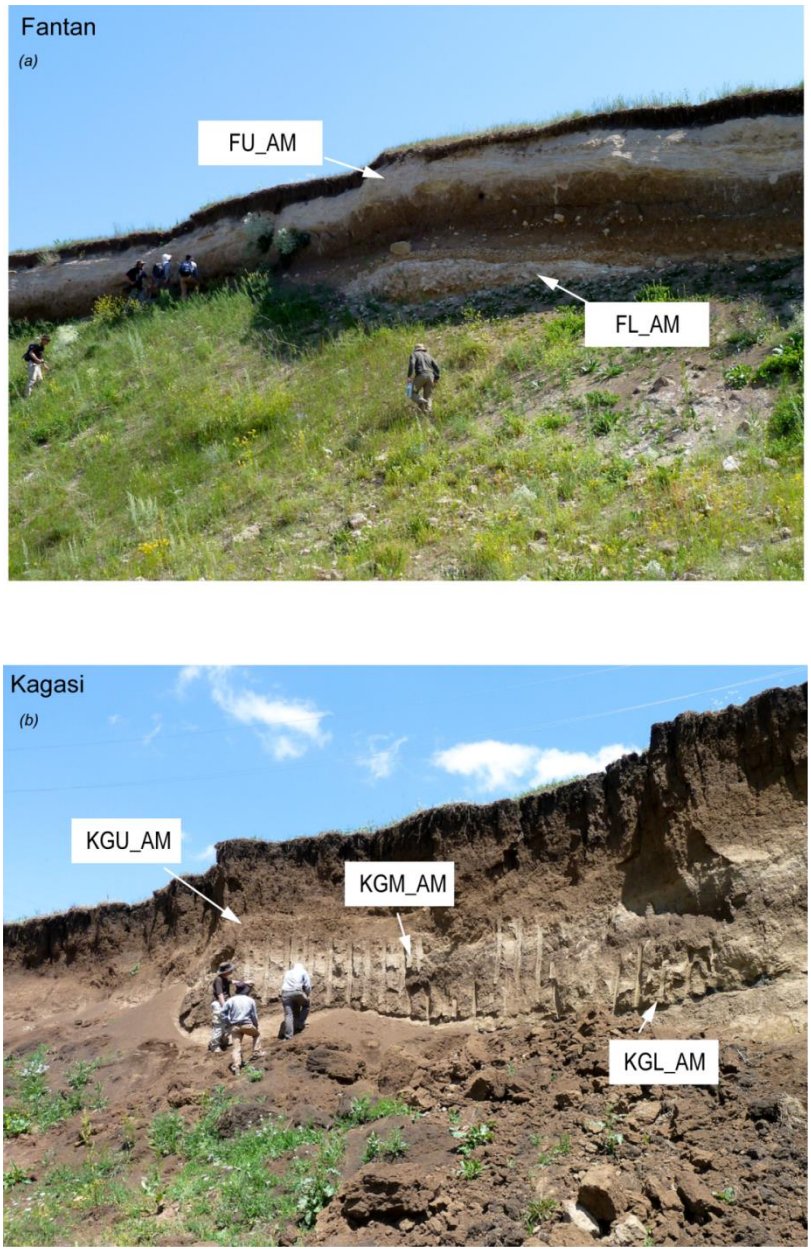

Figure 8.33. (a), photograph of the section at Fantan; the two visible tephra deposits labelled and shown. (b), the three visible deposits that are preserved at the quarry site of Kagasi.

The two youngest tephras in each profile (FU_AM and KGU_AM) are both distinguishable from other tephras in composition (Figure 8.34). FU_AM is a calc-alkaline rhyolite that has ~75-77 wt. % SiO_2 and low FeOt (~0.64-0.97 wt. %). KGU_AM is basaltic trachy-andesite that has the lowest SiO_2 composition of all tephras (~53.49–54.93 wt. %), and it has a high TiO_2 content (~1.68-2.24 wt. %; Figure 8.35a-j).

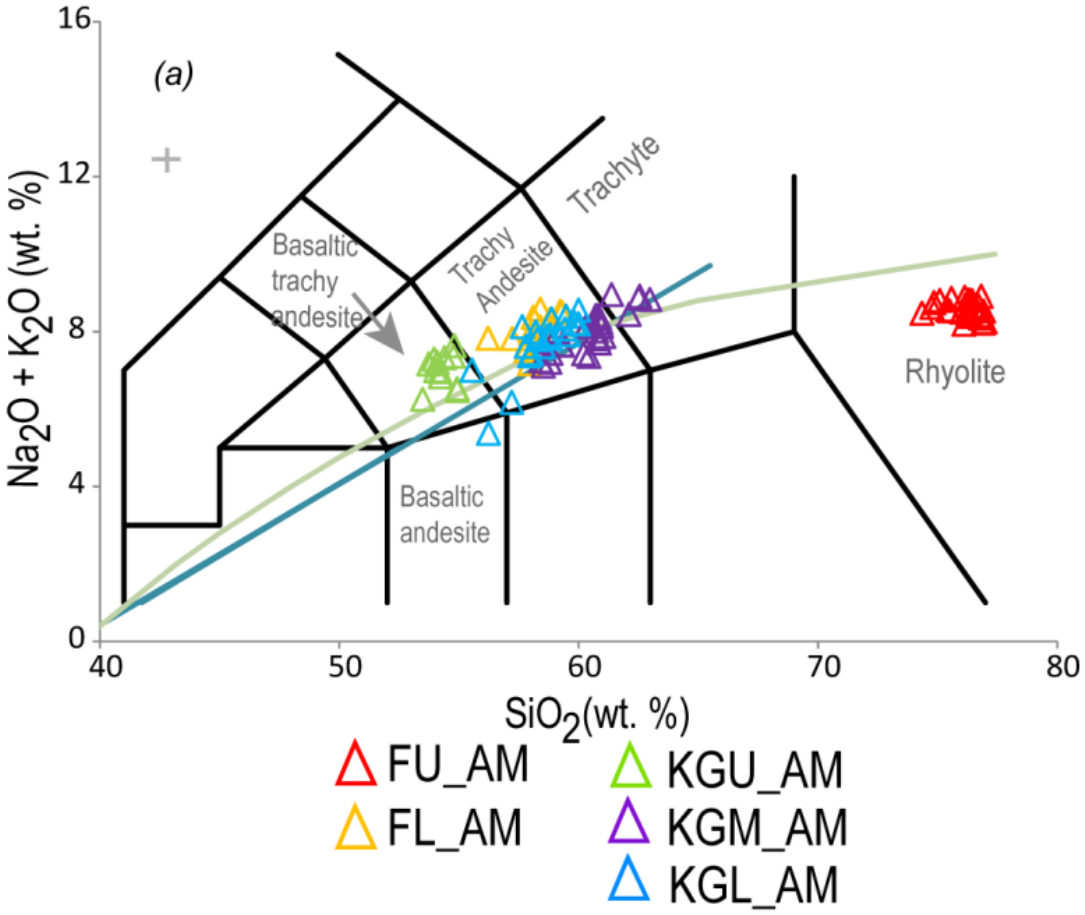

Figure 8.34. Glass compositions of tephras in Fantan and Kagasi. KGU_AM and FU_AM (the only rhyolite) are distinguishable on TAS plot from the other three tephras.

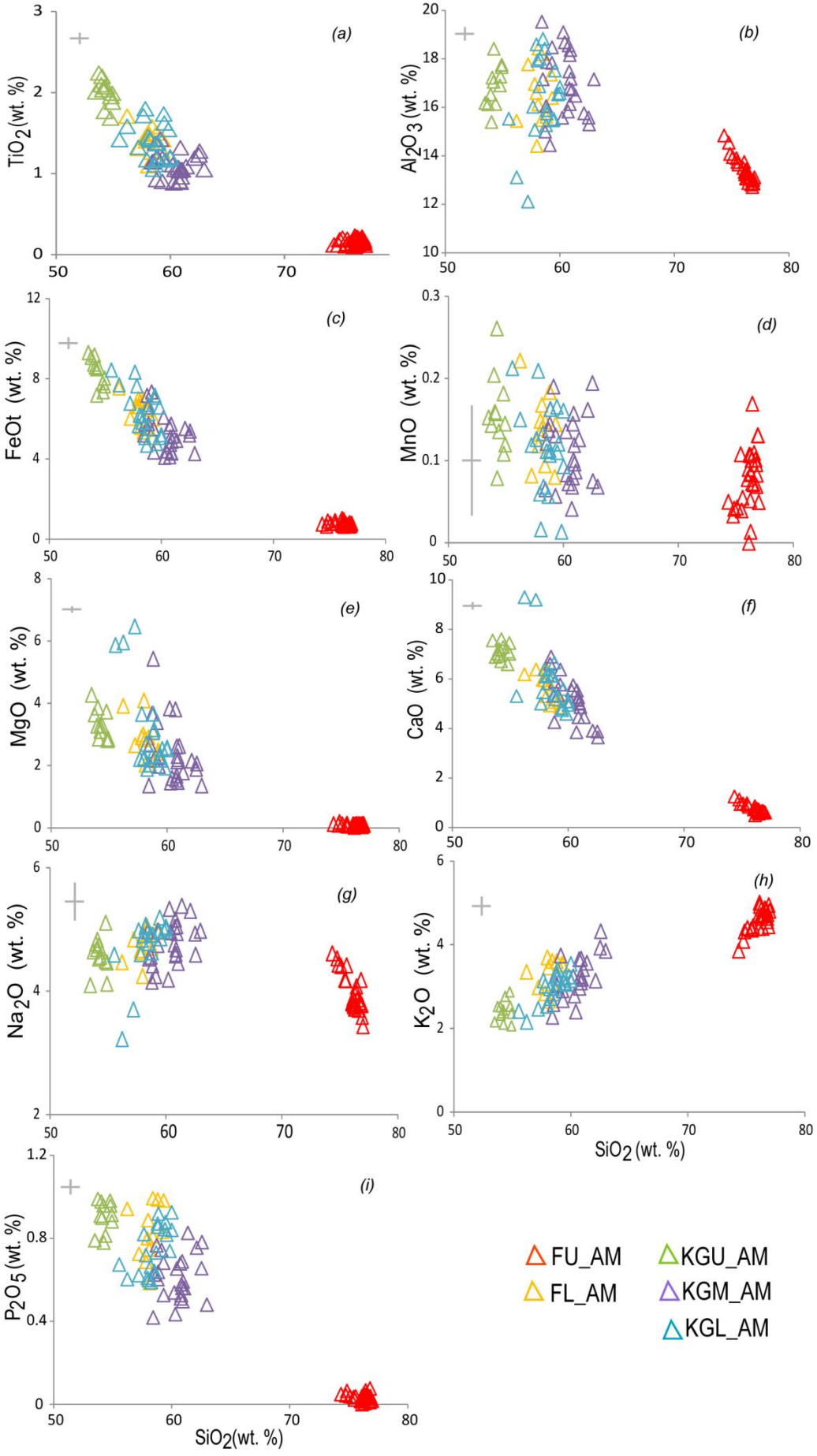

Figure 8.35. Glass compositions of tephras in Fantan and Kagasi.

KGL_AM, KGM_AM and FL_AM share the same major element compositions (Figure 8.35). All three tephras are trachy-andesite and have high CaO and MgO compositional contents (~3.6-9.3 and ~1.5–6.5 wt. %, respectively; Figure 8.35), but KGM_AM has the largest SiO_2 compositional range of ~58.72–62.98 wt. %, while KGL_AM and FL_AM do not exceed 60 wt. % SiO_2 (Table 8.12).

Table 8.12. Average glass compositional data (with 1σ) from Fantan and Kagasi open air sites.

Sample No.	FU_AM n=27	1σ	FL_AM n=12	1σ	KGU_AM n=12	1σ
Major (wt. %)						
SiO_2	76.13	*0.70*	58.14	*0.85*	54.30	*0.48*
TiO_2	0.17	*0.04*	1.42	*0.16*	2.00	*0.16*
Al_2O_3	13.38	*0.52*	16.56	*1.23*	16.89	*0.85*
FeOt	0.79	*0.10*	6.34	*0.75*	8.33	*0.72*
MnO	0.08	*0.04*	0.14	*0.04*	0.15	*0.05*
MgO	0.10	*0.03*	2.86	*0.64*	3.32	*0.47*
CaO	0.76	*0.18*	5.70	*0.61*	7.11	*0.32*
Na_2O	3.95	*0.30*	4.78	*0.24*	4.58	*0.28*
K_2O	4.60	*0.27*	3.24	*0.40*	2.42	*0.25*
P_2O_5	0.04	*0.02*	0.83	*0.13*	0.90	*0.08*

Sample No.	KGM_AM n=24	1σ	KGL_AM n=19	1σ
Major (wt. %)				
SiO_2	60.46	*1.30*	58.45	*1.19*
TiO_2	1.10	*0.15*	1.39	*0.22*
Al_2O_3	17.01	*1.38*	16.29	*1.73*
FeOt	5.26	*0.89*	6.34	*1.14*
MnO	0.11	*0.04*	0.12	*0.05*
MgO	2.38	*0.98*	3.07	*1.40*
CaO	5.07	*0.89*	5.90	*1.29*
Na_2O	4.78	*0.35*	4.74	*0.48*
K_2O	3.22	*0.49*	2.95	*0.37*
P_2O_5	0.61	*0.11*	0.75	*0.12*

8.10.1. Trace data for KGL_AM, KGM_AM, FL_AM and KGU_AM

Samples KGL_AM, KGM_AM, FL_AM and KGU_AM were prepared for trace element analysis. Due to the high proportion of microcrystals in the glass matrix, a number of ablations had to be discarded. FU_AM and KGU_AM are both easily distinguishable from other tephras on major element chemistry (see above). On a mantle normalised diagram KGU_AM tephra looks to be associated with subduction or post subduction volcanism (Figure 8.36) with large negative anomalies at Nb, Ta and Ti. No traces were obtained for FU_AM.

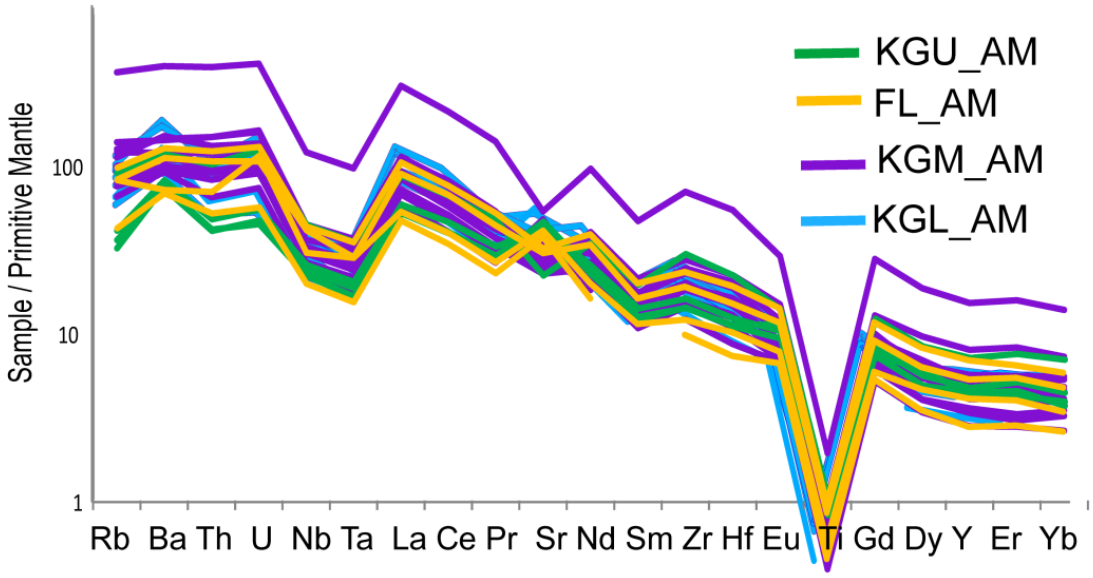

Figure 8.36. Primitive mantle normalised diagram of glass shards. Sample values are normalised to primitive mantle compositions (Sun & McDonough, 1989). Tephras show similar profiles and are suggestive of crustal contamination in the magma melt. Green and yellow show more pronounced Ba and U positive anomalies.

Trace element data for FL_AM (n=4), KGL_AM (n=8), and KGM_AM (n=11) are all compositionally similar in both compatible and incompatible elements, apart from one data point in KMG_AM that is significantly enriched in all trace elements (e.g. 3103 ppm Ba, with 213 ppm La and elevated Sr, 1219 ppm; Figure 8.38a-f).

Compositional values for the remaining tephras (FL_AM, KGL_AM and KGM_AM) are heterogeneous with similar compositional ranges; ~29-96 ppm Rb, 4-12 Th ppm, 525–1409 Ba ppm, 508–1245 ppm Sr, and 50-96 ppm La (Figure 8.37; Appendix 1).

Mantle normalised diagrams for FL_AM, KGL_AM and KGM_AM are all similar and show negative anomalies for Nb and Ta with a deep Ti trough (indicative of post or subduction volcanism) and have slight positive anomalies in Ba and U (pronounced in KGM_AM; Figure 8.37b-d).

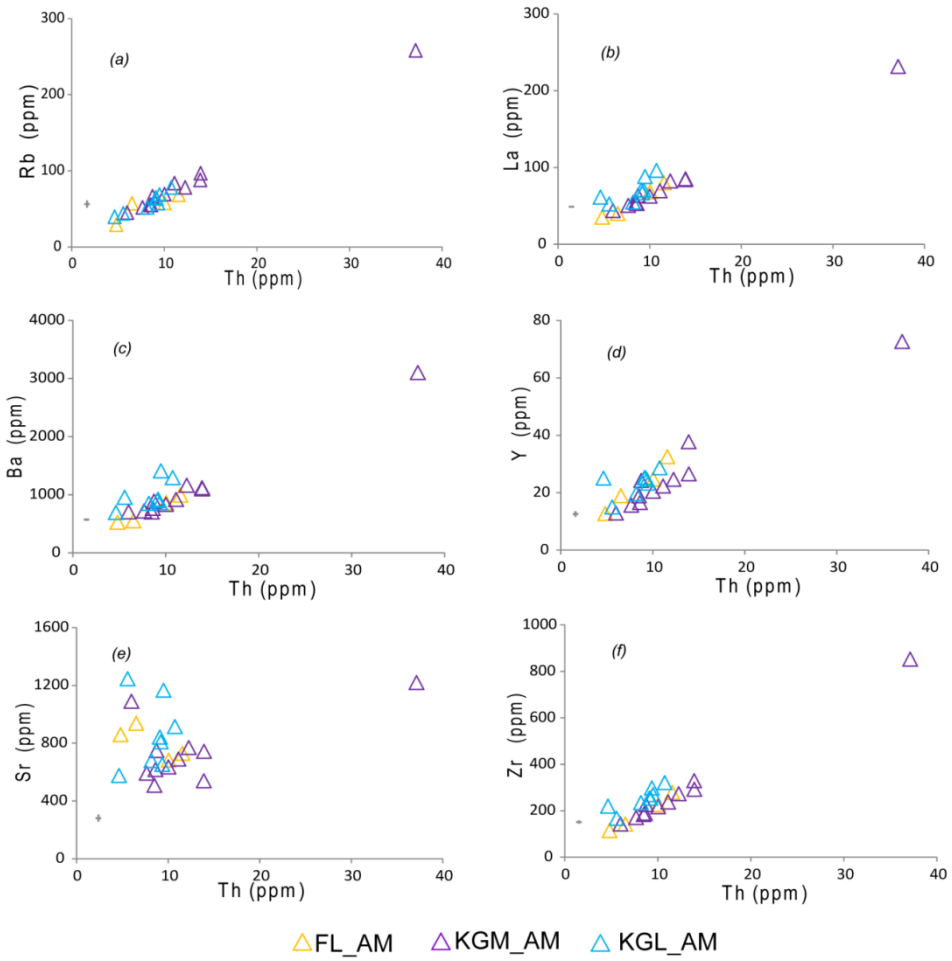

Figure 8.37. Selected bi-plots for incompatible (left a, c, e) and compatible (right; b, d, f) glass shards from FL_AM, KGM_AM and KGL_AM. KGL_AM may show slight deviation from FL_AM and KGL_AM (within errors) seen most pronounced in Zr (f).

8.10.2. Discrimination of primary and secondary deposition

Tephra layers from the sites of Kagasi (KGL_AM, KGM_AM and KGU_AM) and Fantan (FL_AM and FU_AM) are primary deposits that are generally thick (> 1 m in some cases). The basaltic trachy andesite and trachy andesite tephras are not likely to be far-travelled. FU_AM and KGU_AM are readily distinct from the other tephras in these two sites (based on major element analysis) and could be from different volcanic sources/eruptions. KGL_AM, KGM_AM and FL_AM and have similar major and trace elements compositions, and are likely to be from the same / similar, nearby source volcano. The larger grain size would also suggest a nearby source volcano for these tephra deposits (see Chapter 3.1).

8.11. Gubs rock shelter (northern Caucasus), site No. 13

Cryptotephra was located in Layer 2 and Layer 3 of Gubs rock shelter, with a maximum shard count of ~8 s/g in Layer 3 (Figure 8.38). Shards were ~70-90 micrometres in size and had an irregular morphology with expanded and some closed vesicles (Figure 8.38). Layers 2 and 3 contain UP type archaeological artefacts. Samples were collected as part of the EFCHED project, and taken at low resolution (~5–10 cm) but were contiguous. Consequently, further low resolution analysis of sediment was not possible.

Tephra shards were isolated from Layer 3 (Gub_3) for WDS-EPMA analysis. Only 3 analyses of glass shards were obtained for Gub_3 although multiple extractions were performed. The data indicated it is a calc-alkaline rhyolite with glass compositions of 75.29-78.11 wt. % SiO_2 and they generally higher in K_2O wt. % (>4.69 wt. %) than Na_2O (3.34-4.07 wt. %; Figure 8.39; Table 8.13).

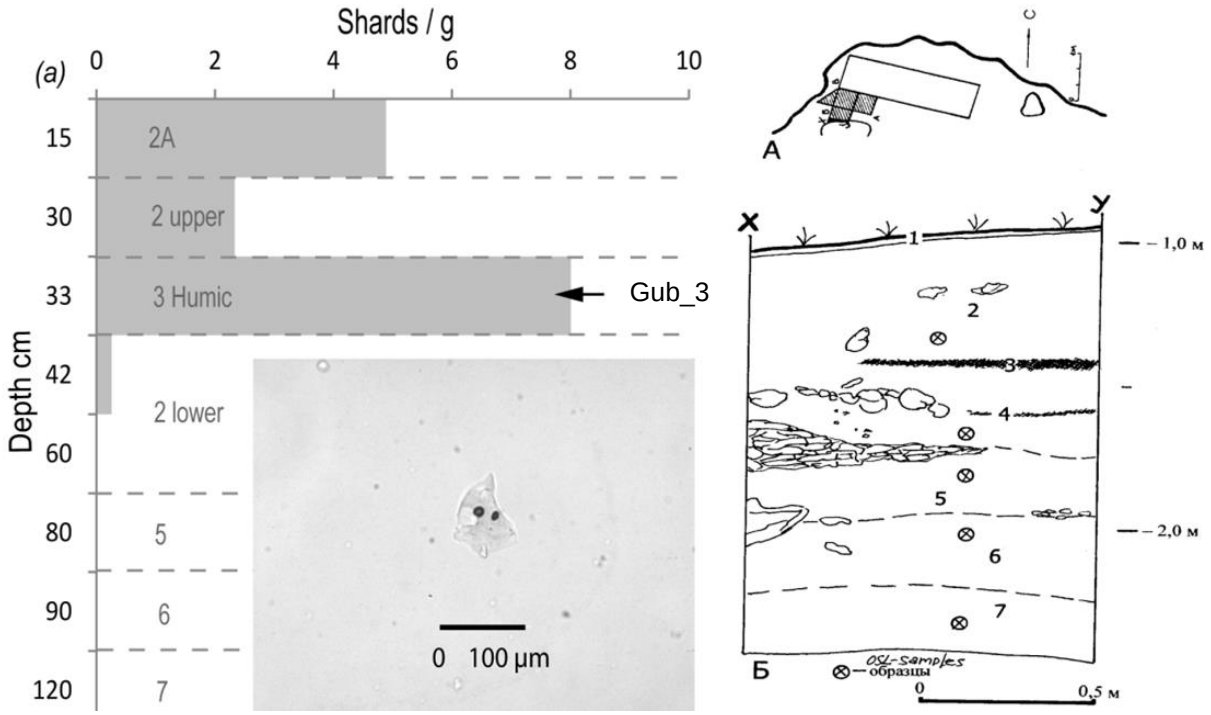

Figure 8.38. Site (right) and tephra profile (left) of Gubs rock shelter. Image shows morphology of glass shards found in Layer 3.

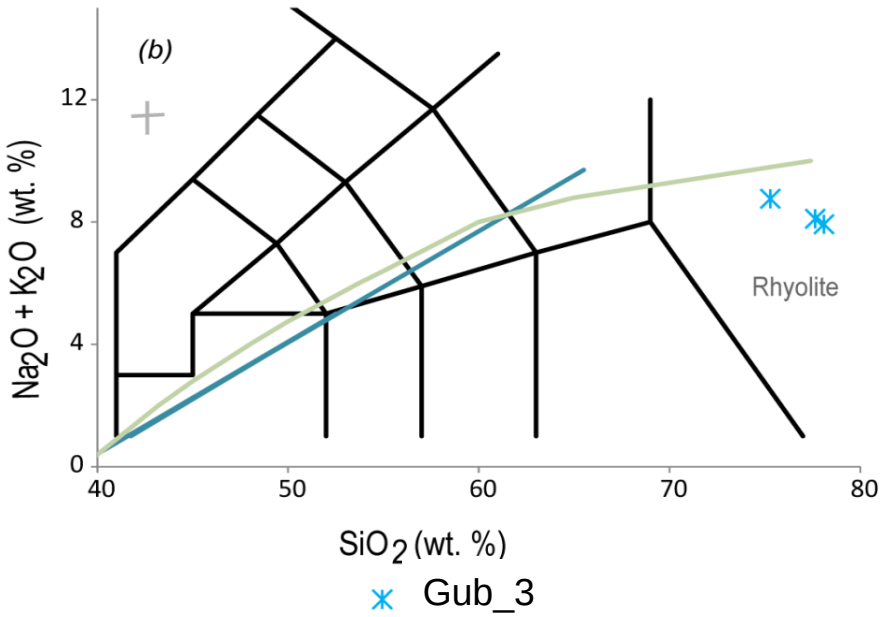

Figure 8.39. Glass compositional data from Gubs rock shelter.

Table 8.13. Glass compositions of three tephra shards extracted from Layer 3, Gubs rock shelter.

Major element (wt. %)	Shard 1	Shard 2	Shard 3
SiO_2	75.29	78.11	77.64
TiO_2	0.12	0.10	0.06
Al_2O_3	13.47	12.78	12.47
FeOt	1.16	0.16	0.77
MnO	0.01	0.03	0.00
MgO	0.11	0.08	0.11
CaO	0.81	0.75	0.75
Na_2O	4.07	2.54	3.34
K_2O	4.69	5.38	4.77
P_2O_5	0.06	0.02	0.00
Cl	0.19	0.04	0.10

8.11.1. Discrimination of primary and secondary deposition

Layer 3 is buried soil that formed during milder climatic conditions before reestablishment of the Layer 2 matrix (Burbidge et al., 2005; section 4.3.9). The highest concentration of tephra was found in this Layer. This suggests the primary input occurred during the formation of Layer 3, with mobilisation of shards upwards a result of bioturbation or the reworking of shards from the landscape post the eruptive event. There was little dislocation of shards downwards.

8.12. Myshtulagty Lagat (Northern Caucasus), site No. 21

Sub-samples from Layers 12-10 and 4-3, from the east profile of Dormouse hall (the main chamber at the site), and samples from Layers 10-11 and 5-4 in the north profile were collected from the site of Myshtulagty Lagat (Weasel Cave). Sampling was conducted by the site excavators and the samples were sent to Royal Holloway, as part of the EFCHED project. The stratigraphy of Myshtulagty Lagat is incredibly complex and the profiles do not contain the full suite of Layers.

Consequently, Layers 9-6 were not sampled. The resolution of the individual bag samples are ~5-20 cm and samples were collected contiguously. Codes for samples prepared for chemical analysis are formatted at follows, WC_Profile/Layer. The east profile (Layer 12-10 and 4-3) contained tephra with the highest shard concentrations spread across ~50 cm in Layer 12. The tephra peak is located at the contact with Layer 11 (WC_EP/12, 11s/g, Figure 8.40) and minimal amounts of tephra found in Layers 3 and 4 are Late Glacial and Holocene in age (respectively) so no further work has been carried out on these two samples. No tephra was found in the north profile. Visual analysis of WC_EP/12 showed shards range from 40 to 150 micrometres in length across the longest axis (Figure 8.40). Shards were colourless and irregular in form with expanded and often enclosed vesicles. Two samples were taken from Layer 12, one from the top and one from the base (~50 cm apart) for WDS-EPMA analysis (see Figure 8.41). Both samples were compositionally identical and are now referred to collectively as WC_EP/12. WC_EP/12 is a homogeneous calc-alkaline rhyolite (Figure 8.42; Table 8.14) that has ~77.60-78.93 wt. % SiO_2, K_2O compositional values of < 4.49 wt. % and has CaO values (~0.50 -0.80 wt. %).

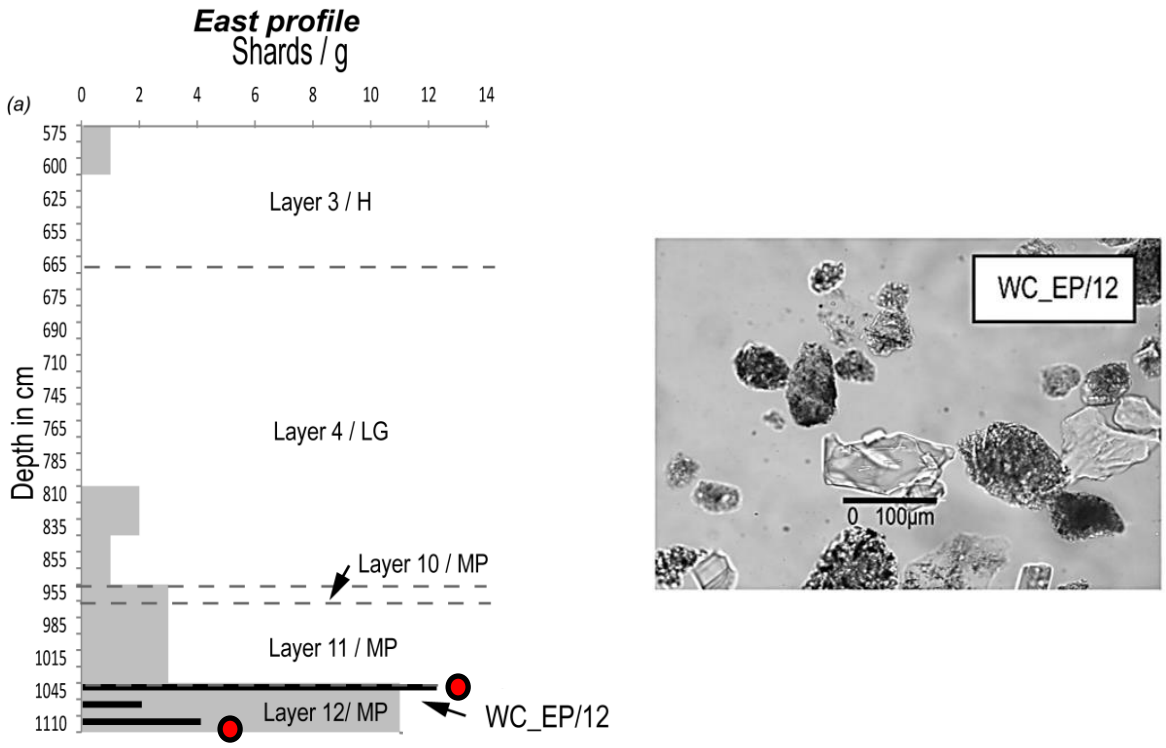

Figure 8.40. The tephra profile from the east profile in the site of Myshtulagty Lagat (North Ossetia) is shown left. Layers 12-10 are associated with the MP (Hidjrati et al., 2003). Red dots are the location of tephra sample that were extracted for WDS-EPMA. Image of glass shards is shown right.

Two samples collected from visible tephra deposits much lower in the sites stratigraphy (thought to be >150 ka; Hidjrati et al., 2003; see section 4.3.10) were prepared for chemical analysis. They are distinguishable from glass shards in Layer 12 (Figure 8.41). As such re-working from these older deposits into the younger layers from the surrounding landscape or through taphonomic processes in the site is unlikely.

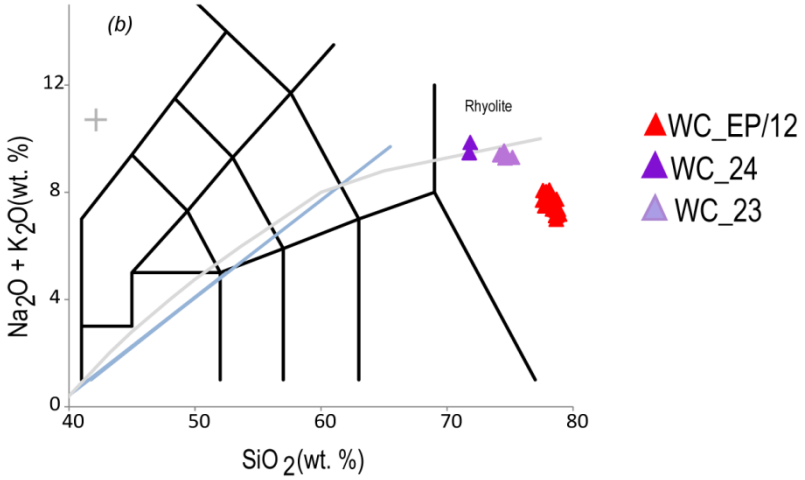

Figure 8.41. Glass compositions from Layer 12 (associated with the MP) and older layers (Layer 23 and 24; WC_23 and WC_24). The older tephras are easily distinguishable from tephra found in Layer 12.

Table 8.14. Glass compositions of tephras extracted from the top and base of Layer 12 in the north profile in Myshtulagty Lagat.

	SiO_2	TiO_2	Al_2O_3	FeOt	MnO	MgO	CaO	Na_2O	K_2O	P_2O_5	Cl
Top of Layer 12	78.70	0.15	11.98	0.65	0.01	0.09	0.51	3.63	4.10	0.05	0.12
	78.51	0.21	12.08	0.75	0.01	0.14	0.73	3.62	3.82	0.00	0.13
	77.62	0.19	12.42	0.76	0.03	0.12	0.65	3.92	4.14	0.00	0.15
	78.54	0.16	11.99	0.76	0.05	0.09	0.62	3.64	3.97	0.02	0.14
	78.20	0.16	11.96	0.79	0.01	0.12	0.69	3.95	3.86	0.03	0.22
	77.60	0.24	12.43	0.84	0.00	0.18	0.83	4.08	3.62	0.04	0.15
	77.97	0.14	12.36	0.84	0.00	0.15	0.75	3.98	3.64	0.03	0.13
	78.00	0.20	12.19	0.85	0.00	0.15	0.79	3.22	4.49	0.00	0.11
	77.82	0.23	12.12	0.91	0.00	0.15	0.79	3.85	3.88	0.00	0.25
	78.71	0.21	12.06	0.92	0.01	0.15	0.67	3.62	3.53	0.00	0.12
	77.87	0.18	12.02	0.93	0.00	0.12	0.73	3.78	4.24	0.03	0.10
Base of Layer 12	77.76	0.23	12.35	0.99	0.01	0.16	0.80	3.77	3.72	0.02	0.19
	78.84	0.18	11.95	0.75	0.02	0.11	0.69	3.83	3.52	0.00	0.10
	78.80	0.14	11.85	0.83	0.07	0.09	0.72	3.77	3.60	0.01	0.11
	78.62	0.18	12.10	0.88	0.07	0.12	0.76	3.70	3.42	0.00	0.14
	78.42	0.19	11.97	0.80	0.00	0.14	0.78	3.97	3.55	0.03	0.14
	78.54	0.19	11.87	0.96	0.04	0.15	0.78	3.76	3.59	0.00	0.12
	78.38	0.13	12.08	0.97	0.00	0.15	0.75	3.95	3.42	0.03	0.14
	78.93	0.18	11.85	0.83	0.06	0.11	0.61	3.40	3.77	0.03	0.22
	78.67	0.16	12.26	0.78	0.03	0.13	0.77	3.46	3.53	0.01	0.19
	78.13	0.12	12.01	0.72	0.07	0.11	0.56	3.59	4.49	0.01	0.19
	78.69	0.21	12.08	0.83	0.05	0.10	0.47	3.02	4.30	0.03	0.22

8.12.1. Discrimination of primary and secondary deposition

Tephra shards are well constrained in Layer 12 (Layer 11-10 above in the same profile have only ~3 s/g and ~1 s/g, respectively) and are fresh appearance with a homogeneous composition. These data would suggest this is a primary event restricted to Layer 12. Location of the isochron is likely towards the top of the Layer with dislocation of shards below the main peak attribute to anthropogenic activity and / or bioturbation.

8.13. Summary of results

In total, nine cave sites and two open air sites have tephra (visible and cryptotephra) preserved in their sedimentary profiles. With the exception of Azhok cave, Gubs rock shelter, Undo Cave, and Ortvale Cave multiple tephra horizons were found at sites and tephra are shown to be associated with both Upper Palaeolithic and Middle Palaeolithic techno-complexes. Some archaeological horizons contain a mix of tephra compositions that span the peralkaline to calc-alkaline index, that suggest different volcanic sources are depositing tephras in the sites; but compositionally homogeneous layers were also found. Tephras were more commonly found in sites south of the Greater Caucasus range.

Chapter 9

Discussion

9.1. Introduction

This chapter brings together all the data presented in the previous chapters to constrain the chronology and correlations between sites across the Caucasus, to further understand the Neanderthal and AMH occupation in the region. The chapter has been divided into three parts: Discussion part I is a comparative discussion of the tephra found in the M72/25-GCI Black Sea core and the archaeological sites; Discussion part II introduces the tephrostratigraphic framework for the southeast Black Sea and the Caucasus; and the third and final section (Discussion part III) discusses how the archaeology of the Caucasus fits into a wider, regional context in light of new data produced in this study.

Discussion part I – comparative discussion of the tephra

9.2. Tephra in the M72/25-GCI Black Sea core

Results from this study reveal that there are 21 cryptically-preserved tephra layers in the M72/5-25-GC1 Black Sea core. Major element chemical analysis of these tephra layers shows that they are predominantly calc-alkaline, high-silica rhyolites. The exceptions are a visible tephra layer that is trachytic in composition and one population of the tephra BSC_651 (see summary Table 9.1).

Table 9.1. Visible tephra and cryptotephra layers in the M72/5-25-GC1 core

Group	Tephra	Composition	Source Volcano	Eruption	Age	Age reference	Published proximal glass chemistry data
Group C	**BSC_008**	CAR	Erciyes Dagi? and CAVP?		unknown		
	BSC_022	CAR	Santorini	Minoan (marine Z2)	3.68 - 3.58 ka cal BP / 3.63 - 3.6 ka cal BP	Friedrich et al., 2006 / Manning et al ., 2006 (^{14}C)	Tomlinson et al., 2014a; This study
	BSC_079	CAR	Erciyes Dagi	Karagüllü or Perikartini	9.97 - 9.56 ka cal BP ; 10.2 - 7.9 ka	Sarikaya et al., 2006 (^{14}C / ^{36}Cl)	Hamann et al., 2010; Tomlinson et al., 2014a
	BSC_139	CAR	Acigöl and CAVP?		~14.4 ka (INT)		
	BSC-154	CAR	Acigöl and CAVP?		~14.6 ka (INT)		
	BSC-158	CAR	Acigöl and CAVP?		~14.6 ka (INT)		
	BSC-179	CAR	Acigöl and CAVP?		~14 - 16 ka (INT)		
Group B	**BSC-394**	CAR	Acigöl	Guneydağ or Korudağ	23.8 ± 2.1 ka or 24.9 ± 2.1 ka	Schmitt et al., 2011 (U-Th/He)	Tomlinson et al., 2014a
	BSC-411	CAR	Acigöl	Guneydağ or Korudağ	23.8 ± 2.1 ka or 24.9 ± 2.1 ka	Schmitt et al., 2011 (U-Th/He)	Tomlinson et al., 2014a
Group A2 tephras	**BSC-651**	CAR / PR	Unknown CAVP/ Nemrut?		After the 34.5 ± 0.65 ka Mono Lake	Kissel et al., 2011 (^{40}Ar/^{39}Ar and K/Ar)	
	BSC-660	CAR	Unknown		~ 34.4 ka (INT)		
	BSC-674	CAR	Unknown		~ 35.6 ka (INT)		
	BSC-683	CAR	Unknown		~ 36.4 ka (INT)		

	BSC-694	CAR	Unknown		~ 37.5 ka (INT)		
	BSC-698	CAR	Unknown		~ 37.8 ka (INT)		
	BSC-705	CAR	Unknown		~ 38.4 ka (INT)		
Visible layer	**BSC-721**	TR	Campi Flegrei	CI (marine Y-5)	39.28 ± 0.11 ka	De Vivo et al., 2001 ($^{40}Ar/^{39}Ar$)	Tomlinson et al., 2012b
Group A1	**BSC-729**	CAR	Unknown		~40 ka (INT)		
	BSC-740	CAR	Unknown		~ LGE 40.7 ± 950 ka	Singer et al., 2009 ($^{40}Ar/^{39}Ar$)	
	BSC-752	CAR	Unknown		~42.1 ka (INT)		
	BSC-778	CAR	Unknown		~44.5 ka (INT)		
	BSC-807	CAR	Unknown		~48.3 ka (INT)		
	Base of core				~60 - 63 ka (INT)		

Footnote: References that have glass shard compositional data are listed. Approximate ages from the tuned Nowaczyk et al. (2012) age model are listed alongside unknown tephras (INT, interpolated from age model). BSC, Black Sea Core; CAR, calc-alkaline rhyolite; CAVP, Central Anatolian Volcanic Province; LGE, Laschamp excursion; PR, Peralkaline rhyolite; TR, trachyte.

9.2.1. Campanian Ignimbrite

Previous work by Nowaczyk et al. (2012) identified the BSC_721 visible tephra layer as the CI tephra. To verify this we have compared our new major element data of the BSC_721 glass shards to the detailed CI glass geochemical dataset of Tomlinson et al. (2012b) and glass compositional data from Cycle III of the Gölcük volcano (WAVP; see section 6.5.2, Chapter 6) that is known to have erupted a trachytic tephra between ~24 – 73 ka (Platevoet et al., 2008; Tomlinson et al., 2014a). The new BSC_721 data sits well within the geochemical field for the CI, and it is easily distinguished from Gölcük on FeOt concentrations (Figure 9.1). The glass composition also confirms that BSC_721 has both fall and flow components of the CI eruption (Figure 9.1; Lowe et al., 2012; Tomlinson et al., 2012b).

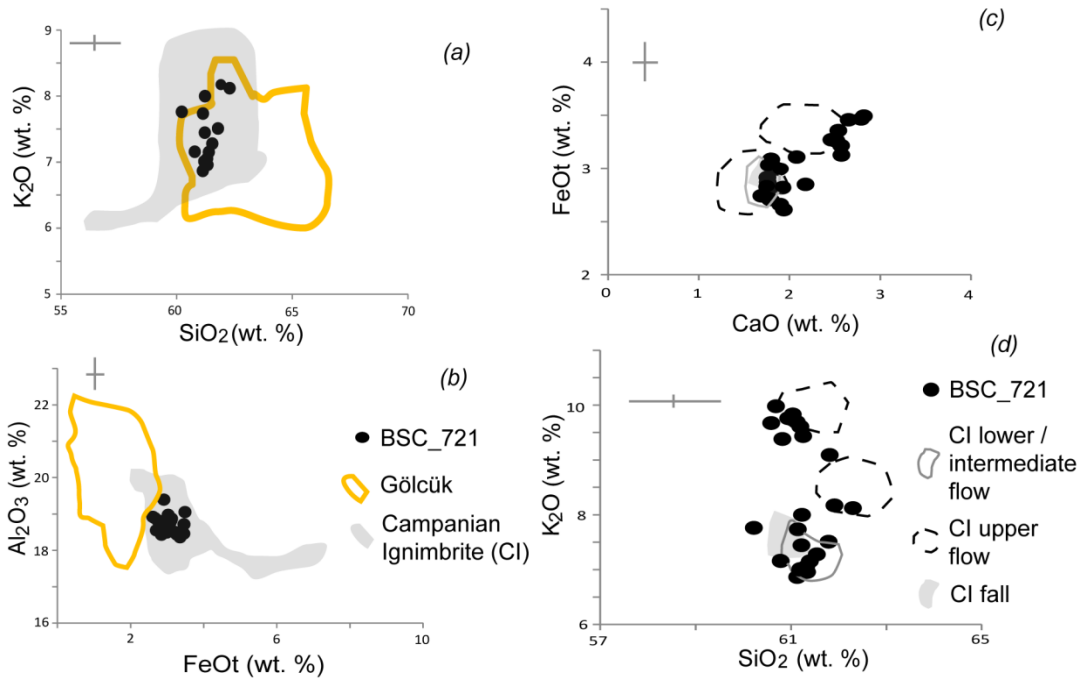

Figure 9.1. Glass compositions of BSC_721 compared to those of the CI (Tomlinson et al., 2012b) and tephra from Gölcük volcano (Tomlinson et al., 2014a). BSC_721 has similarities with trachytic tephra from the Gölcük, Cycle III (a). It is clear that BSC_721 correlates to the CI on major element composition (a-d) and both fall and flow deposits from the ~39 ka CI eruption are preserved (c, d).

9.2.2. The Acigöl rhyolite complex

The major and trace element data of the compositionally homogeneous BSC_394 and BSC_411 tephras (Group B) sit well within the Guneydağ compositional field and one of the populations of the bimodal Korudağ eruption from the Acigöl rhyolite complex (Tomlinson et al., 2014a, Figure 9.2). Both eruptions are from the second eruptive phase, as outlined by Siebel et al. (2011) and Schmitt et al. (2011), and are rhyolitic with >77 wt. % SiO_2 and low CaO contents (<0.6 wt. %; Siebel et al., 2011; see section 6.5.1.1).

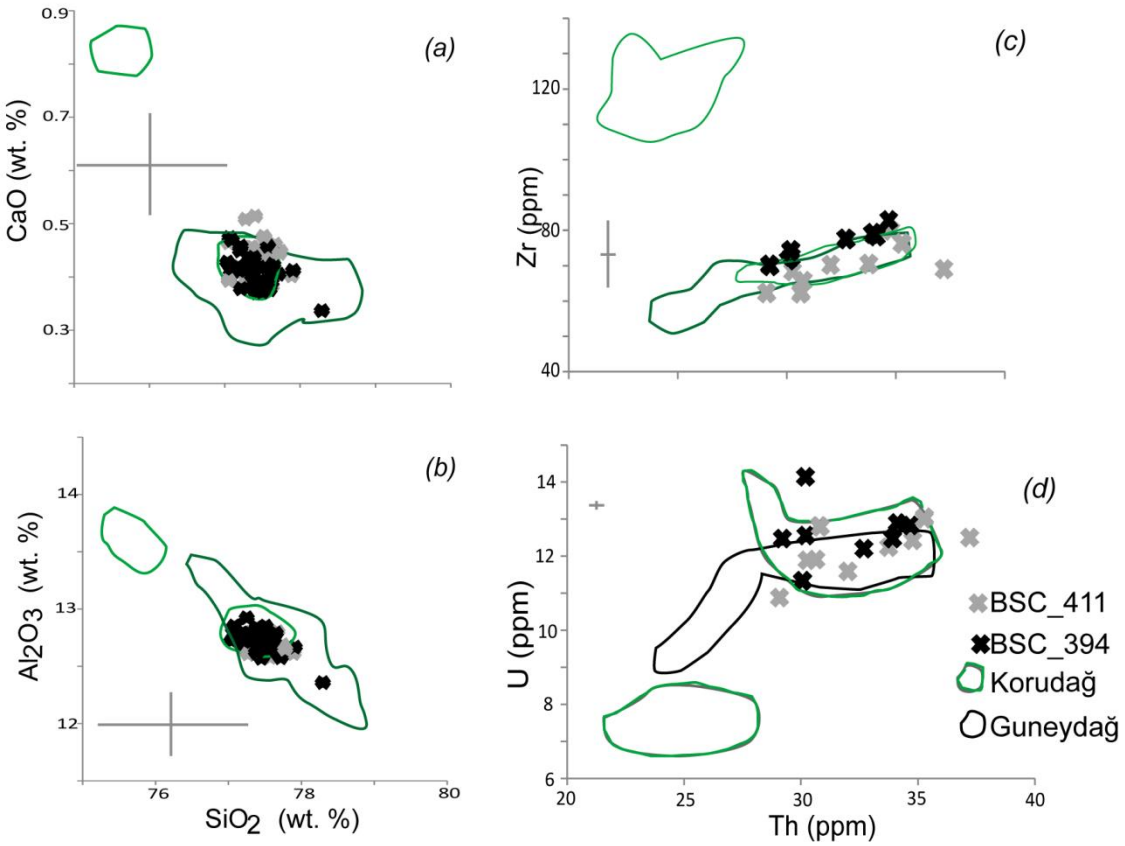

Figure 9.2. Major element (a, b) and trace element glass data (c, d) from BSC_411 and BSC_394. The cryptotephra layers are compositionally indistinguishable from the Guneydağ eruption and one population of the bimodal Korudağ eruption (plotted as geochemical envelopes) from the Acigöl rhyolite complex (data from Tomlinson et al., 2014a).

The (U-Th)/He zircon ages of these eruptions are 24.9 ± 0.9 ka for Korudağ and 23.8 ± 0.9 ka for Guneydağ (Schmitt et al., 2011). Based on the glass compositions of these units, either eruption could be responsible for the BSC_394 and BSC_411 cryptotephra layers (Figure 9.2). BSC_139, BSC_154, BSC_158 and BSC_179 of Group C tephra layers also have some shards that sit within the Acigöl compositional field suggesting that they represent a number of closely spaced, younger eruptions from the Acigöl field (see Figure 9.5).

9.2.3. Erciyes Dagi

BSC_079 is chemically identical to two Holocene eruptions, Karagüllü and Perikartini, from the Erciyes Dagi volcano in the CAVP (Figure 9.3; Hamann et al., 2010; Tomlinson et al., 2014a; section 6.5.1.2). Compositionally, both eruptions are identical (major and limited trace element data; Tomlinson et al., 2014a). Thus, BSC_079 could be a product of either of these eruptions. Both eruptions have been dated and the age ranges overlap: 9971-9594 ka cal BP and 9984-9596 ka cal BP (charcoal, 94.5% confidence, Sarikaya et al., 2006). Cosmogenic ^{36}Cl ages of respective lavas yield ages between 10.3 ka and 7.3 ka (Sarikaya et al., 2006). The stratigraphic relationship between these two tephra is not clear in the literature. Finding this tephra in the Black Sea implies that one of these eruptions (Perikartini or Karagüllü) was dispersed to the northeast. A third Holocene eruption from the same volcano (Dikkarin, ~ 8.8 ka cal BP, Hamann et al., 2010) is easily distinguishable from the other units based on its compositional homogeneity and lower SiO_2 composition (Figure 9.3). Dikkarin tephra is not found in the Black Sea core, which is consistent with its southeasterly dispersal (Hamann et al., 2010).

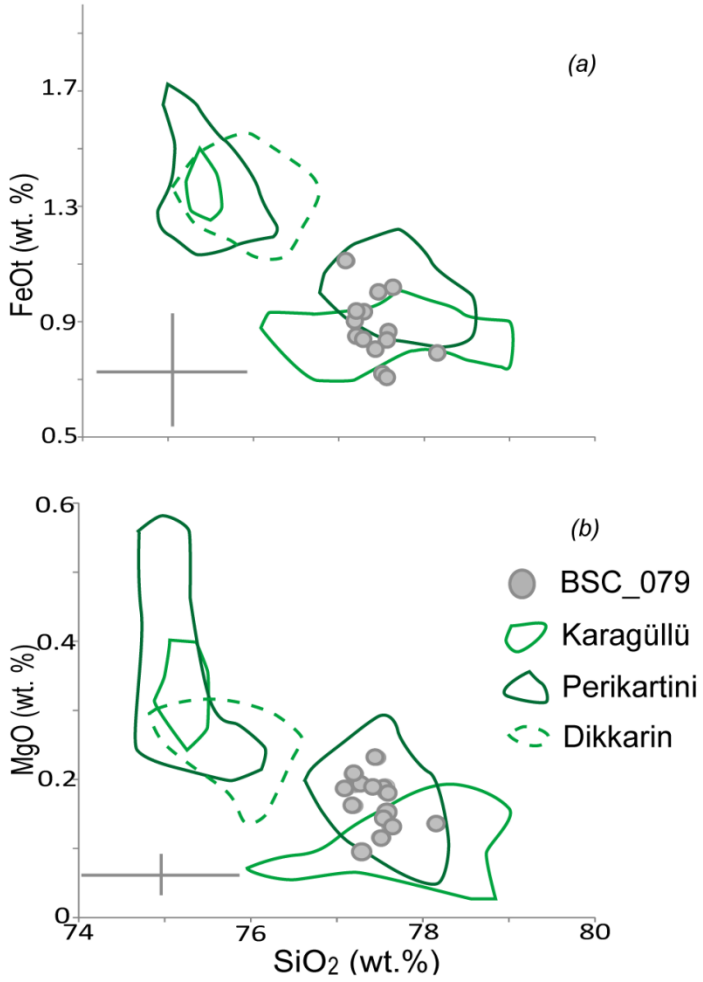

Figure 9.3. BSC_079 with glass compositional data from the three Holocene eruptions (Dikkarin, Karagüllü and Perikartini) of Erciyes Dagi in the CAVP (data from Hamann et al., 2010; Tomlinson et al., 2014a). BSC_079 is chemically identical to the one population of Karagüllü and Perikartini tephras and could be a product of either. Trace element data from the Karagüllü and Perikartini eruptions are unable to differentiate between the eruptions (see Tomlinson et al., 2014a).

9.2.4. Minoan eruption

The glass composition of BSC_022 is identical to that of the 3627 to 3600 ka cal BP (2σ) eruption of Thera volcano, Santorini (Friedrich et al., 2006; Manning et al., 2006; Figure 9.4), also known as the Bronze Age Minoan eruption or the marine Z-2 tephra (Keller et al., 1978; section 6.4.1). Deposits of this eruption have been previously identified in marine cores across the eastern Mediterranean (see Johnston et al., 2012), in the southwest Black Sea (e.g. Guichard et al., 1993), and intercalated with alluvial fan sediments in Acigöl basin, western Turkey (Sulpizio et al., 2013). This BSC_022 layer is the most easterly deposited of the

Minoan eruption. This extends the known fallout area across Turkey and the Black Sea, making it an increasing important regional Holocene tephra marker.

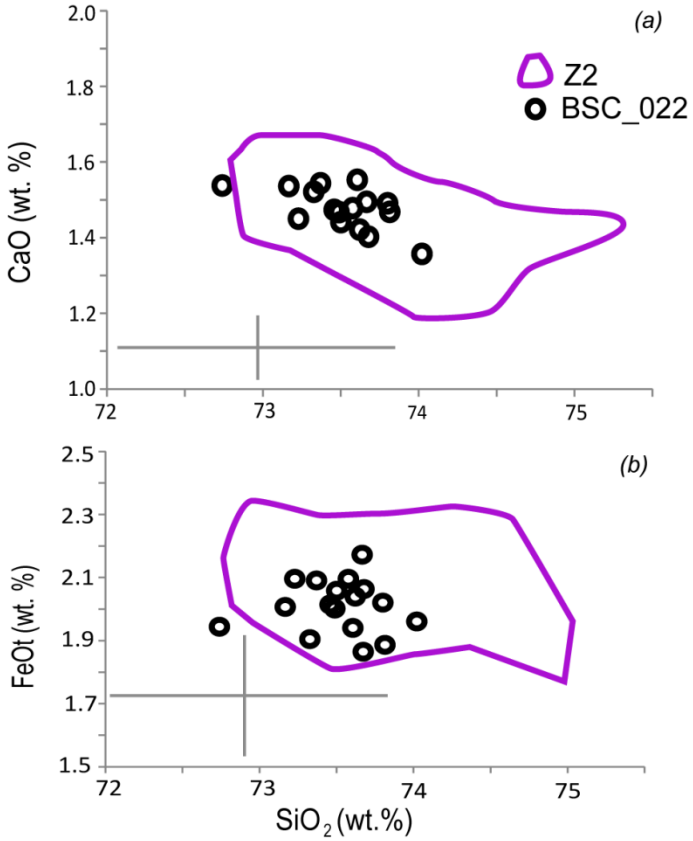

Figure 9.4. Glass compositions of BSC_022 compared to those of the Minoan Z2 eruption from Santorini (Tomlinson et al., 2014a; this study). BSC_022 clearly correlates to the Z2 on major element composition (a and b).

9.2.5. Uncorrelated tephras

Most of the tephra horizons in the Black Sea core that have not been correlated to other tephras (above) typically have SiO_2 concentrations >75 wt. % (with the exception of SiO_2 poor population of BSC_651) and they are typically low in CaO (<1.2 wt. %) and FeOt (<1.5 wt. %). These glass compositions indicate that they are not associated with eruption from the Younger Turia (Romania) or from Italian sources (see sections 6.3.1 and 6.6.1). Eruptions from the Aeolian Islands such as Vulcano typically have < 62 wt. % SiO_2 and those from Lipari generally have > 1.5 wt. % FeOt (Albert et al., 2012a, b). Glasses from Pantelleria are very distinct,

characterised by low SiO_2 compositions (~56.61 - 72.97 wt. %) and high FeOt (> 7 wt. %; Tamburrino et al., 2012). Tephra from some of the Hellenic arc volcanoes can also be excluded. Eruptions from Yali (Ya-3L and YA-3H) have <72 wt. % SiO_2 and CaO contents >1.55 wt. % (Aksu et al., 2008), and Nisyros deposits have high FeOt contents (>1.1 wt. %; Tomlinson et al., 2012a; section 6.4). The lack of a High-K phonolitic compositions and total alkali values of >13 wt. % suggests that the remaining cryptotephras in the M72/5-25-GC1 core are not from the Gölcük (WAVP, see above).

The least evolved population of BSC_651 (<76 wt. %) is compositionally peralkaline. This suggests that it is not from the CAVP but could be from the EAVP (e.g. Nemrut; Sumita and Schmincke, 2013a; section 6.5.3). The least evolved population of BSC_651 (<76 wt. % SiO_2) is similar to the alkaline rhyolite compositional field of Nemrut Formation (NF; Sumita & Schmincke, 2013a; see Figure 6.5 in Chapter 6). However, the two rhyolitic tephras have different Al_2O_3 concentrations; BSC_651 has ~12-15 wt. % and NF ~11 wt. % (Sumita & Schmincke, 2013a; section 6.5.3.1) and BSC_651 is generally lower in FeOt concentrations. These data suggest a more easterly dispersal of the NF, in accordance with prevailing wind directions and it has not been found in the M72/5-25-GC1 core. Given the location and compositional data obtained, remaining sources for the unidentified, calc-alkaline tephras are likely to be those from Turkey, specifically the CAVP, the east Carpathians and possibly Süphan volcano in eastern Turkey (see Figure 9.5; see Table 6.1).

Erciyes Dag and Hasan Dagi show a distinct compositional division from remaining, unidentified tephras recorded in the Black Sea, with consistently lower alkali compositions (Figure 9.5). The Göllü Dagi and the Older Turia deposits have

some compositional similarities to the remaining calc-alkaline tephras (Figure 9.5). However, the majority of the unidentified Black Sea rhyolites have FeOt concentrations > 0.7 wt. % which distinguish them from Older Turia, and deposits from this volcano are not thought to be widely dispersed. Presently there are too many repeat compositions in the Black Sea data and there is not a sufficient glass chemical dataset of other central Anatolia volcanic sources (and from Süphan volcano) with older eruptions from the east Carpathians against which to compare.

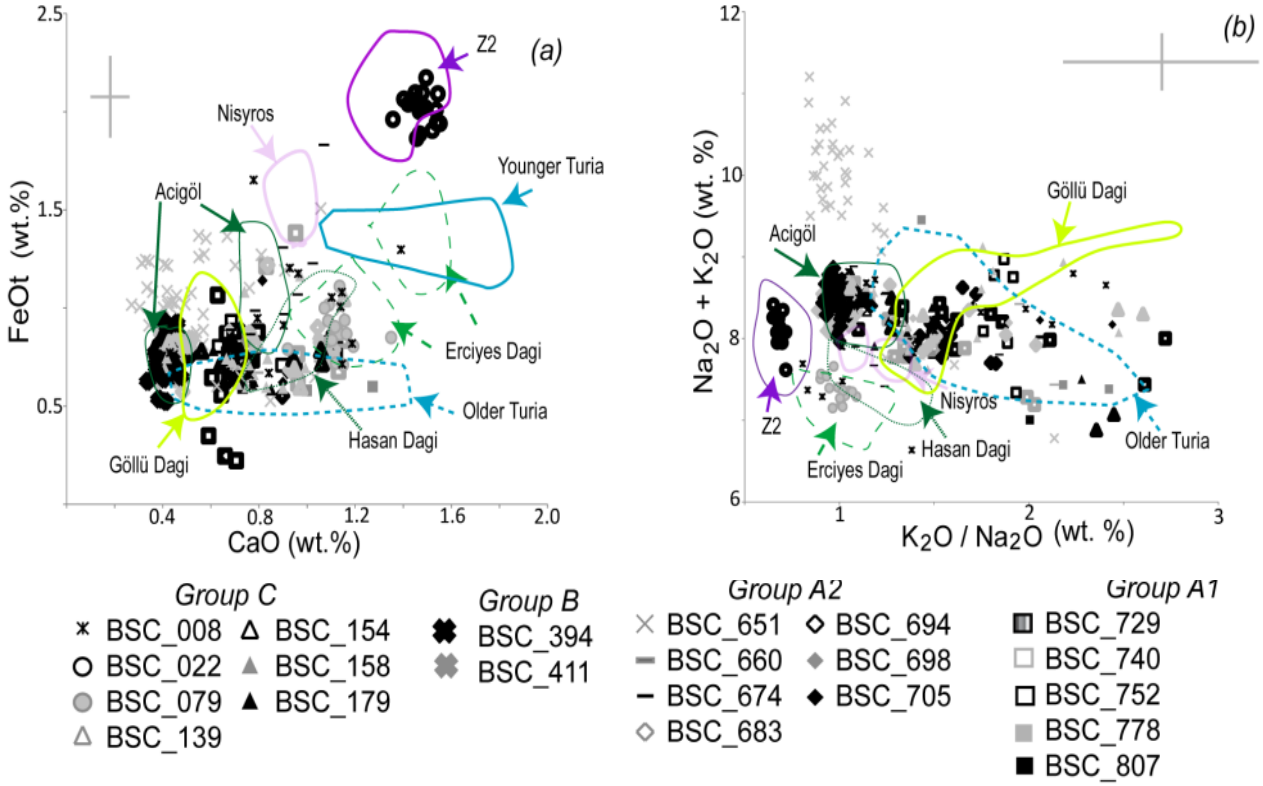

Figure 9.5. Glass compositions (shown as envelopes) of Quaternary eruptions in the eastern Mediterranean and the east Carpathians. Compositional data from specific eruptions has been used where possible, but some chemical envelopes represent data from other smaller eruptions from the volcano. Data from the Upper and Lower Nisyros pumice is from Tomlinson et al. (2012a). Glass data from the Z2 (Minoan) is from Tomlinson et al. (2014a) and was produced in this study. The CAVP compositional data is from Hamann et al. (2010), Tryon et al. (2009), Tomlinson et al. (2014a) and the Romanian data (the Younger and Older Turia) are from Veres and Wulf (pers comms, 2014) and this study.

9.2.6. Age model for the Black Sea core

Ideally, age models for archives should be constructed using only independently dated age makers (e.g. varve, tephra, and radiocarbon ages) without a prior assumption of synchronicity to other disparate records (see Blaauw, 2012; Blockley et al., 2012). In the case of the M72/5-25-GC1 core, the fundamental assumption was that the fluctuations in palaeoenvironmental data (IRD and $CaCO_3$; Nowaczyk et al., 2012) were synchronous to fluctuations observed in the Greenland ice cores so that the GICC05 $\delta^{18}O$ time scale could be used (see Nowaczyk et al., 2012). The current age model for the M72/5-25-GC1 core includes the $^{40}Ar/^{39}Ar$ age of the CI eruption (39.28 ± 0.11 ka; De Vivo et al., 2001) and reservoir-corrected radiocarbon ages from the parallel M72/5-25-GC3 core (correlated to M72/5-25-GC1 using magnetic susceptibility profiles; described in section 4.4). An independently dated age model for the Black Sea core was constructed to try to assess the reliability of the Nowaczyk et al. (2012) tuned age model. After construction (see Appendix 1 for the full details of the age model construction and Figure 9.6), it was found that the new model was unable to integrate the full prior information, the insertion of two recorded hiatuses at the base of the core, one at 180cm and one at 50cm (see Figure 9.6b). This was due to the lack of securely dated markers around these hiatuses. Therefore, the new age model is not able to robustly test the Nowaczyk et al. (2012) age model, but some comments can be made.

The sedimentation rates of the new age model are similar to that of Nowaskey et al. (2012), but there are changes in the timing of deposition in the upper part and lower part of the core (Figure 9.6a, b). In both instances, this new model has produced slightly younger age estimates (modelled BP, 95 % confidence) for the

BSC_079 and BSC_807 tephras (~4-8 ka and 40-45 ka, respectively) than estimates of ~13 ka and ~48 ka from the age model of Nowaczyk et al. (2012). Discrepancies in the younger part of the model may be a result of the two hiatuses that could not be inserted into the OxCal model (see Figure 9.6a). The age for the BSC_079 tephra (from Erciyes Dagi) produced by this new model (~8- 4 ka) overlaps with the eruption ages of ~10- 7 ka from Sarikaya et al. (2006). The agreement of these ages implies that the tuned age model may not be accurate for the upper section of the core.

The Nowaczyk et al. (2012) age model has better constrained ages for the two closely spaced Acigöl eruptions that are preserved in the core (BSC_394 and BSC_411; see Figure 9.6b) of ~24 -22 ka that are close to the ages from Schmitt et al. (2011; see above). The new age model provided an age range of ~32- 18 ka for these same two deposits. The agreement between the Nowaczyk et al. (2012) ages and the Schmitt et al. (2011) ages, provide some reassurances on the accuracy on the central parts of the original model by Nowaczyk et al. (2012). Interpolated, re-calibrated radiocarbon ages with the reservoir correction factor from Kwiecien et al. (2008; see section 4.4.4 and Nowaczyk et al., 2012 supplementary information) are also similar in age to the Acigöl tephras ages (~21 ka cal BP at ~340 cm depth and 26 ka cal BP at 500 cm depth; see Figure 6.9b) and suggest the ~1450 ka correction factor (calculated by independent means, using the age of the Y2 tephra; section 4.4) for sediments around 30-20 ka is reliable. Nowaczyk et al. (2012) model was also constrained with the ~39 ka CI tephra age and it is likely ages around this (between the recorded Laschamp and Mono Lake geomagnetic excursions) are also accurate. As such, the age model produced by Nowaczyk et al. (2012) has been used to provide age estimates for

the tephra groupings in the M72/5-25-GC1 core, but approximate ages of tephras that had some independent age control have also been retained (e.g. Sarikaya et al. (2006) of ~10-7 ka for the Erciyes Dagi eruptions and the ~3.6 ka cal BP for the Minoan tephra; see Table 9.1).

The Nowaskey et al. (2012) age model suggests that Group A tephras are associated with eruptions between ~48 and 31 ka, Group B between ~24 and 22 ka, and the deposition of Group C tephras started between ~16 and 14 ka (Table 9.1; Nowaskey et al., 2012). These groupings of tephra could suggest distinct periods of frequent volcanic activity followed by periods of quiescence. Group A and B tephras were deposited during periods of increased climate instability as recorded by IRD and $CaCO_3$ (see section 4.4 and Figure 7.2). This correlation could indicate increased volcanic activity in times of increased climate instability but as tephras are also deposited in more stable climates (Group B tephras) the deposition of tephras cannot be related to climate, but could reflect other changes such as wind direction. The subtropical jet and polar front jet control prominent wind directions across the region and the seasonal migration of these results in wind directions been different in the summer and winter months (see Stockhecke et al., 2014b). The deposition of tephra in the south-east Black Sea could reflect these changes and dispersal could also be influenced by orographic effects of the mountains around the Black Sea. The situation is complex and taphonomic considerations also need to be considered when looking for patterns of volcanism in distal archives as not all tephras that are erupted downwind of the archive will be recorded. Finding these tephras in other archives and more detailed proximal work in the region will help to understand more about the volcanism and provide a more robust age model for the M72/5-25-GC1 core.

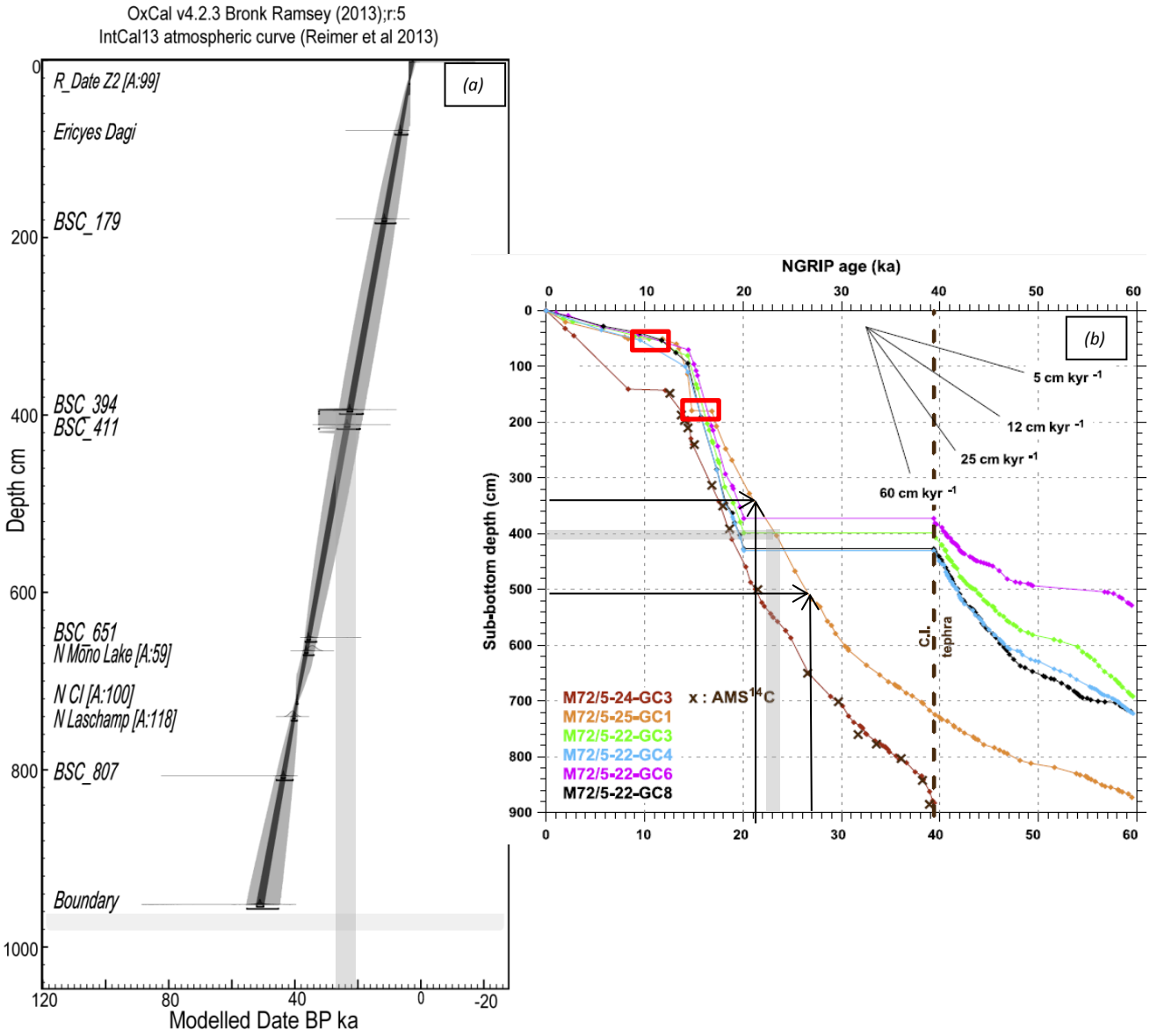

9.6a is the Independent age model for the M72/5-25-GC1 core. The model was created in OxCal v4.2.3 using the IntCal13 calibration curve (Reimer et al., 2013) and a variable k, P sequence was used (Bronk Ramsey, 2008; Bronk Ramsey and Lee, 2013). This model therefore contained depth information alongside the known age markers, and was programmed to assume the deposition of sediments was not uniform. Model a only used independent age markers, the Laschamp and Mono Lake geomagnetic excursions and the CI and Z2 tephra marker layers, and was run without prior information of the two recorded hiatuses (~180 and 50 cm, outlined in red on b). Model b is the Nowaskey et al. (2012) age model (see section 4.4). Vertical and horizontal grey boxing shows the age estimated from the Group b tephras for both models. Model a has a wider age range ~18-32 ka, model b is more tightly constrained (~23-24 ka) and ages are closer to the eruption ages from Acigöl by Schmitt et al. (2011). Black arrows show the relevant radiocarbon ages that were interpolated from the M72/5-24-GC3 sister core (shown as black crosses). These ages were recalibrated with IntCal13 (Reimer et al., 2013) and the reservoir correction factor used by Nowaskey et al. (2012) for these was applied. These ages are also similar to the Acigöl dates. See Appendix 1 for full details of the age model construction.

9.3. Origin of the tephra in the Archaeological sites

Table 9.2. Tephra layers (visible and cryptotephra) in the archaeological sites studied in the Caucasus.

Site	Tephra	Composition	Source volcano	Age*	Techno-complex	Proximal glass chemistry data
Ortvale Klde	OK_3 p1 OK_3 p2	PR CAR	Nemrut Unknown	~30 ka NF / ~25-30 ka ca, BP (Sumita and Schmincke 2013 a, b/ Adler et al., 2008, ^{14}C)	EUP	Sumita and Schmincke, 2013 a, b
	OK_4c p1 OK_4c p2 OK_4c p3	CAR PR D	Unknown Nemrut LCVP?	start ~43 -48ka cal BP end ~36 – 46 ka cal BP (This study, ^{14}C)	EUP	
	OK_5/6	CAR	Unknown	> 50 ka (This study/remodelled Adler et al., 2008 ^{14}C)	LMP	
	OK_7	TD	LCVP?	>50 ka (This study/remodelled Adler et al., 2008, ^{14}C)	MP	
Sakajia Cave	SK_2t(p1,2,3) SK_2b	CAR CAR	CAVP? CAVP?	start 34-39 ka cal BP end ~25-35ka cal BP (Pinhasi et al., 2012, ^{14}C)	UP	
	SK_3a	CAR	Unknown	start 39-45 ka cal BP end 34-39ka cal BP (Pinhasi et al., 2012, ^{14}C)	LMP	
Ortvale Cave	OT_3	CAR	Unknown	>41 ka (Pinhasi et al., 2012, ^{14}C)	LMP	
Lusakert Rock shelter	LKI_3	TR	Nemrut	< 30 ka	MP	

	LKI_4.1 p1	TR	Nemrut		MP	This study
	LKI_4.1 p2	TR	Nemrut? EAVP?			
	LKI_4.1 p3	TR	Nemrut	~30 ka NF (Sumita and Schmincke 2013 a, b.)		Sumita and
	LKI_4.1 p4	PR	Nemrut	~30 ka NF (Sumita and Schmincke 2013 a, b.)		Schmincke, 2013 a, b
	LKI_4.1 p5	CAR	Unknown/LCVP	start ~43 -48ka cal BP end ~36 – 46 ka cal BP		Sumita and
	LKI_4.1 p6	D	LCVP	(correlation to OK_4c, p1 and p3)		Schmincke, 2013 a, b
	LKI_5.1 p1	TR-Ph	Nemrut? EAVP?		MP	
	LKI_5.1 p2	TR	Nemrut? EAVP?			
	LKI_5.1 p3	CAR	Unknown			
	LKI_5.2B p1	TR-Ph	Nemrut? EAVP?		MP	
	LKI_5.2B p2	CAR	Unknown			
	LKI_6.5	TA-TD	LCVP		MP	
	LKI_7 p1	TR-Ph	Nemrut? EAVP?		MP	
	LKI_7 p2	CAR	Unknown			
Lusakert 1	LKO_CT	CAR	Gutansar	Possibly re-worked? Or 2X eruptions ~31-36 ka	MP	This study
	LKO_CB	CAR	Gutansar	(Adler et al., 2012 ^{14}C, OSL)		
	LKO_D	CAR	Unknown		MP	
Azokh	AZ_2a/1	CAR	Unknown	start 39-45 ka cal BP end 34-39ka cal BP (correlation to SK_3a)	UP	
Aghitu 3	AG3_8A	BA-TD	LCVP	30-31ka cal BP (Kandel pers comms, 2014 ^{14}C)	EUP	
	AG3_8D	BA-TD	LCVP	30-31ka cal BP (Kandel pers comms, 2014 ^{14}C)	EUP	
Fantan	FU_AM	CAR	Unknown		MP	

	FL_AM	TA	LCVP		MP	
Kagasi	KGU_AM	BTA	Gutansar		MP	This study
	KGM_AM	TA-TD	LCVP		MP	
	KGL_AM	TA	LCVP		MP	
Gubs rock shelter	Gub_3	CAR	Unknown		EUP	
Myshtulagty Lagat	WC_EP12	CAR	Greater Caucasus range (Elbrus?)	~70-128 ka (Hidjrati et al., 2003, environmental proxies)	MMP	

*Footnote: * Approximate ages for the unknown tephras listed are taken from chronological data from the archaeological units in which the tephra were found and based on correlations to other sites or dated eruptions (radiocarbon ages have been recalibrated and modelled; see below). NF, Nemrut Formation eruption; CAR, Calc-alkaline rhyolite; PR, Peralkaline rhyolite; TR, trachyte; TR-Ph, trachytic that extends to phonolite; TA, trachy andesite; D, dacite; BTA, basaltic trachy andesite; TD trachy dacite; BA, basaltic andesite; CAVP, Central Anatolian Volcanic Province; LCVP, Lesser Caucasus Volcanic Province; EAVP, East Anatolian Volcanic Province. Notation 'p' refers to the number of compositionally distinct tephra populations found in some layers; these reflect either different source volcanoes and/or different eruptions from the same volcano. For example, Layer 3 of Ortvale Klde contains a population of glasses with a peralkaline composition (p1) and a population that is calc-alkaline (p2; see Chapter 8).These populations indicate two different source volcanoes.*

9.3.1. The Nemrut formation tephra, Nemrut volcano, eastern Turkey

The Nemrut Formation (NF) tephra is from the Nemrut volcano in eastern Turkey (see section 6.5.3.1). There are three phases of the NF caldera eruption: the initial plinian fallout (lower NF; L-NF) erupted peralkaline rhyolite, the middle phase (Middle NF; M-NF) is rhyolitic to trachytic, and the PDC and final fall and surge deposits (Upper NF; U-NF) are trachytic. In Layer 3 of Ortvale Klde (Georgia) two compositional glass populations were found (see section 8.3). Population 1 (p1), the peralkaline rhyolite, is a match to the rhyolitic fall (L-NF) and flow (Ignimbrite phase; M-NF) of the ~30 ka Nemrut Formation. Major element data from glasses in Unit 4.1 (p3 & 4) in Lusakert rock shelter (Armenia) also sit well within the distinctive NF compositional field (see Figure 9.7). Lusakert rock shelter contains the trachyte component (U-NF; LKI_4.1, p3) as well as the rhyolitic Ignimbrite (LKI_4.1, p4).

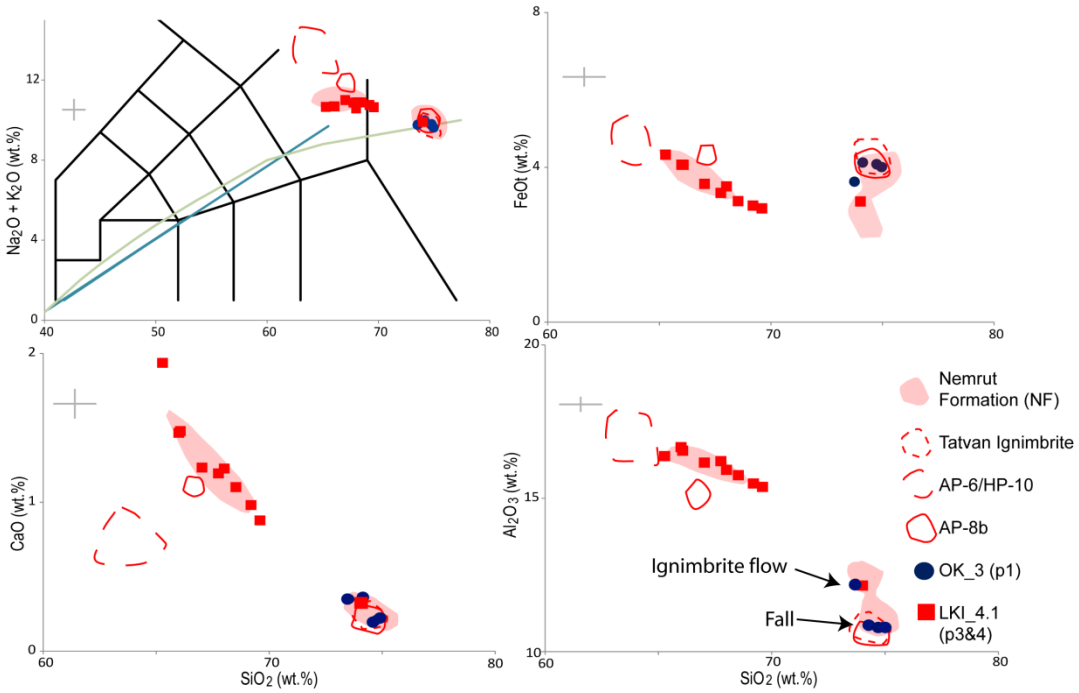

Figure 9.7. Selected glass compositions of OK_3 (p1) and LKI_4.1 (p3&4) compared to those of the NF (Sumita and Schmincke, 2013 a, b) and older Nemrut glasses (see section 6.5.3.1). OK_3 (p1) is identical to the rhyolitic fall and ~12 wt.% Al_2O_3 ignimbrite flow component of the caldera-forming NF eruption and

LKI_4.1 (p3&4) shows the ~12 wt.% Al_2O_3 ignimbrite phase to trachyte compositional range. Therefore, both tephras correlate to the ~30 ka NF on major element compositions and are distinct from the Tatvan ignimbrite, AP-8b or the AP-6/HP-10 eruption.

Rhyolitic and trachytic compositions typically produce high elevation Plinian columns that are able to disperse ash over greater distances. The sole presence of the rhyolite component in Georgia could therefore be an artefact of wind change during the eruption. These deposits are the first recorded distal deposits of this eruption, extending its known fallout. The NF has an average age of ~30 ka that is based on single crystal laser dating of two proximal deposits; 29.7 ± 4.2 and 28.6 ± 3.0 ka (see Sumita and Schmincke, 2013a), with a tuned age of 32.70 ± 2.55 ka derived from the Lake Van palaeoenvironmental record (Sumita and Schmincke 2013b). The re-calibrated age for the start of Layer 3 in Ortvale Klde (charcoal ages with an ABA pre-treatment; likely to be underestimates) is ~30-25 ka and sits well with the current NF age data. These data suggest a north-northeasterly axis of dispersal rather than directly east as previous thought (Sumita and Schmincke, 2013a).

9.3.2. Nemrut volcano, eastern Turkey

The Nemrut volcano is known to have produced a number of variably peralkaline trachyte and alkaline rhyolite tephras through time (see Sumita and Schmincke, 2013a, b), but the full range of geochemical variation in some larger eruptions is unknown (Sumita and Schmincke, pers comms, 2014). The HP-10/AP-6 eruption is older than the NF (61.60 ± 2.55 ka) and also comes from the Nemrut volcano (Sumita and Schmincke, 2013b). The current dispersal axis for the HP/10-AP/6 is to the east-southeast of the Nemrut volcano; proximal/medial deposits have not

been located to the north (Sumita and Schmincke, 2013a, b). In the archaeological site of Lusakert rock shelter (Armenia), glass population 1 from Unit 4.1 (LKI_4.1, p1) and glasses in Unit 3 (LKI_3; that is stratigraphically distinct; see section 8.7.1) have compositions that are similar to the HP-10/AP-6 eruption deposits from Nemrut (see Figure 9.8). Unit 3 that contain tephra LKI_3 is stratigraphically above Unit 4.1 that preserves the NF (both units are also separated by another layer, Unit 4.6). The LKI_3 tephra is too young (<30 ka) to be associated with the HP-10/AP-6 eruption. Furthermore, the majority of LKI_3 glasses have compositions that are higher in CaO and lower in FeOt relative to the HP/10-AP/6 tephra (see Figure 9.8). It is likely that the LKI_3 tephra is from a younger Nemrut eruption. The LKI_4.1 (p1) is a compositional match to the HP-10/AP-6 eruption (Figure 9.8).

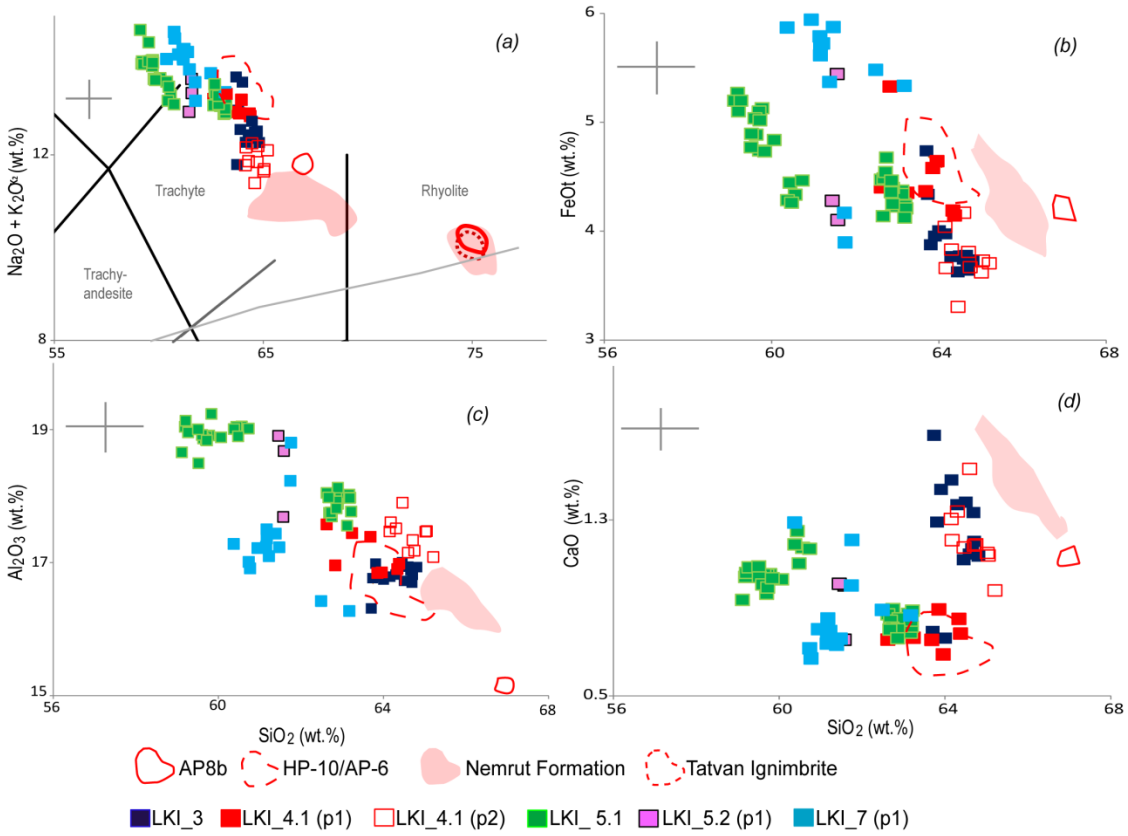

Figure 9.8. TAS (a) and selected Harker diagrams (b-d) with Lusakert rock shelter peralkaline glass compositions compared to glasses from the Nemrut volcano

(shown as envelopes). Both the LKI_4.1 (p1) and LKI_3 have tephra compositions that are similar to the HP-10/AP-6 tephra from Nemrut. The AP8b and Nemrut Formation trachyte tephras are clearly distinct from all Lusakert tephras.

As a similar composition to the HP-10/AP-6 tephra was also found in Unit 3 and in Unit 4.1 the correlation of LKI_ 4.1 p1 with the with the HP-10/AP-6 tephra is not robust but this tephra (LKI_4.1, p1) comes from the Nemrut volcano.

9.3.3. Gutansar volcano, Armenia

Tephra KGU_AM is the upper visible deposit in the site of Kagasi, Armenia (see Figure 4.9 in Chapter 4). Glasses from this layer sit well within the compositional field for both the AM13_13 and AM13_14 fall deposits from the base of the Gutansar volcano (see Figure 9.9) that is situated close to the site (see Figure 6.11). These tephra compositions are distinct from all other tephras analysed in this study (proximal and from the archaeological sites). Ages for AM13_13 and AM13_14 are unknown, but the KGU_AM tephra was associated with MP tools (see Chapter 4.3.8) and suggests the volcano was explosively active during the MP in Armenia. There are no trace data available AM13_13 and AM13_14 due to the presence of numerous microcrystal inclusions in the glassy matrix. However, limited trace data from KGU_AM shards indicate this tephra has a subduction character (see Chapter 8 and below), which is consistent with an Armenian source (e.g. Neill et al., 2013). This confirms that KGU_AM is likely to be associated with an eruption from the Gutansar volcano.

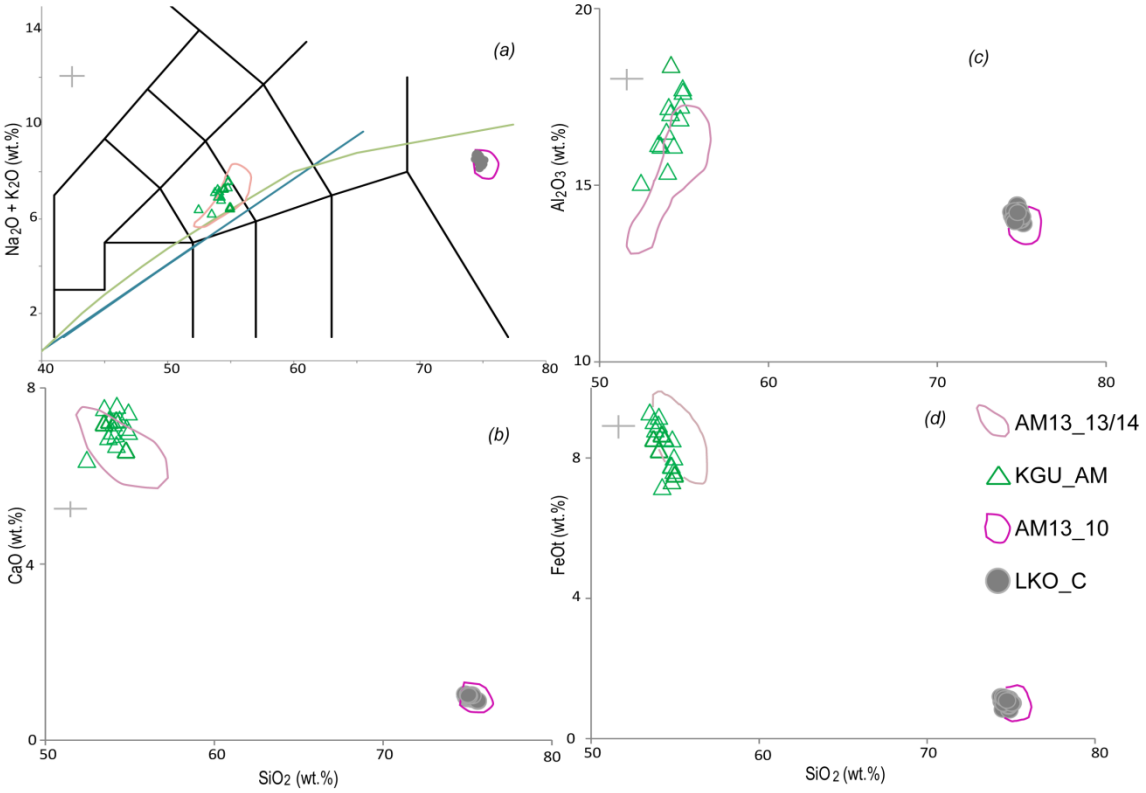

Figure 9.9. Major element glass data (a-d) from KGU_AM and LKO_C compared to the fall (AM13_13 and AM_14) and the block and ash flow (AM13_10) deposits from Gutansar volcano (shown as envelopes). The KGU_AM and LKO_C cryptotephra layers are compositionally indistinguishable from proximal Gutansar deposits.

Glasses found at the base of Layer C outside the Lusakert rock shelter (Lusakert 1; LKO_C) sits well within the Gutansar calc-alkaline glass compositional field (AM13_10; Figure 9.9). These glasses are compositionally distinct from other calc-alkaline glasses found in the archaeological sites, with Al_2O_3 compositions between ~13.96 – 14.25 wt. % (Figure 9.11) and strongly suggest Gutansar as the source. Lusakert 1 is situated a few kilometres southwest of the block and ash fall where the AM13_10 ash was collected and both sites are located in the Hrazdan river gorge. Age estimates for the pyroclastic block and ash flow from Gutansar are not well constrained, but are thought to be part of a larger flow deposit that has ages of ~1.5.Ma and 300 ka (see Frahm et al., 2014), indicating some serious

discrepancies with the dating of this deposit. Layer C was formed from alluvial deposits and it is possible the river could have scoured ash from this block and ash flow and re-deposited glasses at Lusakert 1. As such, these glasses could be a result of secondary deposition in the site at ~36-31 ka (formation of Layer C). However, the same glass composition was not found below in Layer D and suggests the same ash was not continually reworked in the landscape. Consequently, it is possible the river course may have been different during the formation of both layers (D and C), or the glasses in Layer C (that had a shard concentration profile with two peaks) derived from two, younger eruptive event from Gutansar volcano.

9.3.4. Uncorrelated tephras in the Archaeological Sites

The following discussion of potential source volcanoes for the remaining tephras has been split based on their TAS classification to simplify comparisons to proximal data (see Table 9.2 for summary of findings).

9.3.4.1. Peralkaline tephras (trachyte, phonolite and alkaline rhyolites)

The sources of peralkaline tephras include volcanoes in the CVZ, Vulcano in the Aeolian Islands, and volcanoes in the WAVP and EAVP (see Table 6.1, Chapter 6). The remaining trachyte and phonolite tephras from Lusakert rock shelter are compositionally distinct from tephras derived from the Italian provinces, Gölcük phase III and EAVP eruptions (Figure 9.10). Italian and WAVP deposits are generally lower in FeOt, with the exception of deposits from Vulcano (Figure. 9b) and have higher CaO concentrations (~1.2 wt. %) than the Lusakert rock shelter tephras (Figure. 9a). Tephras from Vulcano have CaO concentrations >4 wt. % and are easily differentiated from the Lusakert rock shelter glasses.

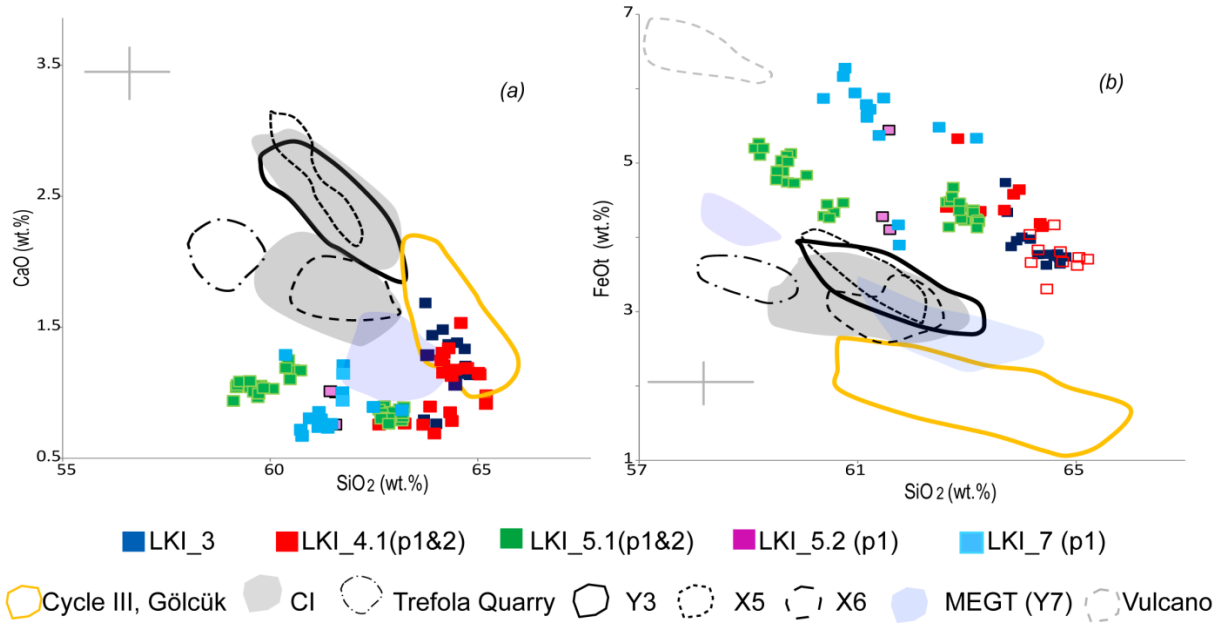

Figure 9.10. (a and b) Glass compositions (shown as envelopes) of large Quaternary eruptions in the central and eastern Mediterranean. The Italian field includes data from the CI, pre-CI (units in Trefola Quarry), X6, X5 and Y3 eruptions from Campania (Albert et al., 2014; Tomlinson et al., 2012a; Wulf et al., 2012), and the MEGT from Ischia (Tomlinson et al., 2014b). Peralkaline deposits from Vulcano in the Aeolian Islands (Albert et al., 2012a, b) and Cycle III eruptive deposits from Gölcük in western Turkey (Tomlinson et al., 2014a) are also shown. Compositional data from specific eruptions have been used where possible, but some chemical envelopes represent data from other smaller eruptions from the volcano (e.g. Vulcano data is ~2.1 ka BP Palizzi A eruption from Albert et al., 2012a, b). The Lusakert rock shelter tephras are clearly distinct from the known proximal glass compositions.

The Nemrut volcano is known to repeatedly produce trachyte and alkaline rhyolite tephras (Sumita and Schmincke 2013 a, b). Its proximity to the Lusakert rock shelter (~300 km S/W of the site) and known, frequent explosive activity suggest it is a likely source for the eight remaining peralkaline tephras in the Lusakert rock shelter, and could also be a source for the alkaline rhyolite in Layer 4c of Ortvale Klde (OK_4c, p2; see Table 9.1). The identification of these eight Nemrut tephras in the Lusakert rock shelter and Ortvale Klde indicates the explosive history is starting to be resolved distally. How this compares to the proximal record is unknown and there is limited EPMA glass data published for eruptions that are

older and younger than the ~30 ka NF. Sumita and Schmincke (2013a) suggest that the proximal record is likely to be incomplete due to erosion (especially for older outcrops) and because of the scouring of landscape during in glacial periods by winds. Additionally, deposits from smaller eruptions may be removed due to subsequent larger eruptive events in the proximal setting, and there are a number of thin units that are undated and not compositionally characterised (Sumita and Schmincke 2013 a, b). Thus, the number of proximal tephra layers documented in the literature are not fully representative of the eruption frequency from this active volcano and it is possible that distal archives are able to shed more light on the eruption history. However, other sources for some of these units should be considered. For example, there is no glass geochemical data from the peralkaline Tendürek volcano (also part of the EAVP), which is also thought to have been active in the Quaternary (Yilmaz et al., 1998)

9.3.4.2. Calc-alkaline rhyolites

The remaining calc-alkaline rhyolite glasses typically have Al_2O_3 compositions <14 wt. %, with FeOt compositions <1.2 wt. %. This distinguishes them from the Hellenic arc, Salina (Aeolian Islands) and the Pantelleria units (Figure 9.11), and also indicates that they are not associated with the Younger Turia eruption from Romania, Gutansar, or the Upper and Lower Nisyros pumices (see Figure 9.11). The remaining potential source volcanoes to be considered (and those that have comparable glass EPMA data) are the volcanoes located in the CAVP and the Ciomadul volcano in Romania (Older Turia).

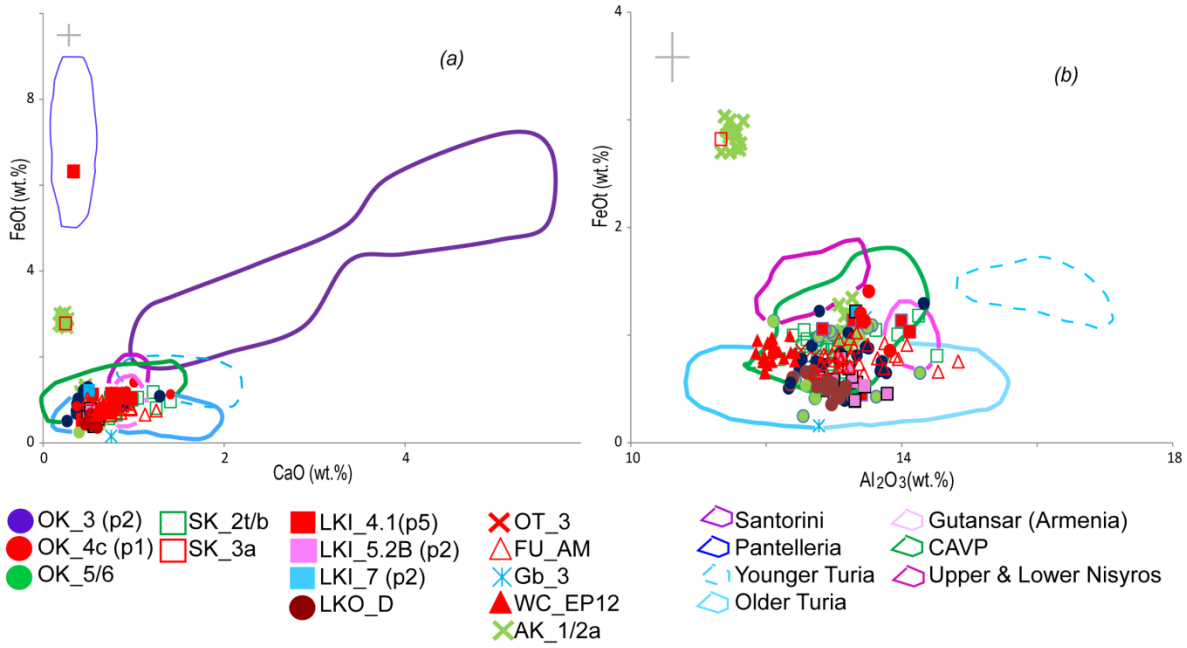

Figure 9.11. Glass compositional data of calc-alkaline proximal deposits (shown as envelopes) from Santorini (data from the Cape Riva and Minoan eruption; Asku et al., 2008; Margari et al., 2007; Tomlinson et al., 2014a; Wulf et al., 2002) and Nisyros (Upper and Lower Pumice eruptions; Tomlinson et al., 2012a). The CAVP compositional data are from Hamann et al. (2010), Tryon et al. (2009), Tomlinson et al. (2014a) with the Younger and Older Turia from Romania curtesy of Veres and Wulf pers comms (2014). Data from Pantelleria, Italy are from Tamburrino et al. (2012). Glasses from the Hellenic Arc and the Younger Turia are clearly distinct from the calc-alkaline rhyolite deposits found in the archaeological sites. One data point from LKI_4.1 (p5) is a pantellerite.

Glasses from WC_EP12 (Layer 12, Myshtulagty Lagat, northern Caucasus) have FeOt compositions between ~0.65 and 0.99 wt. %, CaO concentrations ~0.51-0.83 wt. % and SiO_2 composition ~78 wt. %. These compositions distinguish them from the Hansen Dagi, Older Turia tephra and glasses from Erciyes Dagi (Figure 9.12a). Al_2O_3 concentrations < 12.4 wt. % with K_2O compositions between 3.5 and 4.5 wt. % also show they are not from the Acigöl rhyolite complex or Göllü Dagi (Figure 9.12b). These data suggest this tephra did not derive from the CAVP or the East Carpathians, and are clearly distinct from the Armenia data (Figure 9.11). Given the location of Myshtulagty Lagat, a northern Caucasus source is probable;

e.g. Elbrus volcano ~200 km west of the site, that has known activity between 100-70 ka. This age range is consistent with the age of the WC_EP12 (~128 to 70 ka; Hidjrati et al., 2003; see section 4.3.10), but comparable glass EPMA data are lacking from Elbrus and ages are imprecise.

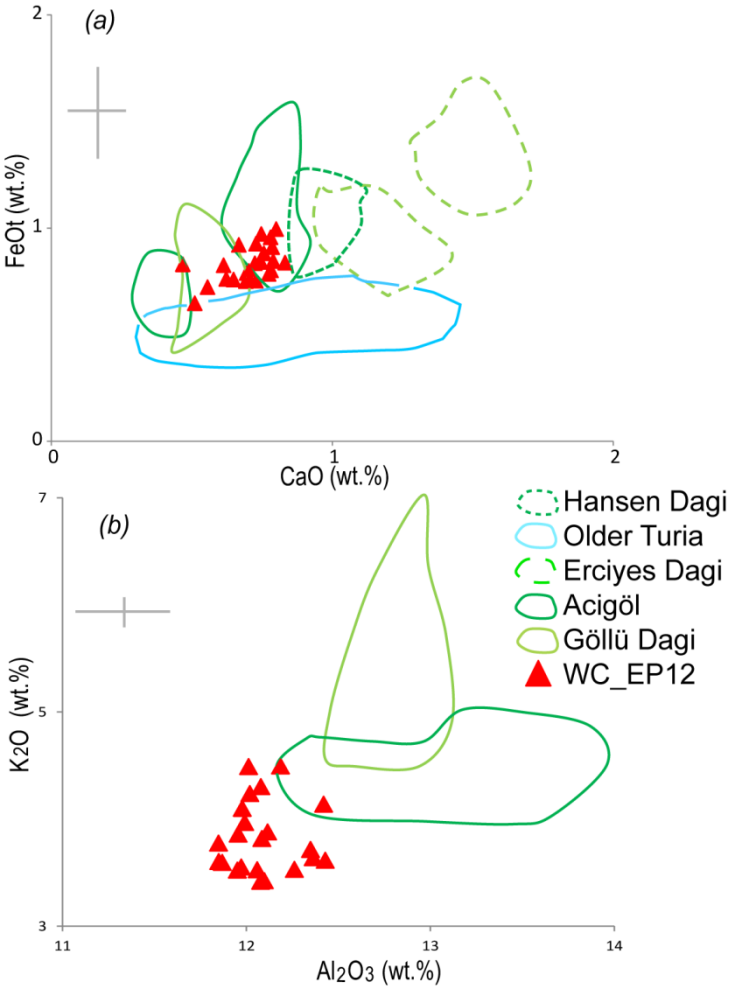

Figure 9.12. Major element glass data (a, b) from WC_EP12. WC_EP12 glasses are more evolved than the older Acigöl glass compositions (~78 wt. %) with CaO concentrations that are too high for the younger Acigöl eruptions (0.51-0.83 wt. %). The cryptotephra layer is compositionally distinct from the CAVP glasses and the Older Turia tephra from the East Carpathians (data Hamann et al., 2010; Tryon et al., 2009; Tomlinson et al., 2014a; Veres and Wulf pers comms, 2014).

AK_2a and AK_1 tephras both have an identical and unique compositional signature. They are the same tephra/s that was deposited in Unit I in Azokh Cave 1 (Azerbaijan; see section 8.8), and are now referred to as AK_1/2a. AK_1/2a is compositionally bimodal, and could represent one eruption or two closely spaced eruptions from similar or the same sources. SK_3a (Layer 3a, Sakajia cave,

Georgia) and one mode of the bimodal AK_1/2a tephra have identical major element glass compositions, and are clearly distinct from all other tephras found in the Caucasus (see Figure 9.11). The second mode has FeOt concentrations >0.8 wt.% and CaO concentrations of ~0.5 wt. % (Figure 9.13), which is similar to Göllü Dagi, but AK_1/2a is generally higher in Al_2O_3 concentration (>13 wt. %). This composition is different from the other CAVP and Older Turia glasses. Both modes are also easily distinguished from the Gutansar glass data (Figure 9.11) and thus the source volcano for AK_1/2a and SK_3a tephras is unknown.

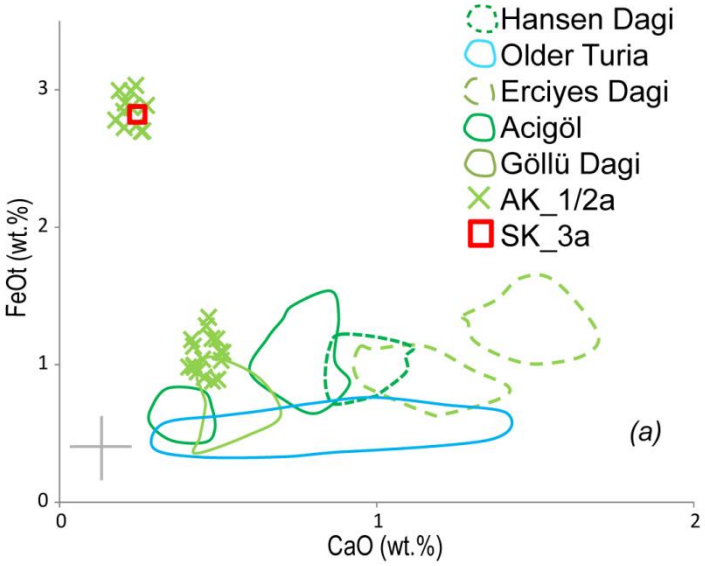

Figure 9.13. Glass compositional data from SK_3a and the AK_1/2a tephras compared to the CAVP and Older Turia (data from Hamann et al., 2010; Tryon et al., 2009; Tomlinson et al., 2014a; Veres and Wulf pers comms, 2014).

Glasses from Layer 2 in Sakajia Cave (SK_2t/b) have CaO concentrations that decrease as the tephras become more evolved (Figure 9.14). This compositional range sits between the Hansen Dagi and Acigöl glass compositions (Figure 9.14), but clearly distinguishes them from Erciyes Dagi deposits. Hansen Dagi typically has glasses with lower K_2O (<4.1 wt. %) than seen in the SK_2t/b glasses, and is unlikely to be the source volcano. FeOt concentration are typically >0.6 wt. % that shows the cryptotephra are not associated with eruptions from Romania with CaO

concentration > 0.7 wt. % that suggest it is not from the Göllü Dagi volcano. It is possible SK_2t/b derives from an unknown Acigöl eruption.

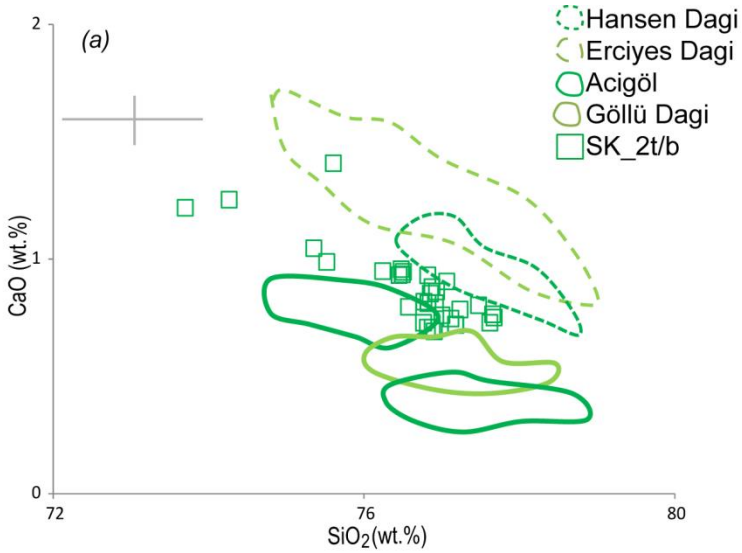

Figure 9.14. Compositional data from SK_2t/b (glass) compared to the CAVP and Older Turia (data from Hamann et al., 2010; Tryon et al., 2009; Tomlinson et al., 2014a; Veres and Wulf pers comms, 2014). There are similarities to the less evolved, Acigöl deposits.

The tephra found at the contact of Layers 5 and 6 in Ortvale Klde (OK_5/6) is bimodal on FeOt concentrations. This tephra is similar to the calc-alkaline rhyolite from Layer 3 and Layer 4c in the same cave (OK_3, p2 and OK_4c, p1), suggesting a similar source volcano with sequential eruptions that are recorded in the Ortvale Klde site (see section 8.3). There are also compositional similarities to calc-alkaline glass populations in Lusakert rock shelter, e.g. LKI_4.1, p5, LKI_5.1 (p3), LKI_5.2B (p2), LKI_7 (p2) and LKO_D from Lusakert 1 (Figure 9.15). Al_2O_3 concentrations are typically < 14 wt. % and show the glasses are not from Gutansar (Figure 9.11). These tephras compositions are spread, but do show similarities to both Acigöl and the Older Turia, and either source could be responsible for these tephra, but there is limited glass data and chronological control for sequential eruptions from either centre to allow for robust correlation. Conversely, it is possible these cryptotephras are from another source/s that produced heterogeneous calc-alkaline rhyolites. At present calc-alkaline glasses

from Lusakert 1 (LKO_D), cannot be used to link the outside of the cave to the Lusakert rock shelter as there are too many repeat compositions.

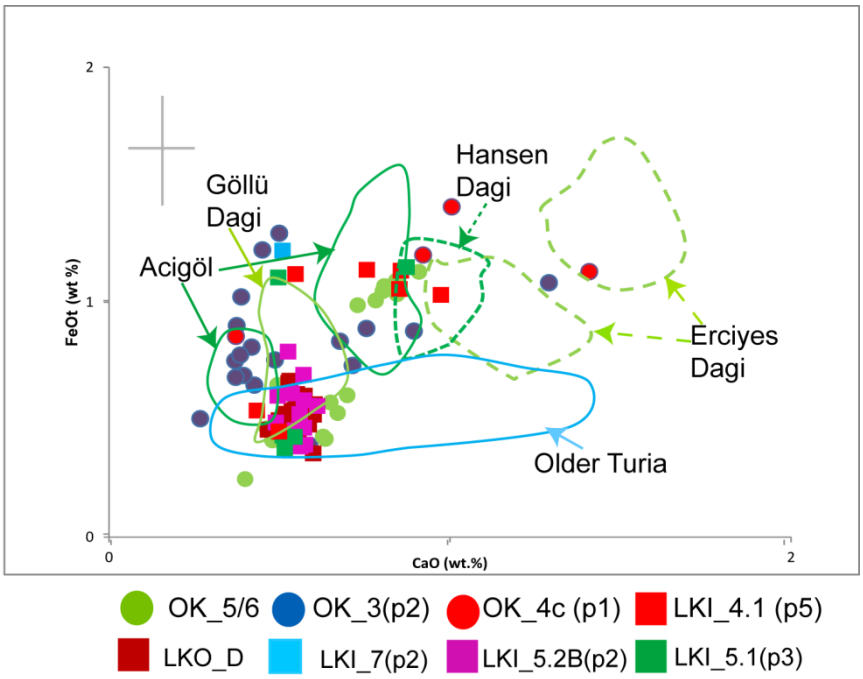

Figure 9.15. Major element glass data from OK_5/6, OK_3 (p2), OK_4c (p1), LKI_4.1 (p5). LKI_5.2B (p2), LKI_7 (p2), LKI_5.1 (p3) and LKO_D. Glass data of all of these cryptotephra are similar to each other and the Acigöl and Romanian deposits (Hamann et al., 2010; Tryon et al., 2009; Tomlinson et al., 2014a; Veres and Wulf pers comms, 2014).

Gub_3 (Gubs rock shelter) and OT_3 (Ortvale Cave) have compositional similarities to the Acigöl rhyolite complex, with CaO concentrations between ~0.7-0.8 wt. % but they are more evolved (~77 wt. % SiO_2) that distinguishes them from this older Acigöl field (see section 6.5.1.1). These compositions are distinct from the CAVP volcanoes and have no known source.

Glasses from the visible, calc-alkaline rhyolite deposit from the upper sequence at Fantan (FU_AM) have FeOt concentrations >0.70 wt. % and typically have Al_2O_3 concentrations ~12 to 13 wt. %. These compositions are different to those from Ciomadul or the Gutansar volcanoes. The tephra shows similarities to the CAVP tephras, specifically the less evolved Acigöl deposits (Figure 9.16) and possibly

Göllü Dagi. However, Göllü Dagi generally has higher K_2O concentrations (>5 wt. %). This tephra was a visible deposit (~1 m thick in some locations) that suggests a nearby source (e.g. the EAVP or the LCVP), but the compositional similarities to the east Acigöl rhyolite field cannot be ruled out. The thickness of the deposit may be indicative of a previously unknown, large explosive eruption with an easterly dispersal axis.

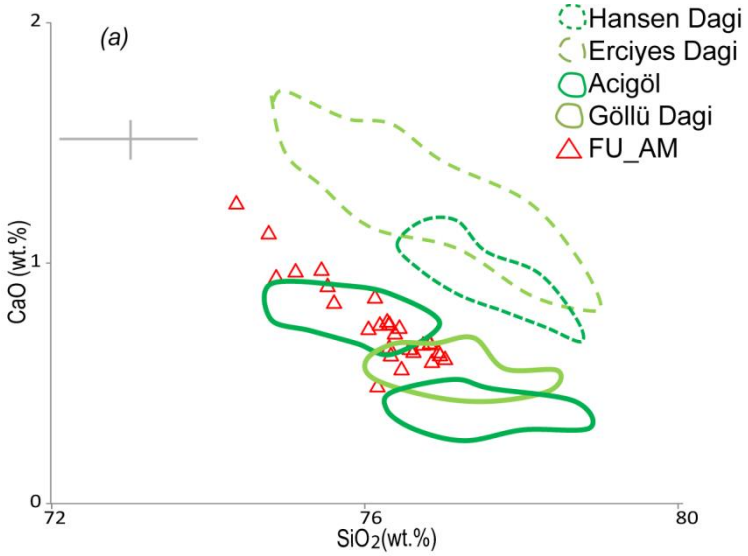

Figure 9.16. FU_AM with glass compositional data from the CAVP (data from Hamann et al., 2010; Tryon et al., 2009; Tomlinson et al., 2014a). FU_AM is chemically similar to deposits from Acigöl (less evolved population.

9.3.4.3. Dacitic tephras

Tephras with glass compositions that are dacitic are population 3 from Layer 4c in Ortvale Klde (OK_4c, p3) and population 6 from Unit 4.1 in Lusakert rock shelter (LKI_4.1, p6). Both these deposits typically have higher TiO_2 concentrations (>1.08 wt. %) than dacitic glasses from the Hellenic arc or the Aeolian Islands (e.g. Salina; Figure 9.17). One data point from LKI_4.1 (p6) is an identical match for OK_4c (p3) across every major element (e.g. Figure 9.17 and see appendix 1). Potential volcanic provinces are the EAVP, LCVP and Dzhavakhe volcanic range in the central southern Caucasus (see Chapter 6, Table 6.1). Dacitic compositions

are also known from Elbrus and the Keli Highlands in the northern Caucasus (see Table 6.1). The extent of explosive volcanism and glass compositions from all these centres is unknown.

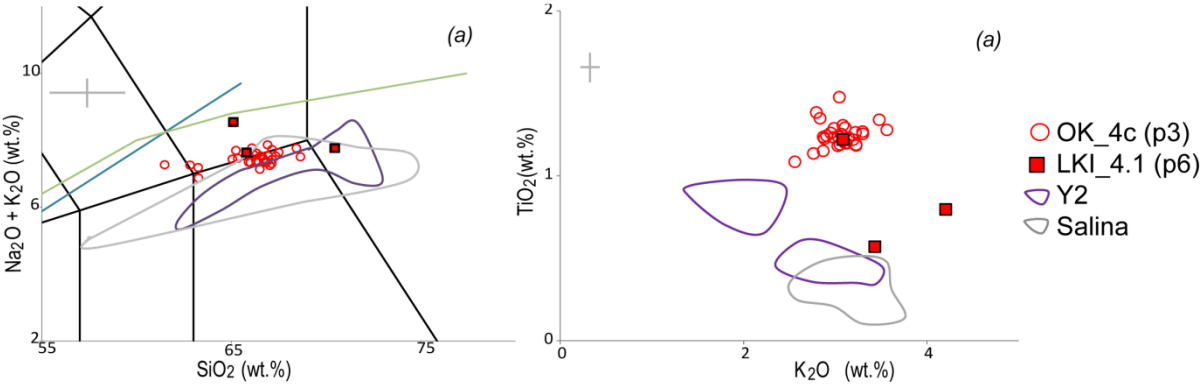

Figure 9.17. TAS (a) and selected bi-plot (b), with cryptotephra glass compositions from LKI_4.1 (p6) and OK_4c (p3). The dacitic glasses are similar to Salina (Aeolian islands; Albert et al., 2012b) and the Y2 tephra from Santorini (Aksu et al., 2008; Margari et al., 2007; Tomlinson et al., 2014a), but typically have higher TiO_2 concentrations (b). The data point from LKI_4.1 (p6) that has lower TiO_2 compositions has higher in total alkali concentrations (a).

9.3.4.4. Trachy-andesite tephras

Tephras from Lusakert rock shelter (LKI_6.5), Aghitue 3 (AG3_8A and AG3_8D), the Fantan lower tephra (FL_AM) and the middle and lower tephras from Kagasi (KGM_AM and KGL_AM) in Armenia are all trachy-andesites. It is unlikely these tephras will be far travelled as eruptions associated with these compositions tend to be less explosive due to lower viscosity of the magmas. These compositions are consistent with volcanic products from Armenia, e.g. Aragats, the Geghama volcanic range, Vardenis volcanic range and the Syunik volcanic range (see section 6.5.3 and 6.7.1) and are likely to derive from an Armenian source.

Unfortunately, there are no glass data for eruptions from these proximal sources to compare to.

Interestingly, trace data from the above tephras all displayed negative anomalies in Ta, Nb and Ti shown in mantle normalised diagrams (see Chapter 8). These depletions are commonly thought to be a result of crustal contamination from subduction processes, but are also found in melts from post-subduction settings (see Tomlinson et al., 2014a). Armenia is no longer an active subduction zone so these negative anomalies are not a result of active subduction occurring in the region. Neill et al. (2013) also identified the same subduction signature in the mantle normalised diagrams of trace data from lavas in northern Armenia. Neill et al. (2013) suggested the 'subduction like characteristics' are derived from a fertile source within the mantle that had a geochemical component inherited from the early subduction processes (see Neill et al., 2013; also see Tomlinson et al. 2014a). Consequently, tephras with a post-subduction trace signature is consistent with an Armenian source which strengthens the link to a local source/s for these tephras.

9.3.5. Ages estimates for tephras found in the archaeological sites

The data indicate that a detailed and complex record of explosive activity is cryptically preserved in the region. The majority of these tephras are only distally defined and documented for the first time and thus age estimate are based on previous radiometric dating of the archaeological units in which they are found (see Table 9.2). The tephras are likely to come from a number of volcanic sources (many of which are unknown). The exception is the ~30 ka NF that has been found in both the Lusakert rock shelter (Unit 4.1) and Ortvale Klde (Layer 3)

archaeological sites and the HP-10/AP-6 tephra in Lusakert rock shelter (~61 ka). Ages for the tephras appear to cluster ~30 to 50 ka, but this could also be an artefact of limited chronology pre-50 ka (radiocarbon limit) in the archaeological sites. A number of tephras are likely to be pre-50 ka in age: Ortvale Klde, Layer 5/6 and 7; deposits in and below LKI_4.1 in Lusakert rock shelter; WC12_EP from Myshtulagty Lagat; and tephra deposits in Fantan and Kagasi. Some tephras are also likely to be younger than 30 ka, e.g. the LKI_3 tephra from Unit 3 in Lusakert rock shelter. These data indicates explosive volcanic activity was prevalent across the region in the timeframe of this study. How the eruption frequency from different volcanoes related to each other is not clear due to a lack of secure correlation to well dated proximal deposits.

Discussion part II- the tephrostratigraphic framework

9.4. Constructing a tephrostratigraphic framework for the Caucasus

Confirmed volcanic sources for tephras found in the M72/5-25-GC1 core include the Hellenic arc (Santorini), the CAVP (Acigöl and Erciyes Dagi) and the CI from the Campi Flegrei (Italy). Deposits from Nemrut (EAVP) and Gutansar volcano (LCVP) have been found in the Caucasus, with some possible unknown CAVP tephras. Although similarities in some of the calc-alkaline rhyolite data exist between the two archives (marine and terrestrial), there are too many repeat compositions and not enough robust chronological or proximal EPMA data to allow robust correlations. Trace data may help to resolve this in the future but it is currently not possible to robustly anchor the archaeological sites to the Black Sea palaeoenvironmental core with a tephra horizon.

Volcanic plumes that deposited glass in the south east Black Sea may not have extended to the archaeological cave sites in the Caucasus (and vice versa) due to a variety of factors: the magnitude of the explosive event was insufficient to disperse tephras across both areas, the wind direction and thus dispersal axis of the plume did not extend to both areas and/or the lack of preservation may just reflect the site's taphonomy (e.g. unknown sedimentary hiatus, low sedimentation rates etc. see Chapter 3). It is also possible that some of the archaeological deposits pre-date the M72/5-25-GC1 core sediments, which only preserve a record up to ~60 ka. Therefore, the M72/5-25-GC1 core cannot be used to help discern a relative stratigraphy for the tephras found in the Caucasus. Archives further east (e.g. the Caspian Sea and possibly Lake Urmia, Iran) are likely to be better candidates for establishing a relative stratigraphy of eruptions recorded in the archaeological sites in the Caucasus.

The M72/5-25-GC1 core is the first marine archive to contain Italian, Hellenic and CAVP tephras and the relative stratigraphy of these tephras extends the Mediterranean tephrochronological framework (Figure 9.18) towards the east (see Figure 9.19). These data can also assist in building inter-regional palaeoclimate correlations over the last ~60 ka.

The CI forms one of the most important geochemical isochrones across the eastern Mediterranean and Eurasia as it is found within numerous palaeoenvironmental and archaeological archives (e.g. Douka et al., 2014; Lowe et al., 2012; Pyle et al., 2006). Climatically, the CI sits in the initial phases of significant cool and dry event that was experienced across Europe, believed to be associated with Heinrich Event 4 cooling event (HE 4) (e.g. Lowe et al., 2012). Unfortunately, the CI eruption is not recorded in the Greenland ice cores, and thus

European palaeoclimate archives (marine, lacustrine and terrestrial) that contain the CI cannot be directly linked to the ice cores to confirm the relative timing of the Heinrich Event. Palaeoenvironmental data on core M72/5-25-GC1 (Nowaczyk et al., 2012) shows the CI sits after the initial stages of a cooling event, recorded by calcium carbonate content (%) with pollen data suggesting cooler and drier conditions around its deposition (~40 ka; Shumilovskikh et al., 2014; see section 2.2.2). Thus the CI's position in the M72/5-25-GC1 core appears to be coincident with that in other terrestrial, marine and lacustrine records in the Mediterranean e.g., the LC-21 marine core (Aegean Sea), and the Lago Grande di Monticchio (Italy) and the Tenaghi Philippon (Greece) terrestrial records (Lowe et al., 2012; Müller et al., 2011; Wutke et al., 2014). This is further indication that the CI was not responsible for the long, widespread cool and dry event that is thought to be HE4 (see Lowe et al., 2012 for more discussion).

The ages of the Korudağ and Guneydağ eruptions (24.9 ± 0.9 ka for Korudağ and 23.8 ± 0.9 ka for Guneydağ; Schmitt et al., 2011) are coincident with a period of cooling and aridity, thought to correspond to Heinrich Event 2 (HE2). These tephra layers could therefore provide important time marker horizons to robustly test the timing of the environmental response (if any) to this climatic downturn in this region. A pronounced cooling and drying episode ~16–31 ka cal BP has been recorded in pollen records (termed pollen zone 6) from cores taken in sediments in Sukhumi, West Georgia (Arslanov et al., 2007; see Table 2.1). IRD and $CaCO_3$ data from the Black Sea core around the BSC_394 and BSC_411 tephra that have been correlated to the Korudağ and Guneydağ eruptions shows small scale fluctuations between cooling and warming episodes but sea surface temperatures are predominantly cool (Nowaczyk et al., 2012; see Figure 7.2). The pollen data

suggest wetter conditions, with an expansion of woodlands, but temperatures remain cool towards the Late Glacial Maximum (LGM) after the eruptions (Shumilovskikh et al., 2014).

Tephra BSC_179 occurs after a short (~2 ka) hiatus in the core, and is located in a period of warming, characterised by decreases in the IRD data (Nowaczyk et al., 2013) and an increase in carbonate precipitation (more productive planktonic activity at the lake surface, Figure 7.2). This tephra represents the start of the final phase of volcanic activity that is recorded in the Black Sea core (Group C). Holocene tephra markers from both the Hellenic arc (3.6 ka cal BP, Minoan) and Erciyes Dagi are preserved within core M72/5-25-GC1 and provide important isochrones to monitor high-frequency climatic changes in the early and mid to late Holocene, anchoring this region to the Mediterranean and the Levant (see Zanchetta et al., 2011; see also Figure 9.19 and 9.20).

The M72/5-25-GC1 core is the first distal record in which many of the other tephra layers are documented (tephras in Group A1-A2 and some in Group C). Some of these layers are compositionally distinct and therefore could be ideal regional marker layers. Furthermore, some are dated and/or located close to climatic transitions and therefore crucial to correlating records and assessing regional response to climatic changes. For example, the least evolved population of BSC_651 has a unique chemical fingerprint that occurs after the ~34 ka Mono Lake excursion and sits towards the end of cooler and wetter condition in this region of the Black Sea (Shumilovskikh et al., 2014). Additionally, BSC_179 has a unique fingerprint (possibly from Acigöl) and dates to ~16-14 ka according the age model in Nowaczyk et al. (2012). The BSC_179 tephra is associated with a warming and increase in moisture in the region (section Figure 7.2). This work

highlights the first occurrence of these tephras in a distal setting, and their relative stratigraphic position, and provides more information on the dispersal and magnitude of these eruptions. Consequently, the identification of the CI (Y5) tephra and the Minoan (Z2) tephras with numerous additional tephras from Anatolia found between them extends the Mediterranean tephra lattice eastwards, but not beyond the Black Sea (see Figure 9.18 for an example of the original lattice by Wulf, 2013 and Figure 9.19 for the extended version).

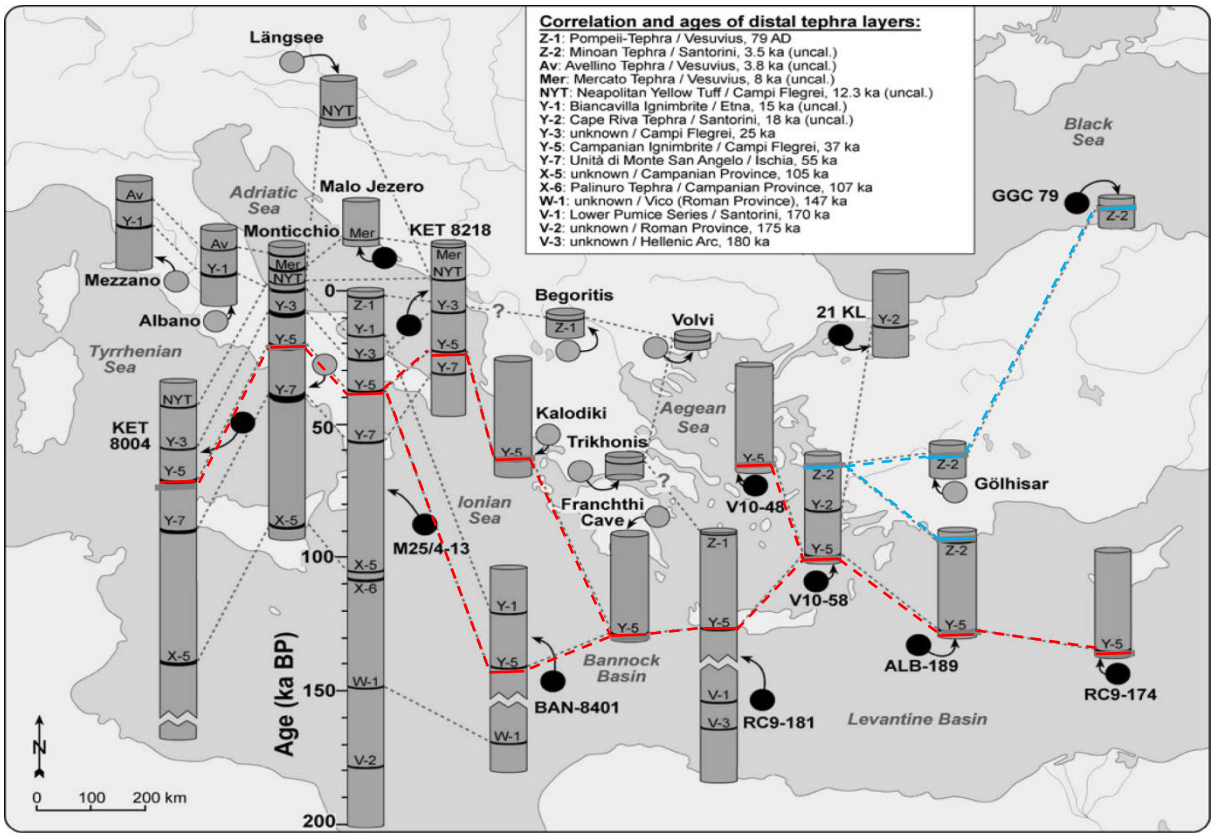

Figure 9.18. The Mediterranean tephrostratigraphic framework for the last ~200 ka. Image shows how marine and terrestrial archives across the Mediterranean can be anchored together via tephra tie lines. Distal deposits of the ~39 ka CI tephra (Y-5) are marked in red, while the ~3.6 ka Minoan eruption (Z-2) is shown in light blue. Both these tephras have now been found in the M72/5-25-GC1 core and can be used to extend this lattice east (see Figure 9.19). Image adapted from Wulf(2013).

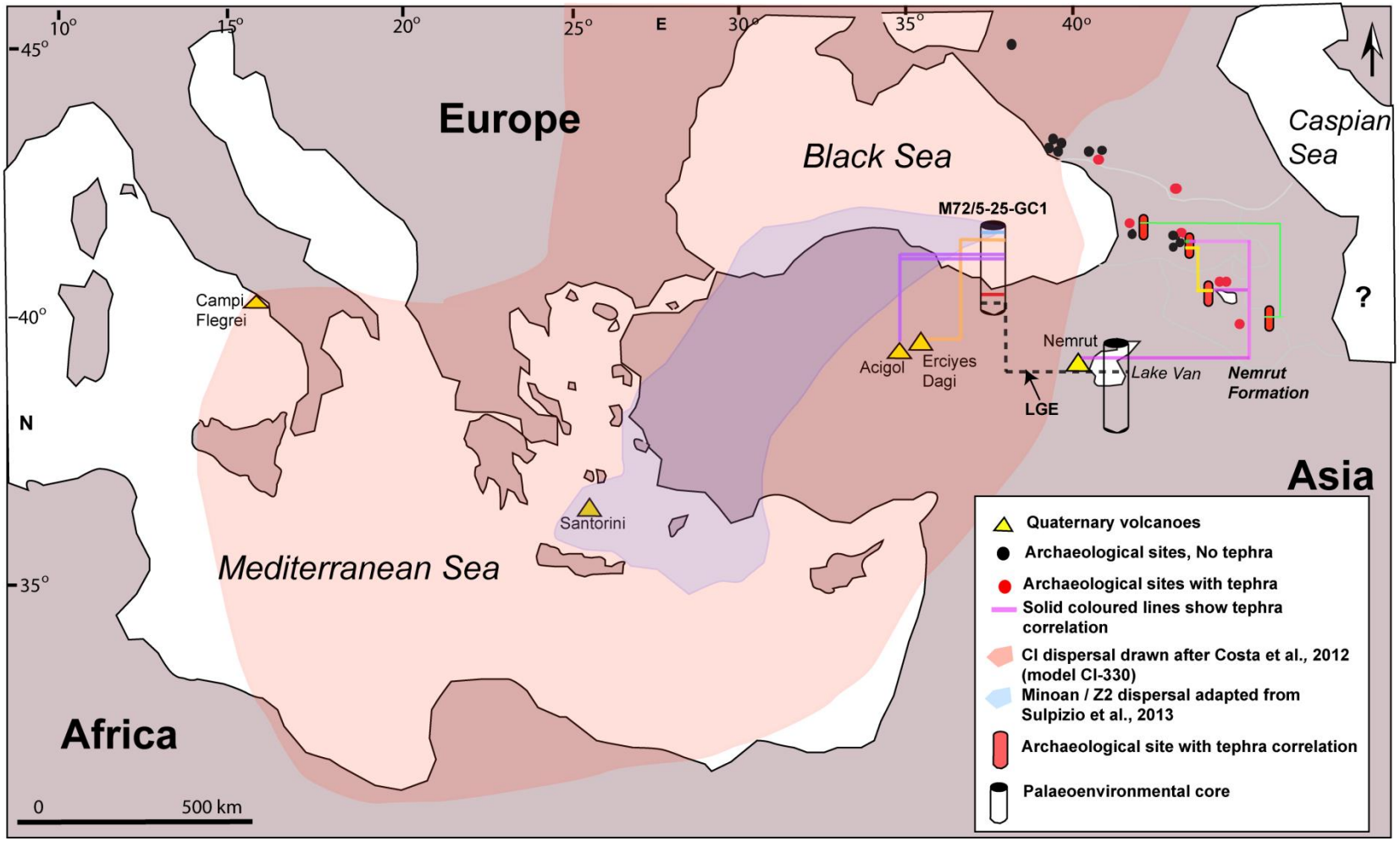

Figure 9.19. Map of the Mediterranean and the Caucasus. The Black Sea core can be anchored to the Mediterranean lattice via the CI and Minoan tephras. New Anatolian tephras can be integrated into the Mediterranean lattice. The Lake Van palaeoenvironmental sequence can be tied to Lusakert rock shelter and Ortvale Klde via the ~30 ka NF (pink solid line). Both the Lake Van and the M72/5-25-GC1 core contain a record for the Laschamp Geomagnetic Excursion (LGE) linking the two archives and consequently the Caucasus data, to the Black Sea record (dotted black line). Tephra correlations in the archaeological data are shown with a green line (Azokh and Sakajia cave) and a yellow line (Ortvale Klde and Lusakert rock shelter).Tephra from the Gutansar volcano, Armenia, to Fantan and Lusakert 1 have also been made.

The reported presence of the Laschamp Geomagnetic Excursion in both the Black Sea and Lake Van palaeoenvironmental records does provide a direct tie to link the newly extended Mediterranean tephra lattice (see Figure 9.19) to the new Caucasus tephrostratigraphy (discussed below). The Laschamp excursion also allows a direct tie to the Greenland ice cores (e.g. Svensson et al., 2006), in which a peak in ^{10}Be indicates the excursion occurred around GI 10. Both palaeoenvironmental cores show warm conditions that are consistent with an interstadial event (see Nowaczyk et al., 2013 and Figure 7.2; Stockhecke et al., 2014a). However at present, there are no robust tephra horizons to connect the two tephrostratigraphic frameworks.

9.4.1. Absence of the CI ash in the Caucasus

The positioning of the CI tephra in archaeological records has shown to be useful in demarcating the relative variations in the end of the Middle Palaeolithic and start of the Upper Palaeolithic techno-complexes (e.g. Lowe et al., 2012; see Figure 1.2). The tephra has been widely used as a marker for this biological transition across Europe and the Mediterranean (e.g. Fedele et al., 2003; Lowe et al., 2012). Presently, the archaeological sites that make up the Kostenki complex (located on the west bank of the Don River, Russia) preserve the most distal, north-easterly deposit of the CI (Pyle et al., 2006), while the Haua Fthea in Libya, Africa, contains the most southerly preserved unit (Douka et al., 2014). The presence of the CI within the Black Sea sediments shows potential for its preservation in archaeological sequences across Anatolia and possibly in the Levant but this study failed to find the CI in the Caucasus.

Costa et al. (2012) modelled dispersal maps for the CI ash plume what show two 'best fit' predictions (see Chapter 6, Figure 6.2). Simulation CI-173R suggests ~0.5 mm of ash could have been deposited across the Caucasus. The second model, CI_330, indicates the plume travelled over the location of the M72/5-25-GC1 Black Sea core (where the CI was found), but does not continue across the Caucasus. The different scenarios are associated with different wind circulation patterns. It is possible the wind direction during the eruption of the CI directed the plume away from the Caucasus, and/or orographic effects of the Lesser Caucasus and East Anatolian Range influenced the dispersal. The situation is complex, and although atmospheric circulation patterns were similar in the past, the displacement, intensity, and seasonal and annual changes between inter-glacial and glacial periods is not well understood. It is also possible that the conditions at the time were not conducive to preservation of such small amounts of tephra at the sites (see taphonomic considerations in caves sites in Chapter 3). Additional factors such as the altitude of the sites (some caves were located in steep, sheltered valleys), and coverage of the cave mouth by foliage at the time of the tephra dispersal could have also hindered tephra from reaching the interior of the caves. Furthermore, low concentrations of shards could have been masked in some sites (e.g. Lusakert rock shelter and potentially Aghitu 3), as they may have been in the tails of other tephra peaks. This study shows that cave mouth direction did not appear to be a limiting factor in the encapsulation of other tephra in the region (see Chapter 8, Figure 8.1). However, given the magnitude of the CI eruption and its known easterly dispersal axis, if the CI plume did traverse the Caucasus it should have been found in the sites analysed.

9.4.2. New regional tephra markers

The absence of the CI in the Caucasus does not allow for the archaeological sites to be directly synchronised to records in the Mediterranean and Africa. However, new tephra correlations between sites in the Caucasus and the Lake Van palaeoenvironmental sequence provide some information on the synchronicity of archaeological occupations on the regional scale.

9.4.2.1. Sakajia Cave Layer 3a and Azokh Cave Unit I

The tephra from Layer 3a in Sakajia cave (Georgia; SK_3a, n=1) is identical to one mode of the Azokh, Unit 1 tephra (Azerbaijan; AZ_1/2an=>40; see Figures 9.11, 9.13 and 9.20). Both tephras are clearly distinctive from all other calc-alkaline rhyolites found in the Caucasus (Figure 9.11) and the source is not known. Based on tool technological assessment from Azokh, which includes an UP end scraper found at the contact of MP Unit II and UP Unit I, and the presence of Neanderthal remains in Layer 3a in Sakajia (Nioradze, 1991), this tephra tie line indicates the co-existence of AMH and Neanderthals in the Caucasus (see Figure 9.20).

The presence of a distinctive tephra directly associated with a layer that contains Neanderthal remains is of significance as it is directly tied to the species, and not just a presumed correlation based on lithic assemblages. Layer 3a (that contains tephra SK_3a) has a boundary start age of ~45- 39 ka cal BP and a boundary end age of ~-39- 34 ka cal BP (95% confidence, data based on a contiguous modelled sequence for Sakajia; Figure 9.23) that suggest the later survival of Neanderthals in this site, but Pinhasi et al. (2012) suggest a possible hiatus between Layer 3b

and 3a in Sakajia cave could be responsible for this younger end age of MP deposits. Currently there are no dates available from Azokh Cave.

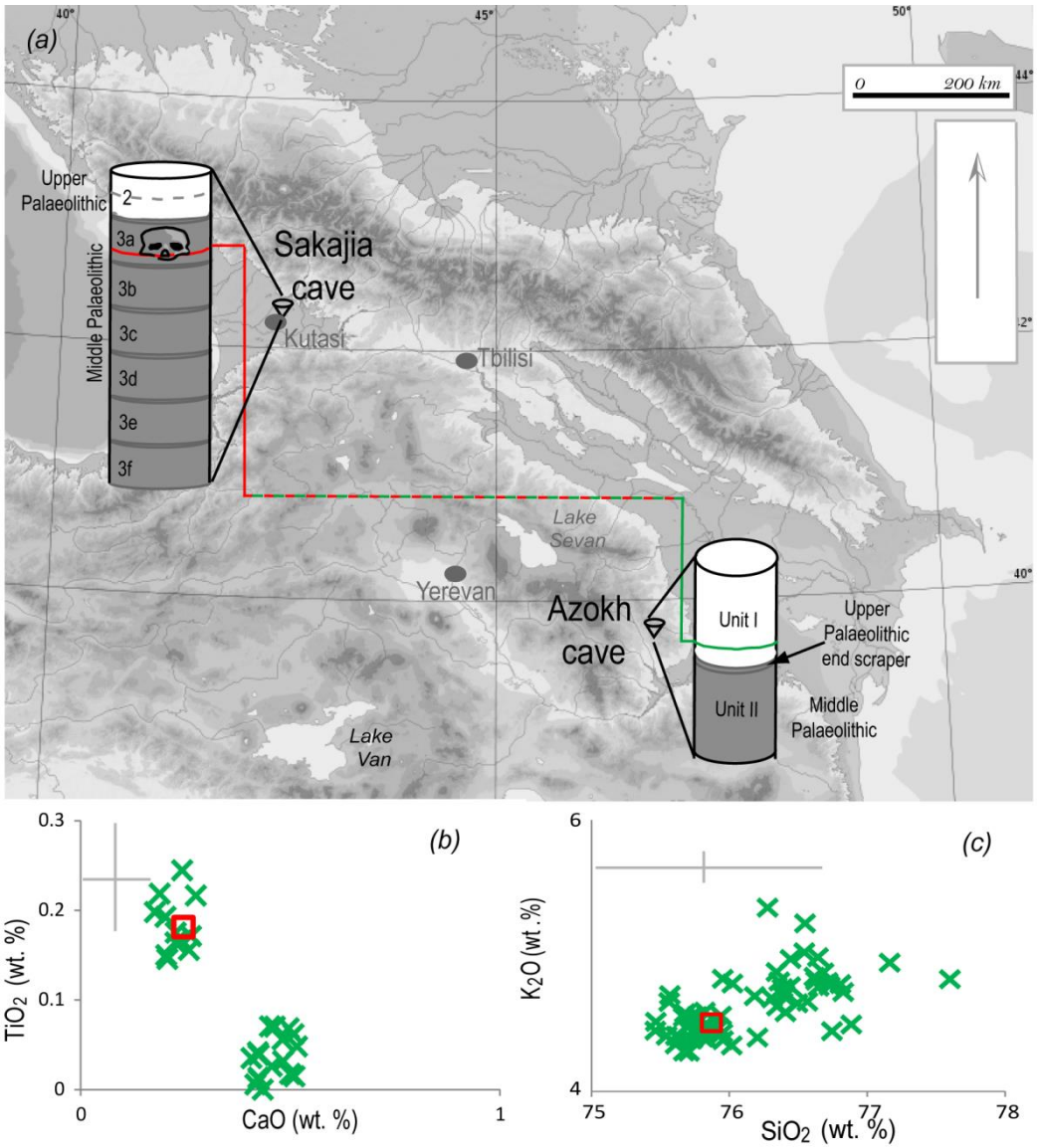

Figure 9.20. Topographical map of the Caucasus with the location of Sakajia cave (Georgia) and Azokh cave in Azerbaijan (a). Glass in Unit I in Azokh is compositional identical to glasses found in Layer 3a in Sakajia cave (b-c), linking the two sites (a). The contact between Unit I and Unit II in Azokh cave contained a UP end scraper associated with AMH, while Layer 3a in Sakajia cave had the partial fragment of a Neanderthal skull suggesting both species were in the region at the same time. Dotted grey line in Layer 2 of Sakajia shows the location of a younger cryptotephra found in the site (see Figure 9.14).

More geochemical data from the tephra in Layer 3a in Sakajia Cave is clearly warranted to strengthen this tephra correlation, as there are potential issues with forming a correlations between archives based on chemical data from one glass shard. For example, the true heterogeneity and / or homogeneity tephra SK_3a is not known and it is possible that additional compositional data from SK_3a would show that this tephra has a different magmatic trend line to that of the AZ_2a/1 tephra. This would indicate the two tephras are from different eruptions from the same source. Trace data could strengthen this correlation (see section 3.1) but the SK_3a shard was too small. At present the unique fingerprint of these tephras that is clearly distinctive from all other calk-alkaline rhyolites found in the Caucasus (see Figure 9.13) suggest there is a good correlation between the Azokh and Sakajia archives. Furthermore, new radiocarbon data also suggests a temporal overlap of AMH with Neanderthals in the region and these data supports this correlation (see section 9.5 below).

9.4.2.2. Ortvale Klde, Lusakert rock shelter and Lake Van.

The dacite tephra of OK_4c is distinctive and is a compositionally indistinguishable from one shard in LKI_4.1 (p6) in Lusakert (Figure 9.21). Furthermore, both layers have a rhyolitic population (OK_4c, p1 and LKI_4.1, p5) that are a compositional match. The presence of two different populations at both sites that are compositionally indistinguishable indicates the tephras are either associated with two coeval eruptions or more likely as both tephras sit on a similar magmatic trend line, one eruption that was compositionally heterogeneous. As both sites contain both compositions this is a robust correlation (see Figure 9.21).

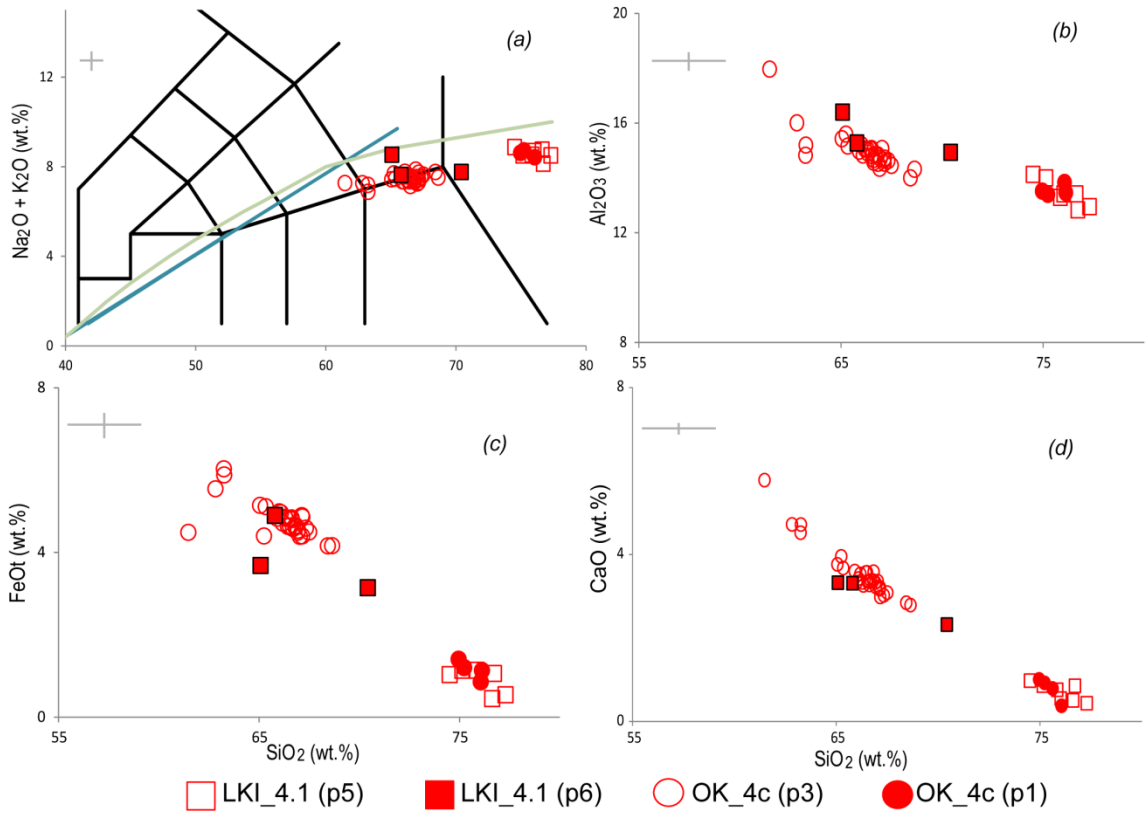

Figure 9.21. a-d Major element glass data from Ortvale Klde (OK_4c p1 and p3) and Lusakert rock shelter(LKI_4.1 p5 and p6). The dacite composition from Ortvale Klde (Layer 4c that is associated with AMH) and one shard from Lusakert rock shelter (Unit 4.1, that has a MP techno-complex) are identical, and rhyolite cryptotephras from the same layers are also compositionally similar (see also Appendix 1).

The dacite tephra in Ortvale Klde occurs just after the earliest evidence for the expansion of AMH into the region (Layer 4d that is stratigraphically below) and contains an Ahmarian type techno-complex that is directly associated with AMH in the Levant (see Chapter 2, section 2.3.2 and Figure 9.22). A more robust radiocarbon age (using an ultra-filtration pre-treatment) for the start of Layer 4c was produced as part of this study and provided an age of 48-43 ka cal BP (modelled age, see Figure 9.24 below). This age is older than the previous age estimates produced by Adler et al. (2008), that ranged from ~41 to 38 ka cal BP for this layer (recalibrated and modelled using OxCal with IntCal13). Consequently, the presence of the distinct dacite (and rhyolite) tephra is an

important marker for the early arrival of modern humans in the region. The same tephra is found in the Lusakert rock shelter and is associated with a MP Levellois and Kombewa flake technology (Adler et al., 2012) that has not been found in any other southern Caucasus MP sites, and authorship of this techno-complex is unknown. This techno-complex is distinct from the Ahmarian-'like' assemblage found in OK_4d and 4c that is associated with AMH. Thus, this tephra tie line shows that there are two distinctive techno-complexes in use in the southern Caucasus at the same time.

The presence of the NF in Ortvale Klde (Layer 3), Lusakert rock shelter (Unit 4.1) and Unit III the Lake Van palaeoenvironmental sequence (e.g. Stockhecke et al., 2014a) allows for all three sites to be correlated (see Figure 9.19 and 22). Palaeoclimate data from Lake Van show the period prior to the NF was relatively warm and humid, with a clear lake level high-stand following the deposition of tephra. A high-stand in the water table is linked to interglacial, warmer climates (see Stockhecke et al., 2014a), but could also be a result of the rapid influx of tephra (Çağatay et al., 2014). Conditions after the NF in Lake Van were cooler and drier (Çağatay et al., 2014). This is presumed to be coincident with the approximate end of MIS 3 and the start of MIS 2 (Unit III to Unit II; Stockhecke et al., 2014a; see Figure 2.5). Sedimentological analysis of Layer 4 in the Lusakert rock shelter suggest a humid environment, and winter ice formation indicates a strong seasonal signal (see summary in Lukich, 2012) consistent with a MIS 3 signal.

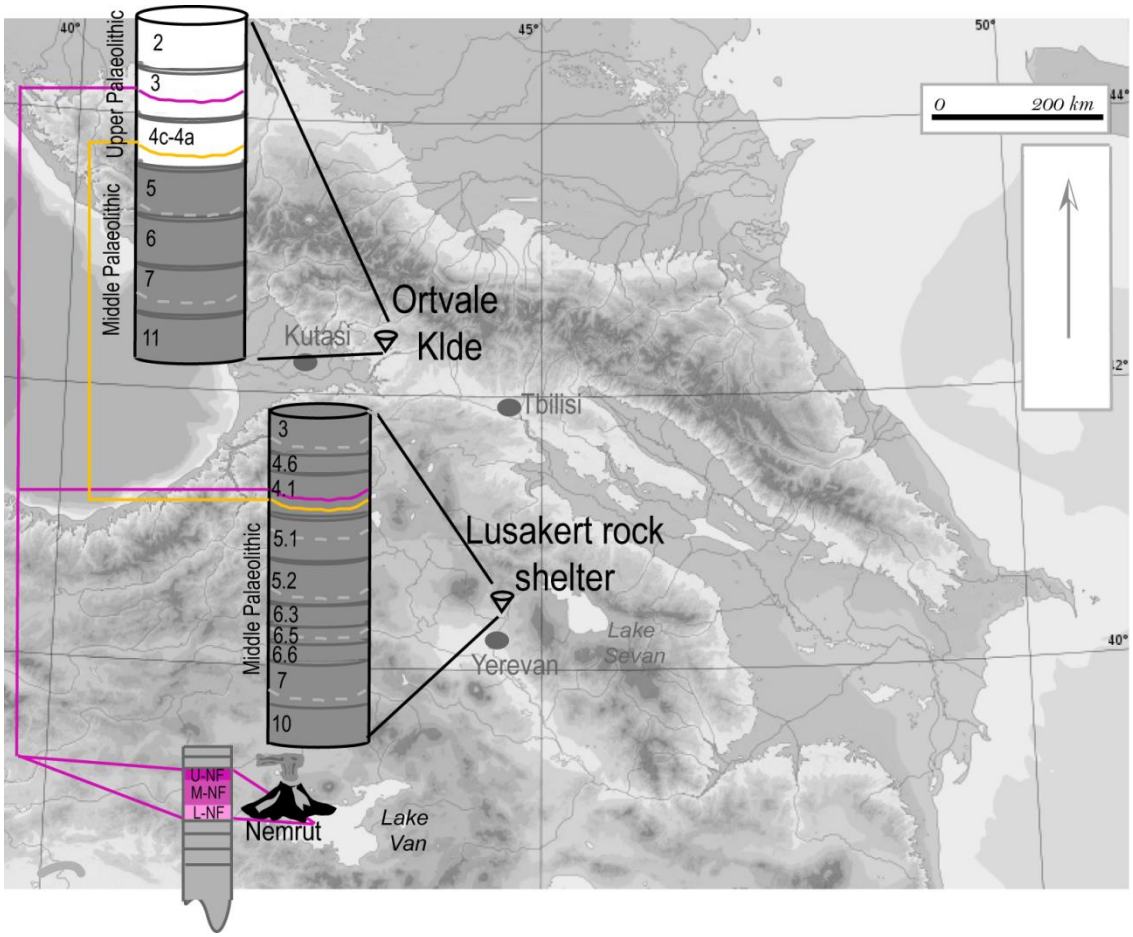

Figure 9.22. A topographical map of the Caucasus with the location of archaeological caves sites Ortvale Klde (Georgia) and the Lusakert rock shelter, Armenia. Both sites contain the same tephras: the ~30 ka NF from Nemrut volcano that links the sites to Lake Van (pink line; see section 9.7), and a compositionally distinct dacite and rhyolite tephra (yellow line). These tephras are found in the EUP Layers in Ortvale Klde (Layer 3 and 4c respectively), but are associated with a MP technology in Layer 4.1 in the Lusakert rock shelter. Grey dotted lines are the locations of other tephras in both sites that are not correlated.

Low resolution pollen data from Layer 5 to Layer 3 in Ortvale Klde indicate warm and wet conditions with a gradual cooling towards Layer 2 (Adler and Tushabramishvili, 2004). Consequently, environmental conditions were similar across the archives and suggest some synchronicity but the low sedimentation rates and proxy data from the archaeological records is not of sufficient resolution to allow the investigation of lead and lags in terrestrial responses. Data from other archives ~30 ka that have not been anchored together also allude to a cooling

across the region; e.g. pollen and faunal records in Georgia (see Table 2.1; Figure 2.4; Aslanov et al., 2007; Shatilova et al., 2011), environmental data in Aghitu 3 (section 4.3.7; Gasparyan et al., 2014a), $CaCO_3$ data from the southeast Black Sea (Figure 7.2; but also wetter; Nowaczyk et al., 2012; Shumilovskikh et al., 2014), and a similar cooling is recorded in the northern Caucasus data with a wet but cooler climate recorded towards the first part of the late Pleniglacial ~30 ka cal BP (see Figure 2.5 and Haesaerts et al., 2010). As this is similar to a cooling recorded in the Greenland ice cores, changes in polar climate likely had an effect on the terrestrial environment across the region, but direct correlation cannot be made. It is likely however that any terrestrial response to any changes in polar climate would have differed (e.g. the duration and intensity of the response) depending on the sub-region, sub-tropical, continental and temperate.

The ~30 ka NF is found in Ortvale Klde EUP, Layer 3 and Lusakert rock shelter, Unit 4.1 (see Figure 9.7 and 9.22). This data suggests the production of the MP Levellois and Kombewa flake technology continued to ~30 ka (and likely after as the same techno-complex is also found above in Layer 3 in the Lusakert rock shelter). Archaeological evidence for the presence of AMH in the Caucasus is no longer restricted to Georgia at this time and extends to Armenia (e.g., Aghitu 3, ~27-35 ka cal BP), and Azerbaijan (Azokh cave, see above), suggesting further migrations or movement in the region by AMH when conditions were becoming cooler (see above).

No skeletal remains have been found in the Lusakert rock shelter sediments, and as it is known that archaic modern humans, AMH and Neanderthals were capable of creating MP tool assemblages (e.g. in the Near East; Grün et al., 2005), it is unclear who made this assemblage (Adler pers comms, 2013). The young age for

this MP type technology, that only changes subtly through the sites stratigraphy, confirm prolonged use of this technology in central Armenia into the latter stages of what is thought to be coincident with the MIS 3 period (e.g., Pinhasi et al., 2008). Cryptotephra analysis of Aghitu 3 (the only stratified UP archaeological site in Armenia; see section 4.3.7) is also warranted as the co-location of the NF would allow for further ties between archaeological sites to be formed, but would also assist in the further development of the tephrostratigraphic framework for the Caucasus.

9.4.2.3. Other potential regional tephra markers

The visible trachy-andesite tephras from Unit 6.5 in Lusakert 1 (LKI_6.5), the lower Fantan tephra (FL_AM) and the middle and lower tephras from Kagasi (KGM_AM and KGL_AM) are all associated with MP techno-complexes (See Chapter 4). These tephras share the same major element glass chemistry and are compositionally similar to the UP visible tephras found in Aghitu 3 (AG3_8A and AG3_8D; see Figure 9.23a and Appendix 1). However, the Aghitu 3 tephras are generally lower in P_2O_5 (<0.45 wt. %) than the other trachy-andesite tephras (0.45-0.99 wt. %; see Chapter 8), and sit on a different compositional trend (based on trace element data) to the MP tephras from Fantan, Kagasi and LKI_6.5 in the Lusakert rock shelter (see Figure 9.23b, c). Similarities in major and trace element data for the MP Fantan, Kagasi (that has two stratigraphically distinct but compositionally alike tephras) and LKI_6.5 tephras likely derive from the same volcanic source and highlight a necessity to supplement the compositional data with other information (e.g. chronology) before any further correlations are made between the MP deposits. Effusive volcanism associated with archaeology during

the MP is known (see Karapetian, 1983, section 6.7.1.1) but these data indicate that there was also explosive activity during the MP of Armenia.

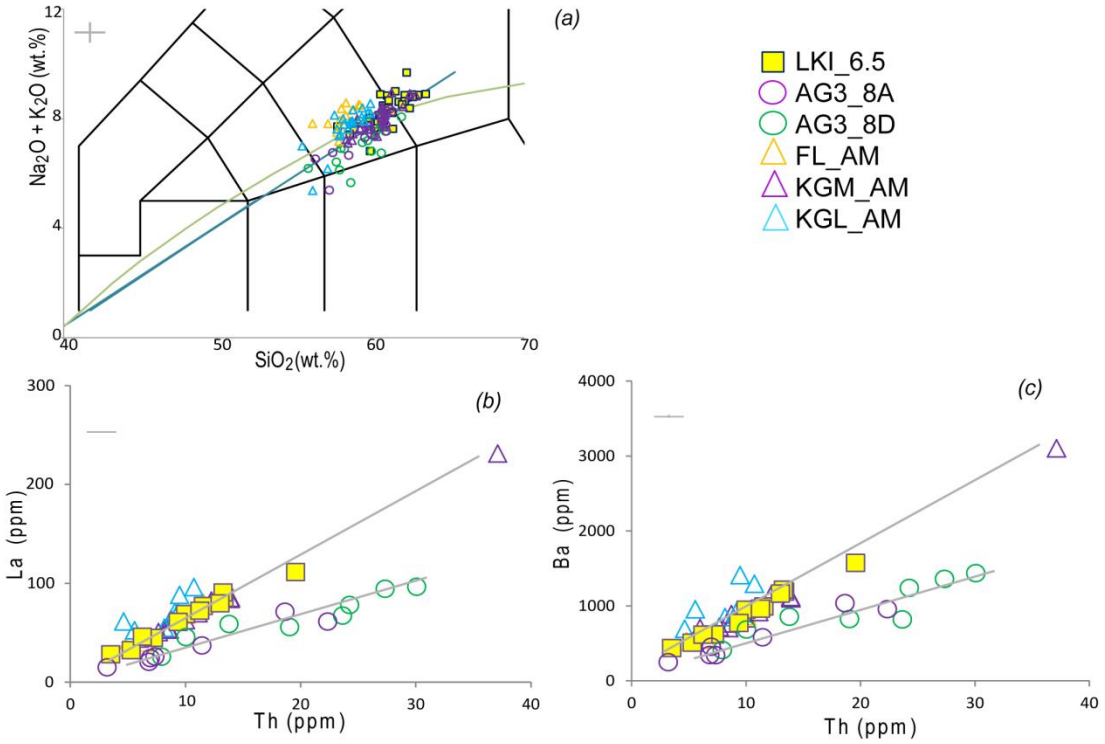

Figure 9.23. Major element (a) and trace element glass data (b, c) from LKI_6.5, AG3_8A, AG3_8D, FL_AM, KGM_AM, KGL_AM. The tephra layers are alike on major element compositions with the exception of P_2O_5. Trace data from AG3_8A and AG3_8D sit along a different fractionation trend, seen clearly on Ba and La versus Th, than the other tephras. Error bars for trace and major element data are ±2σ (determined from standard data, see Appendix 1).

There are similarities in some of the calc-alkaline rhyolites that were found in Gubs rock shelter, Sakajia cave (Layer 2) and Ortvale Cave (Gb_3, SK_2t/b and OT_3). However, the number of repeat rhyolitic compositions could reflect sequential eruptions though time from one volcano and there are not enough robust proximal compositional data or chronological data to allow accurate and precise ties to be formed. Trace data may help to resolve the issue or the co-location of these tephras in stratigraphic order in a long archive would help to elucidate if there are a number of sequential eruptions recorded in the region.

This new framework provided an essential first step in promoting the use of tephra in the Caucasus, and shows the potential for further correlations (in the time frame of this study) that could be made between additional archives that have yet to undergo a cryptotephra investigation (archaeological and palaeoenvironmental). For example, the now known widespread NF may help to discern whether a transgression from the Black Sea to the Caspian Sea occurred at ~30 ka as proposed by Shumilovskikh et al. (2014) and also suggested by Arslanov et al. (2007); deposits are highly likely to be found in the Caspian Sea and possibly in the low-lying Manych-Kerch basin (see Figure 2.8). Future correlations with more robust palaeoenvironmental data and chronological control may also further elucidate terrestrial responses (leads and lags) to changing climates across the region and assist in informing on mechanisms of this change, as seen in other areas (e.g. northern Europe; Lane et al., 2013b).

Discussion part III- archaeological context

9.5. Radiocarbon data and the co-existence of AMH and Neanderthals in the Caucasus

The new IntCal13 calibration curve (Reimer et al., 2013) improves the accuracy of the radiocarbon calibration dataset up to the limit of the technique (~50 ka). All published radiocarbon age estimates for the LMP and EUP in the Caucasus have been recalibrated and modelled using Bayesian statistics with the OxCal (V4.2.3) platform and IntCal13 (see Figure 9.24). New ultra-filtered age determinations on bone from Layers 4c and 4d in Ortvale Klde have also been compared to old ages for these layers. New dates were acquired, not only to produce more robust dates

for the associated tephra in Layer 4c Ortvale Klde (see Table 9.2), but to assess if new and recalibrated radiocarbon data could inform on the occupation of the Caucasus by both Neanderthals and AMH.

Figure 9.24 (next page). Modelled radiocarbon ages for LMP and EUP sites in the Caucasus. A contiguous phase model was produced for each individual site using the OxCal modelling program (V4.2.3; Bronk-Ramsey, 2013; Appendix 1). The exceptions were published data from Ortvale Klde (Adler et al., 2008) that was modelled with a general outlier model as there were both charcoal and bone ages in the same sequence, and the new radiocarbon ages for Ortvale Klde layers 4d-4c that contained a very young date in Layer 4d (likely intrusive or associated with bioturbation, see results Chapter 8). Dates were calibrated using the IntCal13 curve (Reimer et al., 2013). The modelled ages for EUP layers are in orange, and new ages for Ortvale Klde are in red. Ages for LMP deposits are shown in grey. Sakajia Cave, Ortvale Cave, Ortvale Klde (in red) and samples from Layer 2 from Mezmaiskaya cave have radiocarbon samples that have undergone ultrafiltration; all other dates should be assumed to be a minimum ages. Mezmaiskaya cave is located in the northern Caucasus with all other sites located in Georgia. Radiocarbon data from Armenia have not been included as detailed chronological and stratigraphic information is lacking. New ages for the arrival of AMH from Layer 4d and 4c in Ortvale Klde significantly overlap with LMP data from sites Ortvale Cave, Sakajia Cave, Mezmaiskaya Cave and possibly Bondi Cave. Previous radiocarbon ages for Layers 5 and 6 in Ortvale Klde are likely to be > 50 ka (shown in light grey). Uncalibrated radiocarbon ages were taken from Adler et al. (2008), Golovanova et al. (2010b), Pinhasi et al. (2011b; 2012), and Tushabramishvili et al. (2012) and this study

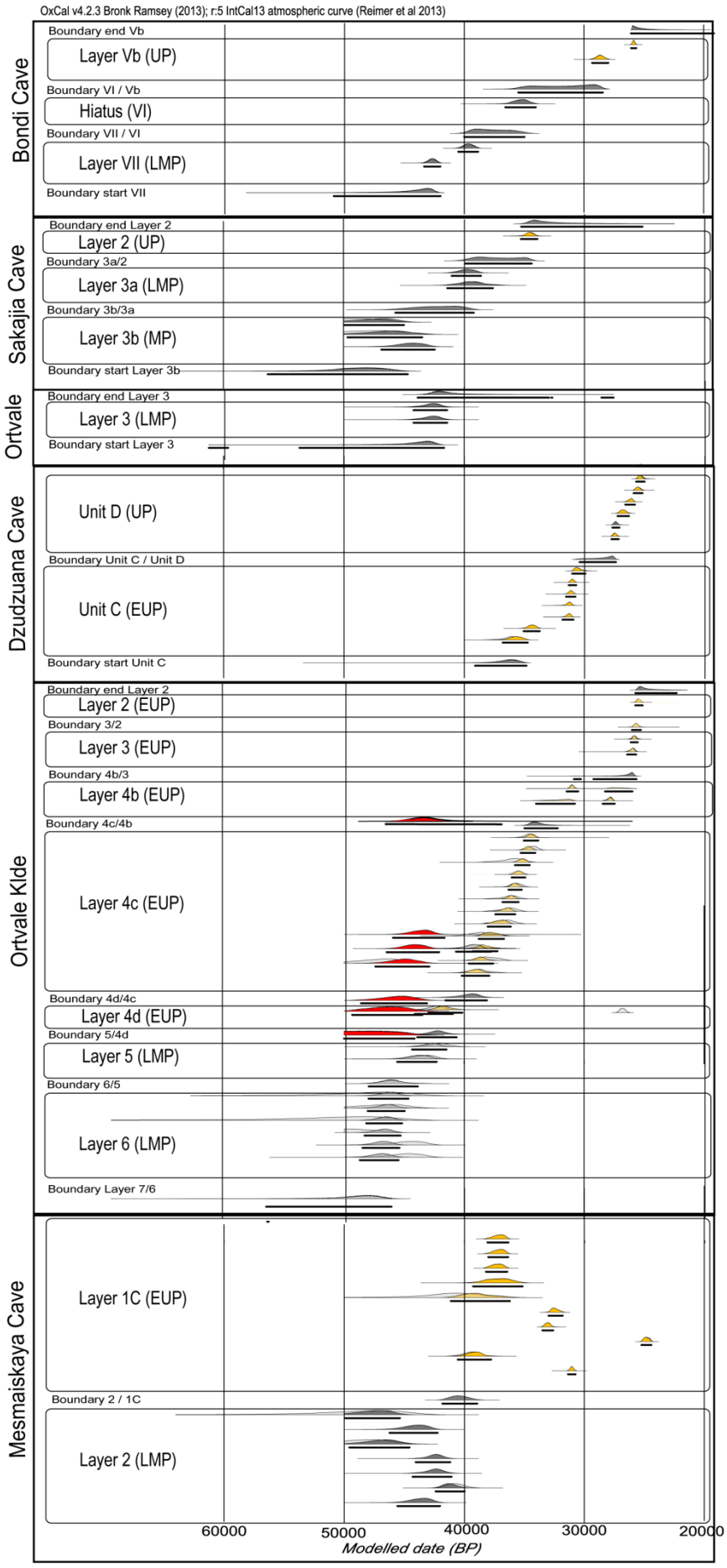
OxCal v4.2.3 Bronk Ramsey (2013); r:5 IntCal13 atmospheric curve (Reimer et al 2013)
Bondi Cave
Boundary end Vb
Layer Vb (UP)
Boundary VI / Vb
Hiatus (VI)
Boundary VII / VI
Layer VII (LMP)
Boundary start VII
Sakajia Cave
Boundary end Layer 2
Layer 2 (UP)
Boundary 3a/2
Layer 3a (LMP)
Boundary 3b/3a
Layer 3b (MP)
Boundary start Layer 3b
Ortvale
Boundary end Layer 3
Layer 3 (LMP)
Boundary start Layer 3
Dzudzuana Cave
Unit D (UP)
Boundary Unit C / Unit D
Unit C (EUP)
Boundary start Unit C
Ortvale Klde
Boundary end Layer 2
Layer 2 (EUP)
Boundary 3/2
Layer 3 (EUP)
Boundary 4b/3
Layer 4b (EUP)
Boundary 4c/4b
Layer 4c (EUP)
Boundary 4d/4c
Layer 4d (EUP)
Boundary 5/4d
Layer 5 (LMP)
Boundary 6/5
Layer 6 (LMP)
Boundary Layer 7/6
Mesmaiskaya Cave
Layer 1C (EUP)
Boundary 2 / 1C
Layer 2 (LMP)
60000
50000
40000
30000
20000
Modelled date (BP)

Figure 9.24 shows the end of the LMP, linked to Neanderthals, in the Caucasus occurs at ~40 ka cal BP. These data are broadly synchronous with European radiocarbon data (see Higham et al., 2014); with the exception of Layer 3a, Sakajia Cave and Bondi Cave that collectively have an age range of ~41–34 ka cal BP for the end of Neanderthal occupation (see Figure 9.25), but unknown sedimentary hiatuses in both sites could account for these young ages. New modelled age estimates for the arrival of AMH in Ortvale Klde (Layer 4d with a distinctive bone and stone techno-complex) suggest an earlier expansion into the region between 50 and 44 ka cal BP (start of Layer 4d; Figure 9.24). Collectively, the new radiocarbon data suggest the period of technological replacement is longer than proposed by Pinhasi et al. (2012) and Adler et al. (2008), between 50 ka and 40 ka cal BP (95% confidence). These new data also suggest some significant temporal overlap of the AMH with Neanderthals as Neanderthal skeletal remains have been found in LMP layers e.g. in Sakajia Cave, Layer 3a, dated between 45-34 ka cal BP and Mesmaiskaya, Layer 2 (Mez 2 infant) which has been directly dated to ~45-42 ka cal BP (Pinhasi et al., 2011b; Pinhasi et al., 2012). The radiocarbon data support the tephra correlations and show that both AMH with Neanderthals occupied the Caucasus at the same time. This refutes claims that Neanderthals were likely extinct or gone from the region prior to the arrival of AMH (e.g. Pinhasi et al., 2012). The migration of AMH to the Caucasus is likely to have occurred first in Georgia (e.g. 50-44 ka cal BP, Ortvale Klde) as previously thought. AMH then appear to have gradually diffused into the Northern Caucasus (e.g. Mesmaiskaya Cave where modern human traversed the greater Caucasus range ~39 ka cal BP) and later then in Azerbaijan/Armenia (~39-35 ka

cal BP, Azokh Cave and ~34-30 ka cal BP, Aghitu 3). But this is based on available data and may change as more information come to light.

The abrupt arrival of a distinctive bone and stone techno-complex found in Ortvale Klde, Dzudzuana and Mesmaiskaya (see section 2.3.2), with similarities to the Levantine Ahmarian suggest that the AMH arrived with the EUP package. As there are no 'transitional' techno-complexes (IUP; see definitions page) in the southern Caucasus there is no clear evidence for acculturation between expanding AMH populations and native Neanderthals (makers of the Lusakert rock shelter techno-complex are not known). Furthermore, EUP techno-complexes (although uncommon) are not mixed or interstratified with any MP techno-complex. This would suggest there was a gap in time before sites previously occupied by Neanderthals were used by AMH (see Chapter 4), suggesting there may not have been temporal overlap between the two at specific sites and a degree of spatial separation between the two existed, as observed in Europe (e.g. Higham et al., 2014). There appears to be occupation of both Neanderthals and AMH throughout periods during which there is considerable environmental change, and as such it is probable that climate change was not a sole driver for the replacement of species.

9.6. Archaeology of the Caucasus put in context

The expansion of AMH at ~50-44 ka cal BP (modelled 95.4 % confidence age, start of Layer 4d) into the Caucasus is earlier than previously thought (~42-41 ka; Adler et al., 2008). The chronology of the expansion is now broadly comparable to dated AMH and early modern techno-complexes from sites in Europe and the Mediterranean; e.g. Kent Cavern in England and from the Grotta de Cavallo, Italy

(~45-41 cal ka BP; Benazzi et al., 2011; Higham et al., 2011); the ~45 ka cal BP Ust'Ishim man from western Siberia (Fu et al., 2014; see Figure 9.26); and the Levantine Ahmarian assemblages in Üçagizli Cave in Turkey (~43-35 cal ka BP; Khun et al., 2009). Earlier dated Ahmarian assemblages have been found at Kebara Cave, Israel dated to ~49- 45 ka cal BP (ABOx-SC on charcoal; Rebollo et al., 2011) and are within the age range for the new Caucasian data presented.

Given the new age for the early arrival of AMH in the Caucasus, with the evidence for co-existence in the region, it is possible the region facilitated not only the meeting of the two species, but could have been a viable, early migration route to the northeast and northwest for AMH from Africa (see Figure 9.25).

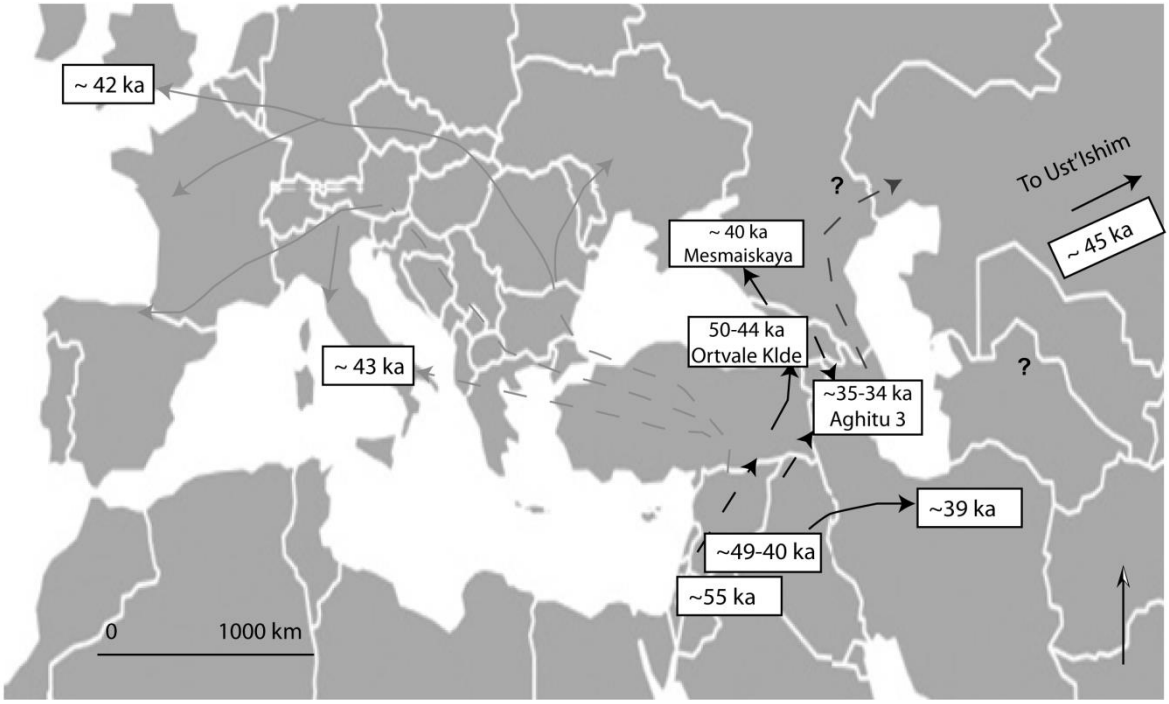

Figure 9.25. Map showing the proposed expansion of AMH through the Caucasus (solid black lines). Ages for the early AMH with a distinctive bone and stone techno-complex (modelled ages; see Figure 9.24) in Ortvale Klde (Georgia) and Mesmaiskaya cave in the northern Caucasus, and from the EUP assemblage in Aghitu 3 in Armenia (Kandel et al., 2011; 2014) are labelled. Grey lines are those from a previous dispersal map of Mellars (2011) with ages for early AMH in Kent Cavern (England) and from the Grotta de Cavallo, Italy (Benazzi et al., 2011; Higham et al., 2011) indicated. The ~55 ka date in the Levant is from the early AMH human skull cap in Manot Cave, Israel (Hershkovitz et al., 2015), with the

~49-40 ka ages ranges from Ahmarian assemblages in the Levant (e.g. Douka et al., 2013; Khun et al., 2009; Rebollo et al., 2011). Dotted black and solid lines are potential dispersal routes west and east. These are based on the technological similarities of the early modern human Baradonstian techno-complex that is found in Iran and the Zargos Mountains to the early Ahmarian (see section 2.3.2). Dispersal routes north to south using the Caspian coast to the east of the Greater Caucasus range is likely, but EUP archaeological data are lacking.

Early dispersal routes for the AMH to Eurasia include an early southern oceanic route (>60 ka; e.g. Dennell and Petraglia, 2012) and northwest dispersal that occurred later (see Mellars, 2011; Figure 1.1). Recently Fu et al. (2014) suggested that the ~45 ka Ust'Ishim man in central Siberia is the ancestor of another group that followed a different route and colonized northern Asia before ~45 ka (after interbreeding with Neanderthals ~60-50 ka; Fu et al., 2014), possibly through the Levant corridor (see Hershkovitz et al., 2015). Collectively, these age data and the scattered locations suggest there were numerous migration routes of early AMH into Europe and Asia from Africa. The Caucasus had not been seriously considered a main, early migration route to northern Eurasia from Africa, as the previous ages were too young, but the new chronological data presented here and the central geographic location indicate that it was a likely early migration route (see Figure 9.26). However, it is possible that AMH did not make it out of the Caucasus (i.e., failed expansion/s) and AMH who made it into northern Asia circumvented the Caucasus via the Caspian Sea.

Chapter 10

Conclusions

10.1. Objective

This project is the first comprehensive, cryptotephra study of archaeological sites in the northern and southern Caucasus, a geographically and archaeologically important region. The main aim of this project was to build a detailed tephrostratigraphy for the Caucasus spanning the Middle to the Middle to Upper Palaeolithic transition (MP-UP, ~125 ka to 30 ka) that could be used to understand AMH and Neanderthal occupations in the region.

10.2. Summary of findings

A total of 21 cryptotephra horizons and one visible tephra layer have been identified in a 952 cm long core that was extracted from the southeast Black Sea (the M72/5-25-GC1 core). The widespread ~39 ka Campanian Ignimbrite tephra from Campi Flegrei, Italy, and the ~3.6 ka cal BP Minoan tephra (marine Z2) from Santorini, Greece, facilitated the extension of the Mediterranean tephrostratigraphic framework further east. Three of the cryptotephra layers have distinct rhyolite compositions and have been correlated to late glacial maximum (LGM) eruptions from Acigöl and early Holocene eruptions from the Erciyes Dagi volcano (both volcanoes are in central Turkey), extending the known dispersal area for all these volcanic ash units. A further 17 tephras were found in the Black Sea core, some of which are compositionally distinct e.g. a cryptotephra found at a depth of 651 cm (BSC_651) that is peralkaline. These latter tephras have been chemically defined for the first time, and with the exception of the BSC_651

tephra, likely derived from the Central Anatolian Volcanic Province (CAVP, Turkey) but data from specific eruptions in this region sre lacking. This is the first marine core to contain Hellenic, Turkish and Italian tephras together and these data provide a new relative stratigraphy for all these tephras. The glass chemistry of the tephra layers has been characterised so all these marker horizons can be correlated to other records across the Mediterranean but the absence of more detailed proximal work hindered further robust comparisons. The palaeoenvironmental proxy data from the Black Sea core shows that the region around the southeast Black Sea also experienced a cooling around the deposition of the CI. This cooling is thought to be a result of the Heinrich Event 4 climatic downturn. Tephras are deposited independent of fluctuations in climate and the range of compositions indicate that there must have been an increase in volcanic activity at volcanoes downwind of the Black Sea followed by periods of quiescence. Data presented in the Black Sea core suggests the volcanic activity that can be grouped between ~48-31 ka, ~24-22 ka and <16-14 ka with further eruptions identified from Acigöl (the latter frequent activity was previously proposed by Kuzucuoglu et al., 1998).

This work adds to a previous NERC funded consortium project (RESET) and has further demonstrated cryptotephras are preserved as isochronous markers in archaeological cave sites (e.g. Lowe et al., 2012). Detailed on-site sampling methodologies and laboratory procedures adapted to cave earth environments were developed in the RESET project by the author and colleagues (see Lane et al., 2014 and Methods Chapter 5), and continued through this project. New developments in this work highlight the ability to identify exotic tephra deposits in sediments that are composed of volcanic material (endogenous sedimentation in

caves formed in lava flows). Lava eroded from the cave walls forms the background cave earth in these sites, but exotic shards that were brought in to the cave could be differentiated with detailed optical analysis, compositional analysis and from the archives, shard concentration profile. This multifaceted approach has extended the use of the technique from karstic cave environments to caves formed in lava. Similarly in sites where stone tools were produced from obsidian (a rhyolitic lava flow), it was hypothesised that anthropogenic activity (knapping/trampling of tools) could produce artificial glass horizons that could mimic tephra layers. The optical analysis of small shards of obsidian glass that were made from crushing obsidian flakes showed the shards had conchoidal fracture marks, rough edges and were devoid of large cuspate features (see Chapter 3.6 and sections 8.7.1 and Figure 8.18). These characteristics were used to differentiate them from explosively erupted glasses. Compositional analysis of obsidians tools in the site was a further control and it was demonstrated that glass shards made by anthropogenic activity could be distinguished from tephra.

Major element data from glasses (tephra) found in archaeological sites showed the Caucasus contains tephras from what appear to be more local volcanic sources e.g. the Lesser Caucasus Volcanic Province (LCVP), the East Anatolian Volcanic Province (EAVP) and some tephras may derive from the CAVP. None of the widespread marker layers from the Mediterranean (e.g. the CI) was found. The lack of tephras commonly found across the Mediterranean in the Caucasus (see Chapter 6) indicate the new regional, tephrostratigraphic framework is independent to the Mediterranean framework. The new Caucasus tephrostratigraphy is in it's infancy of construction (see Figure 10.1), but this study has laid the foundations for its future development by chemically characterising a

total of 30 new cryptotephras and eight visible deposits that were found in eleven of the archaeological sites (Gubs rock shelter and Weasel Cave in the northern Caucasus; Ortvale Klde, Undo Cave, Ortvale Cave and Sakajia Cave in Georgia; Aghitu 3, Lusakert rock shelter/1, Fantan and Kagasi in Armenia and Azokh cave in Azerbaijan). This work has begun to elucidate an explosive eruptive history during the MP to the UP with some sites containing multiple, compositionally distinct tephra layers in stratigraphic order (e.g. Ortvale Klde contains 4 tephra horizons that were deposited between 25-30 ka - >50 ka). Although many of these new tephras cannot be placed on an absolute chronology the suitability for future tephra research work in the region is encouraging.

The most important tephra in this new tephra framework appears to be the ~30 Ka Nemrut Formation (NF) tephra from Nemrut volcano (EAVP). Tephra from this caldera-forming eruption was found to be widespread after deposits were identified in two archaeological sites, Ortvale Klde that is ~400 km away from the volcano and Lusakert rock shelter that is ~ 250 km away. Therefore the NF is an ideal regional tephra marker (see section 3.4.2). This tephra was previously identified in the Lake Van palaeoenvironmental sequence, eastern Turkey (e.g. Stockhecke et al., 2014a; see Figure 9.20) where it is deposited just before a recorded cooling in the archive. Other trachytic tephras from the frequently active Nemrut volcano are also thought to be preserved in the Lusakert rock shelter. These tephras from Nemrut highlight the regional importance of this volcano for future tephra investigations. Another confirmed volcanic source is the Gutansar volcano, Armenia (LCVP). New proximal EPMA data produced in this study showed glasses from this volcano were deposited in Lusakert 1 (Layer C, outside the rock shelter) and Kagasi (uppermost visible tephra). This is the first example of

tephras from a local volcanic source shown to be deposited in the region and has connotations for future hazard assessment in the Caucasus, which are often focussed on effusive activity (e.g. Karakhanian et al., 2003; see section 6.7).

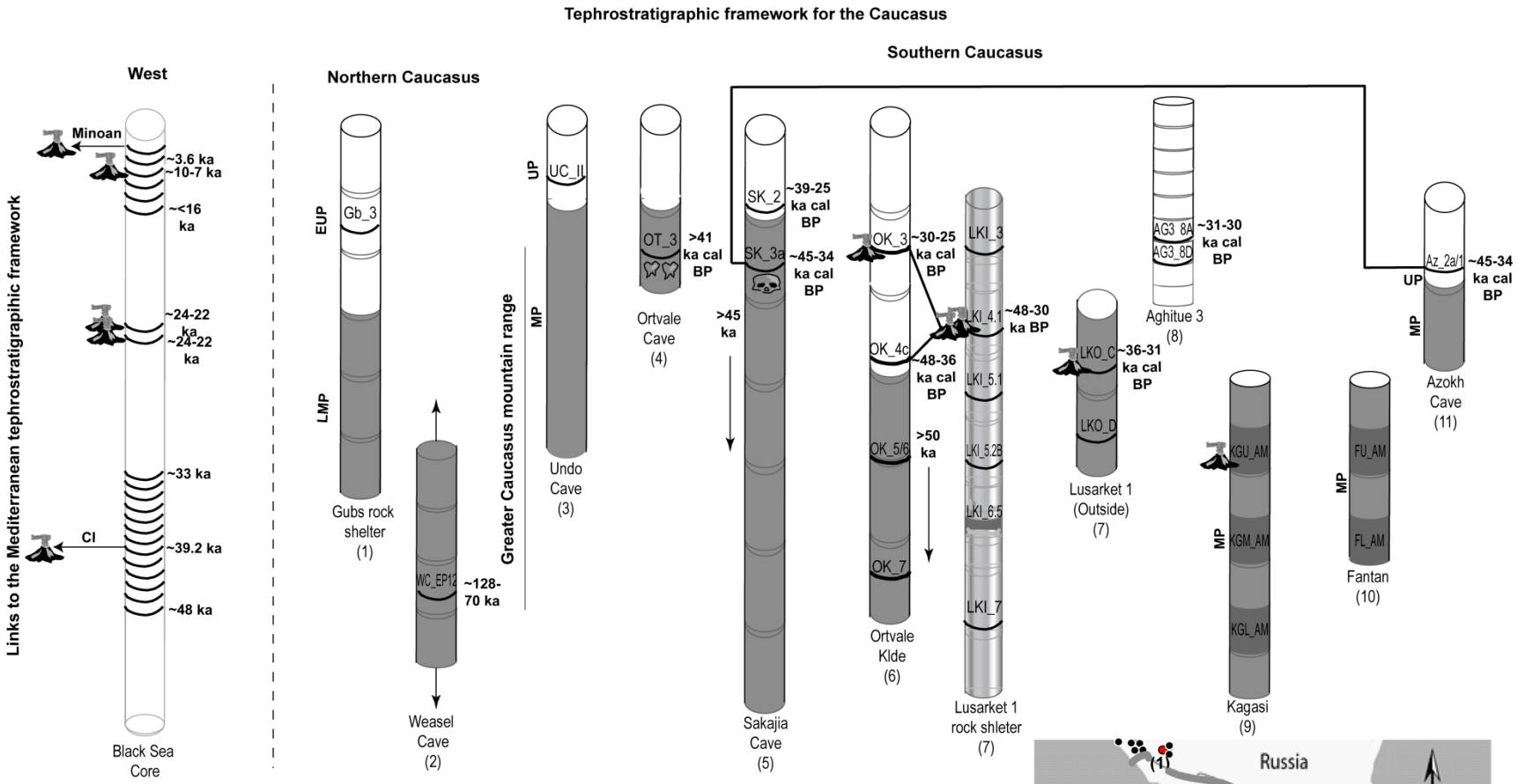

Figure 10.1. The Caucasus tephrostratigraphic framework (right), with the Black Sea core tephra record that shows period of frequent volcanic activity. Black, semicircle line shows the position of tephra layers in each archive; multiple compositions were found in some layers. Black lines between sites show correlations. Volcano symbol indicates the source volcano was identified, for example the tephra OK_3 in Ortvale Klde is the NF, from Nemrut volcano (see text and Chapter 9). Grey colouring denote archaeological layers with a MP techno-complex that is associated with Neanderthals (a skull fragment and two teeth were located in Sakajia Cave, Layer 3a and Ortvale Cave, Layer 3a). White colouring is the EUP techno-complexes that are associated with AMH. Lusakert rock shelter has a MP techno-complex, but authorship is not known and is shown with grey banding. Approximate ages for tephra layers are

A correlation between Azokh Cave in Azerbaijan and Sakajia Cave in Georgia, ~ 600 km away, show that AMH were in the region the same time as Neanderthals. The tephra (AK_1/2a) in Azokh cave is situated just after the contact of sediment beds Unit II and Unit I, where a UP end scraper was found. A single glass shard in Layer 3a in Sakajia cave (SK_3a tephra) is identical in composition and is associated with a Neanderthal skull fragment. A new radiocarbon-based age model that combines new dates with published (but recalibrated) ages for the sites within the Caucasus also show a temporal overlap between AMH and Neanderthals in the region. New ultrafiltered, radiocarbon ages were produced for Layers 4d - 4c in Ortvale Klde. These layers contain the earliest known evidence for AMH in the region and push back the arrival of modern humans in Georgia to ~50- 44 ka cal BP (modelled age for the start of Layer 4d). This age significantly overlaps with existing ultrafiltered ages for Neanderthal occupations in Sakajia Cave, Ortvale Cave and Mesmaiskaya Cave (ages from each site were recalibrated with IntCal13 and modelled using the OxCal 4.2 platform; see Figure 9.25). The arrival of AMH in Georgia is now broadly contemporary to other early AMH sites in Eurasia. Consequently, new chronological constrains on the sites challenges the previous idea that Neanderthals were not in the region when AMH arrived (see Pinhasi et al., 2012).

Correlations between Ortvale Klde (Layer 4c) and Lusakert rock shelter (Layer 4.1) showed AMH who were using a distinctive bone and stone techno-complex in Ortvale Klde were contemporary with hominids that were using a MP-type stone techno-complex in Lusakert rock shelter, Armenia. The makers of this MP stone tool assemblage are not known as diagnostic tools and/or skeletal remains have not been recovered in the Lusakert rock shelter site. The NF is also found within

the MP stone package indicating the prolonged use at this site, up to ~30 ka. The implications of this are that an MP techno-complex was in use at the same time as a more diverse bone and stone technology was being used elsewhere. Both technologies persisted with no signs of interstratification between the tool assemblages indicating technical variability across the region.

This study identified a number of tephras that had similar glass compositions. These data imply a number of volcanoes in and downwind of the region had melts that followed a similar fractionation and mixing pattern prior to each eruption resulting in repeat compositions. Volcanic centres that repeatedly produced tephras with indistinguishable major element chemistry are not uncommon e.g. Katla in Iceland (Lane et al., 2012b) and Campi Flegrei in Naples, Italy (Smith et al., 2011b). In these locations corroborating information such as the tephra stratigraphic position in relation to climatic events and/or robust chronological data are used to assist in forming correlations between sites (e.g. see Lane et al., 2012b). The quality of corroborating information available (e.g. robust stratigraphic palaeoenvironmental information and / or robust dating control) for each archaeological site studied in the Caucasus is different, with many glass shards too small to obtain reliable trace data that could further assist in the discrimination between deposits (see section 3.1 and 3.2). These factors have inhibited the ability to make additional robust correlations between the archives. Although the discovery of a number of repeat compositions limits the use of tephrochronology in the region at present, it has been shown that many of these tephras are stratigraphically spaced in time and as more chronological / palaeoenvironmental and proximal data is obtained the situation will improve.

In summary, this work was able to extend the existing and detailed Mediterranean tephrostratigraphic framework into the southeast Black Sea, but showed that the Caucasus contains none of the widespread Mediterranean tephras and a new tephra framework needs to be developed for the region. A total of 38 tephras were found and chemically characterised in the Caucasus, including 21 discrete tephra layers from the Black Sea core. Tephras mainly derive from volcanoes in central and eastern Turkey and those in the Caucasus, but no correlations between tephras in the Black Sea and the Caucasus could be made. A key marker layer in the new Caucasus tephra framework is the widespread Nemrut Formation (NF) that was found in two archaeological sites and the Lake Van palaeoenvironmental sequence. The new Caucasus tephrostratigraphy with new radiocarbon data has contributed to the understanding of the replacement of Neanderthals by AMH in the Caucasus and demonstrates that both species co-existed. This challenges previous claims that the two species did not occupy the region at the same time. The arrival of AMH in the Caucasus was also earlier and is now temporally similar to other, early ages for AMH migrations in northern Eurasia. The identification of the 30 ka NF in Lusakert rock shelter also showed the prolonged use of an MP - stone tool package in Armenia. This work adds to tephra studies by providing the foundations for future development of a new tephrostratigraphic framework in the Caucasus and for regions further east (e.g. the Caspian Sea).

10.3. Suggestions for future work

The detailed tephra analysis of a long palaeoenvironmental sequence east of the Caucasus (e.g. the Caspian Sea) has the potential to better resolve a relative

order of tephras found in the archaeological sites. Tephras deposited in the Caspian Sea are likely to be from volcanoes in the Caucasus, and also glasses from the frequently active and explosive Nemrut volcano and others in Turkey. Tephra layers from Nemrut could be used to anchor the regional tephra framework to an absolute timescale as the deposits are well dated (e.g. Sumita and Schmincke, 2013a, b). Tephras that are found to be common to the Lake Van and Caspian Sea could inform on leads and lags in terrestrial responses to climate change between the two palaeoclimate records. There are no published palaeoenvironmental records older than ~ 20 ka from the Caspian Sea (e.g., Leroy et al., 2014), but long cores have been extracted for industrial means (e.g. oil prospecting), suggesting there is potential for a long sediment profile from this sea.

Re-dating the early AMH assemblages in Ortvale Klde using ultrafiltration pre-treatments showed that the modern humans were in the region much earlier than previously thought. Other sites that contain evidence for early AMH expansions, e.g. Dzudzuana and Bondi cave (Bar-Yosef et al., 2011, Tushabramishvili et al., 2012) may also benefit from more rigorous radiocarbon pre-treatment methods. This would strengthen the evidence for co-existence in the region, as transitional sites are still uncommon. The re-dating of Lusakert 1 and Lusakert rock shelter with other independent mean is also needed to further substantiate the prolonged use of MP techno-complexes (new OSL data are underway). Additionally, Golovanova et al. (2010a) indicated that there could be at least two tephras preserved in the site of Mesmaiskaya in the northern Caucasus, Layer 2b-1 associated with MP Micoquian industry and 1D a sterile layer situated between the last MP evidence and earliest UP activity at the site. Single shard analyses of

these glasses could lead to further correlations between sites, linking sites in the north to those in the southern Caucasus. This could further inform on movement across and occupation of Neanderthals and AMH on the other side of the Greater Caucasus range.

The work presented has highlighted a significant gap in tephra (glass) compositional data from many eruptions of volcanoes in Turkey and the Caucasus proper. These proximal deposits need to be dated and geochemically characterised to aid correlations of their tephras. This is of course a massive undertaking in both time and cost, and would involve collaboration of many experts. It is a positive to see some new work on the elucidation of the Armenia volcanism is ongoing. This is driven by the need for more robust hazard assessment in the region due to the presence of a nuclear power plant and the complex tectonic setting that has formed the region. This thesis has demonstrated there is significant potential for tephrostratigraphy and tephrochronology in the region, with more explosive eruptions during the MP to the UP that previously identified. As such, further data and future collaboration will allow a more robust tephrostratigraphic framework for the Caucasus archives to be formulated. Such a tephra framework will be able to test archaeological and climatic questions posed for the region.

References

Abbott, P.M., Davies, S.M., Austin, W.E.N., Pearce, N.J.G., and Hibbert, F.D. (2011) Identification of cryptotephra horizons in a North East Atlantic marine record spanning marine isotope stages 4 and 5a (~60,000–82,000 a b2k). *Quaternary International*, 246: 177-189.

Adler, D. (2013) Professor in Anthropology, University of Connecticut. Conversations at the Lusakert 1 rock shelter and the Fantan and Kagasi archaeological sites, Armenia. Field work, 25th -29th June. Personal communication.

Adler, D.S., and Bar-Oz, G. (2009). Seasonal Patterns of Prey Acquisition and Inter-group Competition During the Middle and Upper Palaeolithic of the Southern Caucasus. In: Hublin, J-J., and Richards, M.P. eds. *The evolution of Hominin diets: integrating approaches to the study of Palaeolithic subsistence*. Dordrecht, Springer: 127-140.

Adler, D.S., and Jöris, O. (2008) Dating the Middle to Upper Palaeolithic Boundary across Eurasia. *Eurasian Prehistory*, 5: 5-18.

Adler, D.S., and Tushabramishvili, N. (2004) Middle Palaeolithic patterns of settlement and subsistence in the southern Caucasus. In: Conard, N. ed. *Settlement dynamics of the Middle Paleolithic and Middle Stone Age, Volume II*. Tubingen, Kerns Verlag: 91-132.

Adler, D.S., Belfer-Cohen, A., and Bar-Yosef, O. (2006a) Between a Rock And A Hard Place: Neanderthal-Modern Human Interactions In The Southern Caucasus. In: Conard, N. ed. *Neanderthals and Modern Humans meet. Tübingen Publications in Prehistory*. Tübingen, Kerns Verlag: 165-187.

Adler, D.S., Bar-Oz, G., Belfer-Cohen, A., and Bar-Yosef, O. (2006b) Ahead of the Game: Middle and Upper Palaeolithic Hunting Behaviours in the Southern Caucasus. *Current Anthropology*, 47: 89-117.

Adler, D.S., Bar-Yosef, O., Belfer-Cohen, A., Tushabramishvili, N., Boaretto, E., Mercier, N., Valladas, H., and Rink, W.J. (2008) Dating the demise: Neanderthal extinction and the establishment of modern humans in the southern Caucasus. *Journal of Human Evolution*, 55(5): 817-833.

Adler, D.S., Yeritsyan, B., Wilkinson, K., Pinhasi, R., Bar-Oz, G., Nahapetyan, S., Bailey, R., Schmidt, B.A., Glauberman, P., Wales, N., and Gasparyan, B. (2012) The Hrazdan Gorge Palaeolithic project, 2008-2009. In: Avetisyan, P., and Bobokhyan, A. eds. *Archaeology of Armenia in regional context, proceedings of the international conference dedicated to the 50th anniversary of the institute of archaeology and ethnography held on September 15-17, 2009 in Yerevan.* Yerevan, National Academy of Sciences of the Republic of Armenia, "Gitutyun" Publishing house: 21-37.

Aksu, A.E., Jenner, G., Hiscott, R.N., and Isler, E.B. (2008) Occurrence, stratigraphy and geochemistry of Late Quaternary tephra layers in the Aegean Sea and the Marmara Sea. *Marine Geology*, 252: 174-192.

Albert, P.A. (2014) Post-doctoral researcher, University of Oxford. Conversations and training in the reduction of data for LA-ICP-MS. 25-28th March. Personal communication.

Albert, P.A. (2012b) *Volcanic Glass Geochemistry of Italian Proximal Deposits Linked to Distal Archives in the Central Mediterranean Region*. Unpublished Ph.D thesis, Department of Earth sciences, Royal Holloway, UCL.

Albert, P.G., Tomlinson, E.L., Smith, V.C., Di Roberto, A., Todman, A., Rosi, M., Marani, M., Muller, W., and Menzies, M.A. (2012a) Marine-continental tephra correlations: Volcanic glass geochemistry from the Marsili Basin and the Aeolian Islands, Southern Tyrrhenian Sea, Italy. *Journal of Volcanology and Geothermal Research*, 229-230: 74-94.

Albert, P.G., Hardiman, M., Keller, J., Tomlinson, E.L., Smith, V.C., Bourne, A.J., Wulf, S., Zanchetta, G., Sulpizio, R., Müller, U.C., Pross, J., Ottolini, L., Matthews, I.P., Blockley, S.P.E., and Menzies, M.A. (2014) Revisiting the Y-3 tephrostratigraphic marker: a new diagnostic glass geochemistry, age estimate, and details on its climatostratigraphical context. [Online] *Quaternary Science Reviews*, in press, corrected proof, 30 April 2014. doi:10.1016/j.quascirev.2014.04.002.

Amirkhanov, K.A. (1986) The Upper Palaeolithic of Prikubanye (in Russian). Moscow, Nauka.(Cited in Burbidge et al., 2005).

Anghelinu, M., and Niţă, L. (2014). What's in a name: The Aurignacian in Romania. *Quaternary International*, 351: 171-192.

Arslanov, K.A., Dolukhanov, P.M., and Gei, N.A. (2007) Climate, Black Sea levels and human settlements in Caucasus Littoral 50,000 - 9000BP. *Quaternary International*, 167-168: 121-127.

Arutyunyan, E.V., Lebedev, V.A., Chernyshev, I.V., and Sagatelyan, A.K. (2007) Geochronology of Neogene–Quaternary Volcanism of the Geghama Highland (Lesser Caucasus, Armenia). *Doklady Earth Sciences*, 416: 1041-1046.

Arz, H. (2014). Researcher at the Leibniz-Institute for Baltic Sea Research. Correspondence over the M72/5-25-GC1 Black Sea core and Journal article. Various in 2014. Personal communications.

Badertscher, S., Fleitmann, D., Cheng, H., Edwards, R.L., Gokturk, O.M., Zumbuhl, A., Leuenberger, M., and Tuysuz, O. (2011) Pleistocene water intrusions from the Mediterranean and Caspian seas into the Black Sea. *Nature Geoscience*, 4: 236-239.

Bahr, A., Lamy, F., Arz, H., Kuhlmann, H., and Wefer, G. (2005) Late glacial to Holocene climate and sedimentation history in the NW Black Sea. *Marine Geology*, 214: 309-322.

Barberi, F., Innocenti, F., Lirer, L., Munno, R., Pescatore, T., and Santacroce, R. (1978) The Campanian Ignimbrite: a Major Prehistoric Eruption in the Neapolitan Area (Italy). *Bulletin of Volcanology*, 41: 10-31.

Bar-Oz, G., and Adler, D.S. (2005) Taphonomic History of the Middle and Upper Palaeolithic Faunal Assemblage from Ortvale Klde, Georgian Republic. *Journal of Taphonomy*, 3: 185-212.

Bar-Yosef, O. (1998) On the Nature of Transitions: the Middle to Upper Palaeolithic and the Neolithic Revolution. *Cambridge Archaeological Journal*, 8(02): 141-163.

Bar-Yosef, O. (2002). The Upper Paleolithic revolution. *Annual review of Anthropology*, 31: 363-393.

Bar-Yosef, O., and J-G, Bordes. (2010) Who were the makers of the Châtelperronian culture? *Journal of Human Evolution,* 59: 586-593.

Bar-Yosef, O., Belfer-Cohen, A., and Adler, D.S. (2006) The Implications of the Middle - Upper Paleolithic Chronological Boundary in the Caucasus to Eurasian Prehistory. *Anthropologie*, 44: 49-60.

Bar-Yosef, O., Belfer-Cohen, A., Mesheviliani, T., Jakeli, N., Bar-Oz, G., Boaretto, E., Goldberg, P., Kvavadze, E., and Matskevich, Z. (2011) Dzudzuana: an Upper Palaeolithic cave site in the Caucasus foothills (Georgia). *Antiquity*, 85: 331-349.

Bazgir, B., Otte, M., Tumung, L., Ollé, A., Deo, S.G., Joglekar, P., López-García, J.M., Picin, A., Davoud, D., and van der Made, J. (2014) Test excavations and initial results at the Middle and Upper Paleolithic sites of Gilvaran, Kaldar, Ghamari caves and Gar Arjene Rockshelter, Khorramabad Valley, western Iran. *Comptes Rendus Palevol*, 13: 511-525.

Beliaeva, E.V., and Liubin, V.P. (1998) The Caucasus-Levant-Zargos: Possible relations in the Middle Palaeolithic. In: Otte, M. ed. *Préhistoire d'Anatolie: Genèse de deux mondes, vol. I, Liège, Univ*. de Liège: 39–55. (ERAUL; vol. 85).

Benazzi, S., Douka, K., Fornai, C., Bauer, C.C., Kullmer, O., Svoboda, J., Pap, I., Mallegni, F., P.Bayle, Coquerelle, M., Condemi, S., Ronchitelli, A., Harvati, K., and Weber, G.W. (2011) Early dispersal of modern humans in Europe and implications for Neanderthal behaviour. *Nature*, 479: 525-528.

Bergman, C.A, and Stringer, C.B. (1989) Fifty years after: Egbert, an early Upper Palaeolithic juvenile from Ksar Akil, Lebanon. *Paléorient*, 15: 99-111.

Bigazzi, G., Yeğingil, Z., Ercan, T., Oddone, M., and Özdoğan, M. (1993) Fission track dating obsidians in Central and Northern Anatolia. *Bulletin of Volcanology*, 55: 588-595.

Bird, M.I., Ayliffe, L.K., Fifield, L.K., Turney, C.S.M., Cresswell, R.G., Barrows, T.T., and David, B. (1999) Radiocarbon dating of "old" charcoal using a wet oxidation, stepped-combustion procedure. *Radiocarbon*, 41: 127-140.

Birtwistle, R.J., and Yeritsyan, B.G. (2012) Late Middle Palaeolithic Neanderthal networks and assemblage variability in Armenia: lithic evidence from Lusarket I rockshelter. *Lithics: the Journal of the Lithic Studies Society,* 33: 5–16.

Blaauw, M. (2012) Out of tune: the dangers of aligning proxy archives. *Quaternary Science Reviews*, 36: 38-49.

Blockley, S.P.E., Pyne-O'Donnell, S.D.F., Lowe, J.J., Matthews, I.P., Stone, A., Pollard, A.M., Turney, C.S.M., and Molyneux, E.G. (2005) A new and less destructive laboratory procedure for the physical separation of distal glass tephra shards from sediments. *Quaternary Science Reviews*, 24: 1952-1960.

Blockley, S.P.E., Ramsey, C.B., and Higham, T.F.G. (2008) The Middle to Upper Paleolithic transition: dating, stratigraphy, and isochronous markers. *Journal of Human Evolution*, 55: 764-771.

Blockley, S.P.E., Lane, C.S., Hardiman, M., Rasmussen, S.O., Seierstad, I.K., Steffensen, J.P., Svensson, A., Lotter, A.F., Turney, C.S.M., Bronk Ramsey, C., and INTIMATE members. (2012) Synchronisation of palaeoenvironmental records over the last 60,000 years, and an extended INTIMATE event stratigraphy to 48,000 b2k. *Quaternary Science Reviews*, 36: 2-10.

Blockley, S.P.E., Bourne, A.J., Brauer, A., Davies, S.M., Hardiman, M., Harding, P.R., Lane, C.S., MacLeod, A., Matthews, I.P., Pyne-O'Donnell, S.D.F., Rasmussen, S.O., Wulf, S., and Zanchetta, G. (2014) Tephrochronology and the extended intimate (integration of ice-core, marine and terrestrial records) event stratigraphy 8–128 ka b2k. *Quaternary Science Reviews*, 106: 88-100.

Bourne, A.J., Lowe, J.J., Trincardi, F., Asioli, A., Blockley, S.P.E., Wulf, S., Matthews, I.P., Piva, A., and Vigliotti, L. (2010) Distal tephra record for the last ca 105,000 years from core PRAD 1-2 in the central Adriatic Sea: implications for marine tephrostratigraphy. *Quaternary Science Reviews,* 29: 3079-3094.

Brauer, A., C. Endres., C. Günter., T. Litt., M. Stebich., and Negendank, J.F.W. (1999) High resolution sediment and vegetation responses to Younger Dryas climate change in varved lake sediments from Meerfelder Maar, Germany. *Quaternary Science Reviews,* 18: 321-329.

Bronk Ramsey, C. (2008) Deposition models for chronological records. *Quaternary Science Reviews*, 27: 42-60.

Bronk Ramsey, C. (2009) Bayesian analysis of radiocarbon dates. *Radiocarbon*, 51: 337-360.

Bronk Ramsey, C., and Lee, S. (2013). Recent and Planned Developments of the Program OxCal. *Radiocarbon*, 55: 720-730.

Bronk Ramsey, C., Albert, P.G., Blockley, S.P.E., Hardimann, M., Housley, R.A., Lane, C.S., Lee, S., Matthews, I.P., Smith, V.C., and Lowe, J. (2014) Improved age estimates for key Late Quaternary European tephra horizons in the RESET lattice. [Online] *Quaternary Science Reviews*, in press, corrected proof, 23 December 2014. doi:10.1016/j.quascirev.2014.11.007.

Brown, R.J., Orsi, G., and de Vita, A. (2008) New insights into Late Pleistocene explosive volcanic activity and caldera formation on Ischia (southern Italy). *Bulletin of Volcanology*, 70(5): 583-603.

Burbidge, C.J, Allsworth Jones, P., Housley, R.A., Sanderson, D.C.W., Pyle, D., Bazely, O., McCave, N., and van Andel, T. (2005) *Neanderthal climate preferences and tolerances: the need for a better chronology. Middle Palaeolithic sites in Russia and Ukraine: site summaries and fieldwork 2004*. Glasgow, University of Glasgow, Unpublished Project Report.

Çağatay, M.N., Öğretmen, N., Damci, E., Stockhecke, M., and Sancar, Ü. (2014) Lake level and climate records of the last 90 ka from the Northern Basin of Lake Van, eastern Turkey. *Quaternary Science Reviews*, 104: 97-116.

Capron, E., Landais, A., Chappellaz, J., Schilt, A., Buiron, D., Dahl-Jensen, D., Johnsen, S. J., Jouzel, J., Lemieux-Dudon, B., Loulergue, L., Leuenberger, M., Masson-Delmotte, V., Mayer, H., Oerter, H., and Stenni, B. (2010) Millennial and sub-millennial scale climatic variations recorded in polar ice cores over the last glacial period. *Climate of the Past*, 6: 135-183.

Carter, L., Nelson, C.S., Neil, H.L., and Froggatt, P.C. (1995) Correlation, dispersal, and preservation of the Kawakawa Tephra and other late Quaternary tephra layers in the Southwest Pacific Ocean. *New Zealand Journal of Geology and Geophysics*, 38: 29-46.

Chataigner, C., and Gratuze, B. (2014) New Data on the Exploitation of Obsidian in the Southern Caucasus (Armenia, Georgia) and eastern Turkey, part 1: Source Characterization. *Archaeometry*, 56: 25-47.

Chernyshev, I.V., Lebedev, V.A., Bubnov, S.N., Arakelyants, M.M., and Gol'tsmann, Y.V. (2002) Isotopic Geochronology of Quaternary Volcanic Eruptions in the Greater Caucasus. *Geochemistry International*, 40: 1042-1055.

Costa, A., Folch, A., Macedonio, G., Giaccio, B., Isaia, R., and Smith, V.C. (2012) Quantifying volcanic ash dispersal and impact of the Campanian Ignimbrite super-eruption. *Geophysical Research Letters*, 39: doi:10.1029/2012GL051605.

Crisci, G.M., Delibrias, G., De Rosa, R., Mazzuoli, R., and Sheridan, M.F. (1983) Age and Petrology of the Late-Pleistocene Brown Tuffs on Lipari, Italy. *Bulletin of Volcanology*, 46, 241–391

Crisci, G.M., De Rosa, R., Esperança, S., Mazzuoli, R., and Sonnino, M. (1991) Temporal evolution of a three component system: the island of Lipari (Aeolian Arc, southern Italy). *Bulletin of Volcanology*, 53: 207-221.

Davies, W. (2001) A Very Model of a Modern Human Industry: New Perspectives on the Origins and Spread of the Aurignacian in Europe. *Proceedings of the Prehistoric Society*, 67: 195-217.

Davies, S.M., Abbott, P.M., Pearce, N.J.G., Wastegård, S., and Blockley, S.P.E. (2012) Integrating the INTIMATE records using tephrochronology: rising to the challenge. *Quaternary Science Reviews*, 36: 11-27.

Demaison, G.J., and Moore, G.T. (1980) Anoxic Environments and Oil Source Bed Genesis. *Organic Geochemistry*, 2: 9-31.

Demidenko, Y.E. (2008) The Early and Mid-Upper Palaeolithic of the North Black Sea region: an overview. *Quartär*, 55: 99-114.

Deniel, C., Aydar, E., and Gourgaud, A. (1998) The Hasan Dagi stratovolcano (central Anatolia, Turkey): evolution from calc-alkaline to alkaline magmatism in a collision zone. *Journal of Volcanology and Geothermal Research*, 87: 275-302.

Dennell, R., and Petraglia, M.D. (2012) The dispersal of *Homo sapiens* across southern Asia: how early, how often, how complex? *Quaternary Science Reviews*, 47: 15-22.

d'Errico, F., Henshilwood, C., Lawson, G., Vanhaeren, M., Tillier, A.-M., Soressi, M., Bresson, f., Maureille, B., Nowell, A., Lakarra, J., Backwell, L., and Julien, M. (2003) Archaeological Evidence for the Emergence of Language, Symbolism, and Music–An Alternative Multidisciplinary Perspective. *Journal of World Prehistory*, 17: 1-70.

De Vivo, B., Rolandi, G., Gans, P.B., Calvert, A., Bohrson, W.A., Spera, F.J., and Belkin, H.E. (2001) New constraints on the pyroclastic eruptive history of the Campanian volcanic Plain (Italy). *Mineralogy and Petrology*, 73: 47-65.

Di Paola, G.M. (1974) Volcanology and Petrology of Nisyros Island (Dodecanese, Greece). *Bulletin of Volcanology*, 38: 944-987.

Dibble, H.L., and Rolland, N. (1990) A New Synthesis of Middle Paleolithic Variability. *Antiquity,* 55: 480-499.

Djamali, M., de Beaulieu, J.-L., Shah-hosseini, M., Andrieu-Ponel, V., Ponel, P., Amini, A., Akhani, H., Leroy, S.A.G., Stevens, L., Lahijani, H., and Brewer, S. (2008) A late Pleistocene long pollen record from Lake Urmia, NW Iran. *Quaternary Research*, 69: 413-420.

Doronichev, V.B. 1993. Mustierskie industrii Bol'shogo Kavkaza (The Mousterian Industries of the Great Caucasus). *Peterburgurskiy Arkheologicheskiy Vestnik (St.Petersburg Archaeology News)*, 7: 14-24.

Douka, K., Hedges, R.E.M., and Higham, T.F.G. (2010) Improved AMS ^{14}C Dating of Shell Carbonates Using High-Precision X-Ray Diffraction and a Novel Density Separation Protocol (CarDS). *Radiocarbon*, 52: 735-751.

Douka, K., Bergman, C.A., Hedges, R.E.M., Wesselingh, F.P., and Higham, T.F.G. (2013) Chronology of Ksar Akil (Lebanon) and Implications for Colonization of Europe by Anatomically Modern Humans. [Online] *PLoS ONE*, 8: e72931. doi:72910.71371/journal.pone.0072931.

Douka, K., Jacobs, Z., Lane, C., Grün, R., Farr, L., Hunt, C., Inglis, R.H., Reynolds, T., Albert, P., Aubert, M., Cullen, V., Hill, E., Kinsley, L., Roberts, R.G., Tomlinson, E.L., Wulf, S., and Barker, G. (2014) The chronostratigraphy of the Haua Fteah cave (Cyrenaica, northeast Libya). *Journal of Human Evolution*, 66: 39-63.

Druitt, T.M., Mellors, R.A., Pyle, D.M., and Sparks, S.R.J. (1989) Explosive volcanism on Santorini, Greece. *Geological Magazine*, 126: 95-126.

Druitt, T.H., Brenchley, P.J., Gökten, Y.E., and Francaviglia, V. (1995) Late Quaternary rhyolitic eruptions from the Acigöl complex, central Turkey. *Journal of the Geological Society, London*, 152: 655-677.

Druitt, T.H., Edwards, L., Mellors, R.M., Pyle, D.M., Sparks, R.S.J., Lanphere, M., Davies, M., and Barriero, B. (1999) *Santorini Volcano*. Geological Society of London, Memoir, 19.

Dugmore, A.J., Larsen, G., Newton, A.J. (1992a) Thin Tephra Layers in Peat Revealed by X-Radiography. *Journal of Archaeological Sciences*, 19: 163-170.

Dugmore, A.J., Newton, A.J., Sugden, D.E., and Larsen, G. (1992b) Geochemical stability of fine-grained silicic Holocene tephra in Iceland and Scotland. *Journal of Quaternary Science,* 7: 173-183.

Ewing, J.F. (1947) Preliminary Note on the Excavations at the Palaeolithic Site of Ksâr 'Akil, Republic of Lebanon. *Antiquity*, 21: 186-196.

Faerman, M., Zilberman, U., Smith, P., Karitonov, V., and Batsevitz, V. (1994) A Neanderthal infant from the Barakai Cave, western Caucasus. *Journal of Human Evolution*, 27: 405-415.

Faulks, N.R., Kimball, L.R., N.Hidjrati., and Coffey, T.S. (2011) Atomic force microscopy of microwear traces on Mousterian tools from Myshtylagty Lagat (Weasel Cave), Russia. *Scanning*, 33: 304-315.

Fedele, F.G., Giaccio, B., and Hajdas, I. (2008) Timescales and cultural process at 40,000 BP in the light of the Campanian Ignimbrite eruption, Western Eurasia. *Journal of Human Evolution*, 55: 834-857.

Federman, A.N., and Carey, S.N. (1980) Electron microprobe correlation of tephra layers from Eastern Mediterranean abyssal sediments and the island of Santorini. *Quaternary Research*, 13: 160-171.

Fernández-Jalvo, Y., King, T., Andrews, P., Yepiskoposyan, L., Moloney, N., Murray, J., Domínguez-Alonso, P., Asryan, L., Ditchfield, P., van der Made, J., Torres, T., Sevilla, P., Díaz, M.N., Cáceres, I., Allué, E., Marín Monfort, M.D., and Sanz Martín, T. (2010) The Azokh Cave complex: Middle Pleistocene to Holocene human occupation in the Caucasus. *Journal of Human Evolution*, 58: 103-109.

Ferring, C.R., Swisher, C.C., Bosinski, G., Gabunia, L., Kikodze, Z., Lordkipanidze, D., Tvalchrelidze, M., and Tutberidze, B. (1996) Progress report on the geology of the Plio-Peistocene Dmanisi site and the Diliska Gorge, Republic of Georgia. *Paleanthropology Society, New Orleans*: 5-6.

Finsinger, F.G., C.S.Lane, van Den Brand, G.J., Wagner-Cremer, F., Blockley, S.P.E., and Lotter, A.F. (2011) The lateglacial *Quercus* expansion in the southern European Alps: rapid vegetation response to a late Allerød climate warming? *Journal of Quaternary Science*, 26: 694-702.

Fisher, R.V., Orsi, G., Ort, M., and Heiken, G. (1993) Mobility of a large-volume pyroclastic flow - emplacement of the Campanian ignimbrite, Italy. *Journal of Volcanology and Geothermal Research*, 56: 205-220.

Fletcher, W.J., Sánchez Goñi, M.F.S., Allen, J.R.M, Cheddadi, R., Combourieu-Nebout, N., Huntley, B., Lawson, I., Londeix, L., Magri, D., Margari, V., Müller, U.C., Naughton, F., Novenko, E., Roucoux, K., and Tzedakis, P.C. (2010). Millennial-scale variability during the last glacial in vegetation records from Europe. *Quaternary Science Reviews*, 29: 2839-2864

Fourloubey, C., Beauval, C., Colonge, C., Liagre, D., Ollivier, J., and Chataigner, C. (2003) Le Paléolithique en Arménie : état des connaissances acquises et données récentes. *Paléorient,* 29: 5-18.

Frahm, E. (2013) Research scientist, University of Minnesota. Discussions while on tour of the Geghama volcanic Rage, Armenian. Field work, 25th-29th June. Personal communication.

Frahm, E., Feinberg, J.M., Schmidt-Magee, B.A., Wilkinson, K., Gasparyan, B., Yeritsyan, B., Karapetian, S., Meliksetian, K., Muth, M.J., and Adler, D.S. (2014) Sourcing geochemically identical obsidian: multiscalar magnetic variations in the Gutansar volcanic complex and implications for Palaeolithic research in Armenia. *Journal of Archaeological Science*, 47: 164-178.

Friedrich, W.L., Kromer, B., Friedrich, M., Heinemeier, J., Pfeiffer, T., and Talamo, S. (2006) Santorini Eruption Radiocarbon Dated to 1627-1600 B.C. *Science*, 312: 548.

Froggatt, P.C. (1992) Standardization of the chemical analysis of tephra deposits. Report of the ICCT working group. *Quaternary International*, 13-14: 93-96.

Fu, Q., Li, H., Moorjani, P., Jay, F., Slepchenko, S.M., Bondarev, A.A., Johnson, P.L.F., Aximu-Petri, A., Prufer, K., de Filippo, C., Meyer, M., Zwyns, N., Salazar-Garcia, D.C., Kuzmin, Y.V., Keates, S.G., Kosintsev, P.A., Razhev, D.I., Richards, M.P., Peristov, N.V., Lachmann, M., Douka, K., Higham, T.F.G., Slatkin, M., Hublin, J.-J., Reich, D., Kelso, J., Viola, T.B., and Paabo, S. (2014) Genome sequence of a 45,000-year-old modern human from western Siberia. *Nature*, 514: 445-449.

Fytikas, M., Innocenti, F., Manetti, P., Mazzuoli, R., Peccerillio, A., and Vallari, L. (1984) Tertiary to Quaternary evolution of volcanism in the Aegean region. *Geological Society, London Special Publications*, 17: 687-699.

Gabunia, L.K., and Vekua, A. (1990) L'évolution du paléoenvironment au cours de l'Anthropogène en Géorgie (Transcaucasie). *L'Anthropologie*, 94: 643-650.(Cited in Pinhasi et al., 2012)

Garcea, E.A.A. (2012) Successes and failures of human dispersals from North Africa. *Quaternary International*, 270: 119-128.

Gasparyan, B., Kandel, A.W., and Montoya, C. (2014a) Living the High Life: The Upper Paleolithic Settlement of the Armenian Highlands. In: Gasparyan, B., and Arimura, M. eds. *Stone age Armenia: A Guide-book to the Stone Age Archaeology in the Republic of Armenia.* Japan, Centre for Cultural Resource Studies, Kanazawa University: 107-134.

Gasparyan, B., Egeland, C.P., Adler, D.S., Pinhasi, R., Glaubermann, P. and Haydosyan, H. (2014b) The Middle Paleolithic Occupation of Armenia: Summarizing Old and New Data. In: Gasparyan, B., and Arimura, M. eds. *Stone age Armenia: A Guide-book to the Stone Age Archaeology in the Republic of Armenia.* Japan, Centre for Cultural Resource Studies, Kanazawa University: 65-106.

Gehrels, M.J., Newnham, R.M., Lowe, D.J., Wynne, S., Hazell, Z.J., and Caseldine, C. (2008) Towards rapid assay of cryptotephra in peat cores: Review and evaluation of various methods. *Quaternary International*, 178: 68-84.

Geraga, M., Tsaila-Monopolis, S., Ioakim, C., Papatheodorou, G., and Ferentinos, G. (2005) Short-term climate changes in the southern Aegean Sea over the last 48,000 years. *Palaeogeography Palaeoclimatology, Palaeoecology*, 220: 311-332.

Giaccio, B., Nomade, S., Wulf, S., Isaia, R., Sottili, G., Cavuoto, G., Galli, P., Messina, P., Sposato, A., Sulpizio, R. and Zanchetta, G. (2012) The late MIS 5 Mediterranean tephra markers: a reappraisal from peninsular Italy terrestrial records. *Quaternary Science Reviews*, 56: 31-45.

Gillot, P.Y., Chiesa, S., Pasquaré, G. and Vezzoli, L. (1982) <33000 yr K-Ar dating of the volcano-tectonic horst of the Isle of Ischia, Gulf of Naples. *Nature*, 229: 242-245.

Gioncada, A., Mazzuoli, R., Bisson, M., and Pareschi, M.T. (2003) Petrology of volcanic products younger than 42 ka on the Lipari–Vulcano complex (Aeolian Islands, Italy): an example of volcanism controlled by tectonics. *Journal of Volcanology and Geothermal Research*, 122: 191-220.

Golovanova, L.V., and Doronichev, V.B. (2003) The Middle Paleolithic of the Caucasus. *Journal of World Prehistory*, 17: 71-140.

Golovanova, L.V., Hoffecker, J.F., Kharitonov, V.M., and Romanova, G.P. (1999) Mezmaiskaya cave: a Neanderthal occupation in the northern Caucasus. *Current Anthropology,* 40: 77-86.

Golovanova, L.V., Doronichev, V.B., Cleghorn, N.E., Koulkova, M.A., Sapelko, T.V., and Shackley, M.S. (2010a) Significance of Ecological Factors in the Middle to Upper Paleolithic Transition. *Current Anthropology*, 51: 655-691.

Golovanova, L.V., Doronichev, V.B., and Cleghorn, N.E. (2010b) The emergence of bone-working and ornamental art in the Caucasian Upper Palaeolithic. *Antiquity*, 84(324): 299-320.

Grapes, R., Rieser, U., and Wang, N. (2010) Optical luminescence dating of a loess section containing a critical tephra marker horizon, SW North Island of New Zealand. *Quaternary Geochronology*, 5: 164-169.

Green, R.E., Krause, J., Briggs, A.W., Maricic, T., Stenzel, U., Kircher, M., Patterson, N., Li, H., Zhai, W., Fritz, M.H.-Y., Hansen, N.F., Durand, E.Y., Malaspinas, A.-S., Jensen, J.D., Marques-Bonet, T., Alkan, C., Prüfer, K., Meyer, M., Burbano, H.A., Good, J.M., Schultz, R., Aximu-Petri, A., Butthof, A., Höber, B., Höffner, B., Siegemund, M., Weihmann, A., Nusbaum, C., Lander, E.S., Russ, C., Novod, N., Affourtit, J., Egholm, M., Verna, C., Rudan, P., Brajkovic, D., Kucan, Ž., Gušic, I., Doronichev, V.B., Golovanova, L.V., Lalueza-Fox, C., de la Rasilla, M., Fortea, J., Rosas, A., Schmitz, R.W., Johnson, P.L.F., Eichler, E.E., Falush, D., Birney, E., Mullikin, J.C., Slatkin, M., Nielsen, R., Kelso, J., Lachmann, M., Reich, D., and Pääbo, S. (2010) A Draft Sequence of the Neandertal Genome. *Science*, 328: 710-722.

Griggs, A.J., Davies, S.M., Abbott, P.M., Rasmussen, T.L., and Palmer, A.P. (2014) Optimising the use of marine tephrochronology in the North Atlantic: a detailed investigation of the Faroe Marine Ash Zones II, III and IV. *Quaternary Science Reviews*, 106: 122-139.

Grün, R., Stringer, C., McDermott, F., Nathan, R., Robertson, S., Taylor, L., Mortimer, G., Eggins, S., and McCulloch, M. (2005) U-series and ESR analysis of bones and teeth relating to the human burials from Skhul. *Journal of Human Evolution,* 49: 316-334.

Guichard, F., Carey, S., M.A. Arthur, Sigurdsson, H., and Arnold, M. (1993) Tephra from the Minoan eruption of Santorini in sediments of the Black Sea. *Nature*, 363: 610-612.

Haesaerts, P., Borziak, I., Chirica, V., Damblon, F., Koulakovska, L., and Van der Plicht, J. (2003) The east Carpathian loess record: a reference for the middle and late pleniglacial stratigraphy in central Europe. *Quaternaire*, 14: 163-188.

Haesaerts, P., Borziac, I., Chekha, V.P., Chirica, V., Damblon, F., Drozdov, N.I., Orlova, L.A., Pirson, S., and Van der Plicht, J. (2009) Climatic Signature and Radiocarbon Chronology of Middle and Late Pleniglacial Loess from Eurasia: Comparison with the Marine and Greenland records. *Radiocarbon*, 51: 301-318.

Haesaerts, P., Borziac, I., Chekha, V.P., Chirica, V., Drozdov, N.I., Koulakovska, L., Orlova, L.A., Van der Plicht, J., and Damblon, F. (2010) Charcoal and wood remains for radiocarbon dating Upper Pleistocene loess sequences in Eastern Europe and Central Siberia. *Palaeogeography, Palaeoclimatology, Palaeoecology*, 291: 106-127.

Hall, A., 1996. *Igneous Petrology*. 2nd ed. London. Longman Group.

Hamann, Y., Wulf, S., Ersoy, O., Ehrmann, W., Aydar, E., and Schmiedl, G. (2010) First evidence of a distal early Holocene ash layer in Eastern Mediterranean deep-sea sediments derived from the Anatolian volcanic province. *Quaternary Research*, 73: 497-506.

Harangi, S., Molnár, M., Vinkler, A.P., Kiss, B., Jull, A.J.T., and Leonard, A.G. (2010) Radiocarbon Dating the Last Volcanic Eruptions of Ciomadul Volcano, Southeast Carpathians, Eastern-Central Europe. *Radiocarbon*, 52: 1498-1507.

Hardiman, J.C. (1999) Deep sea tephra from Nyisyros Island, eastern Agean Sea, Greece. In: Firth, C.R., and McGuire, W.J. eds. *Volcanoes in the Quaternary, Geological Society Special Publications, 161.* London, The Geological Society: 69-88.

Hershkovitz, I., Marder, O., Ayalon, A., Bar-Matthews, M., Yasur, G., Boaretto, E., Caracuta, V., Alex, B., Frumkin, A., Goder-Goldberger, M., Gunz, P., Holloway, R.L., Latimer, B., Lavi, R., Matthews, A., Slon, V., Mayer, D.B.-Y., Berna, F., Bar-Oz, G., Yeshurun, R., May, H., Hans, M.G., Weber, G.W., and Barzilai, O. (2015) Levantine cranium from Manot Cave (Israel) foreshadows the first European modern humans. [Online] *Nature*, advanced online publication, 28 January 2015: doi:10.1038/nature14134.

Hidjrati, N.I., Kimball, L.R., and Koetje, T. (2003) Middle and Late Pleistocene investigations of Myshtulagty Lagat (Weasel Cave) North Ossetia, Russia. *Antiquity*, *Project Gallery*, 77(298).

Higham, T.F.G., Jacobi, R.M., and Ramsey, C.B. (2006) AMS radiocarbon dating of ancient bone using ultrafiltration. *Radiocarbon*, 48: 179-195.

Higham, T., Brock, F., Peresani, M., Broglio, A., Wood, R., and Douka, K. (2009) Problems with radiocarbon dating the Middle to Upper Palaeolithic transition in Italy. *Quaternary Science Reviews*, 28: 1257-1267.

Higham, T., Compton, T., Stringer, C., Jacobi, R., Shapiro, B., Trinkaus, E., Chandler, B., Gröning, F., Collins, C., Hillson, S., O'Higgins, P., FitzGerald, C., and Fagan, M. (2011) The earliest evidence for anatomically modern humans in northwestern Europe. *Nature*, 479: 521-524.

Higham, T., Douka, K., Wood, R., Ramsey, C.B., Brock, F., Basell, L., Camps, M., Arrizabalaga, A., Baena, J., Barroso-Ruiz, C., Bergman, C., Boitard, C., Boscato, P., Caparros, M., Conard, N.J., Draily, C., Froment, A., Galvan, B., Gambassini, P., Garcia-Moreno, A., Grimaldi, S., Haesaerts, P., Holt, B., Iriarte-Chiapusso, M.-J., Jelinek, A., Jorda Pardo, J.F., Maillo-Fernandez, J.-M., Marom, A., Maroto, J., Menendez, M., Metz, L., Morin, E., Moroni, A., Negrino, F., Panagopoulou, E., Peresani, M., Pirson, S., de la Rasilla, M., Riel-Salvatore, J., Ronchitelli, A., Santamaria, D., Semal, P., Slimak, L., Soler, J., Soler, N., Villaluenga, A., Pinhasi, R., and Jacobi, R. (2014) The timing and spatiotemporal patterning of Neanderthal disappearance. *Nature*, 512: 306-309.

Hoffecker, J.F., and Cleghorn, N. (2000) Mousterian Hunting Patterns in the Northwestern Caucasus and the Ecology of the Neanderthals. *International Journal of Osteoarchaeology*, 10: 368-378.

Housley, R.A., C.S. Lane, Cullen, V.L., Weber, M.-J., Riede, F., Gamble, C.S., and Brock, F. (2012) Icelandic volcanic ash from the Late-glacial open-air archaeological site of Ahrenshöft LA 58 D, North Germany. *Journal of Archaeological Science*, 39: 708-716.

Hublin, J-J. (2012) The earliest modern human colonization of Europe. *Proceedings of the National Academy of Sciences*, 109: 13471-13472.

Innocenti, F., Mazzuoli, R., Pasquare, G., Radicati, D., Brozolo, F., and Villari, L. (1975) The Neogene calc-alkaline volcanism of central Anatolia: geochronology data on Kayseri-Niğde area. *Geological Magazine*, 112: 349-360.

Joannin, S., Cornée, J.-J., Münch, P., Fornari, M., Vasiliev, I., Krijgsman, W., Nahapetyan, S., Gabrielyan, I., Ollivier, V., Roiron, P., and Chataigner, C. (2010) Early Pleistocene climate cycles in continental deposits of the Lesser Caucasus of Armenia inferred from palynology, magnetostratigraphy, and $^{40}Ar/^{39}Ar$ dating. *Earth and Planetary Science Letters,* 291: 149-158.

Jochum, K.P., Stoll, B., Herwig, K., Willbold, M., Hofmann, A.W., Amini, M., Aarburg, S., Abouchami, W., Hellebrand, E., Mocek, B., Raczek, I., Stracke, A., Alard, O., Bouman, C., Becker, S., Dücking, M., Brätz, H., Klemd, R., Bruin, D.d., Canil, D., Cornell, D., Hoog, C.-J.d., Dalpé, C., Danyushevsky, L., Eisenhauer, A., Gao, Y., Snow, J.E., Groschopf, N., Günther, D., Latkoczy, C., Guillong, M., Hauri, E.H., Höfer, H.E., Lahaye, Y., Horz, K., Jacob, D.E., Kasemann, S.A., Kent, A.J.R., Ludwig, T., Zack, T., Mason, P.R.D., Meixner, A., Rosner, M., Misawa, K., Nash, B.P., Pfänder, J., Premo, W.R., Sun, W.D., Tiepolo, M., Vannucci, R., Vennemann, T., Wayne, D., and Woodhead, J.D. (2006) MPI-DING reference glasses for in situ microanalysis: new reference values for element concentrations and isotope ratios. [Online]. *Geochemistry Geophysics Geosystems*, 7: Q02008, doi:10.1029/2005GC001060.

Johnston, E.N., Phillips, J.C., Bonadonna, C., and Watson, I.M. (2012) Reconstructing the tephra dispersal pattern from the Bronze Age eruption of Santorini using an advection–diffusion model. *Bulletin of Volcanology*, 74: 1485 - 1507.

Kandel, A. (2014) Researcher at the University of Tübingen. Email correspondence regards the Aghitu 3 cave. Samples and figures exchanged. Personal communication. 15-16th January (Samples received November 2013).

Kandel, A.W., Gasparyan, B., Bruch, A.A., Weissbrod, L., and Zardaryan, D. (2011) Introducing Aghitu-3, the first Upper Paleolithic cave site in Armenia. *ARAMAZD*, *Armenian Journal of Near Eastern Studies,* 6(2): 7-23.

Kandel, A.W., Gasparyan, B., Nahepetyan, S., Taller, A., and Weissbrod, L. (2014) The Upper Paleolithic Settlement of the Armenian Highlands. In: Otte, M. ed. *Modes of Contacts and Mobility during the Eurasian Palaeolithic.* Luxembourg, Université de Liège: 39–60. (ERAUL 140)

Karakhanian, A., Djrbashian, R., Trifonov, V., Philip, H., Arakelian, S., and Avagian, A. (2002) Holocene-historical volcanism and active faults as natural risk factors for Armenia and adjacent countries. *Journal of Volcanology and Geothermal Research*, 113: 319-344.

Karakhanian, A., Jrbashyan, R., Trifonov, V., Philips, H., Arakelian, S., Avagyan, A., Baghdassaryan, H., Davtian, V., and Ghoukassyan, Y. (2003) Volcanic hazards in the region of the Armenian Nuclear Power Plant. *Journal of Volcanology and Geothermal Research*, 126: 31-62.

Karapetian, K.I. (1983) On the use of archaeological data in stratigraphical descriptions of Quaternary volcanic rocks in Armenia SSR. In: *The issues of Quaternary period geology in Armenia*. Publishing house of the Armenian SSR academy of sciences, Yerevan (in Russian). (Cited in Karakhanian et al., 2003)

Karkanas, P., White, D., Lane, C.S., Cullen, V.L., Stringer, C., Davies, W., Cullen, V,L., Smith, V.C., Ntinou, M., Tsartsidou, G. and Kyparissi-Apostolika, N. (2014) Tephra correlations and climatic events between the MIS6/5 transition and the beginning of MIS3 in Theopetra Cave, central Greece. [Online]. *Quaternary Science Reviews*, in press, corrected proof, 17 June 2014. doi:10.1016/j.quascirev.2014.05.027

Keller, J., Ryan, W.B.F., Ninkovich, D., and Altherr, R. (1978) Explosive volcanic activity in the Mediterranean over the past 200,000 yr as recorded in deep-sea sediments. *Geological Society of America Bulletin*, 89: 591-604.

Kempema, E.W. (1998) *Nearshore ice formation and sediment transport in southern Lake Michigan.* Unpublished PhD Thesis, Oceanography, University of Washington.

Keskin, M., Pearce, J.A., and Mitchell, J.G. (1998) Volcano-stratigraphy and geochemistry of collision-related volcanism on the Erzurum–Kars Plateau, northeastern Turkey. *Journal of Volcanology and Geothermal Research*, 85: 355-404.

Kissel, C., Guillou, H., Laj, C., Carracedo, J.C., Nomade, S., Perez-Torrado, F., and Wandres, C. (2011) The Mono Lake excursion recorded in phonolitic lavas from Tenerife (Canary Islands): Paleomagnetic analyses and coupled K/Ar and Ar/Ar dating. *Physics of the Earth and Planetary Interiors*, 187: 232-244.

Kozlowski, J.K. (1998) The Middle and the Early Upper Paleolithic around the Black Sea. In: Akazawa, T., Aoki, K., and Bar-Yosef, O. eds. *Neanderthals and Modern Humans in western Asia*. New York, Plenum Press: 461-482.

Kraml, M. (1997) *Laser-^{40}Ar/^{39}Ar-Datierungen an distalen marinen Tephren des jung-quartären Mediterranen vulkanismus (Ionisches Meer, METEOR-Fahrt 25/4).* Unpublished Ph. D. Thesis, Albert-Ludwigs-Universität, Freiburg. (Cited in Giaccio et al., 2012; Wulf et al., 2012)

Krause, J., Orlando, L., Serre, D., Viola, B., Prüfer, K., Richards, M.P., Hublin, J-J., Hänni, C., Derevianko, A.P., and Pääbo, S. (2007) Neanderthals in central Asia and Siberia. *Letters to Nature*, 449: 902-904.

Kuhn, S.L., Stiner, M.C., and Güleç, E. (1999) Initial Upper Palaeolithic in south-central Turkey and its regional context: a preliminary report. *Antiquity*, 73: 505-517.

Khun, S.L., Stiner, M.C., Güleç, E., Özer, I., Yilmaz, H., Baykara, I., Açikkol, A., Goldberg, P., Martínez Molina, M., Ünay, E., and Suata-Alpaslan, F. (2009) The early Upper Paleolithic occupations at Üçağizli Cave (Hatay, Turkey). *Journal of Human Evolution*, 56: 87-113.

Kuzucuoglu, C., Pastre, J.F., Black, S., Ercan, T., Fontugne, M., Guillou, H., Hatté, C., Karabiyikoglu, M., Orth, P., and Türkecan, A. (1998) Identification and dating of tephra layers from Quaternary sedimentary sequences of Inner Anatolia, Turkey. *Journal of Volcanology and Geothermal Research*, 85:153-172.

Kwiecien, O., Arz, H.W., Lamy, F., Wulf, S., Bahr, A., Röhl, U., and Haug, G.H. (2008) Estimated Reservoir Ages of the Black Sea since the Last Glacial. *Radiocarbon*, 50: 99-118.

Lamy, F., Arz, H.W., Bond, G.C., Bahr, A., and Pätzold, J. (2006) Multicentennial-scale hydrological changes in the Black Sea and northern Red Sea during the Holocene and the Arctic/North Atlantic oscillation. [Online]. *Paleoceanography*, 21: PA1008, doi:10.1029/2005PA001184.

Lane, C.S., Andric, M., and Cullen, V.L. (2011a) The occurrence of distal Icelandic and Italian tephra in the Lateglacial of Lake Bled, Slovenia. *Quaternary Science Reviews*, 30: 1013-1018.

Lane, C.S., Haslam, M., Petraglia, M., Ditchfield, P., Smith, V., and Korisettar, R. (2011b) Cryptotephra from the 74 ka BP Toba super-eruption in the Billa Surgam caves, southern India. *Quaternary Science Reviews*, 30: 1819-1824.

Lane, C.S., De Klerk, P., and Cullen, V.L. (2012a) A tephrochronology for the Lateglacial palynological record of the Endinger Bruch (Vorpommern, north-east Germany). *Journal of Quaternary Science*, 27: 141-149.

Lane, C.S., Blockley, S.P.E., Mangerud, J., Smith, V.C., Lohne, Ø.S., Tomlinson, E.L., Matthews, I.P., and Lotter, A.F. (2012b) Was the 12.1 ka Icelandic Vedde Ash one of a kind? *Quaternary Science Reviews*, 33: 87-99.

Lane, C.S., Chorn, B.T., and Johnson, B.T. (2013a) Ash from the Toba supereruption in Lake Malawi shows no volcanic winter in East Africa at 75 ka. *Proceedings of the National Academy of Sciences*, 110: 8025- 8029.

Lane, C.S., Brauer, A., Blockley, S.P.E., and Dulski, P. (2013b) Volcanic ash reveals time-transgressive abrupt climate change during the Younger Dryas. *Geology*, 41: 1251-1254.

Lane, C.S., Cullen, V.L., White, D., Bramham-Law, C.W.F., and Smith, V.C. (2014) Cryptotephra as a dating and correlation tool in archaeology. *Journal of Archaeological Sciences*, 42: 42-50.

Le Bas, M.J., Le Maitre, R.W., Streckeisen, A., and Zanettin, B. (1986) A Chemical Classification of Volcanic Rocks Based on the Total Alkali-Silica Diagram. *Journal of Petrology*, 27: 745-750.

Lebedev, V.A., Chernyshev, I.V., Arakelyant, M.M., Gol'tsman, Y. V., Dudauri, O.Z., and Vashakidze, G.T. (2004a) Geochronology of the Neogene-Quaternary Dacitic Volcanism in the Northwestern Lesser Caucasus (Georgia). *Stratigraphy and Geological Correlations,* 12: 85-101.

Lebedev, V.A., Chernyshev, I.V., Arutyunyan, E.V., Bubnov, S.N., Dudauri. O.Z., and Vashakidze, G.T. (2004b) Chronology of Quaternary Volcanism of the Keli Highland, Greater Caucasus: Evidence from K-Ar Isotopic Dating. *Doklady Earth Sciences*, 399: 1227-1231.

Lebedev, V.A., Chernyshev, I.V., Chugaev, A.V., and Vashakidze, G.T. (2007) Geochronology of Quaternary Volcanism of the Krestovyi Pass Region, Kazbek Neovolcanic Area, Greater Caucasus. *Doklady Earth Sciences*, 413: 272-276.

Lebedev, V.A., Vasakidze, G.T., and Sakhno, V.G. (2008) Potential Volcanic Danger in the Keli Highland (Greater Caucasus): Evidence from Isotopic-Geochronological Study of the Youngest Lavas. *Doklady Earth Sciences*, 418: 169-173.

Lebedev, V.A., Chernyshev, I.V., Chugaev, A.V., Gol'tsman, Y.V. and Bairova, E.D. (2010) Geochronology of Eruptions and Parental Magmas Sources of Elbrus Volcano, the Greater Caucasus: K-Ar and Sr-Nd-Pb Isotope Data. *Geochemistry International*, 48: 41-67.

Lebedev, V.A., Chernyshev, I.V., and Sharkov, E.V (2011a) Geochronological Scale and Evolution of Cenozoic Magmatism within the Caucasian Segment of the Alpine Belt. *Doklady Earth Sciences,* 441: 1656-1660.

Lebedev, V.A., Vashakidze, G.T., Arutyunyan, E.V. and Yakushev, A.I. (2011b) Geochronology and Evolution of Quaternary Volcanism at the Keli Highland, Greater Caucasus. *Geochemistry International*, 49: 1120-1144.

Lebedev, V.A., Chernyshev, I.V., Shatagin, K.N., Bubnov, S.N., and Yakushev, A.I. (2013) The Quaternary Volcanic Rocks of the Geghama Highland, Lesser Caucasus, Armenia: Geochronology, isotopic Sr-Nd Characteristics, and Origin. *Journal of Volcanology and Seismology*, 7: 204-229.

Le Bourdonnec, F-X., Nomade, S., Poupeau, G., Guillou, H., Tushabramishvili, N., Moncel, M-H., Pleurdeau, D., Agapishvili, T., Voinchet, P., Mgeladze, A., and Lordkipanidze, D. (2012) Multiple origins of Bondi Cave and Ortvale Klde (NW Georgia) obsidians and human mobility in Transcaucasia during the Middle and Upper Palaeolithic. *Journal of Archaeological Sciences*, 39: 1317-1330.

Leng, M.J., and Marshall, J. D. (2004) Palaeoclimate interpretation of stable isotope data from lake sediment archives. *Quaternary Science Reviews*, 23: 811-831.

Leroy, S.A.G., López-Merino, L., Tudryn, A., and Chalié, F. (2014) Late Pleistocene and Holocene palaeoenviroments in and around the middle Caspian basin as reconstructed from a deep-sea core. *Quaternary Science Reviews*, 101: 91-110.

Lewis, L., Ditchfield, P., Pal, J.N., and Petraglia, M. (2012) Grain size distribution analysis of sediments containing Younger Toba tephra from Ghoghara, Middle Son valley, India. *Quaternary International*, 258: 180-190.

Limburg, E.M., and Varekamp, J.C. (1991) Young pumice deposits on Nisyros, Greece. *Bulletin of Volcanology*, 54: 68-77.

Litt, T., Pickarski, N., Heumann, G., Stockhecke, M., and Tzedakis, P.C. (2014) A 600,000 year long continental pollen record from Lake Van, eastern Anatolia (Turkey). *Quaternary Science Reviews*, 104: 30-41.

Liubin, V.P. (1977) Mustierskie kul'turi Kavkaza (Mousterian Cultures of the Caucasus). Nauka, Leningrad. (Cited in Adler and Tushabramishvili, 2004, Golovanova and Doronichev, 2003 and Pinhasi et al., 2012).

Liubin, V.P. (1989) Paleolit Kavkaza (Paleolithic of the Caucasus). In: P.I. Boriskovski (Editor), Paleolit Kavkaza i Sredney Azii (Paleolithic of the Caucasus and Northern Asia). Nauka, Leningrad, p 9-144. (Cited in Adler and Tushabramishvili, 2004, Golovanova and Doronichev, 2003 and Pinhasi et al., 2012).

Lowe, D.J. (2011) Tephrochronology and its application: A review. *Quaternary Geochronology*, 6: 107-153.

Lowe, D.J., and Hunt, J.B. (2001) A summary of terminology used in tephra-related studies. In: Juvigné, J-P., and Raynal, J-P. eds. *Tephras: Chronology, Archaeology. Les Dossiers de l'Archeo-Logis 1*. Archeo-Logis/CDERAD: 17-22.

Lowe, J.J., and Walker, M.J.C. (1997) *Reconstructing Quaternary Environments*. 2nd ed. Harlow, Addison Wesley Longman LtD.

Lowe, J., Barton, N., Blockley, S., Ramsey, C.B., Cullen, V.L., Davies, W., Gamble, C., Grant, K., Hardiman, M., Housley, R., Lane, C.S., Lee, S., Lewis, M., MacLeod, A., Menzies, M., Müller, W., Pollard, M., Price, C., Roberts, A.P., Rohling, E.J., Satow, C., Smith, V.C., Stringer, C.B., Tomlinson, E.L., White, D., Albert, P., Arienzo, I., Barker, G., Borić, D., Carandente, A., Civetta, L., Ferrier, C., Guadelli, J-L., Karkanas, P., Koumouzelis, M., Müller, U.C., Orsi, G., Pross, J., Rosi, M., Shalamanov-Korobar, L., Sirakov, N., and Tzedakis, P.C. (2012) Volcanic ash layers illuminate the resilience of Neanderthals and early modern humans to natural hazards. *Proceedings of the National Academy of Sciences*, 109: 13532-13537.

Lucchi, F., Tranne, C.A., De Astis, G., Keller, J., Losito, R., and Morche, W. (2008) Stratigraphy and significance of Brown Tuffs on the Aeolian Islands (southern Italy). *Journal of Volcanology and Geothermal Research*, 177: 49-70.

Lukich, V. (2012) *Single grain OSL dating of the Middle Palaeolithic site Lusakert in Armenia*. Unpublished MSc thesis, Department of Geography, Royal Holloway, UCL.

Mangerud, J., Lie, S.E., Furnes, H., Kristiansen, I.L., and Lømo, L. (1984) A Younger Dryas Ash Bed in western Norway, and its possible correlations with tephra in cores from the Norwegian Sea and the North Atlantic. *Quaternary Research*, 21: 85-104.

Mangerud, J., Jakobsson, M., Alexanderson, H., Astakhov, V., Clarke, G.K.C., Henriksen, M., Hjort, C., Krinner, G., Lunkka, J.-P., Möller, P., Murray, A., Nikolskaya, O., Saarnisto, M., and Svendsen, J.I. (2004) Ice-dammed lakes and rerouting of the drainage of northern Eurasia during the Last Glaciation. *Quaternary Science Reviews*, 23: 1313-1332.

Manning, S.W., Ramsey, C.B., Kutschera, W., Higham, T., Kromer, B., Steier, P., and Wild, E.M. (2006) Chronology for the Aegean Late Bronze Age 1700-1400 B.C. *Science*, 312: 565-569.

Margari, V., Pyle, D.M., Bryant, C., and Gibbard, P.L. (2007) Mediterranean tephra stratigraphy revisited: results from a long terrestrial sequence on Lesvos Island, Greece. *Journal of Volcanology and Geothermal Research*, 163: 34-54.

Mark, D.F., Petraglia, M., Smith, V.C., Morgan, L.E., Barfod, D.N., Ellis, B.S., Pearce, N.J., Pal, J.N., and Korisettar, R. (2014) A high-precision $^{40}Ar/^{39}Ar$ age for the Young Toba Tuff and dating of ultra-distal tephra: Forcing of Quaternary climate and implications for hominin occupation of India. *Quaternary Geochronology*, 21: 90-103.

Matthews, N.E., Smith, V.C., Costa, A., Durant, A.J., Pyle, D.M., and Pearce, N.J.G. (2012) Ultra-distal tephra deposits from super-eruptions: Examples from Toba, Indonesia and Taupo Volcanic Zone, New Zealand. *Quaternary International*, 258: 54-79.

Mellars, P. (2004) Neanderthals and the modern human colonization of Europe. *Nature*, 432: 461-465.

Mellars, P. (2005) The impossible coincidence. A single-species model for the origins of modern human behaviour in Europe. *Evolutionary Anthropology*, 14: 12-27.

Mellars, P. (2006) A new radiocarbon revolution and the dispersal of modern humans in Eurasia. *Nature*, 439: 931-935.

Mellars, P. (2011) Palaeoanthropology: The earliest modern humans in Europe. *Nature*, 479: 483-485.

Mercier, N., Valladas, H., Meignen, L., Joron, J-L., Tushabramishvilli, N., Adler, D.S., and Bar-Yosef, O. (2011) Dating the Early Middle Palaeolithic Laminar Industry from Djruchula Cave, Republic of Georgia. *Paléorient*, 36: 163-173.

Meyer, M., Kircher, M., Gansauge, M.-T., Li, H., Racimo, F., Mallick, S., Schraiber, J.G., Jay, F., Prüfer, K., de Filippo, C., Sudmant, P.H., Alkan, C., Fu, Q., Do, R., Rohland, N., Tandon, A., Siebauer, M., Green, R.E., Bryc, K., Briggs, A.W., Stenzel, U., Dabney, J., Shendure, J., Kitzman, J., Hammer, M.F., Shunkov, M.V., Derevianko, A.P., Patterson, N., Andrés, A.M., Eichler, E.E., Slatkin, M., Reich, D., Kelso, J., and Pääbo, S. (2012) A High-Coverage Genome Sequence from an Archaic Denisovan Individual. *Science*, 338: 222-226.

Moncel, M.-H., Pleurdeau, D., Tushabramishvili, N., Yeshurun, R., Agapishvili, T., Pinhasi, R., and Higham, T.F.G. (2013) Preliminary results from the new excavations of the Middle and Upper Palaeolithic levels at Ortvale Klde-north chamber (South Caucasus Georgia). *Quaternary International*, 316: 3-13.

Morche, W. (1988) *Tephrochronologie der Aolischen Inseln*. Unpublished PhD Thesis, Albert-Ludwigs-Universitat Freiburg, Germany.

Morley, M.W., and Woodward, J.C. (2011) The Campanian Ignimbrite (Y5) tephra at Crvena Stijena Rockshelter, Montenegro. *Quaternary Research*, 75: 683-696.

Mouralis, D., Pastre, J.-F., Kuzucuoglu, C., Türkecan, A., Atici, Y., Slimak, L., Guillou, H., and Kunesch, S. (2002) Les complexes volcaniques Rhyolithiques quaternaires d'Anatolie centrale (Göllü Dag et Acigöl, Turquie): genèse, instabilité, contraintes environnementales. *Quaternaire*, 13: 219-228.

Murray, J., Domíngues-Alonso, P., Fernández-Jalvo, Y., King, T., Lynch, E.P., Andrews, P., Yepiskoposyan, L., Moloney, N., Cacères, I., Allué, E., Asryan, L., Ditchfield, P., and Williams, D.M. (2010) Pleistocene to Holocene stratigraphy of Azokh 1 Cave, Lesser Caucasus. *Irish Journal of Earth Sciences*, 28: 75-91.

Müller, U.C., Pross, J., Tzedakis, P.C., Gamble, C., Kotthoff, U., Schmiedl, G., Wulf, S., and Christanis, K. (2011) The role of climate in the spread of modern humans into Europe. *Quaternary Science Reviews,* 30: 273-279.

Narcisi, B., and Vezzoli, L. (1999) Quaternary stratigraphy of distal tephra layers in the Mediterranean - an overview. *Global and Planetary Change*, 21: 31-50.

Neill, I., Meliksetian, Kh., Allen, M.b. Navarsardyan, G., and Karapetyan, S. (2013) Pliocene-Quaternary volcanic rocks of NW Armenia: magmatism and lithospheric dynamics within an active orogenic plateau. *Lithos*, 180-181: 200-215.

Nioradze, M. (1991) *Altsteinzeitliche Höhlenfundplätze in Zchalzitela-Tal*. Tbilisi, Die Akademie der Wissenschaften des Georgiens.

Nioradze, M. (1992) Peshernie paleoliticheskie stoyanki ushelia r. Tskhaltsitela (Palaeolithic cave sites of the Tskhaltsitela River gorge). In: Tushabramishvili, D. ed. Paleolit Kavkaza i sopredel'nikh territory (Palaeolithic caves of the Caucasus and adjacent regions). Tbilisi, Metsnereba: 55-60. (Cited in Adler and Tushabramishvili, 2004, and Pinhasi et al., 2012)

Nioradze, M.G., and Otte, M. (2000) Paléolithique supérieur de Géorgie. *L'Anthropologie*, 104: 265-300.

North Greenland Ice Core Project members. Anderson, K., Azuma, N., Barnola, J.-M., Bigler, M., Biscaye, P., Caillon, N., Chappellaz, J., Clausen, H.B., Dahl-Jensen, D., Fischer, H., Flückiger, J., Fritzsche, D., Fujii, Y., Goto-Azuma, K., Grønvold, K., Gundestrup, N.S., Hansson, M., Huber, C., Hvidberg, C.S., Johnsen, S.J., Jonsell, U., Jouzel, J., Kipfstuhl, S., Landais, A., Leuenberger, M., Lorrain, R., Masson-Delmotte, V., Miller, H., Motoyama, H., Narita, H., Popp, T., Rasmussen, S.O., Raynaud, D., Rothlisberger, R., Ruth, U., Samyn, D., Schwander, J., Shoji, H., Siggard-Andersen, M.-L., Steffensen, J.P., Stocker, T., Sveinbjörnsdóttir, A.E., Svensson, A., Takata, M., Tison, J-L., Thorsteinsson, T., Watanabe, O., Wilhelms, F., and White, J.W.C. (2004) High-resolution record of Northern Hemisphere climate extending into the last interglacial period. *Nature*, 431: 147-151.

Nowaczyk, N.R., Arz, H.W., Frank, U., Kind, J., and Plessen, B. (2012) Dynamics of the Laschamp geomagnetic excursion from Black Sea sediments. *Earth and Planetary Science Letters*, 351-352: 54-69.

Nowaczyk, N.R., Frank, U., Kind, J., and Arz, H.W. (2013) A high-resolution paleointensity stack of the past 14 to 68 ka from Black Sea sediments. *Earth and Planetary Science Letters*, 384: 1-16.

Ollivier, V., Nahapetyan, S., Roiron, P., Gabrielyan, I., Gasparyan, B., Chataigner, C., Joannin, S., Corée, J-J., Guillou, H., Scaillet, S., Munch, P., and Krijgsman, W. (2010) Quaternary volcano-lacustrine patterns and palaeobotanical data in the southern Armenia. *Quaternary International*, 223-224: 312-326.

Orsi, G., Vita, S.D., and Vito, M.A.D. (1996) The restless, resurgent Campi Flegrei nested caldera (Italy): constraints on its evolution and configuration. *Journal of Volcanology and Geothermal Research*, 74: 179-214.

Otte, M., Shidrang, S., Zwyns, N., and Flas, D. (2011) New radiocarbon dates for the Zagros Aurignacian from Yafteh cave, Iran. *Journal of Human Evolution*, 61(3): 340-346.

Pappalardo, L., Civetta, L., D'Antonio, M., Deino, A., Di Vito, M., Orsi, G., Carandente, A., de Vita, S., Isaia, R., and Piochi, M. (1999) Chemical and Sr-isotopical evolution of the Phlegraean magmatic system before the Campanian Ignimbrite and the Neapolitan Yellow Tuff eruptions. *Journal of Volcanology and Geothermal Research*, 91: 141-166.

Pasquarè, G., Poli, S., Vezzoli, L., and Zanchi, A. (1988) Continental arch volcanism and tectonic setting in Central Anatolia, Turkey. *Tectonophysics,* 146: 217-230.

Paterne, M., Guichard, F., Duplessy, J.C., Siani, G., Sulpizio, R., and Labeyrie, J. (2008) A 90,000-200,000 yrs marine tephra record of Italian volcanic activity in the Central Mediterranean Sea. *Journal of Volcanology and Geothermal Research*, 177: 187-196.

Patou-Mathis, M. (2012) Interactions Between Neanderthals and Carnivores in Eastern Europe. *Journal of Taphonomy*, 10(3-4): 277-290.

Payne, R., and Gehrels, M. (2010) The formation of tephra layers in peatlands: an experimental approach. *CATENA*, 81: 12-23.

Pearce, J.A., Bender, J.F., De Long, S.E., Kidd, W.S.F., Low, P.J., Güner, Y., Saroglu, F., Moorbath, S., and Mitchell, J.G. (1990) Genesis of collision volcanism in eastern Anatolia, Turkey. *Journal of Volcanology and Geothermal Research*, 44: 189-229.

Pearce, N.J.G., Westgate, J.A., Perkins, W.T., and Preece, S.J. (2004) The application of ICP-MS methods to tephrochronological problems. *Applied Geochemistry*, 19: 289-322.

Pécskay, Z., Lexa, J., Szakács, A., Seghedi, I., Balogh, K., Konečný, V., Zelenka, T., Kovacs, M., Póka, T., Fülöp, A., Márton, E., Panaiotu, C., and Cvetković, V. (2006) Geochronology of Neogene magmatism in the Carpathian arc and intra-Carpathian area. *Geologica Carpathica,* 57:511–530.

Perkins, W.T., Pearce, N.J.G., and Weatgate, J.A. (1997) The Development of Laser Ablation ICP-MS and Calibration Strategies: Examples from the Analysis of Trace Elements in Volcanic Glass Shards and Sulfide Minerals. *Geostandards Newsletters*. 21: 175-190.

Petraglia, M.D. (2011) Archaeology: Trailblazers across Arabia. *Nature*, 470: 50-51.

Pinhasi, R., Gasparian, B., Wilkinson, K., Bailey, R., Bar-Oz, G., Bruch, A., Chataigner, C., Hoffmann, D., Hovsepyan, R., Nahapetyan, S., Pike, A.W.G., Schreve, D., and Stephens, M. (2008) Hovk 1 and the Middle and Upper Paleolithic of Armenia: a preliminary framework. *Journal of Human Evolution*, 55: 803-816.

Pinhasi, R., Gasparian, B., Nahapetyan, S., Bar-Oz, G., Weissbrod, L., Bruch, A.A., Hovsepyan, R., and Wilkinson, K. (2011a) Middle Palaeolithic human occupation of the high altitude region of Hovk-1, Armenia. *Quaternary Science Reviews*, 30: 3846-3857.

Pinhasi, R., Higham, T.F.G., Golovanova, L.V., and Doronichev, V.B. (2011b) Revised age of late Neanderthal occupation and the end of the Middle Paleolithic in the northern Caucasus. *Proceedings of the National Academy of Sciences*, 108: 8611–8616.

Pinhasi, R., Nioradze, M., Tushabramishvili, N., Lordkipanidze, D., Pleurdeau, D., Moncel, M-H., Adler, D.S., Stringer, C., and Higham, T.F. (2012) New chronology for the Middle Palaeolithic of the southern Caucasus suggests early demise of Neanderthals in this region. *Journal of Human Evolution*, 63: 770-780.

Platevoet, B., Scillet, S., Guillou, H., Blamart, D., Nomade, S., Massault, M., Poisson, A., Elitok, Ö., Özgür, N., Yagmurlu, F., and Yilmaz, K. (2008) Pleistocene eruptive chronology of the Gölcük volcano, Isparta Angle, Turkey. *Quaternaire*, 19: 147-156.

Pleurdeau, D., Touchabramichvili, N., Nioradze, M., de Lumley, H., and Lordkipanidze, D. (2007) Les assemblages lithiques du Paléolithique moyen de Géorgie (Lithic assemblages of Middle Palaeolithic from Georgia). *L'anthropologie*, 111: 400-431.

Pollard, A.M., Blockley, S.P.E., and Ward, K.R. (2003) Chemical alteration of tephra in the depositional environment: theoretical stability modelling. *Journal of Quaternary Science*, 18: 385-394.

Prufer, K., Racimo, F., Patterson, N., Jay, F., Sankararaman, S., Sawyer, S., Heinze, A., Renaud, G., Sudmant, P.H., de Filippo, C., Li, H., Mallick, S., Dannemann, M., Fu, Q., Kircher, M., Kuhlwilm, M., Lachmann, M., Meyer, M., Ongyerth, M., Siebauer, M., Theunert, C., Tandon, A., Moorjani, P., Pickrell, J., Mullikin, J.C., Vohr, S.H., Green, R.E., Hellmann, I., Johnson, P.L.F., Blanche, H., Cann, H., Kitzman, J.O., Shendure, J., Eichler, E.E., Lein, E.S., Bakken, T.E., Golovanova, L.V., Doronichev, V.B., Shunkov, M.V., Derevianko, A.P., Viola, B., Slatkin, M., Reich, D., Kelso, J., and Paabo, S. (2014) The complete genome sequence of a Neanderthal from the Altai Mountains. *Nature*, 505: 43-49.

Pyle, D.M., Ricketts, G.D., Margari, V., van Andel, T.H., Sinitsyn, A. A., Praslov, N.D., and Lisitsyn, S. (2006) Wide dispersal and deposition of distal tephra during the Pleistocene 'Campanian Ignimbrite/Y5' eruption, Italy. *Quaternary Science Reviews*, 25: 2713-2728.

Pyne-O'Donnell, S.D.F., Blockley, S.P.E., Turney, C.S.M., and Lowe, J.J. (2008) Distal volcanic ash layers in the Lateglacial Interstadial (GI-1): problems of stratigraphic discrimination. *Quaternary Science Reviews*, 27: 72-84.

Rasmussen, S.O., Andersen, K.K., Svensson, A.M., Steffensen, J.P., Vinther, B.M., Clausen, H.B., Siggaard-Anderson, M-L., Johnsen, S.J., Larsen, L.B., Dahl-Jensen, D., M. Bigler, Röthlisberger, R., Fischer, H., Goto-Azuma, K., Hansson, M.E., and Ruth., U. (2006) A new Greenland ice core chronology for the last glacial termination. [Online]. *Journal of Geophysical Research*, 111: D06102, doi:10.1029/2005JD006079.

Rasmussen, S.O., Bigler, M., Blockley, S.P., Blunier, T., Buchardt, S.L., Clausen, H.B., Cvijanovic, I., Dahl-Jensen, D., Johnsen, S.J., Fischer, H., Gkinis, V., Guillevic, M., Hoek, W.Z., Lowe, J.J., Pedro, J.B., Popp, T., Seierstad, I.K., Steffensen, J.P., Svensson, A.M., Vallelonga, P., Vinther, B.M., Walker, M.J.C., Wheatley, J.J., and Winstrup, M. (2014) A stratigraphic framework for abrupt climatic changes during the Last Glacial period based on three synchronized Greenland ice-core records: refining and extending the INTIMATE event stratigraphy. *Quaternary Science Reviews*, 106: 14-28.

Rebollo, N.R., Weiner, S., Bronk, F., Meignen, L., Goldberg. P., Belfer-Cohen, A., Bar-Yoself, O., and Boaretto, E. (2011) New radiocarbon dating of the transition from the Middle to the Upper Paleolithic in Kebara Cave, Israel. *Journal of Archaeological Science,* 38: 2424-2433.

Reich, D., Green, R.E., Kircher, M., Krause, J., Patterson, N., Durand, E.Y., Viola, B., Briggs, A.W., Stenzel, U., Johnson, P.L.F., Maricic, T., Good, J.M., Marques-Bonet, T., Alkan, C., Fu, Q., Mallick, S., Li, H., Meyer, M., Eichler, E.E., Stoneking, M., Richards, M., Talamo, S., Shunkov, M.V., Derevianko, A.P., Hublin, J.-J., Kelso, J., Slatkin, M., and Paabo, S. (2010) Genetic history of an archaic hominin group from Denisova Cave in Siberia. *Nature*, 468: 1053-1060.

Reimer, P.J., Baillie, M.G.L., Bard, E., Bayliss, a., Beck, J.W., Blackwell, P.G., Ramsey, C.B., Buck, C.E., Burr, G.S., Edwards, R.L., Friedrich, M., Grootes, P.M., Guilderson, T.P., Hajdas, I., Heaton, T.J., Hogg, A.G., Hughen, K.A., Kaiser, K.F., Kromer, B., McCormac, F.G., Manning, S.W., Reimer, R.W., Richards, D.A., Southon, J.R., Talamo, S., Turney, C.S.M., van der Plicht, J., and Weyhenmeyer, C.E. (2009) IntCal09 and Marine09 Radiocarbon Age Calibration Curves, 0-50,000 years cal BP. *Radiocarbon*, 51: 1111-1150.

Reimer, P.J., Bard, E., Bayliss, A., Beck, J.W., Blackwell, P.G., Bronk Ramsey, C., Buck, C.E., Cheng, H., Edwards, R.L., Friedrich, M., Grootes, P.M., Guilderson, T.P., Haflidason, H., Hajdas, I., Hatté, C., Heaton, T.J., Hoffmann, D.L., Hogg, A.G., Hughen, K.A., Kaiser, K.F., Kromer, B., Manning, S.W., Niu, M., Reimer, R.W., Richards, D.A., Scott, E.M., Southon, J.R., Staff, R.A., Turney, C.S.M., and van der Plicht, J. (2013) IntCal13 and Marine13 Radiocarbon Age Calibration Curves 0–50,000 years cal BP. *Radiocarbon*, 55: 1869-1887.

Riede, F., Bazely, O., Newton, A.J., and Lane, C.S. (2011) A Laacher See-eruption supplement to Tephrabase: Investigating distal tephra fallout dynamics. *Quaternary International*, 246: 134-144.

Rivals, F., and Arellano, A. (2010) Les faunes des sites du Pléistocène supérieur du Caucase méridional : Grotte de Sakažhia, Grotte d'Ortvala et Grotte du Bronze (République de Géorgie). *L'anthropologie*, 114: 305-323.

Roland, T.P., Mackay, H., and Hughes, P.D.M. (2015) Tephra analysis in ombrotrophic peatlands: A geochemical comparison of acid digestion and density separation techniques. *Journal of Quaternary Science*, 30: 3-8.

Rolandi, G., Bellucci, F., Heizler, M.T., Belkin, H.E., and De Vivo, B. (2003) Tectonic controls on the genesis of ignimbrites from the Campanian Volcanic Zone, southern Italy. *Mineralogy and Petrology*, 79: 3-31.

Rollinson, H. (1993) *Using geochemical data: evaluation, presentation, interpretation*. Harlow, London, Longman Scientific & Technical.

Rose., N.L., Golding, P.N.E., and Battarbee, R.W. (1996) Selective concentration and enumeration of tephra shards from lake sediment cores. *Holocene* 6: 243-246.

Rosi, M., Vezzoli, L., Castelmenzano, A., and Grieco, G. (1999) Plinian pumice fall deposit of the Campanian Ignimbrite eruption (Phlegraean Fields, Italy). *Journal of Volcanology and Geothermal Research*, 91: 179-198.

Salgueiro, E., Voelker, A.H.L., de Abreu, L., Abrantes, F., Meggers, H., and Wefer, G. (2010) Temperature and productivity changes off the western Iberian margin during the last 150 ky. *Quaternary Science Reviews*, 29: 680-695.

Santacroce, R., Cioni, R., Marianelli, P., Sbrana, A., Sulpizio, R., Zanchetta, G., Donahue, D.J., and Joron, J.L. (2008) Age and whole rock–glass compositions of proximal pyroclastics from the major explosive eruptions of Somma-Vesuvius: A review as a tool for distal tephrostratigraphy. *Journal of Volcanology and Geothermal Research*, 177: 1-18.

Sarikaya, M.A., Zreda, M., Desilets, D., Çiner, A., and Şen, E. (2006) *Correcting for nucleogenic ^{36}Cl in cosmogenic ^{36}Cl dating of volcanic rocks from Erciyes volcano, central Turkey*. Eos Trans. American Geophysical Union Conference, San Francisco, USA, December 11-15: V21A-0553.

Scaillet, S., Vita-Scaillet, G., and Rotolo, S.G. (2013) Millennial-scale phase relationships between ice-core and Mediterranean marine records: insights from high-precision ^{40}Ar/^{39}Ar dating of the Green Tuff of Pantelleria, Sicily Strait. *Quaternary Science Reviews*, 78: 141-154.

Scandone, R., Bellucci, F., Lirer, L. and Rolandi, G. (1991) The structure of the Campanian Plain and the activity of the Neapolitan volcanoes (Italy). *Journal of Volcanology and Geothermal Research*, 48: 1-31.

Schmincke, H-U., Park, C., and Harms, E. (1999) Evolution and environmental impacts of the eruption of Laacher See Volcano (Germany) 12,900 a BP. *Quaternary International*, 61: 61-72.

Schmitt, A.K., Danišik, M., Evans, N.J., Siebel, W., Kiemele, E., Aydin, F., and Harvey, J.C. (2011) Acigöl rhyolite field, central Anatolia (part 1): high-resolution dating of eruption episodes and zircon growth rates. *Contributions to Mineralogy and Petrology*, 162: 1215-1231.

Schmitt, A.K., Danišík, M., Aydar, E., Şen, E., Ulusoy, İ., and Lovera, O.M. (2014) Identifying the Volcanic Eruption Depicted in a Neolithic Painting at Çatalhöyük, Central Anatolia, Turkey. [Online]. *PLoS ONE*, 9: e84711. doi:84710.81371/journal.pone.0084711.

Schrader, H-J. (1979) Quaternary Paleoclimatology of the Black Sea basin. *Sediment Geology*, 23: 165-180.

Scott, R.B. (1971) Alkali exchange during Devitrification and Hydration of glasses in Ignimbrite Cooling Units. *The Journal of Geology*, 79: 100-110.

Scott, J.E., and Marean, C.W. (2009) Paleolithic hominin remains from Eshkaft-e Gavi (southern Zagros Mountains, Iran): description, affinities, and evidence for butchery. *Journal of Human Evolution*, 57: 248-259.

Shane, P. (2000) Tephrochronology: a New Zealand case study. *Earth-Science Reviews*, 49(1-4): 223-259.

Shatilova, I., Mchedlishvili, N., Rukhadze, L., and Kvavadze, E. (2011) *The History of the flora and Vegetation of Georgia (South Caucasus)*. Tbilisi, Georgian National Museum.

Shea, J.J. 2013. *Stone tools in the Paleolithic and Neolithic Near East*. New York, Cambridge University Press.

Shumilovskikh, L.S., Fleitmann, D., Nowaczyk, N.R., Behling, H., Marret, F., Wegwerth, A., and Arz, H.W. (2014) Orbital- and millennial-scale environmental changes between 64 and 20 ka BP recorded in Black Sea sediments. *Climate of the Past*, 10: 939-954.

Siebel, W., Schmitt, A.K., Kiemele, E., Danišik, M., and Aydin, F. (2011) Acigöl rhyolite field, central Anatolia (part II): geochemical and isotopic (Sr–Nd–Pb, $\delta^{18}O$) constraints on volcanism involving two high-silica rhyolite suites. *Contributions to Mineralogy and Petrology*, 162: 1233-1247.

Singer, B.S., Guillou, H., Jicha, B.R., Laj, C., Kissel, C., Beard, B.I., and Johnson, C.M. (2009) $^{40}Ar/^{39}Ar$, K–Ar and $^{230}Th–^{238}U$ dating of the Laschamp excursion: a radioisotopic tie-point for ice core and climate chronologies. *Earth and Planetary Science Letters*, 286: 80-88.

Smith, P.E., York, D., Chen, Y., and Evensen, N.M. (1996) Single crystal $^{40}Ar–^{39}Ar$ dating of a Late Quaternary paroxysm on Kos, Greece: Concordance of terrestrial and marine ages. *Geophysical Research Letters*, 23: 3047-3050.

Smith, F.H., Jankovic, I., and Karavanic, I. (2005) The assimilation model, modern human origins in Europe, and the extinction of Neanderthals. *Quaternary International*, 137: 7-19.

Smith, V.C., Mark, D.F., Staff, R.A., Blockley, S.P.E., Bronk Ramsey, C., Bryant, C.L., Nakagawa, T., Han, K.K., Weh, A., Takemura, K., Danhara, T., and Suigetsu 2006 project members. (2011a) Toward establishing precise $^{40}Ar/^{39}Ar$ chronologies for Late Pleistocene palaeoclimate archives: an example from the Lake Suigetsu (Japan) sedimentary record. *Quaternary Science Reviews*, 30: 2845-2850.

Smith, V.C., Isaia, R., and Pearce, N.J.G. (2011b) Tephrostratigraphic and glass compositions of post- 15 kyr Campi Flegrei eruptions: implications for eruption history and chronostratigraphic markers. *Quaternary Science Reviews*, 30: 3638-3660.

Smith, V.C., Staff, R.A., Blockley, S.P.E., Bronk Ramsey, C., Nakagawa, T., Mark, D.F., Takemura, K., and Danhara, T. (2013) Identification and correlation of visible tephras in the Lake Suigetsu SG06 sedimentary archive, Japan: chronostratigraphic markers for synchronising of east Asian/west Pacific palaeoclimatic records across the last 150 ka. *Quaternary Science Reviews*, 67: 121-137.

Stockhecke, M., Kwiecien, O., Vigliotti, L., Anselmetti, F.S., Beer, J., Çağatay, M.N., Channell, J.E.T., Kipfer, R., Lachner, J., Litt, T., Pickarski, N., and Sturm, M. (2014a) Chronostratigraphy of the 600,000 year old continental record of Lake Van (Turkey). *Quaternary Science Reviews,* 104: 8-17.

Stockhecke, M., Strum, M., Brunner, I., Schmincke, H-U., Sumita, M., Kipfer, R., Cukur, D., Kwiecien, O., and Anselmetti, F.S. (2014b) Sedimentary evolution and environmental history of Lake Van (Turkey) over the past 600 000 years. *Sedimentology*, 61:1830-1861.

Sulpizio, R., Zancehtta, G., D'Orazio, M.D., Vogel, H., and Wagner, B. (2010) Tephrostratigraphy and tephrochronology of lakes Ohrid and Prespa, Balkans. *Biogeosciences*, 7: 3931-3967.

Sulpizio, R., Alçlçek, M.C., Zanchetta, G., and Solari, L. (2013) Recognition of the Minoan tephra in the Acigöl Basin, western Turkey: implications for inter-archive correlations and fine ash dispersal. *Journal of Quaternary Science*, 28: 329-335.

Sumita, M., and Schmincke, H-U. (2013a) Impact of volcanism on the evolution of Lake Van I: evolution of explosive volcanism of Nemrut Volcano (eastern Anatolia) during the past >400,000 years. *Bulletin of Volcanology*, 75: 1-32.

Sumita, M., and Schmincke, H-U. (2013b) Impact of volcanism on the evolution of Lake Van II: Temporal evolution of explosive volcanism of Nemrut Volcano (eastern Anatolia) during the past ca. 0.4 Ma. *Journal of Volcanology and Geothermal Research*, 253: 15-34.

Sumita M., and Schmincke, H-U. (2013) Researchers working on the Nemrut Volcano, Turkey. Email correspondence regarding the eruptive history of the Nemrut Volcano. Various, throughout the year. Personal communication.

Sumita M., and Schmincke, H-U. (2014) Researchers working on the Nemrut Volcano, Turkey. Email correspondence regarding the eruptive history of the Nemrut Volcano. Samples sent to authors for WDS-EPMA analysis. Various throughout the year. Personal communication.

Sun, S., and McDonough, W.F. (1989) Chemical and isotopic systematics of oceanic basalts: implications for mantle composition and processes. *Geological Society, London, Special Publications*, 42: 313-345.

Svensson, A., Andersen, K.K., Bigler, M., Clausen, H.B., Dahl-Jensen, D., Davies, S.M., Johnsen, S.J., Muscheler, R., Rasmussen, S.O., Röthlisberger, R., Peder Steffensen, J., and Vinther, B.M. (2006) The Greenland ice core chronology 2005, 15–42 ka. Part 2: comparison to other records. *Quaternary Science Reviews*, 25: 3258-3267.

Szakacs, A., Seghedi, I., and Pécskay, Z. (2002) The most recent volcanism in the Carpathian-Pannonian Region. Is there any volcanic hazard? *Geologica Carpathica Special Issue, Proceedings of the XVIIth Congress of Carpathian-Balkan Geological Association*, 53:193-194.

Tamburrino, S., Insinga, D.D., Sprovieri, M., Petrosino, P., and Tiepolo, M. (2012) Major and trace element characterization of tephra layers offshore Pantelleria Island: insights into the last 200 ka of volcanic activity and contribution to the Mediterranean tephrochronology. *Journal of Quaternary Science*, 27: 129-140.

Thorarinsson, S. (1954) The Eruptions of Hekla 1947– 1948. The Tephra Fall from Hekla. *Vis Islendinga*, *Reykjavik*, 2: 68.

Todd, J.A., Austin, W.E.N., and Abbott, P.M. (2014) Quantifying bioturbation of a simulated ash fall event. *Geological Society of London Special Publication*, 398: doi:10.1144/SP398.9

Tokçaer, M., Agostini, S., and Savaşçin, M.Y. (2005) Geotectonic Setting and Origin of the Youngest Kula Volcanics (Western Anatolia), with a New Emplacement Model. *Turkish Journal of Earth Sciences*, 14: 145-166.

Tomlinson, E.L. (2014). Assistant Professor, Geology, School of Natural Sciences, Trinity College Dublin. Excel software for the reduction of LA-ICP-MS data given to Author via Albert, P. 25-28th March. Personal communication.

Tomlinson, E.L., Thordarson, T., Müller, W., Thirlwall, M., and Menzies, M.A. (2010) Microanalysis of tephra by LA-ICP-MS - Strategies, advantages and limitations assessed using the Thorsmörk ignimbrite (Southern Iceland). *Chemical Geology*, 279: 73-89.

Tomlinson, E.L., Kinvig, H.S., Smith, V.C., Blundy, J.D., Gottsmann, J., Müller, W., and Menzies, M.A. (2012a) The Upper and Lower Nisyros Pumices: Revisions to the Mediterranean tephrostratigraphic record based on micro-beam glass geochemistry. *Journal of Volcanology and Geothermal Research*, 243-244: 69-80.

Tomlinson, E.L., Arienzo, I., Civetta, L., Wulf, S., Smith, V.C., Hardiman, M., Lane, C.S., Carandente, A., Orsi, G., Rosi, M., Müller, W., and Menzies, M.A. (2012b) Geochemistry of the Phlegraean Fields (Italy) proximal sources for major Mediterranean tephras: Implications for the dispersal of Plinian and co-ignimbritic components of explosive eruptions. *Geochimica et Cosmochimica Acta*, 93: 102-128.

Tomlinson, E.L., Smith, V.C., Albert, P.G., Aydar, E., Civetta, L., Cioni, R., Çubukçu, E., Gertisser, R., Isaia, R., Menzies, M.A., Orsi, G., Rosi, M., and Zanchetta, G. (2014a) The major and trace element glass compositions of the productive Mediterranean volcanic sources: tools for correlating distal tephra layers in and around Europe. [Online] *Quaternary Science Reviews*, In press, corrected proof, 29 November 2014. doi:10.1016/j.quascirev.2014.10.028

Tomlinson, E.L., Albert, P.G., Wulf, S., Brown, R.J., Smith, V.C., Keller, J., Orsi, G., Bourne, A.J., and Menzies, M.A. (2014b) Age and geochemistry of tephra layers from Ischia, Italy: constraints from proximal-distal correlations with Lago Grande di Monticchio. *Journal of Volcanology and Geothermal Research*, 287: 22-39.

Tryon, C.A., Logan, M.A.V., Mouralis, D., Kuhn, S., Slimak, L., and Balkan-Atli, N. (2009) Building a tephrostratigraphic framework for the Paleolithic of Central Anatolia, Turkey. *Journal of Archaeological Sciences*, 36: 637-652.

Tsanova, T. (2013) The beginning of the Upper Paleolithic in the Iranian Zagros. A taphonomic approach and techno-economic comparison of early Baradostian assemblages from Warwasi and Yafteh (Iran). *Journal of Human Evolution*, 65: 39-64.

Turney, C.S.M., Harkness, D.D., and Lowe, J.J. (1997) The use of microtephra horizons to correlate Late-glacial lake sediment successions in Scotland. *Journal of Quaternary Science*, 12: 525-531.

Tushabramishvili, D.M. (1978) *Arkheologicheskie panyatniki Tsutskhvatskogo mnogoetajnogo peshernogo kompleska (archaeological sites of the Tsutskhvati Cave complex)*. Metsniereba, Tbilisi. (Cited in Adler and Tushabramishvili, 2004)

Tushabramishvili, N., Pleurdeau, D., Moncel, M.H., Agapishvili, T., Vekua, A., Bukhsianidze, M., Maureille, B., Muskhelishvili, A., Kapanadze, N., and Lordkipanidze, D. (2012) Human remains from a new Upper Pleistocene sequence in Bondi Cave (Western Georgia). *Journal of Human Evolution*, 62: 179-185.

Van Daele, M., Moernaut, J., Silversmith, G., Schmidt, S., Fontijn, K., Heirman, K., Vandoorne, W., De Clercq, M., Van Acker, J., Wolff, C., Pino, M., Urrutia, R., Roberts, S.J., Vincze, L., and De Batist, M. 2014. The 600 yr eruptive history of Villarrica Volcano (Chile) revealed by annually laminated lake sediments. *Geological Society of America Bulletin*, 126: 481-498.

Van den Bogaard, P., and Schminke, H-U. (1985) Laacher See tephra: A widespread isochronous late Quaternary tephra layer in central and northern Europe. *Geological Society of America Bulletin*, 96: 1554-1571.

Villa, P., and Roebroeks, W. (2014) Neanderthal Demise: An Archaeological Analysis of the Modern Human Superiority Complex. [Online]. *PLoS ONE*, 9(4). e96424. doi:10.1371/journal.pone.0096424.

Volodicheva, N. (2002) The Caucasus. In: Shahgedanova, M. eds. *The physical geography of northern Eurasia*. Oxford, Oxford University Press: 350-376.

Watts, W.A., Allen, J.R.M., and Huntley, B. (1996) Vegetation history and palaeoclimate of the last glacial period at Lago Grande di Monticchio, Southern Italy. *Quaternary Science Reviews*, 15: 133-153.

Wilkinson, K. (2013) Reader in Environmental Archaeology, University of Winchester. Conversations at the Lusakert 1 rock shelter, Armenia. Field work, 25th -29th June. Personal communication.

Wolpoff, M.H., Hawks, J., Frayer, D.W., and Hunley, K. (2001) Modern Human Ancestry at the Peripheries: A test of the Replacement Theory. *Science*, 291: 293-297.

Wood, R.E., Douka, K., Boscato, P., Haesaerts, P., Sinitsyn, A., and Higham, T.F.G. (2012) Testing the ABOx-Sc method: dating known-age charcoals associated with the Campanian Ignimbrite. *Quaternary Geochronology*, 9.

Wulf, 2013. Tephrochronologie des 133 ka Sedimentprofils des Lago Grande di Monticchio [internet]. GFZ, Helmholtz-Zentrum, Potsdam. Available from < http://www.gfz-potsdam.de/forschung/ueberblick/departments/department-5/klimadynamik-und-landschaftsentwicklung/projekte/lago-grande-di-monticchio-palaeoklima-umwelt-und-tephrochronologie-archiv/tephrochronologie-des-133-ka-sedimentprofils-des-lago-grande-di-monticchio/#top> [Accessed on 02/12/2014]

Wulf, S., Kraml, M., Kuhn, T., Schwarz, M., Inthorn, M., J. Keller., I, Kuscu., and Halbach, P. (2002) Marine tephra from the Cape Riva eruption (22 ka) of Santorini in the Sea of Marmara. *Marine Geology*, 183: 131-141.

Wulf, S., Kraml, M., Brauer, A., Keller, J., and Negendank, J.F.E. (2004) Tephrochronology of the 100 ka lacustrine sediment record of Lago Grande di Monticchio (southern Italy). *Quaternary International*, 122: 7-30.

Wulf, S., Keller, J., Paterne, M., Mingram, J., Lauterbach, S., Opitz, S., Sottili, G., Giaccio, B., Albert, P.G., Satow, C., Tomlinson, E.L., Viccaro, M., and Brauer, A. (2012) The 100–133 ka record of Italian explosive volcanism and revised tephrochronology of Lago Grande di Monticchio. *Quaternary Science Reviews*, 58: 104-123.

Wulf, S., and Veres, D. (2014). Scientific researchers, studying the Ciomadul volcano, Romania. Correspondence (email and conversations) regarding tephra compositions from two eruptions from the Ciomadul Volcano. 24th -27th April and 9th -14th May.

Wutke, K., Wulf, S., Tomlinson, E.L., Hardiman, M., Dulski, P., Luterbacher, J., and Brauer, A. (2014) Geochemical properties and environmental impacts of seven Campanian tephra layers deposited between 40 and 38 ka BP in the varved lake sediments of Lago Grande di Monticchio, southern Italy. [Online]. *Quaternary Science Reviews*, in press, corrected proof, 22 August 2014. doi:10.1016/j.quascirev.2014.05.017.

Yilmaz, Y., Güner, Y., and Şaroğlu, F. (1998) Geology of the quaternary volcanic centres of the east Anatolia. *Journal of Volcanology and Geothermal Research*, 85: 173-210.

Yilmaz, Y. (1990) Comparison of young volcanic associations of western and eastern Anatolia formed under a compressional regime: a review. *Journal of Volcanology and Geothermal Research*, 44: 69-87.

Zanchetta, G., Sulpizio, R., Giaccio, B., Siani, G., Paterne, M., Wulf, S., and D'Orazio, M. (2008) The Y-3 tephra: A Last Glacial stratigraphic marker for the central Mediterranean basin. *Journal of Volcanology and Geothermal Research*, 177: 145-154.

Zanchetta, G., Sulpizio, R., Roberts, N., Cioni, R., Eastwood, W.J., Siani, G., Caron, B., Paterne, M., and Soantacroce, R. (2011) Tephrostratigraphy, chronology and climatic events of the Mediterranean basin during the Holocene: an overview. *The Holocene,* 21: 33 - 52.

Zilhão, J. (2006) Neanderthals and moderns mixed, and it matters. *Evolutionary Anthropology: Issues, News, and Reviews*, 15: 183-195.

Project webpages mentioned in text

EFCHED, Environmental Factors in the Chronology of Human Evolution & Dispersal. Funded by the Natural Environment Research Council.
<http://www.gla.ac.uk/projects/efched/>

INTIMATE, INTergrating Ice cores, MArine and TErrestrial records. COST Action group 2010-2014, (ES0907)**.** INQUA recognised Focus Group.<http://cost-es0907.geoenvi.org/>

RESET, Response of Humans to Abrupt Environmental Transitions. Funded by the Natural Environment Research Council.<http://c14.arch.ox.ac.uk/reset/embed.php?File=>

Appendix 1 (CD)

Geochemical data and OxCal outputs

(Email author – victoria.cullen@rlaha.ox.ac.uk)

References for papers produced as part of this DPhil research:

Cullen, V.L. Smith, V.C., and Arz, H. (2014) The detailed tephrostratigraphy of a c ore from the south-east Black Sea spanning the last ~60 ka. *Journal of Quaternary Science*, 29: 675-690.

Lane, C.S., Cullen, V.L., White, D., Bramham-Law, C.W.F., and Smith, V.C. (2014) Cryptotephra as a dating and correlation tool in archaeology. *Journal of Archaeological Sciences*, 42: 42-50.